DEVELOPMENT OF METHODOLOGIES TOWARD PHOSGENE-FREE SYNTHESES OF MORPHOLOGICALLY TUNABLE POLYURETHANES AND INVESTIGATION OF A SOLVATOCHROMIC CARBONATE

A Dissertation

by

CHRISTOPHER HOUSTON KOMATSU

Submitted to the Office of Graduate and Professional Studies of
Texas A&M University
in partial fulfillment of the requirements for the degree of

DOCTOR OF PHILOSOPHY

Chair of Committee,	Karen L. Wooley
Committee Members,	Emily B. Pentzer
	David E. Bergbreiter
	Melissa A. Grunlan
Head of Department,	Simon North

August 2020

Major Subject: Organic Chemistry

ABSTRACT

Polyurethanes (PUs) comprise an important class of polymers that are used for a multitude of industrial applications. However, the toxicity of certain metal-containing catalysts and diisocyanate reagents, as well as the nonrenewability of many common multifunctional hydroxyl monomers, have led to the investigation of environmentally friendly and sustainable alternatives. Additionally, the use of nonbiodegradable and nonrecyclable polymers has led to astonishing accumulation of waste in the world's oceans, prompting an increasing outcry from the public. The work presented in this dissertation focuses on replacing nonrenewable starting materials such as metal-containing catalysts and multifunctional hydroxyl monomers with natural products or organically derived reagents.

A synthetic methodology was developed employing relatively benign reagents that allows for the incorporation of carbohydrate-based natural products into functional PUs under mild conditions, resulting in nearly quantitative macrocycle formation, as extensively verified using matrix-assisted laser desorption/ionization – time-of-flight mass spectrometry (MALDI-TOF MS). This work involved screening of conditions for PU synthesis using hexamethylene-1,6-di(*p*-nitrophenyl)carbamate (HMDNC), a 1,8-diazabicyclo[5.4.0]undec-7-ene (DBU) organobase, and the biosourced diol, methyl 4,6-O-benzylidene-α-(D)-glucopyranoside. Unlike many previous PU syntheses involving dicarbamates, this system achieved polymerization under relatively mild conditions, *e.g.*, attaining a molar mass of up to *ca.* 9 kDa in 8 h at 40 °C at ambient pressure. This chemistry has potential applicability to a wide range of di(*p*-nitrophenyl)carbamates and diols that should create broad interest in the PU community for sustainability and hazard mitigation.

Additionally, this dissertation examines the unusual selectivity for cyclization that the glucopyranoside dihydroxyl monomer imparts on the system using Raman spectroscopy and molecular modeling. A structural difference was indicated by Raman spectroscopy, but its identity remains inconclusive by molecular modeling. Third, multiple synthetic schemes were attempted toward an antibiofouling PU using a capsaicinoid molecule as a sensory deterrent for marine and microbial antibiofouling. The conjugation *via* the carbonate linkage appears most promising, but all synthetic routes were complicated by several factors and, thus, remain incomplete. Lastly, a solvatochromic carbonate was realized, and molecular modeling indicates that it undergoes electron transfer in polar, heteroatom-containing solvents, giving rise to a solvent-induced "redoxochromic" effect that has potential applicability in radical-mediated reactions and polymerizations.

DEDICATION

I dedicate this dissertation to my family, especially my grandfather, Albert Komatsu, and to my grandparents who are no longer with us and who have supported me all of my life. Also included are my parents and my brother who have supported me. I cannot leave out my dog, Ginger, who supported me since elementary school, through my most difficult years in middle school, and was with me through high school, college, and my first year of graduate school. I would also like to dedicate this to my high school chemistry teacher, Marsha Stripe, for inspiring me to pursue a degree in chemistry and to thank her for all of the time and support that she provided me. Additionally, I dedicate this dissertation to all of my other mentors, teachers, and professors who have helped me along the way including: Mr. Walter Hearnes, Mr. Rupert Crabb, Coach Mark Cox, Dr. William Fanning Jr., Coach Blake Brockermeyer, Ms. Ann Baldwin, Dr. Bart Pointer, Mrs. Amy Martin-Nelson, Mr. Wallace Worden, Mr. Greg Nowlin, Dr. Gary Defotis, Dr. Christopher Abelt, Dr. Kristin Wustholz, Dr. Jonathan Scheerer, Dr. Elizabeth Arsenault, and Dr. David Kranbuehl. I'd also like to thank Dr. Tracy Underwood for all of her guidance for many years. This dissertation is also dedicated to anyone else I may have forgotten off the top of my head and who made me who I am today.

ACKNOWLEDGEMENTS

I would first like to thank my advisor, Prof. Karen L. Wooley, for her support, guidance, and help throughout my graduate education at Texas A&M. None of the work done in this dissertation would be possible without her, and none of the spectacular opportunities that I have had during my PhD would likely have been available. I have met two Nobel Laureates, presented my work at some of the most prestigious conferences, and have traveled across the Atlantic to do research in Bordeaux, France because of doors that she opened for me. I am the researcher that I am today because of her, and my abilities reflect directly on her mentorship and instruction. As such, I am honored to join the prestigious alumni that have graduated from her group.

I would also like to thank my committee members, Prof. Emily B. Pentzer, Prof. Melissa A. Grunlan, and Prof. David E. Bergbreiter, for their guidance and support throughout my time at Texas A&M. Prof. Pentzer was especially gracious to join my committee in my final year shortly after she joined Texas A&M University, for which I am particularly thankful. I would also like to thank Prof. Kevin Burgess for his support throughout my time at Texas A&M as well.

In particular, I would like to thank Prof. Henri Cramail and Prof. Etienne Grau for graciously inviting me to the University of Bordeaux to conduct research as part of a collaboration between our groups. Not only did I get a chance to visit France for the first time, they lent me their time and funding to host me at their lab to teach me about CO_2 chemistry. I look forward to seeing them, as well as my other friends in France, again soon, and I hope that this collaboration yields results for our two groups soon. I would also like to thank Dr. Fiona Maggliozzi, who was my mentor while there, as well as Leah Spitzer, Nicolas Longhitano, and Dr. Christopher Costa for advice, for helping me with my French, and for showing me around Bordeaux.

Thanks is given to my collaborators, who not only assisted me with specific problems, but also helped expand my chemistry expertise. McKenna J. Redding in Prof. Scott Grayson's group at Tulane University gave significant advice on mass spectrometry, as did Prof. David Russell and his group. Dr. Yohannes Rezenom and Mike Raulerson were also helpful in working with me on mass spectrometry data. Dr. Daniel Dobbins in Prof. Brent Sumerlin's group at the University of Florida helped run a few samples from Chapter 5 on their size exclusion chromatography instrument for which I am also thankful. Dr. Gregory P. Wylie, Dr. Douglas Elliott, and Dr. Vladimir Bakhmoutov were all very helpful with specialized nuclear magnetic resonance spectroscopy techniques. I would also like to thank Prof. Lisa Perez and Andreas Ehnbom in Prof. Hall's group for assisting and advising me in the molecular modeling work, as well as for Andreas performing conformational sampling for Chapter 3.

Special thanks need to be given to my mentors and colleagues. Dr. Samantha Kristufek and Dr. Kevin Wacker were my co-mentors for most of this dissertation. Both provided instruction, valuable techniques, advice, and direction. Both have continued to correspond with me and provide advice late in my time here as a PhD student after they have graduated. This dissertation would not exist without them. Prof. Rachel Letteri, who is now faculty at the University of Virginia, also mentored me to great extent, for which I'm thankful. Dr. Letteri provided crucial support, advice, and direction and lifted me up when things were not going well. Dr. Alex Kosanovich provided me with not only with advice and support, but he also provided productive conversations that led to significant findings and research collaborations. Dr. Guorong Sun has supported me since I arrived at Texas A&M and has provided advice and productive conversations and has even offered to help complete some of my work after I leave, for which I am immensely grateful. I would like to thank everyone in Prof. Wooley's lab who provided

general support as well. I would also like to thank Prof. Quentin Michaudel for his advice, productive conversations, and support and for his family hosting me for dinners while I was in Bordeaux, France.

Lastly, I must thank my friends in my cohort, in what I'll call "the dirty dozen" for the purpose of this dissertation, who kept me (mostly) sane during my time here by sharing food, drinks, and crawfish on weekends and grading nights. Additionally, they sometimes even provided personal advice and career advice and helped me keep a positive outlook. These friends are Dr. Alexandra Trott, Chris Watson, Dr. Thomas Malinski, Dr. Joshua Winner, Dr. Corey Burns, Dr. Seth Cory, Dr. Lauren Washburn, Dr. Kelsey Schulte, Dr. Greg Waetzig, Dr. Tom O'Loughlin, Ryan Sarkisian, and Dr. Alex Kalin.

FUNDING SOURCES

Funding Sources

This work was made possible in part by the National Science Foundation under grant number CHE-1610311. Additionally, a grant supplement was awarded for an international collaboration. Its contents are solely the responsibility of the authors and do not necessarily represent the official views of the National Science Foundation.

This work was also made possible in part by the W.T.-Doherty Welch Foundation under grant number A-0001. Its contents are solely the responsibility of the authors and do not necessarily represent the official views of the Welch Foundation.

Part of the work in Chapter 4 was funded by the Office of Naval Research under grant number N00014-14-1-0082. Its contents are solely the responsibility of the authors and do not necessarily represent the official views of the Office of Naval Research or the Department of Defense.

Travel expenses for the 2019 Gordon Research Conference was supported by the Eastman Chemical Travel Award through the Department of Chemistry.

NOMENCLATURE

1,8-DHA	1,8-dihydroxyanthraquinone
2D	two-dimensional
acac	acetylacetonate
ACS	American Chemical Society
AM1	Austin Model 1
ATR-FTIR	attenuated total reflectance – Fourier transform infrared
ATRP	atom transfer radical polymerization
BA	benzoic acid
BG	blocking group
BPA	bisphenol A
BSA	bovine serum albumin
CPCM	conductor-like polarizable continuum model
CV	cyclic voltammetry
DABCO	diazabicyclo[2.2.2]octane
DBTDL	dibutyltin dilaurate
DBU	1,8-diazabicyclo[5.4.0]undec-7-ene
DCM	dichloromethane
DCTB	*trans*-2-[3-(4-*tert*-butylphenyl)-2-methyl-2-propylidene]malononitrile
DFT	density functional theory
DIPEA	*N*,*N*-diisopropyl-*N*-ethylamine
DMA	*N*,*N*-dimethylaniline

DMAc	*N*,*N*-dimethylacetamide
DMF	*N*,*N*-dimethylformamide
DMOPA	dimethylolpropionic acid
DMPA	2,2-dimethyoxy-2-phenylacetophenone
DMSO	dimethylsulfoxide
DMTDA	dimethyltin diacetate
DMTDL	dimethyltin dilaurate
DMTMA	dimethyltin methoxy acetate
DSC	differential scanning calorimetry
EPR	electron paramagnetic resonance
ESI	electrospray ionization
EtOH	Ethanol
gCOSY	gradient-selected homonuclear correlation
GIAO	gauge-independent atomic orbital
GVL	γ-valerolactone
HABA	2-(4-hydroxyphenylazo)benzoic acid
HF	Hartree-Fock
HFIP	1,1,1,3,3,3-hexafluorisopropan-2-ol
HMBC	heteronuclear multiple bond correlation
HMDI	hexamethylene-1,6-diisocyanate
HMDNC	hexamethylene-1,6-di(*p*-nitrophenyl)carbamate
HMQC	heteronuclear multiple quantum coherence
HOMO	highest occupied molecular orbital

HRMS	high-resolution mass spectrometry
IPDI	isophorone diisocyanate
IR	infrared
LCAO	linear combination of all atomic orbitals
LED	light-emitting diode
LiHMDS	lithium bis(trimethylsilyl)amide
LMS	Laboratory for Molecular Simulation
LUMO	lowest unoccupied molecular orbital
MALDI-TOF MS	matrix-assisted laser desorption/ionization – time-of-flight mass spectrometry
MDI	4,4’-methylene diphenyl diisocyanate
MO	molecular orbital
MP2	Møller-Plesset perturbation 2
MTBD	7-methyl-1,5,7-triazabicyclo[4.4.0]dec-5-ene
NaTFA	sodium trifluoroacetate
NHC	*N*-heterocyclic carbene
NMP	1-methyl-2-pyrollidinone
NMR	nuclear magnetic resonance
PBS	phosphate-buffered saline
PCM	polarizable continuum model
PCR	polymerase chain reaction
PEG	poly(ethylene glycol)
PET	photoinduced electron transfer

PGU	poly(glucose urethane)
PHU	poly(hydroxyurethane)
PIE	pulsed ion extraction
PLA	poly(lactic acid)
PM6	Parametric Model 6
PM7	Parametric Model 7
PMMA	poly(methyl methacrylate)
PTMG	poly(tetramethylene glycol)
PTMO	poly(tetramethylene oxide)
PU	polyurethane
RAFT	reversible addition-fragmentation chain transfer
RDS	rate-determining step
REACH	Registration, Evaluation, Authorization, and Restriction of Chemicals
ROP	ring-opening polymerization
SEC	size-exclusion chromatography
SMD	solvation model based on density
SPS	Solvent Purification System
TBD	1,5,7-triazabicyclo[4.4.0]dec-5-ene
TBDMS	*tert*-butyldimethylsilyl
TBDMSCl	*tert*-butyldimethylsilyl chloride
T_d	degradation temperature
TDI	toluene diisocyanate
TEA	*N*,*N*,*N*-triethylamine

TFA	trifluoroacetic acid
TFMI	bis(trifluoromethanesulfonyl)imide
T_g	glass transition temperature
TGA	thermogravimetric analysis
THAP	2,4,6-trihydroxyacetophenone
THF	tetrahydrofuran
TLC	thin-layer chromatography
T_m	melting temperature
TMS	tetramethylsilane
TMXDI	*m*-tetramethylxylylene diisocyanate
UMMS	unit-mass mass spectrometry
US	United States
UV	ultraviolet
UV-VIS	ultraviolet–visible spectroscopy
VOC	volatile organic compound

TABLE OF CONTENTS

Page

Page

Page

LIST OF FIGURES

FIGURE Page

FIGURE Page

FIGURE Page

FIGURE Page

FIGURE Page

FIGURE Page

LIST OF TABLES

1. INTRODUCTION: A REVIEW OF POLYURETHANE CHEMISTRY

1.1. Introduction

PUs are an important polymer class featuring carbamate [R(H)N-C(O)-OR'] linkages, most commonly derived from the addition reaction of a multifunctional isocyanate (O=C=N-R-N=C=O) with a multifunctional polyol (HO-R'-OH).[1] These polymerizations result in materials with wide-ranging applications in coatings, adhesives, sealants, elastomers, and foams, among others.[2-4] The ability of highly varied functional groups to be co-incorporated (ureas, isocyanurates, etc.) and the resultant tunability of these materials helped PU production to surpass 2.6 million tons in 2017 alone.[1-7] With this in mind, it is not unreasonable to assume that when Otto Bayer first discovered PUs in 1937, he likely did not anticipate exactly how widely used and diverse these materials would become, let alone the chemistries that have spawned from their production.[8] Although nonrenewable diols, such as poly(ethylene glycol) (PEG) and poly(tetramethylene glycol) (PTMG), are commonly used, the current industrial trend has moved toward more biosourced and renewable diols, including naturally derived oils.[9-12] While isocyanates occupy a whole field of chemistry themselves that includes and goes well beyond PUs, their notable reactivity and toxicity have come under increased regulatory scrutiny, and outsize efforts are being undertaken to develop alternative methods and reagents that allow access to analogous reactivity for PU production.[8,13-15] Additionally, many metal catalysts used industrially are regarded as toxic and nonrenewable, thus offering opportunities for improvement.[16]

General synthetic methods involve three primary components: a multifunctional diol, a multifunctional isocyanate, and a catalyst. Solvent conditions vary widely, and reaction temperatures are typically mild and range from room temperature to 120 °C.[1,17-20] The catalysts

primarily employed in industrial production are variations of tin (Sn), such as dibutyltin dilaurate (DBTDL) or dimethyltin dilaurate (DMTDL).[4,16] PUs are manufactured as linear thermoplastics, cross-linked thermosets, or a mixture of both depending on the desired application.[12] This review surveys current PU applications and conventional and recent PU synthetic methodologies and comments on the challenges posed by making PUs sustainable industrially.

1.2. Polyurethane Applications

Linear, thermoplastic PUs are used for coatings, solid elastomers, packaging, and biomedical applications.[1] The precise synthetic procedures can vary for these thermoplastic systems, but they typically involve the reaction of a macrodiol (a polyether- or polyester-based diol) with an excess of diisocyanate to form a PU prepolymer that is diisocyanate-terminated, allowing it to undergo subsequent reactions.[12] Such PU prepolymers can be applied in "moisture-cure urethane coating applications," where they can be spray-coated onto a surface, the ambient moisture in the air reacts with the diisocyanate termini (liberating carbon dioxide [CO_2] and forming an amine) in the presence of a catalyst to form urea [R(H)N-C(O)-N(H)R] linkages, and the final polymer is a poly(urethane-urea).[18] One other end use of this macro-prepolymer is for PU elastomers by adding a difunctional "chain extender" such as a low-molar-mass diamine (which introduces urea linkages) or a diol.[12] These chain extenders include ethylene glycol, 1,4-butanediol, 1,6-hexanediol, diethyltoluenediamine, and methylenebis(*p*-aminobenzene).[1] Typically, PU elastomers contain alternating flexible "soft" segments, composed of long, flexible macrodiols, and more rigid "hard" segments, made of urethane groups formed from an aromatic isocyanate, small-molecule chain extenders, or urea linkages.[4,21-23]

It is well documented that these hard and soft segments phase-separate into nanodomains, where the hard segments can self-assemble and crystallize while the soft segments assemble

amorphously so that they can uncoil when a stress is applied to the system.[21,22] In this regard, hard segments can also be formed from urethane—and especially urea—groups themselves, even with flexible diisocyanates, because of both the formation of strong hydrogen bond interactions between chains and significant differences in polarity between the polar urethane groups and a less-polar diol.[4,23] Because these polymers are linear and are only pseudo-cross-linked *via* noncovalent interactions (sometimes referred to as "physical cross-linking"), the shape-memory behavior is thermoreversible, and there have been reports of self-healing upon heating as well.[21,22] Phase-separated materials are notable for exhibiting two glass transition temperatures (T_g) and sometimes two different melting temperatures (T_m) corresponding to the hard and soft segments.[23] The addition of diamines as chain extenders increases material properties such as Young's modulus, both through increased hydrogen bonding of the resulting urea linkages and an increased ratio of hard to soft segments per chain.[4,7] In the case of Spandex, the hard segments are actually urea linkages, and the strength of the hydrogen bonds formed in the hard domains allow for large, reversible deformations.[22] Mechanical properties, and even the dielectric constant as recently shown,[24] can be tuned by changing the structures and ratios of both the diisocyanates and the diols.[12]

PUs manufactured as cross-linked networks find use as foams and other solids in applications such as heat insulation and vibrational dampening, among others.[12,25] To make a cross-linked network, tri- and polyfunctional monomers are used, such as polyhydroxyl compounds, commonly referred to as "polyols."[1,12] In order to form a foam, a "blowing agent" is required to create bubbling.[12,26] Having replaced freon ($CFCl_3$) for environmental reasons, physical blowing agents such as *n*-pentane—which evaporate at reaction temperatures and form bubbles—fill this role for certain applications such as building insulation due to its low thermal

conductivity.[12,26] Water (H_2O) behaves as a chemical blowing agent that liberates CO_2 during the reaction with an isocyanate to form an amine and subsequent urea linkage.[1,27] Longer, more-flexible polyols typically result in more-flexible foams, while shorter-chain polyols, the addition of chain extender units, or more-rigid diisocyanate monomers favor more-rigid foams.[1,12] A surfactant is also added as an essential component to stabilize and control the size and dispersity of the gas bubbles caused by the blowing agent.[26] It has been demonstrated that covalently cross-linked systems typically result in superior mechanical properties compared to noncovalently cross-linked systems in the form of higher toughness, recovery stresses, and cyclic recoverable strains, as well as being more thermally resilient and wear resistant for use in harsh environments.[25,28,29] For vibrational dampening applications, especially under harsh conditions, cross-linked PU solids can be made from the same process as for foams but without blowing agents.[22,29] Having discussed the synthesis and structure of PUs and their applications, it is important to briefly mention a recent development into how these resulting materials are formulated for consumer use.

In the past decade or so, industry has refined techniques for waterborne PU dispersions, which are sometimes referred to as "solvent-less waterborne PUs" in order to address concerns regarding volatile organic compounds (VOCs) in PU end-use items.[20,30] These systems can be formulated with polyols to form resins or diols to form thermoplastic films or coatings.[20,31] These systems comprise external or internal emulsifying groups that cause a PU—or PU prepolymer—to form dispersions/colloids of micelles once the prepolymer is dispersed in water. The addition of internal emulsifying groups at the polymer termini or randomly in the main chains, such as dimethylolpropionic acid (DMOPA) for anionic dispersions or quaternary ammonium species for cationic dispersions, is preferred over adding an external emulsifier, which requires strong shear forces to disperse the macromolecule and generates coarse particles and poor dispersion

stability.[20,31] Sometimes, PEG is used as the hydrophilic internal emulsifying species.[20] Dispersions containing DMOPA moieties also have the ability to undergo cross-linking, such as with aziridines or by using hexa(methoxymethyl) melamine.[20] If the polymers in these dispersions are terminated by hydroxy or carboxylic acid moieties, they can undergo further reaction with diisocyanates in applications such as "two-component" wood coatings.[20] For these systems, *m*-tetramethylxylylene diisocyanate (TMXDI) is sometimes used because it exhibits low reactivity with water.[14] With the introduction of generalized methods for industrial PUs, it becomes necessary to delve deeper into the chemistry underlying these processes and the construction of the monomers that constitute the backbone of PU technology.

1.3. New Polyurethane Applications

While the diversity of PUs in the aforementioned applications is well established, there have emerged recent developments that have expanded the applicability of PUs into nontraditional applications. Biomedical applications have emerged as an increasingly attractive application industrially because of their inherent biocompatibility.[32] Additionally, stimuli-responsive PUs and reversibly cross-linked PUs have surfaced as a way to bridge the advantages of physically cross-linked and covalently cross-linked systems. Several other miscellaneous applications have been reported, such as infrared (IR) "cloaking" for military use and CO_2 capture, among others.

1.3.1. Biomedical Applications

PUs have been used for ligament and meniscus reconstruction, blood-contacting materials, infusion pumps, heart valves, insulators for pacemaker leads, nerve guidance channels, and dental applications because of their inherent bio- and blood compatibility and easy modification.[33,34] Biofilm formation, induced blood coagulation, and other biological responses on the surfaces of medical devices are a serious problem that can result in device failure and bacterial

infections.[32,33,35] PEG containing PUs has been shown to be particularly effective in deterring protein adhesion and biofilm formation because of the formation of a hydration layer.[32,35,36] Güner and coworkers synthesized a PU using PEG and castor oil that was modified by grafting acrylic acid *via* plasma treatment to modify the surface morphology; they concluded that surface morphology ("roughness") has more of an effect on protein adhesion than hydrophilicity.[36] Ye and coworkers synthesized a PU by first ring-opening 2-ethyl-2oxazoline and then end-capping with bis(hydroxymethyl)propionic acid to form a diol that could be made into a branched architecture by reacting it with 4,4'-methylene diphenyl diisocyanate (MDI) and polycaprolactone.[33] The resulting PU-*g*-poly(2-ethyl-2-oxazoline) showed higher resistance to protein adhesion with higher graft density and longer branch lengths; it also showed that protein adhesion could be reduced by 97% relative to unmodified PU.[33] Tan, He, and coworkers reported the synthesis of a cross-linked PU made with PEG or poly(tetramethylene oxide) (PTMO) and L-lysine containing gemini quaternary ammonium salts; this system killed 99.99% of the Gram-positive *S. aureus* bacteria in the surrounding environment while leaving no surviving bacteria on its surface for more than 150 d.[35] The use of PUs as antibiofouling coatings has continued to develop significantly from simple systems relying on PEG for amphiphilicity, and there is certainly more investigation needed with regard to zwitterionic PUs for this purpose.

1.3.2. Dynamic Cross-Linked Networks and Polyurethane Vitrimers

A recently emerging application for PUs is the incorporation of reversible covalent cross-linked networks triggered by stimuli such as heat or light. Work has been done on the ability to synthesize materials that possess both the desired mechanical properties of nonprocessable thermoset materials and the thermal processability of physically cross-linked thermoplastic polymers.[25,37,38] Dynamic cross-linked networks fall into two broad categories: 1) networks that

undergo dynamic exchange interactions by dissociative processes and 2) networks that are dynamic because of associative exchange interactions, referred to as "vitrimers."[39]

It is important to recall that the urethane bond formation is inherently reversible, especially at elevated temperatures.[14] Dichtel and coworkers showed that urethane bonds in traditional cross-linked PU networks can be reversible at temperatures of 140 °C in the presence of certain catalysts, as evidenced by their ability to undergo rapid stress relaxation at this temperature—a diagnostic sign of a dynamic covalent network.[40] Samples containing the bismuth catalyst had the most rapid relaxation times at all temperatures, while the iron catalyst was the only one that showed signs of irreversible degradation.[40] While interesting fundamentally, this work also has significant implications for PU foam recyclability.

This dissociative exchange process can be contrasted with PU networks that can undergo an associative exchange process at elevated temperatures (vitrimers).[39] Dichtel, Hillmyer, Cramer, and coworkers synthesized a cross-linked poly(hydroxy urethane) vitrimer material that became dynamic at 111 °C and exhibited postfracture recoveries of Young's modulus and ultimate strain, as well as tensile strengths of 76%, 69%, and 74%, respectively, after heating to 160 °C, indicating that the material was self-healing.[39] There has been and will be plenty more work done in thermally reversible PU networks, but these works are some of the recent ones.[41]

A different and slightly less prevalent flavor of this emerging application is the ability to reprocess cross-linked PU systems by exposure to varying wavelengths of light. Li and coworkers recently reported the synthesis of a linear PU from toluene diisocyanate (TDI), poly(ethylene propylene adipate) diol, and 2,2-bis(hydroxymethyl)butyl-3-phenylacrylate—made from glycerol and cinnamoyl chloride.[25] Upon ultraviolet (UV) irradiation at 300 nm, double bonds on the cinnamoyl groups underwent a [2+2] cycloaddition and formed a cross-linked network, as

evidenced by dramatic increases in strain at break, tensile strength, Young's modulus, and toughness correlating with irradiation times up to 72 h, as well as the loss of the cinnamoyl absorption by ultraviolet–visible spectroscopy (UV-VIS).[25] However, insolubility of the materials was achieved after 120 h coinciding with a loss in ultimate strain, indicating a full transition to a gel.[25] On the other hand, irradiation at 250 nm corresponded with the cycloreversion back to the linear PU.[25] There has been less research in this area of reversible cross-linking for PUs, so this should remain an intriguing target for researchers going forward.

1.3.3. Miscellaneous Applications: CO_2 Capture and Infrared Cloaking

The scope of PU chemistry and its applications far exceed the capacity of this review. However, there have been two interesting works published on rather novel applications for which PUs have not been traditionally used and for which additional attention is deserved: the first being CO_2 capture *via* a poly(ionic liquid) PU and the second being a PU-based IR invisibility cloaking material for potential military applications.

The first work by Mecerreyes and coworkers reported the synthesis of ionic liquid PUs made from four different ionic diols based on ammonium, quinuclidinium, diquinuclidinium, and imidazolium cations and a series of diisocyanates and anions for CO_2 capture. The resulting PUs had T_g values ranging from 30 to 78 °C, as well as high thermal stability up to 275 °C.[42] It was determined that the PU containing the diquinuclidinium cationic diol, 4,4'-methylene bis(cyclohexyl isocyanate), and acetate or tetrafluoroborate (BF_4) anions exhibited the highest CO_2 sorption of 18.25 and 24.76 mg/g at 273 K and 1 bar of CO_2, which is reportedly higher than the highest known value for cross-linked mesoporous poly(ionic liquids) at 20.24 mg/g under the same conditions.[42] It is also notable that this PU was more difficult to regenerate by CO_2 desorption than some of the other systems discussed.[42] Thus, it is clear for future work in this area that a

balance must be reached between the CO_2 sorption capacity and ease of desorption for regeneration in order to avoid the energy costs present with current CO_2 scrubbing technology.[43]

Another interesting innovation is the recent report by Ju, Park, and coworkers[44] on the synthesis of a PU composite material for use as a cloaking fabric that obscures "hot" objects from thermal imaging sensors.[44] All objects with a surface temperature near room temperature and above emit IR radiation that can be detected and imaged by devices known as "thermal cameras," which have been used by military and police forces for some time now.[44] A PU solution containing tin(IV) oxide (SnO_2) nanoparticles was then extruded into a "coagulation bath" of deionized water to precipitate as a fiber in a process known as "wet spinning" to create a cavity in the center of the extruded fiber.[44] The resulting hollow fiber composite was thus able to thermally insulate a hot object on one side of the fiber from the other side of it, while the SnO_2 nanoparticles are known to be reflective in the IR region.[44] The authors demonstrated that an electrically heated object was almost entirely indistinguishable from the background when using thermal imaging equipment, even after allowing the material to thermally equilibrate with the object for 30 min, while a polyester control material showed a significant thermal signature of the underlying object.[44] This is yet another application among many for which PUs can be used.

1.4. Diols and Polyols

The conventional diols used industrially are petrochemical-based polyethers or polyesters, as shown in Figure 1-1.[26] Polyester diols and polyols generally impart better toughness, oil resistance, and thermal stability to the PU product while also being readily biodegraded and hydrolyzed.[22,26] These benefits are given by varying degrees of crystallinity within the polyester backbones, which can limit elasticity and transparency.[26,45] Examples of this category include macrodiols such as poly(ethylene adipate), poly(ε-caprolactone), and polysuccinates.[12,45]

Polyether-based diols have lower T_g and greater hydrolytic resistance and include PEG, PTMG, and poly(propylene glycol), among others.[22,46] While both types have traditionally been produced from petrochemicals, some production has been achieved from biobased starting materials (i.e., a method for producing ethylene oxide from ethanol).[26,47] Although the PUs made from polyester-based diols have shown varying degrees of biodegradability due to ester-linkage hydrolysis, PUs made from the polyether diols have typically been regarded as nonbiodegradable.[48] Reports in the media and in the polymer community have brought to light significant concern over polymer accumulation in the environment, and PUs are no exception.[48-50]

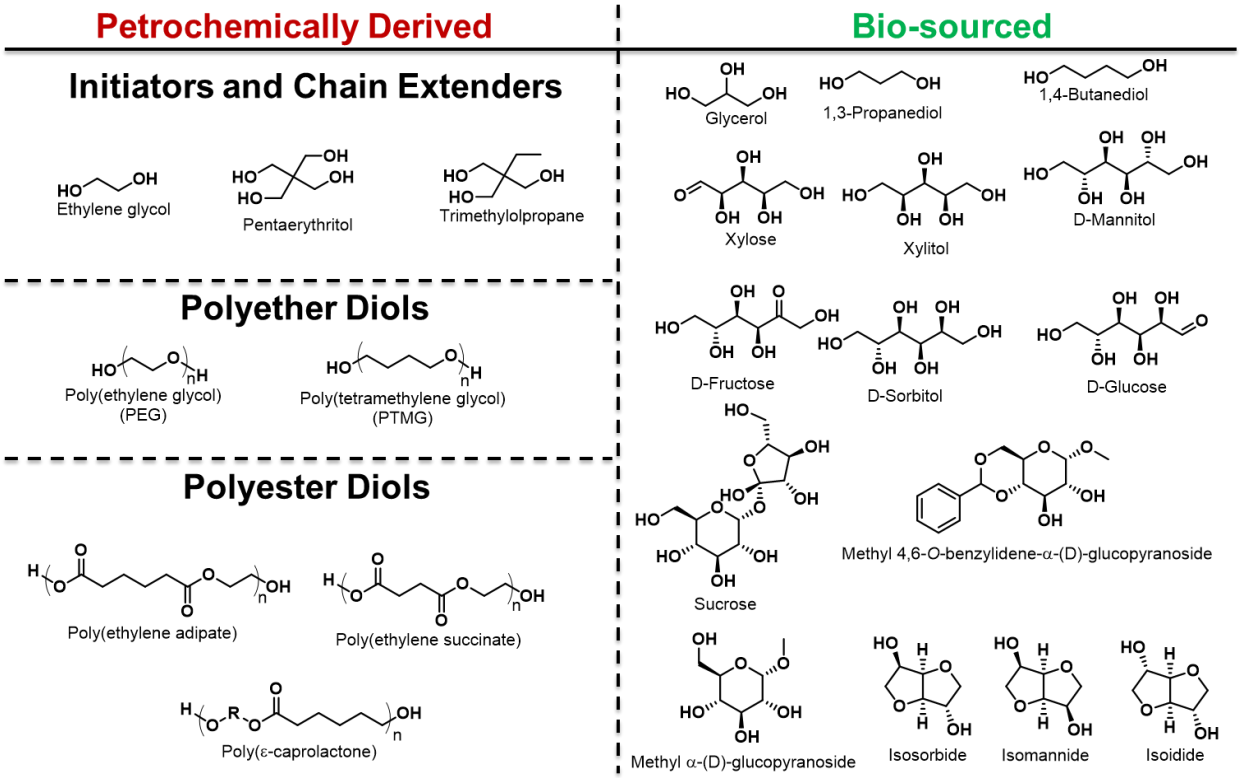

Figure 1-1. Diols that are made from petrochemical feedstocks and ones that are biosourced.

The PU community has sought biosourced and readily biodegradable alternatives to the diols used in PU synthesis. First, it is worth mentioning that chain extenders such as 1,3-propanediol, 2,3-propanediol, and 1,4-butanediol are actually biosourced and can be obtained by biomass fermentation.[26] Glucose-derived diols have been investigated and incorporated to impart orthogonal functionality and other properties.[41,51-55] Isosorbide is one such derivative that has been applied industrially and that results in polymers with high T_g but low crystallinity.[47,56] These mechanical properties can be tuned by blending with another, more-flexible diol.[57] Kennemur and coworkers used 2,5-bis(hydroxymethyl)furan attained from the reduction of hydroxymethylfurfural as the diol for a PU system.[58] Still, other naturally occurring ester compounds have been modified to form diols for PUs. For instance, Hillmyer and coworkers synthesized and incorporated a biobased poly(δ-decalactone) diol into a thermoplastic PU, resulting in a completely amorphous system giving thermal and mechanical properties similar to that of polyether diol–based PUs.[45] The monomer δ-decalactone is found in plants, but large quantities are produced by enzymatic hydroxylation, lactonization, and hydrogenation of fatty acids and essential oils.[59] In a slightly different approach, interesting work has been done with diols based on β-thioesters that form PUs that can undergo fast hydrolysis at the carbamate linkage at a range of pH values.[60] While the diols mentioned thus far produce linear PUs, there is an even greater diversity surrounding the chemistry of higher-order polyols for the synthesis of cross-linked PUs.

Polyols containing multiple hydroxyl functionalities along the backbone produce cross-linked systems for multiple applications. One of the simplest and most abundant polyols that also happens to be biosourced is glycerol.[26] Glycerol is often used as an additive into other polyol systems to increase the hydroxyl for increased rigidity, cross-linked density, and yield.[12,26] Several

other small-molecule polyol compounds used in PU procurement are shown in Figure 1-1.[26] Polyester and polyether polyols are typically produced by starting from small, multifunctional alcohols, termed "starters" or "chain initiators," and then performing a ring-opening polymerization (ROP), either with an alkylene oxide for polyether-based polyols or with a lactone, lactide, or cyclic carbonate for polyester polyols, as shown in Figure 1-2.[26] One area of significant interest has been polyols derived from vegetable oils, such as castor, soybean, rapeseed, sunflower, and palm, because they contain unsaturated triglycerides that can be converted into polyols with various chemical modifications.[26] Castor oil is of particular interest because it does not compete with food sources, but it is biosourced and biodegradable and actually contains some hydroxyl groups without modification.[26] Karak and coworkers were able to convert neat castor oil to a polymerizable, hyperbranched polyol by reacting it with diethanolamine at 120 °C for 4 h.[61] There have also been reports of naturally derived aromatic polyols, such as the polyphenolic, hyperbranched, tannic acid used by Karak and coworkers, to produce a PU that can be biodegraded by bacteria.[62] Lastly, significant interest has been found in converting waste CO_2 into polycarbonate-based diols. DeBolt and coworkers incorporated CO_2-based polycarbonate polyols derived from the copolymerization of CO_2 and epoxides into PU foams with little change in density relative to conventional polyols.[63] These polyols are already manufactured from waste CO_2 by companies like Huntsman International, DOW Chemical, and Novomer for incorporation into PUs for various applications.[63] It is important for more biosourced and biodegradable polyols to be discovered and utilized in order to continue making PU syntheses more sustainable and stay within evolving regulatory guidelines as demand for such products grows.

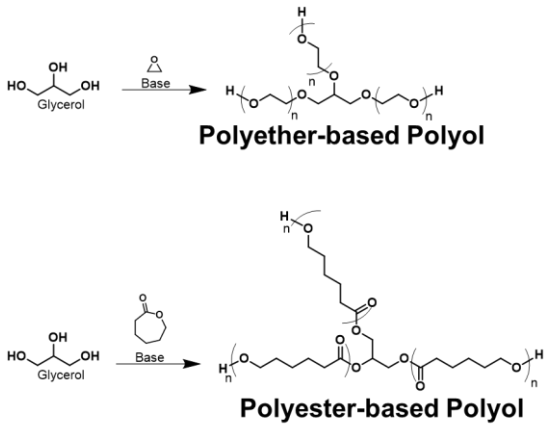

Figure 1-2. Synthesis of polyols from multifunctional "initiator" molecules.

1.5. Diisocyanates: Their Production, Chemistry, and Hazards

Isocyanates (R-N=C=O) are highly reactive compounds—with a general structure shown in Figure 1-3—that show enormous utility in the literature. For PU synthesis, the four most common diisocyanates used in industry are hexamethylene-1,6-diisocyanate (HMDI), isophorone diisocyanate (IPDI), bis(4-isocyanatocyclohexyl)methane, 2,4-toluene-diisocyanate and 2,6-toluene-diisocyanate (2,4- or 2,6-TDI), MDI, and TMXDI, as shown in Figure 1-3.[1,12,14]

The aliphatic and aromatic diisocyanates—shown in Figure 1-4—differ in two major aspects: their reactivity and the physical properties they impart into PUs. Aromatic diisocyanates (TDI and MDI) are markedly more reactive toward nucleophiles and more easily self-dimerize to form functionalities such as uretdiones and isocyanurates compared with their aliphatic counterparts (HMDI and IPDI).[14,23,64] This reactivity is easily explained by the more-electron-deficient nature of the isocyanate carbon due to the electron-withdrawing effect of the aromatic groups. Additionally, the more-rigid, planar structure of the aromatic diisocyanates allows for more compact packing of the urethane and urea moieties, as well as the hydrogen bonds formed between them, resulting in the hard segments that phase-separate from the flexible and amorphous

soft segments if large, flexible diols are used.[12,21,22] The terminology can be somewhat confusing in the literature because, in some cases, ureas derived from flexible isocyanate moieties can also form the hard segments through strong hydrogen bonding and, in turn, cause some degree of phase separation.[4,23] Given such variable reactivity, it is important to examine the different reactions that isocyanates can undergo.

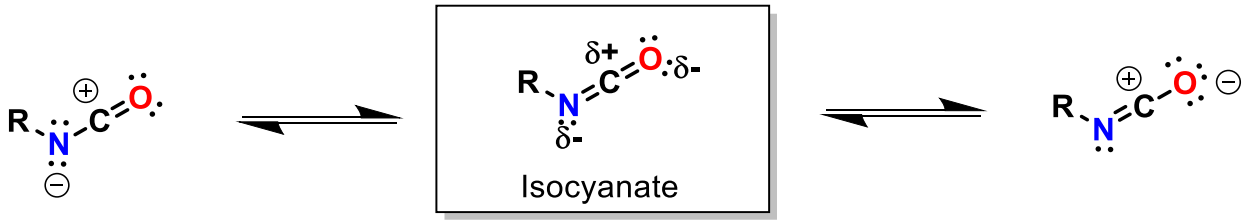

Figure 1-3. The structure of the isocyanate functional group with resonance electronic structures shown.

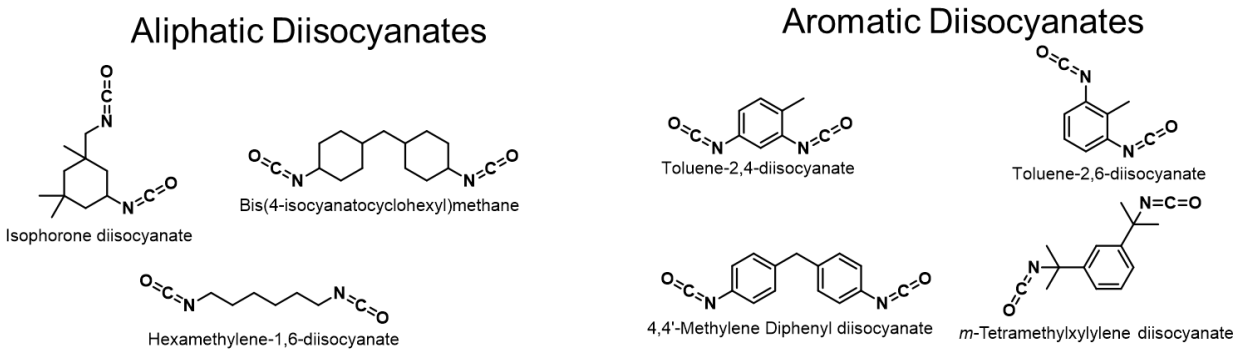

Figure 1-4. A list of aliphatic and aromatic diisocyanates used industrially.

Isocyanates have a rich and diverse body of chemistry, making them ubiquitous in a number of chemical transformations, as well as in materials chemistry. As shown in Figure 1-5, isocyanates, first and foremost, can undergo reactions with alcohols to form urethane linkages. It

is important to note that all of these urethane linkages are reversible upon heating to varying extents starting at 150 °C and above.[14] At sufficiently high temperatures, alternate degradation pathways can be accessed, as shown in Figure 1-6.[14] The main degradation pathway depends on the equilibrium of the urethane bonds and the starting material functional groups, which can be significantly influenced by electronic effects.[14] For instance, aromatic substituents tend to favor reversion to the diol and isocyanate starting materials, while aliphatic groups tend to favor dissociation into primary amine and alkenes.[14] For instance, *N*-alkyl-*O*-phenyl urethanes have been reported to undergo exchange with hydroxyl-bearing reagents at as low as 90 °C with a tin catalyst *in vacuo*.[65] In the presence of a bismuth triflate catalyst, *N*-alkyl-*O*-methyl urethanes could undergo exchange reactions at 122 °C under atmospheric pressures with alcohols.[66] However, the formation of a urethane bond is only one of many reactions that isocyanates can undergo.

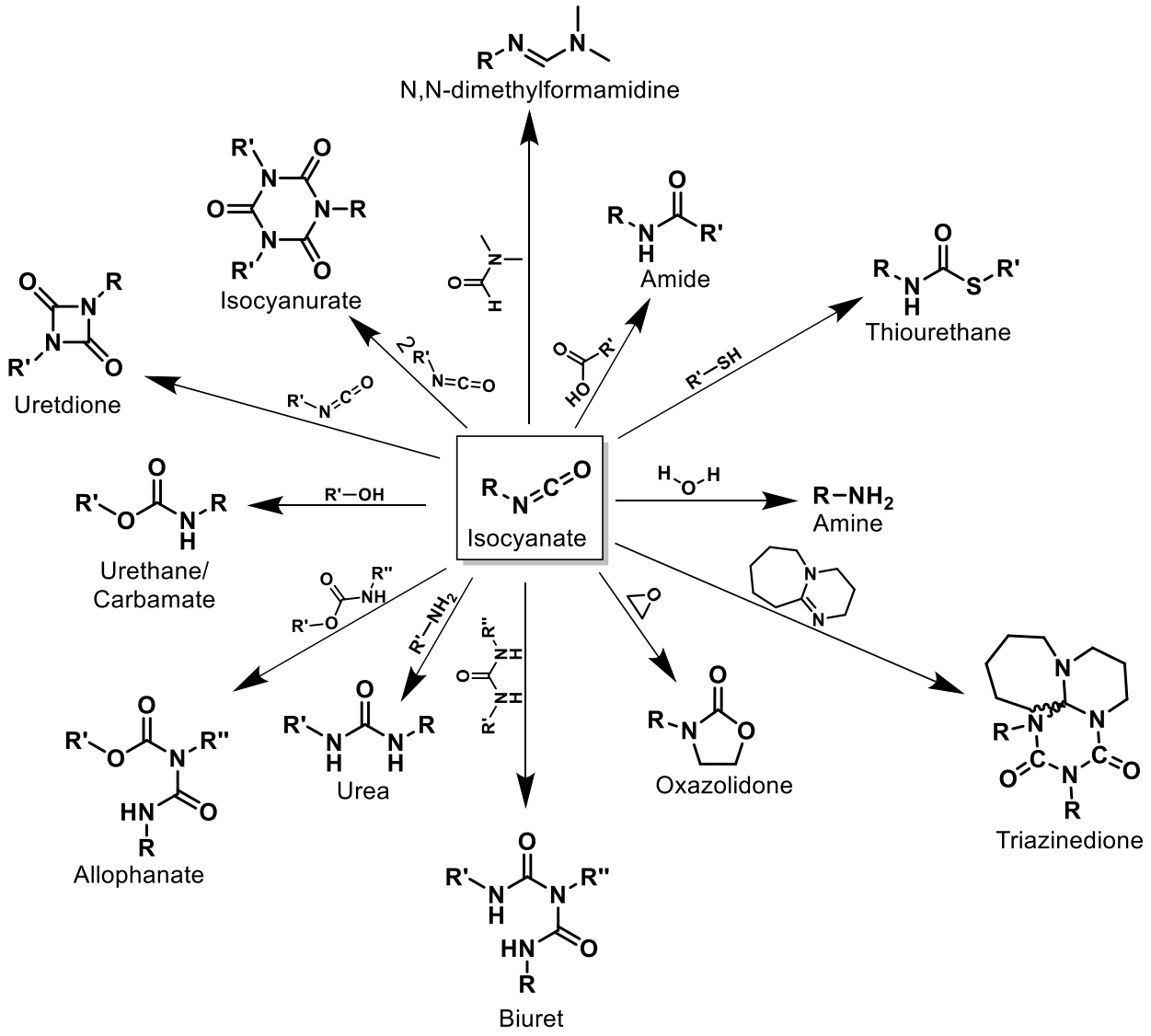

Figure 1-5. A sample of the multiple reactions that isocyanates can undergo with different reagents.

As also shown in Figure 1-5, an isocyanate can undergo several side reactions, not only with itself, but also with urethane groups and the recurring villain to many organic chemists and PhD students writing dissertations in organic chemistry: water.[8,14] Aliphatic isocyanates are relatively stable upon standing at room temperature, while aromatic isocyanates slowly undergo a self-dimerization to form a four-membered, cyclic linkage known as a uretdione, as shown in Figure 1-5.[67] Uretdione is known to form from aliphatic diisocyanates in the presence of trialkyl

phosphines, substituted pyridines, or trialkyl amines.[14,67] Aromatic diisocyanates can self-polymerize *via* uretdione linkages by simply heating them above 43 °C, producing a material with a yellow color.[23,67] This is one of the reasons that aromatic diisocyanates, in particular, require refrigeration for long-term storage.[64] The aromatic adduct can dissociate back to starting material above 150 to 165 °C, while the aliphatic adduct can be dissociated at *ca.* 200 °C.[14]

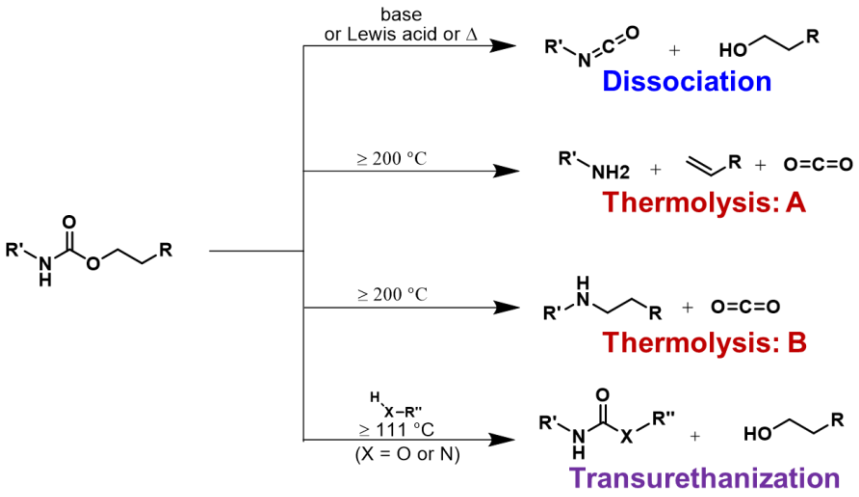

Figure 1-6. Degradation pathways for the urethane bond. Note that Thermolysis: A is only possible for *O*-aliphatic linkages**.** Figure adapted from Reference 14.

The other major product that isocyanates can form with themselves is a cyclic, six-membered trimer known as an isocyanurate, also shown in Figure 1-5. Isocyanurates typically only form with catalysts such as alkali metal alkoxides, alkali metal acetates, certain tertiary amines, tin(II)acetylacetonate, aluminum complexes, alkali metal fluorides, *N*-heterocyclic carbenes (NHCs), trialkyl phosphines, and even basic impurities.[5,6,14,67-69] These six-membered adducts are more thermodynamically stable than uretdiones and have higher dissociation temperatures: 441 °C for poly(aromatic isocyanurate) and 410 °C for poly(aliphatic isocyanurate).[14] In fact, poly(aromatic isocyanurate)s are reported to form a nonvolatile char upon

degradation, making them potentially suitable for fire-resistant applications.[14,26] Lastly, expanding on previous statements, isocyanates can undergo a reaction with water to form a carbamic acid ($RN\text{-}CO_2H$) intermediate, which rapidly decomposes into CO_2 and the amine.[26] The resulting amines can react with other isocyanate groups to form ureas, and it is indeed by this route that urea linkages can be introduced into a PU backbone.[1] While by no means exhaustive, these are the primary reactions of concern with respect to the isocyanate reagents alone for the scope of this dissertation.

During polymerization of diisocyanates with diols or polyols, there are two other side reactions that can occur under certain conditions: the formation of allophanate and biuret linkages, as shown in Figure 1-5. Allophanate groups are branching functionalities that form when an isocyanate reacts with the nitrogen lone pair in a urethane linkage.[1] Biuret linkages are the urea analog of an allophanate and occur when the nitrogen atom of a urea functional group reacts with an isocyanate to form a branched chain.[1] Typically, these reactions only occur at temperatures in excess of 110 °C, and the kinetics for biuret formation are significantly faster than those of the corresponding allophanate formation—while urethane formation is faster than both.[14] Below 60 °C, the reaction rate for either of these pathways is negligible.[14,70] The thermal stability series for the products discussed thus far follows: uretdione ~ allophanate < biuret < urethane < urea < isocyanurate.[14,71] The products from isocyanate reactions discussed thus far are the ones typically encountered in conventional PU synthesis.

However, as Figure 1-5 shows, more functional groups are accessible with isocyanate chemistry. Above 60 °C, *N*,*N*-dimethylformamide (DMF) can react with phenylisocyanate to form *N*,*N*-dimethyl-N'-phenylformamidine.[72] Amidine and guanidine bases such as DBU can react exothermically with two equivalents of isocyanate groups to form cyclic, six-membered

triazinedione heterocyclic adducts.[11,13] When diisocyanates are used, oligomers containing this adduct form have been indicated to be thermally reversible at 130 °C in the case of an oligomer made with HMDI.[13] When isocyanates are heated to 50 to 60 °C in the presence of an epoxide functional group and certain catalysts, oxazolidones can form, which are essentially cyclic carbamates.[14,26] Lastly, isocyanates can react with carboxylic acids to form an unstable anhydride that then decarboxylates to form an amide and CO_2.[5,26] Now that isocyanate chemistry has been elaborated upon, it is important to examine some intrinsic properties and environmental effects.

Despite their rich and interesting chemistry, isocyanates are toxic and hazardous and exhibit varying degrees of volatility, leading both industrial PU manufacturers and researchers in academia to find better synthetic methods or alternatives to diisocyanates altogether.[64,69,73,74] The effects of isocyanate exposure vary and range from asthma to pulmonary edema by inhalation while causing sensitization and dermatitis upon skin contact.[73,75] The toxicity and reactivity of isocyanates wreaked devastation in the Bhopal, India disaster in 1984 when a storage container for methyl isocyanate was leaking and, along with a host of other operator errors, allowed water to be introduced to the storage container—ultimately resulting in the large-scale release of methyl isocyanate, thousands of deaths, and many more suffering long-term health effects.[76] It is this toxicity, combined with the reactivity of isocyanates, that necessitates specialized containment vessels and, in some cases, refrigeration for transport and storage.[73,77] Temperature control and containment during storage and handling is especially important for the more-reactive aromatic diisocyanates like TDI and MDI.[5,12,26,64] Even further complicating their safety and environmental impact, isocyanates are often synthesized from phosgene ($COCl_2$), an even-more-toxic reagent that adds risks in production, as shown in Figure 1-7.[74,78-80] The toxicity and hazards of phosgene alone have led to investigations into alternative synthetic routes for isocyanate reagents.

As shown in Figure 1-7, numerous alternative synthetic routes have been reported—the Curtius rearrangement of acyl azides,[80] the Hofmann rearrangement of amides,[79] and the Lossen rearrangement of hydroxamic acids[78]—but these routes each has drawbacks.[5] The Curtius rearrangement uses explosive and toxic acyl azides, making it unappealing for industrial use despite the fact that it has been used to convert fatty acid and glucose derivatives to diisocyanates.[5,58,81,82] The Hofmann and Lossen rearrangements suffer from poor atom economy and the use of corrosive reagents such as bromine (Br_2) and acetic anhydride or acyl chloride.[5] Somewhat more promising is the conversion of nitro aryl compounds to aromatic isocyanates using reductive carbonylation with carbon monoxide (CO) in the presence of a catalyst—typically transition metals of groups VIII-X or compounds of group XVI.[5] Recently, Cramail, Landais, and coworkers reported generating isocyanates by reacting oxamic acids with a photocatalyst and a hypervalent iodine source with a light-emitting diode (LED) *via* a radical mechanism.[83] While these alternative syntheses alleviate the use of phosgene, they do little to address the toxicity and hazards of the storage, handling, and use of diisocyanates themselves.

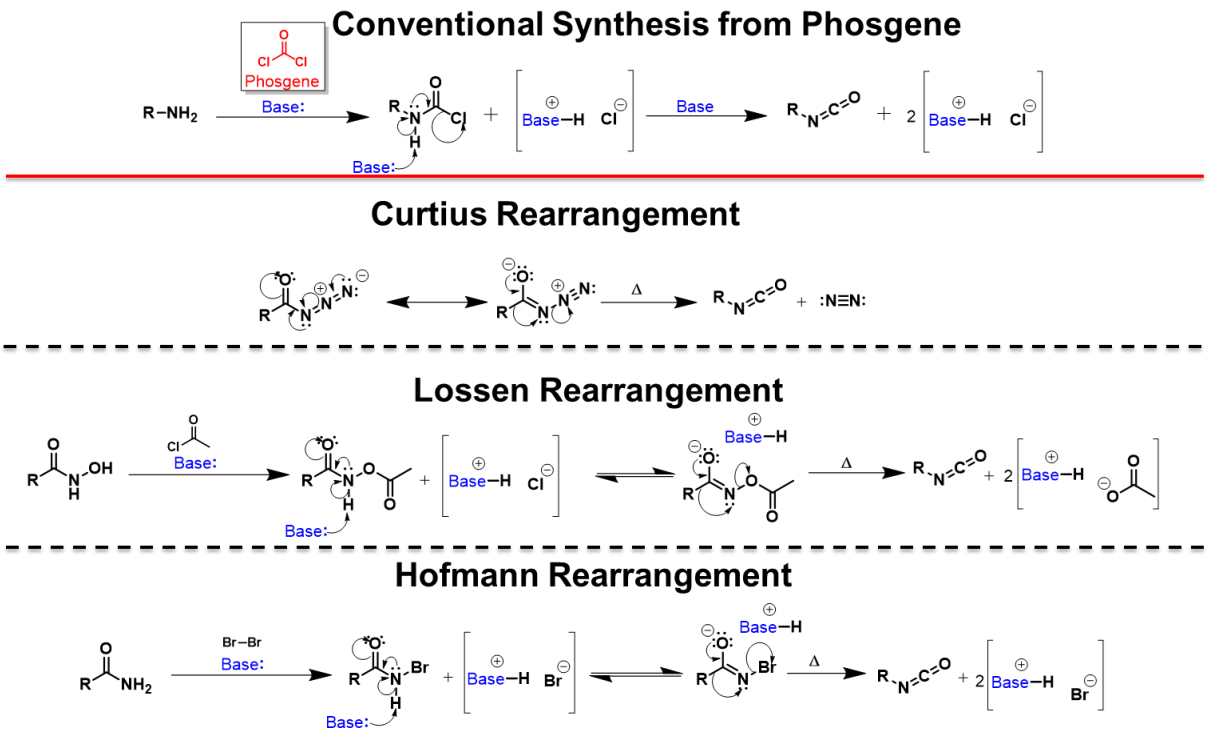

Figure 1-7. Schemes for the synthesis of diisocyanates *via* phosgene, Curtius rearrangement, Lossen rearrangement, and Hofmann rearrangement.

Industry has devoted significant resources toward developing larger, less-volatile diisocyanate and polyisocyanate compounds for thermoplastic and foam formulations. This goal specifically addresses the VOCs that have drawn concern from the public and from regulatory agencies.[30,69,84] As mentioned previously, some PU formulations involve the formation of an isocyanate-terminated prepolymer prior to subsequent spray-coating in the presence of a catalyst to undergo moisture cure.[18] One advantage of forming a diisocyanate prepolymer is that it is significantly less volatile than the original diisocyanate monomers, and, indeed, this is exploited as one way to mitigate their toxicity during handling and manufacturing.[18,23,69] Another industrial remedy is the formation of polyisocyanates that contain isocyanurate or uretdione linkages in the backbone rather than forming prepolymers with diols.[69] Isocyanurate linkages allow for multifunctional polyisocyanates with isocyanate functionalities higher than two and form cross-

linked networks when combined with diols or polyols.[69] Additionally, higher thermal stability, flame resistance, and mechanical strength are achieved with isocyanurate linkages, though at the cost of heightened viscosity.[6,23,69] Polyisocyanate prepolymers made with uretdione linkages are also less volatile and have the advantage of lower viscosities than their isocyanurate-based counterparts, but they are less thermally stable.[69] However, the reactivity of the uretdione groups in the backbone can be manipulated by reacting them with primary amines at room temperature or with alcohols at 125 to 160 °C to form biuret- or allophanate-based dendrimers or branched systems.[14,85]

There have been several recent reports of using biobased feedstocks to synthesize less-volatile diisocyanates. Lysine- and lysine ester–based diisocyanates have been industrially available for some time and have been incorporated into PUs, making them biodegradable and more biocompatible.[26,27,54] These diisocyanates have been synthesized using the previously described method with phosgene.[27] Fatty acid–based polyisocyanates have also been developed using various methods such as bromination and the subsequent reaction with excess silver cyanate (AgNCO) of soybean oil.[26] Diisocyanates have been produced *via* the Curtius rearrangement from dimethyl sebacate and methyl 10-undecenoate, which are both natural products contained in castor oil, by Cramail and coworkers.[82] Vanillic acid,[86] isosorbide,[81] isomannide,[81] and isoidide[81] have also been converted to diisocyanates *via* the Curtius rearrangement. Kennemur and coworkers later showed that the optical rotation of PUs can be tuned based on the amount of chiral isomannide- and isosorbide-derived diisocyanates incorporated.[58] While these systems offer only a small sample of the ongoing research into less-volatile, biosourced diisocyanate and polyisocyanates, it remains clear that there is more progress to be made in making PU production sustainable.

1.5.1. Diisocyanate Alternatives

Diisocyanate and polyisocyanate starting materials are coming under increased regulatory scrutiny, such as by the European Union's Registration, Evaluation, Authorization, and Restriction of Chemicals (REACH) regulations.[87,88] Additionally, industry has continued interest in finding ways to reduce the use of VOCs in PU formulation given concerns of residual, volatile content in the finished product.[69] Therefore, desirable properties of diisocyanate alternatives should be that they are relatively less toxic, nonvolatile, and preferably biosourced while maintaining reactivity, efficiency, and atom economy.

As shown in Figure 1-8 (adapted with permission from Sardon *et al.*),[16] there are four major methods to prepare PUs without the use of isocyanates: condensation of diamines with dicyclic carbonates forming poly(hydroxyurethane)s (PHUs),[15,89] condensation of diamines with linear dicarbonates,[90] ROP of cyclic carbamates,[91] and condensation of linear carbamates with diols.[92] There have been extensive studies of polycondensation of diamines with dicyclic carbonates to produce PHUs because the carbonates may be prepared from CO_2.[89] However, high reaction temperatures and long reaction times are typically required to achieve high conversion, and the resulting PHUs are only soluble in polar organic solvents, such as DMF.[15,74,93] Polycondensation of diamines with linear dicarbonates derived from expensive bis(pentafluorophenyl)carbonate has been demonstrated to proceed readily at room temperature to produce PUs of relatively high molar mass, overcoming the solution processability of PHUs.[90] Thomas, Li, and coworkers recently reported the ROP of five-membered cyclic carbamates initiated by *n*-butyl lithium.[94] While interesting mechanistically, this approach requires a pyrophoric initiator and cyclic monomers often achieved *via* multistep syntheses.[91,95] Given the drawbacks associated with these methods, focus is directed toward the condensation of linear dicarbamates and diols.

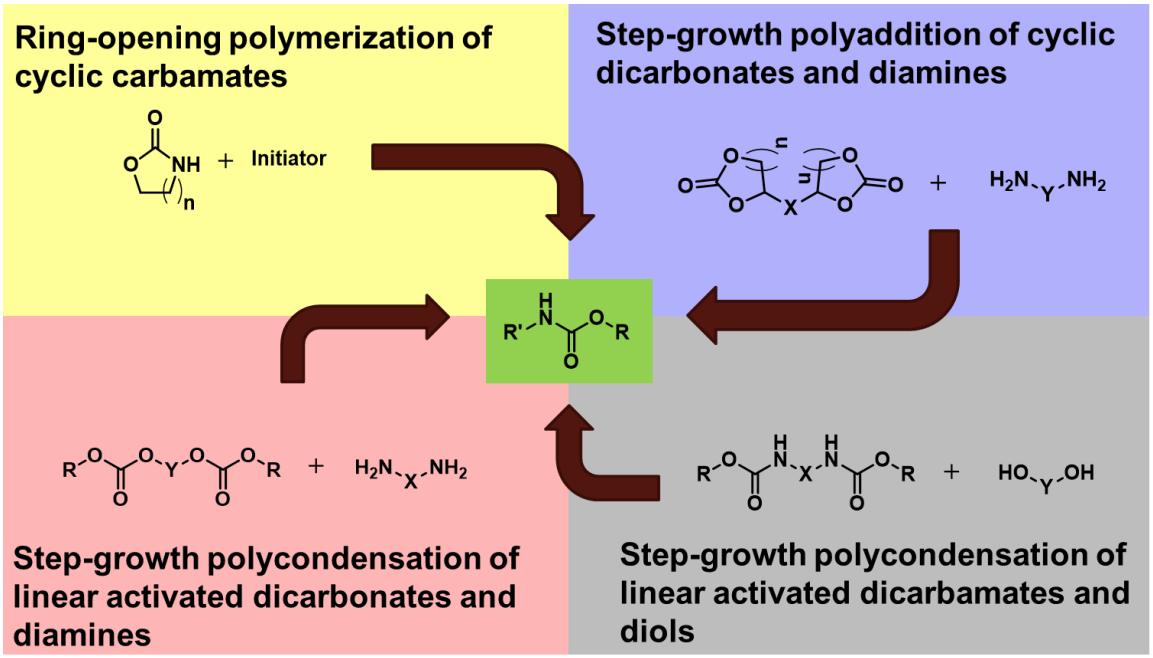

Figure 1-8. The four main types of diisocyanate-free polymerization methods. Figure adapted with permission from Sardon and coworkers. [16]

Polymerizations involving the reaction of diols with methyl or phenyl dicarbamates have been studied extensively. Depending on the conditions and substrate, the polycondensation of linear dicarbamates and diols is reported to occur either *via* transurethanization or by "deblocking" to form a diisocyanate *in situ*, as shown in Figure 1-9.[14,74] Dimethyl carbamates are reported to react with diols through a transurethanization reaction and are attractive because the dimethyl carbonate precursor can be synthesized from methanol and carbon dioxide, enhancing sustainability.[74,96] However, these systems typically require reaction temperatures in excess of 100 °C, along with a catalyst and vacuum to remove methanol.[74,97,98] In contrast, displacement of phenol as a better leaving group facilitates reaction at temperatures as low as 90 °C with catalyst and *in vacuo*.[65] In one example, a reaction with phenol-based carbamates proceeded *via* a

transurethanization route at 100 °C, while at temperatures above 170 °C, a deblocking reaction occurred where phenol was eliminated, forming isocyanate.[99]

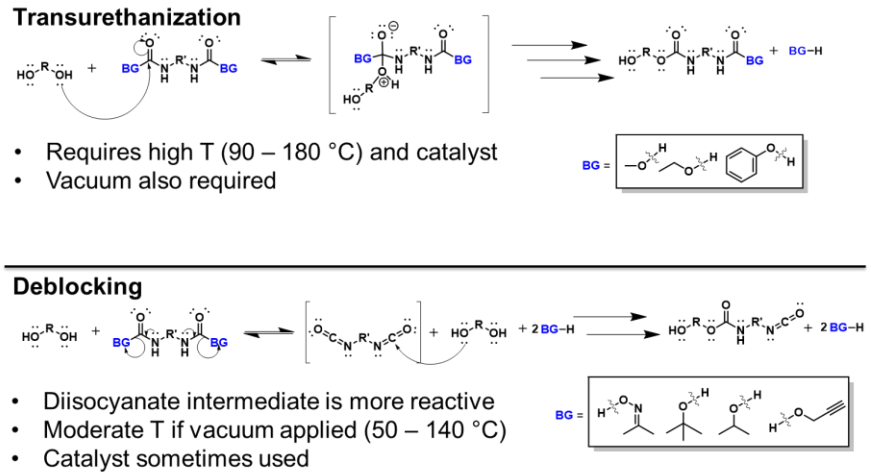

Figure 1-9. Of the two types of polymerization mechanisms for linear dicarbamates, the deblocking mechanism appears to proceed under milder conditions (BG: blocking group).

Deblocking methodology has received more attention recently for the potential to produce diisocyanates *in situ* while mitigating risks and costs for storage and transport of isocyanates themselves.[8] Recently, Emrick and coworkers demonstrated that fluoride salts could catalyze the deblocking of alcohol or oxime-blocked TDI and react with diols to form PUs in a one-pot reaction.[92] Documented research has been performed using alcohols, phenols, oximes, and pyrazoles as blocking groups.[5,14,100,101] While most of this research has involved identifying a deblocking temperature by its "onset," it is important to note that deblocking is an equilibrium reaction with an associated rate, making it difficult to compare reported deblocking temperatures because of wide variations in analytical techniques and conditions.[14,101] For instance, deblocking temperatures for phenol-blocked aliphatic carbamates are reported to be 170 °C in bulk or 240 °C

in diphenyl ether.[99,102] Given that the deblocking temperatures reported for oxime- and phenol-blocked isocyanates are well in excess of 100 °C, the question has turned to the potential deblocking behavior of more-electron-deficient phenolic groups.[100,102] Indeed, adding electron-withdrawing substituents to the phenol blocking group has been reported to lower the deblocking temperature to 35 °C in the case of *o*-nitrophenol-blocked TDI, one of the lowest deblocking temperatures for thermal dissociation.[14,103] However, there is little information regarding *p*-nitrophenol-blocked diisocyanates.

Katsarava and coworkers first reported the synthesis of HMDNC and observed slow deblocking at 30 °C in *N*,*N*-dimethylacetamide (DMAc), while dissociation occurred rapidly in the presence of tertiary amines.[104] This carbamate readily produced polyureas when allowed to undergo reaction with diamines, but did not produce PUs when combined with diols at 60 °C in DMF.[104,105] Petillo and coworkers reported the synthesis of an AB-type hydroxyl (*p*-nitrophenyl)carbamate derived from a glucopyranoside that was self-condensed by adding sodium hydride (NaH) at 43 °C, yielding cyclized trimers and tetramers.[106] The synthesis of the monomer involved multiple steps and was tailored to form cyclodextrin analogs. Despite the use of such a strong base, this system required long reaction times, and the premature cyclization was claimed to be caused by coordination of urethane groups to sodium ions.[106] These results indicate that a di(*p*-nitrophenyl)carbamate might be used as a general strategy for PU synthesis.

In a rather groundbreaking work, Gnanou, Feng, and coworkers were able to synthesize PUs directly from a series of dialkyl and dibenzyl amines and CO_2 in the presence of dialkyl or dibenzyl halides.[107] The mechanism for this transformation is shown in Figure 1-10 and requires that the diamine be allowed to react with CO_2 at room temperature in the presence of the cesium carbonate (Cs_2CO_3) first before adding the dihalide and heating in order to prevent unwanted side

reactions.[107] The conditions require a pressure vessel at a moderate pressure of 10 bar, a quaternary ammonium salt, and 1-methyl-2-pyrollidinone (NMP).[107] The system is heated to 80 °C for 24 h after the dihalide is added.[107] This chemistry is rather new and untested but has significant potential in improving the sustainability of PU synthesis given that it provides a way of remediating atmospheric CO_2 by using it as a feedstock. One significant obstacle that needs investigation is how to make this process more selective for PU formation, as all systems studied were reported to produce a certain amount of carbonate linkages in the backbone.[107] Additionally, near-stoichiometric amounts of quaternary ammonium salt and the use of highly polar and toxic organic solvents like NMP could create concerns in both profit margin and end-use toxicity as compared to conventional methods.[107]

1.6. Polyurethane Catalysis

The third component of PU synthesis is the catalyst. While aromatic diisocyanates can react with polyols and diols without catalyst,[25] it is more practical for most applications to use a

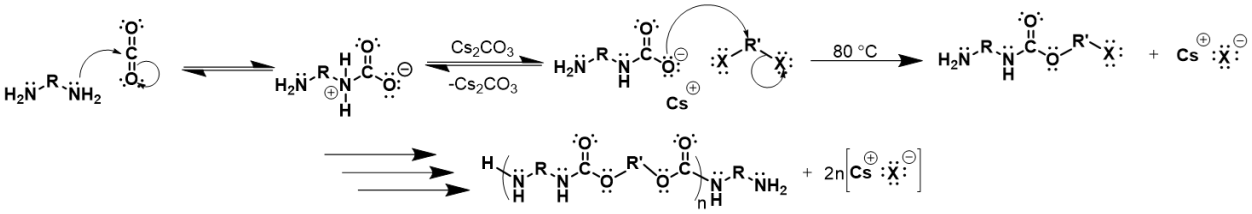

Figure 1-10. The mechanism for synthesis of PUs directly from diamines and dihalides using CO_2 requires the formation of an anionic carbamate intermediate. X = Cl or Br.

catalyst to control cure times and to ensure full conversion so that no VOCs remain in the material.[84,108] On the other hand, polymerization with aliphatic diisocyanates requires a catalyst for any significant conversion to take place at moderate temperatures.[109] By far, the most common catalysts used are tin-based Lewis acids such as DBTDL or DMTDL, but Lewis bases such as

diazabicyclo[2.2.2]octane (DABCO) have also been used industrially.[4,16] However, the use of tin-based catalysts has presented challenges in a number of industrial applications.

Tin-based catalysts can be problematic as a result of their nonrenewability, toxicity, and difficulty in removal from PU materials.[16,19] Firstly, tin-based catalysts are toxic and nonrenewable, and there have been numerous reports of tin accumulation in the world's oceans inflicting irreversible harm to marine organisms.[11,108-111] Moreover, lingering tin in PU materials can be especially problematic for biomedical applications, as DBTDL specifically accumulates in and damages the liver, having an IC_{50} of 1.33 μmol/L for liver cell viability.[112] If not removed, these tin-containing catalysts can induce adverse effects on the material, for instance promoting side reactions, altering the dielectric constant and increasing the conductivity.[16,113] Certain metal-containing catalysts, such as DBTDL, are typically removed with multiple tedious procedures such as precipitations with potassium fluoride (KF), strong bases, or hydrogen peroxide that can have deleterious effects on the polymer.[113,114] It is for these reasons that efforts are underway to find alternatives to tin-based catalysts for PU synthesis.

Before examining the alternative catalysts, it is important to examine the mechanism by which catalysts such as DBTDL facilitate conversion of isocyanates with alcohols. The actual catalytic mechanism has been debated for years, and as late as 2015,[16] the mechanism proposed by Bloodworth, Davies, and coworkers[115] was still argued to be the accepted mechanism, as shown in Figure 1-11. However, the mechanism of Bloodworth and coworkers involving metal coordination by the isocyanate nitrogen was derived from their work on aromatic isocyanates

exclusively and was derived from indirect data analysis due to the lack of both computational and experimental techniques to monitor and model reactions.[115]

More recently, Sohnel and coworkers performed a comprehensive molecular modeling study using density functional theory (DFT) along with experimental kinetic studies to posit that an alternative mechanism appears likelier in which the carbonyl oxygen coordinates to the tin as shown in Figure 1-11. [17,18] The mechanism involving the diisocyanate oxygen coordinating to the tin center—of either a dimethyltin diacetate (DMTDA) or dimethyltin methoxy acetate (DMTMA)—is well supported for both aliphatic and aromatic isocyanates by empirical data while being somewhat supported by molecular modeling.[17,18]

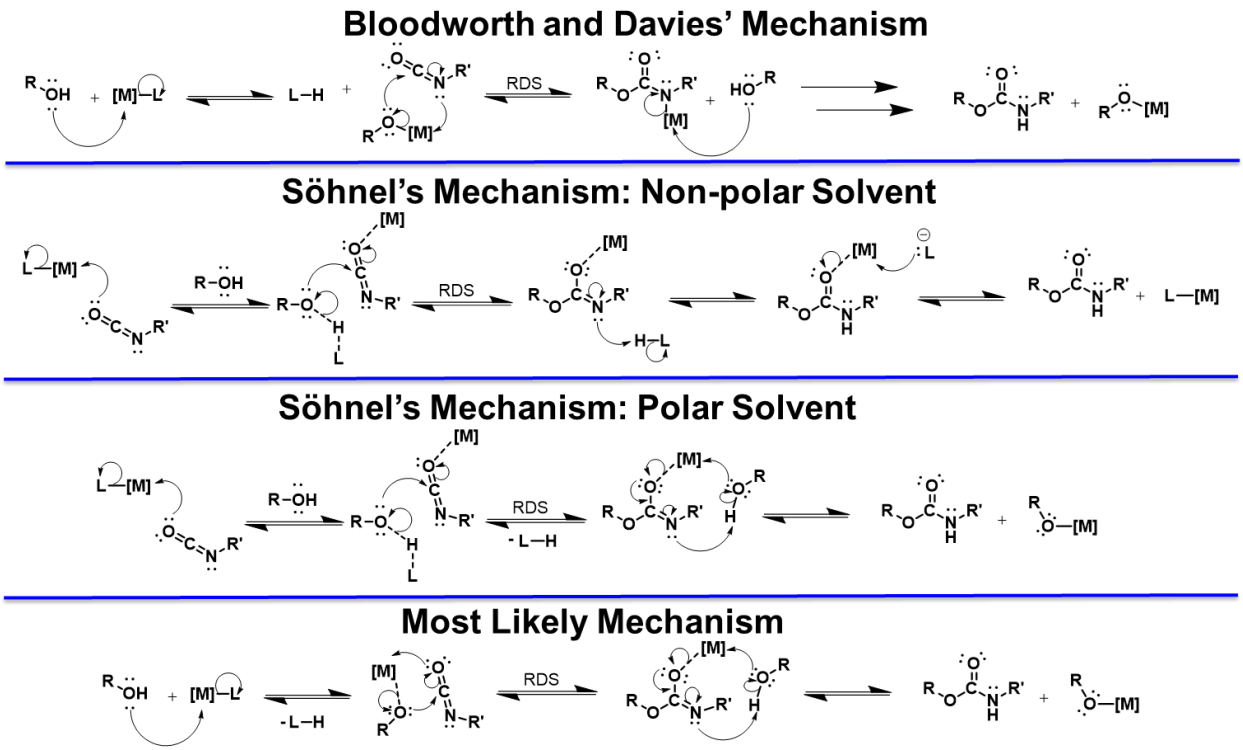

Figure 1-11. The actual mechanism by which Lewis acid complexes can catalyze PU synthesis from isocyanates is most likely a variation of the mechanism proposed by Sohnel and coworkers.[17,18]

However, the authors' claims that that the mechanism changes in polar solvents for aliphatic isocyanates after the first cycle—forming a DMTMA complex on subsequent cycles—and that the DMTMA complex cannot form first are more questionable.[17,18] The problem with the proposed mechanism in polar solvents, as shown in Figure 1-11, for aliphatic isocyanates is twofold: 1) the conductor-like polarizable continuum (CPCM) solvation model does not account for the effects of solvent cavitation, dispersion, or repulsion and is only stabilizing the electrostatic charges of each atom that are more pronounced in the gas phase,[116,117] and 2) the authors do not use explicit solvation with a polar solvent molecule that could shuttle protons, thereby preventing the acetic acid from being optimized further away from the complex and significantly lowering the energy of this transition state.[17,18,116] The authors' result may change when using the solvation

model based on density (SMD)[117] solvation parameter—containing the nonelectrostatic terms—and explicit solvation for their conclusion about the aliphatic isocyanate.[17,18] Secondly, the energy barrier for the overall reaction *via* DMTMA was lower in all cases than for the pathway *via* the DMTDA, meaning that the DMTMA is the preferred pathway.[17,18] The positive free energy of formation for the DMTMA intermediate (3.4 kcal/mol)—from methanol and DMTDA—is irrelevant for DMTMA to form first, as it is not the rate-determining step (RDS) per the Curtin-Hammet principle.[17,118] The attack by methanol is the RDS.[17] Thus, the proper catalytic cycle in all cases could reasonably be the last mechanism shown in Figure 1-11.

For biomedical applications or whenever a less-toxic catalyst is required, industrial manufacturers of PUs typically turn to the nontoxic or low-toxicity bismuth-based catalysts such as $BiPh_3$, $Bi(O\text{-}(C{=}O)\text{-}C_7H_{15})_2$, or $Bi(O\text{-}(C{=}O)\text{-}C_9H_{19})_2$.[19,66] However, the bismuth catalysts have generally been regarded as not being as catalytically active as the tin-based catalysts, and they are not as soluble in some of the common solvents used for PU synthesis.[19] The systems containing bismuth catalysts are generally more susceptible to moisture and have longer cure times.[19] However, catalytic activity comparable to some tin catalysts was reported by Jousseaume and coworkers with bismuth triflate.[66] While bismuth catalysts are currently the industry's "go-to" catalyst when the toxicity of the resulting PUs is to be minimized, several other catalysts are being investigated.

There have been several investigations on other transition-metal catalysts and ligands for PU synthesis. Okamoto and coworkers reported that the less-toxic manganese(II) acetylacetonate [$Mn(acac)_2$] compound combined with DABCO approaches the catalytic activity of DBTDL with HMDI and diethylene glycol.[109] $Mn(acac)_2$ catalyst exhibits a particularly interesting characteristic in that it activates isocyanates to form urethane linkages with diols, preferentially

over attack by water-forming urea groups, while zirconium(IV) acetylacetonate [$Zr(acac)_4$] exhibits the highest urethane selectivity.[119] Chawiwannakorn and coworkers further examined copper and zinc catalysts with different ligands and found that copper(II) acetylacetonate [$Cu(acac)_2$] complexed with triethylenetetramine exhibits foaming characteristics similar to the commercially used *N*,*N*-dimethylcyclohexylamine.[108] While many of these metal-based catalysts are of interest industrially because they are nonvolatile and result in fewer VOCs in PU materials, the metals themselves are not renewable from organic or biosourced feedstocks, which has fueled investigations into catalysts that are.[19]

Other efforts have investigated more-renewable organocatalysts such as organic bases, organic acids, "latent organic catalysts," and, to a lesser extent, NHCs.[16] Cramail, Landais, and coworkers performed a comprehensive study on a series of amidine and guanidine base catalysts.[11] They found DBU to exhibit the highest catalytic activity with isophorone isocyanate and PEG, even over 1,5,7-triazabicyclo[4.4.0]dec-5-ene (TBD) and especially over DABCO.[11] They convincingly concluded that DBU catalyzes the reaction via a general base catalysis mechanism as a result of its relatively high (*ca.* 24 in acetonitrile [CH_3CN] and *ca.* 12 in H_2O), as shown in Figure 1-12.[11,120] On the other hand, 7-methyl-1,5,7-triazabicyclo[4.4.0]dec-5-ene (MTBD) was found to be a better general catalyst for PUs because it is not only a strong base (pK_a of *ca.* 25 in CH_3CN), but the cyclic adduct that it forms with diisocyanates is strained and reversible, unlike the cyclic adduct that DBU forms, and its catalytic activity is second only to DBU when either PEG or PTMO is used.[11] Both DBU and MTBD have been found to have a higher catalytic activity than DBTDL.[11] While organic bases are attractive because they can be removed from PUs and are organically derived, they make the polymerization system more susceptible to water, which can be exploited if the reaction of water with isocyanate groups is desired, as is done industrially with

DABCO.[11,26] If only the diol-isocyanate reaction is desired, then the base needs to be dried first, often by distillation to minimize water contamination.[26] Organobase catalysts are some of the more-discussed types of organic catalysts in the literature, but there is still more investigation to be had into less-toxic ones.[121,122]

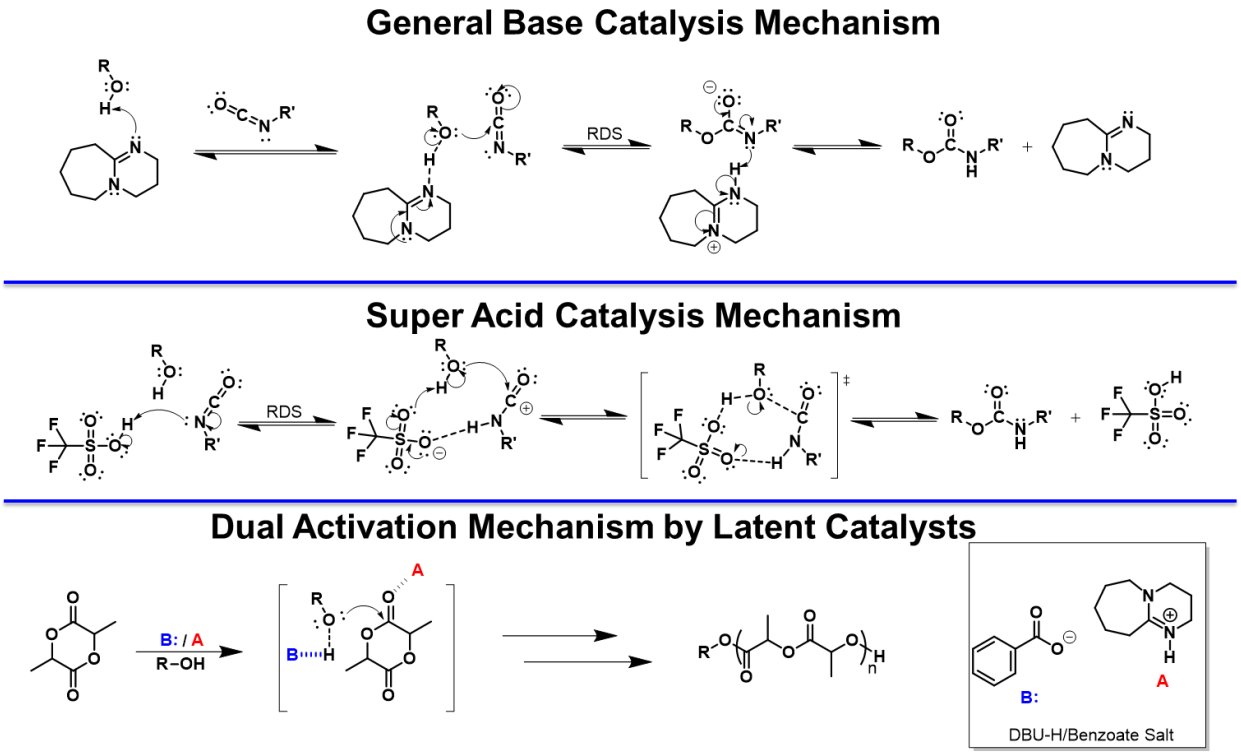

Figure 1-32. Mechanisms for catalysis of PU synthesis by metal-free methods. The latent catalyst system has been applied to PLA, but has potential for PUs.

Complementary to organobases is the use of organic "super acids" in PU synthesis.[16] Hedrick, Horn, Sardon, and coworkers[123] experimented with a series of acidic compounds and found that 5 mol% triflic acid and bis(trifluoromethanesulfonyl)imide (TFMI) achieved near quantitative conversion of hexamethylene diisocyanate and PEG in 6 h at 20 °C.[123] By comparison, DBU and DBTDL only achieved 86% and 82% conversion, respectively, after 24 h.[123] The authors reported after computational analysis that the catalytic mechanism likely

involved a “dual activation” of both the isocyanate nitrogen by the acidic proton and the alcohol lone pair *via* the conjugate base coordinating with the hydroxyl proton, as shown in Figure 1-12.[123] The transition state of the RDS had an N-H bond that was mostly formed while the C-O bond formed later.[123] This mechanism was supported by an inverse correlation with regard to the pK_a and the reaction rate.[123] Additionally, these organic acids did not show degradation of the resulting PUs that DBU and DBTDL can induce on the resulting PUs long term.[123] While these acid catalysts appear to be promising alternatives to DBTDL, they may not be applicable when diols or diisocyanates with acid-sensitive pendant groups are used or with ester-based diols or polyols.

Expanding on both the base and acid catalysts are what have been termed latent catalysts, which typically involve an organic base, such as DBU, being neutralized by an organic acid, thereby producing a salt that can exhibit properties of the conjugates of both ions during polymerization due to microreversibility or a dual-activation mechanism of the organic salt.[16] Hedrick and coworkers showed that when DBU was combined with benzoic acid (BA) in equal amounts, it produced a DBU-H/BA salt that could catalyze the ROP of (L)-lactide to near quantitative conversion in 24 h at room temperature with a dispersity of 1.06.[124] Changing the base to MTDB afforded virtually identical results, but in only 16 h instead of 20 h.[124] Another kind of latent catalyst is the urea anions. Waymouth and coworkers showed that a urea anion formed by the reaction of potassium methoxide and an electron-deficient urea, shown in Figure 1-13, could affect the ROP of (L)-lactide forming poly(lactic acid) (PLA) in 6 s for 94% conversion and a dispersity of 1.06.[125] The proposed mechanism was similar to that of the DBU-H/BA compound.[125] While neither of these latent catalysts have been used in PU synthesis yet, their potential for PU applications appears promising as well.

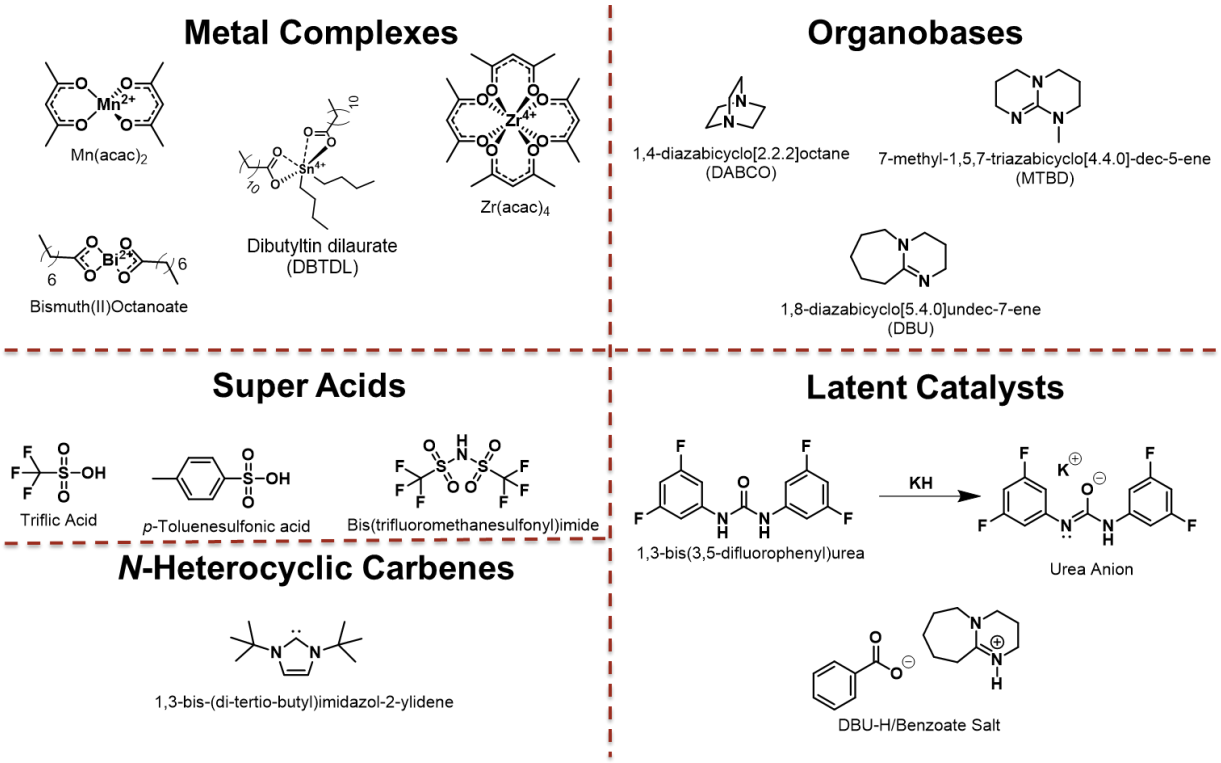

Figure 1-4. A series of catalysts used for PU synthesis. Note that the latent catalysts have yet to be used on PU systems, but show potential.

Finally, NHCs, which possess a neutral divalent carbon atom with only six electrons in their valence shell and can act as both nucleophiles and electrophiles, are worthy of brief mention.[16] NHCs have been known to catalyze both chain polymerizations and step-growth polymerizations, including for PUs.[16,126,127] However, formation of uretdiones and isocyanurates and low-molecular-weight species were reported if the NHC was added to the diisocyanate first rather than adding the NHC first to the diol and then adding the diisocyanate.[126] Thus, the primary catalytic mechanism was determined to be the activation of the diol.[126] There appears to be less literature on using NHCs for PU synthesis than some of the other catalysts discussed herein, so more investigation is warranted in this area.

Additionally, the role of the solvent has a large impact on kinetics. Multiple reports have claimed that increasing the polarity of the solvent drastically increases the kinetics of polymerizations for aliphatic diisocyanates, but Sohnel and coworkers indicated that solvent polarity has little effect on the reaction for aromatic isocyanates.[14,17,18] Common solvents used industrially are toluene, xylene, "white spirit," butyl acetate, methyl pentanone, acetone, and methoxypropyl acetate.[19] One area where research into alternative means of PU synthesis could improve significantly is the use of "green" solvents during polymerization. For example, γ-valerolactone (GVL) is a polar, aprotic, organic liquid that is a component in fruit and is nontoxic ($LD_{50,rat}$ = 8,800 mg/kg), high-boiling (207 °C), miscible with water, and biodegradable and does not form peroxides, contrary to 2-methyltetrahydrofuran.[128] Therefore, more investigation into greener solvent systems and their effect on the rates of polymerization should be pursued.

1.7. A Perspective on Polyurethane Sustainability and Reconciling Priorities of Academia and Industry

Now that the chemistry behind PUs has been elaborated upon, it is important to consider how sustainability in PU production might be realistically achieved. Specifically, there are some competing interests between academia and industry that need to be addressed and resolved. The guiding principles for both academia and industry for making chemical processes more green and sustainable are as follows: safer chemicals and solvents, atom economy, utilization of renewable resources, and metabolism of industrial products.[128] This section provides a contrast between the industrial and academic perspectives on sustainable catalysis, atom economy, industrial metabolism, and use of biosourced feedstocks in PU production.

1.7.1. Overlooked Hazards with Organic Catalysts

First and foremost, there exists somewhat of a conflict between academia and industry when it comes to using organocatalysts versus metal catalysts. As mentioned previously, there exists a wide range of scientific research into organic catalysts for PU synthesis such as organic bases, organic acids, latent organic catalysts, and NHCs.[16] The benefits often claimed in academic research for organic polymer catalysts are that they are less toxic, are more removable, and have potential for selectivity.[16,129] However, the industrial perspective does not necessarily agree. As stated previously, an increasing concern by PU manufacturers is the presence of VOCs in end-use materials.[84] This concern is partially driven by increased attention and public outcry regarding VOCs in commodity products, some of which may not be entirely warranted.[30] Nonetheless, industry must accommodate these concerns in order to sell products. Adding organic catalysts such as DBU or triflic acid just incorporates another VOC that needs to be accounted for and removed from the polymer. Even a simple extraction step adds cost to the overall production when done on a ton scale and requires solvent. Moreover, many literature reports that present these alternatives and decry the toxicity of DBTDL do not list the toxicity of compounds such as DBU or triflic acid.[11,16,123] Industry actually prefers the use of nonvolatile metal catalysts for applications like bed mattresses because, being nonvolatile, they do not require removal because the material does not come into contact with subcutaneous tissue.[19,84,113] It is for this reason that industry has largely opted to use bismuth catalysts instead of organocatalysts when minimal toxicity is paramount, such as in biomedical applications.[19,84] A possible reconciliation between these competing interests is the ongoing work with latent organic catalysts in the form of acid-based salts, but research pertaining to PU synthesis is scarce.[124,129]

Going forward, academic literature will need to consider these aspects in order to reasonably expect new sustainable methods to be adopted industrially.

1.7.2. Atom Economy

The second aspect that needs to be addressed when adopting new synthetic procedures for PUs is atom economy. Every atom in a raw material used industrially costs money, and discarding waste products during a process results in a material loss, resulting in higher cost and potential environmental hazards.[128] It is indeed this aspect where the polyaddition chemistry of PUs shines rather than producing a by-product *via* polycondensation.[1] While diisocyanate alternatives, such as dicarbamates and dicarbonates, have significant potential to make PU synthesis safer and potentially more environmentally friendly, the loss in atom economy may make these alternatives industrially impractical, and the alkoxy, phenol, oxime, or other by-products may present concerns with their own toxicity.[8,130] Academic researchers should account for the atom economy of new PU synthetic methods when attempting to find viable diisocyanate-free methods.

1.7.3. Polyurethane Metabolism

As has been discussed in the media and the scientific community, the problem of PU accumulation is becoming a real concern.[49] It has been estimated that PUs can take up to hundreds of years to completely metabolize in the environment.[48] In 2014, more than 25.8 million tons of postconsumer plastic ended up in waste upstream, 30.8% of which was deposited in landfills.[48] As PU production increases and more uses are found for these materials, remediation of PUs themselves will need to be addressed.[20] A significant number of reports have been published recently seeking to find ways to either recycle PU materials or affect their biodegradation, as has been discussed previously, but academia needs to consider more carefully how these goals are to

be actually implemented in addition to how their findings of recyclability and biodegradability are reported.

Because the technology for biodegradable PUs—and polymers more generally—is rather young and complex, industry has focused more on the recyclability of polymers.[26] The preferred PU waste remediation methods currently employed are chemical and biochemical recycling.[26] As mentioned previously, polyester-based macrodiols can undergo hydrolysis and other biologically driven cleavage reactions at the ester linkage, whereas the corresponding polyether-based diols cannot.[1,26,45] For recycling PUs made from both types of diols, glycolysis is the most developed remediation method presently employed.[26,131] This method involves heating the PU foams to 180 to 220 °C in the presence of amino alkanols or glycols and a catalyst in a "split phase" reactor where the lighter polyols are separated into the upper phase while the rest of the heavier material remains in the lower phase.[26,131] The PU carbamate bonds undergo transurethanization by the hydroxyl groups, and the liberated polyols separated into the upper phase can be reintroduced into formulations for PU foams.[26] Although this method works for both polyether and polyester diols and polyols, it is rather energy-intensive.

While industry is more focused on improving methods for recycling PUs, academic literature has found methods to potentially biodegrade existing PU materials. Recently, there have been advances in using microorganisms to biodegrade PUs, but this has generally been seen as practical only for polyester-based PUs.[26] However, a recent report indicated that polyether-based PUs can, in fact, be biodegraded by the fungi *C. pseudocladosporioides* at up to 65% of its dry mass after 21 d, while this same strain can also degrade polyester-based PUs at up to 87% after 14 d.[48] While this discovery shows novel potential, this method of waste PU remediation requires

more investigation to be industrially scalable. Instead, both industry and academia have invested a significant amount of resources into synthesizing PUs that are more readily biodegradable.

However, the means by which biodegradable PUs are to be implemented industrially need to be considered more carefully in scientific research when trying to address the metabolism issues of PUs and polymers more generally. The accumulation of polymer waste in the environment has been the motivation of a plethora of literature claiming to have synthesized "biodegradable" polymers, but it is noteworthy that some of these research papers have presented no evidence of biodegradation.[49] There are at least two reports claiming the synthesis of a biodegradable PU but are ambiguous as to whether the main chains are degrading or cleavage is occurring in the labile side-chains.[33,132] In some cases, a polymer is reported to be biodegradable when the evidence presented shows that the polymer is only degradable under harsh laboratory conditions such as high temperature, low/high pH values, or other artificial chemical environments.[49] While some polymers may be biodegradable under specific laboratory conditions, they may not be in field conditions. For instance, an enzyme or organism in a natural environment may prefer another substrate with alternate nutrients than the polymer in question, or the required organism may not predominate in the environment in question.[49] PLA, for example, is a commonly used, biodegradable polymer in living human tissue, but it is not biodegradable in seawater and even shows drastically different degradation rates at different composting sites correlating with average humidities and temperatures.[49] When biodegradability is desired in a polymer for any given application, it is thus important to consider how the waste of the application will be disposed of in order to ensure that the polymer is degraded; otherwise, the accumulation problem will remain unsolved. The toxicity and remediation of the initial degradation products need to be taken into account. For instance, it has been reported that free isocyanate groups have been liberated using

fungi to depolymerize PUs.[48] If this method were to be incorporated into a landfill, the release of diisocyanate small molecules could be harmful to the environment and local populations. Therefore, it is important that researchers use caution when using the term biodegradable to describe their systems and qualify the conditions under which their system can be degraded.[49] More generally, the PU community needs to define what exactly is meant by biodegradable versus polymers that require an artificially administered chemical or physical stimulus for degradation.[49]

1.7.4. Biosourced and CO_2 Feedstocks Versus Practical Feedstocks

The last aspect that needs to be reconciled by academia for sustainable PU synthesis is to more carefully consider the proposed biosourced feedstocks in terms of the practicality of using these sources on the ton scale, as well as their use in existing and vital functions such as sources of food. Many novel diols and diisocyanate precursors have been proposed using derivatives from glucose, extracts from plants, cellulose, and even vegetable oils.[26,133] However, the practicality and means by which these feedstocks could be exploited for PU synthesis on the ton scale has often gone unconsidered. The question should be asked as to how incorporating these feedstocks affects their uses in existing, and in some cases vital, functions such as sources of food and what the total life-cycle cost is, starting with their extraction from the environment.

Natural products, such as syringaresinol derived from lilacs and magnolias, have been reported to be used as diols for PHUs with the goal of potentially replacing petrochemical diphenols like bisphenol A (BPA).[134] While the chemistry and material properties are indeed novel and interesting, the question should be asked whether it is practical for industrial manufacturers to harvest magnolia trees just to extract syringaresinol for PHUs and whether this would actually be sustainable on a ton scale.[134] DBU is another example because it is produced by the marine sponge *Niphates digitalis*, but again, there is little chance industry would source natural products like it

this way.[135] Researchers should also consider whether using food sources on a ton scale for PU manufacturing would negatively impact the availability and cost of foods given malnourishment being a significant problem in certain parts of the world.[128] For instance, glucose derivatives have been incorporated as diols and, even in some cases, as diisocyanates as biosourced feedstocks.[51,52,58] But perhaps the biggest hurdle for industry to adopt many biosourced feedstocks for use is the extremely low cost and widespread availability of ethylene due to advances in—and increasing expansion of—fracking.[136] Ethylene is the main feedstock for chemicals like PEG (*ca.* $29/kg) used in PU synthesis, and indeed products like PEG are far cheaper than biosourced compounds like methyl-α-(D)-glucopyranoside (*ca.* $128/kg), especially on a ton scale.[137-139]

To overcome most of these issues, there have been a few intriguing investigations into biosourced products that are produced as waste from existing industrial processes. For instance, the use of castor oil as a feedstock for PUs does not intrude on other industries or commodities of vital importance—such as food—because neither castor oil nor the castor bean from which it is derived is edible.[26] Using other vegetable oils such as soy, palm, rapeseed, or sunflower could impede on their other uses such as for food commodities.[26] Limonene is another biosourced waste product in the citrus industry that has been incorporated as a feedstock for PUs.[133] Additionally, the work done by DeBolt and coworkers on using waste CO_2 to synthesize polyols with epoxide could also significantly capitalize on an existing industrial waste product.[63] However, even a waste compound like CO_2 is not necessarily sourced as such when used as an industrial feedstock.

Industrial CO_2—including the cylinders used by academic researchers—primarily comes from calcium carbonate taken from the ground in the form of limestone, from plants that produce hydrogen or ammonia from coal, natural gas, or other hydrocarbon.[140] These methods are not green or sustainable. Thus, even some of the methods incorporating CO_2 as a starting material for

PU or PHU synthesis discussed herein are not necessarily sustainable yet.[107,141] Only when more-efficient and -economical CO_2 capture technology is adopted will most of the intriguing chemistry incorporating CO_2 into PUs and PHUs become sustainable. Presently, amine solvents are primarily used as "CO_2 scrubbers" industrially, but a significant cost/energy barrier exists because a large amount of heat is required to release the captured CO_2 in the regeneration step, thwarting widespread adoption.[43] This problem is why continuing research on CO_2 capture, as performed by Mecerreyes, Shaplov, and coworkers with their poly(ionic liquid) PU, is so important for the rest of the CO_2 feedstock chemistry to be sustainable.[42] The PU researchers in academia need to consider more carefully where feedstocks—including ones claiming to be "waste" or biosourced—used in their research originate and use feedstocks that do not reduce the availability of vital commodities such as food in order for them to be realistically adopted as sustainable PU starting materials.

1.8. Conclusion

The tunability of PU materials by altering the monomer components and reaction conditions has led to applications far exceeding the scope of this review. In addition to their traditional roles as elastomers, vibrational dampeners, and various kinds of foams, PUs have found applicability as biomedical materials and even thermal cloaking materials. New types of hybrid materials, some of which are known as vitrimers, have recently been developed to bridge the properties of both thermoplastic and thermosetting PUs. The synthetic chemistry has been expanded to not only include biosourced and biodegradable starting materials, but also entirely different methods of polymerization through condensation reactions of linear dicarbamates, condensation of diamines with bis(cyclic carbonates), ROP of cyclic carbamates, and condensation of diamines with linear dicarbonates so as to avoid the transport and handling of toxic

diisocyanates and their derivatization from the even-more-toxic phosgene. Academia has begun a wide array of investigations into alternative and renewable catalysts to replace the toxic and nonrenewable tin catalysts most commonly used. However, attempts in the academic literature to find sustainable alternatives to existing PU manufacturing methods should be analyzed critically with regard to whether the proposed alternatives are actually less toxic, whether any loss of atom economy makes said alternatives impractical on an industrial scale, any complications associated with mass consumption of "renewable" resources, and whether biodegradable alternatives can realistically be degraded in all ambient environments.

2. AN EFFICIENT AND MILD SYNTHESIS FOR POLYURETHANES USING GLUCOSE AS A BIORENEWABLE COMONOMER

2.1. Introduction

PUs have become important materials for applications ranging from packaging, footwear, electronics, construction, adhesives, and numerous others, causing their production to surpass 26 million metric tons and generating an end-use market of $297 billion in the United States (US) alone in 2017.[2] The versatility of PUs is a result of the tunability of the primary components, generally including multifunctional diols and multifunctional isocyanates, and the polymerization conditions, which determine the morphology and introduce ureas and other functional groups.[1,5-7] Although nonrenewable diols, such as PEG and PTMG, are commonly used, the current industrial trend has moved toward more biosourced and renewable diols, including naturally derived oils.[9-12] Additionally, the metal catalysts and isocyanates used industrially are regarded as toxic and nonrenewable and, therefore, offer opportunities for improvement.[16] Moreover, certain metal-containing catalysts, such as DBTDL, are typically removed with multiple tedious procedures, such as precipitations with KF, strong bases, or hydrogen peroxide, that can have deleterious effects on the polymer.[113,114] If not removed, these tin-containing catalysts can induce adverse effects on the material.[16,113] Lingering catalysts could be especially problematic for biomedical applications, as DBTDL specifically accumulates in and damages the liver.[112]

Four major methods exist to prepare PUs without the use of isocyanates: condensation of diamines with dicyclic carbonates forming PHUs,[15,89] condensation of diamines with linear dicarbonates,[90] ROP of cyclic carbamates,[91] and condensation of linear carbamates with diols.[92]

We focused on the condensation of linear dicarbamates and diols for this work because of the potential for shorter reaction times, lower temperatures, cheaper and safer reagents, and the ability to process the resulting PUs with nonpolar solvents unlike the alternative methods (*vide supra*).[15,74,90,91,93-95]

Polymerizations involving the reaction of diols with methyl or phenyl dicarbamates have been studied extensively. Depending on the conditions and substrate, the polycondensation of linear dicarbamates and diols has been reported to occur either via transurethanization or by deblocking to form a diisocyanate *in situ*.[14,74] Dimethyl carbamates react via transurethanization, but typically require temperatures higher than 100 °C, a catalyst, and a vacuum.[74,97,98] On the other hand, diphenyl carbamates tend to undergo deblocking under certain conditions.[99]

This deblocking methodology has received more attention recently for its potential to produce diisocyanates *in situ* while mitigating the risk and cost of storing and transporting isocyanates themselves. [8] A significant amount of research has been performed using alcohols, phenols, oximes, and pyrazoles as blocking groups.[5,14,92,100,101] Given that deblocking temperatures reported for oxime- and phenol-blocked isocyanates are well in excess of 100 °C, the question has turned to the potential deblocking behavior of more-electron-deficient phenolic groups.[100,102] Indeed, adding electron-withdrawing substituents on the phenol-blocking group has been reported to lower the deblocking temperature to 35 °C in the case of *o*-nitrophenol–blocked TDI, one of the lowest deblocking temperatures for thermal dissociation. [14,103] However, there is little information regarding *p*-nitrophenol–blocked diisocyanates.

Katsarava and coworkers first reported the synthesis of HMDNC (**1**) and observed slow deblocking at 30 °C in DMAc and rapid dissociation in the presence of tertiary amines.[104] This carbamate readily produced polyureas when allowed to undergo reaction with diamines, but did

not produce PUs when combined with diols at 60 °C in DMF.[104,105] Petillo and coworkers reported the synthesis of an AB-type hydroxyl-(*p*-nitrophenyl)carbamate derived from a glucopyranoside that was self-condensed by adding NaH at 43 °C, yielding cyclized trimers and tetramers.[106] The synthesis of the monomer involved multiple steps and was tailored to form cyclodextrin analogues. Despite the use of such a strong base, this system required long reaction times and premature cyclization, claimed to be caused by the coordination of urethane groups to sodium ions.[106] These results indicate that a di(*p*-nitrophenyl)carbamate might be used as a general strategy for PU synthesis.

This chapter details the one-pot condensation polymerization of **1** with methyl 4,6-*O*-benzylidene-α-(D)-glucopyranoside (**2**) at room temperature, 40 °C, and 60 °C in the presence of DBU (Scheme 1). This diol was chosen as a diol because it is biosourced and can undergo a postpolymerization deprotection of the benzylidene group for future studies.[142] We hypothesized that combining **1** with a diol and an appropriate base would produce a PU with a similar molar mass, tunability, and other properties as the analogous PU produced using HMDI (**3**).

2.2. Experimental Details

2.2.1. Materials

All materials were purchased from ChemImpex, Sigma-Aldrich, or VWR. Unless noted, reagents were used as received. Nuclear magnetic resonance (NMR) solvents were purchased from Cambridge Isotope Laboratories. Dichloromethane (DCM) and DMF were purified and dried by a J.C. Meyer Solvent System, also known as a solvent purification system (SPS). DBU was distilled over calcium hydride (CaH_2) and stored under dry nitrogen over activated 3-Å molecular sieves. Methyl 4,6-*O*-benzylidene-α-(D)-glucopyranoside was stored and handled under dry conditions using one of two methods: 1) storing under an active vacuum (*ca.* 50 mT by

Hg gauge) in a vacuum desiccator, with Drierite® and SICAPENT® phosphorous pentoxide (P_2O_5) as desiccants, for 48 to 144 h prior to dispensing or 2) drying under a vacuum in an oven at *ca.* 108 °C for 12 min before quickly weighing out and adding to the reaction flask and returning the reaction flask to the vacuum oven at *ca.* 108 °C for another 20 min before use. Reaction flasks were kept in a 110-°C drying oven when not in use.

2.2.2. Molecular Modeling

Molecular modeling calculations were performed using the Gaussian09 software package.[143] All systems were optimized at either the B3LYP or the cam-B3LYP level of theory using the 6-311++G(d,p) basis set. Calculations performed with solvation used the SMD parameterization. Predictions for NMR spectroscopy chemical shifts were carried out using the gauge-independent atomic orbital (GIAO) method and referenced to tetramethylsilane (TMS), which was optimized and analyzed *via* NMR-GIAO using the same parameters.

2.2.3. Characterization

2.2.3.1. Nuclear Magnetic Resonance Spectroscopy

Recorded on a Varian Inova500 spectrometer were ^{1}H, ^{13}C, heteronuclear multiple bond correlation (HMBC), heteronuclear multiple quantum coherence (HMQC), and gradient-selected homonuclear correlation spectroscopy (gCOSY) spectra (500 MHz for ^{1}H and 125 MHz for ^{13}C). Where noted, a Varian NMRS500 was used to acquire spectra (500 MHz for ^{1}H and 125 MHz for ^{13}C). Chemical shifts were referenced to signals from residual protons of the deuterated solvents.

To investigate the effect of DBU equivalents on **1**, HMDNC was weighed before being transferred into a glove box with a dry argon atmosphere. Each sample (**1**) was dissolved in dimethylsulfoxide (DMSO)-d_6 from a freshly opened bottle of anhydrous solvent, ensuring that a

concentration range of 25 to 26 mg/mL was maintained among the three samples. Each NMR tube was capped with a septum before being transferred out of the glove box, where the DBU was added using a 25-μL syringe. The tube was shaken vigorously to ensure homogeneity before acquisition of the ^{1}H-NMR spectrum, both 8 to 15 min and then 8 h after DBU addition. Notably, upon addition of the DBU, each solution immediately changed color from faint yellow to very dark yellow. For each sample, it was ensured that the time between DBU addition and collection of the ^{1}H-NMR spectrum was kept within a tolerance of 8 to 15 min. The relaxation delay for the ^{1}H-NMR spectrum was extended to 10 s to ensure more-accurate integrations and proportional peak heights between the different species as determined by a relaxation experiment.

2.2.3.2. Attenuated Total Reflectance – Fourier Transform Infrared Spectroscopy

A Shimadzu IR Prestige attenuated total reflectance – Fourier transform infrared (ATR-FTIR) spectrophotometer was used to acquire FTIR spectra, in conjunction with IR Solution v. 1.40 software. All spectra were further analyzed using Origin 2018 data analysis software. The spectra presented in absorbance mode were baseline-subtracted using the Origin baseline subtraction function and were normalized for proportional comparison. Peak-height ratios were calculated from the baseline-subtracted spectra before normalization by dividing the maximum peak height at the apex of the urethane peak at 1709 to 1713 cm^{-1} by the intensity at the apex of the urea peak at 1668 cm^{-1}, shown in Appendix A where the urea peaks appear in Figures A-6, A-73, and A-74 and are in agreement with similar systems.[2] All transmittance spectra in the appendices are presented without baseline correction or normalization. Eight scans were used for all spectra.

2.2.3.3. Size-Exclusion Chromatography

Size-exclusion chromatography (SEC) data were collected using a Tosoh Co. Model HLC-8320 EcoSEC system equipped with two TSK Super AW 4000 PMMA columns and a TSKgel Super AW-H guard column, operated at 50 °C with a flow rate of 0.35 mL/min. DMF with 0.01-M lithium bromide (LiBr) was used as the eluent. The polymer solutions were prepared at 1 to 1.5 mg/mL and were analyzed relative to a calibration curve derived from Agilent poly(methyl methacrylate) (PMMA) reference standards ranging from 550 to 1,568,000 Da.

2.2.3.4. Matrix-Assisted Laser Desorption/Ionization – Time-of-Flight Mass Spectrometry

MALDI-TOF mass spectra were collected on a Bruker Microflex™ LRF mass spectrometer (Bruker Corporation, Billerica, MA) in positive linear or positive reflectron modes. Ionization was induced by a pulsed nitrogen laser (337 nm, 25 kV) at 200 laser pulses per spectrum. *Trans*-2-[3-(4-*tert*-butylphenyl)-2-methyl-2-propylidene]malononitrile (DCTB) and sodium trifluoroacetate (NaTFA) were used as a matrix and doping agent, respectively. The samples and DCTB solutions were prepared as 1- and 25-mg/mL solutions in chloroform, respectively. The NaTFA solution was prepared at 1 mg/mL in acetone. The sample, DCTB, and NaTFA solutions were premixed at a volumetric ratio of 2:2:1 (volume ratio of x:y:z), respectively, in a 0.2-mL polymerase chain reaction (PCR) tube before spotting. From this mixture, 1 μL of solution was spotted onto the MALDI plate and was allowed to air-dry prior to the measurement. All spectra were calibrated to Bruker Peptide II and Protein I Calibration standards. The voltages of sources 1 and 2 were 20 and 18.35 kV, respectively, with a default pulsed ion extraction (PIE) delay time of 220 ns in linear mode unless otherwise specified. The voltages of sources 1 and 2 were 19 and 15.65 kV, respectively, with a default PIE delay time of

110 ns in reflectron mode unless otherwise specified. The voltage of reflector 1 was 20 kV. Reflector 1 was only used in reflectron mode. All spectra were analyzed in flexAnalysis by smoothing and subtracting the baseline.

2.2.3.5. Electrospray Ionization Mass Spectrometry

Electrospray ionization (ESI) samples were run with a Thermo Fisher Scientific Q Exactive Focus.

2.2.3.6. Thermogravimetric Analysis

Thermogravimetric analysis (TGA) was performed under an $N_{2(g)}$ atmosphere using a Mettler-Toledo TGA2/1100/464 instrument, with a heating rate of 10 °C/min from 25 to 500 °C. Data were analyzed using Mettler-Toledo STAR^e v.15.00a software.

To determine the content of water in glucose, the TGA method contained a 30-s isotherm at 25 °C followed by a ramp from 25 to 300 °C at a rate of 3 °C/min under $N_{2(g)}$. The thermograms, showing percent mass loss, were analyzed using Origin 2018 data analysis software by plotting the mass as a percentage of the starting mass, taken as the average mass measured from 25 to 40 °C, and then calculating the average percent mass loss between 111 and 115 °C.

2.2.3.7. Differential Scanning Calorimetry

Differential scanning calorimetry (DSC) was performed with a Mettler-Toledo DSC 3® calorimeter under $N_{2(g)}$. The measurement method for the polymer samples consisted of three heating and cooling cycles with a 10-°C/min ramp from 60 to 180 °C. For small molecules, the measurement included three heating and cooling cycles with a 10-°C/min ramp from 60 to 200 °C for **1** and from 25 to 120 °C for the triazinedione compound. T_g was determined from the midpoint

of the inflection tangent of the third heating cycle, and T_m was determined from the first heating cycle using the "onset of slope" application in Origin.

2.2.4. Synthetic Procedures and Results

2.2.4.1. Synthesis of Hexamethylene-1,6-Di(*p*-Nitrophenyl)Carbamate (1)

This synthesis follows the procedure by Katsarava and coworkers.[104] A 250-mL, round-bottomed flask was charged with di(*p*-nitrophenyl)carbonate (6.0045 g, 19.738 mmol) before purging with dry $N_{2(g)}$. Then, tetrahydrofuran (THF) (32 mL) was added, and the mixture was cooled to 0 °C. Hexamethylene-1,6-diamine (0.9165 g, 7.887 mmol) was dispersed in dry THF (11 mL) in an N_2-purged vial fitted with a septum. The diamine suspension was then added dropwise *via* syringe over the course of *ca.* 30 min to the carbonate solution. Subsequently, another 4 mL of dry THF was added to the diamine vial to rinse and was subsequently added to the reaction mixture over the course of 1 min. The reaction was allowed to warm to room temperature. After 19 h, the reaction mixture was poured into ice water (750 mL) and was vacuum-filtered, leaving behind a white solid precipitate. The white solid was mixed with acetone (300 mL) and stirred thoroughly, followed by the addition of hexanes (180 mL) to cause precipitation. The precipitate was vacuum-filtered using a large excess of acetone to rinse the solid precipitate, removing the di(*p*-nitrophenyl)carbonate. The precipitate was collected in a

vial and left under a vacuum at 40 °C overnight, giving product HMDNC (**1**) (2.990 g, 85% yield). This synthesis of dicarbamate monomer **1** is shown in Figure 2-1.

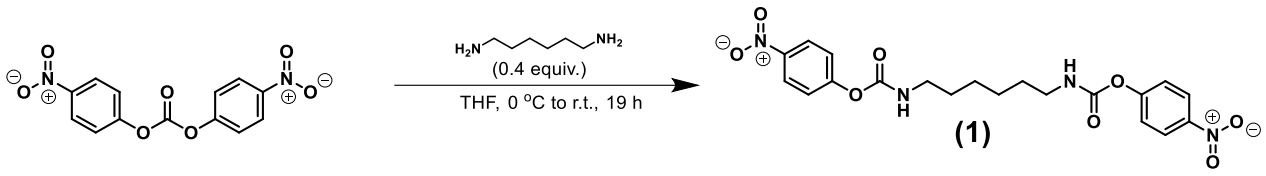

Figure 2-1. Synthesis of dicarbamate monomer **1**.

^{1}H-NMR (500 MHz, DMSO-d_6, δ, ppm): 8.25 (4H, ½AB$_q$, $J_{AA'-XX'}$ = 9 Hz, ***ortho-H*** to NO_2), 8.05 (2H, t, J = 6 Hz, R-CH_2-C***H***$_2$-CH_2-**N*H***-CO-O-Ar), 7.39 (4H, ½AB$_q$, $J_{AA'-XX'}$ = 9 Hz, **ortho-*H*** to -O-CO-R), 3.09 (4H, td, J = 6 Hz, 7 Hz, R-CH_2-C***H***$_2$-**C*H*$_2$**-NH-CO-O-Ar), 1.50 (4H, t, J = 7 Hz, R-CH_2-**C*H*$_2$**-CH_2-NH-CO-O-Ar), 1.34 (4H, m, R-**C*H*$_2$**-CH_2-CH_2-NH-CO-O-Ar). ^{13}C-NMR (125 MHz, DMSO-d_6, δ, ppm): 156.28, 153.07, 144.03, 125.11, 122.38, 40.47, 28.99, 25.87. ATR-FTIR (cm^{-1}): 3341, 3175 – 3049, 2992 – 2810, 1701, 1668, 1620, 1526, 1487, 1350, 1256, 1207, 1107, 1036, 1013, 995, 966, 874, 860, 818, 764, 716. High-resolution mass spectrometry (HRMS) (ESI$^+$): $[M+Na]^+$: $C_{20}H_{22}O_8N_4Na$ expected: 469.1330 amu; found: 469.1326. T_m = 175 °C. T_d = 207 – 253 °C, with 96% mass loss at 315 °C.

2.2.4.2. Synthesis of 1,8-Diazabicyclo[5.4.0]undec-7-ene-H *p*-Nitrophenoxide Salt (4)

In an oven-dried, 100-mL, round-bottomed flask, *p*-nitrophenol (0.5013 g, 3.604 mmol) was purged twice with $N_{2(g)}$. Dry DCM (13 mL) was added, followed by dry DBU (0.54 mL, 3.6 mmol). The reaction mixture immediately turned bright yellow, and no precipitate formed. After 14 min, the reaction flask was opened and condensed *in vacuo* to form a highly viscous liquid that did not self-crystallize at room temperature. The liquid was cooled to 4 °C for 5 h, at which point it crystallized. The solid was rinsed with cold hexanes over an aspirator vacuum before being dried *in vacuo* at *ca.* 50 mT for 5 h, giving product DBU-H *p*-nitrophenoxide salt (**4**) (0.9370 g, yield: 89%). The synthesis of DBU-H *p*-nitrophenoxide salt **4** is shown in Figure 2-2.

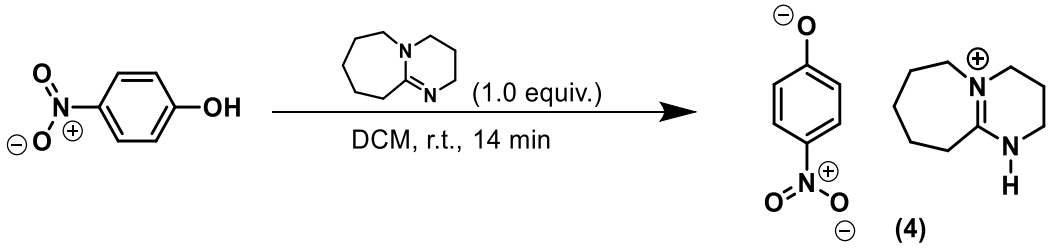

Figure 2-2. Synthesis of DBU-H *p*-nitrophenoxide salt **4.**

^{1}H-NMR (500 MHz, DMSO-d_6, δ, ppm): 10.50 – 9.73 (1H, br. s, -N_{tert} = C_{quart}-**N*H***-CH_2-CH_2-CH_2-), 7.73 (2H, ½AB_q, , $J_{AA'\text{-}XX'}$ = 10 Hz, **ortho-*H*** to NO_2), 5.94 (2H, ½AB_q, $J_{AA'\text{-}XX'}$ = 10 Hz, **ortho-*H*** to O^-), 3.53 (2H, m, -**C*H₂***-N_{tert} = C_{quart}-CH_2-CH_2-CH_2-CH_2-), 3.46 (2H, t, *J* = 6 Hz, -N_{tert} = C_{quart}-NH-CH_2-CH_2-**C*H₂***-), 3.24 (2H, t, *J* = 6 Hz, -N_{tert} = C_{quart}-NH-**C*H₂***-CH_2-CH_2-) 2.63 (2H, m, -CH_2-N_{tert} = C_{quart}-**C*H₂***-CH_2-CH_2-CH_2-), 1.90 (2H, quin., *J* = 6 Hz, -N_{tert} = C_{quart}-NH-CH_2-**C*H₂***-CH_2-), 1.66 (2H, m, -CH_2-N_{tert} =

C_{quart}-CH_2-CH_2-**C*H*$_2$**-CH_2-), 1.63 – 1.55 (4H, br. m, -CH_2-N_{tert} = C_{quart}-CH_2-**C*H*$_2$**-CH_2-**C*H*$_2$**-). ^{13}C-NMR (125 MHz, DMSO-*d*$_6$, δ, ppm): 179.84, 165.14, 128.16, 127.41, 119.12, 53.28, 47.84, 37.82, 31.78, 28.27, 26.01, 23.44, 19.03. ATR-FTIR (cm^{-1}): 3248, 3150 – 2025, 2025 – 1738, 1643, 1622, 1576, 1543, 1510, 1477, 1454, 1441, 1416, 1377, 1352, 1323, 1314 – 1211, 1198, 1161, 1102, 1090, 984, 957, 932 – 872, 866, 845, 810, 793, 760, 706, 692. HRMS (ESI^+): $[M]^+$: $C_9H_{17}N_2^+$ expected: 153.1386 amu; found: 153.1383. HRMS (ESI^-): $[M]^-$: $C_6H_4NO_3^-$ expected: 138.0197 amu; found: 138.0184. T_m = 110 °C. T_d = 245 – 260 °C, with 47% mass loss at 300 °C.

2.2.4.3. Synthesis of Diethyl Triazinedione Adduct (5)

In a flame-dried, 10-mL, two-necked flask, ethyl isocyanate (0.1770 mL, 2.236 mmol) was added to dry DCM (0.50 mL), followed by the addition of DBU (0.1350 mL, 0.9027 mmol). Reaction progress was monitored by thin-layer chromatography (TLC), using 1:1 DCM:ethyl acetate as the eluent, for 25 h before the reaction mixture was run through a silica gel plug using 50 mL 1:1 DCM:ethyl acetate as the eluent. The filtrate was concentrated *in vacuo* and dried under a vacuum in an oil bath at 40 °C overnight to afford **5** (0.2423 g, 91% yield). The synthesis of ethyl isocyanate cyclic adduct **5** with DBU is shown in Figure 2-3.

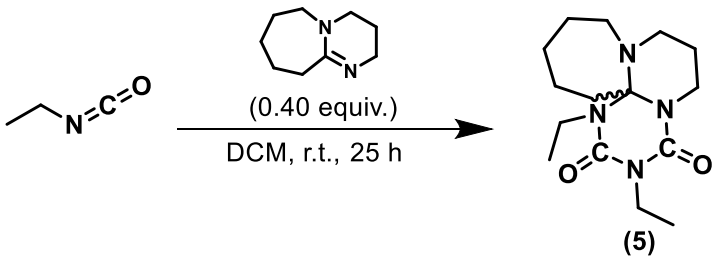

Figure 2-3. Synthesis of ethyl isocyanate cyclic adduct **5** with DBU.

^{1}H-NMR (500 MHz, $CDCl_3$, δ, ppm): 4.38 (1H, ddd, *J* = 14 Hz, 10 Hz, 1 Hz, N_{tert}-CH_2-CH_2-**C*H₂***-N_{tert}), 3.79 (2H, q, *J* = 7 Hz, N_{tert}-**C*H₂***-CH_3 [farthest from DBU ring]), 3.69 (1H, dq, *J* = 13 Hz, 7 Hz, N_{tert}-**C*H₂***-CH_3 [closest to DBU ring]), 3.57 (1H, dq, *J* = 14 Hz, 7 Hz, N_{tert}-**C*H₂***-CH_3 [closest to DBU ring]), 3.13 (1H, m, N_{tert}-**C*H₂***-CH_2-CH_2-CH_2-CH_2-C_{quart}), 3.11 (1H, m, N_{tert}-**C*H₂***-CH_2-CH_2-N_{tert}), 3.01 (1H, m, N_{tert}-**C*H₂***-CH_2-CH_2-CH_2-CH_2-C_{quart}), 2.86 (1H, ddd, *J* = 14 Hz, 10 Hz, 8 Hz, N_{tert}-CH_2-CH_2-**C*H₂***-N_{tert}), 2.76 (1H , ddd, *J* = 14 Hz, 8 Hz, 1 Hz, N_{tert}-**C*H₂***-CH_2-CH_2-N_{tert}), 2.10 (1H, m, N_{tert}-CH_2-CH_2-CH_2-CH_2-**C*H₂***-C_{quart}), 1.92 (1H, m, N_{tert}-CH_2-CH_2-CH_2-CH_2-**C*H₂***-C_{quart}), 1.75 - 1.85 (2H, m, N_{tert}-CH_2-**C*H₂***-CH_2-CH_2-CH_2-C_{quart}, N_{tert}-CH_2-**C*H₂***-CH_2-N_{tert}), 1.90 (1H, m, N_{tert}-CH_2-**C*H₂***-CH_2-N_{tert}), 1.70 (1H, m, N_{tert}-CH_2-CH_2-**C*H₂***-CH_2-CH_2-C_{quart}), 1.64 (1H, m, N_{tert}-CH_2-**C*H₂***-CH_2-CH_2-CH_2-C_{quart}), 1.60(1H, m, N_{tert}-CH_2-CH_2-CH_2-**C*H₂***-CH_2-C_{quart}), 1.45 (1H, m, N_{tert}-CH_2-CH_2-CH_2-**C*H₂***-CH_2-C_{quart}), 1.31 (1H, m, N_{tert}-CH_2-CH_2-**C*H₂***-CH_2-CH_2-C_{quart}), 1.19 (3H, t, *J* = 7 Hz, **-C*H₃*** [farthest from DBU ring]), 1.16 (3H, t, *J* = 7 Hz, **-C*H₃*** [closest to DBU ring]). ^{13}C-NMR (125 MHz, $CDCl_3$, δ, ppm): 152.97, 151.54, 90.72, 52.04, 45.48, 38.63, 36.80, 35.41, 34.60, 31.53, 29.57, 22.64, 21.58, 15.00, 14.23. ATR-FTIR (cm^{-1}): 2978 – 2855, 1686, 1645, 1483 – 1454, 1422, 1391, 1368, 1321, 1275, 1234, 1198, 1175, 1152, 1088, 1045, 1014, 984, 972, 937, 881, 868, 851, 826, 781, 764, 750. HRMS (ESI^+): $[M+H]^+$: $C_{15}H_{27}O_2N_4$ expected: 295.2129 amu; found: 295.2119. T_m = 108 °C. T_d = 169 – 209 °C with 93% mass loss at 275 °C.

2.2.4.4. Synthesis of Poly(Glucose Urethane)s from 1 and 2 (Entries 6 to 9 in Table 2-2) Under Different Conditions

In a 5-mL, round-bottomed flask, **2** (126.5 mg, 0.4481 mmol) and **1** (201.5 mg, 0.4514 mmol) were combined, and the apparatus was purged with dry $N_{2(g)}$. Dry DMF (0.28 mL) was

subsequently added, and the flask was immersed in a 40 °C oil bath, and DBU (135 μL, 0.903 mmol) was added dropwise using a microsyringe. The DBU addition rate was held constant by timing each drop with a stopwatch: 1 drop/2 min for an average rate of 3 μL/min and 1 drop/min for 6 μL/min, with the rapid addition taking no longer than 10 s to complete. The drop size was determined by counting the total number of drops to dispense the whole volume of DBU and was thus an average drop size of 5 μL/drop. After 8 h from the end of the DBU addition, the reaction was quenched with methanol (MeOH) (1 mL). The round-bottomed flask was rinsed four times with DCM (10 mL) and was washed with 0.1-M aqueous sodium chloride (NaCl) (30 mL). The organic phase was washed with 0.05M NaCl (30 mL × 2) and H_2O (30 mL) and was concentrated *in vacuo*. The resulting solution was then precipitated into cold diethyl ether (Et_2O) (20 mL) and was centrifuged at 9800 RPM for 12 min at 3 °C. The solid precipitate was transferred to a vial and dried under a vacuum at 40 °C. The general procedure for poly(glucose urethane) (PGU) synthesis from dicarbamate **1** is shown in Figure 2-4.

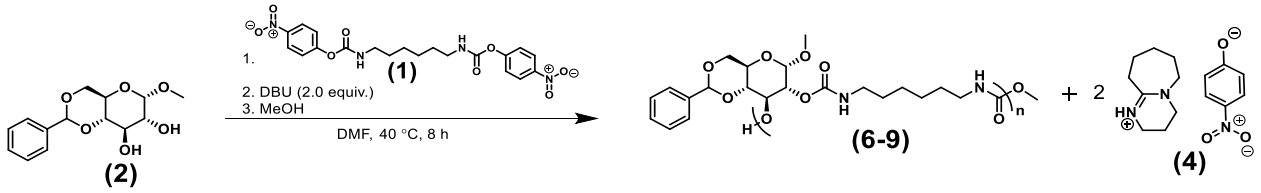

Figure 2-4. General procedure for PGU synthesis from dicarbamate **1**.

PU(**6a**): ^{1}H-NMR (500 MHz, $CDCl_3$, δ, ppm): 7.52 – 7.37 (2H, br), 7.37 – 7.27 (3H, br), 5.69 – 5.26 (3H, br), 5.26 – 4.87 (3H, br), 4.87 – 4.74 (1H, br), 4.28 (1H, s), 3.97 – 3.85 (1H, br), 3.85 – 3.72 (1H, br), 3.72 – 3.57 (1H, br), 3.40 (3H, s), 3.22 – 2.85 (4H, br), 1.51 – 1.32 (3H, br), 1.32 – 1.00 (5H, br). ^{13}C-NMR (125 MHz, $CDCl_3$, δ,

ppm): 156.21, 155.77, 137.18, 129.21, 128.32, 126.42, 101.71, 98.53, 79.51, 72.18, 70.08, 69.04, 62.57, 55.49, 41.01, 29.62, 26.15. ATR-FTIR (cm^{-1}): 3717 – 3140, 3113 – 3020, 2932, 2859, 1709, 1669, 1518, 1454, 1373, 1333, 1312, 1238, 1182, 1146, 1119, 1094, 1047, 989, 918, 876, 752, 698, 673. Yield: 79% (0.1588 g). T_g = °C. TGA in N_2: 289 – 336 °C, 78% mass loss at 375 °C. SEC (DMF, PMMA standards): M_n = 3.80 kDa, Đ = 2.9. MALDI-TOF MS M_p = 3,008.89 amu.

PU(**7a**): ^{1}H-NMR (500 MHz, $CDCl_3$, δ, ppm): 7.52 – 7.38 (2H, br), 7.38 – 7.27 (3H, br), 5.59 – 5.17 (5H, br), 5.14 – 4.87 (2H, br), 4.86 – 4.74 (1H, br), 4.28 (1H, s), 3.96 – 3.86 (1H, br), 3.86 – 3.72 (1H, br), 3.72 – 3.58 (1H, br), 3.40 (3H, s), 3.22 – 2.84 (4H, br), 1.51 – 1.31 (3H, br), 1.31 – 1.00 (5H, br). ^{13}C-NMR (125 MHz, $CDCl_3$, δ, ppm): 155.77, 137.21, 129.21, 128.32, 126.43, 101.68, 98.53, 79.52, 72.19, 70.12, 69.01, 62.55, 55.50, 41.00, 29.77, 26.21. ATR-FTIR (cm^{-1}): 3732 – 3142, 3107 – 3022, 2932, 2860, 1711, 1518, 1454, 1375, 1314, 1238, 1184, 1146, 1117, 1094, 1047, 991, 918, 876, 752, 698, 673. .Yield: 75% (0.1515 g). T_g = 127 °C. TGA in N_2: 289 – 335 °C, 84% mass loss at 375 °C. SEC (DMF, PMMA standards): M_n = 5.39 kDa, Đ = 2.0. MALDI-TOF MS M_p = 3,908.89 amu.

PU (**8a**): ^{1}H-NMR (500 MHz, $CDCl_3$, δ, ppm): 7.51 – 7.37 (2H, br), 7.37 – 7.27 (3H, br), 5,59 – 5.19 (2H, br), 5.19 -4.90 (br, 2H), 4.87 4.73 (1H, br), 4.27 (1H, s), 3.98 – 3.85 (1H, br), 3.85 – 3.72 (1H, br), 3.72 – 3.57 (1H, br), 3.40 (3H, s), 3.21 – 2.82 (4H, br), 1.55 – 1.32 (3H, br), 1.32 – 0.98 (5H, br). ^{13}C-NMR (125 MHz, $CDCl_3$, δ, ppm): 155.76, 137.20, 129.21, 128.31, 126.42, 101.67, 98.53, 79.52, 72.16, 70.11, 68.99, 62.57, 56.48, 55.50, 40.99, 29.73, 26.37. ATR-FTIR (cm^{-1}): 3746 – 3150, 3132 – 3021, 2932, 2860, 1711, 1518, 1454, 1373, 1335, 1314, 1238, 1182, 1146, 1117, 1094, 1047, 989, 918, 876,

752, 698, 673. Yield: 79% (0.1588 g). T_g = 126 °C. TGA in N_2: 292 – 345 °C, 79% mass loss at 375 °C. SEC (DMF, PMMA standards): M_n = 6.38 kDa, Đ = 2.4. MALDI-TOF MS M_p = 3,458.96 amu.

PU (**9b**): ^{1}H-NMR (500 MHz, $CDCl_3$, δ, ppm): 7.52 – 7.38 (2H, br), 7.38 – 7.27 (3H, br), 5.59 5.21 (3H, br), 5.18 – 4.89 (3H, br), 4.89 – 4.74 (1H, br), 4.28 (1H, s), 3.99 – 3.85 (1H, br), 3.85 – 3.73 (1H, br), 3.73 – 3.59 (1H, br), 3.40 (3H, s), 3.22 – 2.90 (4H, br), 1.50 – 1.33 (3H, br), 1.33 – 1.02 (5H, br). ^{13}C-NMR (125 MHz, $CDCl_3$, δ, ppm): 155.80, 137.21, 129.20, 128.31, 126.43, 101.68, 98.52, 79.59, 72.18, 70.11, 69.01, 62.55, 55.50, 40.99, 29.77, 26.19. ATR-FTIR (cm^{-1}): 3753 – 3169, 3125 – 3022, 2932, 2859, 1713, 1651, 1516, 1454, 1371, 1335, 1314, 1236, 1182, 1146, 1119, 1094, 1047, 989, 918, 876, 752, 698, 673. Yield: 69% (0.1393 g). T_g = 118 °C. TGA in N_2: 289 – 335 °C, 77% mass loss at 375 °C. SEC (DMF, PMMA standards): M_n = 5.82 kDa, Đ = 2.3. MALDI-TOF MS: M_p = 3,626.32 amu.

2.2.4.5. Synthesis of Poly(Glucose Urethane)s (10)

In an oven-dried, 5-mL, round-bottomed flask, $Mn(acac)_2$ (5.7 mg, 0.023 mmol) and DABCO (12.3 mg, 0.110 mmol) were combined, and the flask was purged with dry $N_{2(g)}$. HMDI (72.0 μL, 0.448 mmol) was added, and the reaction flask was immersed in an oil bath set to 40 °C. In a separate vial, methyl 4,6-*O*-benzylidene-α-(D)-glucopyranoside (126.5 mg, 0.4481 mmol) was placed in a vacuum oven at 108 °C for 15 min before weighing on a balance, dispensing into a separate vial, and returning to the vacuum oven at 108 °C for 20 min. The vial was removed from the oven, capped with a septum, purged twice with $N_{2(g)}$, and charged with DMF (0.28 mL) to dissolve **2**. The solution of **2** was added to the HMDI (**3**) mixture, and the reaction was allowed to stir for 1 h before a 0.16-mL aliquot (**10-1**) was taken and immediately

quenched into a vial with 2 mL of methanol. The rest of the reaction mixture (**10-8**) was allowed to stir for a total of 8 h before quenching with 1 mL of methanol. After 20 min, both solutions were concentrated *in vacuo*. Both of the quenched reaction mixtures were transferred with 5 mL of DCM (four times) and were washed with 15 mL of 0.1-M aqueous NaCl. The organic phases were then washed with 0.05-M $NaCl_{(aq)}$ (15 mL × 2) and H_2O (15 mL) and were concentrated *in vacuo*. The resulting solution was then precipitated into cold Et_2O (10 mL) and centrifuged at 9800 RPM for 12 min at 3 °C. The solids from both precipitations were transferred to a vial and dried under a vacuum overnight at 40 °C. The recovered yield at 8 h was 70% (0.0803 g). The general procedure for the conventional synthesis of PGU **10-1a** and **10-8a** is shown in Figure 2-5.

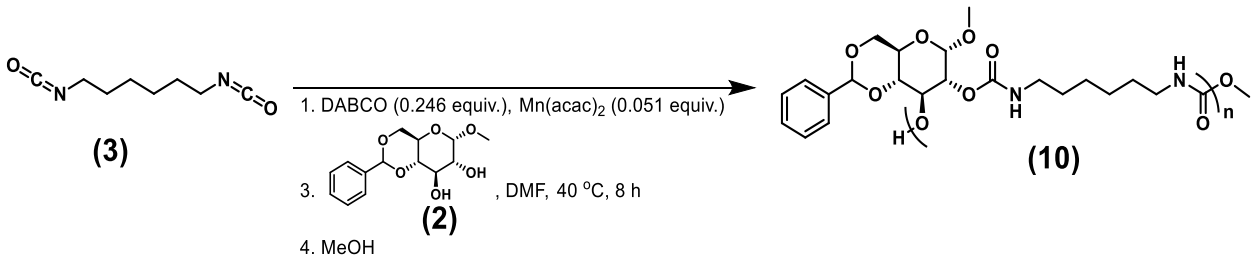

Figure 2-5. General procedure for the conventional synthesis of PGU **10-1a** and **10-8a**.

PU(**10-1a**): ^{1}H-NMR (500 MHz, $CDCl_3$, δ, ppm): 7.54 – 7.39 (2H, br), 7.39 – 7.27 (3H, br), 5.67 – 5.45 (1H, br), 5.45 – 5.16 (2H, br), 5.16 – 4.87 (2H, br), 4.87 – 4.58 (1H, br), 4.28 (1H, s), 4.00 – 3.85 (1H, br), 3.85 – 3.72 (1H, br), 3.72 – 3.54 (2H, br), 3.40 (3H, s), 3.15 – 2.84 (4H, br), 1.62 – 1.34 (3H, br), 1.34 – 0.92 (6H, br). ^{13}C-NMR (125 MHz, $CDCl_3$, δ, ppm): 155.78, 137.21, 129.21, 128.32, 126.42, 101.69, 98.56, 79.63, 72.19,

70.13, 69.05, 62.57, 55.50, 52.15, 41.00, 29.77, 26.35. ATR-FTIR (cm^{-1}): 3807 – 3169, 3127 – 3021, 2932, 2860, 2347, 1711, 1518, 1454, 1373, 1312, 1238, 1184, 1146, 1119, 1094, 1047, 991, 918, 878, 820, 752, 698, 673. Yield: 58% (0.0505 g). T_g = 106 °C. TGA in N_2: 265 – 320 °C, 85% mass loss at 375 °C. SEC (DMF, PMMA standards): M_n = 3.32 kDa, Đ = 1.4. MALDI-TOF MS M_p = 2,956.91 amu.

PU(**10-8a**): ^{1}H-NMR (500 MHz, $CDCl_3$, δ, ppm): 7.54 – 7.37 (2H, br), 7.37 – 7.27 (3H, br), 5.65 – 5.44 (1H, br), 5.44 – 5.23 (2H, br), 5.23 – 4.88 (2H, br), 4.88 – 4.64 (1H, br), 4.27 (1H, s), 3.99 – 3.84 (1H, br), 3.84 – 3.72 (1H, br),), 3.72 – 3.57 (1H, br), 3.39 (3H, s), 3.19 – 2.83 (5H, br), 1.51 – 1.31 (4H, br), 1.31 – 0.91 (6H, br). ^{13}C-NMR (125 MHz, $CDCl_3$, δ, ppm): 155.75, 137.20, 129.21, 128.31, 126.42, 101.71, 98.51, 79.60, 72.17, 70.11, 69.00, 62.56, 55.49, 41.00, 29.70, 26.17. ATR-FTIR (cm^{-1}): 3730 – 3169, 3125 – 3022, 2932, 2859, 1711, 1666, 1524, 1454, 1375, 1312, 1238, 1182, 1146, 1119, 1094, 1047, 989, 918, 876, 752, 698, 675. Yield: 70% (0.0803 g). T_g = 131 °C. TGA in N_2: 266 – 324 °C, 72% mass loss at 375 °C. SEC (DMF, PMMA standards): M_n = 17.3 kDa, Đ = 2.8. MALDI-TOF MS M_p = 2,869.67 amu.

2.3. Results and Discussion

2.3.1. Synthesis of Dicarbamate

The synthesis of the HMDNC comonomer **1** proceeded in good yield (*ca.* 85%). With slight modification to the procedure described by Katsarava *et al.*,[104] a dispersion of 1,6-diaminohexane in THF was added to a solution of di(*p*-nitrophenyl)carbonate at 0 °C and was allowed to warm to room temperature while stirring for 19 h. Product **1** was obtained as a white solid by a series of precipitations. Chromatographic purification was complicated by the solubility properties of **1**, together with its relative reactivity (*e.g.*, for the silica gel stationary

phase). It was insoluble in water, chloroform, DCM, and methanol, but was sparingly soluble in acetone and was soluble in polar aprotic organic solvents, such as DMF, DMAc, and DMSO. Multiple batches afforded a clean product according to NMR spectroscopy, with minor amounts of urea observed (*ca.* 7%), as measured by ^{1}H-NMR spectroscopy comparing the methylene proton signals alpha to the urethane and urea functionalities (see Figure A-1 in Appendix A). A fuller picture of Scheme 1 is shown in Figure 2-6.

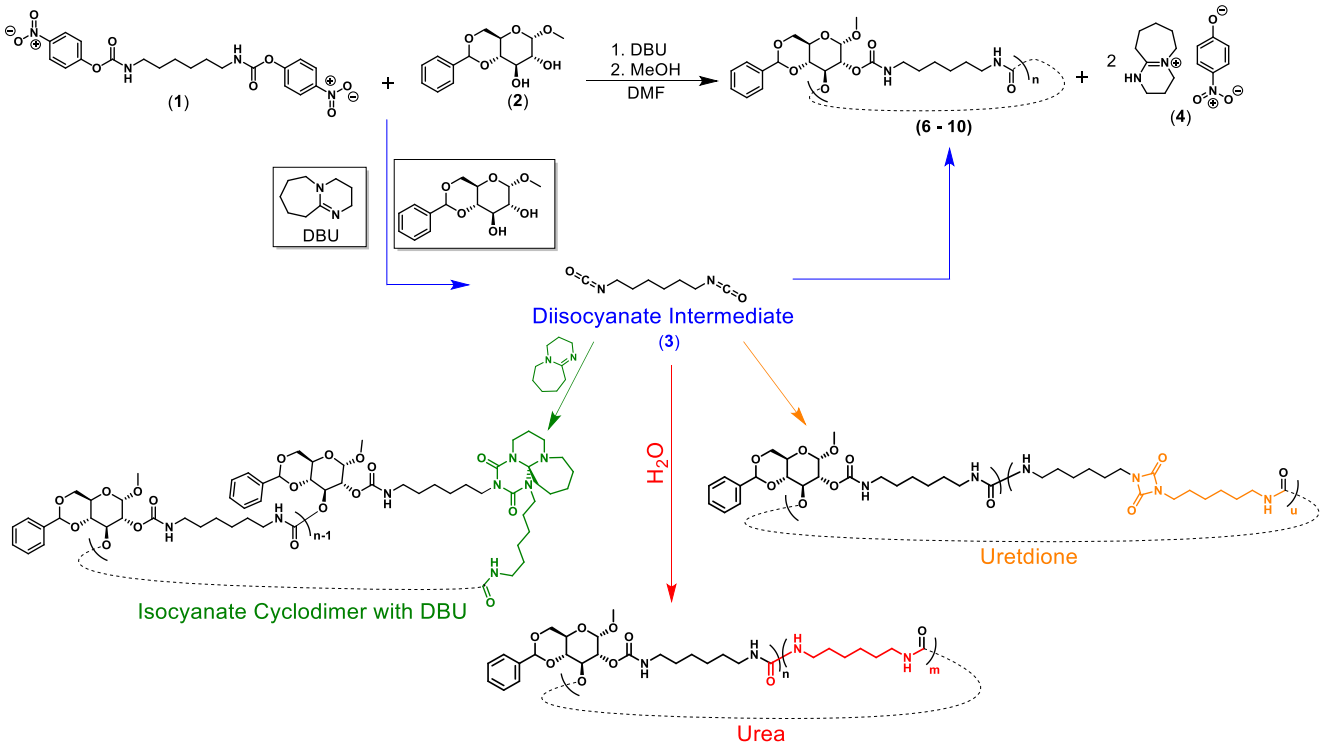

Figure 2-6. Scheme 1—Deblocking dicarbamate (**1**) with DBU to form a diisocyanate intermediate (**3**) can form a cyclic PU in the presence of a diol (**2**) or can form urea, uretdione, or an isocyanate cyclodimer with DBU, depending on the reaction conditions.

Dicarbamate **1** was found to undergo deblocking at room temperature over time without added catalyst to produce *p*-nitrophenol and diisocyanate in solvents in which it is soluble. As shown in Figure A-5 in Appendix A, **1** was 1%, 15%, and 28% dissociated at 15 min, 8 h, and 24

h, respectively, as determined by ^{1}H-NMR spectroscopy in DMSO-d_6 (see Table A-1 and Figure A-5 in Appendix A). The ability of blocked isocyanates to deblock at room temperature has been rarely reported, despite the abundance of literature on the design of isocyanate blocking groups that dissociate at low temperatures.[14,92,103] One such system is the photocatalyzed decarboxylation of oxamic acids reported by Landais, Cramail, and coworkers, proceeding through a protonated isocyanate intermediate at room temperature.[83] Patton and coworkers employed another ambient deblocking scheme with azole-*N*-carboxamides as polymer pendant groups for postpolymerization modification by thiols using DBU as a catalyst.[144] Thus, the reactivity of **1** appeared unique because deblocking could occur with no other stimulus other than adding a suitable solvent.

Given the labile nature of the end groups on **1**, the stability of the solid was probed in regard to long-term storage and safety. ^{1}H-NMR spectroscopy showed no significant change in composition of **1** after storage as a solid for more than a year in a vial under ambient conditions (Figure A-9 in Appendix A). The vial was stored primarily in a cabinet in the absence of light and was opened periodically to collect samples for analysis and further chemical transformations. Therefore, it can be concluded that **1** is stable under ambient conditions in the solid state.

2.3.2. The Effect of 1,8-Diazabicyclo[5.4.0]undec-7-ene on Carbamate Dissociation

The intentional deblocking of **1** was then examined to afford a diisocyanate *in situ* for condensation polymerization with diols. DBU was selected as the deblocking base for three reasons: 1) DBU is a bulky base, hampering its nucleophilic addition to isocyanates; 2) DBU is a strong organic base with an experimental pK_a of 11.5 to 11.9 in water and 24.3 in CH_3CN, which

may force the equilibrium to favor deblocking,[120] and 3) DBU was shown by Cramail, Landais, and coworkers to be a more-active catalyst than DBTDL when used with IPDI and diols.[11] Given the inherent deblocking of **1** that occurred under ambient conditions in the solution, it was anticipated that DBU may provide accelerated deblocking at substoichiometric amounts. A screening study was, therefore, conducted to measure carbamate dissociation at 0, 0.48, 0.99, and 2.0 equivalents of DBU relative to carbamate. ^{1}H-NMR spectroscopy in DMSO-d_6 was used to observe the extent of dissociation of **1** in the presence of DBU immediately after addition (t = 15 to 20 min), followed by 8 and 24 h after addition (see Figures A-28 and A-29 in Appendix A). The relaxation delay for the ^{1}H-NMR spectrum was extended to 10 s to ensure more-accurate integrations and proportional peak heights between the different species, as determined by a relaxation experiment (Figure A-17 in Appendix A). Figure 2-7 shows a stark contrast in the intensities of the carbamate phenyl protons (labeled A and B, resonating at 8.25 and 7.39 ppm, respectively) and the *p*-nitrophenoxide phenyl protons (labeled P and Q, resonating at 7.96 to 7.68 and 6.48 to 5.89 ppm, respectively), with increasing relative intensities of the *p*-nitrophenoxide phenyl proton signals at progressively upfield chemical shifts as the DBU equivalents increased at t = 15 to 20 min. Quantification of the normalized intensities are included in Table A-5 in Appendix A, allowing for determination of the extent of deblocking. The *p*-nitrophenoxide Q proton signals not only increased in relative intensity with increasing DBU equivalents, but also shifted upfield and became more resolved. These observations indicate an increase in dissociation and a decrease in phenolic proton exchange between nitrophenols and nitrophenoxides as equivalents of DBU approached stoichiometric amounts. Concomitant with this result, the carbamate D peak intensity progressively decreased in intensity relative to the isocyanate G and J peaks as the reaction proceeded to a greater extent. The

isocyanate peaks are only barely visible on the baseline of the system without DBU. Most importantly, these spectra show that the dicarbamate is only 81% dissociated, by integration of the B and Q peaks, at 15 to 20 min after 0.99 equivalents of DBU were added (see Table A-5 in Appendix A). While the presence of unreacted DBU is seen in the sample with 2.0 DBU equivalents, the dicarbamate is 93% dissociated 15 to 20 min after addition. Therefore, two equivalents of DBU were needed for conversion of **1** to approach completion essentially just after addition of DBU, absent any other nucleophiles.

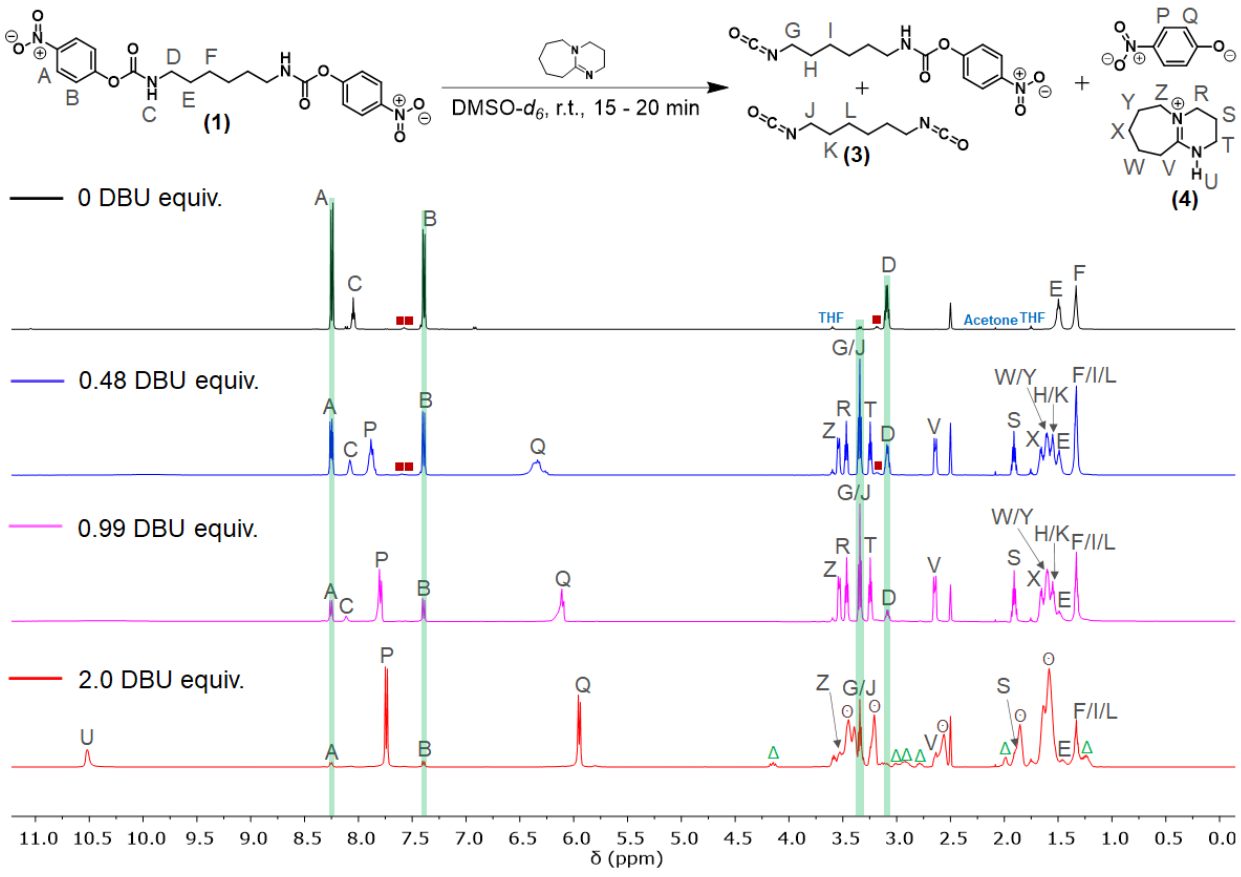

Figure 2-7. ^{1}H-NMR spectra (500 MHz, DMSO-d_6) show the reaction of DBU with carbamate (**1**) forming the DBU-H *p*-nitrophenoxide salt at 15 to 20 min after DBU addition. Signals for protons associated with carbamates (labeled "A" to "F") nearly vanished with addition of 2.0 equivalents of DBU, while some residual DBU (Θ) appeared, along with another by-product, a cyclodimer of HMDI with DBU (Δ). A small amount of urea (red boxes) was also visible.

In the ranges of 1.0 to 2.0 ppm and 2.6 to 4.5 ppm, broad, low-intensity peaks (Δ) appeared after 2.0 DBU equivalents were added. Previous works have shown that cyclic amidine and guanidine bases could act as nucleophiles with electrophilic IPDI to form a six-membered adduct analogous to an isocyanurate well below room temperature.[11,13] The cyclic adduct forms irreversibly, persisting in the presence of primary alcohols in refluxing THF.[11] During polymerization, formation of this adduct could render some of the diols unreacted and potentially limit the degree of polymerization. However, coordination of these bases to a hydroxyl proton reportedly suppresses cycloadduct formation during polymerization.[11] Thus, DBU could preferentially abstract a proton from **1,** forming the DBU-H amidinium species before it attacks free isocyanate groups. However, Figure 2-7 suggests that some cyclic adduct might form. Even if a slight excess of free DBU were present, cycloadduct formation was hypothesized to be even more suppressed in the presence of a diol under polymerization conditions.

Figure A-28 and Table A-6 in Appendix A show ^{1}H-NMR spectra of these same systems after 8 h and indicate little decrease in the composition of carbamate A and B peaks from their initial values. However, one significant change is the appearance of the isocyanate cyclodimer with DBU in the sample with 0.99 DBU equivalents. This study demonstrates that complete carbamate dissociation occurs only as the number of DBU equivalents approaches 2.0 relative to **1**. However, these results also suggest that 2.0 equivalents of DBU would be likelier to favor cyclic adduct formation with free isocyanate groups. Therefore, we next sought to determine whether such an adduct could form in a small molecule study to help elucidate its spectral properties for identification in a polymer backbone.

2.3.3. Isocyanate Cyclodimer with 1,8-Diazabicyclo[5.4.0]undec-7-ene

To assign the observed impurity peaks (Δ) in Figure 2-7, a model reaction was conducted between ethyl isocyanate and DBU (Scheme 2). This reaction included adding DBU to 2.5 equivalents of ethyl isocyanate in DCM at room temperature to realize the diethyl triazinedione product **5** after 25 h in 91% yield. The peaks from 1.16 to 2.10 ppm, from 2.76 to 3.69 ppm, and at 4.38 ppm (shown in Figure A-30 in Appendix A) appear to correlate with the minor peaks observed in Figures 2-7 and A-28 (in Appendix A) given the polymeric peak broadening. For brevity, this structure in a polymer backbone is hereafter referred to as a "Δ-adduct" (shown in Figure 2-8).

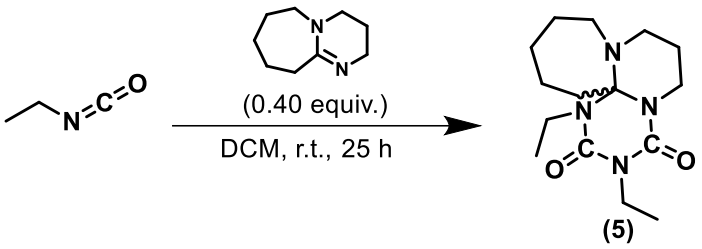

Figure 2-8. Scheme 2, synthesis of DBU-isocyanate cyclodimer (**5**) (Δ-adduct).

2.3.4. Polymerization

Given the results of these small molecule studies, we hypothesized that the addition of DBU to a one-pot mixture of diol and **1** would produce a PU by deblocking the dicarbamate to yield **3** *in situ*. While deblocking schemes generally allow for more-benign conditions relative to the transurethanization routes, different reaction parameters were optimized to determine the efficiency of this chemistry relative to other diisocyanate alternatives and to conventional methods.[14,74] Therefore, we conducted two screening studies to optimize conditions limiting the

formation of other side-products; namely polyurea and Δ-adducts in the backbone. We first hypothesized that the slow addition of DBU would allow time for liberated diisocyanate groups to react with alcohols rather than with free DBU to form Δ-adducts. Secondly, we hypothesized that altering the water content of the diol (**2**) starting material would alter the urea content in the resulting polymer. Thus, the slower rates of addition (1.8 to 2.8 μL/min) were used to screen the effect of water content in **2** on the PU urea composition first before screening DBU addition rates. However, for this chemistry to be relevant as a replacement for conventional PU synthesis methods using diisocyanates, we also needed to explore how this chemistry compares to a system synthesized using conventional methods. Finally, we screened the effects of time and temperature on this dicarbamate route to optimize molar mass.

To optimize both molar mass and identify side-products, SEC and FTIR spectroscopy were found to be inadequate as stand-alone techniques. Polymer distributions of the same molar mass but with different functional groups on the backbone or cyclic instead of linear forms can show drastically different retention times by SEC.[145-147] While FTIR spectroscopy is a robust analytical method for determining the identity of functional groups, it is generally not quantitative unless steps are taken to incorporate an internal standard or reference. Using these two techniques together can help compensate for the shortcomings of either technique, but a more-robust and absolute method was necessary.

MALDI-TOF MS allows not only precise determination of the identity of polymer chains and their end groups, but it also can give an absolute and accurate determination of mass distributions.[148] MALDI-TOF MS further provides analyte sensitivity down to picomoles.[149] In an uncontrolled, polycondensation reaction without defined end groups, MALDI-TOF MS is one of the few characterization methods that can give reliable and absolute information about molar

mass distributions. Therefore, MALDI-TOF MS was used primarily to investigate various aspects of the one-pot, DBU-mediated copolymerization of dicarbamates and diols, while SEC and FTIR were used to supplement and corroborate the results.

2.3.5. Tunability of Urea Content Based on Diol Water Content

It was realized that polyurea formation could be a major undesired product of polymerization with this dicarbamate system. Indeed, it has been well documented that some amount of urea formation occurs during PU synthesis because of even small amounts of water present.[1] However, Cramail, Landais, and coworkers demonstrated that base catalysts, such as guanidines, make the polymerization system more susceptible to urea production from water contamination compared to systems using catalysts, such as DBTDL.[11] Thus, all polymerizations were conducted with distilled DBU that was stored with 3-Å molecular sieves under dry $N_{2(g)}$.

Because water can be introduced to these polymerizations *via* the glucose-based diol, we used TGA to determine the water content in **2** subject to various drying methods. Table 2-1 shows that storing **2** in a desiccator under a constant vacuum of *ca.* 50 mT in the presence of both Drierite® and SICAPENT® P_2O_5 for at least 72 h yielded a diol monomer with 0.82% water. However, applying a vacuum at 108 °C to dry **2** for 15 min resulted in a 0.03% water concentration.

Table 2-1. Water content of glucose diol **1** by TGA.

Method	Drying Time	Water Loss (%)	T_D (°C)
Vac. desiccator	72 h	0.82±0.02	151±5
Vac. oven 108 °C	15 min	0.03*	167*

*Performed single trial

Table 2-2 shows the resulting analysis of two polymer systems made as follows: a) **2** having different water contents achieved by drying in a vacuum desiccator for 48 h (entry **6**) and b) drying first in a vacuum oven at 108 °C for 15 min before weighing, adding to the reaction flask, and putting the flask with **2** back in the vacuum oven at 108 °C for another 20 min (entry **7**). Both systems were duplicated (a and b) and involved purging the reaction flask with $N_{2(g)}$ after **1** was added. As previously mentioned, slow DBU addition rates were used for the two systems, **6** and **7**, to determine the effect of water content in diol **2**. The M_n values appear to increase slightly from 3.68 to 3.80 kDa for the system using diol dried in the vacuum desiccator (**6**) to 4.89 to 5.39 kDa for the oven-dried diol system (**7**). This result could be because either the polymer distribution moved to a higher molar mass for **7** or there was a change in the identity of the functional group on the polymer chains with different hydrodynamic volumes resulting from the formation of urea linkages for **6**.[147,150] ATR-FTIR of these samples (Figure 2-9) showed a pronounced increase in the relative intensity of the urea C = O stretch at 1668 cm^{-1} relative to the urethane peak (1709 to 1713 cm^{-1}) in **6** compared with **7**. Additionally, the ratio listed in Table 2-2 uses the baseline-subtracted spectra to divide the peak height of the urethane peak by that of the urea peak at a fixed value of 1668 cm^{-1} (see Figures A-6, A-57, and A-58 in Appendix A). This wavenumber value for the urea peak is in agreement with literature values for similar systems.[89] From this ratio, it was observed that the drier polymer (**7)** contains less urea than **6**.

Table 2-2. Polymerization conditions for selected PUs.

Entry	Conc. (M)	Base (equivalents)†	Base	Base Addition Rate (μL/min)	M_n (kDa)	Đ	M_p (amu)**	Urethane:Urea (height:height)††
6a	3.2	2.0	DBU	1.8	3.80	1.7	3008.89	2.9
6b	3.2	2.0	DBU	1.9	3.68	1.7	3149.02	3.2
7a	3.2	2.0	DBU	2.8	5.39	2.0	3908.85	4.2
7b	3.2	2.0	DBU	2.8	4.89	2.0	3458.62	3.9
8a	3.2	2.0	DBU	5.6	6.38	2.4	3458.96	3.9
8b	3.2	2.0	DBU	5.6	6.36	2.2	3909.29	4.2
9a	3.2	2.0	DBU	R	9.06	2.4	3626.76	4.6
9b	3.2	2.0	DBU	R	5.82	2.3	3626.32	4.1
10-1	3.2	0.25	DABCO	N/A	3.32	1.4	2956.91	4.1
10-8	3.2	0.25*	DABCO	N/A	17.3	2.8	2869.67	3.4

All reactions conducted at 40 °C; †Relative to carbamate; DBU was added rapidly over the course of 10 s; *DABCO relative to HMDI; ††Urea peak values taken at 1668 cm^{-1}; **Value taken from MALDI-TOF mass spectra as the most intense peak in the distribution

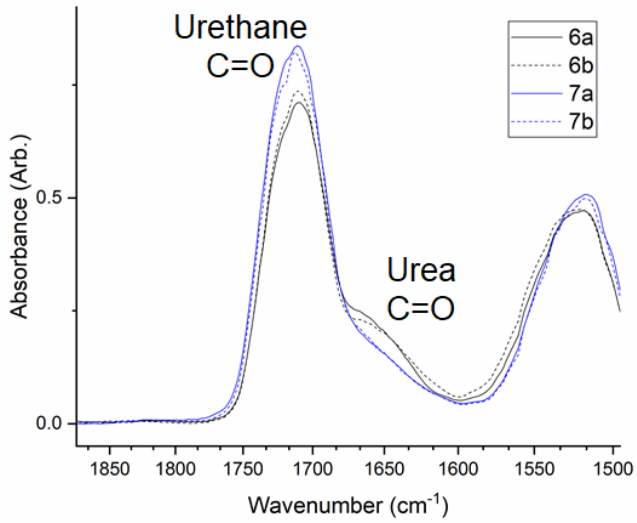

Figure 2-9. FTIR spectra of **6a**, **6b**, **7a**, and **7b** shows the very stark increase in urea content of the wet diol (**6a**, **6b**) due to insufficient drying in a vacuum desiccator relative to the system produced from diols dried in a 108-°C vacuum oven (**7a**, **7b**). For comparison, the ATR-FTIR spectra are shown as absorbance with the baseline subtracted and absorbance normalized.

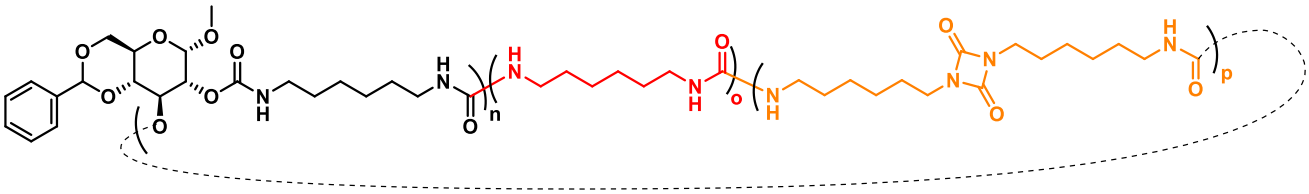

Figure 2-10. The generic structure of macrocyclic PGU can contain urea or uretdione by-products in the polymer backbone.

Surprisingly, MALDI-TOF MS shows that both **6a** and **7a** consisted of predominantly cyclized species in Figure 2-11 and Table 2-3. Kricheldorf and coworkers[151,152] showed that cyclization is favored at high conversion for step-growth polymerizations as a result of "self-dilution." Our group's previous work also indicated a tendency for cyclization when attempting a step-growth synthesis of hyperbranched systems.[153]

Table 2-3. Labels and expected masses for main cyclic structures.

Population	o units	p units	q[b] units	Counterion	n=2 Average Mass (amu)	n=6 Average Mass (amu)	n=2 Exact Mass (amu)[a]	n=6 Exact Mass (amu)[a]
A	0	0	0	Na^+	923.97	2725.92	923.390	2725.194
B	1	0	0	Na^+	1066.17	2868.12	1065.500	2867.305
C	2	0	0	Na^+	1208.37	3010.32	1207.611	3009.415
D	3	0	0	Na^+	1350.57	3152.52	1349.722	3151.526
E	4	0	0	Na^+	1492.77	3294.73	1491.832	3293.636
F	5	0	0	Na^+	1634.98	3434.74	1633.943	3435.747
UB	0	1	0	Na^+	1092.16	2894.11	1091.480	2893.284
UC	1	1	0	Na^+	1234.36	3036.32	1233.590	3035.394
$C\Delta^A$	0	0	1	Na^+	1222.42	3024.37	1221.629	3023.433

[a]Masses listed are highest abundance monoisotopic masses; [b]See Figure 2-16 for structure of $C\Delta^A{}_n$

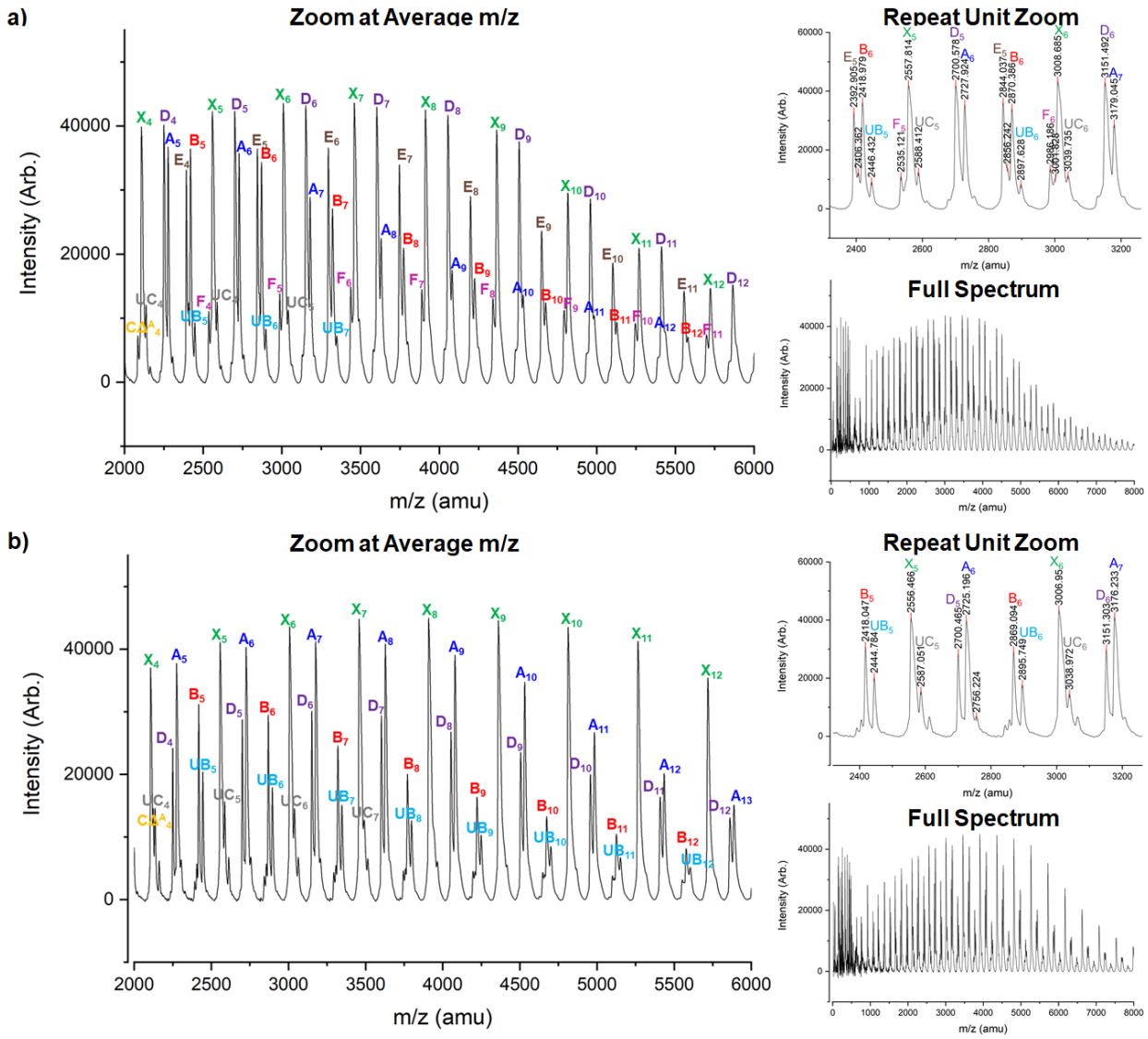

Figure 2-11. Increased urea content caused by higher water content in monomers, as shown by MALDI-TOF mass spectra of a) polymer **6a**, of which monomers were dried in a vacuum desiccator and b) polymer **7a**, of which monomers were dried using a vacuum oven, resulting in less water content. Because of peak overlap, $x_n = C_n + G_n$.

Moreover, MALDI-TOF MS was used to determine whether the presence of more urea linkages had actually shifted the distribution to a lower molar mass or the added urea linkages in the backbone merely resulted in a decreased hydrodynamic volume. The spectra in Figure 2-11 clearly show that the molar mass distribution of the drier PU (**7a**) shifted to a slightly higher

mass relative to **6a**. Additionally, the spectrum of **7a** shows significantly reduced urea populations, denoted D, E, and F corresponding to three, four, and five urea linkages in the chain, respectively. Indeed, the E and F species are completely absent in the **7a** spectrum, consistent with the ATR-FTIR spectra. While recognizing that MALDI-TOF MS is not quantitative in terms of absolute concentration because of differing ionizabilities of different species, it is an accepted practice to compare the relative intensities of the same species to one another from sample to sample as long as the laser intensity and sample preparations are kept constant.[154,155] Not only do these results show that urea content can be tuned based on the drying method of the diol, but they also show that a one-pot polymerization of dicarbamates and diols mediated by DBU can occur.

Another noteworthy aspect of the **7a** spectrum is the presence of the uretdione species UB_n (corresponding to a cyclic PU with one uretdione linkage) and UC_n (a cyclic PU with one uretdione and one urea linkage). In ATR-FTIR spectra, the uretdione carbonyl stretch at 1767 cm^{-1}, as reported in literature for HMDI,[67] was not observed, possibly because of overlap with the broadened urethane peak or because too little of the species was present to detect. Uretdione is known to form from aliphatic diisocyanates in the presence of trialkyl phosphines, substituted pyridines, or trialkylamines.[14,67] Aromatic diisocyanates can form uretdiones by simply heating them above 43 °C.[23,67] The absence of uretdione in the **6a** spectrum is noteworthy given that the presence of water likely competes more effectively as a nucleophile than any agent that may be acting as a catalyst for uretdione formation.

The uretdione formation during polymerization could be the result of either a nucleophilic mechanism with DBU, analogous to previous reports with tertiary amines or substituted pyridines, or a nucleophilic mechanism involving *p*-nitrophenol or the *p*-

nitrophenoxide anion, which might be operative.[14,67] The precise mechanism for uretdione formation requires further investigation in future work.

The X peaks in Figure 2-11 were verified to contain overlapping polymer populations by further examination with the more-precise reflectron mode of MALDI-TOF MS. Species C and G are resolved in reflectron mode, but appear as one peak in linear mode. Figure B-2 in Appendix B shows the expanded spectra of **6a** and **7a** acquired in reflectron mode. Because species G_n is slightly lower in mass than C_n, as shown in Table 2-4 and Figure 2-12, the broadened peak observed in linear mode appears biased to a slightly lower mass than expected. Thus, X_n is labeled as $X_n = C_n + G_n$.

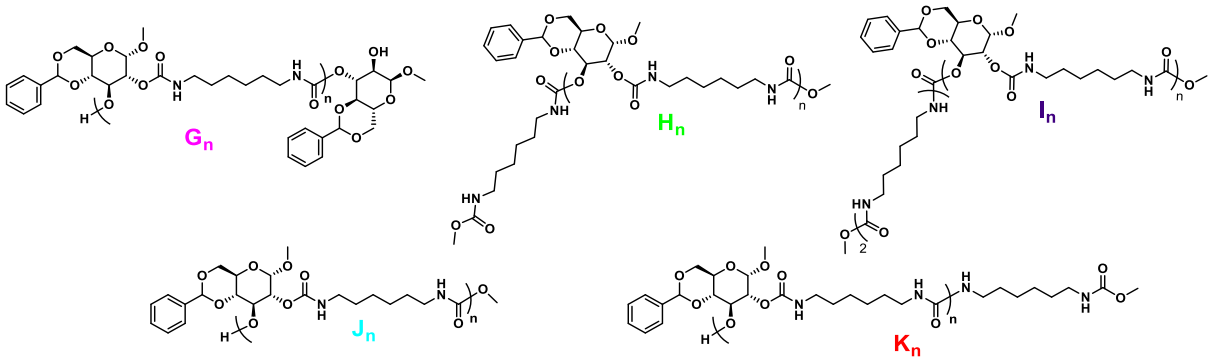

Figure 2-12. The G_n structure is the only linear chain observed in the dicarbamate-derived systems, while the other linear species are found in the conventionally derived polymer after 1 h but not 8 h.

Table 2-4. Labels and expected masses for main linear species.

Population	Counterion	n=2 Average Mass (amu)	n=6 Average Mass (amu)	n=2 Exact Mass (amu)[a]	n=6 Exact Mass (amu)[a]
G	Na^+	1206.26	3008.21	1205.500	3007.304
H	Na^+	1156.25	2958.20	1155.532	2957.336
I	Na^+	1298.45	3100.40	1297.643	3099.447
J	Na^+	956.01	2757.96	955.416	2757.220
K	Na^+	1098.21	2900.16	1097.527	2899.331

[a]Masses listed are highest abundance monoisotopic masses

Figure 2-13 shows the ^{1}H-NMR spectra for PUs **6a** and **7a**. To aid in assignments, ^{13}C, ^{1}H-^{13}C-HMQC, and ^{1}H-^{13}C-HMBC NMR were run on **7a** in Figures A-73 to A-76 in Appendix A. While all spectra showed good, general agreement, there are some subtle differences. For instance, there is a significant downfield shoulder at 3.08 ppm ascribed to the alpha urea (ζ) protons in Figure 2-14a. This result corroborates the MALDI-TOF and FTIR data showing that PU **6a** displayed the highest urea content of all PUs discussed. The urea shoulder is significantly less pronounced in most of the other systems. Additional singlets appear at 4.68 and 5.54 ppm in all spectra, except for the spectrum shown in Figure 2-14e. Given the results from MALDI-TOF MS, these signals were ascribed to the end groups for the linear G_n species corresponding to the λ and κ protons on the cyclized species in Figure 2-14. As shown in Table A-9 in Appendix A, the area of these peaks is highest in **6a**. With more consumption of free isocyanates to form urea linkages, it follows that the linear species, G_n, would increase in abundance as a result.

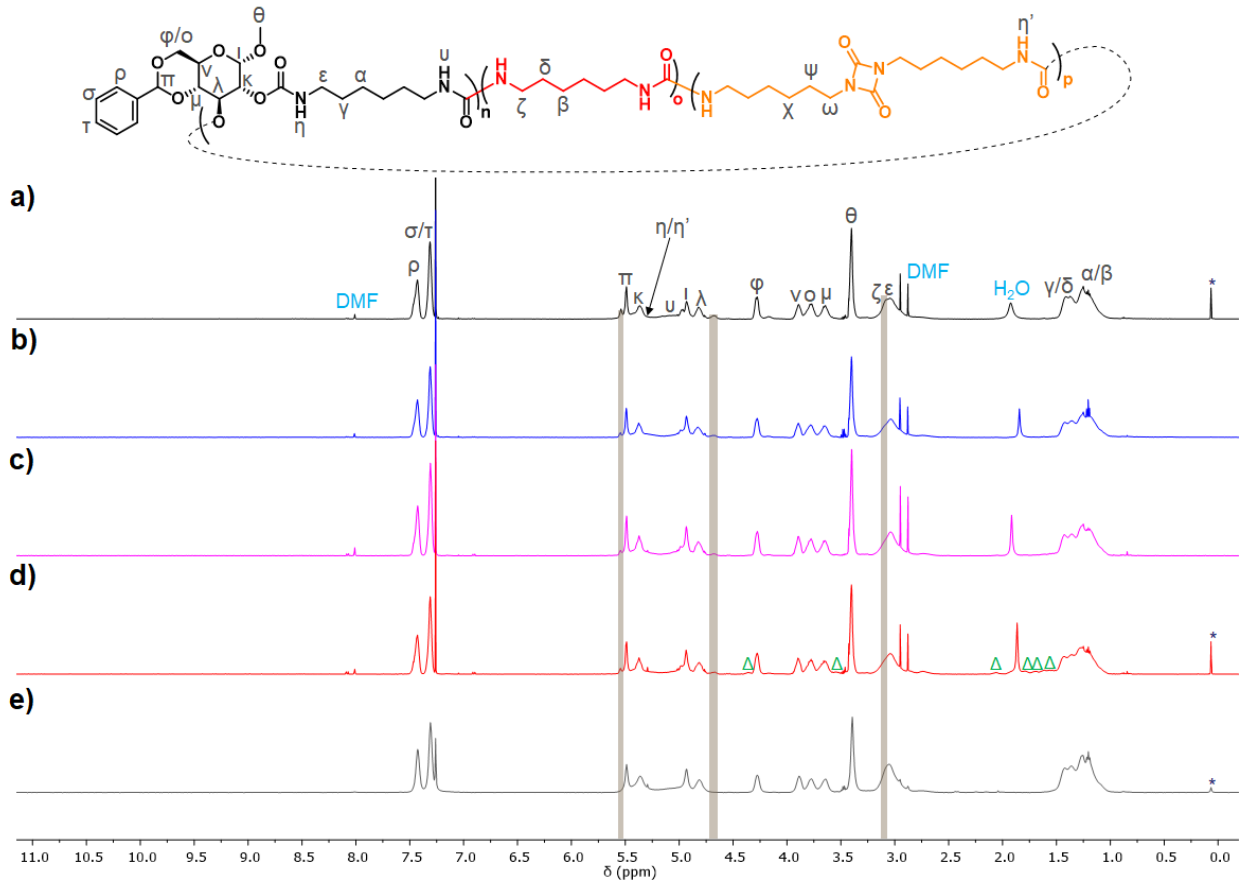

Figure 2-13. ^{1}H-NMR spectra in deuterated chloroform ($CDCl_3$), showing a surprising similarity between the different reaction conditions except for the pronounced urea shoulder seen at 3.08 ppm for a) **6a**. There are also peaks at 4.68 and 5.54 ppm in polymers a) **6a**, b) **7a**, c) **8a**, and d) **9b**, but not e) **10-8a**. In e), PU **9b** shows the faint presence of Δ-adduct (Δ). *Vacuum grease contamination.

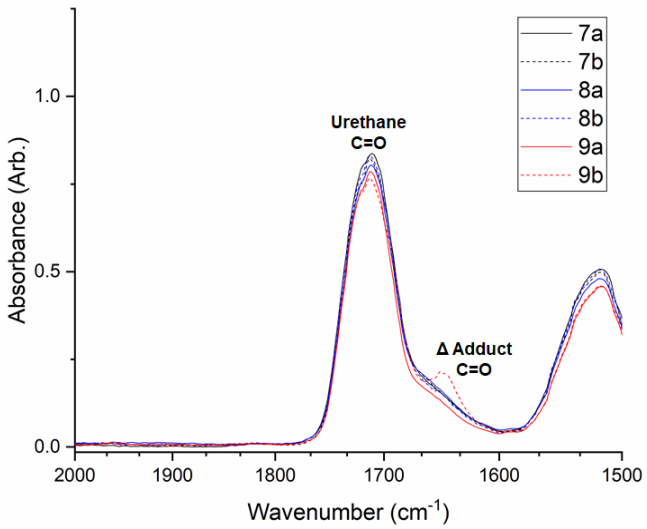

Figure 2-14. Normalized FTIR showing the presence of the Δ-adduct in PU **9b** while being absent in PGUs **7a**, **7b**, **9a**, **8a**, and **8b**.

These data confirm the tunability of the urea content in the polymer based on the water content of diol monomer **2**. The duplicate reactions, **6b** and **7b**, indeed mirror these results (see Figures A-36 and A-40 in Appendix A). It is well known that adding urea linkages to a PU backbone increases material properties such as Young's modulus through increased hydrogen bonding.[7,21,89] PUs with significant urea content and a long, flexible polyol tend to undergo phase separation into hard segments consisting of hydrogen-bonded urea linkages and soft segments consisting of the polyol and non–hydrogen-bonded urethanes, resulting in tunable hydrophobicity and morphologies of great interest to the PU community.[15,21,88,89] Industrial PU manufacturers sometimes add chain extenders, such as diamines, or small amounts of water to a conventional polymerization to induce urea formation for applications requiring improved material or thermal properties.[1,7] Only a few diisocyanate alternatives have shown the ability to tune urea formation in the PU product.[89] Recently, Sardon and coworkers reported a route to

synthesize and tune poly(urethane-ureas) by copolymerization of dicyclic carbonate with diamines, but this method required heating to 120 °C and at least 10 h before any urea signal was detected.[89] Thus, the ability to tune the urea content demonstrated here under benign conditions should enhance the appeal of this method for conventional PU production.

2.3.6. Tunability of Δ-Adduct and Uretdione Formation *via* 1,8-Diazabicyclo[5.4.0]undec-7-ene Addition Rate

Given the urea content tunability, we were also interested in tuning the uretdione and the cyclic isocyanate-DBU adduct (Δ-adduct) by-products. We hypothesized that by-product formation would be suppressed if the DBU addition rate were kept relatively slow. Considering Scheme 1, if the diisocyanate (**3**) intermediate's concentration is kept low throughout the polymerization, then there should be a low probability of isocyanate groups reacting with each other to form uretdiones and will preferentially react with diol **2**. Additionally, the slow addition of DBU should limit the free DBU concentration throughout the polymerization, suppressing its reactions with free isocyanate groups for two reasons: 1) there is more time for the liberated diisocyanates to react with diols before more DBU is added, and 2) more time is allowed for the system to become homogeneous, allowing the DBU to reach equilibrium and favoring protonation. It is worth noting that at this concentration in DMF at 40 °C, **1**, was not entirely dissolved before DBU was added and was more of an opaque white slurry. With each drop of DBU, the slurry became more yellow, more transparent, and less viscous. Upon addition of *ca.* 63% of the total DBU volume, the system became transparent yellow at 40 °C. Therefore, three DBU addition rates were screened while holding all other variables constant.

While screening for water and urea content as previously discussed, the lowest DBU addition rates (1.8 to 2.8 μL/min) were employed. In these experiments, the DBU addition rate

was controlled by manually timing each drop from a 250-µL microsyringe and increasing the drop rate to increase the overall addition rate going from polymer **7** (2.8 µL/min) to **8** (5.6 µL/min), as shown in Table 2-2. For the synthesis of polymer **9**, DBU was added rapidly over the course of 5 to 10 s. We hypothesized that this condition would be likeliest to induce Δ-adduct formation (*vide supra*).

First, the SEC M_n values in Table 2-2 give very little information other than the apparent trend of increasing hydrodynamic volume with increasing DBU addition rate. Additionally, there appears to be some scatter with the M_n values between polymers **9a** and **9b**. We attributed the scatter seen between the duplicate polymerizations of system **9** to the inhomogeneities inherent in the rapid addition of DBU, which might make consistency challenging. Thus, further evaluation was needed by ATR-FTIR and MALDI-TOF MS.

ATR-FTIR spectroscopy was used to determine the uretdione or Δ-adduct content as a function of DBU addition rate (Figure 2-14). A pronounced peak at 1651 cm^{-1} in the polymer **9b** spectrum indicates Δ-adduct formation when DBU is added rapidly, consistent with the hypothesis. This peak matches well with the 1645-cm^{-1} peak observed for **5** (see Figure A-27 in Appendix A), as well as the 1654-cm^{-1} peak of the previously reported Δ-adduct structure using benzyl isocyanate by Cramail, Landais, and coworkers.[11]

The structure of the Δ-adduct–containing species, shown in Figure 2-15, was determined by the MALDI-TOF spectra of polymers **7a** and **9b**, as shown in Figure 2-16. These spectra showed two entirely different compositions. The Δ-adduct population, denoted $C\Delta^{A}_{n}$, was very pronounced in the **9b** spectrum, while the corresponding peaks were barely detectable in polymer **7a**, consistent with the IR spectroscopy results. While the Δ-adduct population is clearly present, it is not the most intense population in the spectrum and only corresponds to one Δ-adduct per

polymer chain. Given the relative intensity of $C\Delta^{A}_{n}$ to the A_n (corresponding to the pure urethane species) and X_n (corresponding to the linear G species and the C population consisting of two urea linkages) populations in the MALDI-TOF MS spectra, this result is also consistent with the relatively low intensity of the Δ-adduct peak relative to the urethane peak observed by ATR-FTIR in Figure 2-14. The other contrasting feature is the increased intensities of the uretdione peaks UB and UC in **9b** relative to the X population. Concomitant with the intensity increase of these peaks in Figure 2-16a, the D population (corresponding to three urea linkages) intensity was significantly suppressed relative to the X population. In theory, it would follow that an increase in uretdione and Δ-adduct formation would result in fewer free isocyanate groups available for urea formation given the same amount of isocyanate (or blocked isocyanate) available. These results strongly support our hypothesis that more free DBU and isocyanate groups, created by rapid DBU addition, significantly increases the formation of both Δ-adducts and uretdione side-products.

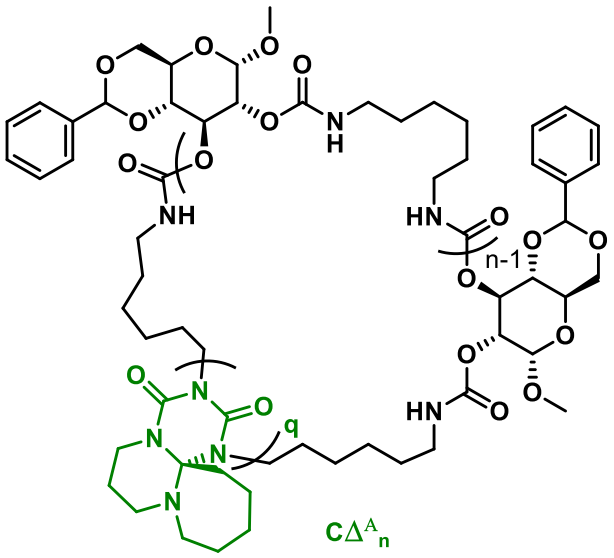

Figure 2-15. The structure of $C\Delta^{A}_{n}$ is a macrocycle containing a single Δ-adduct and no urea or uretdione units.

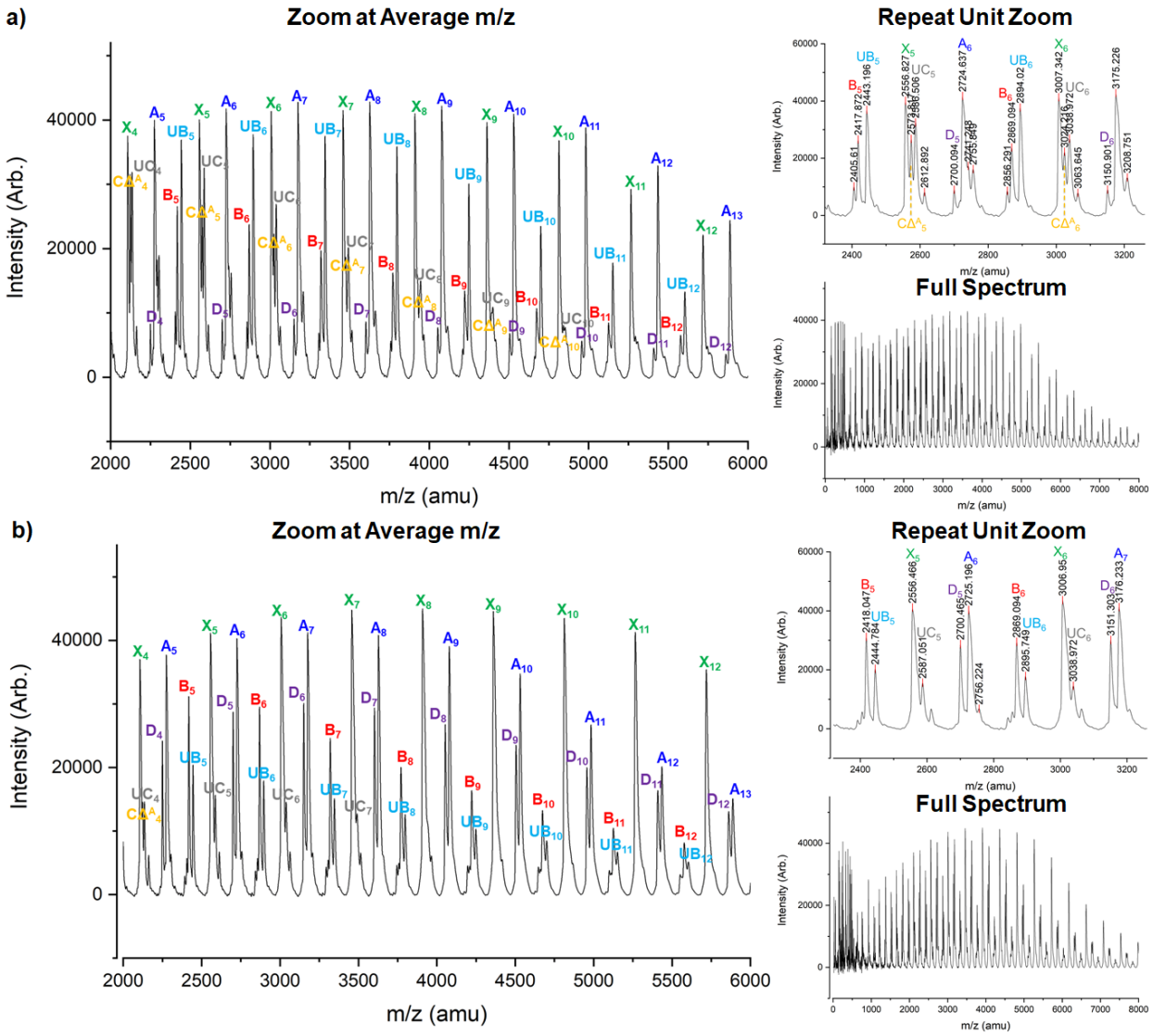

Figure 2-16. MALDI-TOF clearly shows that the increase in DBU addition rate causes more Δ-adduct and uretdione formation as seen in a) polymer **9b** with a rapid DBU addition over the course of 5 to 10 s and b) polymer **7a** with a DBU addition rate of 2.8 μL/min.

Interestingly, the molar mass distributions of the A population (corresponding to the macrocycle species with no urea linkages) in Figure 2-16a appear to have shifted to slightly higher m/z relative to polymer **7a** in Figure 2-16b. The A peak for **9b** in Figure 2-16a is also more intense than the X population, whereas the opposite is seen in Figure 2-16b for polymer **7a**.

Subpopulations aside, the overall molar mass distributions, determined by MALDI-TOF MS, appear roughly the same for both polymer systems, and it is unlikely that a one repeat unit shift to higher m/z by the A population is the cause of the significant increase in hydrodynamic volume observed by SEC in Table 2-2 for **9b**. Rather, we attribute the higher observed hydrodynamic volume to the presence of the Δ-adducts and uretdione linkages along the backbone. Also, different interactions with the stationary phases of the SEC for the different functional groups between the two systems cannot be ruled out.

Also of note is the presence of broad, low-intensity singlets (Δ) that correlate with Δ-adduct formation in PU **9b** in Figure 2-13d (see Figure A-81 in Appendix A). These same peaks are also present in Figure 2-13c for PU **8a**, but they are difficult to resolve from the baseline, showing that it contains more than **7a** but less than **9b** as expected for the intermediate addition rate. These results correlate with what we observed by both ATR-FTIR and MADLI-TOF MS.

Concluding that by-product formation is tunable based on DBU addition rate, it is important to point out the significance of the tunability of uretdione or Δ-adduct formation. While for these purposes these by-products were seen as problematic for this chemistry, there are numerous potential applications for incorporating either by-product into a polymer backbone. Polenz and coworkers reported that a polymer made from DBU and **3** can thermally deblock at 130 °C, potentially allowing for orthogonal deblocking of systems such as **9b**.[13] The onset of degradation temperature (T_d) for **5** is 169 °C (see Figure A-25 in Appendix A), while the onset of T_d for **9b** with more Δ-adduct is 289 °C, with an anomalous onset of mass loss at 191 °C (see Table A-13 and Figure A-90 in Appendix A). On the other hand, the uretdione linkage is a strained four-membered ring that is chemically labile. A uretdione of HDMI is reported to thermally decompose at 200 °C (without catalyst) and can react with primary amines at room

temperature to form "biuret" branches.[14,85] Alcohols have been reported to react with uretdiones of TDI at 90 °C to give diurethanes.[14] Thus, the ability to tune the uretdione content allows for the potential of postpolymerization modification such as grafting via orthogonal polymerization methods, attachment of bioactive or spectroscopically active small molecules, or the formation of dendrimers or other branching architectures.

2.4. Comparison to Conventional Polymerization Methods

We then compared the polymerization method presented here to a conventional PU synthetic method using the same diol (**2**) with **3** and a catalyst system consisting of DABCO and $Mn(acac)_2$. Okamoto and coworkers demonstrated that a DABCO-$Mn(acac)_2$ system approaches the activity of DBTDL while being less toxic.[109] It is also worth noting that the $Mn(acac)_2$ catalyst has been reported to have higher selectivity for urethane vs. urea than DBTDL.[119] Given that 40 °C was the optimal temperature for the carbamate-derived PU, we performed this reaction at the same temperature. An aliquot was taken at 1 h of reaction time.

Table 2-2 shows the observed M_n by SEC and the urethane:urea ratio for the conventionally synthesized PU at 1 h (**10-1**) and 8 h (**10-8**). SEC alone indicated that this conventional system (**10-8**) is nearly double the size of **7**. Figure 2-17 shows the MALDI-TOF mass spectra of PU **10a** after polymerization for 1 and 8 h. Surprisingly, the **10-8a** system in Figure 2-17b does not show an increase in the M_p or an increase in the m/z of the molar mass distribution in general. In fact, the M_p and all populations appear to be centered at a lower m/z than all of the dicarbamate-based PUs previously discussed. However, PU **10-8a** does show a complete absence of uretdione and Δ-adduct by-products. In addition, the MALDI-TOF MS reflectron spectra in Figures C-1 and C-2 in Appendix C indicate that there is also no linear G_n population in **10-8a** or **10-8b**. This absence of G_n in **10-8a** is further supported by the absence of

corresponding peaks (4.68 and 5.54 ppm) in Figure 2-13e. Therefore, it is possible that the unusually large hydrodynamic volume indicated by SEC was a result of the absence of low-molar-mass by-product populations, as seen in the spectra for the dicarbamate-derived systems.

A likelier cause of the unusually high molar mass of **10-8** compared to other systems is aggregation. We were able to determine the occurrence of a high degree of aggregation and noncovalent interactions with the species in **10-8** that is not present in the other systems, either because of the presence of the Lewis acidic $Mn(acac)_2$ species and its two coordination sites or because fewer by-products allow for a higher probability of dimer formation at high conversion (see Appendix C). This effect would explain why the molar mass of **10-8**, shown by SEC, appears much larger than all other systems. Furthermore, the polymer failing to ionize can be ruled out based on the study conducted in Appendix F.

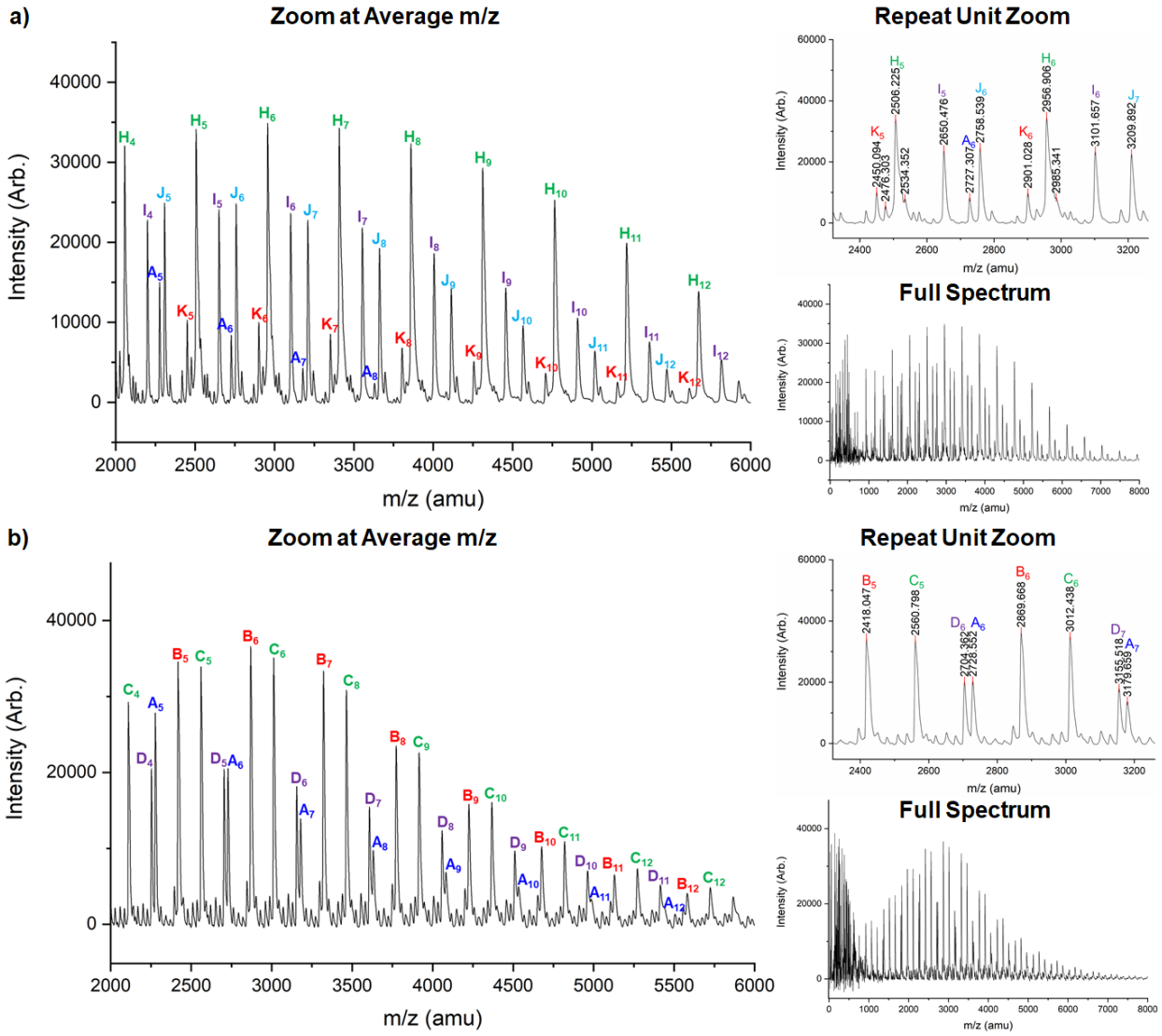

Figure 2-17. The MALDI-TOF spectra of PU **10a** synthesized using conventional methods: a) 1-h reaction time shows mostly linear species; b) 8-h reaction time shows mostly cyclic species.

Of particular note in Figure 2-17a is that the **10-1a** system consists mostly of new linear species, as described in Table 2-4. Table A-15 in Appendix A also shows that the **10-1** systems have a T_g *ca.* 20 °C lower than almost all of the other PUs presented, further corroborating a different morphology. These new linear species indicate an incomplete polymerization at 1 h and conform to normal kinetic behavior expected from polycondensation reactions because

cyclization occurs near complete conversion.[152] This result also confirms that if there were linear species present in our dicarbamate systems, the quenching time with methanol is sufficient to endcap most isocyanate end groups. Additionally, no PU in Figure 2-13 shows a methoxy end group such as that present in **10-1a** (see Figure A-93 in Appendix A). Although difficult to resolve, this resonance was identified with ^{13}C and two-dimensional (2D) NMR techniques in Figures A-82 to A-85 in Appendix A. Thus, this system allows for the direct comparison of cyclic verses linear species of the same molar mass simply by altering the reaction time.

2.5. Broader Impacts

Although not fully optimized, this system exhibits advantages over conventional PU synthetic methods, as well as many diisocyanate alternatives, investigated previously. This system can produce a polymer of a higher molar mass, shown by MALDI-TOF MS, than some conventional methods without the use of a metal-containing catalyst and without a diisocyanate starting material. While the system is not diisocyanate-free *per se*, the costs and hazards associated with the storage and transport of diisocyanates can be avoided. One of the key criticisms of this chemistry relative to conventional methods is the lack of atom economy associated with the loss of the DBU-H *p*-nitrophenoxide salt (**4**) by-product. However, a method has been patented to synthesize di(*p*-nitrophenyl) carbonate from *p*-nitrophenol, dimethyl carbonate, and a combination of catalysts.[156] This method could allow for the *p*-nitrophenoxide by-product to be recycled, mitigating the loss of atom economy, incorporating CO_2 remediation into the overall process, and bypassing the use of phosgene as a precursor to diisocyanates altogether.

This polymerization method also allows for tuning of the urea content for different applications analogous to industrial processes where urea formation is induced by simply adding

varying amounts of water.[1] Additionally, the PUs produced using this method are soluble in common, nonpolar organic solvents (*e.g.*, DCM and chloroform), while PHUs made from dicyclic carbonates are typically only soluble in highly polar organic solvents such as DMF, which would make niche applications such as spraycoating difficult.[74]

Several similar one-pot deblocking methods for PU synthesis have been investigated and show their own advantages. Recently, Emrick and coworkers used catalytic amounts of fluoride to deblock various TDI-derived dicarbamates to synthesize PUs *in vacuo* for 6 h at 50 °C.[92] While fundamentally interesting, the hydrofluoric acid intermediate is corrosive and requires a vacuum. Sablong and coworkers used *t*-butyl alcohol-protected IPDI with catalytic potassium *t*-butoxide to produce PUs at 130 °C for 12 h *in vacuo*.[157] In comparison, the dicarbamate system discussed herein requires no vacuum and could potentially be optimized at room temperature. Cramail, Landais, and coworkers, as well as Patton and coworkers, recently reported fascinating deblocking methodologies that take place at room temperature, but these methods have yet to be applied to produce PUs.[83,144] Nevertheless, further optimization with respect to concentration, base type, and base equivalents could improve the efficiency of this chemistry relative to conventional methods, and screening of other diols and diamines could demonstrate the broader applicability needed to realistically replace conventional methods.

2.6. Conclusion

This work has demonstrated that a one-pot reaction using HMDNC with a biosourced secondary diol and DBU produces PU at 40 °C without a vacuum and without a metal catalyst. This work presents a one-pot PU synthesis that can achieve appreciable molar masses at ambient pressure without using diisocyanates as a starting material. Moreover, the work has demonstrated that this synthetic methodology allows for tuning of side-products such as urea,

uretdione, and an isocyanate cyclodimer with DBU in the final material analogous to conventional PU synthetic methods. Future investigation includes screening polymerization conditions for reaction time, different bases, fewer equivalents of base, concentration, and screening the reactivity on other diols. Although an extra synthetic step may increase costs, require additional reagents, and use non–environmentally benign solvents, this chemistry mitigates hazards and costs of transporting and storing diisocyanate starting materials. The volatility and reactivity of **1** are certainly less than that of **3**, indicating that it is less likely to react as an alkylating agent or induce sensitization by skin contact or inhalation. Therefore, this work is anticipated to be of significant interest to the PU community and the larger polymer community as well.

3. THE QUALIFICATION AND QUANTIFICATION OF POLYURETHANE MACROCYCLE FORMATION BY RAMAN SPECTROSCOPY AND MOLECULAR MODELING

3.1. Introduction

The formation of cyclized polymers larger than *ca.* 20 atoms in the ring were once considered highly improbable, if not impossible, by the original derivations of Carothers and Flory for "ordinary bifunctional condensations."[151,152] However, numerous examples of macrocyclic polymers have since been reported, including work by our group,[153,158] leading Hans Kricheldorf and coworkers to develop a new mathematical treatment demonstrating that polymer cyclization is not only possible but indeed likely at high conversion for both thermodynamically and kinetically controlled polycondensation reactions.[151,152] It is this historical perspective that makes the macrocyclization of the polymer systems in Chapter 2 significant in and of itself.

Cyclized polymers tend to exhibit lower melt viscosities, higher T_g, higher thermal stabilities, and even reduced cell toxicities compared to their linear counterparts, but their conclusive identification requires specialized analytical techniques.[146,151] The rapidly expanding use of MALDI-TOF MS for polymer characterization over the past two decades has allowed for the definitive verification of cyclic or linear species in various polymer systems.[151,152] Macrocyclic polymers also typically exhibit lower hydrodynamic volumes by SEC, but the use of SEC alone is inconclusive as to whether or not the species is cyclized.[145,151,159] In 2016, Kertesz, Casado, and coworkers published an interesting work where they elucidated a discreet "ring-breathing-type" motion at low wavenumbers for cyclic *p*-phenylenes that was absent in the analogous linear *p*-phenylenes with the same number of repeat units for a range of ring sizes.[160] Thus, we

hypothesized that an analogous ring-breathing-type band might be observable using Raman spectroscopy for the PGU synthesized in Chapter 2 using the conventional polymerization method. In this chapter, the properties of both linear and cyclic PUs made from HMDI and **2** using a conventional catalyst are explored using Raman spectroscopy and molecular modeling in addition to the other forms of characterization, such as MALDI-TOF MS, done in Chapter 2.

3.2. Experimental Details

3.2.1. Materials

All materials were purchased from ChemImpex, Sigma-Aldrich, or VWR. Unless noted, reagents were used as received. NMR solvents were purchased from Cambridge Isotope Laboratories. DMF was purified and dried by a solvent purification system (J.C. Meyer Solvent System). DBU was distilled over CaH_2 and stored under dry nitrogen over activated 3-Å molecular sieves. Methyl 4,6-*O*-benzylidene-α-(D)-glucopyranoside was dried under a vacuum in an oven at *ca.* 108 °C for 12 min before quickly weighing out and adding to the reaction flask and returning the reaction flask to the vacuum oven at *ca.* 108 °C for another 20 min before use. Reaction flasks were kept in a 110-°C drying oven when not in use.

3.2.2. Molecular Modeling

Molecular modeling calculations were performed using the Gaussian16 software package.[161] Calculations were performed using the Vici high-performance computing in the Laboratory for Molecular Simulation (LMS) at Texas A&M University. For semiempirical calculations, the Austin Model 1 (AM1) or Parametric Models 6 and 7 (PM6 and PM7) levels of theory were used.[162] For the DFT calculations, BP86, B3LYP, and cam-B3LYP levels of theory were used. For the *ab initio* calculations, the HF level of theory was used. Basis sets of 6-311++G(d,p), 6-31+G(d), and 3-21+G(d) were used. Calculations were performed mostly in the

gas phase and were frequency checked with Raman frequency calculations performed for all levels of theory. Andreas Ehnbom assisted by performing conformational annealing using Materials Studio to acquire global minimum conformations from 4,000 possible conformations for the head-to-tail structure and 400 possible conformations of the head-to-head structure. Of these, 150 structures were retained and the three structures, lowest in energy, were further optimized by DFT or HF.

Molecular mechanics simulations using MMFF94 were done using the ChemDraw and ChemDraw 3D software packages on a standard personal computer. Typically, the structure was optimized after being drawn and then conformationally sampled for 100 conformations using the default parameters.

3.2.3. Characterization

3.2.3.1. Nuclear Magnetic Resonance Spectroscopy

Recorded on a Varian Inova500 spectrometer were ^{1}H, ^{13}C, HMBC, HMQC, and gCOSY spectra (500 MHz for ^{1}H and 125 MHz for ^{13}C). Where noted, a Varian NMRS500 was used to acquire spectra (500 MHz for ^{1}H and 125 MHz for ^{13}C). Chemical shifts were referenced to signals from residual protons of the deuterated solvents.

3.2.3.2. Raman Spectroscopy

A BWTek iRaman spectrometer coupled with a BAC151A microscope camera was used to take spectra at a preset incident wavelength of 785 nm. The solid samples were placed on an aluminum foil sample substrate. The scans were conducted with a laser intensity of 50%, the integration time set for 30 s, the multiplier set to 10, and the time averaging set to a value of 4. A reference scan was taken of the bare aluminum foil substrate using the same parameters. The data were subsequently worked up in Origin, where the reference scan was subtracted from the

raw data, and the resulting spectra were smoothed and baseline-subtracted. For directly comparing multiple spectra, normalization of the two spectra was also conducted in Origin.

3.2.4. Synthesis of Poly(Glucose Urethane)s (10)

PUs **10b** discussed in this section are the same materials discussed in Chapter 2. See Chapter 2.2.4.5 for the synthesis of these systems.

3.2.5 Time-Dependent Study on Poly(Glucose Urethane)s (11)

To an oven-dried, 5-mL, round-bottomed flask, methyl 4,6-*O*-benzylidene-α-(D)-glucopyranoside (0.1265 g, 0.4481 mmol) was combined with hexamethylene-1,6-di(*p*-nitrophenyl carbamate) (0.2010 g, 0.4503 mmol) and the system was purged two times with $N_{2(g)}$. The flask was immersed in a 40-°C oil bath, and dry DMF (0.28 mL) was added. DBU (0.135 mL, 0.9027 mmol) was added all at once over a few seconds from a 250-µL microsyringe. Aliquots of 0.20 mL were taken at reaction times of 2 min (**11-2**), 10 min (**11-10**), and 30 min (**11-30**) and were immediately quenched into MeOH (2 mL). A final aliquot was taken by quenching the whole reaction mixture at 1 h (**11-60**) with MeOH (2 mL). The MeOH was removed *in vacuo* at 60 °C within a window of 45 min to 1 h and 15 min after quenching. All aliquots were dissolved with DCM (*ca.* 4.5 mL) and extracted with 0.1-M NaCl solution (13 mL), followed by 0.05-M NaCl solution (13 mL), and lastly with distilled water (13 mL) before condensing the organic phase *in vacuo*. The solid samples were put under vacuum overnight at 45 °C to dry. MALDI-TOF MS was the only characterization done on these samples. Only MALDI-TOF MS was performed on these samples.

3.3. Results and Discussion

In line with the work done in Chapter 2, a time-dependent study was carried out where a polymerization at 40 °C was monitored by taking aliquots at 2 min (**11-2**), 10 min (**11-10**), 30

min (**11-30**), and 1 h (**11-60**) and immediately quenching them in methanol. The samples were worked up in the same manner as before but scaled per the quantity of material. MALDI-TOF MS was again run on each aliquot using the same technique as in Chapter 2. Some of the same linear species were observed as in Chapter 2, but there was an additional species identified as H'_n, as shown in Figure 3-1. This species has an unreacted isocyanate group at one terminus, whereas the regular H_n species has both termini reacted with methanol. Otherwise, the other species observed in this study were the same as in Chapter 2.

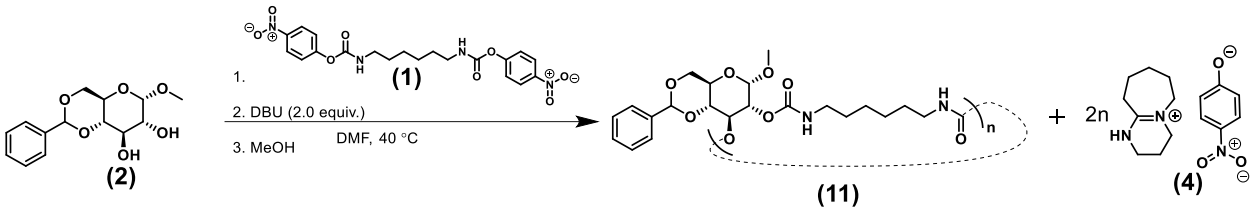

Figure 3-1. The synthesis of PGU (**11**) at 2 min, 10 min, 30 min, and 1 h.

The resulting MALDI-TOF spectra in Figure 3-2 appear to show a gradual increase in the average molar mass in going from **11-2** aliquot to the **11-60** aliquot. Additionally, it is notable that all of the lower-molar-mass species below 2,500 amu appear suppressed, and the distribution becomes more Gaussian at 1 h of polymerization. However, this is not the most exciting aspect of these spectra.

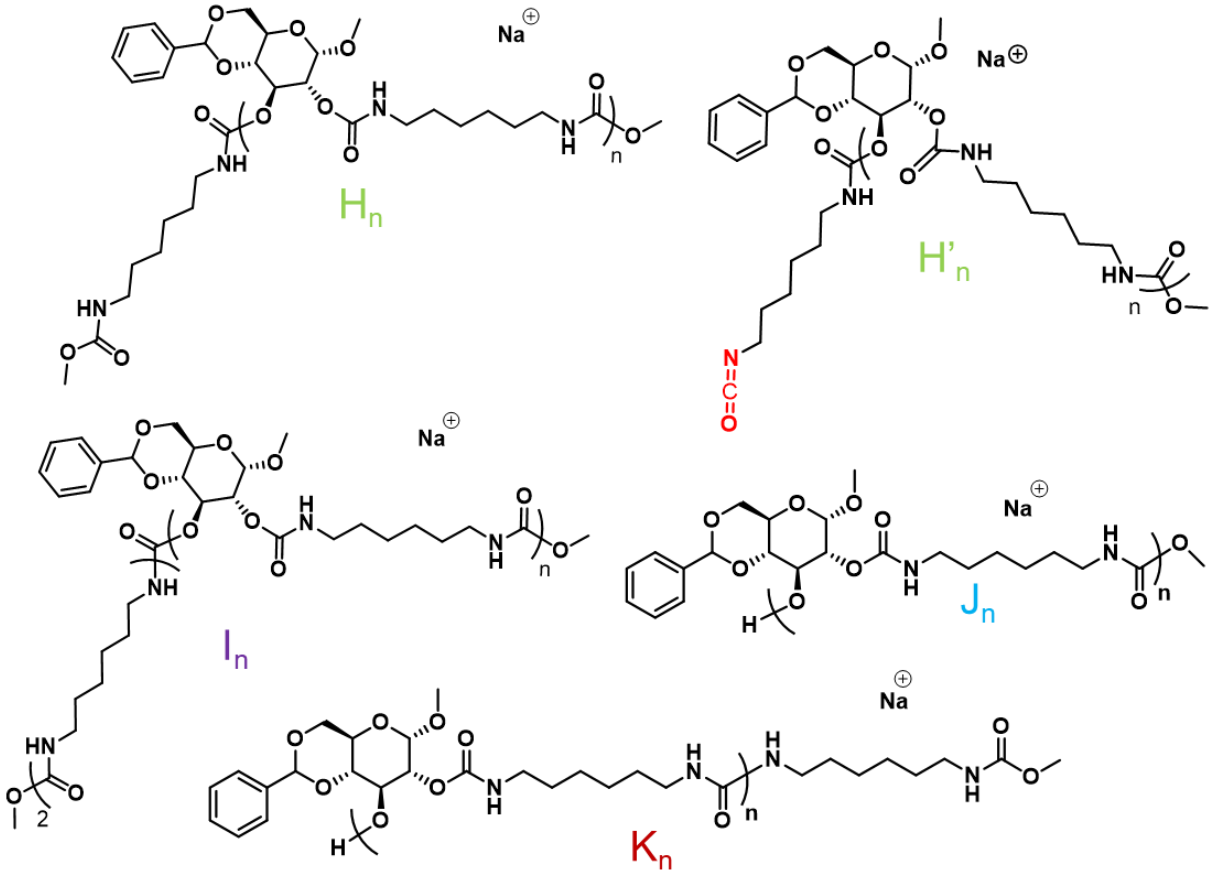

Figure 3-2. Some of the linear species from Chapter 2 but with the addition of the H' species. These species were observed by MALDI-TOF MS in a time-dependent study done up to 1 h for the dicarbamate-derived system.

Upon examining the zoomed-in MALDI-TOF MS spectra in Figure 3-3, it can be clearly seen that the linear species (J_n, H_n, and H'_n) gradually decrease in intensity as reaction time proceeds to 1 h. In fact, these peaks corresponding to linear species appear entirely suppressed at 1 h, indicating that cyclization is complete. Kricheldorf and coworkers[151,152] showed that cyclization is favored at high conversion for step-growth polymerizations as a result of self-dilution. So it would follow that complete cyclization at 1 h is indicative that conversion is also approaching completion. This should be contrasted to the model system in Chapter 2, where the

polymer still comprised mostly linear chains at 1 h of polymerization at the same temperature. Thus, the kinetics of the system in Chapter 2 are indicated to be remarkably fast compared with conventional methods of polymerization.

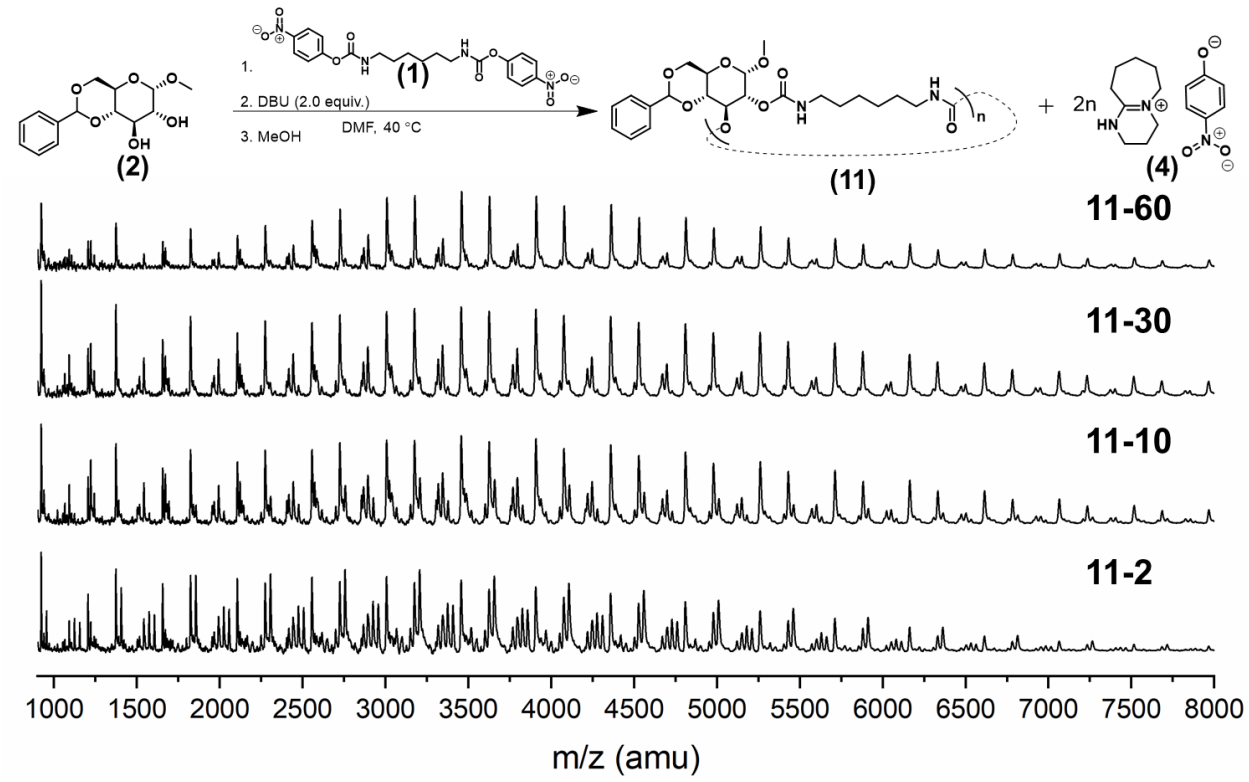

Figure 3-3. MALDI-TOF MS shows what appears to be a slight increase in the average molar mass of the macrocyclic PUs with times 2 min (**11-2**), 10 min (**11-10**), 30 min (**11-30**), and 1 h (**11-60**).

However, this begs the question as to whether macrocyclization can be quantified in these systems. MALDI-TOF MS is certainly diagnostic of macrocyclization, as has been shown. However, as also stated, MALDI-TOF MS can only be used quantitatively in the manner performed by comparing the relative intensities of peaks to one another to determine composition

from sample to sample.[155] To get absolute quantities, an internal standard must be used to create a calibration curve to compensate for differences in ionization efficiency of different species, which can be quite tedious when high throughput is necessary.[155] ^{1}H-NMR spectroscopy could be used to quantify macrocyclization, but as shown in Figure A-82 (see Appendix A), peak overlap can complicate quantification or impede it entirely. Kricheldorf also reported that macrocyclic systems exhibit markedly different material and thermal properties than their linear counterparts, notably that cyclic systems have smaller hydrodynamic volumes, lower melt viscosities, and higher thermostabilities.[151] But indirect techniques like viscosity measurements or dynamic mechanical analysis would neither be quantitative or diagnostic unless there was some known reference material that was entirely linear or cyclic with which to calibrate to. This requirement again would complicate high-throughput characterization. The question then turned to whether some other form of spectroscopy could be used to both diagnose and quantify macrocyclization.

By MALDI-TOF MS, the model polymers (**10**) from Chapter 2 at 1 h and 8 h of reaction time have distributions centered at roughly the same average molar mass. However, the system at 1 h is nearly entirely composed of linear species, while the 8-h system is composed entirely of macrocyclic species. These two systems would theoretically provide suitable reference materials by which to explore a different technique to quantify cyclization. Given the difference in the thermal properties between the 1-h and 8-h systems, we intended to explore the material properties by dynamic mechanical analysis and hypothesized that the degree of cyclization could be quantified by Raman spectroscopy coupled with molecular modeling of linear and cyclic species to identify the Raman bands.

It is well known that Raman spectroscopy is significantly more quantitative than FTIR, partly because of fewer overtone and combination vibrations, and we hypothesized that there was

likely some sort of symmetric ring vibration band that would be Raman-active.[163] The work by Kertesz, Casado, and coworkers[160,164] is very instructive on how Raman could potentially be used on cyclic systems. In this work, the authors synthesized and modeled linear and cyclic *p*-phenylene systems from 4 to 20 repeat units.[160] Their results using both the B3LYP level of theory and observed Raman measurements of their systems indicated that for all cycle sizes, there was a band at around 500 cm^{-1} corresponding to a symmetric, ring-breathing-type motion.[160] Both experimentally and computationally, their results showed that this band's Raman shift not only was not altered to any significant extent in the range of 5 to 12 repeat units, but that its intensity was only significantly suppressed when going above 14 repeat units or so.[160] Additionally, the authors performed a molecular modeling study on how distortions or bending of the rings would disrupt the Raman bands' intensity and Raman shift values and found that the twisted geometries had no significant effect on the low-wavenumber ring-breathing bands other than a slight increase in intensity.[160] Another interesting work was conducted by Tykwinski and coworkers[165] where a similar computational and Raman study was done on linear and cyclic polyynes to determine how the distortion of their linearity affected their Raman spectra. This work focused only on bands above 2000 cm^{-1}, which correlate more to individual bonds rather than structural vibrations at lower wavenumbers.[165,166] However, this work showed that distorting the linearity of the polyyne systems caused some Raman modes to be active in the IR and *vice versa* while only changing their Raman shift values to a small degree.[165] Thus, it was deemed feasible that a symmetric ring vibration could be observed in the Raman spectra of the **10-1** and **10-8** materials from Chapter 2.

As shown in Figure 3-5, both the **10-1b** and **10-8b** systems have a carbonyl stretch centered around 1710 cm^{-1} by FTIR. This is important to note because upon examining the predicted Raman spectra by computational methods, the spectra have correction factors applied to them

using mostly this peak as a reference in order to compensate for the harmonic oscillators used by DFT and semiempirical methods as applied to the anharmonic oscillators of most compounds.[167] While this peak was the main point of reference, a "best-fit" approach was applied to the whole FTIR spectrum when deciding upon scaling factors listed with each spectrum.

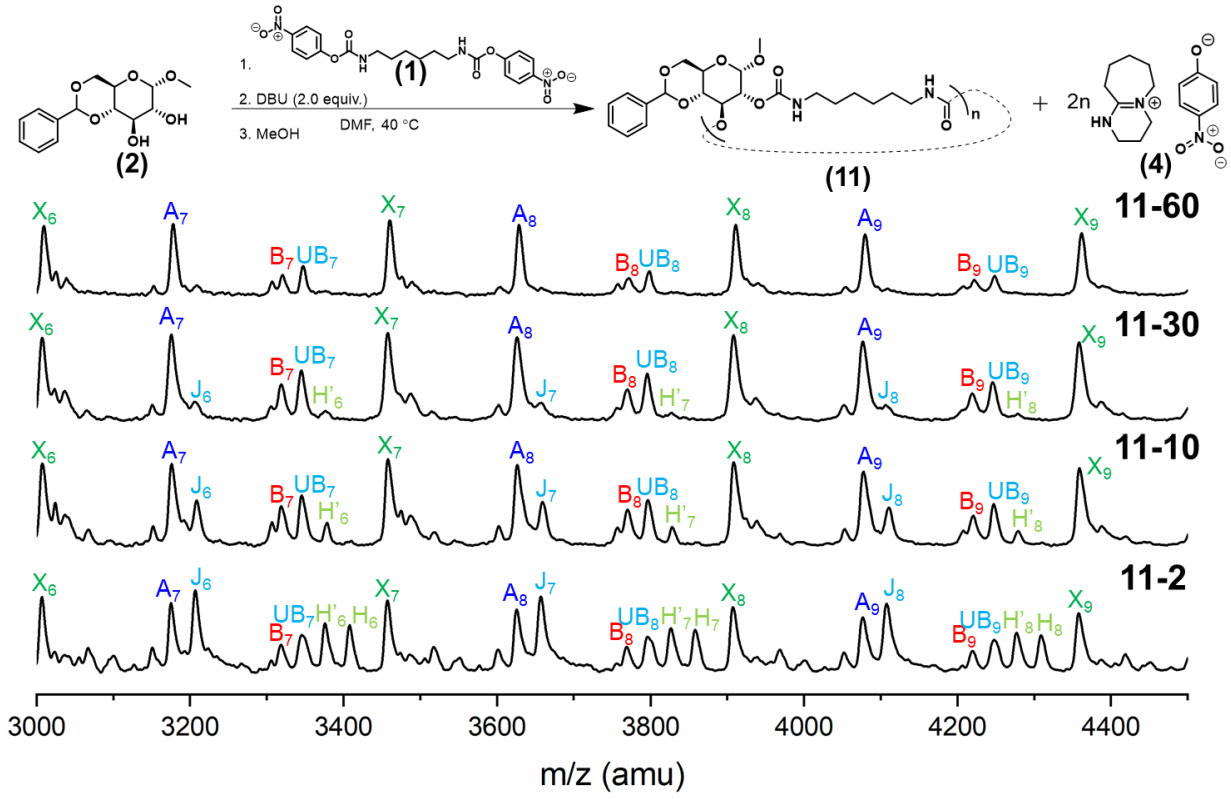

Figure 3-4. MALDI-TOF MS shows the disappearance of the linear species H_n, H'_n, and J_n as reaction time approaches 1 h in PUs **11-2** (2 min), **11-10** (10 min), **11-30** (30 min), and **11-60** (1 h).

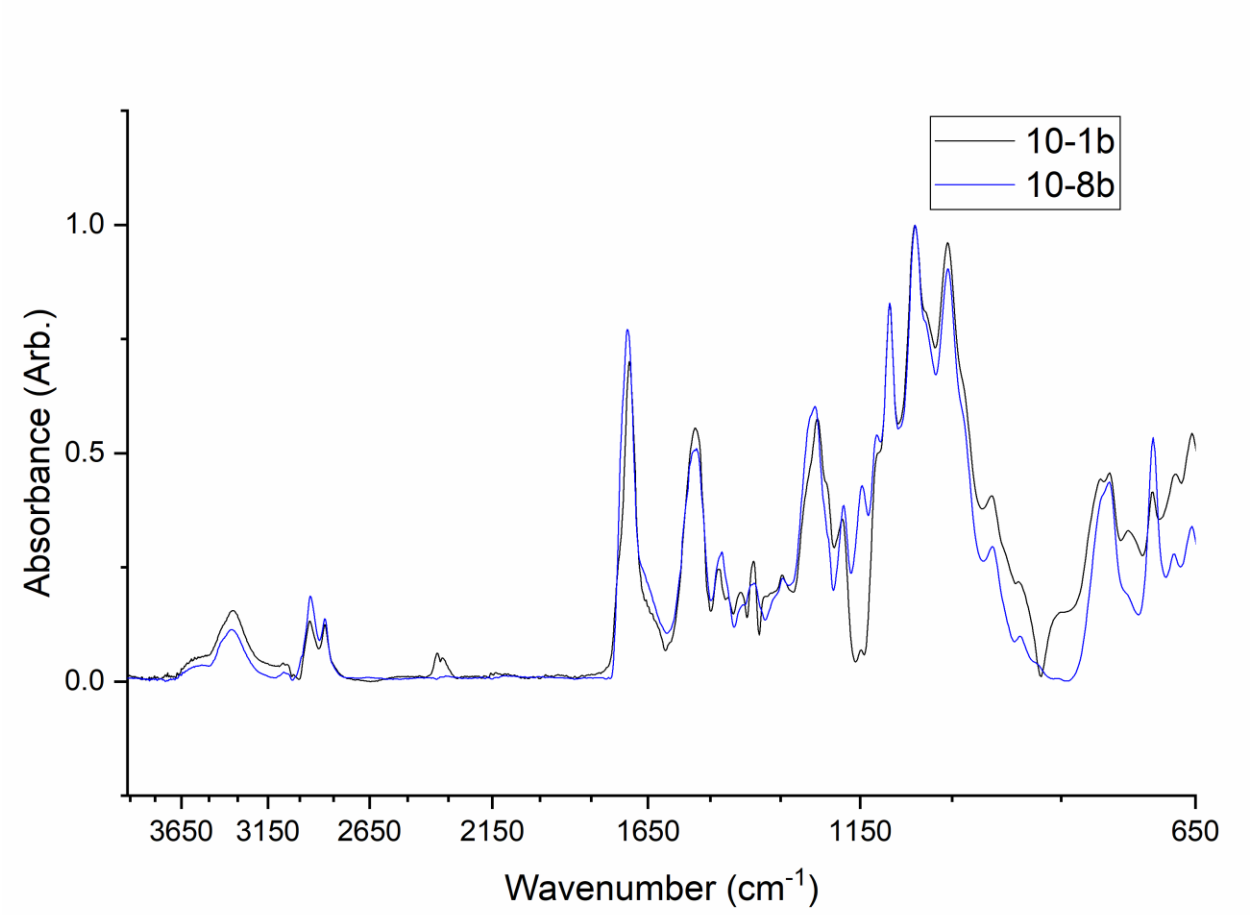

Figure 3-5. The ATR-FTIR absorbance spectra of both **10-1b** and **10-8b** corresponding to the 1-h and 8-h polymerization times, respectively.

On the other hand, Raman spectroscopy conducted on solid samples of **10-1b** and **10-8b** shows almost identical spectra except for one region. In the 100- to 500-cm^{-1} range, there appears to be a marked contrast for two distinct peaks in the Raman spectra. Typically, bands arising at low wavenumbers such as these are indicative of structural vibrations rather than the motions of individual bonds.[166] Sometimes, these bands are referred to as "acoustic vibrations" and extend into the range of Brillouin scattering versus normal Raman phenomena.[166] Therefore, it is entirely possible that one or both of these bands could correspond to cycle vibrations versus linear ones.

In an attempt to determine what type of mode these bands could correlate to, several dozen structures were optimized and had subsequent frequency analysis using semiempirical, DFT, and HF methods in the gas phase. First, it was necessary to conduct an analysis of the two predominant linear species that were identified by MALDI-TOF MS to get a point of reference. The H_1 linear species was optimized and subsequently had a frequency analysis conducted using the HF/6-311++G(d,p) level of theory, as shown in Figure 3-6, as the H_n species predominate in the **10-1** systems. As shown by the predicted Raman spectrum in Figure 3-7, there is no observable vibrational modes below 500 cm^{-1} for this structure, as expected.

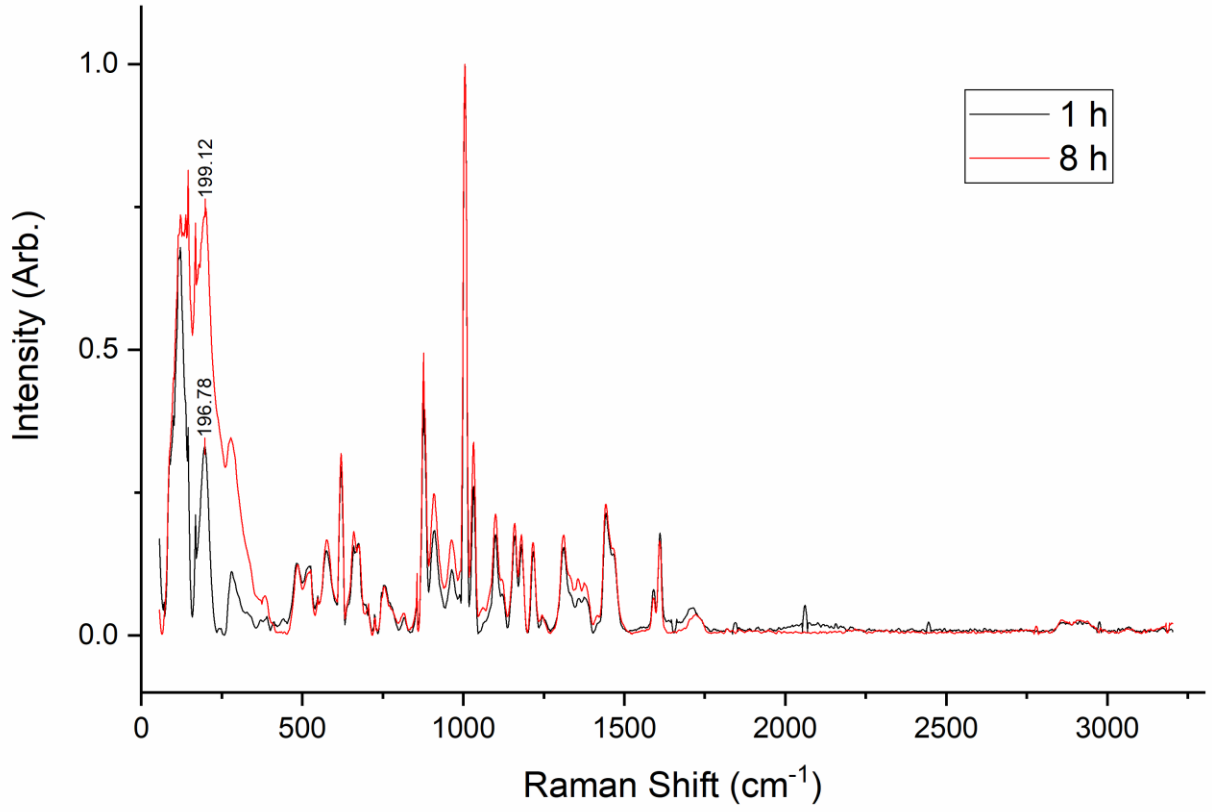

Figure 3-6. The Raman spectra of **10-1b** (1-h polymerization time) and **10-8b** (8-h polymerization time) appear almost identical except for the region around 200 cm^{-1}.

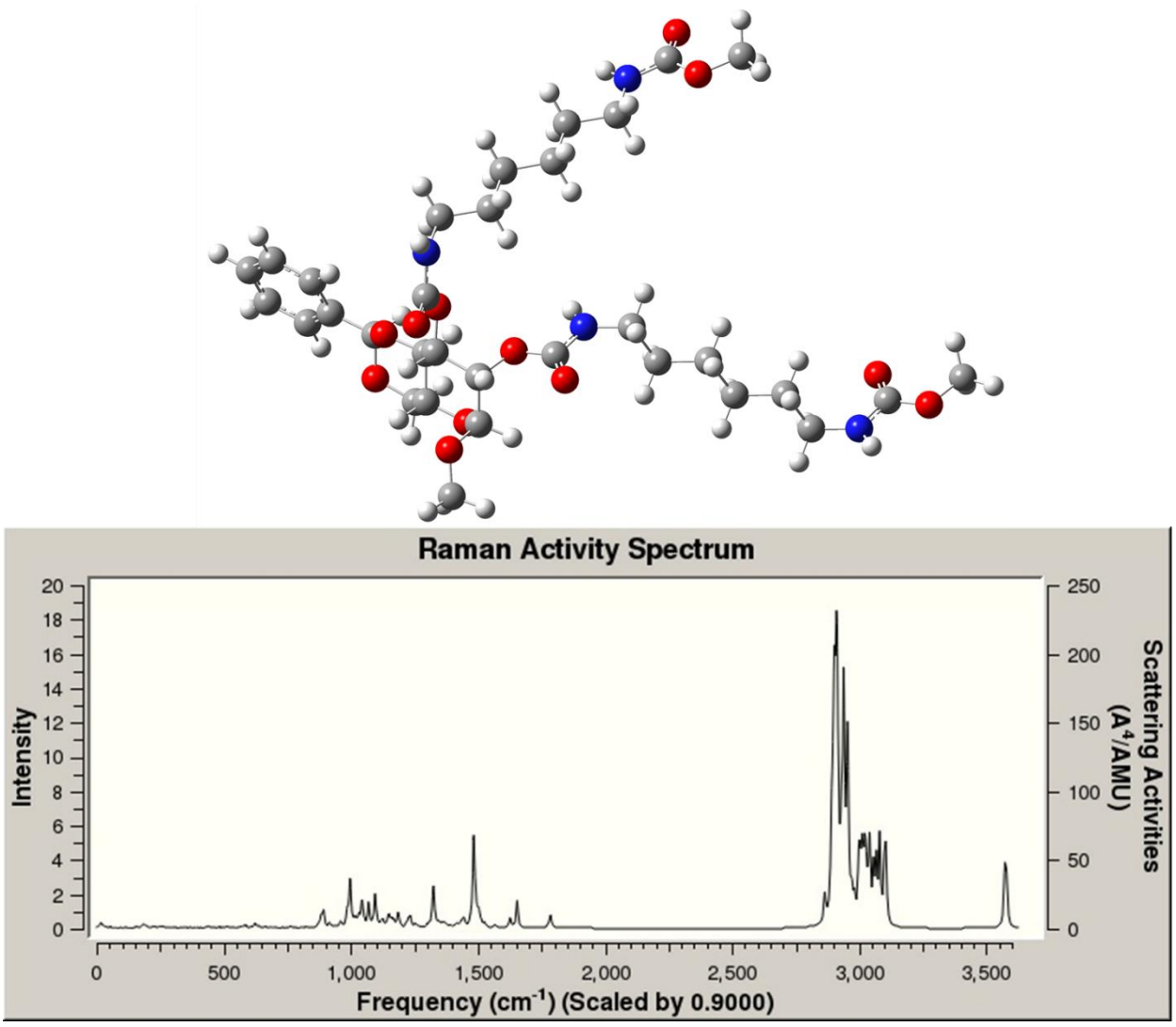

Figure 3-7. The predicted Raman spectra for the H_1 linear species as optimized and calculated using HF with the 6-311++G(d,p) basis set. The frequency correction factor was set for 0.90.

Next, we modeled the diol-terminated G_2 linear structure that was present in the dicarbamate-derived systems from Chapter 2 but was not found in the conventionally derived systems. As shown in Figure 3-8, there are no noticeable Raman bands below 500 cm^{-1}, as expected. This would be important to determine if Raman were to be used to monitor cyclization

in situ with the dicarbamate-derived PUs in the future. At least from the preliminary results from both of these linear structures, such an *in situ* method might still be possible.

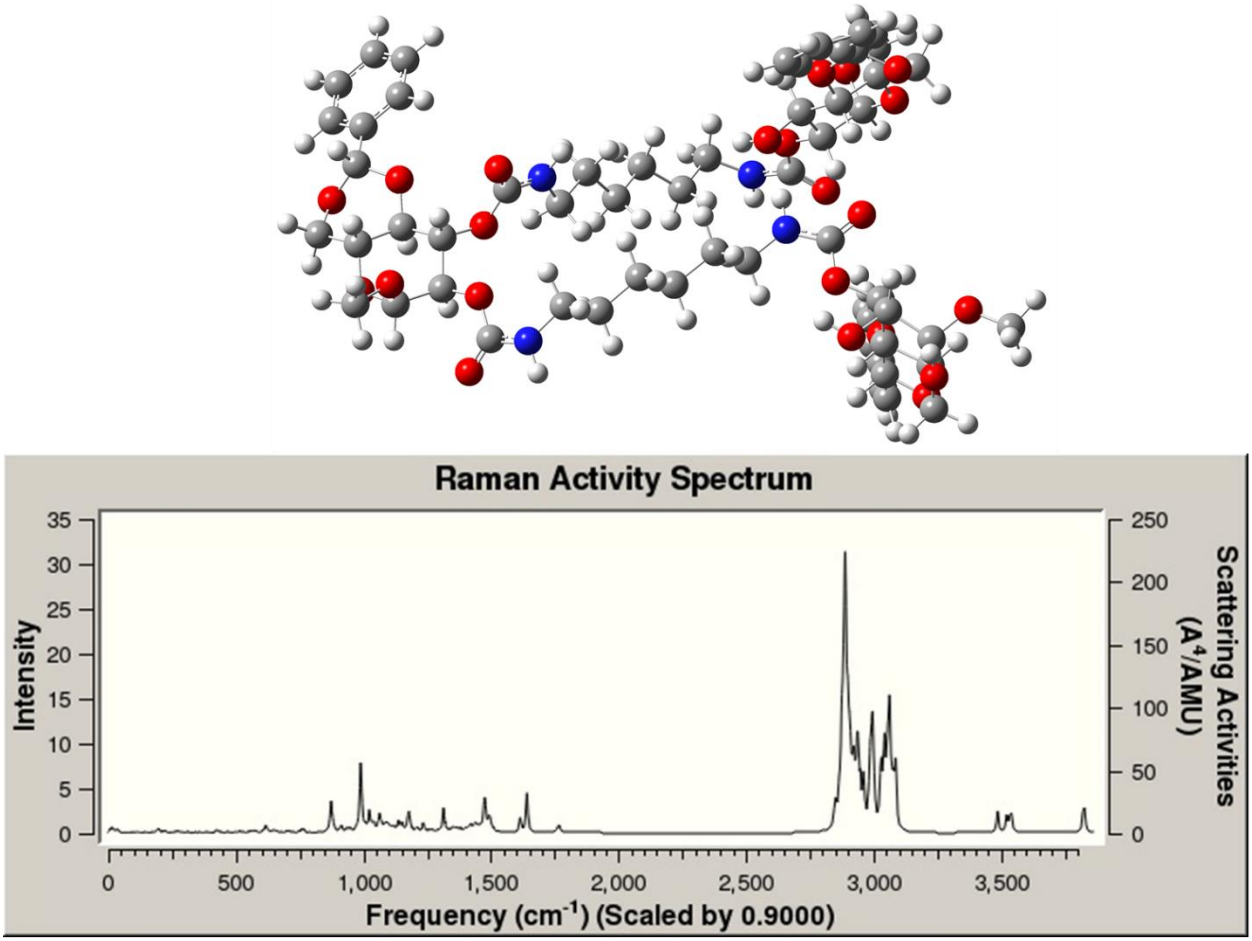

Figure 3-8. An HF-optimized G_2 linear structure using the 6-311++G(d,p) basis set. The frequency correction factor was 0.90.

For the first cyclic structure that was optimized, we modeled the A_2 cyclic species by HF in Figure 3-9. While the vibrational analysis indicated that there was a ring-breathing vibration at *ca.* 200 cm^{-1}, the intensity of that mode on the scale of the overall spectrum was virtually nonexistent. It was hypothesized that the "hoop" geometry displayed a degree of symmetry that would allow for highly symmetric ring-breathing vibrations, but this result indicated otherwise.

This may be a result of the limitations of the basic HF level of theory, so we explored alternative computational methods.

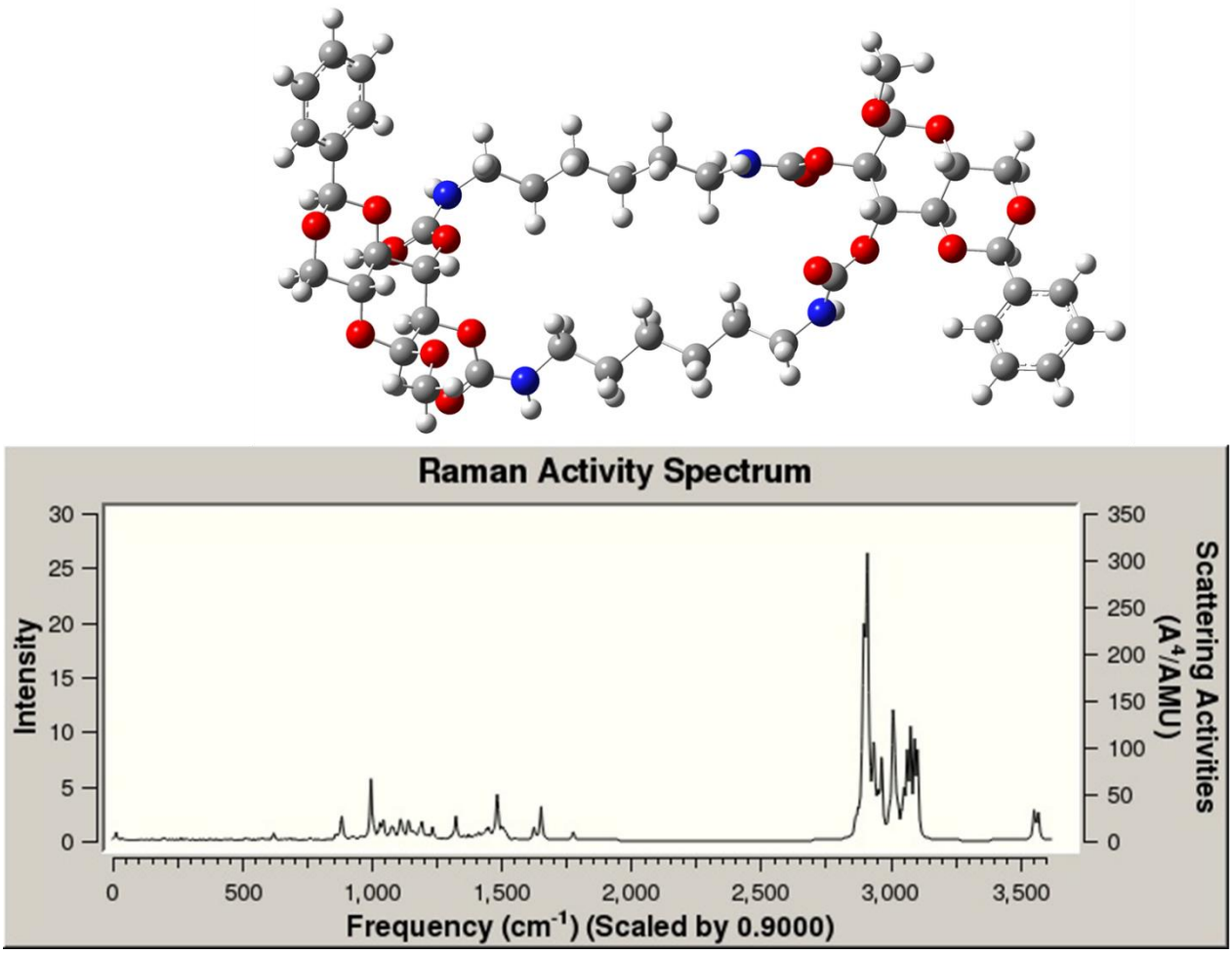

Figure 3-9. An HF-optimized A_2 cyclic structure and the predicted Raman spectrum with a 0.90 correction factor. The basis set used was 6-311++G(d,p).

As shown in Figure 3-10, the same A_2 hoop structure modeled previously by HF was optimized using the cam-B3LYP level of theory and the 6-311++G(d,p) basis set. Unfortunately, the predicted Raman spectrum was very similar to the HF-derived one from Figure 3-9. It became

clear that some sort of high-throughput conformational sampling approach was needed to cover all possible conformations that these macrocyclic structures could acquire in the solid state. Neither Gaussian09 nor Gaussian16 has this capability. Additionally, we thought it necessary to explore alternative regioisomers such as "head-to-head" macrocycles.

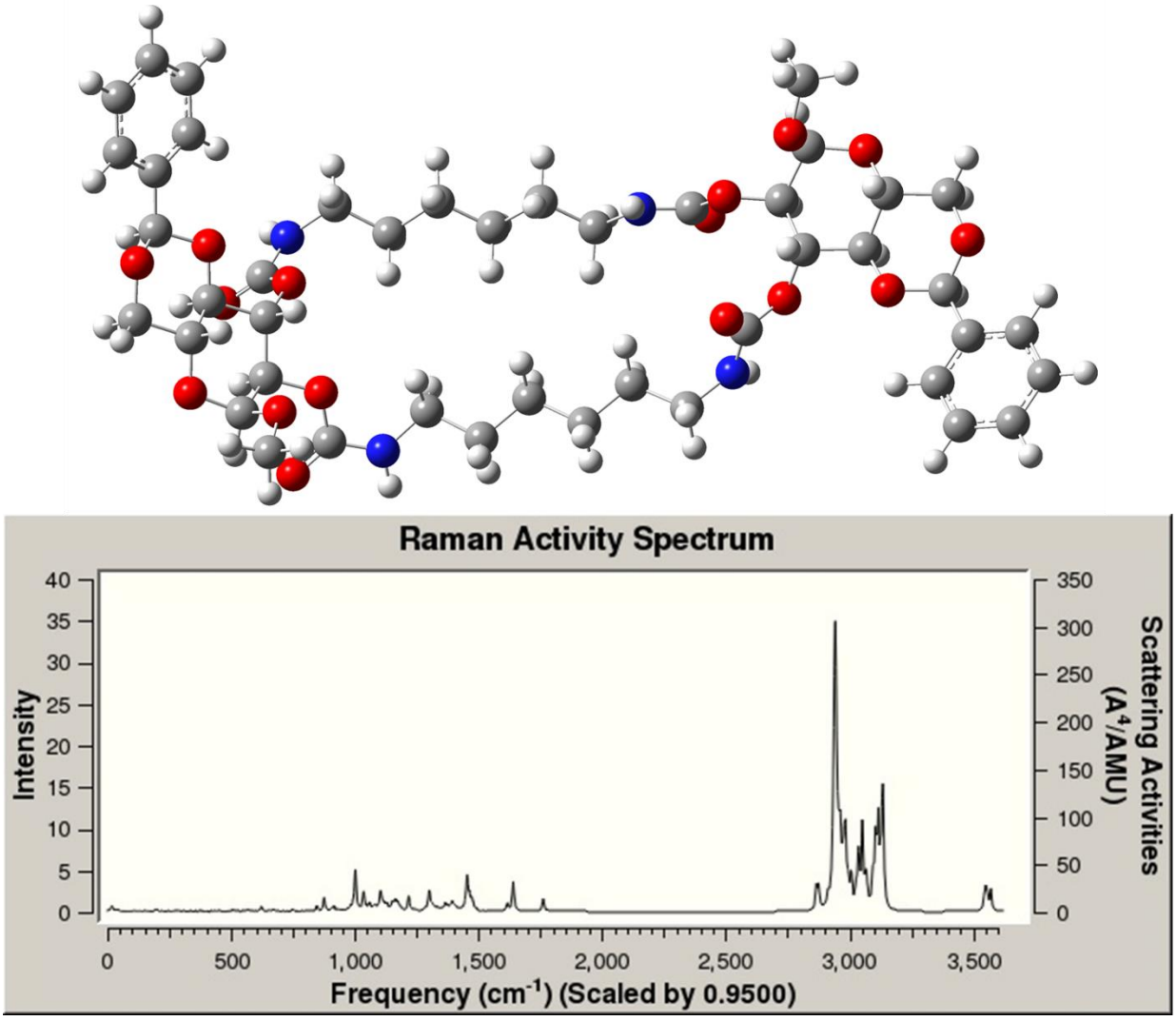

Figure 3-10. A cam-B3LYP optimized structure of the head-to-tail A_2 cyclic system and the predicted Raman spectrum. The 6-311++G(d,p) basis set was used.

Andreas Ehnbom in the LMS was able to assist in using Materials Studio to conformationally anneal more than 4,000 possible conformations for the head-to-tail and 400 conformations for the head-to-head regioisomers as shown in Figure 3-11. Three of the lowest-energy conformers were modeled for the head-to-tail regiochemistry, while two of the lowest-energy conformers were further analyzed for that which was head-to-head.

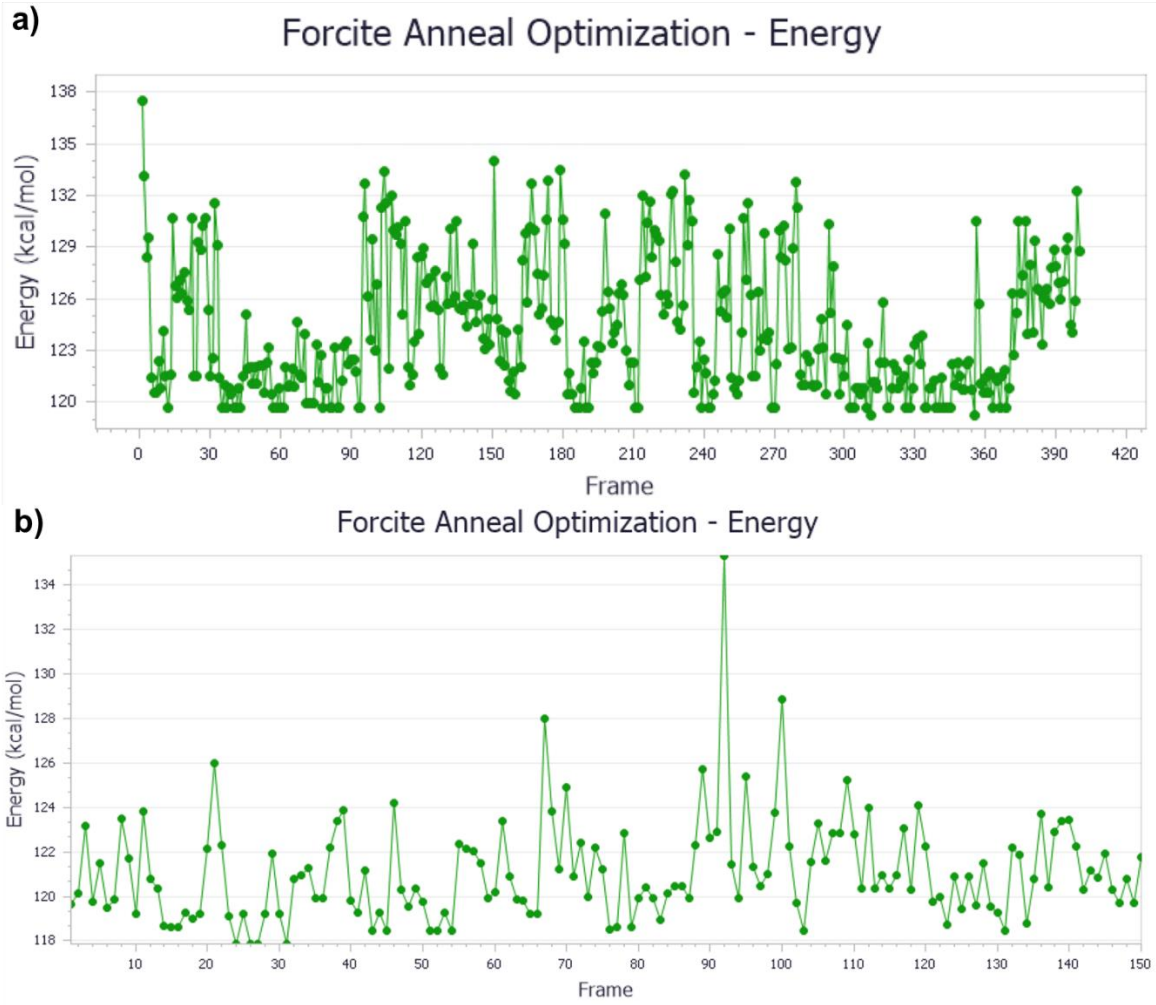

Figure 3-11. Conformational "annealing" as performed by Andreas Ehnbom using Materials Studio for: a) 4,000 conformations for the head-to-tail structure and; b) 400 conformations for the head-to-head regioisomer of the A_2 species.

One of the head-to-tail regioisomers was modeled using the BP86 level of theory and the 6-31+G(d) basis set, along with the d3bj empirical dispersion correction applied, and is shown in Figure 3-12. This new level of theory was done to try and reduce the enormous computational cost and computing times that the HF and cam-B3LYP required with the higher basis sets. While BP86 gave results very similar to those of cam-B3LYP and HF, there were still no noticeable Raman peaks below 500 cm^{-1} for any of these optimized structures. However, it is notable that the structure derived from conformational annealing takes on a "knotted ball" conformation rather than a hoop as shown previously.

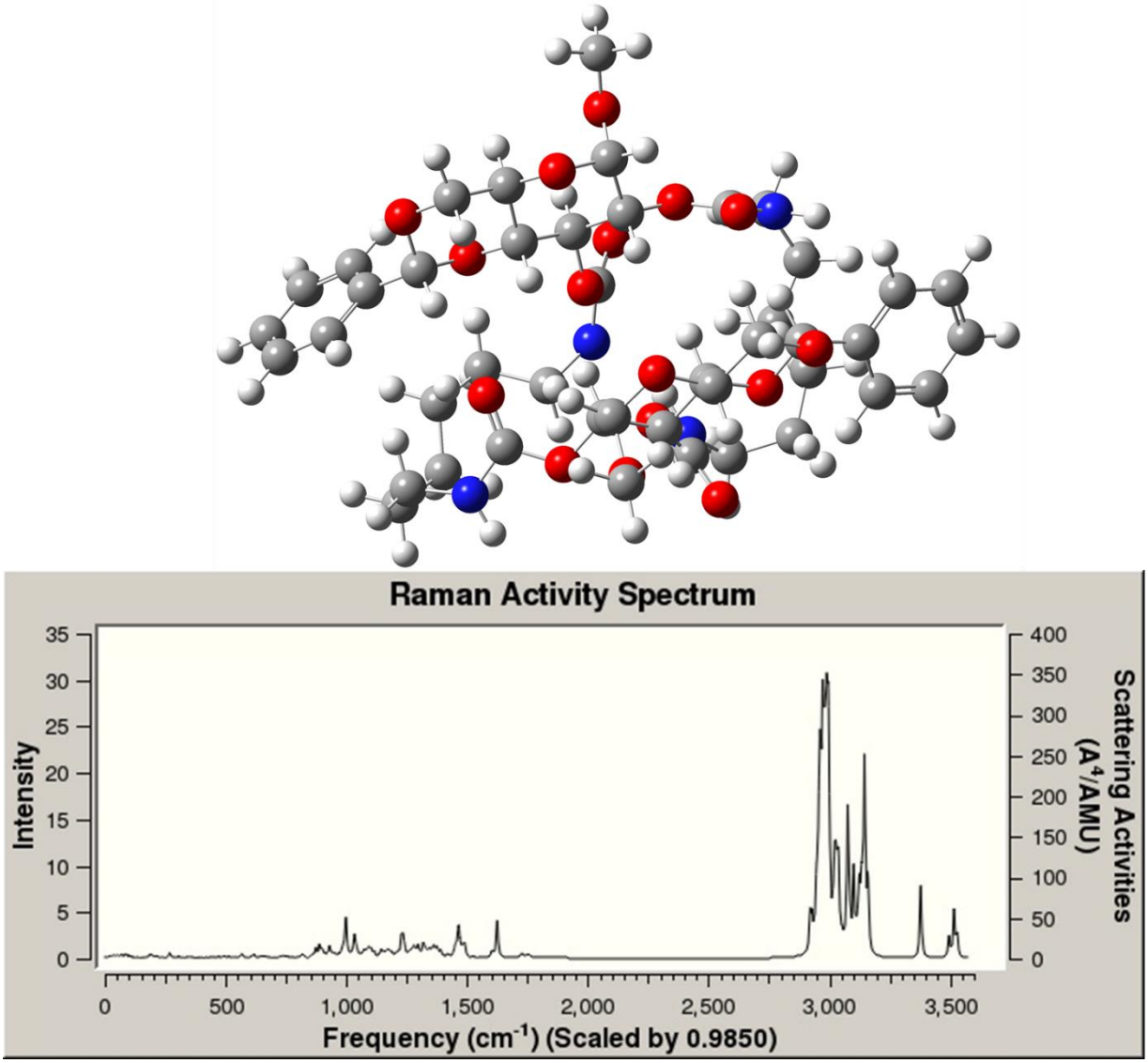

Figure 3-12. An optimized structure using BP86 with the 6-31+G(d) basis set using structure 102 from the head-to-tail conformational sampling results. The d3bj empirical dispersion correction was applied.

Many more structures were optimized and had frequency calculations performed to obtain predicted Raman spectra on them, including stacked dimers of the A_2 species, as well as interlocked catenane forms of two A_2 rings. Many of these many atom calculations were done using the semiempirical method, PM7, which gave surprisingly similar geometries to both the DFT

and HF methods mentioned previously. It became somewhat apparent that whatever structural feature was giving rise to the observed Raman bands around 200 cm^{-1} must be something entirely different than the simple hoop or even the knotted ball geometry of the conformationally annealed systems. Thus, in a last effort to try and find some kind of positive result, it was hypothesized that the acac ligands on the manganese(II) Lewis acid catalyst for these conventionally derived systems might be coming off at long reaction times, which might allow the carbonyl groups on these macrocycles to complex to the manganese(II) center. A surprisingly symmetric geometry resulted, as shown in Figure 3-13, for the A_2-Mn(II) complex. Additionally, there seemed to be some Raman activity in the low-band region of the predicted Raman spectrum. Thus, it was hypothesized that perhaps another carbonyl group from a separate macrocyclic system could complex to the exposed coordination site on this new A_2-Mn structure.

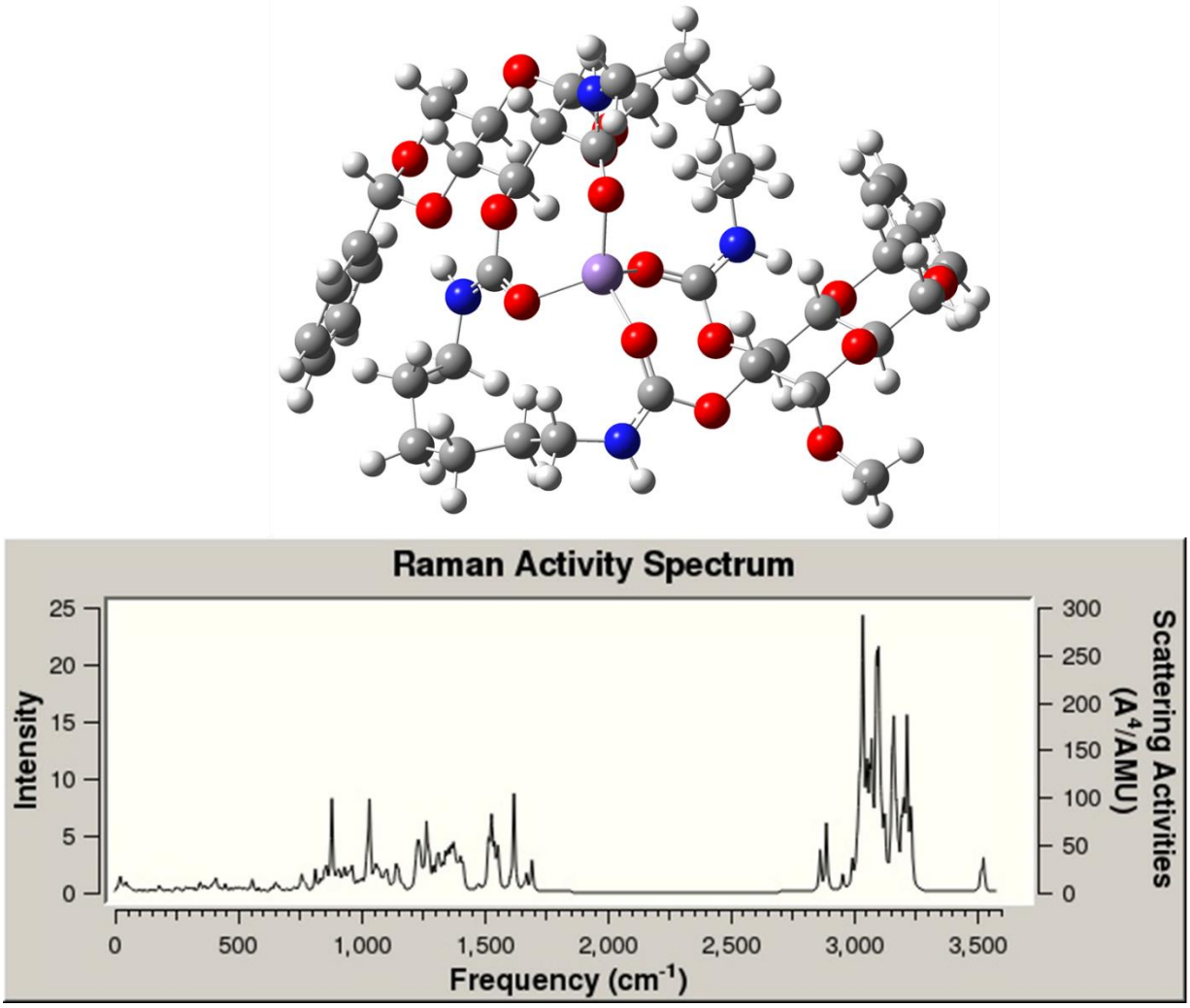

Figure 3-13. An optimized A_2 cyclic structure complexed to Mn(II) in the center with a 2+ overall charge using BP86 with the 3-21G* basis set. The predicted Raman spectrum has no correction factor.

As shown in Figure 3-14, a DMF molecule was used as a model ligand in this case, was optimized as coordinated to the Mn(II) center of the previous structure, and was optimized using BP86 with the d3bj empirical dispersion parameter. The DMF molecule, in this case, serves to reduce the computational cost of placing another macrocycle just to incorporate the carbonyl group

as a ligand, but it is entirely possible that the DMF solvent from the reaction could form such a complex that would not dissociate with vacuum during workup. However, it is worth noting that the Raman activity in the low-wavenumber region of the predicted Raman spectrum has increased in intensity ever so slightly, indicating that this could be a potential lead as to the actual structural phenomenon giving rise to the observed Raman spectrum experimentally.

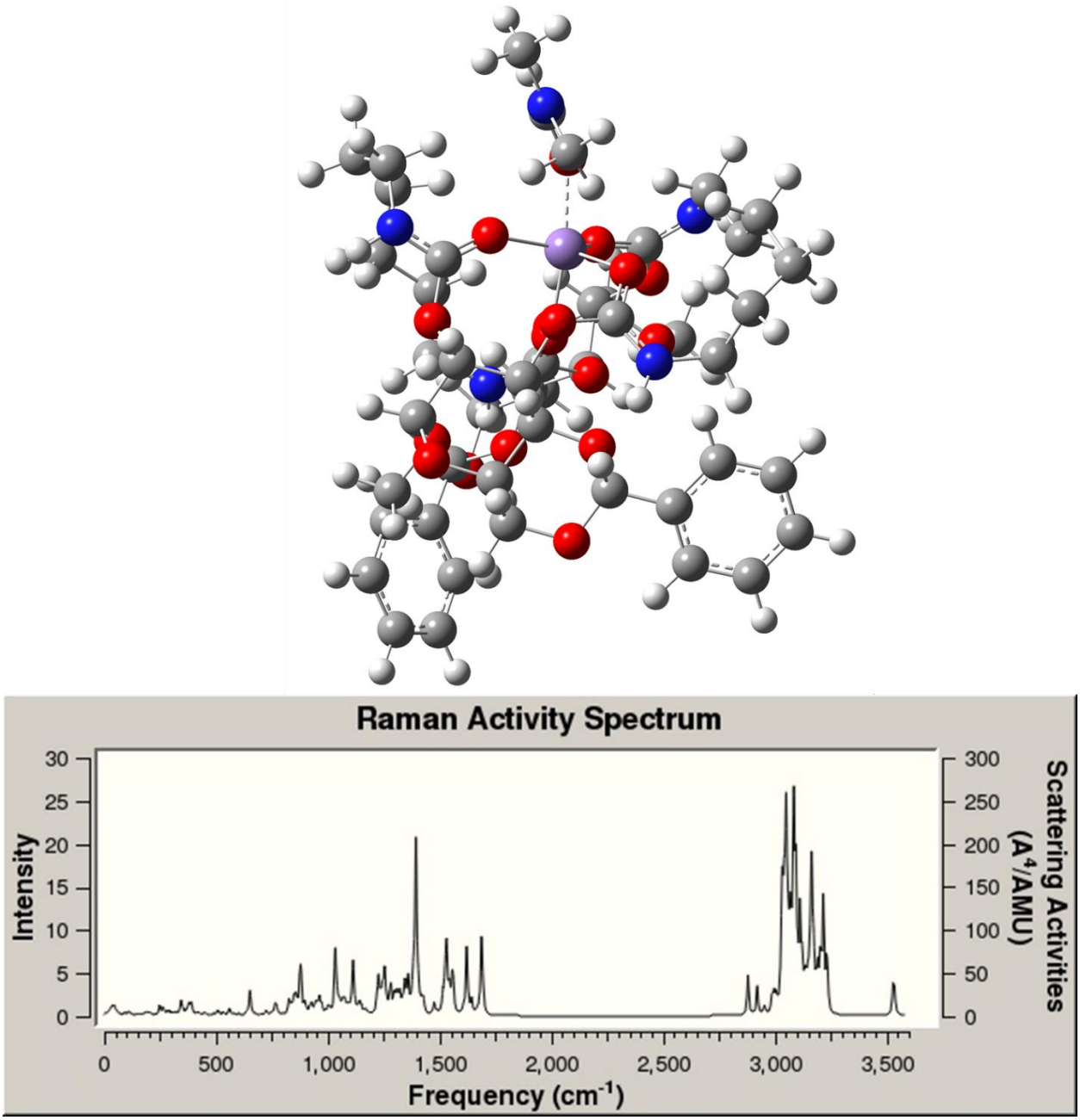

Figure 3-14. An optimized A_2 cyclic structure complexed to Mn(II) in the center with 2+ overall charge and an additional DMF molecule complexed to the exposed coordination site using BP86 with the 3-21G* basis set. The predicted Raman spectrum has no correction factor.

While the structure shown in Figure 3-14 may be a potential lead as to what might be inducing the spectral bands at *ca.* 200 cm^{-1} in the experimental Raman spectrum, it is far from

certain. While it is entirely plausible that a single macrocycle could entropically displace two weak acac ligands during the course of the polymerization, it is rather curious why the NMR spectra in Figures A-82 to A-86 (see Appendix A) are not more severely distorted by the presence of such a paramagnetic compound. It is possible that the concentration, in this case, is simply too low for any significant distortion to take place, but this would require more experimentation to confirm. It is also possible that Mn(II) may not be the metal cation that these macrocycles are coordinating to, as such complexes are not observed in any of the MALDI-TOF MS spectra. However, what is observed in the MALDI-TOF MS spectra in Figure G-8 (see Appendix G) for PU **10-8b** are peaks corresponding to complexes with potassium when no potassium salts were used to dope the MALDI-TOF MS samples. Only NaTFA was used to dope these MALDI-TOF samples. So it is conceivable that these macrocycles are complexing to potassium ions. Ultimately, more structures need to be optimized and analyzed, and more experimentation needs to be done. At the present time, current calculations are underway for A_2 macrocycles complexed to K^+ and Na^+ species.

3.4. Conclusion

It is clear from the experimental Raman spectra that there is some structural difference between the model PUs (**10b**) at 1 h versus those at 8 h. It cannot be concluded at this time what that structural difference is, but preliminary computational data suggest that it arises from some sort of complexation to a metal cation by a symmetric macrocycle like the A_n populations. More experimentation and molecular modeling is required to elucidate what this structural difference is.

4. ANTIBIOFOULING POLYURETHANES USING BIOSOURCED POLYHYDROXYLS CONJUGATED TO CAPSAICINOID SENSORY DETERRENTS

4.1. Introduction

In the maritime shipping industry, the hydrodynamic drag created on equipment reduces efficiency and significantly increases operating costs because of increased fuel consumption and the ultimate removal of organisms from surfaces.[110] Current antibiofouling methodologies have advantages and disadvantages that this work attempted to address. Antibiofouling agents such as tributyltin and the currently used Sea-Nine™ 211 pose significant nonselective toxicity to marine life.[168] In response, a large amount of research has been conducted into cationic, zwitterionic, and amphiphilic polymers as active and passive deterrents to both marine biofouling and also for use in biomedical devices.[169-171] Some cationic and zwitterionic systems suffer from being very hydrophilic and will dissolve or delaminate in aqueous environments unless they are bonded to the substrate in question or are spray-coated on top of an "undercoat" polymer substrate.[169,170,172] The amphiphilic fluoropolymers studied extensively in the Wooley group were shown to be 60% less susceptible to bovine serum albumin (BSA) attachment and up to an *ca*. 80% lower Ulva zoospore settlement.[173,174] However, these systems are drawn mostly from petrochemical feedstocks and suffer detrimental morphology changes over time that negate their amphiphilic morphology.[173,175] The Wooley group has also explored a coating that makes use of an active, sensory deterrent called noradrenaline, which is also a natural product.[171] While the system has displayed enhanced inhibition of attachment *via* oyster hemocyte and barnacle cyprid assays, only 39% of the available chain-end functionalities on the surface have reacted with noradrenaline.[171] Greater inhibition of

fouling may be possible through the incorporation of higher percentages of covalently linked, active, deterrent moieties.

Capsaicin, the compound responsible for the burning sensation of chili peppers, exhibits anti-inflammatory, antibacterial, anticancer, antifungal, and antimarine biofouling properties.[111,176,177] It has been reported that some zwitterionic groups on polymers are not hydrophobic enough to penetrate the membranes of bacteria; the significant hydrophobicity of capsaicinoids should eliminate this problem.[170] Both capsaicin and its less-expensive analog, pseudocapsaicin, are relatively nontoxic and are both used as food additives, in addition to pain relief agents in the pharmaceutical industry.[178-180] Capsaicin, pseudocapsaicin, and a range of capsaicinoid-like molecules also show significant inhibition of zebra mussels attaching to submerged surfaces when in solution without any detectable lethality.[111] In fact, the capsaicinoids in question have showed antibiofouling activity at significantly lower concentrations than the LC_{50} for the non–target organism *Daphnia magna*.[111] As of this writing, there is little precedent for using capsaicinoids covalently bonded onto polymers for any purpose, and this approach could prove useful in antibiofouling and antimicrobial applications.

An attempted synthesis of a capsaicinoid conjugated PGU as an antibiofouling coating for marine or biomedical applications is discussed herein. Continuing the Wooley group's work synthesizing novel polycarbonates using functionalized glucose monomers as a biorenewable feedstock, this research sought to functionalize methyl α-(D)-glucopyranoside, or one of its derivatives, with a capsaicinoid functional group *via* ether, thioether, ester, or carbonate linkages and subsequently react the remaining diols with a diisocyanate to form a PU.[142,181,182] Specifically, this research attempted to avoid the postpolymerization functionalization issues that have hindered previous work using conjugated sensory deterrents and focused on prepolymerization

functionalization of monomers.[171] This research was intended to add to the literature on using glucose as a biorenewable monomer for PUs and explore the use of a capsaicinoid as a biorenewable, cost-efficient, nontoxic conjugate for polymers with a range of biomedical and industrial applications.[51,52]

4.2. Experimental Details

4.2.1. Reagents

All materials were purchased from ChemImpex, Sigma-Aldrich, or VWR. Unless noted, reagents were used as received. NMR solvents were purchased from Cambridge Isotope Laboratories. The DCM and DMF used as reaction solvents came from either a SPS (J.C. Meyer Solvent System) or were purchased as EMD Millipore DriSolv® bottles from VWR. The DMAc was obtained as an EMD Millipore DriSolv® bottle from VWR.

4.2.2. Instrumentation

4.2.2.1. Nuclear Magnetic Resonance Spectroscopy

^{1}H, ^{13}C, HMBC, HMQC, and gCOSY spectra were recorded on a Varian Inova500 spectrometer (500 MHz for ^{1}H and 125 MHz for ^{13}C), a Varian NMRS500 (500 MHz for ^{1}H and 125 MHz for ^{13}C), a Mercury Plus spectrometer (300 MHz for ^{1}H and 70 MHz for ^{13}C), or a Varian Inova300 (300 MHz for ^{1}H and 70 MHz for ^{13}C). Chemical shifts were referenced to signals from residual protons of the deuterated solvents.

4.2.2.2. Attenuated Total Reflectance – Fourier Transform Infrared Spectroscopy

A Shimadzu IR Prestige ATR-FTIR spectrophotometer was used to acquire FTIR spectra in conjunction with IR Solution v. 1.40 software. All spectra were further analyzed using Origin 2018 data analysis software.

4.2.2.3. Electrospray Ionization Mass Spectrometry and Matrix-Assisted Laser Desorption/Ionization – Time-of-Flight Mass Spectrometry

ESI samples were run with a Thermo Fisher Scientific Q Exactive Focus and MALDI-TOF MS samples were run by the Chemsitry Mass Spectrometry facility on a Bruker Microflex™ LRF mass spectrometer (Bruker Corporation, Billerica, MA).

4.2.2.4. Karl Fischer Titration

A Mettler-Toledo C20 coulometric Karl Fischer titrator was used with the HYDRANAL™ Coulomat E electrolyte solution for both the catholyte and the anolyte cells to determine the water content of solvents and bases.

4.2.3. Synthetic Procedures

4.2.3.1. Synthesis of Pseudocapsaicin Chloroformate

This synthesis followed the procedure by Wooley and coworkers as shown in Figure 4-1.[158] In a 25-mL Schlenk flask, pseudocapsaicin (0.5050 g, 1.721 mmol), *N*,*N*-dimethylaniline (DMA) (0.390 mL, 3.08 mmol), and a catalytic amount (0.0084 g) of activated charcoal were mixed in 10.0 mL of dry DCM. The reaction was cooled to –46 ^{o}C in a dry ice/cyclohexanone bath. Diphosgene (0.1241 mL, 1.028 mmol) was added dropwise over 40 min. The reaction was taken off the ice bath and allowed to warm up to room temperature and react. After *ca.* 26 h, the reaction was quenched using a vacuum trap filled with potassium hydroxide (KOH) pellets. The reaction mixture was immediately gravity-filtered with excess DCM into a flask filled with 1.6 g of silica gel and condensed *in vacuo*. The sample was packed into a 25-g load column and run on the CombiFlash instrument using a 40-g flash column with a solvent system of hexanes:ethyl acetate. The solvent gradient was increased from 10% to 50% ethyl acetate. The product was isolated in a 15.4% yield.

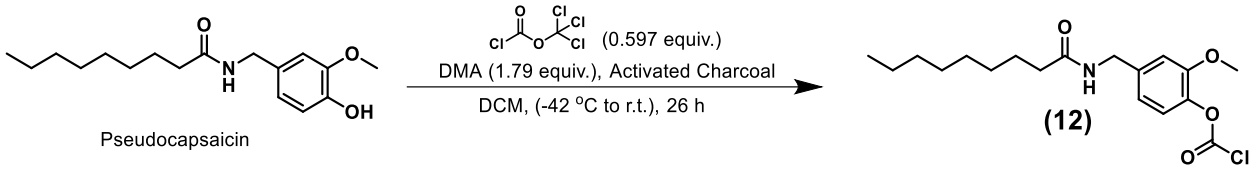

Figure 4-1. Synthesis of pseudocapsaicin chloroformate (**12**).

^{1}H-NMR (300 MHz, $CDCl_3$, δ, ppm): 7.09 (1H, d, *J* = 8 Hz, -(CO_2Cl)C-**C*H***-CH-C(-R)-CH-C(OCH_3)-), 6.93 (1H, s, -(CO_2Cl)C-CH-CH-C(-R)-**C*H***-C(OCH_3)-), 6.84 (1H, d, *J* = 8 Hz, -(CO_2Cl)C-CH-**C*H***-C(-R)-CH-C(OCH_3)-), 6.10 - 5.85 (1H, br. s, R-**N*H***-R'), 4.41 (2H, d, *J* = 4 Hz, $R_{aliph.}$-C=O-NH-**C*H₂***-R_{Ar}), 3.85 (3H, s, -(CO_2Cl)C-CH-CH-C(-R)-CH-C(O**C*H₃***)-), 2.22 (2H, t, *J* = 8 Hz, -C_{amide}-**C*H₂***-CH_2-CH_2-CH_2-CH_2-CH_2-CH_2-CH_3), 1.78 – 1.52 (2H, m, C_{amide}-CH_2-**C*H₂***-CH_2-CH_2-CH_2-CH_2-CH_2-CH_3), 1.41 – 1.10 (10H, br. m, -C_{amide}-CH_2-CH_2-**C*H₂***-**C*H₂***-**C*H₂***-**C*H₂***-**C*H₂***-CH_3), 0.87 (3H, t, *J* = 6 Hz, -C_{amide}-CH_2-CH_2-CH_2-CH_2-CH_2-CH_2-**C*H₃***). ^{13}C-NMR (70 MHz, $CDCl_3$, δ, ppm): 173.39, 150.68, 149.25, 140.03, 139.20, 121.85, 119.93, 112.51, 56.18, 43.39, 36.84, 31.93, 29.44, 29.28, 25.92, 22.76, 14.21. HRMS (ESI^+): [$M+H^+$]: $C_{18}H_{27}ClNO_4$ expected: 356.1623 amu; found: 356.1549 amu. HRMS (ESI^-): [$M+Cl^-$]: $C_{18}H_{26}Cl_2NO_4$: 390.1244 amu; found 390.1349 amu.

4.2.3.2. Synthesis of 1-Chloroethyl-2-(*p*-Toluenesulfonate) (13)

The procedure by Kornfield and coworkers was used as shown in Figure 4-2.[183] In a 250-mL, two-necked flask, *p*-toluenesulfonyl chloride (70.6547 g, 370.60 mmol), and pyridine (24.45 mL, 302.3 mmol) were combined in 73.0 mL of DCM. The flask was put on an ice bath for 10 min before adding 1-chloroethanol (13.25 mL, 197.6 mmol) dropwise. After the addition of 1-chloroethanol, the reaction was taken off the ice and allowed to warm up to room temperature.

After 22 h, the reaction mixture was washed twice in 150 mL of distilled water containing 25 mL of pyridine. The reaction mixture was subsequently washed twice in 150-mL 2-M hydrochloric acid (HCl). The organic phase was condensed *in vacuo*. The resulting yellowish, viscous liquid was put under Schlenk vacuum overnight and briefly heated under vacuum to 50 °C. A subsequent ^{1}H-NMR revealed a small amount of DCM present from integration; no DCM was visible from the ^{13}C-NMR spectra. The overall yield of 2-chloroethyl-p-toluenesulfonate product was 82%. This yield accounted for 14% of irremovable DCM impurity of the otherwise 95% mass recovery.

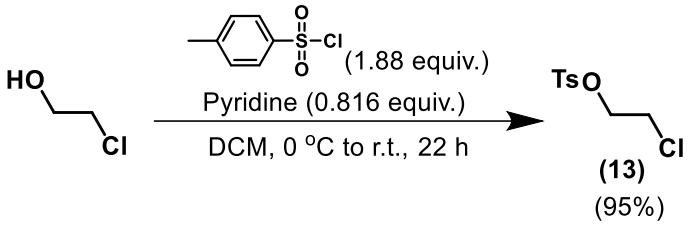

Figure 4-2. Synthesis of 1-chloroethyl-2-(*p*-toluenesulfonate) (**13**) from 1-chloroethan-2-ol.

^{1}H-NMR (300 MHz, $CDCl_3$, δ, ppm): 7.80 (2H, d, *J* = 8 Hz, -(CH_3)CH-**C*H***-C(SO_3-R)-), 7.36 (2H, d, *J* = 8 Hz, -(CH_3)**C*H***-CH-C(SO_3-R)-), 4.23 (2H, t, *J* = 6 Hz, TsO-**C*H₂***-CH_2-Cl), 3.65 (2H, t, *J* = 6 Hz, TsO-CH_2-**C*H₂***-Cl), 2.45 (3H, s, -(**C*H₃***)CH-CH-C(SO_3-R-)-). ^{13}C-NMR (70 MHz, $CDCl_3$, δ, ppm): 145.37, 132.58, 130.07, 128.08, 69.04, 40.87, 21.78. HRMS (ESI^+): [M+Na^+]: expected: $C_9H_{11}O_3SClNa$ expected: 257.0010 amu; found: 256.9993 amu; [M+K^+]: expected: $C_9H_{11}O_3SClK$ expected: 272.9749 amu; found: 272.9804 amu.

4.2.3.3. Synthesis of 1-Chloroethyl-2-*O*-Pseudocapsiacin (14)

This synthesis followed the procedure by Kornfield and coworkers as shown in Figure 4-3.[183] In a 500-mL, two-necked flask, pseudocapsaicin (5.0056 g, 17.061 mmol) and potassium carbonate (K_2CO_3) (3.5974 g, 26.028 mmol) were added to 100 mL of dry DMF. **13** (7.2816 g, 26.621 mmol) was added dropwise at room temperature initially. The reaction was monitored by TLC using hexanes:ethyl acetate (1:1) as an eluent and was gradually heated to 80 °C over 75 h. After 75 h, the heat was cut off. A total of 5.1389 g (68.930 mmol) of KCl was added from 76 to 136 h while monitoring by TLC until all 1-chloroethyl-2-(*p*-toluenesulfonate) had been consumed. The temperature began at 90 ^{o}C, but high conversion was achieved at 100 ^{o}C.

The reaction mixture was first poured into distilled water (300 mL) and extracted first with 2-butanone (200 mL) and then three times with 2-butanone (100 mL). The collected organic phase was extracted four times with distilled water (100 mL). The organic phase was condensed *in vacuo*, leaving a whitish cake-like substance. There appeared to be some sort of residual salt remaining, so the solid was redissolved in DCM (400 mL) and extracted three times with distilled water (100 mL). The solution was condensed *in vacuo* and then put on a high-vacuum rotary evaporator (20 to 50 mTorr) at 60 ^{o}C to remove any residual DMF. The remaining solid was rinsed with cold distilled water on a vacuum filter to remove small remaining DMF droplets and left to dry. The remaining white powder was put under vacuum overnight.

All of the solid sample was put back into a two-necked flask with KCl (5.9563 g, 79.895 mmol). The flask was purged, and DMF (50 mL) was added. The reaction was heated to 85 ^{o}C for 24 h. The cooled reaction mixture was then poured into a separatory funnel with distilled water (300 mL). The reaction was first extracted with DCM (200 mL). Then, the reaction was

extracted with DCM (300 mL). The organic phase was collected and extracted three times with distilled water (100 mL) and then three more times with distilled water (200-mL water). The organic phase was then gravity-filtered with excess DCM. The reaction was then condensed *in vacuo*. The dried white cake was again put on high vacuum at 60 ^{o}C for 2 h. Product was obtained in 93% yield.

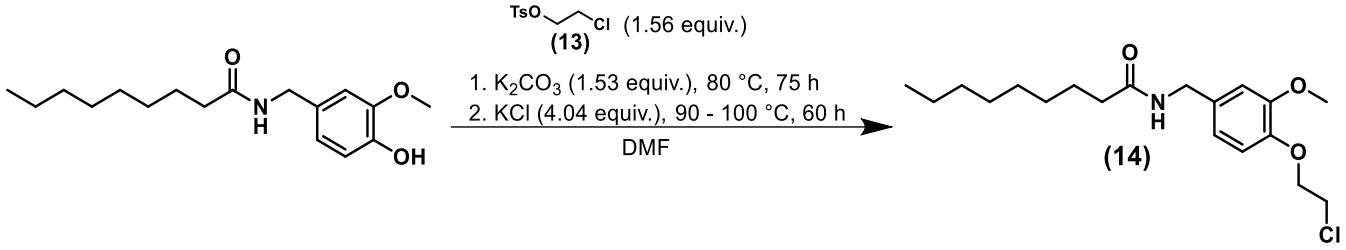

Figure 4-3. Synthesis of 1-chloroethyl-O-pseudocapsaicin (**14**) from pseudocapsaicin.

^{1}H-NMR (300 MHz, $CDCl_3$, δ, ppm): 6.86 (1H, dd, J_{ABX} = 8 Hz, 2 Hz, -(Cl-CH_2-CH_2-O-)C-**C*H***-CH-C(-R)-CH-C(OCH_3)-), 6.83 (1H, d, J_{ABX} = 2 Hz, -(Cl-CH_2-CH_2-O-)C-CH-CH-C(-R)-**C*H***-C(OCH_3)-), 6.78 (1H, dd, J_{ABX} = 8 Hz, 2 Hz, -(Cl-CH_2-CH_2-O-)C-CH-**C*H***-C(-R)-CH-C(OCH_3)-), 5.80 – 5.62 (1H, br. s, R-**N*H***-R'), 4.37 (2H, d, *J* = 5 Hz, $R_{aliph.}$-C=O-NH-**C*H₂***-R_{Ar}), 4.25 (2H, t, J = 6 Hz, -(Cl-CH_2-**C*H₂***-O-)C-CH-CH-C(-R)-CH-C(OCH_3)-), 3.85 (3H, s, -(Cl-CH_2-CH_2-O-)C-CH-CH-C(-R)-CH-C(O**C*H₃***)-), 3.81 (2H, t, *J* = 6 Hz, -(Cl-**C*H₂***-CH_2-O-)C-CH-CH-C(-R)-CH-C(OCH_3)-), 2.20 (2H, t, *J* = 8 Hz, -C_{amide}-**C*H₂***-CH_2-CH_2-CH_2-CH_2-CH_2-CH_2-CH_3), 1.71 – 1.57 (2H, m, C_{amide}-CH_2-**C*H₂***-CH_2-CH_2-CH_2-CH_2-CH_2-CH_3), 1.40 – 1.14 (10H, br. m, -C_{amide}-CH_2-CH_2-**C*H₂***-**C*H₂***-**C*H₂***-**C*H₂***-**C*H₂***-CH_3), 0.87 (3H, m, -C_{amide}-CH_2-CH_2-CH_2-CH_2-CH_2-CH_2-CH_2-**C*H₃***).

^{13}C-NMR (70 MHz, $CDCl_3$, δ, ppm): 173.07, 150.15, 147.07, 132.81, 120.21, 114.92,

112.14, 105.15, 69.62, 56.15, 43.45, 41.78, 36.99, 31.94, 29.45, 29.29, 25.93, 22.77, 14.23. HRMS (ESI^+): [$M+H^+$]: $C_{19}H_{31}ClNO_3$ expected: 356.1987 amu; found: 356.2038 amu; [$M+K^+$]: $C_{19}H_{30}ClNO_3K$ expected: 394.1546 amu; found: 394.1651 amu; [$M+Cl^-$]: $C_{19}H_{30}ClNO_3Cl$ expected: 390.1608 amu; found: 390.1562 amu.

4.2.3.4. Synthesis of 1-Iodoethyl-2-*O*-Pseudocapsaicin (15)

The procedure used for this synthesis was previously discussed by Clark and coworkers as shown in Figure 4-4.[184] In a nitrogen-purged, two-necked flask, **14** (1.0015 g, 2.814 mmol), and potassium iodide (KI)-alumina (9.0139-g KI-alumina, 9.8339-mmol KI) were mixed in dry toluene. The reaction was heated to 95 ^oC for 6 h. The reaction was monitored via TLC using hexanes:ethyl acetate (1:1) as the eluent.

The reaction mixture was mixed with Celite and gravity-filtered with excess DCM. The solution was condensed *in vacuo* at 60 °C. Then, the reaction mixture was put on a high-vacuum rotary evaporator until all toluene was removed. No further purification was necessary. The recovered yield was 59%.

KI-alumina used in this reaction was made by dissolving KI (3.0256 g, 18.226 mmol) in a beaker with distilled water (50 mL) and alumina powder (12 g). The KI-alumina mixture was 20% KI by mass. The mixture was heated to 100 °C until all water evaporated. The sample was then put in a vacuum oven at 80 °C for 5 h. The recovered white powder was crushed up with a spatula and quickly put into a sealed vial.

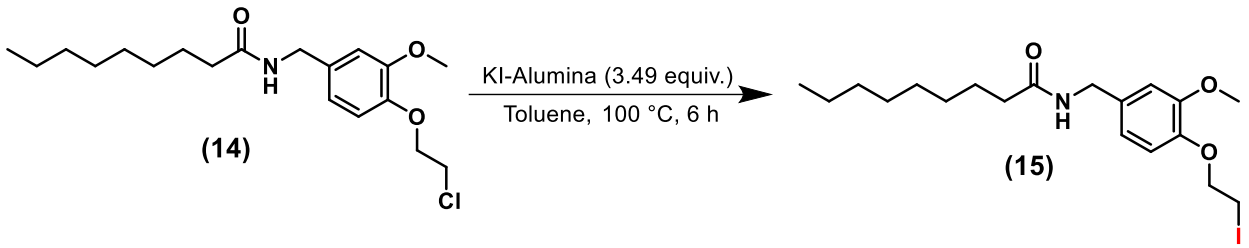

Figure 4-4. Synthesis of 1-iodoethyl-2-*O*-pseudocapsaicin (**15**) from **14**.

^{1}H-NMR (300 MHz, $CDCl_3$, δ, ppm): 6.87 – 6.72 (3H, m, -(I-CH_2-CH_2-O-)C-**C*H***-**C*H***-C(-R)-**C*H***-C(OCH_3)-), 5.89 – 5.53 (1H, br. s, R-**N*H***-R'), 4.36 (2H, d, *J* = 6 Hz, $R_{aliph.}$-C=O-NH-**C*H*$_2$**-R_{Ar}), 4.26 (2H, t, J = 7 Hz, -(I-CH_2-**C*H*$_2$**-O-)C-CH-CH-C(-R)-CH-C(OCH_3)-), 3.85 (3H, s, -(I-CH_2-CH_2-O-)C-CH-CH-C(-R)-CH-C(O**C*H*$_3$**)-), 3.41 (2H, t, *J* = 7 Hz, -(I-**C*H*$_2$**-CH_2-O-)C-CH-CH-C(-R)-CH-C(OCH_3)-), 2.19 (2H, t, *J* = 8 Hz, -C_{amide}-**C*H*$_2$**-CH_2-CH_2-CH_2-CH_2-CH_2-CH_2-CH_3), 1.69 – 1.53 (2H, m, C_{amide}-CH_2-**C*H*$_2$**-CH_2-CH_2-CH_2-CH_2-CH_2-CH_3), 1.42 – 1.11 (10H, br. m, -C_{amide}-CH_2-CH_2-**C*H*$_2$**-**C*H*$_2$**-**C*H*$_2$**-**C*H*$_2$**-**C*H*$_2$**-CH_3), 0.87 (3H, m, -C_{amide}-CH_2-CH_2-CH_2-CH_2-CH_2-CH_2-CH_2-**C*H*$_3$**). ^{13}C-NMR (70 MHz, $CDCl_3$, δ, ppm): 173.07, 150.10, 146.74, 132.80, 120.21, 114.97, 112.15, 105.12, 70.39, 56.16, 43.45, 36.98, 31.94, 29.45, 29.29, 25.93, 22.77, 14.23, 1.13. HRMS (ESI^+): [$M+H^+$]: expected C_{19} $H_{31}INO_3$: 448.1343 amu; found 448.1421 amu; [$M+K^+$]: expected C_{19} $H_{30}INO_3K$: 486.0902 amu; found 486.1087 amu. HRMS (ESI^-): [$M+Cl^-$]: expected C_{19} $H_{30}IClNO_3$: 482.0964 amu; found: 482.1014 amu; [$M+I^-$]: expected C_{19} $H_{30}I_2NO_3$: 574.0321 amu; found: 574.0308 amu**.**

4.2.3.5. Synthesis of 2-Tosylethyl-1-*O*-Pseudocapsaicin (16)

In a flame-dried, 250-mL, two-necked flask equipped with a reflux column, pseudocapsaicin (1.0094 g, 3.4404 mmol), K_2CO_3 (0.7185 g, 5.199 mmol), and 1,2-bis(tosyloxy)ethane (3.7880 g, 10.226 mmol) were combined, and the apparatus was purged

under nitrogen. DMF (20.0 mL) was added to the flask, and the oil bath temperature was immediately set to 60 ^{o}C while stirring. The reaction was allowed to stir for 23 h while monitoring by TLC. The optimum TLC solvent system appeared to be 8:2 (DCM:ethyl acetate) using a potassium permanganate ($KMnO_4$) stain. After 23 h, a small amount of starting material still appeared in the reaction mixture, so the temperature was increased to 70 °C. After 6 h, the reaction appeared complete by TLC, and the reaction was taken off of heating after a total of *ca.* 28 h.

The reaction mixture was extracted twice into distilled water (75 mL) with DCM (50 mL). The collected organic phase was then extracted with distilled water (75 mL). The organic phase was then vacuum-filtered twice with some Celite and excess DCM. The solid precipitate collected was discarded. The filtrate was concentrated *in vacuo* and was placed into a centrifuge tube with DCM (25 mL). The solution was left in a –20-^{o}C freezer overnight. A solid precipitate had separated from the rest of the solution at the top of the tube the next day, and the mixture was vacuum-filtered using excess cold DCM, leaving a clear filtrate solution.

Before running the filtered organic phase on a column, a TLC run indicated that starting material was present in the reaction mixture that apparently was not seen in the last time point. The organic phase was condensed *in vacuo* onto 22 g of silica gel and loaded onto an empty 25-g load column. The column sample was run on a 330-g flash column using DCM:ethyl acetate as the eluent. The collected product was put under vacuum for *ca.* 48 h, and the product was confirmed using both ^{1}H-NMR and ^{13}C-NMR, indicating a clean spectrum. The overall isolated yield of the product is 74%. The overall reaction is illustrated in Figure 4-5.

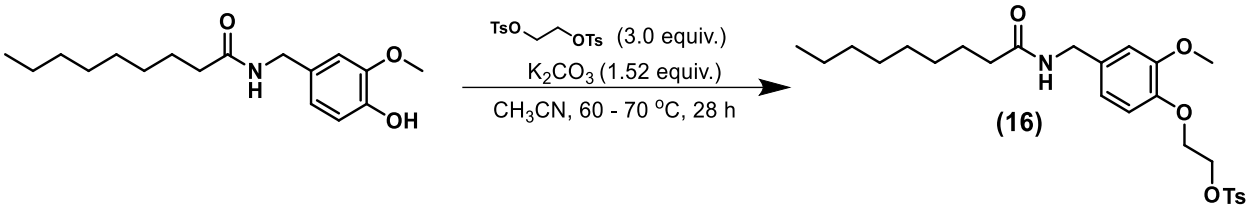

Figure 4-5. Synthesis of 2-tosylethyl-1-O-pseudocapsaicin (**16**) from pseudocapsaicin.

^{1}H-NMR (500 MHz, $CDCl_3$, δ, ppm): 7.80 (2H, d, J_{ABX} = 8 Hz, 9 Hz, -(CH_3)C-CH-**C*H***-C(SO_3-R_{Ethyl})-), 7.32 (2H, d, J_{ABX} = 8 Hz, 9 Hz, -(CH_3)C-**C*H***-CH-C(SO_3-R_{Ethyl})-), 6.83 – 6.70 (3H, m, -(TsO-CH_2-CH_2-O-)C-**C*H***-**C*H***-C(-R)-**C*H***-C(OCH_3)-), 5.85 – 5.73 (1H, br. s, R-**N*H***-R'), 4.39 – 4.29 (4H, m, $R_{aliph.}$-C=O-NH-**C*H₂***-R_{Ar}, TsO-**C*H₂***-CH_2-O-R_{Ar}), 4.19 (2H, t, *J* = 5 Hz, TsO-CH_2-**C*H₂***-O-R_{Ar}), 3.80 (3H, s, -(TsO-CH_2-CH_2-O-)C-CH-CH-C(-R)-CH-C(O**C*H₃***)-), 2.44 (3H, s, J_{ABX} = 8 Hz, -(**C*H₃***)C-CH-CH-C(SO_3-R_{Ethyl}-)-), 2.20 (2H, t, *J* = 7 Hz, -C_{amide}-**C*H₂***-CH_2-CH_2-CH_2-CH_2-CH_2-CH_2-CH_3), 1.70 – 1.57 (2H, m, -C_{amide}-CH_2-**C*H₂***-CH_2-CH_2-CH_2-CH_2-CH_2-CH_3), 1.37 – 1.17 (10H, br. m, -C_{amide}-CH_2-CH_2-**C*H₂***-**C*H₂***-**C*H₂***-**C*H₂***-**C*H₂***-CH_3), 0.87 (3H, t, *J* = 7 Hz, -C_{amide}-CH_2-CH_2-CH_2-CH_2-CH_2-CH_2-CH_2-**C*H₃***). ^{13}C-NMR (125 MHz, $CDCl_3$, δ, ppm): 172.19, 150.17, 147.00, 145.06, 132.91, 129.98, 128.13, 120.19, 115.19, 112.15, 68.22, 67.27, 56.07, 43.46, 36.94, 31.93, 29.45, 29.44, 29.28, 25.94, 22.76, 21.80, 14.22. HRMS (ESI^+): [$M+H^+$]: expected: C_{26} $H_{38}NO_6S$: 492.2414 amu; found 492.2570 amu; [$M+Na^+$]: expected C_{26} $H_{37}NO_6SNa$: 514.2234 amu; found 514.2363 amu; [$M+K^+$]: expected C_{26} $H_{37}NO_6SK$: 530.1973 amu; found: 530.2170 amu. HRMS (ESI^-): [$M+Cl^-$]: expected: C_{26} $H_{37}NO_6SCl$: 526.2036 amu; found: 526.2574 amu.

4.2.3.6. Synthesis of Methyl 2,3-*O*-Diallyl-4,6-*O*-Benzylidene-α-(D)-Glucopyranoside (17)

In a 25-mL, round-bottomed flask, NaH (0.2597 g, 6.493 mmol) was washed in 3.0 mL of dry THF. Then, 7.4 mL of dry DMF was added, and the flask was purged by briefly purging

three times with nitrogen, being careful not to bump the solvent. Simultaneously in a purged vial, methyl 4,6-*O*-benzylidene-α-(D)-glucopyranoside (**2**) (0.3017 g, 1.069 mmol) was dissolved in 1.8 mL of dry DMF. The original round-bottomed flask was put in an ice bath, and the benzylidene glucose solution was added dropwise over 10 min. Then, allyl bromide (0.460 mL, 5.32 mmol) was dissolved in 0.720 mL of DMF and added dropwise over 10 min. The reaction was taken off the ice bath and allowed to warm up to room temperature and react. After 20 h, the reaction was quenched by adding 6 mL of isopropanol dropwise over 8 min.

The reaction mixture was put on a standard rotary evaporator at 60 °C for several hours. The reaction flask was subsequently put on a high-vacuum rotary evaporator (20 to 50 mTorr) at 60 °C for *ca.* 1 h. The reaction mixture was extracted twice with DCM (30 mL) and distilled water (30 mL). The collected organic phase was extracted again with 30 mL of deionized water. The organic phase was then condensed *in vacuo* to a reddish, oily liquid that crystallized upon cooling.

The sample was recrystallized seven times by adding no more than hexanes (4 mL), heating until all solid dissolved, and allowing some solvent to evaporate. A mineral oil impurity appeared by ^{1}H-NMR. The overall yield was 96% with trace amounts of mineral oil impurity, as seen in the ^{1}H and ^{13}C-NMR spectra. This reaction is illustrated in Figure 4-6.

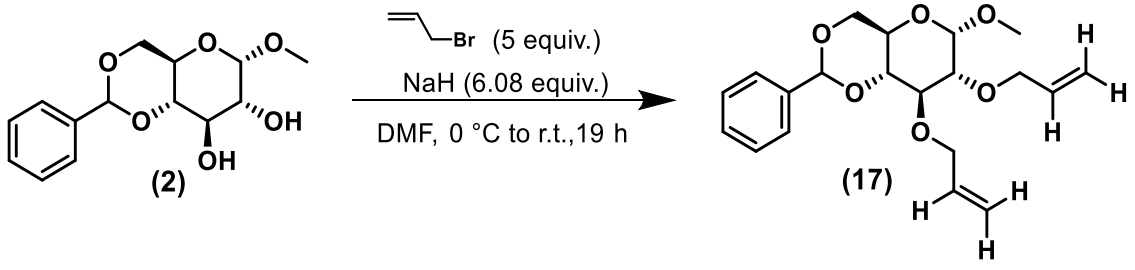

Figure 4-6. Synthesis of methyl 2,3-*O*-diallyl-4,6-*O*-benzylidene-α-(D)-glucopyranoside (**17**) from **2**.

^{1}H-NMR (500 MHz, $CDCl_3$, δ, ppm): 7.49 (2H, m, -CH-CH-**C*H***-C_{tert}(CH(O-R)(O-R'))-), 7.40 – 7.31 (2H, m, -**C*H***-**C*H***-CH-C_{tert}(CH(O-R)(O-R'))-), 6.01 – 5.88 (2H, m, $R_{ring\text{-}C2+C3}$-O-CH_2-**C*H*$_{down}$**=C(H_{up})(H_{down})), 5.54 (1H, s, -CH-CH-CH-C_{tert}(**C*H***(O-R)(O-R'))-), 5.32 – 5.30 (1H, m, $R_{ring\text{-}C3}$-O-C(H)(H')-CH_{down}=**C**(H_{up})(***H*$_{down}$**)), 5.29 – 5.26 (1H, m, $R_{ring\text{-}C2}$-O-CH_2-CH_{down}=**C**(H_{up})(***H*$_{down}$**)), 5.22 – 5.18 (1H, m, $R_{ring\text{-}C3}$-O-C(H)(H')-CH_{down}=**C**(***H*$_{up}$**)(H_{down})), 5.16 – 5.12 (1H, m, $R_{ring\text{-}C2}$-O-CH_2-CH_{down}=**C**(***H*$_{up}$**)(H_{down})), 4.78 (1H, d, *J* = 4 Hz, -(O)(OCH_3)**C*H***-CH(-O-R_{allyl})-CH(-O-R_{allyl})-CH(-O-R_{benz})-CH(-C(H)(H')-O-R_{benz})-), 4.39 – 4.33 (1H, m, $R_{ring\text{-}C3}$-O-**C**(***H***)(H')-CH_{down}=C(H_{up})(H_{down})), 4.32 – 4.24 (3H, m, $R_{ring\text{-}C2}$-O-**C*H*$_2$**-CH_{down}=C(H_{up})(H_{down}), -(O)(OCH_3)CH-CH(-O-R_{allyl})-CH(-O-R_{allyl})-CH(-O-R_{benz})-CH(-**C**(***H***)(H')-O-R_{benz})-), 4.22 – 4.15 (1H, m, $R_{ring\text{-}C3}$-O-**C**(H)(***H'***)-CH_{down}=C(H_{up})(H_{down})), 3.87 (1H, t, *J* = 9 Hz, -(O)(OCH_3)CH-CH(-O-R_{allyl})-CH(-O-R_{allyl})-**C*H***(-O-R_{benz})-CH(-C(H)(H')-O-R_{benz})-), 3.84 – 3.77 (1H, m, -(O)(OCH_3)CH-CH(-O-R_{allyl})-CH(-O-R_{allyl})-CH(-O-R_{benz})-CH(-**C**(H)(***H'***)-O-R_{benz})-), 3.72 (1H, t, J = 10 Hz, -(O)(OCH_3)CH-CH(-O-R_{allyl})-**C*H***(-O-R_{allyl})-CH(-O-R_{benz})-CH(-C(H)(H')-O-R_{benz})-), 3.55 (1H, t, *J* = 9 Hz, -(O)(OCH_3)CH-CH(-O-R_{allyl})-CH(-O-R_{allyl})-CH(-O-R_{benz})-**C*H***(-C(H)(H')-O-R_{benz})-), 3.47 (1H, m, -(O)(OCH_3)CH-**C*H***(-O-R_{allyl})-CH(-O-R_{allyl})-CH(-O-R_{benz})-CH(-C(H)(H')-O-R_{benz})-). ^{13}C-NMR (125 MHz, $CDCl_3$, δ, ppm): 137.55, 135.34, 134.97, 129.03, 128.34, 126.16, 117.86, 116.89, 101.41, 99.41, 82.19, 79.15, 78.09, 74.12, 73.25, 69.22, 62.45, 55.40. HRMS (ESI^+): [M+H^+]: expected $C_{20}H_{27}O_6$: 363.1802 amu; found: 363.1861 amu; [M+Na^+]: expected $C_{20}H_{26}O_6Na$: 385.1622 amu; found: 385.1638 amu.

4.2.3.7. Synthesis of Ethyl-2-Thiobenzoate-1-*O*-Pseudocapsaicin (18)

This procedure followed the work of Kornfield and coworkers as shown in Figure 4-7.[183] The tabulated amount of thiobenzoic acid (0.150 mL, 1.27 mmol) was added dropwise to the tabulated amounts of 1-chloroethyl-2-*O*-pseudocapsaicin (0.2228 g, 0.6260 mmol), sodium bicarbonate base (0.1449 g, 1.725 mmol), and DMF (2.5 mL) in a round-bottomed flask. The reaction was allowed to stir until most of the CO_2 evolution ceased, and the reaction was heated to 45 °C for 19 h while monitoring *via* TLC using 8:2 (chloroform [$CHCl_3$]:ethyl acetate) as the eluent and $KMnO_4$ stain.

The reaction mixture was extracted four times with DCM (10 mL) and distilled water (30 mL). Then, the organic phases were collected and washed two times with distilled water (30 mL) before condensing. The mixture was then recrystallized in 14-mL ethanol, and the procedure was repeated for the filtrate two times, decreasing the volume of ethanol by half each time. The recovered pink solid was put under vacuum overnight at 40 °C to dry, giving an 84% overall yield.

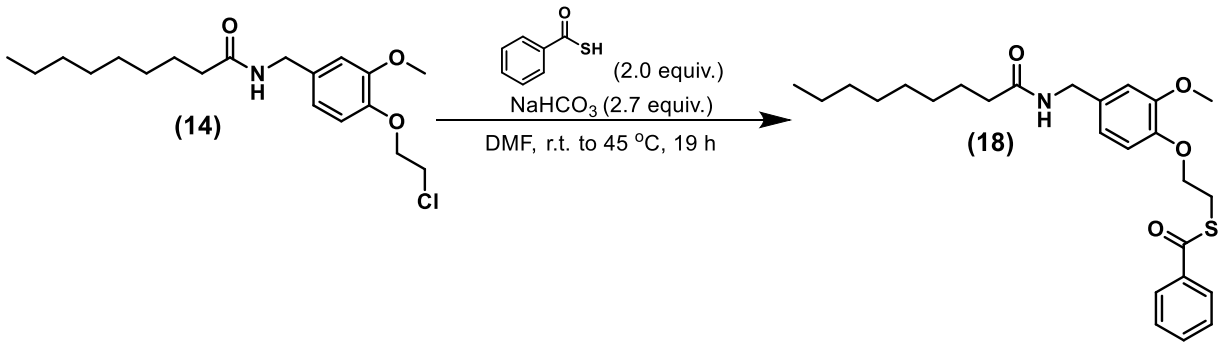

Figure 4-7. Synthesis of ethyl-2-thiobenzoate-1-*O*-pseudocapsaicin (**18**) from **14**.

^{1}H-NMR (500 MHz, $CDCl_3$, δ, ppm): 7.97 (2H, dd, *J* = 8 Hz, 1 Hz, -CH-CH-**C*H***-C(CO-S-CH_2-CH_2-O-R_{Ar})-), 7.58 (1H, t, *J* = 7 Hz, -**C*H***-CH-CH-C(CO-S-CH_2-CH_2-O-R_{Ar})-), 7.45 (2H, t, *J* = 8 Hz, -CH-**C*H***-CH-C(CO-S-CH_2-CH_2-O-R_{Ar})-), 6.95 (1H, d, *J* = 8 Hz, -(R_{Ar}-CO-S-CH_2-CH_2-O-)C-**C*H***-CH-C(-R)-CH-C(OCH_3)-), 6.84 – 6.75 (2H, m, -(R_{Ar}-CO-S-CH_2-CH_2-O-)C-CH-**C*H***-C(-R)-**C*H***-C(OCH_3)-), 5.72 (1H, s, R-**N*H***-R'), 4.36 (2H, d, *J* = 6 Hz, $R_{aliph.}$-C=O-NH-**C*H₂***-R_{Ar}), 4.23 (2H, t, *J* = 7 Hz, -CH-CH-CH-C(CO-S-CH_2-**C*H₂***-O-R_{Ar})-), 3.85 (3H, s, -(R_{Ar}-CO-S-CH_2-CH_2-O-)C-CH-CH-C(-R)-CH-C(O**C*H₃***)-), 3.48 (2H, t, *J* = 7 Hz, -CH-CH-CH-C(CO-S-**C*H₂***-CH_2-O-R_{Ar})-), 2.23 – 2.14 (2H, m, -C_{amide}-**C*H₂***-CH_2-CH_2-CH_2-CH_2-CH_2-CH_3), 1.69 – 1.58 (2H, m, -C_{amide}-CH_2-**C*H₂***-CH_2-CH_2-CH_2-CH_2-CH_2-CH_3), 1.37 – 1.17 (11H, br. m, -C_{amide}-CH_2-CH_2-**C*H₂***-**C*H₂***-**C*H₂***-**C*H₂***-**C*H₂***-CH_3), 0.86 (3H, t, *J* = 7 Hz, -C_{amide}-CH_2-CH_2-CH_2-CH_2-CH_2-CH_2-CH_2-**C*H₃***). ^{13}C-NMR (125 MHz, $CDCl_3$, δ, ppm): 191.60, 173.03, 149.85, 147.31, 136.85, 133.72, 132.14, 128.78, 127.42, 120.30, 114.07, 111.98, 67.94, 56.13, 43.50, 36.99, 31.94, 29.46, 29.45, 29.28, 28.14, 25.93, 22.77, 14.23. HRMS (ESI^+): [$M+Na^+$]: expected: C_{26} $H_{35}NO_4SNa$: 480.2179 amu; found 480.2240 amu. HRMS (ESI^-): [$M+Cl^-$]: expected: C_{26} $H_{35}NO_4SCl$: 492.1981 amu; found: 492.1994 amu.

4.2.3.8. Synthesis of 2-Thioethyl-1-*O*-Pseudocapsaicin (19)

The procedure by Kornfield and coworkers was used for this synthesis as shown in Figure 4-8.[183] To a round-bottomed flask, hydrazine hydrochloride (0.1515 g, 2.211 mmol), sodium acetate (0.2892 g, 3.526 mmol), and **18** (0.2019 g, 0.4412 mmol) were added, and the flask was

purged with $N_{2(g)}$. Then, DMF (12.5 mL) was added and the reaction was stirred for 32 h while monitoring by TLC using 8:2 (DCM:ethyl acetate) as the eluent.

After 32 h, the reaction mixture was extracted two times with DCM (6 mL) into distilled water (20 mL). The organic phase was collected and washed four times with distilled water (30 mL). The organic phase was then condensed down, purged with $N_{2(g)}$, and put under Schlenk vacuum in a 40-^{o}C oil bath to dry overnight. The product was confirmed *via* ^{1}H-NMR and ^{13}C-NMR. The recovered yield was 96%, with a 2.7% disulfide impurity–derived ^{1}H-NMR integration. The disulfide impurity was intractable but considered inert for the next step.

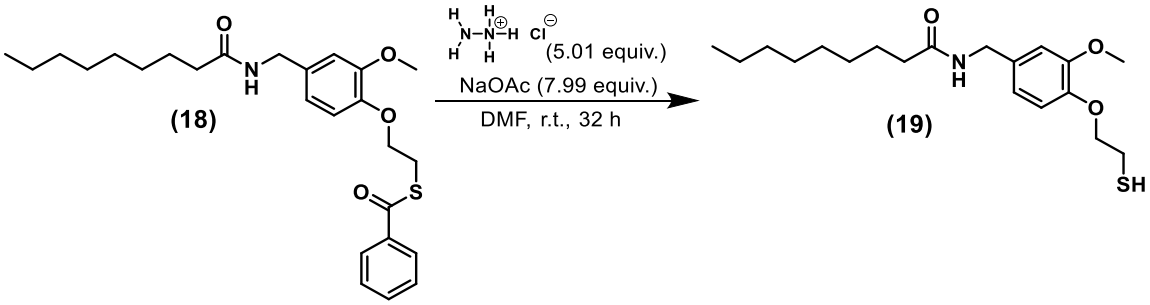

Figure 4-8. Synthesis of 2-thioethyl-1-*O*-pseudocapsaicin (**19**) from **18**.

^{1}H-NMR (500 MHz, $CDCl_3$, δ, ppm): 6.86 – 6.76 (3H, m, -(HS-CH_2-CH_2-O-)C-**C*H*-C*H*-**C(-R)-**C*H*-**C(OCH_3)-), 5.69 (1H, s, R-**N*H*-**R') 4.37 (2H, d, *J* = 6 Hz, $R_{aliph.}$-C=O-NH-**C*H*$_2$-R_{Ar}), 4.13 (2H, t, *J* = 7 Hz, -(HS-CH_2-**C*H*$_2$-O-)C-CH-CH-C(-R)-CH-C(OCH_3)-), 3.85 (3H, s, -(HS-CH_2-CH_2-O-)C-CH-CH-C(-R)-CH-C(O**C*H*$_3$)-), 2.90 (2H, dt, *J* = 7 Hz, 8 Hz, -(HS-**C*H*$_2$-CH_2-O-)C-CH-CH-C(-R)-CH-C(OCH_3)-), 2.23 – 2.17 (2H, m, -C_{amide}-**C*H*$_2$-CH_2-CH_2-CH_2-CH_2-CH_2-CH_3), 1.69 (1H, t, *J* = 8 Hz, -(***H*S**-CH_2-CH_2-O-)C-CH-CH-C(-R)-CH-C(OCH_3)-), 1.69 – 1.60 (2H, m, -C_{amide}-CH_2-**C*H*$_2$-CH_2-

CH_2-CH_2-CH_2-CH_2-CH_3), 1.34 – 1.18 (11H, br. m, -C_{amide}-CH_2-CH_2-**C*H₂*-C*H₂*-C*H₂*-C*H₂*-C*H₂*-**CH_3), 0.87 (3H, t, *J* = 7 Hz, -C_{amide}-CH_2-CH_2-CH_2-CH_2-CH_2-CH_2-**C*H₃***). ^{13}C-NMR (125 MHz, $CDCl_3$, δ, ppm): 173.04, 150.01, 147.36, 132.28, 120.23, 114.29, 112.00, 71.20, 56.12, 43.51, 37.01, 31.95, 29.47, 29.46, 29.29, 25.94, 23.92, 22.78, 14.23. Unit Mass (UM) MS (ESI^+): [M+Na^+]: expected $C_{19}H_{30}NO_3SNa$: 376.1917 amu; found: 376.22 amu. Unit-mass mass spectrometry (UMMS) (ESI^-): [M+Cl^-]: expected: C_{19} $H_{30}NO_3SCl$: 388.1719 amu; found 388.50 amu.

4.2.3.9. Synthesis of Methyl 4,6-*O*-Benzylidene-2,3-O-Bis(3-Thiopent-5-*O*-Pseudocapsaicin)-α-(D)-Glucopyranoside (20)

In a 20-mL scintillation vial, **19** (0.0586 g, 0.1658 mmol), **17** (0.0151 g, 0.0417 mmol), and 2,2-dimethoxy-2-phenylacetophenone (DMPA) (0.0094 g, 0.037 mmol) were combined, and the vial was purged with $N_{2(g)}$. DMAc (0.9 mL) was added, and the reaction mixture was sparged with $N_{2(g)}$ for 30 min. The vial was then placed in a UV oven (365 nm) for 2 h with stirring.

After 2 h, a time point was taken, and a TLC was run using 8:2 (DCM:ethyl acetate), indicating no remaining allylated glucose starting material and what appeared to be a product spot. The DMAc was taken off on a high-vacuum rotary evaporator at 40 °C. The reaction mixture was then loaded onto a 2.5-g prefilled load column using a few milliliters of DCM. The sample was then run on the CombiFlash instrument using a 12-g flash column and DCM:ethyl acetate as the eluent. The product fraction was condensed *in vacuo* and put under vacuum at 40 °C overnight. ^{1}H- and ^{13}C-NMR indicated one or more regioisomers with respect to the alkene groups in the product. The overall yield by mass recovery was 61%, including all regioisomers. This reaction is illustrated in Figure 4-9.

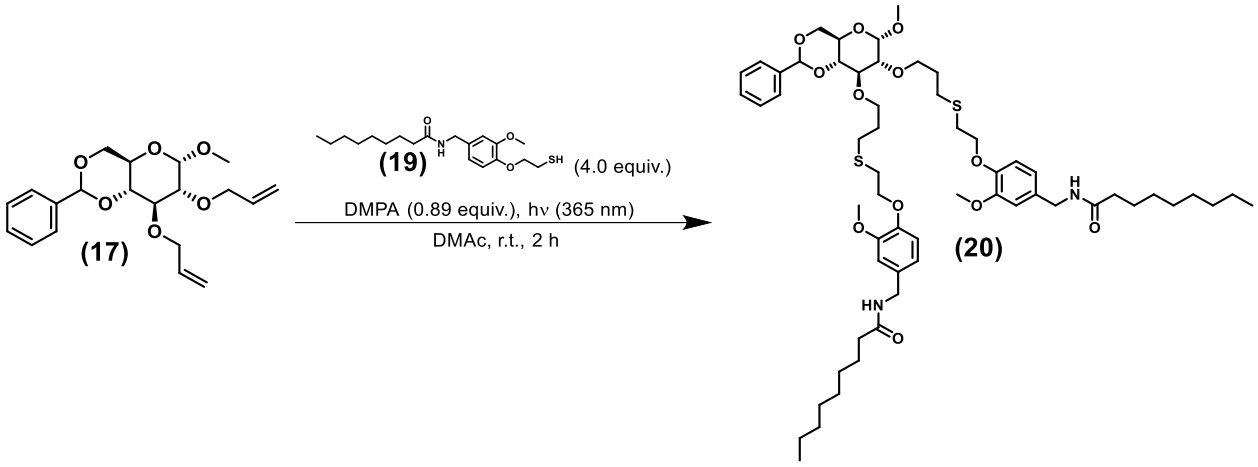

Figure 4-9. Synthesis of methyl 4,6-O-benzylidene-2,3-O-bis(3-thiopent-5-O-pseudocapsaicin)-α-(D)-glucopyranoside (**20**) from **19** and **17**.

^{1}H-NMR (500 MHz, $CDCl_3$, δ, ppm): See Figures H-1 to H-10 in Appendix H for complex assignment. ^{13}C-NMR (125 MHz, $CDCl_3$, δ, ppm): See Figures H-1 to H-10 in Appendix H for complex assignment. LRMS (ESI^+): [$M+Na^+$]: expected $C_{58}H_{88}N_2O_{12}S_2Na$: 1,091.5671 amu; found: 1,091.62 amu. LRMS (ESI^-): [$M+Cl^-$]: expected: $C_{58}H_{88}N_2O_{12}S_2Cl$: 1,103.5473 amu; found 1,103.84 amu.

4.3. Results and Discussion

4.3.1. Synthesis

The first method attempted was to directly conjugate a pseudocapsaicin molecule to a glucose-based PU backbone using the route in Figure 4-10. We hypothesized that this route would allow for a slow or delayed release of the pseudocapsaicin molecule due to the degradable and hydrolyzable carbonate linkage. This would be potentially beneficial should the antibiofouling activity be predicated upon the phenolic proton moiety of the molecule. The fact that the TRPV1 receptor, for which capsaicin is an agonist, is also activated by acidic protons in mammals indicates that the phenolic proton may play a role in its antibiofouling activity.[185] However, Angarano and

coworkers[111] indicated that the hydrophobic tail attached to the amide moiety appears to have a more-variable effect, which would be in line with the work of Domene and coworkers[186] indicating a stereoselective binding to the TRPV1 channel. Thus, the methodology for synthesizing a pseudocapsaicin chloroformate used in some of our group's previous work was attempted.[158] However, the yields for the synthesis of the chloroformate, the first step, were shockingly low. Numerous alterations to the reaction setup and even the nitrogen manifold were attempted before the problem was realized. Upon testing the DMA base by coulometric Karl Fischer titration, it was discovered that the stock bottle of the base had just over 800 ppm of water—well above EMD Millipore's (now Millipore Sigma) standard for dry solvent (50 ppm).[187] It became clear that the DMA needed to be distilled given that phosgene reactions such as this one are very susceptible to the presence of water. Unfortunately, this aspect was realized after this part of the project had been temporarily tabled.

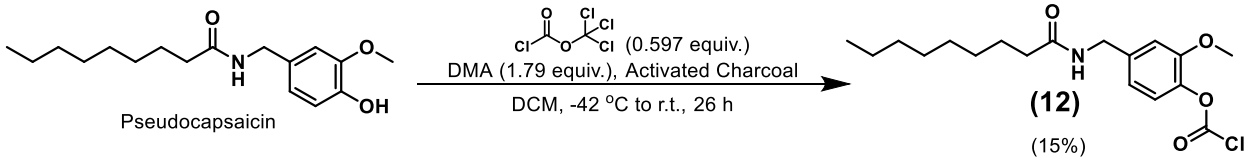

Figure 4-10. The attempted synthesis of the pseudocapsaicin chloroformate (**12**) produced a very low yield that was found to be the result of wet DMA. This should be remedied by distillation.

Before the problem was identified in the previous synthetic route, an alternative synthetic route was attempted where the pseudocapsaicin molecule would be permanently attached to the glucose backbone of the PU *via* either an ether linkage or a thioether linkage. The first route attempted was the synthesis of an ether-linked pseudocapsaicin-glucopyranoside monomer. Following the work of Kornfield and coworkers,[183] the synthesis of the 1-chloroethyl-2-*O*-

pseudocapsaicin (**14**) proceeded smoothly and in good yield with no column purification, as shown in Figure 4-11 from 1-chloroethyl-2-(*p*-toluenesulfonate) (**13**). First, an attempt was made to react **14** with the tetrafunctional methyl α-(D)-glucopyranoside using pyridine as the solvent and the base, but even gradually heating the system to 80 °C resulted in no product formation. It was expected that at a sufficiently high temperature, there would be conversion of the alkyl chloride moieties with selectivity for the 2,6-protected methyl glucopyranoside from the selective acylation work of Roberts and coworkers[188] and the pivaloylation done by Scharf and coworkers.[189] So, triethylamine (TEA) in acetone and lithium bis(trimethylsilyl)amide (LiHMDS) in DMF were then tried by monitoring and gradually heating the reactions to 90 °C over the course of weeks. However, no intended product was recovered. An ethyl-2-triethylammonium-1-*O*-pseudocapsaicin (**21**) product was recovered with the reaction using TEA and the LiHMDS reaction resulted in an intractable mixture, as shown in Table 4-1 and Figure 4-12. Thus, it appeared that a more sterically hindered yet weak base was needed in a polar solvent like DMF.

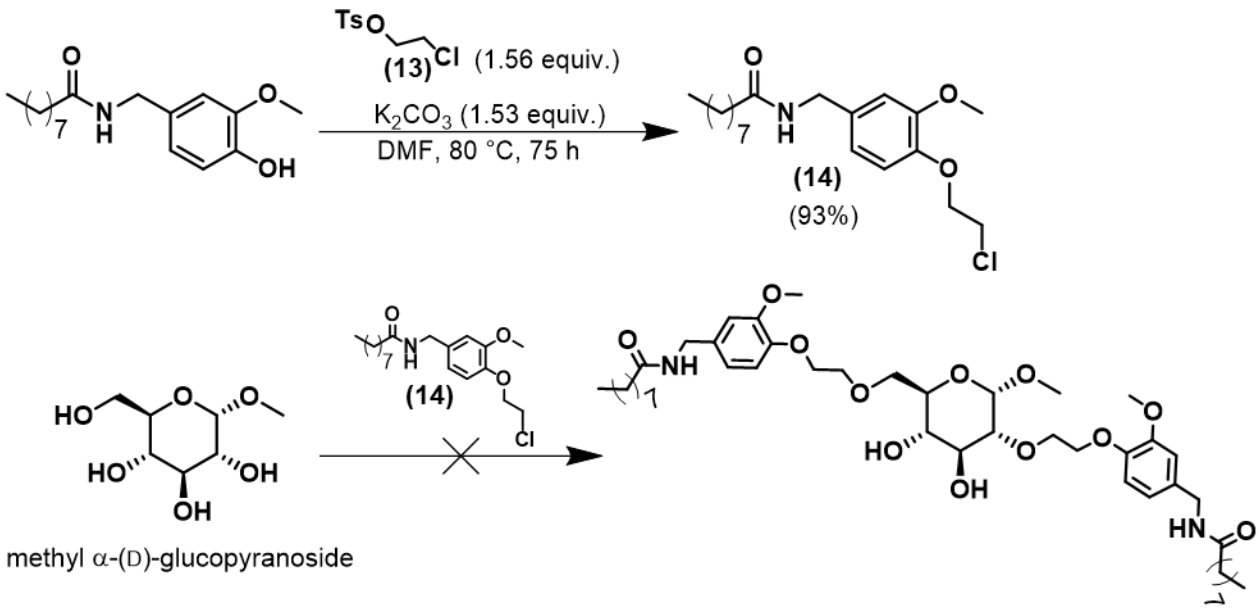

Figure 4-11. The attempted 2,6 protection of methyl α-(D)-glucopyranoside using **14** resulted in no product being recovered.

Table 4-1. Conditions for the attempted 2,6 protection of methyl α-(D)-glucopyranoside.

Capsaicinoid	*Base*	*Solvent*	*T (°C)*	*Time (h)*	*Product*
14/NaI	Pyridine	Pyridine	0 to 80	144	No reaction
14/NaI	TEA	Acetone	0 to 90	351	**21**
14/NAI	LiHMDS	DMF	–42 to 90	214	Intractable
14/KI-Alumina	DIPEA	DMF	100	21	**22** + **23**

Lastly, an attempt was made to effect the conversion by using *N*,*N*,*N*-diisopropylethylamine (DIPEA) in DMF with an alumina support for the KI Finkelstein catalyst. However, upon heating to 100 °C, the major products were 1-formylethyl-2-*O*-pseudocapsaicin (**22**) and the 1-hydroxyethyl-2-*O*-pseudocapsaicin (**23**), as shown in Table 4-1 and Figure 4-12. Apparently, as reported by Brace and coworkers,[190] this side reaction occurs with DMF in the presence of water as the reaction temperature approaches 150 °C. Nevertheless, it was clear that

the chloride moiety was too poor of a leaving group to undergo conversion with these bases, even in polar solvents like DMF.

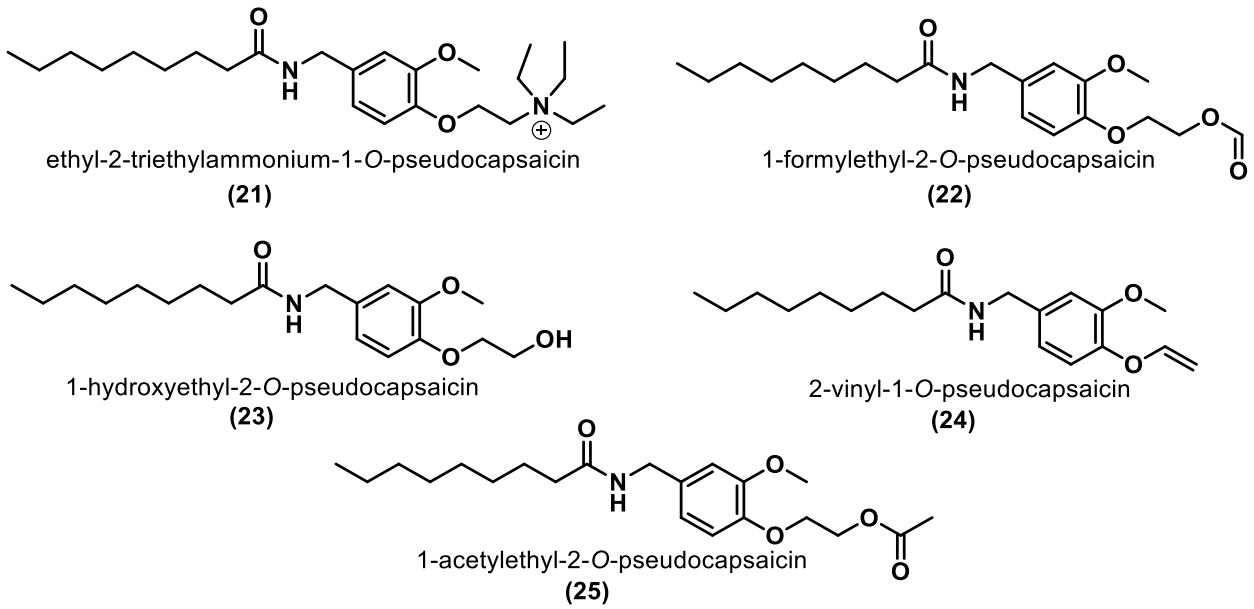

Figure 4-12. The by-products from attempted synthesis of ether-linked pseudocapsaicin to glucopyranoside consisted of the formylate and hydroxy functional groups when DMF was used at high temperatures, the acetate and hydroxy functional groups when DMAc was used at high temperatures, and the vinyl functional group when strong bases like NaH were used.

Thus, a simpler reaction was attempted with the difunctional methyl 4,6-*O*-benzylidene-α-(D)-glucopyranoside (**2**) and an even stronger base, NaH, as shown in Figure 4-13 and Table 4-2. However, no difunctionalized product was recovered, and instead, a significant amount of vinyl-*O*-pseudocapsaicin (**24**) was recovered, as shown in Figure 4-12 and Table 4-2, because of elimination. Significant gas evolution when attempting to wash the NaH led to a startling finding. Both sources of DMF had significant water contamination. The EMD Millipore DrySolv bottles that some lab members used contained more than 300 ppm of water by Karl Fischer titration (even when fresh from the factory and unopened), and the DMF from the group's own SPS system was

being dispensed with large amounts of water contamination in excess of 100 ppm at the time. The problem with the SPS was eventually remedied. While a significant amount of sodium hydroxide (NaOH) being present could contribute to the formation of this **24** elimination product, the other issue with using NaH as a base is that it also is likely deprotonating the amide moiety on the capsaicin molecule. The deprotonated, anionic amide moiety is perhaps likeliest to induce elimination with the alkyl chloride moiety under most conditions. Thus, any similar reaction using NaH with capsaicin present was deemed likely not feasible going forward.

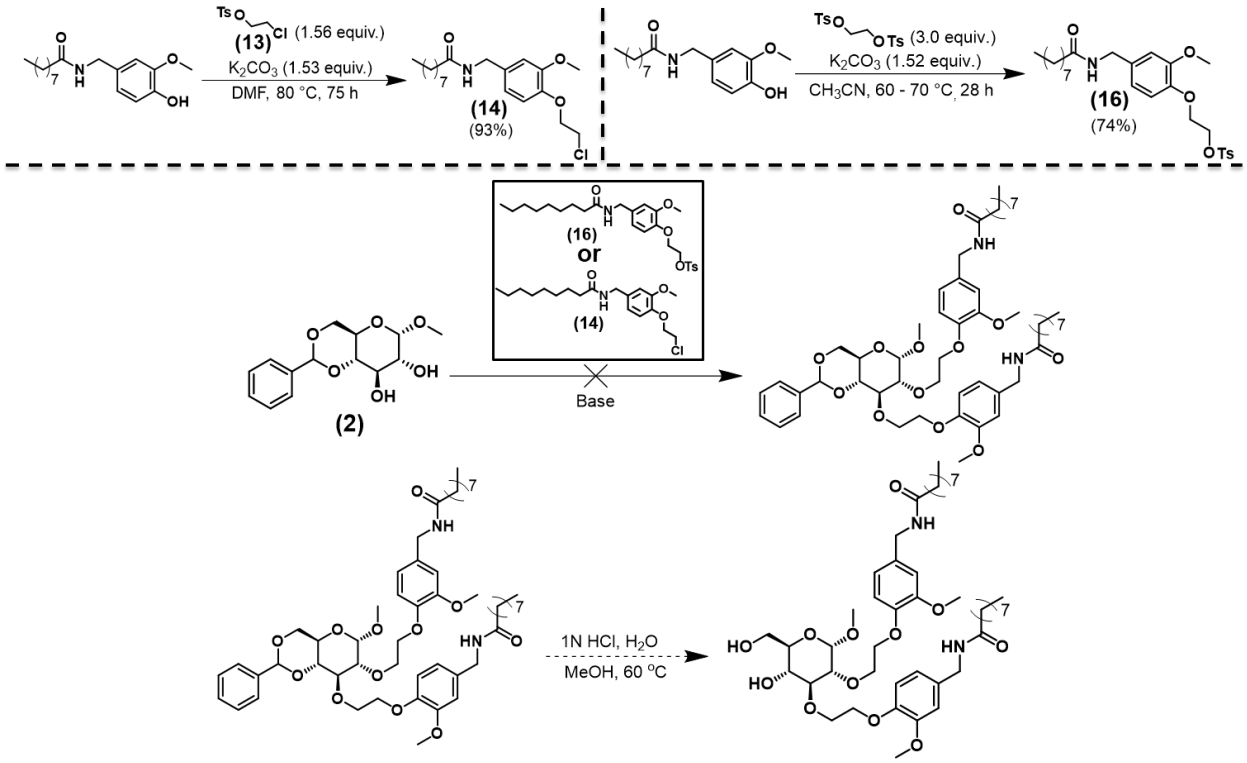

Figure 4-13. The attempted synthesis of the ether-conjugated pseudocapsaicin onto diol **2** *via* either the tosylate or the chloride did not produce the intended product while trying numerous conditions.

Subsequently, a modified approach was taken where the 2-tosylethyl-1-*O*-pseudocapsaicin (**16**) was synthesized and attempted to be combined with the benzylidene

glucopyranoside substrate under a number of conditions, as shown in Figure 4-13 and Table 4-2. Even when using dry (< 50 ppm H_2O) DMF as a solvent, the major products were **22** and **23**, as shown in Table 4-2. Adding 3-Å molecular sieves to a DMF reaction mixture to ensure that there was no water present with **16** still resulted in no product being recovered, and both **22** and **23** still appeared in the reaction mixture, as shown in Table 4-2. Attempting to carry out this reaction in a more sterically hindered yet polar solvent such as DMAc resulted in significant formation of the 1-acetylethyl-2-*O*-pseudocapsaicin (**25**) product and **23,** also shown in Table 4-2 and Figure 4-12. Thus, it became clear that any of the *N*,*N*-alkyl amide solvents were unsuitable to carry out this reaction.

Table 4-2. Conditions for the synthesis of methyl 2,3-*O*-bis(ethyl-*O*-pseudocapsaicin)-4,6-*O*-benzylidene-α-(D)-glucopyranoside.

Capsaicinoid	*Base*	*Solvent*	*T (°C)*	*Time (h)*	*Product*
14	NaH	DMF	0 to r.t.	66	**24**
14	NaH	THF	0 to r.t.	46	**24**
16	K_2CO_3	DMF/sieves	80 to 116	68	**22** + **23**
16	K_2CO_3	DMAc	50 o 100	48	**23** + **25**
16	K_2CO_3	Cyclohexanone	90 o 155	45	Intractable
16	K_2CO_3	CH_3CN	Reflux	48	Intractable
16	K_2CO_3/alumina	CH_3CN	Reflux	136	Intractable
16	K_2CO_3/18-c-6	Toluene	40 to 90	89	**23**[*]

[*]Trace direacted product detected by MALDI-TOF MS but not observable by ^{1}H-NMR spectroscopy
r.t. = room temperature

The last attempts to effect the etherification from **16** and the benzylidene glucopyranoside substrate involved the use of different solvents like cyclohexanone, acetonitrile (CH_3CN), and toluene, as shown in Table 4-2. However, none of these reactions produced any significant amount of product. The one exception was that a trace amount of product was detected in the system using toluene as a solvent and K_2CO_3/18-c-6 as a base after heating up to 90 °C. Based upon the work

of Maia and coworkers,[191] it was hypothesized that a less-polar solvent could increase the reaction rate because of a relatively nonpolar transition state of the tosylate leaving group and because of the expected decrease in solvation of the attacking alcohol relative to more-polar solvents. The product was detected by MALDI-TOF MS after recrystallization, but it was too low in intensity to be resolved by ^{1}H-NMR spectroscopy as **23** was the major product by far. It was not until later when performing the work in Chapter 2 that it was realized that the significant source of water in these reactions was likely from the diol (**2**) and not the solvents. For this project, **2** was merely stored in an ambient-pressure glass desiccator with KOH pellets, which contained 1.45% (14,500-ppm) H_2O by TGA when conducting the tests for the data shown in Table 2-1. Therefore, drying **2** in a vacuum oven prior to these reactions would likely improve the results. However, at the time, this route was viewed as not worth pursuing any further, so alternatives to the etherification route were investigated

Alternatively, the attempt was then made was to follow the original approach that Kornfield and coworkers[183] had attempted with their system to conjugate the pseudocapsaicin molecule to the glucopyranoside starting material *via* the thioether linkage, as shown in Figure 4-14. Thiol-ene click chemistry has been studied in the literature to a great extent by Hawker and coworkers and has been reported to be simple, efficient, regioselective, and able to occur in benign solvents.[192] Continuing from **14**, we synthesized ethyl-2-thiobenzoate-1-*O*-pseudocapsaicin (**18**) in reasonable yield and again with no column purification. The subsequent deprotection with hydrazonium chloride to form the 2-thioethyl-1-*O*-pseudocapsaicin (**19**) product also went relatively smoothly with no column purification and only a minor amount of disulfide by-product that was presumed to be inert for the next step.

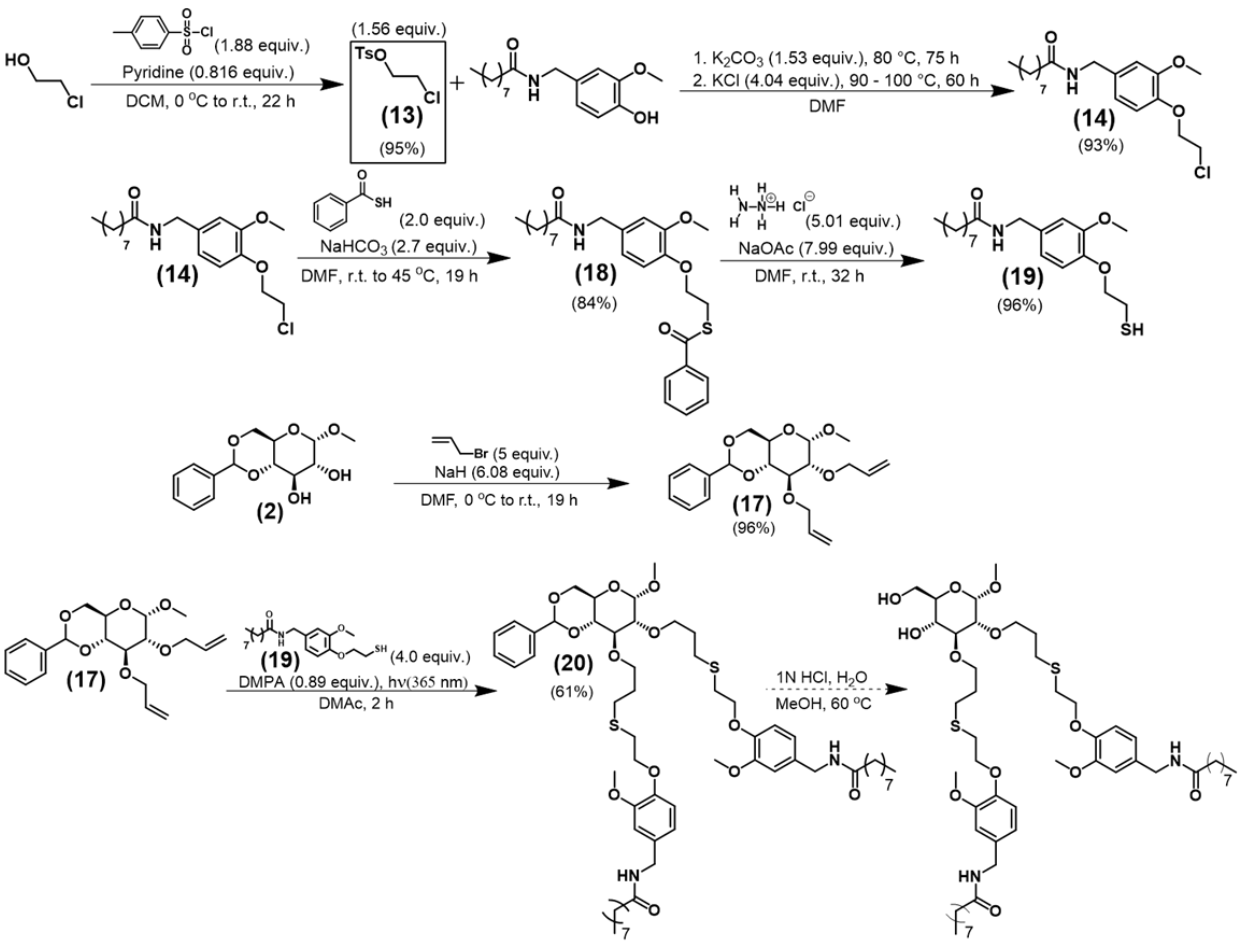

Figure 4-14. The attempted conjugation of pseudocapsaicin to the benzylidene glucose monomer *via* the thioether linkage reached an impasse when the proliferation of regioisomers for the thiol-ene click reaction hindered characterization.

The thiol-ene click step itself presented several challenges to obtaining product. After trying the reaction in ethanol and methanol where no product was recovered partly due to solubility problems, the reaction was done in DMAc at a relatively high concentration and with an excess of **19** where the product was recovered. However, as shown in Figures H-1 to H-10 (see Appendix H), the recovered product mixture was somewhat of a mess even after column purification, which made characterization by NMR spectroscopy difficult. There appeared to be some amount of disulfide eluted with the product (**20**) fraction that could not be separated as well. Because this

product took so long to characterize, further synthesis was tabled until full characterization could be carried out. In retrospect, the disulfide impurity was relatively minor and could probably have been ignored because it was likely to separate upon deprotection of the benzylidene group in the next step. However, there did appear to be some signals in the ^{13}C-NMR spectra indicating that possible regioisomers had formed (see Figures H-1 to H-10 in Appendix H). For the purposes of this project, this route might be refined further, but some of the criticisms of radical thiol-ene reactions as click chemistry seemed apparent with this system and could hinder progress going forward.[193]

4.4. Conclusion

While it would be fair to say that the findings of this project are only examples of conditions that cannot obtain product, there are two routes that are still viable. The original route to produce a carbonate linkage between pseudocapsaicin and the glucopyranoside substrate is still very plausible, and indeed likely, if the dimethylaniline base is distilled. In fact, this is probably the recommended route going forward. The other potentially viable route is the thiol-ene click method. However, the thiol-ene click step itself will require significant refining if it is to be used. Chloride leaving groups should be avoided when attempting to synthesize ether linkages with secondary alcohols at all costs.

5. THE REALIZATION, CHARACTERIZATION, AND MODELING OF A SOLVATOCHROMIC AND SOLVATOREDOX BISCARBONATE FOR PHOTOSENSING AND POTENTIAL PHOTOINDUCED ELECTRON TRANSFER INITIATION

5.1. Introduction

The synthesis and characterization of a solvatochromic carbonate for chemical-sensing applications and for photoinitiated polymerizations were explored. These properties could allow its use as both a highly sensitive probe for identification of organic solvents and as a transition metal-free photocatalyst in longer wavelengths of the visible spectrum than has been previously shown.[194,195] A longer-wavelength photocatalyst can improve existing free-radical and reversible addition-fragmentation chain transfer (RAFT) polymerization methods, as well as other radical-mediated reactions by using less energy than current UV-initiated reactions.[196] UV light can also lead to significant formation of side-products and alterations to nontargeted functional groups in some photoinitiated reactions and polymerizations.[193,195] This project emphasized both the synthesis and the characterization of the proposed anthraquinone carbonate. The molecular modeling provided insight into the solvatochromism, charge transfer, and electron transfer chemistry it possesses.

There exists a need for quick and inexpensive identification of organic solvents for qualitative analysis in the event of chemical spills and industrial accidents. One innovative method is the use of colorimetric sensor arrays as a kind of "optoelectronic nose" for the identification of unknown organic substances.[194] Rankin *et al.*[194] used a series of solvatochromic dyes embedded in polymer matrices to qualitatively identify unknown organic solvents using empirically derived

"difference maps" to correlate the color changes of the dyes based on the differing polarities of organic solvents. Dyes such as the one synthesized by Wang *et al.*[197] can show bathochromic shifts in their UV-VIS absorption spectra of 48 nm or more going from nonpolar to highly polar solvents. Indeed, such dyes are used to measure solvent polarity on scales such as the Kamlet-Taft α, β, and ET(30) scales based on the shift in the λ_{max}.[198] Dyes with a broader range of λ_{max} shifts with respect to solvent polarity could not only allow for more-precise polarity scales but also lead to more-straightforward and more-precise colorimetric sensors based on a single dye.

Recently, Zhang *et al.*[199] reported that 1,8-dihydroxyanthraquinone (1,8-DHA) can efficiently initiate free-radical and RAFT polymerizations in the presence of a redox mediator such as diphenyliodonium hexafluorophosphate, *N*-vinylcarbazole, or triethanolamine with blue light. In turn, a bis(1,8-DHA)carbonate might also possess the same electron transfer mechanism for photoinitiation described by the authors for 1,8-DHA and do so at a longer wavelength of visible light. The thiol-ene click reaction is one notable example where visible photoinitiation, as opposed to UV photoinitiation, could improve reaction efficiency by reducing the side reactions in polymer substrates.[193] Such side reactions are a point of debate, and some suggest that thiol-ene chemistry should be removed from the click category altogether.[193] Recent literature has shown that ruthenium and bismuth organometallic compounds can effectively catalyze thiol-ene click reactions approaching 100% conversion using blue LED and white light, respectively, with no evidence of side reactions.[195,196] Although this methodology bypasses the adverse effects of UV light, the use of rare, expensive, or toxic heavy metals in cross-linking or polymerization of thiol-ene systems will lead to deleterious effects in the polymer product, especially if its end use is a biomedical application.[195] The organic alternative extensively described in literature for thiol-ene click photoinitiators is eosin-Y (λ_{max} = 516 nm in phosphate-buffered saline [PBS]), which has

been shown to be as effective as the ruthenium system when photocatalyzing thiol-ene click reactions under blue LED.[195,200] The challenge to making radical organic photocatalysts more efficient under ambient light and in terms of energy consumption is to design photocatalysts that absorb at longer wavelengths of the visible spectrum. Using light at a longer wavelength should also allow better penetration of thick samples.

This chapter describes the synthesis and characterization of di(1,8-DHA)carbonate that is solvatochromic and, as a result, has tunable absorption wavelengths depending on the solvent. Although 1,8-DHA itself is not solvatochromic, its carbonate dimer has this characteristic. Both the extent of the solvatochromism and the origin of this compound's solvatochromism from solvents were evaluated using molecular modeling with DFT.

5.2. Experimental Details

5.2.1. Instrumentation

5.2.1.1. Nuclear Magnetic Resonance Spectroscopy

^{1}H, ^{13}C, HMBC, HMQC, and gCOSY spectra were recorded on a Varian Inova500 spectrometer (500 MHz for ^{1}H and 125 MHz for ^{13}C), a Varian NMRS500 (500 MHz for ^{1}H and 125 MHz for ^{13}C), a Mercury Plus spectrometer (300 MHz for ^{1}H and 70 MHz for ^{13}C), or a Varian Inova300 (300 MHz for ^{1}H and 70 MHz for ^{13}C). Chemical shifts were referenced to signals from residual protons of the deuterated solvents.

5.2.1.2. $CHCl_3$-Size-Exclusion Chromatography (SEC) Analysis

For some of the initial measurements on the attempted polymerizations, a Tosoh HLC-8320 EcoSEC system was applied with a two-column set of TOSOH Bioscience TSKgel columns (Super HM-M 6.0mm i.d. tme15 cm columns) and a guard column (Super H-H4μm). The system was equilibrated at 40 °C in chloroform (≥99.8% American Chemical Society [ACS] grade with

ethanol [EtOH] stabilizer), which served as the polymer solvent and eluent (flow rate set to 0.600 mL/min). The differential refractometer was calibrated with Polymer Laboratories, Inc. polystyrene standards (580 to 370,000 Da). Polymer solutions were prepared at a concentration of *ca.* 3 mg/mL, and an injection volume of 200 µL was used.

5.2.1.3. Ultraviolet–Visible Spectroscopy Analysis

Samples of the purified product were dissolved in DCM and DMAc to 0.010-mg/mL final concentration. The resulting solutions were transferred to quartz cuvettes with a 1-cm path length and run on the Shimadzu UV-2550 UV-VIS instrument with a scan from 250 to 800 nm.

5.2.1.4. Mass Spectrometry (Electrospray Ionization and Matrix-Assisted Laser Desorption/Ionization –Ttime-of-Flight Mass Spectrometry)

ESI samples were run with a Thermo Fisher Scientific Q Exactive Focus, and MALDI-TOF MS samples were run by the Chemsitry Mass Spectrometry facility on an Applied Biosystems (now called Sciex) Voyager-DE-STR.

5.2.2. Molecular Modeling

All calculations were performed on the Gaussian09 interface using the 6-31G(d) basis set at the B3LYP level of theory.[143] Solvation was applied using both the polarizable continuum model (PCM) and SMD. The empirical dispersion correction, gd3bj, was only applied to the binary system containing bis(1,8-DHA)carbonate. Time-dependent and frequency calculations were done only after optimization. Output files from the time-dependent calculations were worked up in Chemissian to identify the main transitions for each excitation, and the molecular orbital (MO) visualizations were exported. The MO diagrams of the bis(1,8-DHA)carbonate and the DMAc molecule were generated using GaussView 6.0. All isovalues were set to 0.04, and the half-width for the spectra was set to 0.160 eV.

5.2.3. Synthetic Procedures

5.2.3.1. Monobenzylation of 1,8-Dihydroxyanthraquinone

In a two-necked flask equipped with a reflux column, 1,8-DHA (2.0005 g, 8.328 mmol), K_2CO_3 (1.8281 g, 13.23 mmol), and benzyl chloride (1.82 mL, 15.8 mmol) were combined in 50 mL of DMF at 80 ^oC for 17 h. The reaction was monitored by TLC 50:50 hexanes to ethyl acetate.

After 17 h, the DMF was removed on a high-vacuum rotary evaporator. The mixture was then extracted in a separatory funnel with DCM and distilled water. After concentrating the organic phase, the solid mixture was separated by column chromatography using 70:30 chloroform to hexanes. The overall yield was 23%. The reaction is shown in Figure 5-1.

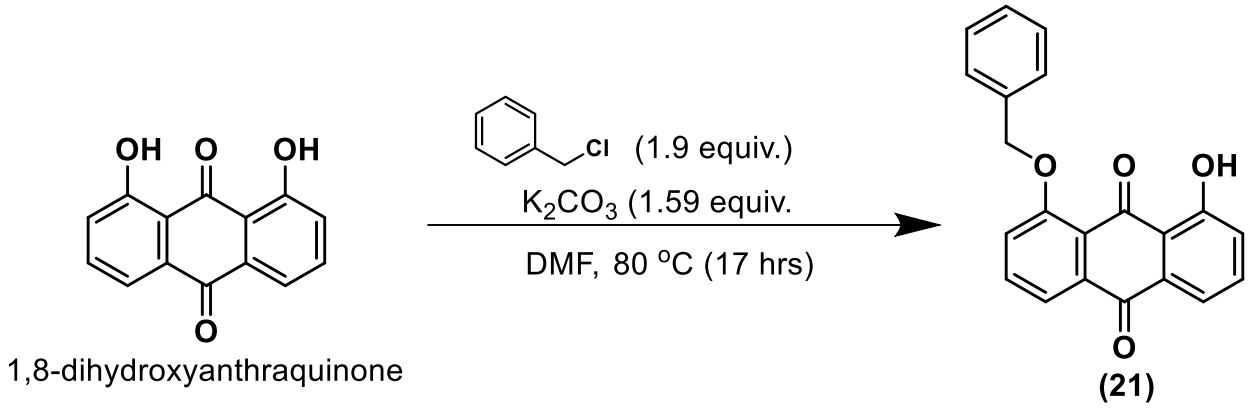

Figure 5-1. Synthesis of 1-benzyl-8-hydroxyanthraquinone (**21**).

^{1}H-NMR (500 MHz, DCM-d_2, δ, ppm): 13.01 (2H, s, -C_{tert}-CH-CH-CH-C(**O*H***)-C_{tert}-), 7.91 (1H, dd, *J* = 1 Hz, 8 Hz, -C_{tert} -(Bn-O)C-**C*H***-CH-CH-C_{tert}-), 7.75 – 7.70 (1H, m, -C_{tert}-**C*H***-CH-CH-C(OH)-C_{tert}-), 7.71 (1H, t, *J* = 9Hz, -C_{tert} -(Bn-O)C-CH-**C*H***-CH-C_{tert}-), 7.64 – 7.58 (3H, m, -C_{tert}-CH-**C*H***-CH-C(OH)-C_{tert}-, CH-$(CH)_2$-(**C*H***)$_2$-C_{tert}-CH_2-O-R_{Ar}), 7.45 (2H, t, *J* = 7 Hz, CH-(**C*H***)$_2$-$(CH)_2$-C_{tert}-CH_2-O-R_{Ar}), 7.40 (1H, d, *J* = 8 Hz, -

C_{tert} -(Bn-O)C-**C*H***-CH-CH-C_{tert}-), 7.37 (1H, t, *J* = 7 Hz), 7.27 (1H, dd, *J* = 8 Hz, 1 Hz, -C_{tert}-CH-CH-**C*H***-C(OH)-C_{tert}-), 5.29 (2H, s, CH-$(CH)_2$-$(CH)_2$-C_{tert}-**C*H*$_2$**-O-R_{Ar}). ^{13}C-NMR (125 MHz, CD_2Cl_2, δ, ppm): 189.13, 183.04, 162.93, 160.36, 136.74, 136.30, 136.20, 133.29, 129.17, 128.56, 127.57, 124.98, 121.63, 120.25, 119.05, 117.65, 71.64. (MALDI-TOF$^+$): [M+Na$^+$]: expected $C_{21}H_{14}O_4Na$: 353.0784 amu; found: 353.05 amu. HRMS (ESI$^-$): [M+Cl$^-$]: expected: $C_{21}H_{14}O_4Cl$: 365.0586 amu; found 365.0347 amu.

5.2.3.2. Synthesis of Bis(1-Benzyl-8-Hydroxy-Anthraquinone) Carbonate (22)

In a 10-mL Schlenk flask, **21** (0.2053 g, 0.6215 mmol) and TEA (0.10 mL, 0.72 mmol), were combined with diphosgene (0.0430 mL, 0.356 mmol) using a microsyringe in 5.0 mL of DCM for 49 h at room temperature. The reaction was quenched with 6 mL of concentrated sodium bicarbonate ($NaHCO_3$).

The reaction mixture was then extracted in a separatory funnel with distilled water before washing with a 0.045-M HCl solution. Because the reaction mixture had some sort of product—likeliest the intended dimer—precipitate out of solution on its own, the chosen workup method was to place the organic phase into a centrifuge tube for precipitation at 9,800 rpm for 10 min at 4 °C. The supernatant was decanted, leaving behind a solid paste-like substance. The rest of the solvent was allowed to evaporate.

The tan-colored powder that was left behind was not soluble in any organic solvents tested except 1,1,1,3,3,3-hexafluoro-propan-2-ol (HFIP) to a limited extent and trifluoroacetic acid (TFA). It was noticed later that the product reacted with TFA, turning from a bright yellow solution initially to a dark green solution, corresponding to the debenzylated dimer. The tan powder was soluble in HFIP without any noticeable reaction at a concentration of at least 2.25 mg/mL. A set of shims was successfully developed for the sample dissolved in HFIP-d_2. The

product was confirmed by dissolving it in HFIP and submitting for MALDI +/– mass spectrometry, which gave good results with the 2,4,6-trihydroxyacetophenone (THAP) matrix. The product was sluggish to ionize by ESI. The yield of this reaction, as shown in Figure 5-2, was 63%.

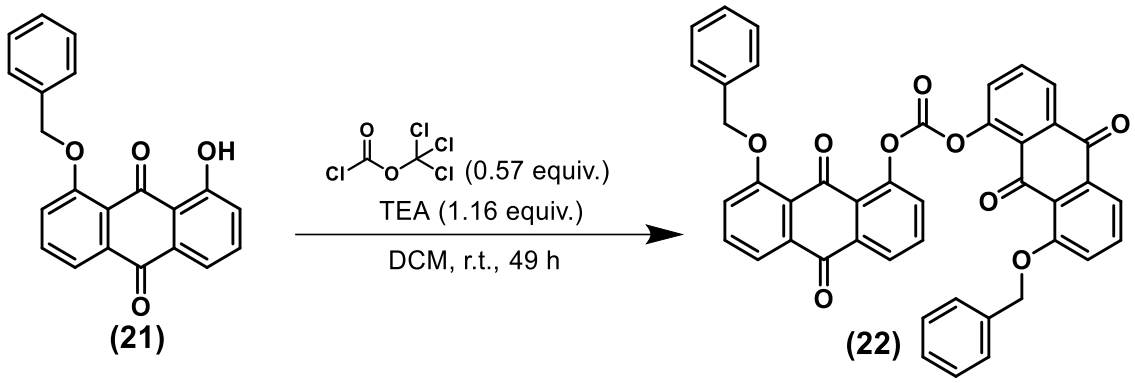

Figure 5-2. Synthesis of bis(1-benzyl-8-hydroxyanthraquinone)carbonate (**22**).

^{1}H-NMR (300 MHz, HFIP-d_2, δ, ppm): 8.17 (2H, ddd, J = 5 Hz, 4 Hz, 1 Hz, -C_{tert}-CH-CH-**C*H***-C(O-CO-O-$R_{Ar'}$)-C_{tert}-), 7.87 (2H, d, J = 8 Hz, -C_{tert}-**C*H***-CH-CH-C(O-CO-O-$R_{Ar'}$)-C_{tert}-) 7.75 (2H, td, J = 1 Hz, 8 Hz, 8 Hz, , -C_{tert}-CH-**C*H***-CH-C(O-CO-O-$R_{Ar'}$)-C_{tert}-), 7.71 – 7.64 (6H, m, -C_{tert}-(Bn-O)C-CH-CH-**C*H***-C_{tert}-, CH-$(CH)_2$-(**C*H***)$_2$-C_{tert}-CH_2-O-R_{Ar}), 7.55 (2H, t, J = 7 Hz, -C_{tert}-(Bn-O)C-CH-**C*H***-CH-C_{tert}-), 7.55 – 7.47 (4H, m, CH-(**C*H***)$_2$-$(CH)_2$-C_{tert}-CH_2-O-R_{Ar}), 7.47 – 7.33 (4H, m, **C*H***-$(CH)_2$-$(CH)_2$-C_{tert}-CH_2-O-R_{Ar}, -C_{tert}-(Bn-O)C-**C*H***-CH-CH-C_{tert}-), 5.35 (4H, s, CH-$(CH)_2$-$(CH)_2$-C_{tert}-**C*H*$_2$**-O-R_{Ar}). ^{13}C-NMR (70 MHz, HFIP-d_2, δ, ppm): 184.71, 183.38, 159.00, 151.79, 148.97, 135.67, 135.29, 134.88, 134.01 133.68, 130.06, 128.35, 128.05, 127.12, 125.95, 125.81, 121.99, 121.46, 120.13, 71.45. (MALDI-TOF$^+$ MS): [M+Na^+]: expected $C_{43}H_{26}O_9Na$: 709.1469 amu; found: 709.32 amu; [M+K^+]: expected $C_{43}H_{26}O_9K$: 725.1208 amu; found: 725.32 amu.

5.2.3.3. Synthesis of Bis(1,8-Dihydroxyanthraquinone)Carbonate (23)

A round-bottomed flask was charged with **22** (0.1021 g, 0.1487 mmol). Subsequently, TFA (4.0 mL, 52 mmol) was added, and the round-bottomed flask was capped with a septum and allowed to stir for 41 h. The progress of the reaction was monitored by TLC using 8:2 ($CHCl_3$:hexanes) as the eluent.

After 41 h, the reaction mixture was extracted with 10 mL of DCM three times into 40-mL, 0.91-M $NaHCO_3$. The organic phase was extracted again with 40 mL of distilled water. Then, the organic phase was vacuum-filtered over Celite using excess DCM before concentrating the organic phase down. The organic solid was then put under Schlenk vacuum at 60 °C overnight. Purification was achieved by recrystallizing the crude reaction mixture and vacuum-filtering one time in $CHCl_3$ and three times in DCM using a $CHCl_3$/dry ice bath, an acetone/dry ice bath, a –20-^oC freezer, and an ether/dry ice bath to cool the solvents and mixture for each recrystallization, respectively. No noticeable impurities were observed by ^{1}H-NMR except for some vacuum grease. The overall yield of the reaction, as displayed in Figure 5-3, was 13%.

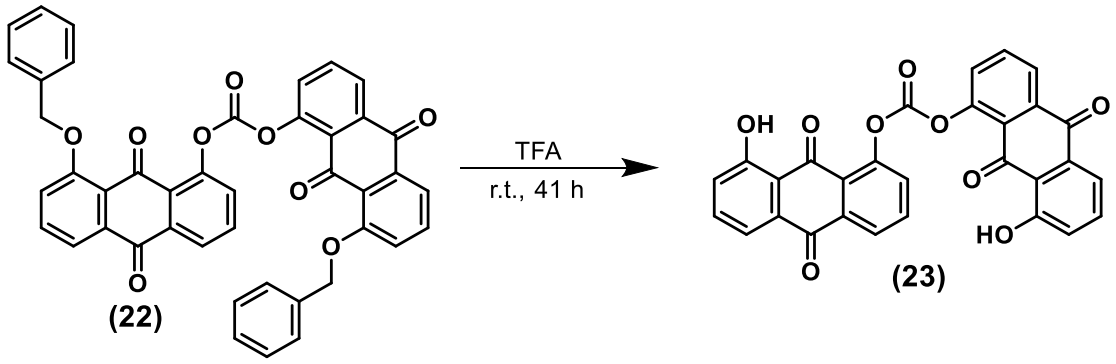

Figure 5-3. Synthesis of the bis(1,8-DHA)carbonate (**23**).

^{1}H-NMR (500 MHz, $CDCl_3$, δ, ppm): 12.62 (2H, s, -C_{tert}-**C**(**O*H***)-CH-CH-CH-C_{tert}-), 8.36 (2H, dd, *J* = 8 Hz, 1 Hz, -C_{tert}-CH-CH-**C*H***-C(O-CO-O-$R_{Ar'}$)-C_{tert}-), 7.93 (2H, t, *J* = 8 Hz, -C_{tert}-CH-**C*H***-CH-C(O-CO-O-$R_{Ar'}$)-C_{tert}-), 7.87 – 7.80 (4H, m, -C_{tert}-C(OH)-CH-CH-**C*H***-C_{tert}-, -C_{tert}-**C*H***-CH-CH-C(O-CO-O-$R_{Ar'}$)-C_{tert}-), 7.74 – 7.67 (2H, m, -C_{tert}-C(OH)-CH-**C*H***-CH-C_{tert}-), 7.35 (2H, dd, J = 8 Hz, 1 Hz, -C_{tert}-C(OH)-**C*H***-CH-CH-C_{tert}-). ^{13}C-NMR (125 MHz, $CDCl_3$, δ, ppm): Carbon spectra was not intense enough. UMMS (MALDI-TOF$^+$): [M+Na^+]: expected $C_{29}H_{14}O_9Na$: 529.0530 amu; found: 528.9753 amu; [M+K^+]: expected $C_{29}H_{14}O_9K$: 545.0269 amu; found: 545.7888 amu. (MALDI-TOF$^-$): [M+Cl^-]: expected $C_{29}H_{14}O_9Cl$: 541.0332 amu; found 540.9027 amu.

5.2.3.4. Synthesis of 1-*tert*-Butyldimethylsiloxy-8-Hydroxyanthraquinone (24)

In a 50-mL, round-bottomed flask, 1,8-DHA (0.5009 g, 2.085 mmol), and imidazole (0.1986 g, 2.917 mmol) were combined, and the flask was purged with $N_{2(g)}$. DCM (7.0 mL) was added to the reaction flask, which was then put on an ice bath. In a separate vial, *tert*-butyldimethylsilyl chloride (TBDMSCl) (0.4556 g, 3.023 mmol) was first purged with N_2 and dissolved in DCM (3.0 mL) before subsequently being added dropwise to the reaction. More DCM (2.5 mL) was used to rinse the TBDMSCl vial for a total of 12.5-mL DCM. The ice melted after 2 h. The reaction was monitored by TLC using 5:5 (hex:DCM) as the eluent for 40 h.

The solvent was removed from the reaction mixture *in vacuo* and extracted with 40 mL of distilled water three times with DCM (10 mL). The organic phase was collected and again extracted with distilled water (40 mL). The organic phase was concentrated and run on a flash column using hexanes:DCM as the eluent. The product fraction was concentrated and put under vacuum at 40 °C overnight. ^{1}H-NMR and ^{13}C-NMR were run on the yellow solid, confirming it to be the product in 69% yield. This reaction is shown in Figure 5-4.

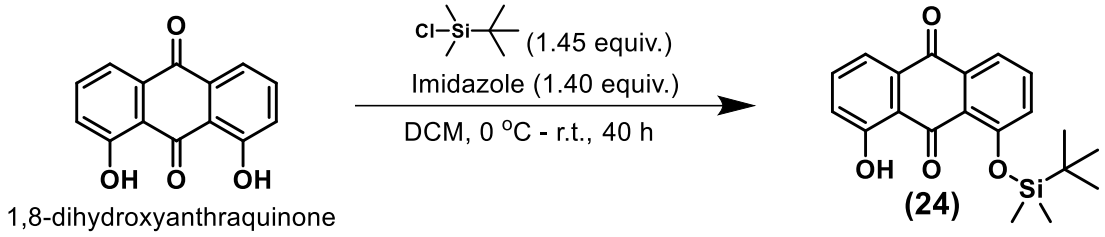

Figure 5-4. General procedure for synthesis of 1-*tert*-butyldimethylsilyloxy-8-hydroxyanthraquinone (**24**).

^{1}H-NMR (500 MHz, $CDCl_3$, δ, ppm): 13.07 (1H, s, -C_{tert}-**C**(**O*H***)-CH-CH-CH-C_{tert}-), 7.96 (1H, ddd, *J* = 8 Hz, 1 Hz, 1 Hz, -C_{tert}-C(OTBS)-CH-CH-**C*H***-C_{tert}-), 7.77 (1H, dt, *J* = 7 Hz, 1 Hz, 1 Hz, -C_{tert}-C(OH)-CH-CH-**C*H***-C_{tert}-), 7.62 (2H, m, -C_{tert}-C(OTBS)-CH-**C*H***-CH-C_{tert}-, -C_{tert}-C(OH)-CH-**C*H***-CH-C_{tert}-), 7.28 (1H, dt, *J* = 8 Hz, 1 Hz, 1 Hz, -C_{tert}-C(OTBS)-**C*H***-CH-CH-C_{tert}-), 7.23 (1H, ddd, *J* = 1 Hz, 1 Hz, 8 Hz, -C_{tert}-C(OH)-**C*H***-CH-CH-C_{tert}-), 1.09 (9H, s, R_{Ar}-O-Si$(CH_3)_2$(C_{tert})-(**C*H*$_3$**)$_3$), 0.30 (6H, s, R_{Ar}-O-Si(**C*H*$_3$**)$_2$(C_{tert})-$(CH_3)_3$). ^{13}C-NMR (125 MHz, $CDCl_3$, δ, ppm): 188.84, 182.91, 162.63, 157.35, 135.89, 135.72, 135.24, 133.13, 128.55, 124.63, 123.20, 121.30, 118.89, 117.17, 25.97, 18.71, -3.89. UMMS (ESI^+): [M+H^+]: expected $C_{21}H_{15}O_4$: 355.1360 amu; found: 355.17 amu. UMMS (ESI^-): [M+e^-]: expected: $C_{21}H_{14}O_4$: 354.1293 amu; found 354.34 amu. UMMS (MALDI-TOF^+) : [M+H^+]: expected $C_{21}H_{15}O_4$: 355.1360 amu; found 355.6534 amu.

5.2.3.5. Synthesis of Di(1-*tert*-Butyldimethylsiloxy-8-Hydroxyanthraquinone)Carbonate

In a 10-mL Schlenk flask, 1-*tert*-butyldimethylsilyl-8-hydroxyanthraquinone (0.1015 g, 0.2863 mmol) was purged with $N_{2(g)}$ before dissolving in DCM (2.5 mL). Then, TEA (0.050 mL, 0.36 mmol) was added. After putting the reaction on an ice bath for 30 min, diphosgene (0.01140 mL, 0.09445 mmol) was added dropwise over the course of 2 min, and the reaction was taken off ice and allowed to stir for 49 h.

After 49 h, the reaction was quenched with 2 mL of saturated $NaHCO_3$ solution. Then, the reaction mixture was extracted twice with DCM (10 mL) into distilled water (25 mL). The organic phase was collected and again extracted in an 0.11-M K_2CO_3 solution (25 mL). Then, the organic phase was collected and concentrated to a viscous oil. The reaction mixture was then dissolved in DCM and condensed onto 0.5 g of silica gel before being loaded onto a 5-g empty load column and run on a 12-g flash column using the CombiFlash instrument. The eluent was DCM:hexanes, but was changed to DCM:acetone later in the run. Upon adding the acetone eluent as a gradient, there was a stark color change on the column, and a darker purple-violet band appeared to elute very quickly, while the rest of the product spot eluted slowly, but slowly changed to a darker purple-violet color, and what was a thin band began to smear and expand. TLC indicated that there was a contaminant in all collected product fractions that could not be identified spectroscopically.

5.3. Results and Discussion

Initially, this project sought to find an alternative polyphenol compound to use as a substitute for BPA in polycarbonates along with other work published recently.[201] One of the target candidates was aloe-emodin, a natural product used in traditional Chinese medicine.[202,203] However, aloe-emodin's high cost led to the testing of a significantly cheaper model compound called 1,8-DHA that only differs from aloe-emodin by the absence of the benzylic alcohol moiety in the three-position.

Upon screening suitable polymerization solvents, this anthraquinone was apparently only soluble in HFIP and 1-chloronaphthalene at *ca.* 100 mg/mL. 1,8-DHA was fairly soluble in chloroform, 1,4-dioxane, and NMP, but only up to 50 to 60 mg/mL. Solvents like dibenzyl ether, DMAc, acetonitrile, and pyridine all required slightly more solvent than chloroform, dioxane, or

NMP. Acetone, methyl ethyl ketone, toluene, carbon tetrachloride, and glycerol were all poor solvents.

Numerous polymerization screenings were attempted. First, 1,8-DHA was attempted to be polymerized at room temperature and 50 °C in chloroform with TEA and *p*-nitrophenyl chloroformate, ethyl chloroformate, and carbonyldiimidazole, but none of these reactions produced any polymer as detected by $CHCl_3$-SEC. Then, polymerization was attempted by combining diphosgene and triphosgene with 1,8-DHA in the presence of stoichiometric amounts of TEA, as shown in Figure 5-5 with reaction times of 3 h, 15 h, 24 h, and 48 h. An insoluble precipitate formed (**25**), which was attempted to be diluted and run on a $CHCl_3$-SEC, but the oligomer/polymer peak was below the calibration range. Later, polymerizations were attempted in pyridine because the condensation product (**26**) appeared slightly more soluble. A sample of **26** was obtained and able to be characterized by MALDI-TOF MS using 2-(4-hydroxyphenylazo)benzoic acid (HABA) as a matrix, indicating that the average degree of polymerization was a pentamer, as shown in Figure I-1 (Appendix I).

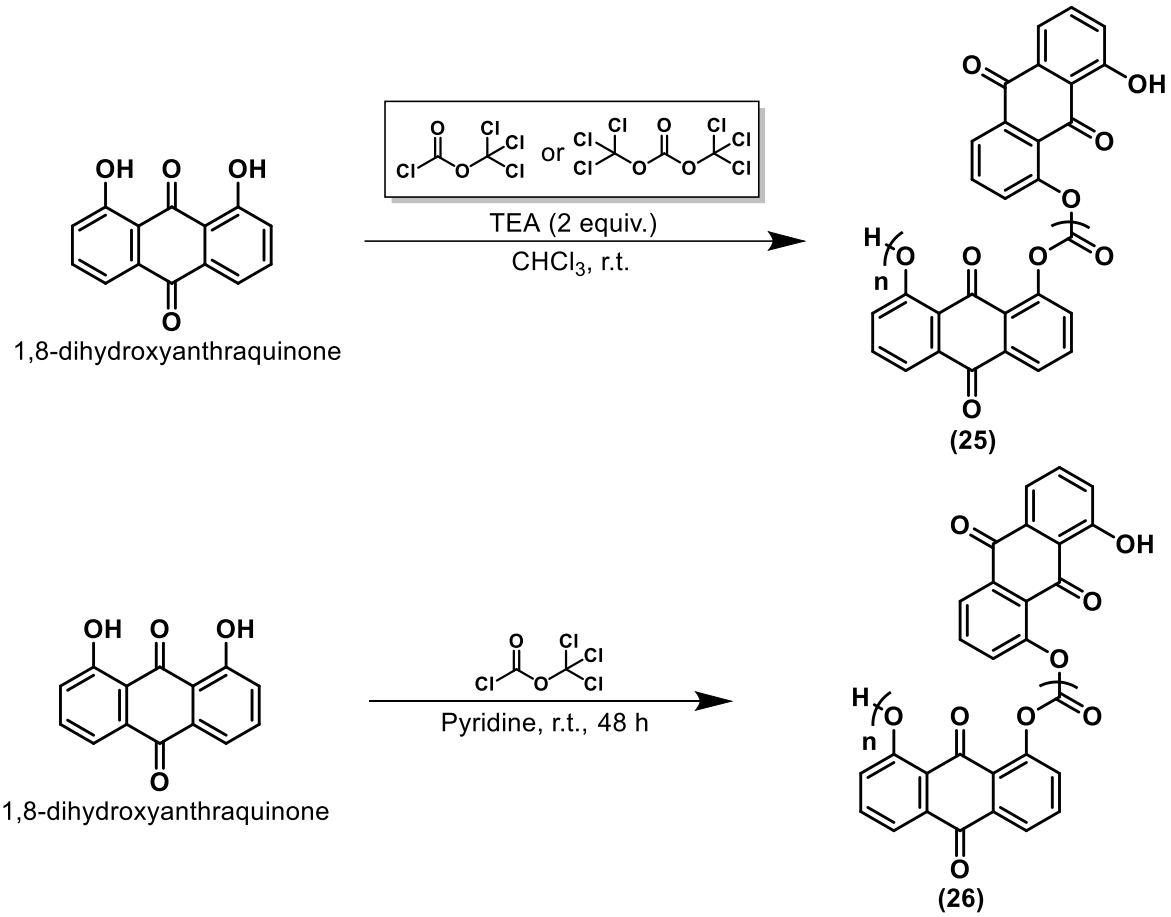

Figure 5-5. Attempted syntheses of the polymer **25** at 3 h, 15 h, 24 h, and 48 h for the reactions in $CHCl_3$ while the reactions done in pyridine were done at 48 h to form **26**.

Despite being low-molar-mass oligomers, an unusual characteristic was noticed about both systems. As shown in Figures 5-6 and 5-7, they appeared to show drastic color changes in multiple solvents. Most notably, **25** displayed a significant a color shift going from red in water to a dark blue in DMSO. This prompted further investigation as to the origin of this solvatochromic effect. However, because these species were oligomers at best, we hypothesized that it would be easier to characterize a small-molecule dimer rather than work with these species that had sluggish solubility forming only suspensions.

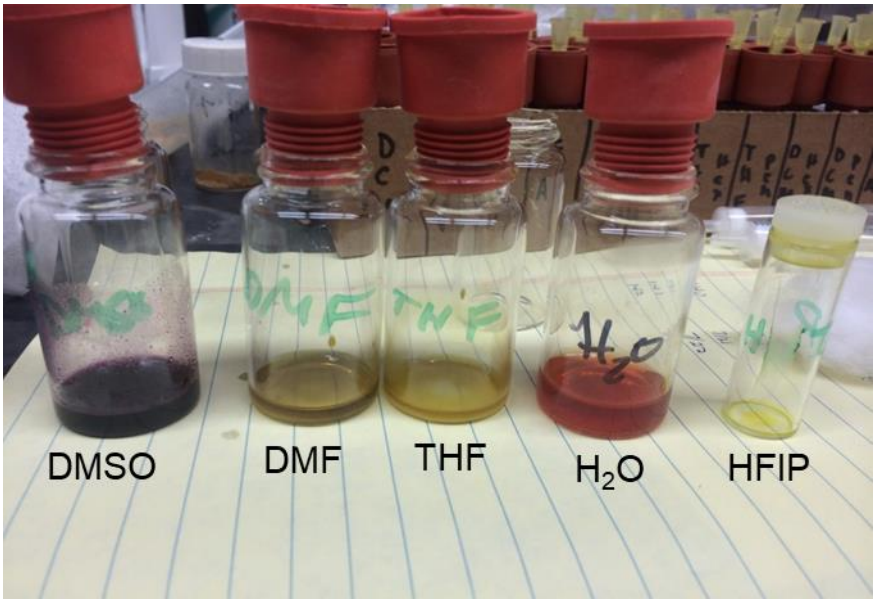

Figure 5-6. Oligomer **25** shows remarkable solvatochromic effect as a suspension in various solvents.

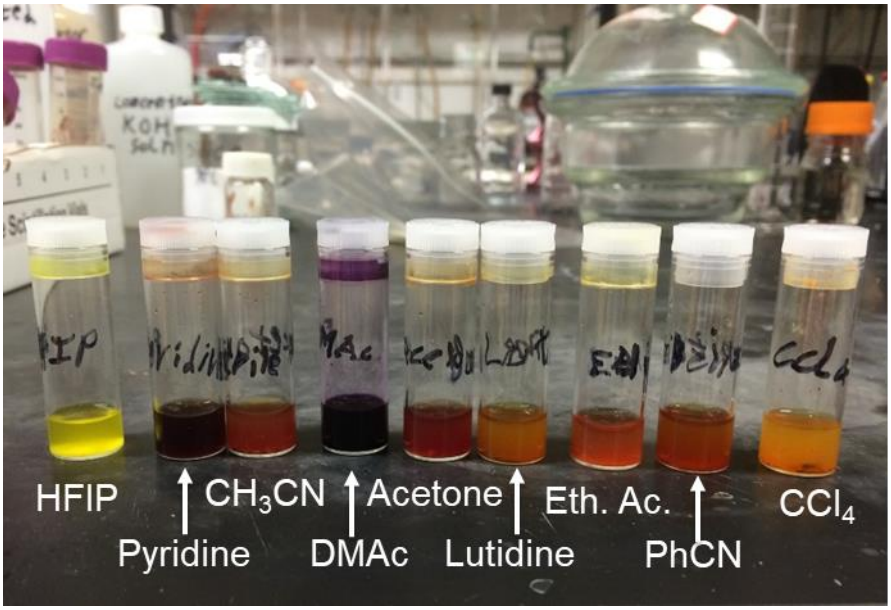

Figure 5-7. Oligomer **26** shows remarkable solvatochromic effect as a suspension in various solvents.

Therefore, we set out to synthesize a dimer carbonate first by utilizing a benzyl-protecting group. As shown in Figure 5-8, a benzyl-protected 1-benzyloxy-8-hydroxyanthraquinone (**21**) was

obtained in a rather low yield. The subsequent reaction of this species with diphosgene yielded the benzylated dimer carbonate (**22**) in a better yield. However, this precursor proved very difficult to characterize as it was even more insoluble in most solvents than the 1,8-DHA starting material. The only methods for characterization that were possible were NMR in HFIP-d_2, where a new shim set had to be developed and by MALDI-TOF MS (see Appendix I). By accident, it was observed that the benzylated dimer could be deprotected when stirred in TFA while leaving the carbonate linkage mostly intact. However, workup by recrystallization of the resulting dimer carbonate product also proved difficult, resulting in a relatively low yield.

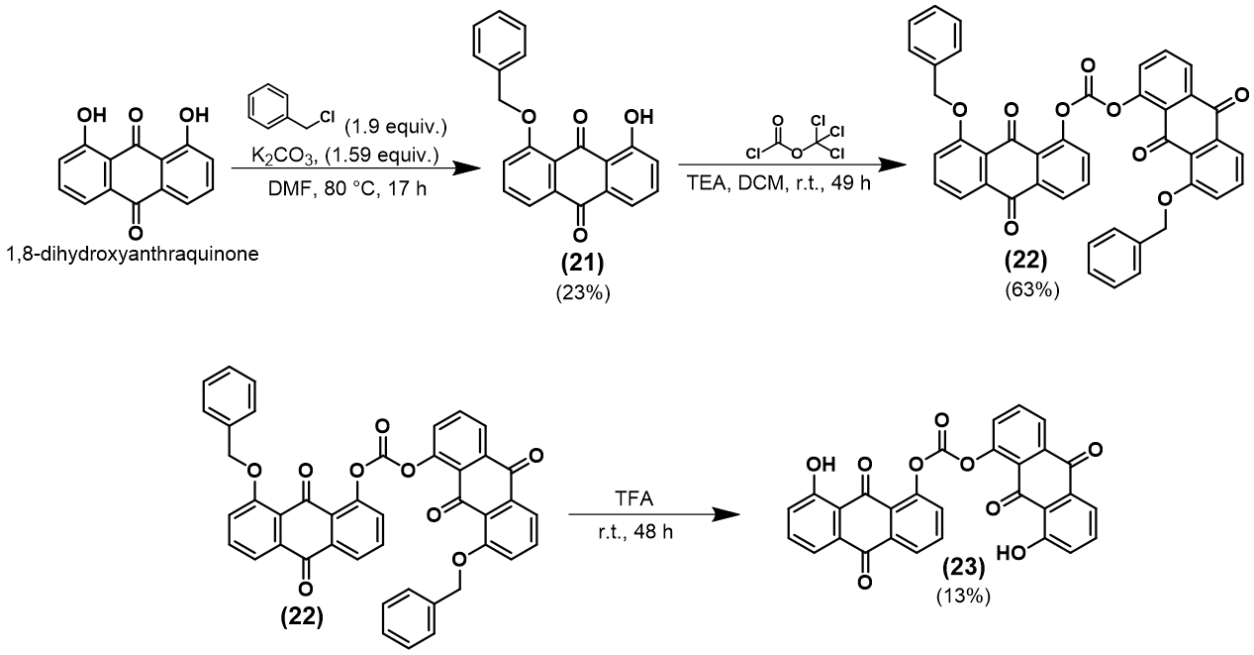

Figure 5-8. The first attempted synthesis of the bis(1,8-DHA)carbonate product (**23**) was difficult to carry out because of the significant insolubility of the benzylated dimer intermediate that made characterization and workup of the final step difficult.

Because of the solubility problems that this original benzylation route imparted, we decided to pursue a different protecting group that improved the solubility of the protected dimer. A route

consisting of a *tert*-butyl dimethylsilyl (TBDMS)–protecting group was attempted, as shown in Figure 5-9. The initial protection step proceeded smoothly and in a decent yield of product **24**. The subsequent dimerization step using diphosgene had an unexpected problem upon workup. During column purification, a gradient solvent eluent was used with DCM and acetone. As soon as the first solvent fraction containing acetone was added to the column, a color change of the expected product band took place from initially a yellow-orange to a darker red-violet, and the eluting product band smeared up and down the column. An unidentifiable compound was in all product fractions, and the NMR instrument was unusually hard to shim for samples of this product. Additional reactions were planned but not attempted using only DCM as the column eluent for separation, which was likely polar enough to effect the separation on a reasonable time scale.

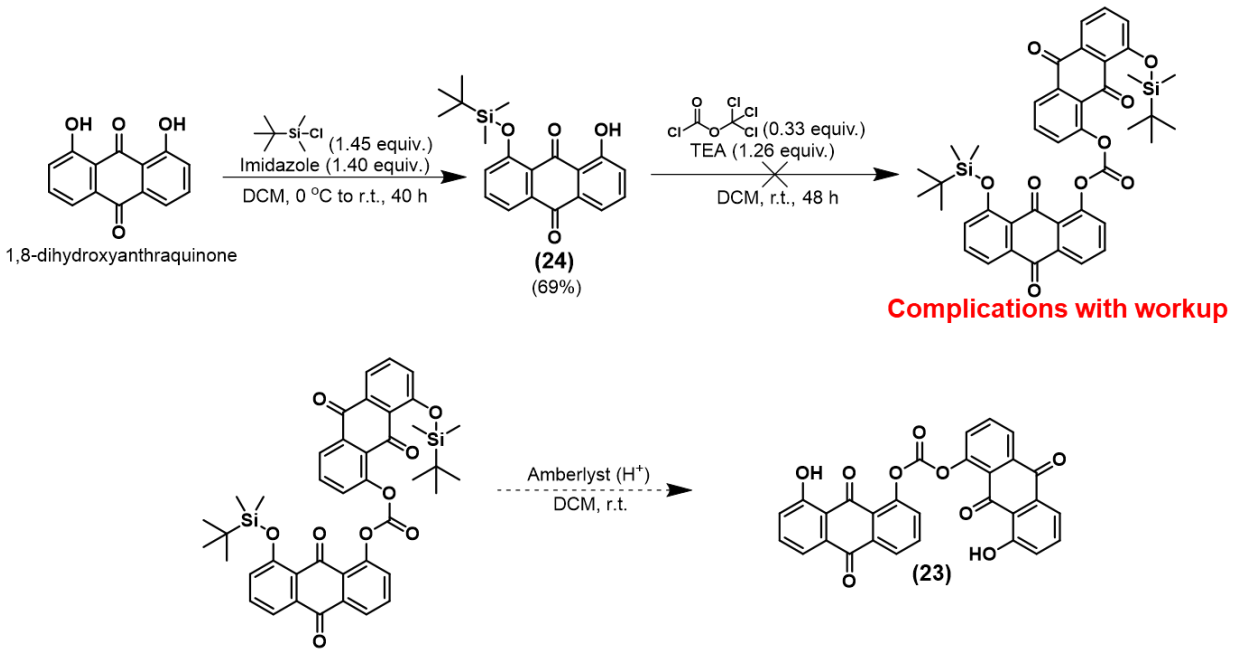

Figure 5-9. The second attempted synthesis of **23** made use of the TBDMS-protecting group to help solubilize the dimer intermediate. Upon reacting **24** with diphosgene to form the dimer carbonate, a chemical transformation appeared to have occurred when trying to separate the product by column chromatography.

What little of the **23** product was obtained from the first synthetic route in Figure 5-9 was dissolved in two solvents at the same concentration. As shown in Figure 5-10, the colors of the two solutions did differ significantly. These two solutions were run on UV-VIS, which surprisingly exhibited a very low molar extinction coefficient for both solutions ($\varepsilon_{DCM} = 3.5\times10^3$ $M^{-1}\bullet cm^{-1}$ and $\varepsilon_{DMAc} = 3.8\times10^3$ $M^{-1}\bullet$ cm^{-1}), as shown in Figure 5-11. However, what Figure 5-11 also shows for the UV-VIS spectrum of the two solutions is a bathochromic, redshift in the λ_{max} of more than 144 nm. This result is remarkable given that many solvatochromic shifts in the UV-VIS spectra of various conjugated, organic, dye molecules were reported on a scale of 48 to 64 nm.[197,204] Large, positive solvatochromic effects in these dyes were reported to be the result of intramolecular charge transfer character between the ground and excited states of the π-π^* transitions.[197,204] These types of effects have been well documented in the literature, so it became clear that there was some other phenomenon causing this dramatic shift.[205]

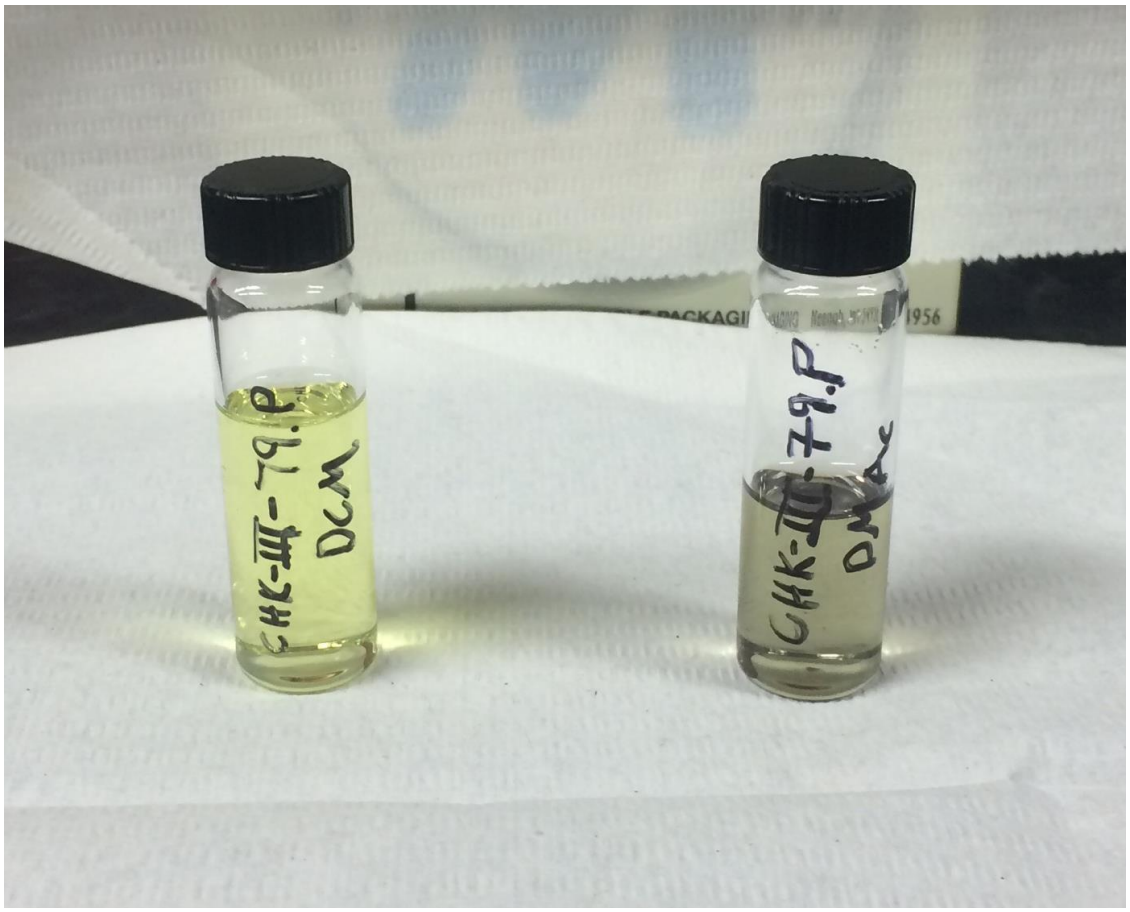

Figure 5-10. Solutions from **23** in DCM (left) and DMAc (right). The purple color of the DMAc solution did appear to fade with time.

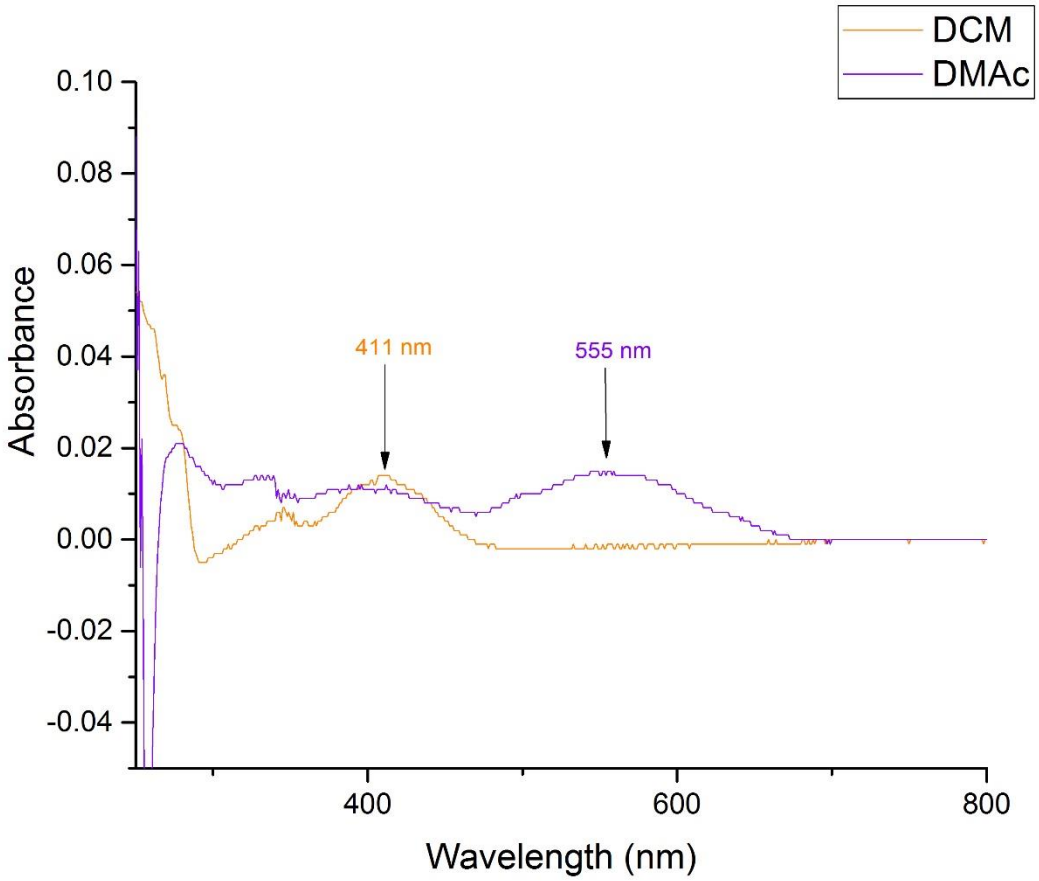

Figure 5-11. The preliminary UV-VIS spectrum taken of **23** shows λ_{max} of 411 nm in DCM (ε_{DCM} = 3.5×10^3 $M^{-1}\bullet cm^{-1}$) and 555 nm in DMAc (ε_{DMAc} = 3.8×10^3 $M^{-1}\bullet$ cm^{-1}).

First, it was worth examining the monomer 1,8-DHA to see if there was a similar effect between the two solvents. As shown in Figure 5-12, there is a solvatochromic change between the two, but it was not as dramatic or as intense as with **23**. The 1,8-DHA samples were dissolved at similar concentration as in Figure 5-10 (0.01 mg/mL). Moreover, Xiao, Stenzel, and coworkers reported on the intramolecular charge transfer nature of 1,8-DHA, but did not report any solvatochromic effects.[199] Thus, it became clear that a more-in-depth analysis was needed of **23** in order to determine the origin of this phenomenon.

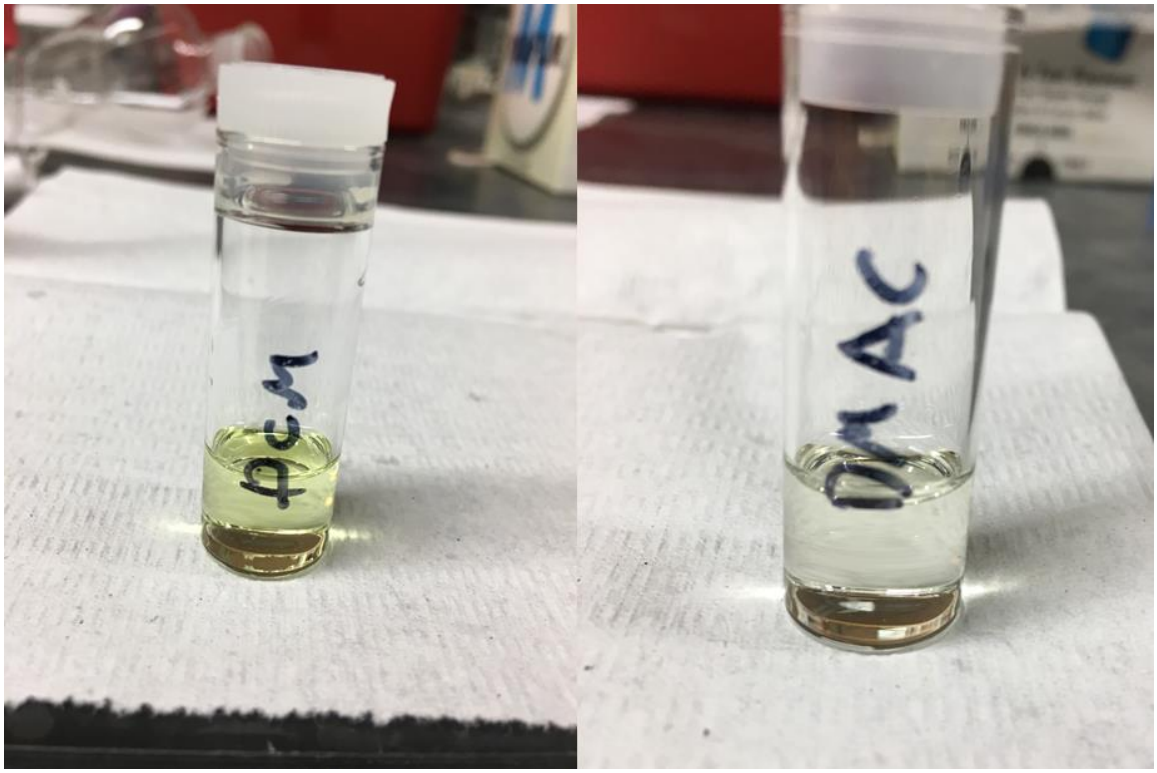

Figure 5-12. Dissolving 1,8-DHA into DCM (left) and DMAc (right) showed almost no change in color except the DMAc solution appears less intense.

Molecular modeling was performed using the DFT with the B3LYP method on **23** utilizing the 6-31G* basis set. First, **23** was geometrically optimized in the gas phase as a ground-state singlet. Then, a time-dependent calculation was performed for 50 excitations. The predicted UV-VIS spectrum for this calculation is shown in Figure 5-13. The λ_{max} at 411 nm correlated almost precisely with that of the carbonate observed in DCM and was indicated to be mostly from the excitation from the highest occupied molecular orbital (HOMO) to the lowest unoccupied molecular orbital (LUMO)+1. This excitation did indeed correlate to an intramolecular charge transfer pattern in that the electron density was localized to one part of an anthraquinone ring in

the ground state and was delocalized across both π systems in the excited state. However, the question then arose as to how this would change with solvation in a solvent like DMAc.

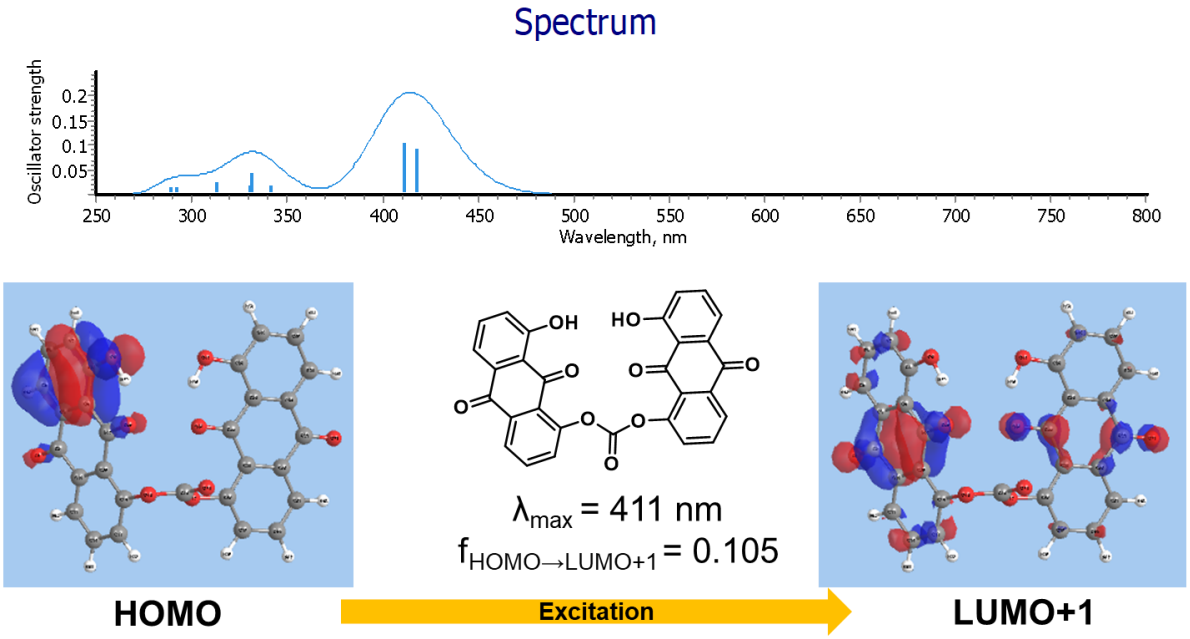

Figure 5-13. A time-dependent DFT simulation on an optimized ground-state molecule of **23** using the uB3LYP level of theory in the gas phase, indicating a transition from the HOMO to the LUMO+1 occurring at 411 nm and matching the experimental spectrum in DCM.

An optimization of **23** was performed in an implicit DMAc solvation shell using the PCM solvation model. The subsequent time-dependent calculation for 50 excited states in DMAc-PCM, with all other parameters the same, gave rise to the spectrum shown in Figure 5-14. The λ_{max} shifted only slightly, going from 411 nm in the gas phase (which should have closely resembled that of a nonpolar solvent) to 418 nm with an implicit solvation shell of DMAc. Although the orbital structures of the excitation did appear to have changed, it was nowhere near the shift that was observed experimentally. Thus, other possible electronic states of this carbonate were screened.

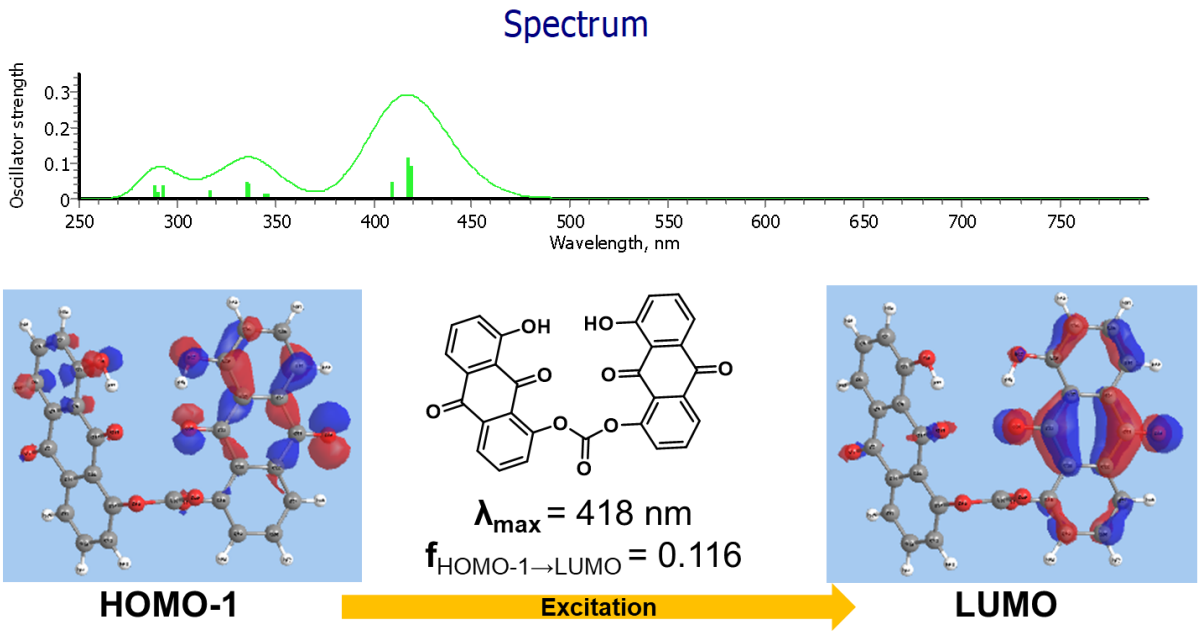

Figure 5-14. A time-dependent simulation of an optimized molecule of the ground state of **23** using the uB3LYP method in DMAc (PCM model) indicated that a transition occurred from the HOMO-1 to the LUMO at 418 nm, only a slight shift from the gas phase.

Upon modeling other electronic states, a striking resemblance to the observed UV-VIS spectrum was found when a time-dependent calculation was performed on the doublet radical anion state of the carbonate in the gas phase, as shown in Figure 5-15. This excitation was indicated to occur from the HOMO to the LUMO+3 and appeared to be an n-π^* transition. The λ_{max} was predicted to be between 528 nm (shown) and 519 nm, which was close but still a bit off from the observed λ_{max} at 555 nm in DMAc. This could potentially have been remedied by adding an implicit solvation shell. But before investigating that, it was worth trying to determine where any electrons could possibly come from in order to induce a radical anion state.

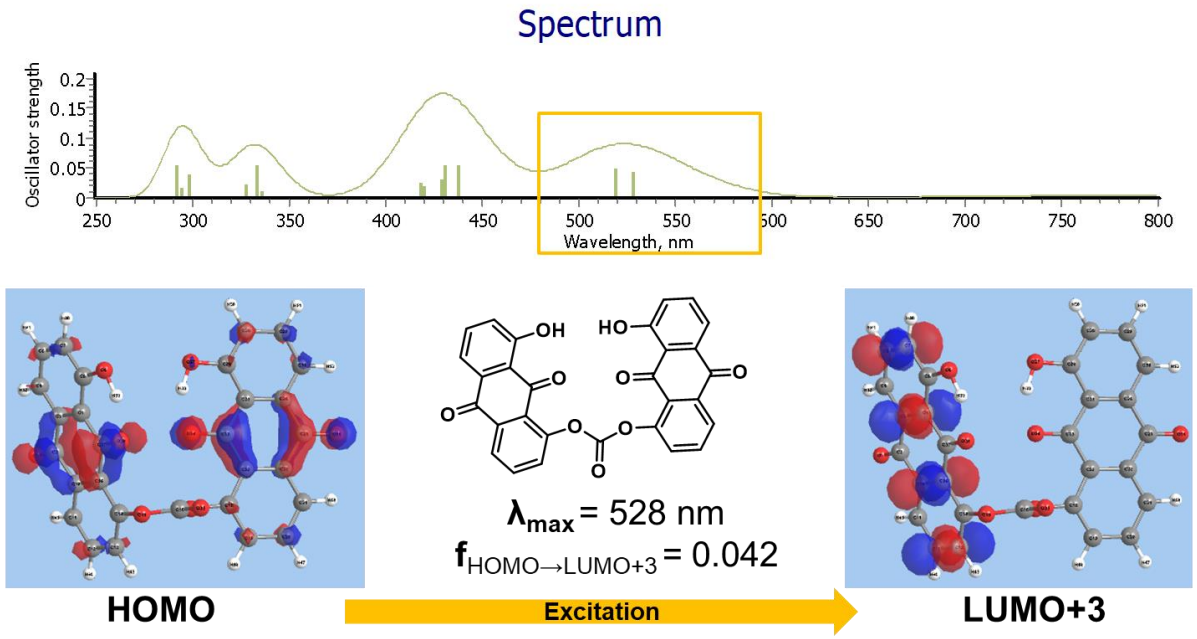

Figure 5-15. A time-dependent simulation of an optimized molecule of the radical anion form of **23** using the uB3LYP method in the gas phase indicated that a transition occurred from the HOMO to the LUMO+3 at 528 nm and 519 nm, approximating the observed spectrum in DMAc.

Anthraquinones are generally known to undergo sequential one-electron transfers or reductions in aprotic solvents (or high-pH aqueous solutions) when an electric potential is applied in cyclic voltammetry (CV).[206,207] In protic solvents, a two-electron wave is commonly observed.[206] These reduced states of anthraquinones are used to produce hydrogen peroxide on an industrial scale in the presence of a proton source such as water.[206,208,209] However, these reports are all with induced, external potentials, and 1,8-DHA is reported to have a reduction potential of –1.05 V versus a ferrocene/ferrocenium redox couple in acetonitrile.[209] There are numerous examples of photoinduced electron transfer (PET) occurring between highly conjugated fluorophores and readily oxidizable species like amines and, in some cases, alcohols.[210,211] The way this process is typically described is that the excited-state species can either act as an acceptor (A^*) from an electron donor (D) if the acceptor's HOMO is lower than the donor's HOMO upon

excitation to A^* or; can be the donor (D^*) if its LUMO is higher than the acceptor molecule's (A's) LUMO.[211,212] Because the radical anion was indicated by DFT; the former case is shown in Figure 5-16. The electron donor becomes a radical cation while the electron acceptor becomes the radical anion, depicted as DMAc and **23**, respectively. However, the question remains as to what precisely the identity of the donor species present in solution could be.

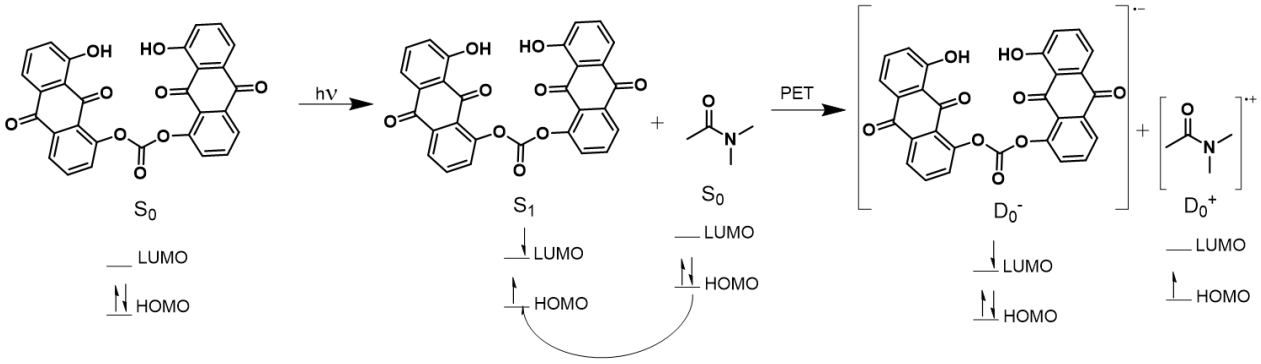

Figure 5-16. Description of how a one-electron PET mechanism might occur with DMAc if the HOMO of DMAc is higher than the HOMO of **23** when it is excited by light.

The first possibility, as of this writing, is that the DMAc molecule could be serving as the electron donor. On its face, this seems unlikely as the reports of DMAc as a radical cation are sparse, but there are two reports of DMAc radical cations forming upon excitation by ^{60}Co γ-ray and X-ray (50 keV) radiation.[213-215] However, turning to molecular modeling once again provided a surprising result. The structures of **23** and DMAc were optimized using the uB3LYP method separately in DMAc with the SMD to more accurately predict the energetics by accounting for the nonelectrostatic terms. Then, using all of the same parameters from optimization, frequency calculations were performed on all relevant species to obtain their Gibbs free energies. As shown in the plot in Figure 5-17, the free energy transition from the singlet excited state to the radical

anion state of the carbonate was downhill by –144.6 kcal/mol. On the other hand, the DMAc molecule had a relatively high endergonic transition that was uphill by +135.6 kcal/mol, as expected. However, the lower energy of the radical anion state outweighed that of the radical cation formation for a net ΔG of –9.0 kcal/mol, indicating that this transformation happened spontaneously and was thermodynamically favored.

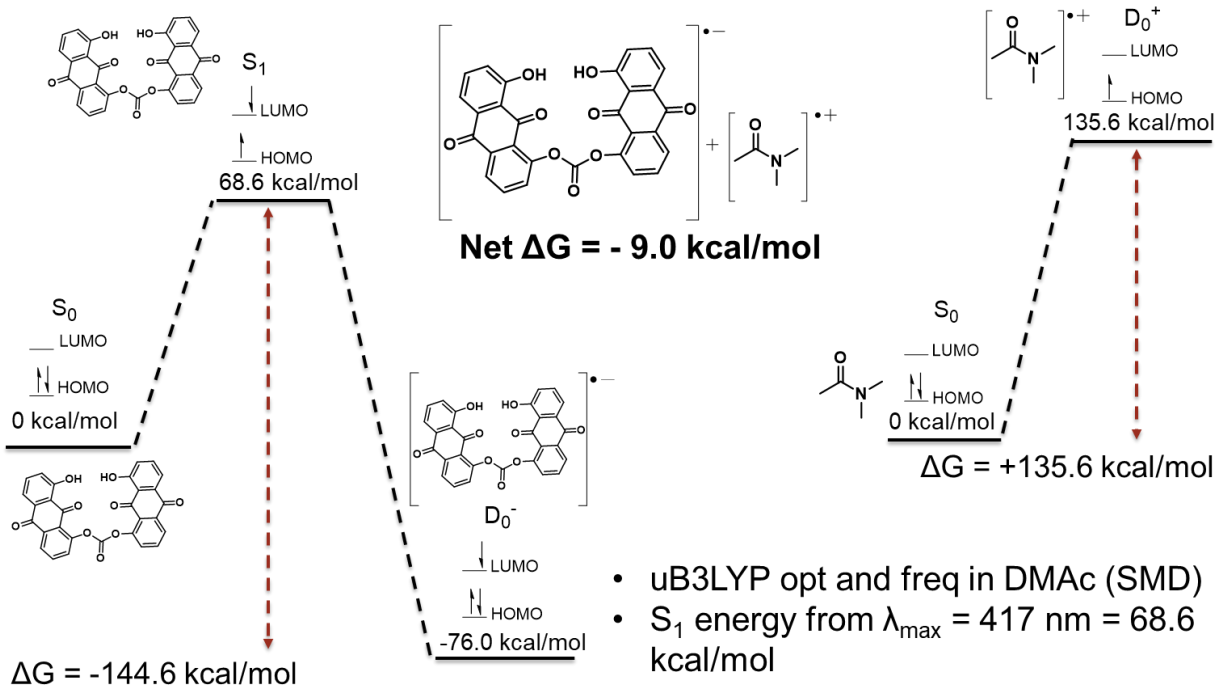

Figure 5-17. Gibbs free energies for hypothesized states of **23** and DMAc molecule suggest that a single electron transfer from DMAc to the excited carbonate species is thermodynamically favorable by 9.0 kcal/mol. The ground states of both the carbonate and DMAc were arbitrarily normalized to zero. The excited-state energy was taken from the λ_{max} predicted by a time-dependent calculation with the same parameters (see Appendix I).

However, there are some assumptions built into this description given the fact that this system is a multireference problem.[211] First, the two species were modeled isolated from each other because basis sets in DFT and higher levels of theory will generate MOs for the whole system

based upon a linear combination of all atomic orbitals (LCAO), present which may or may not be indicative of the actual system.[216] Thus, what is not being accounted for in this case is the lowering of the energy of the system based upon the pairing of the two ions together rather than being optimized as if they were infinitely apart. Thus, the expected error here would be that this result underestimates the negativity of the Gibbs free energy. Second, the energy value from the excited singlet (S_1) of the carbonate was derived from the λ_{max} of the ground state at 417 nm, which was calculated separately by optimizing the molecule with the SMD-DMAc parameter and then performing a time-dependent calculation to obtain the lowest energy excitation in DMAc (see Appendix I). This may not be valid if there is a lower energy excitation. There does appear to be an electronic excitation in the near IR with a considerable oscillator strength at 3087 nm (see Appendix I). However, the oscillator strength of this transition is significantly reduced with solvation (also in Appendix I). Additionally, the electron transfer could occur after some degree of geometric relaxation in the excited state. Current efforts are underway to optimize an excited-state form of the carbonate, but this has proven difficult because the MOs have a tendency to crash to the ground state, even when the MOs are initially permuted. However, if the electron transfer occurs rapidly after excitation, then this would be a moot point. For now, this result is a reasonable indication that this process is indeed favorable.

If the hypothesis about the electron transfer from DMAc is correct, then the corollary based upon the experimental UV-VIS data is that an electron transfer from a DCM molecule would not be thermodynamically favorable. Thus, **23** and a DCM molecule were again optimized independently with a DCM solvation shell *via* the SMD, and frequency calculations were subsequently performed on them with the same parameters. As shown in Figure 5-18, the radical anion doublet state was 140.9 kcal/mol downhill from the excited state, which was again taken

from a separate time-dependent calculation with SMD-DCM (see Appendix I). On the other hand, the radical cation of the DCM molecule, with the same parameters, was unsurprisingly 200.3 kcal/mol uphill. The endergonic process of removing an electron from DCM outweighs the lowering of the energy of the carbonate by 59.4 kcal/mol, making this process highly thermodynamically unfavorable. Therefore, there is no electron source for the carbonate when dissolved in DCM, and the only UV-VIS spectrum observed was that from the ground state to the singlet state. Again, the same assumptions from the DMAc description apply here, but it is not predicted that those assumptions will alter this result significantly.

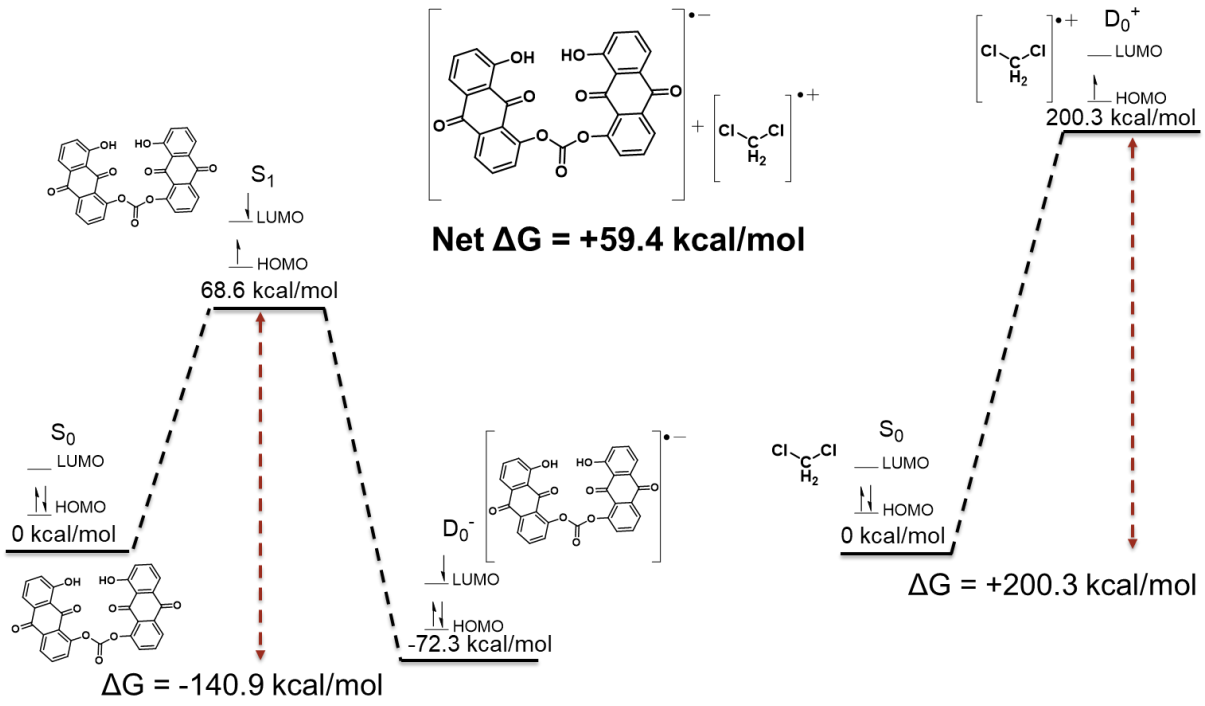

Figure 5-18. After optimizing both **23** and a DCM molecule in an implicit solvation shell of DCM (SMD) for the hypothesized electronic states, the subsequent frequency calculations with the same parameters provided the Gibbs free energies, indicating that a single electron transfer from DCM to the excited carbonate species is thermodynamically unfavorable by 59.4 kcal/mol. The ground states of both the carbonate and DCM were arbitrarily normalized to zero. The excited-state energy was taken from the λ_{max} at 417 nm predicted by a time-dependent calculation with the same parameters (see Appendix I).

Further support for this proposed PET mechanism lies in the examination of the energies of the MOs of the two species in question. It is necessary to reiterate that it is not the HOMO of **23** that contributes the most during the transition at 417 nm in DMAc (see Figure I-6 in Appendix I). Rather, it is the HOMO-1 that is the highest contributor in the ground state for the excitation to the LUMO. As shown in in Figure 5-19, the HOMO-1 of **23** was lower than the HOMO of DMAc by –5.3 kcal/mol. Therefore, the mechanism stated previously requiring that the acceptor MO be lower in energy than the donor MO was satisfied. On the other hand, Figure 5-19 also shows that the HOMO-1 of **23** in in DCM (see Figure I-7 in Appendix I) was higher in energy than the HOMO of DCM (with SMD) by +653.1 kcal/mol. Therefore, any electron donation from DCM to **23** could be ruled out, further supporting the donor-acceptor PET mechanism for **23** in solvents like DMAc but not solvents such as DCM.

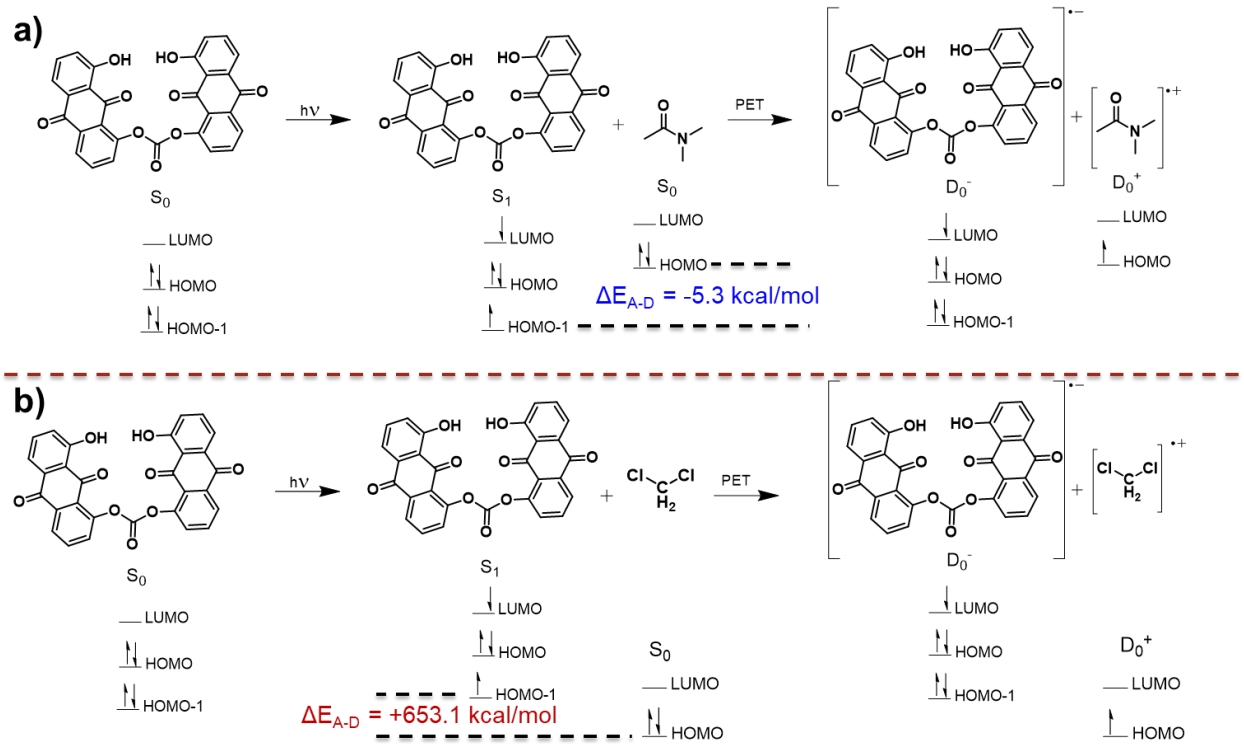

Figure 5-19. Examining the relative energy differences between the relevant MOs shows that a) the HOMO of DMAc is higher in energy by 5.3 kcal/mol than the HOMO-1 of **23** and b) the HOMO of DCM is lower than the HOMO-1 of **23** by 653.1 kcal/mol**.** Thus, a PET process is theoretically possible between an electron acceptor like **23** and an electron donor such as DMAc, but not between **23** as an electron acceptor and DCM as a donor. All species were optimized and frequency-checked using the SMD for the respective solvents separately.

Notwithstanding the multireference problem associated with DFT, we attempted to optimize and perform a time-dependant DFT analysis on **23** and DMAc together. Optimizing a binary system like this by DFT can be difficult because there is a near-infinite number of possible conformations that the DMAc and **23** molecules can take with respect to one another. However, it has been reported before that the triplet ground state (T_1) geometry can approximate the S_1 state and, thus, would potentially limit the number of local minima that the DFT method can clearly identify.[217] Accordingly, **23** and one DMAc molecule were first optimized together as a neutral triplet. Upon finding a geometry that showed spin delocalization on both molecules,

the system was then modeled using time-dependent DFT as a singlet. As shown in Figure 5-20, not only is there a significant excitation at 564 nm, but this excitation corresponds to a transfer of electron density from the DMAc molecule in the HOMO-1 of this system to exclusively the π system of **23** in the LUMO. This value at 564 nm is also the closest approximation to the 555 nm λ_{max} observed experimentally by **23** in DMAc. Thus, this result is further evidence that PET might occur between **23** and DMAc; however, caution must be taken when making inferences.

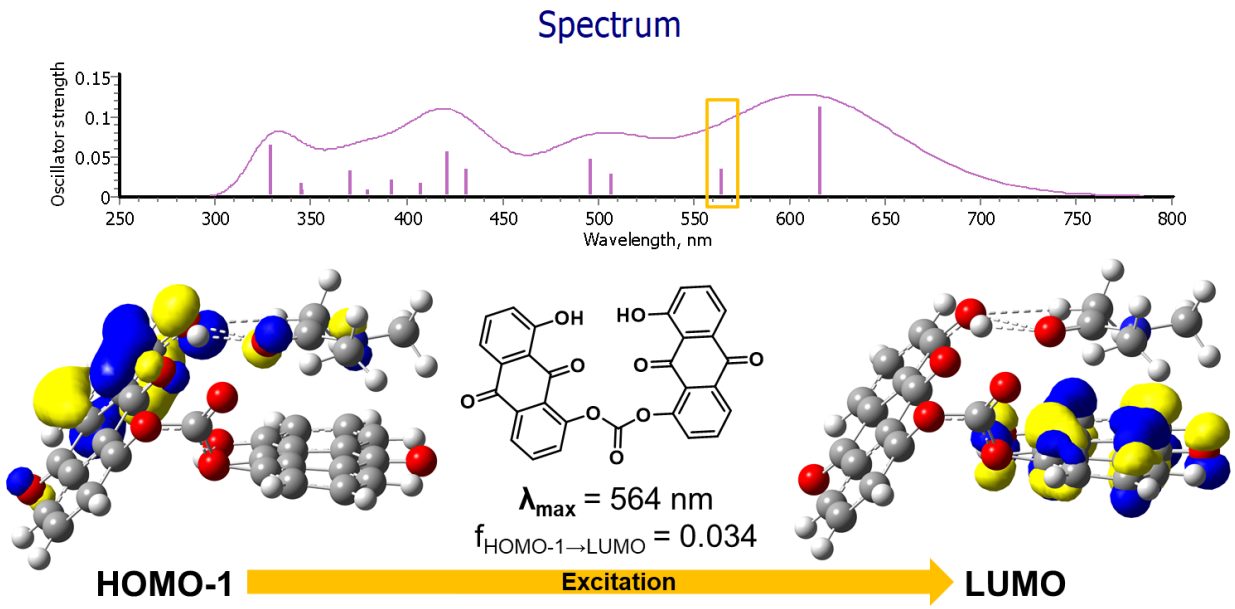

Figure 5-20. The excitation at 564 nm between the HOMO-1 and the LUMO of DMAc and **23**, optimized together, shows electron density moving from the DMAc molecule in the ground state to the π system of **23** exclusively in the excited state. This binary system was optimized initially as a T_1 in an attempt to approximate the geometry of the S_1 excited state and limit the number of potential local minima. The gd3bj empirical dispersion parameter was incorporated into this system in DMAc using the PCM solvation parameter.

As noted before, the system in Figure 5-20 is multireference in nature and may or may not contain significant error from contributions of orbitals and associated electron density on the π system of **23** in the ground state, which is also depicted in Figure 5-20. It can be said that the

B3LYP functional does generate MOs combining the observed atomic orbitals on both DMAc and **23**, indicating significant overlap using the LCAO approach. Perhaps the biggest caveat in Figure 5-20 is that the excitation with the largest oscillator strength actually occurs at 616 nm. As shown in Figure I-11 (see Appendix I), this excitation mainly corresponds to a charge transfer effect in the π system of **23**. It is possible that this excitation is absent when **23** is actually dissolved in DMAc and the two species are constantly colliding as two independent systems in reality. Whether or not this excitation should still present when **23** could be determined by more-complex computational methods is not discussed in this dissertation.[211] Notwithstanding these caveats, the result in Figure 5-20 still contributes support that a PET mechanism can and does occur.

5.4. Implications and Impact

This binary system of **23** and DMAc could theoretically be reversible, as shown in Figure 5-21. However, this would assume that no degradation or side reactions occur between the radical anion of **23** or the radical cation of DMAc. It has been reported that radical cations of DMAc, formed by high energy radiation, do decay into different products by multiple pathways over time when not at low temperatures.[214] Therefore, applying this chemistry for any reaction, requiring such a photocatalyst as a reducing agent in its radical anionic form, would necessitate the use of a stabler electron donor such as triphenylamine perhaps.[218,219] For reactions where a photocatalyst needs to serve as the oxidizing agent, **23** could potentially serve that purpose alone or with a redox mediator.[195] In either case, utilizing **23** as a photocatalyst would make for an interesting future endeavor.

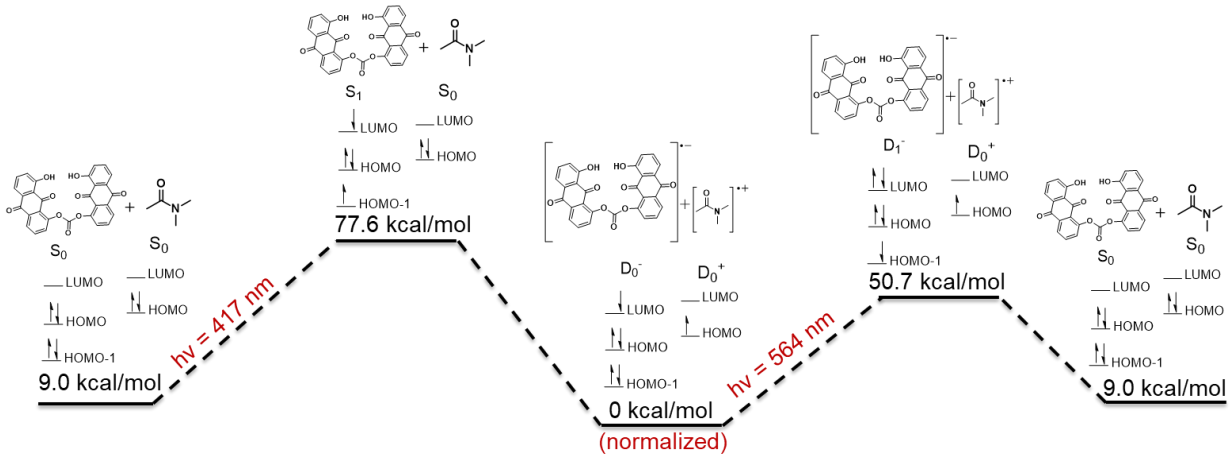

Figure 5-21. A plot of the Gibbs free energy values for the binary **23** and DMAc system together shows a theoretical reversibility between the binary donor and acceptor system assuming no side reactions.

If this PET process occurs as described, the implications could be far-reaching. Lin, Lambert, and coworkers recently reported a PET-mediated functionalization of aryl halides by a voltaic reduction of dicyanoanthracene, followed by photoexcitation of the radical anion as a donor.[218] Duan and coworkers reported the photooxidation of amines and alcohols and a reduction of aryl halides *via* a stacked perylene diimide with zinc.[210] The system presented herein could potentially carry out these transformations in the absence of an electric potential and without the need for readily oxidizable species like amines or alcohols. Additionally, this system could also be used as an initiator for PET polymerizations of alkenes. In fact, the 1,8-DHA starting material has been reported to act as an initiator for such polymerizations when in the presence of diphenyliodonium hexafluorophosphate using blue LED.[199] However, the authors reported that 1,8-DHA initiates as a radical cation, which is somewhat questionable given its reduction potential (–1.05 versus ferrocene/ferrocenium redox couple), and there appears to be insufficient support for this specific mechanism.[199,209] Nevertheless, the authors did report

somewhat controlled polymerization giving dispersities of 1.14 and 1.15.[199] More generally though, the authors used blue light, which can penetrate farther into materials when synthesizing materials like cross-linked networks, and it could be potentially be more selective with fewer side reactions when compared to UV-initiated polymerizations.[193,195,196] Lastly, **23** could be used as a photocatalyst for thiol-ene click reactions, as Boyer and coworkers have demonstrated with their $Ru(bpy)_3Cl_2$ and eosin photo-oxidant catalysts.[195] Thus, **23** could potentially serve as either a photoreducing or photooxidizing catalyst for various reactions.

Additionally, the color change exhibited by this carbonate would not just be solvatochromic, but it would also be solvent-induced redoxochromism if the PET hypothesis holds true. If so, it could still be used as an optoelectronic sensor, but that would be a relatively minor application given the other potential uses.

5.5. Future Work

There is still more work to be done to complete this project. First, the second synthetic scheme should be completed using DCM (or chloroform perhaps) as the eluent for all column separations. The silylated carbonate appears to undergo a type of redox reaction with acetone, so workup should avoid polar solvents with oxygen or nitrogen atoms. Once more of the carbonate is made, the UV-VIS spectrum needs to be retaken at a higher concentration of the solutions to get a better spectrum. Thirdly, it would be worth screening a few more solvents, not only by UV-VIS but also by fluorescence, to show how well (or not) molecular modeling is able to predict this carbonate's behavior. Furthermore, it needs to be verified that aggregation effects, or "excimer" formation, are not inducing this solvatochromism.[220] This can be verified by manipulating the concentrations in one solvent and analyzing the UV-VIS spectra, as has been done for pyrene and bianthryl systems.[220,221] Additionally, the 2D fluorescence measurements will indicate if there are

multiple excitations or electronic states present, as well as any excimer complexes formed.[220] Perhaps the last, but very crucial, study that must take place is the UV-VIS and fluorescence measurements of **23** as a deprotonated anion to determine whether the observed solvatochromism is caused by an excited-state proton transfer to a highly coordinating solvent like DMAc. It has been reported that fluorophores can have a dramatic lowering of their pk_a in the excited state, resulting in a loss of symmetry between absorption and emission spectra.[220] As shown in Figures I-16 to I-18 (see Appendix I), molecular modeling of a deprotonated anion shows that there should be a significant excitation just below 600 nm, but it is considerably more "off" of the observed 555 nm observed experimentally relative to the prediction in Figure 5-20. Additionally, Figure I-19 and Tables I-4 to I-5 show that the reverse proton transfer from the anion ground state is downhill and should compete with further excitation (uphill), but their relative rates are unknown. The complication for investigating this will be to use a base that does not also undergo electron transfer to **23**. These are just the main future considerations that should take place.

Other characterization methods worth looking into would be electron paramagnetic resonance (EPR) and CV in different solvents. One crucial supplement for the molecular modeling data presented herein would be to perform single-point calculations on each of the optimized structures with an *ab initio* method like Møller-Plesset perturbation 2 (MP2) to calibrate the energies to ensure that they are higher/lower than one another as presented. DFT is theoretically *ab initio,* but in practice, it is not because the actual functional is not known, and methods like B3LYP are approximations with empirical parameters added to more closely match the actual theoretical functional.[222] Lastly, it may not go into the initial report on this work, but it would be worth trying to see if this carbonate could photoinitate existing RAFT polymerization, atom transfer radical polymerization (ATRP), or even thiol-ene click polymerization systems.

5.6. Conclusion

From the preliminary data collected, the bis(1,8-DHA)carbonate (**23**) product and its oligomer analogue, appear to exhibit a significant bathochromic redshift in its UV-VIS spectrum when placed in very polar solvents containing heteroatoms due to a redox reaction with the solvent. Specifically, the computational data indicate that a one-electron transfer from DMAc to **23** is thermodynamically favorable, whereas such a transformation is not thermodynamically feasible with DCM. The radical anion that is formed has a different UV-VIS profile with an additional absorption band centered at 555 nm, in addition to the singlet, ground-state excitation band centered at 411 to 417 nm. DFT with the B3LYP method does indicate charge transfer character with these excitations and that the whole π system on both anthraquinone moieties is involved, but that the shift in λ_{max} is caused by the new electronic state generated in polar solvents. The fact that this compound can oxidize a relatively nonredox active molecule like DMAc by photoexcitation indicates that it has a reduction potential either as high as or higher than many of the other PET compounds reported in the literature. However, more experimentation and modeling need to be done in order to be conclusive.

6. CONCLUSIONS

In closing, this work presents significant advancements in the tunable synthesis of PU linear chains and macrocycles, as well as their characterization by MALDI-TOF MS and, potentially, Raman spectroscopy. The use of a new variety of carbamate deblocking chemistry with DBU was shown to produce a high conversion of macrocyclic PUs in a fraction of the time of a corresponding conventional condition using a diisocyanate starting material and a metal-containing catalyst. This synthetic scheme could alleviate the storage and transport concerns of conventional diisocyanate and polyisocyanates currently used in PU procurement, as well as reduced reaction times for conventional polymerizations. As stated in Chapter 1, DBU itself may not be any less toxic than conventional transition metal catalysts for use in commodity products. However, it was shown that the DBU could be removed entirely from the PU materials by aqueous extraction and precipitation, whereas many conventional metal catalysts require harsh conditions for removal. Although no functionalized material was obtained, this work has shown two viable synthetic routes for the procurement of an antibiofouling PU using pseudocapsaicin. Additionally, the work in Chapter 4 showed that conjugation of the pseudocapsaicin molecule using the route *via* the carbonate linkage is likeliest to work and that both the diol and the base must be dried for the formation of the pseudocapsaicin chloroformate in order to obtain sufficiently high yields for the first step. Lastly, the solvatochromism for an oligo- and di(1,8-DHA)carbonate was shown to be likely induced by an electron transfer from polar, heteroatom-containing solvents with more experimentation necessary for conclusive support.

In Chapter 2, it was demonstrated that PU macrocycles could be synthesized using mild conditions such as a DBU organobase in place of metal-containing catalysts. Moreover, the composition of urea, triazinedione, and uretdione functional groups can be tuned in these macrocycles by altering conditions such as the rate of DBU addition and the drying method of the diol. The HMDNC monomer (**1**) can be synthesized in one step with a relatively simple workup procedure and is stable for extended periods of time under ambient conditions. However, this route uses the labile nature of these dicarbamate groups in the presence of a base to form diisocyanate *in situ* to form PU *via* a deblocking mechanism. Thus, this synthetic route could alleviate the concerns and hazards that accompany the storage and transport of diisocyanates. The cost-effectiveness of this methodology relative to conventional industrial methods remains a concern. It is possible that the atom economy deficit of this method relative to industrial techniques could be eliminated if the nitrophenol/nitrophenoxide by-products can be shown to be recycled to regenerate the carbonate starting material. Additionally, there is even more significant potential for this method if it can be shown that **1** can be synthesized using a starting material other than the carbonate. Therefore, this work presents a promising new flavor of the deblocking chemistry already discussed in the literature.

The diagnosis and quantification of macrocyclization with these PU systems was attempted in Chapter 3 by utilizing molecular modeling and Raman spectroscopy to identify any structural ring vibrations in a mostly linear and a cyclic PU. It was demonstrated that cyclization approached completion for the dicarbamate-derived systems (**11**) by MALDI-TOF at 1 h of reaction time, implying a rather unusual kinetic behavior of these systems relative to the industrially derived PUs (**10**) from Chapter 2. Thus, Raman spectroscopy was chosen for its ability to be quantitative, but also for its ability to monitor the cyclization of these systems *in*

situ, given that literature precedent has shown that some macrocyclic systems exhibit some unique, low-frequency, ring-breathing vibrations. PUs **10** showed very minute cycle content at 1 h of reaction time but quantitative cyclization after 8 h, so these two systems were used as preliminary reference materials. The Raman spectra of the conventionally derived PUs (**10b**) at 1 h and 8 h did show significant differences with two Raman bands around 200 cm^{-1}, which is where the anticipated structural modes are reported to occur. Ring-breathing vibrations were observed in the predicted Raman spectra by molecular modeling at *ca.* 200 cm^{-1}, but their intensities relative to the rest of the spectra were remarkably small. Thus, while it is apparent there is some kind of Raman mode that is different between these two systems, it is not clear what structural difference this mode arises from at the present time. More structures and conformations of these macrocycles need to be sampled and modeled to see if the predicted Raman spectra can match those observed in PUs **10b**. If a matching structure and spectra are determined, monitoring the cyclization of the PU systems from Chapter 2 could be done in a high-throughput manner *in situ*. Moreover, if demonstrated for this system, Raman spectroscopy could be another potential tool for polymer chemists to detect and quantify cyclization in other symmetric polymer systems.

An antibiofouling PU was attempted to be synthesized in Chapter 4 using a pseudocapsaicin as a sensory-deterrent molecule. The capsaicinoid family of compounds has been demonstrated in the literature to exhibit antibiofouling activity to numerous organisms while being nontoxic natural products. Pseudocapsaicin was chosen for its relatively low cost. However, attempts at functionalizing pseudocapsaicin to either a methyl α-(D)-glucopyranoside or methyl 4,6-*O*-benzylidene-α-(D)-glucopyranoside substrate was difficult and only moderately successful. Functionalization of the pseudocapsaicin molecule *via* the carbonate linkage was

hindered by water contamination of the DMA base, resulting in abnormally low yields of the pseudocapsaicin chloroformate. The attempt to functionalize pseudocapsaicin to either glucopyranoside substrate through the ether linkage became overly complicated by side reactions induced by polar solvents like DMF. Only a trace amount of the intended difunctionalized product with 4,6-*O*-benzylidene-α-(D)-glucopyranoside was detected for the system using dry toluene as a solvent. Both of these synthetic routes could be realized if the glucopyranoside diol or polyol was dried appropriately, as was discovered with the work in Chapter 2. However, before that was realized, a thioether route was attempted by using thiol-ene click chemistry, and a difunctionalized product was recovered. However, the characterization of this product was difficult, and there was some disulfide impurity, as well as apparent regioisomer formation. The need for a significant excess of thiol also made this route less appealing. While incomplete, this project still shows promise through the carbonate route if both the diol and the dimethylaniline are dried, and the resulting material would be the likeliest to show antibiofouling activity. The potential for a polymer that can slowly release pseudocapsaicin in aqueous environments would not only be a worthy fundamental investigation, but it could also be potentially used as an anti-inflammatory and antimicrobial biomedical material, in addition to marine antibiofouling.

Lastly, oligo(1,8-DHA)carbonates (**25** and **26**) and a di(1,8-hydroxyanthraquinone)carbonate (**23**) were synthesized in Chapter 5. Solubility problems complicated this work. However, it is tentatively concluded that linking 1,8-DHA *via* a carbonate linkage results in an extended π system that exhibits unusual solvatochromism due to an equally unusual electron transfer from polar, heteroatom-containing solvents like DMAc, which does not occur in nonpolar solvents like DCM. The formation of the radical anion in the dicarbonate by electron transfer caused a 144-nm bathochromic shift in the λ_{max} by UV-VIS

spectroscopy when changing solvents from DCM to DMAc and exhibited a brilliant color change to the naked eye. The electron transfer reaction was modeled using the DFT level of theory with the B3LYP method with the SMD solvent correction to show that the overall process is thermodynamically favorable by 9.0 kcal/mol. The addition of an electron to the excited state of the dicarbonate to form the radical anion in DMAc is sufficiently exergonic (by –144.6 kcal/mol) to negate the endergonic (by 135.6 kcal/mol) nature of the abstraction of an electron from a DMAc molecule to form the radical cation. This phenomenon is additionally unusual because previous reports indicate that ultrahigh-energy X-ray or γ-ray radiation is required to form a radical cation in DMAc. More work is necessary, including a more-workable synthesis of the dicarbonate using the TBDMS-protecting group, but care must be taken not to use polar, heteroatom-containing solvents during column purification. Once more of the carbonate is made, a better UV-VIS spectrum should be taken by increasing the concentration in solution because the extinction coefficients are smaller than expected. Further experiments such as fluorescence, EPR, CV, and *ab initio* calibrations of the energetics of the system should be conducted to provide sufficient support for this mechanism. If this electron transfer is indeed occurring with this system, it could have potential use for PET reactions and polymerizations for which there is significant interest in recent reports. Additionally, the solvatochromism could be used as a chemical sensor to readily identify different organic compounds.

REFERENCES

1. Odian, G., Principles of Polymerization. 4th ed.; John Wiley & Sons, Inc.: Hoboken, New Jersey, 2004; pp 130-132.

2. *The Economic Benefits of the U.S. Polyurethanes Industry 2017*; American Chemistry Council: October 2018, 2018; https://polyurethane.americanchemistry.com/Resources-and-Document-Library/Economic-Benefits-of-Polyurethane-Full-Report.pdf (accessed 03/10/2019).

3. Zhang, F.; Hu, C.; Kong, Q.; Luo, R.; Wang, Y., Peptide-/Drug-Directed Self-Assembly of Hybrid Polyurethane Hydrogels for Wound Healing. *ACS Appl. Mater. Interfaces* **2019,** *11* (40), 37147-37155.

4. Allcock, H. R.; Lamp, F. W.; Mark, J. E., Contemporary Polymer Chemistry. 3rd ed.; Pearson Education, Inc.: Upper Saddle River, New Jersey, 2003; pp 51- 52.

5. Kreye, O.; Mutlu, H.; Meier, M. A. R., Sustainable routes to polyurethane precursors. *Green Chem.* **2013,** *15* (6), 1431-1455.

6. Al Nabulsi, A.; Cozzula, D.; Hagen, T.; Leitner, W.; Müller, T. E., Isocyanurate formation during rigid polyurethane foam assembly: a mechanistic study based on in situ IR and NMR spectroscopy. *Polym. Chem.* **2018,** *9*, 4891-4899.

7. Saetung, A.; Tsupphayakorn-ake, P.; Tulyapituk, T.; Saetung, N.; Phinyocheep, P.; Pilard, J.-F., The chain extender content and NCO/OH ratio flexibly tune the properties of natural rubber-based waterborne polyurethanes. *J. Appl. Polym. Sci.* **2015,** *132* (36), 42505.

8. Rolph, M. S.; Markowska, A. L. J.; Warriner, C. N.; O'Reilly, R. K., Blocked isocyanates: from analytical and experimental considerations to non-polyurethane applications. *Polym. Chem.* **2016,** *7* (48), 7351-7364.

9. Adkins, R. I.; England, J.; Wardius, D. S. Novel polymer polyols based on natural oils polyols and preparation of the polyols. WO2014159048A1, 2014.

10. Wardius, D. S.; Albers, R.; Headley, K. J.; Otto, F.; Leyrer, U.; Lorenz, K. Process for the preparation of polyether-ester polyols. CA2610459A1, 2008.

11. Alsarraf, J.; Ammar, Y. A.; Robert, F.; Cloutet, E.; Cramail, H.; Landais, Y., Cyclic Guanidines as Efficient Organocatalysts for the Synthesis of Polyurethanes. *Macromolecules* **2012,** *45* (5), 2249-2256.

12. Cowie, J. M. G.; Arrighi, V., Polymer Chemistry: Chemistry and Physics of Modern Materials. 3rd ed.; CRC Press: Boca Raton, FL, 2008; pp 46-49.

13. Polenz, I.; Laue, A.; Uhrin, T.; Rüffer, T.; Lang, H.; Schmidt, F. G.; Spange, S., Thermally cleavable imine base/isocyanate adducts and oligomers suitable as initiators for radical homo- and copolymerization. *Polym. Chem.* **2014,** *5* (23), 6678-6686.

14. Delebecq, E.; Pascault, J.-P.; Boutevin, B.; Ganachaud, F., On the Versatility of Urethane/Urea Bonds: Reversibility, Blocked Isocyanate, and Non-isocyanate Polyurethane. *Chem. Rev.* **2013,** *113* (1), 80-118.

15. Beniah, G.; Fortman, D. J.; Heath, W. H.; Dichtel, W. R.; Torkelson, J. M., Non-Isocyanate Polyurethane Thermoplastic Elastomer: Amide-Based Chain Extender Yields Enhanced Nanophase Separation and Properties in Polyhydroxyurethane. *Macromolecules* **2017,** *50* (11), 4425-4434.

16. Sardon, H.; Pascual, A.; Mecerreyes, D.; Taton, D.; Cramail, H.; Hedrick, J. L., Synthesis of Polyurethanes Using Organocatalysis: A Perspective. *Macromolecules* **2015,** *48* (10), 3153-3165.

17. Devendra, R.; Edmonds, N. R.; Sohnel, T., Computational and experimental investigations of the urethane formation mechanism in the presence of organotin(IV) carboxylate catalysts. *J. Mol. Catal. A: Chem.* **2013,** *366*, 126-139.

18. Devendra, R.; Edmonds, N. R.; Sohnel, T., Organotin carboxylate catalyst in urethane formation in a polar solvent: An experimental and computational study. *RSC Adv.* **2015,** *5* (60), 48935-48945.

19. Guhl, D., Alternatives to DBTL catalysts in polyurethanes – a comparative study. In *European Coatings Conference*, Berlin, DE, 2008.

20. Panda, S. S.; Panda, B. P.; Nayak, S. K.; Mohanty, S., A Review on Waterborne Thermosetting Polyurethane Coatings Based on Castor Oil: Synthesis, Characterization, and Application. *Polym.-Plast. Technol. Eng.* **2018,** *57*, 500-522.

21. Hermida-Merino, D.; O'Driscoll, B.; Hart, L. R.; Harris, P. J.; Colquhoun, H. M.; Slark, A. T.; Prisacariu, C.; Hamley, I. W.; Hayes, W., Enhancement of microphase ordering and mechanical properties of supramolecular hydrogen-bonded polyurethane networks. *Polym. Chem.* **2018,** *9*, 3406-3414.

22. Odian, G., Principles of Polymerization. 4th ed.; John Wiley & Sons, Inc.: Hoboken, New Jersey, 2004; pp 142-143.

23. Krol, P., Synthesis methods, chemical structures and phase structures of linear polyurethanes. Properties and applications of linear polyurethanes in polyurethane elastomers, copolymers and ionomers. *Prog. Mater. Sci.* **2007,** *52* (6), 915-1015.

24. Xiang, D.; He, J.; Cui, T.; Liu, L.; Shi, Q. S.; Ma, L. C.; Liang, Y., Multiphase Structure and Electromechanical Behaviors of Aliphatic Polyurethane Elastomers. *Macromolecules* **2018,** *51* (16), 6369-6379.

25. Yan, R.; Jin, B.; Luo, Y.; Li, X., Optically healable polyurethanes with tunable mechanical properties. *Polym. Chem.* **2019,** *10* (18), 2247-2255.

26. Furtwengler, P.; Avérous, L., Renewable polyols for advanced polyurethane foams from diverse biomass resources. *Polym. Chem.* **2018,** *9*, 4258-4287.

27. Zhang, J. Y.; Beckman, E. J.; Piesco, N. P.; Agarwal, S., A new peptide-based urethane polymer: synthesis, biodegradation, and potential to support cell growth in vitro. *Biomaterials* **2000,** *21* (12), 1247-1258.

28. Hearon, K.; Nash, L. D.; Volk, B. L.; Ware, T.; Lewicki, J. P.; Voit, W. E.; Wilson, T. S.; Maitland, D. J., Electron Beam Crosslinked Polyurethane Shape Memory Polymers with Tunable Mechanical Properties. *Macromol. Chem. Phys.* **2013,** *214* (11), 1258-1272.

29. Wang, C.; Jia, J., Damping and mechanical properties of polyol cross-linked polyurethane/epoxy interpenetrating polymer networks. *High Perform. Polym.* **2014,** *26* (2), 240-244.

30. Ham, B., Indoor chemical pollution impacts often remain invisible. *Science* **2019,** *366* (6469), 1084-1085.

31. Cakic, S. M.; Spirkova, M.; Ristic, I. S.; B-Simendic, J. K.; M-Cincovic, M.; Poreba, R., The waterborne polyurethane dispersions based on polycarbonate diol: Effect of ionic content. *Mater. Chem. Phys.* **2013,** *138* (1), 277-285.

32. Harding, J. L.; Reynolds, M. M., Combating medical device fouling. *Trends Biotechnol.* **2014,** *32* (3), 140-146.

33. Yang, J.; Li, L.; Ma, C.; Ye, X., Degradable polyurethane with poly(2-ethyl-2-oxazoline) brushes for protein resistance. *RSC Adv.* **2016,** *6* (74), 69930-69938.

34. Sheikh, Z.; Khan, A. S.; Roohpour, N.; Glogauer, M.; Rehman, I. u., Protein adsorption capability on polyurethane and modified-polyurethane membrane for periodontal guided tissue regeneration applications. *Mater. Sci. Eng., C* **2016,** *68*, 267-275.

35. Zhang, Y.; He, X.; Ding, M.; He, W.; Li, J.; Li, J.; Tan, H., Antibacterial and Biocompatible Cross-Linked Waterborne Polyurethanes Containing Gemini Quaternary Ammonium Salts. *Biomacromolecules* **2018,** *19*, 279-287.

36. Akkas, T.; Citak, C.; Sirkecioglu, A.; Guener, F. S., Which is more effective for protein adsorption: surface roughness, surface wettability or swelling? Case study of polyurethane films prepared from castor oil and poly(ethylene glycol). *Polym. Int.* **2013,** *62* (8), 1202-1209.

37. Rolph, M. S.; Inam, M.; O'Reilly, R. K., The application of blocked isocyanate chemistry in the development of tunable thermoresponsive crosslinkers. *Polym. Chem.* **2017,** *8* (46), 7229-7239.

38. Christensen, P. R.; Scheuermann, A. M.; Loeffler, K. E.; Helms, B. A., Closed-loop recycling of plastics enabled by dynamic covalent diketoenamine bonds. *Nat. Chem.* **2019,** *11* (5), 442-448.

39. Fortman, D. J.; Brutman, J. P.; Cramer, C. J.; Hillmyer, M. A.; Dichtel, W. R., Mechanically Activated, Catalyst-Free Polyhydroxyurethane Vitrimers. *J. Am. Chem. Soc.* **2015,** *137* (44), 14019-14022.

40. Fortman, D. J.; Sheppard, D. T.; Dichtel, W. R., Reprocessing Cross-Linked Polyurethanes by Catalyzing Carbamate Exchange. *Macromolecules* **2019,** *52*, 6330-6335.

41. Yang, Y.; Urban, M. W., Self-healing of glucose-modified polyurethane networks facilitated by damage-induced primary amines. *Polym. Chem.* **2017,** *8* (1), 303-309.

42. Morozova, S. M.; Shaplov, A. S.; Lozinskaya, E. I.; Mecerreyes, D.; Sardon, H.; Zulfiqar, S.; Suarez-Garcia, F.; Vygodskii, Y. S., Ionic Polyurethanes as a New Family of Poly(ionic liquid)s for Efficient CO2 Capture. *Macromolecules* **2017,** *50* (7), 2814-2824.

43. Ramdin, M.; de Loos, T. W.; Vlugt, T. J. H., State-of-the-Art of CO2 Capture with Ionic Liquids. *Ind. Eng. Chem. Res.* **2012,** *51* (24), 8149-8177.

44. Ahn, J.; Lim, T.; Yeo, C. S.; Hong, T.; Jeong, S.-M.; Park, S. Y.; Ju, S., Infrared Invisibility Cloak Based on Polyurethane–Tin Oxide Composite Microtubes. *ACS Appl. Mater. Interfaces* **2019,** *11*, 14296-14304.

45. Tang, D.; Macosko, C. W.; Hillmyer, M. A., Thermoplastic polyurethane elastomers from bio-based poly(δ-decalactone) diols. *Polym. Chem.* **2014,** *5* (9), 3231-3237.

46. Miyajima, T.; Nishiyama, K.; Satake, M.; Tsuji, T., Synthesis and process development of polyether polyol with high primary hydroxyl content using a new propoxylation catalyst. *Polym. J.* **2015,** *47* (12), 771-778.

47. Gandini, A.; Lacerda, T. M., From monomers to polymers from renewable resources: Recent advances. *Prog. Polym. Sci.* **2015,** *48*, 1-39.

48. Alvarez-Barragan, J.; Domınguez-Malfavon, L.; Vargas-Suarez, M.; Gonzalez-Hernandez, R.; Aguilar-Osorio, G.; Loza-Tavera, H., Biodegradative activities of selected environmental fungi on a polyester polyurethane varnish and polyether polyurethane foams. *Appl. Environ. Microbiol.* **2016,** *82* (17), 5225-5235.

49. Haider, T. P.; Völker, C.; Kramm, J.; Landfester, K.; Wurm, F. R., Plastics of the Future? The Impact of Biodegradable Polymers on the Environment and on Society. *Angew. Chem., Int. Ed.* **2019,** *58* (1), 50-62.

50. Zhang, S., The Deep Sea Is Full of Plastic, Too. *The Atlantic* 2019.

51. Hashimoto, K.; Yaginuma, K.; Nara, S.-i.; Okawa, H., Synthesis of new hydroxy-bearing polyurethanes: Polyaddition of D-glucose-derived diols with diisocyanates. *Polym. J.* **2005,** *37* (5), 384-390.

52. Garcon, R.; Clerk, C.; Gesson, J. P.; Bordado, J.; Nunes, T.; Caroco, S.; Gomes, P. T.; Da Piedade, M. E. M.; Rauter, A. P., Synthesis of novel polyurethanes from sugars and 1,6-hexamethylene diisocyanate. *Carbohydr. Polym.* **2001,** *45* (2), 123-127.

53. Prompers, G.; Keul, H.; Hocker, H., Polyurethanes with pendant hydroxy groups: polycondensation of 1,6-bis-O-phenoxycarbonyl-2,3[ratio]4,5-di-O-isopropylidenegalactitol and 1,6-di-O-phenoxycarbonylgalactitol with diamines. *Green Chem.* **2006,** *8* (5), 467-478.

54. Zhang, J.-Y.; Beckman, E. J.; Hu, J.; Yang, G.-G.; Agarwal, S.; Hollinger, J. O., Synthesis, biodegradability, and biocompatibility of lysine diisocyanate-glucose polymers. *Tissue Eng.* **2002,** *8* (5), 771-785.

55. Marin, R.; Munoz-Guerra, S., Carbohydrate-based poly(ester-urethane)s: A comparative study regarding cyclic alditols extenders and polymerization procedures. *J. Appl. Polym. Sci.* **2009,** *114* (6), 3723-3736.

56. Braun, D.; Bergmann, M., Polymers from 1,4:3,6-Dianhydrosorbitol. *J. Prakt. Chem.* **1992,** *334* (4), 298-310.

57. Kim, H.-J.; Kang, M.-S.; Knowles, J. C.; Gong, M.-S., Synthesis of highly elastic biocompatible polyurethanes based on bio-based isosorbide and poly(tetramethylene glycol) and their properties. *J. Biomater. Appl.* **2014,** *29* (3), 454-464.

58. Kieber, R. J.; Silver, S. A.; Kennemur, J. G., Stereochemical effects on the mechanical and viscoelastic properties of renewable polyurethanes derived from isohexides and hydroxymethylfurfural. *Polym. Chem.* **2017,** *8* (33), 4822-4829.

59. Martello, M. T.; Burns, A.; Hillmyer, M., Bulk Ring-Opening Transesterification Polymerization of the Renewable δ-Decalactone Using an Organocatalyst. *ACS Macro Lett.* **2012,** *1* (1), 131-135.

60. Rangadurai, P.; Molla, M. R.; Prasad, P.; Caissy, M.; Thayumanavan, S., Temporal and Triggered Evolution of Host-Guest Characteristics in Amphiphilic Polymer Assemblies. *J. Am. Chem. Soc.* **2016,** *138* (24), 7508-7511.

61. Bayan, R.; Karak, N., Renewable resource modified polyol derived aliphatic hyperbranched polyurethane as a biodegradable and UV-resistant smart material. *Polym. Int.* **2017,** *66* (6), 839-850.

62. Gogoi, S.; Karak, N., Biobased Biodegradable Waterborne Hyperbranched Polyurethane as an Ecofriendly Sustainable Material. *ACS Sustainable Chem. Eng.* **2014,** *2* (12), 2730-2738.

63. DeBolt, M.; Kiziltas, A.; Mielewski, D.; Waddington, S.; Nagridge, M. J., Flexible polyurethane foams formulated with polyols derived from waste carbon dioxide. *J. Appl. Polym. Sci.* **2016,** *133* (45), 44086.

64. *VORANATE T-80: Toluene Diisocyanates Safe Handling and Storage Guide*; The Dow Chemical Company: Midland, MI, 2010; http://msdssearch.dow.com/PublishedLiteratureDOWCOM/dh_095b/0901b8038095bf42.pdf?filepath=polyurethane/pdfs/noreg/109-52180.pdf&fromPage=GetDoc (accessed 01/28/2018).

65. Sharma, B.; Ubaghs, L.; Keul, H.; Hoecker, H.; Loontjens, T.; Van Benthem, R., Synthesis and characterization of alternating poly(amide urethane)s from ε-caprolactam, amino alcohols, and diphenyl carbonate. *Polymer* **2004,** *45* (16), 5427-5440.

66. Jousseaume, B.; Laporte, C.; Toupance, T.; Bernard, J. M., Efficient bismuth catalysts for transcarbamoylation. *Tetrahedron Lett.* **2002,** *43* (36), 6305-6307.

67. Hu, J.; Chen, Z.; He, Y.; Huang, H.; Zhang, X., Synthesis and structure investigation of hexamethylene diisocyanate (HDI)-based polyisocyanates. *Res. Chem. Intermed.* **2017,** *43* (5), 2799-2816.

68. Bahili, M. A.; Stokes, E. C.; Amesbury, R. C.; Ould, D. M. C.; Christo, B.; Horne, R. J.; Kariuki, B. M.; Stewart, J. A.; Taylor, R. L.; Williams, P. A.; Jones, M. D.; Harris, K. D. M.; Ward, B. D., Aluminium-catalysed isocyanate trimerization, enhanced by exploiting a dynamic coordination sphere. *Chem. Commun.* **2019,** *55* (53), 7679-7682.

69. Widemann, M.; Driest, P. J.; Orecchia, P.; Naline, F.; Golling, F. E.; Hecking, A.; Eggert, C.; Pires, R.; Danielmeier, K.; Richter, F. U., Structure–Property Relations in Oligomers of Linear Aliphatic Diisocyanates. *ACS Sustainable Chem. Eng.* **2018,** *6* (8), 9753-9759.

70. Dusek, K.; Spirkova, M.; Havlicek, I., Network formation of polyurethanes due to side reactions. *Macromolecules* **1990,** *23* (6), 1774-81.

71. Simon, J.; Barla, F.; Kelemen-Haller, A.; Farkas, F.; Kraxner, M., Thermal stability of polyurethanes. *Chromatographia* **1988,** *25* (2), 99-106.

72. Joel, D.; Müller, P.; Ahl, R., Isocyanate reactions in and with N,N-dimethylformamide. *Angew. Makromol. Chem.* **1992,** *197* (1), 131-139.

73. *Guidance for Working with Aliphatic Diisocyanates*; American Chemistry Council: March 2016, https://adi.americanchemistry.com/Guidance-for-Working-with-ADIs.pdf (accessed 03/10/2019).

74. Maisonneuve, L.; Lamarzelle, O.; Rix, E.; Grau, E.; Cramail, H., Isocyanate-Free Routes to Polyurethanes and Poly(hydroxy Urethane)s. *Chem. Rev.* **2015,** *115* (22), 12407-12439.

75. Pauluhn, J., Analysis of the interrelationship of the pulmonary irritation and elicitation thresholds in rats sensitized with 1,6-hexamethylene diisocyanate (HDI). *Inhalation Toxicol.* **2015,** *27* (4), 191-206.

76. Mandavilli, A., The World's Worst Industrial Disaster Is Still Unfolding. *The Atlantic* 2018.

77. International Diisocyanate Institute. http://www.diisocyanates.org/links-sources-information-tdi-safe-handling-transport-storage-disposal-and-emergency-actions (accessed 02/19/2018).

78. Kürti, L.; Czakó, B., Lossen Rearrangement. In *Strategic Applications of Named Reactions in Organic Synthesis*, Hayhurst, J., Ed. Elsevier Inc.: Burlington MA, 2005; pp 266-267.

79. Kürti, L.; Czakó, B., Hofmann Rearrangement. In *Strategic Applications of Named Reactions in Organic Synthesis*, Hayhurst, J., Ed. Elsevier Inc.: Burlington MA, 2005; pp 210-211.

80. Kürti, L.; Czakó, B., Curtius Rearrangement. In *Strategic Applications of Named Reactions in Organic Synthesis*, Hayhurst, J., Ed. Elsevier Inc.: Burlington MA, 2005; pp 116-117.

81. Zenner, M. D.; Xia, Y.; Chen, J. S.; Kessler, M. R., Polyurethanes from Isosorbide-Based Diisocyanates. *ChemSusChem* **2013,** *6* (7), 1182-1185.

82. More, A. S.; Lebarbé, T.; Maisonneuve, L.; Gadenne, B.; Alfos, C.; Cramail, H., Novel fatty acid based di-isocyanates towards the synthesis of thermoplastic polyurethanes. *Eur. Polym. J.* **2013,** *49* (4), 823-833.

83. Pawar, G. G.; Robert, F.; Grau, E.; Cramail, H.; Landais, Y., Visible-light photocatalyzed oxidative decarboxylation of oxamic acids: a green route to urethanes and ureas. *Chem. Commun.* **2018,** *54* (67), 9337-9340.

84. Eckert, N.; Hart, R. In *Water Soluble Bismuth Based Curatives with Remarkable Activity and Shelf Life*, Polyurethanes Technical Conference 2016, Baltimore, MD, American Chemistry Council: Baltimore, MD, 2016; pp 302-312.

85. Bakhshi, H.; Agarwal, S., Dendrons as active clicking tool for generating non-leaching antibacterial materials. *Polym. Chem.* **2016,** *7* (33), 5322-5330.

86. de Haro, J. C.; Allegretti, C.; Smit, A. T.; Turri, S.; D'Arrigo, P.; Griffini, G., Biobased Polyurethane Coatings with High Biomass Content: Tailored Properties by Lignin Selection. *ACS Sustainable Chem. Eng.* **2019,** *7* (13), 11700-11711.

87. REACH. https://ec.europa.eu/growth/sectors/chemicals/reach_en (accessed 11/27/2019).

88. Beniah, G.; Chen, X.; Uno, B. E.; Liu, K.; Leitsch, E. K.; Jeon, J.; Heath, W. H.; Scheidt, K. A.; Torkelson, J. M., Combined Effects of Carbonate and Soft-Segment Molecular Structures on the Nanophase Separation and Properties of Segmented Polyhydroxyurethane. *Macromolecules* **2017,** *50* (8), 3193-3203.

89. Bossion, A.; Aguirresarobe, R. H.; Irusta, L.; Taton, D.; Cramail, H.; Grau, E.; Mecerreyes, D.; Su, C.; Liu, G.; Müller, A. J.; Sardon, H., Unexpected Synthesis of Segmented Poly(hydroxyurea–urethane)s from Dicyclic Carbonates and Diamines by Organocatalysis. *Macromolecules* **2018,** *51*, 5556-5566.

90. Sardon, H.; Engler, A. C.; Chan, J. M. W.; Coady, D. J.; O'Brien, J. M.; Mecerreyes, D.; Yang, Y. Y.; Hedrick, J. L., Homogeneous isocyanate- and catalyst-free synthesis of polyurethanes in aqueous media. *Green Chem.* **2013,** *15* (5), 1121-1126.

91. Kušan, J.; Keul, H.; Höcker, H., Cationic Ring-Opening Polymerization of Tetramethylene Urethane. *Macromolecules* **2001,** *34* (3), 389-395.

92. Sheri, M.; Choudhary, U.; Grandhee, S.; Emrick, T., Fluoride-Catalyzed Deblocking: A Route to Polymeric Urethanes. *Angew. Chem., Int. Ed.* **2018,** *57* (17), 4599-4602.

93. Lamarzelle, O.; Hibert, G.; Lecommandoux, S.; Grau, E.; Cramail, H., A thioglycerol route to bio-based bis-cyclic carbonates: poly(hydroxyurethane) preparation and post-functionalization. *Polym. Chem.* **2017,** *8* (22), 3438-3447.

94. Zhang, D.; Zhang, Y.; Fan, Y.; Rager, M.-N.; Guérineau, V.; Bouteiller, L.; Li, M.-H.; Thomas, C. M., Polymerization of Cyclic Carbamates: A Practical Route to Aliphatic Polyurethanes. *Macromolecules* **2019,** *52* (7), 2719-2724.

95. Neffgen, S.; Keul, H.; Höcker, H., Cationic Ring-Opening Polymerization of Trimethylene Urethane: A Mechanistic Study. *Macromolecules* **1997,** *30* (5), 1289-1297.

96. Peng, W.; Zhao, N.; Xiao, F.; Wei, W.; Sun, Y., Recent progress in phosgene-free methods for synthesis of dimethyl carbonate. *Pure Appl. Chem.* **2012,** *84* (3), 603-620.

97. Dongdong, P.; Hengshui, T., Polycarbonate polyurethane elastomers synthesized via a solvent-free and nonisocyanate melt transesterification process. *J. of Appl. Polym. Sci.* **2015,** *132* (7).

98. Deepa, P.; Jayakannan, M., Solvent-free and nonisocyanate melt transurethane reaction for aliphatic polyurethanes and mechanistic aspects. *J. Polym. Sci., Part A: Polym. Chem.* **2008,** *46* (7), 2445-2458.

99. Sharma, B.; Ubaghs, L.; Keul, H.; Höcker, H.; Loontjens, T.; Benthem, R. v., Microstructure and Properties of Poly(amide urethane)s: Comparison of the Reactivity of α-Hydroxy-ω-O-phenyl Urethanes and α-Hydroxy-ω-O-hydroxyethyl Urethanes. *Macromol. Chem. Phys.* **2004,** *205* (11), 1536-1546.

100. Check, C.; Imre, B.; Gojzewski, H.; Chartoff, R.; Vancso, G. J., Kinetic Aspects of Formation and Processing of Polycaprolactone Polyurethanes In-situ from a Blocked Isocyanate. *Polym. Chem.* **2018,** *9* (15), 1983-1995.

101. Wicks, D. A.; Wicks, Z. W., Multistep chemistry in thin films; the challenges of blocked isocyanates. *Prog. Org. Coat.* **2001,** *43* (1), 131-140.

102. Lin, W.-H.; Guo, Y.-S.; Dai, S. A., An efficient one-pot synthesis of aliphatic diisocyanate from diamine and diphenyl carbonate. *J. Taiwan Inst. Chem. Eng.* **2015,** *50*, 322-327.

103. Mohanty, S.; Krishnamurti, N., Synthesis and thermal deblocking of blocked diisocyanate adducts. *Eur. Polym. J.* **1998,** *34* (1), 77-83.

104. Katsarava, R. D.; Kartvelishvili, T. M.; Japaridze, N. N.; Goguadze, T. A.; Khosruashvili, T. A.; Tiger, R. P.; Berlin, P. A., Synthesis of polyureas by polycondensation of diamines with active derivatives of carbonic acid. *Makromol. Chem.* **1993,** *194* (12), 3209-3228.

105. Katsarava, R. D.; Kartvelishvili, T. M.; Kharadze, D. P.; Zaalishvili, M. M.; Patsuriya, M. M., Synthesis of polyurethanes by polycondensation of activated diol biscarbonates with diamines under mild conditions. *Vysokomol. Soedin., Ser. A* **1987,** *29* (10), 2069-75.

106. Chong, P. Y.; Petillo, P. A., Synthesis of Carbamate-Containing Cyclodextrin Analogues. *Org. Lett.* **2000,** *2* (8), 1093-1096.

107. Chen, Z.; Hadjichristidis, N.; Feng, X.; Gnanou, Y., Poly(urethane–carbonate)s from Carbon Dioxide. *Macromolecules* **2017,** *50* (6), 2320-2328.

108. Sridaeng, D.; Limsirinawa, A.; Sirojpornphasut, P.; Chawiwannakorn, S.; Chantarasiri, N., Metal acetylacetonate-amine and metal nitrate-amine complexes as low-emission catalysts for rigid polyurethane foam preparation. *J. Appl. Polym. Sci.* **2015,** *132* (31), 42332.

109. Inoue, S.-I.; Nagai, Y.; Okamoto, H., Amine-manganese complex as an efficient catalyst for polyurethane syntheses. *Polym. J.* **2002,** *34* (4), 298-301.

110. Turgut, C.; Newby, B.-m.; Cutright, T. J., Determination of optimal water solubility of capsaicin for its usage as a non-toxic antifoulant. *Environ. Sci. Pollut. Res. Int.* **2004,** *11* (1), 7-10.

111. Angarano, M.-B.; McMahon, R. F.; Hawkins, D. L.; Schetz, J. A., Exploration of structure-antifouling relationships of capsaicin-like compounds that inhibit zebra mussel (Dreissena polymorpha) macrofouling. *Biofouling* **2007,** *23* (5), 295-305.

112. Qiao, X.; Li, Y.; Mai, J.; Ji, X.; Li, Q., Effect of Dibutyltin Dilaurate on Triglyceride Metabolism through the Inhibition of the mTOR Pathway in Human HL7702 Liver Cells. *Molecules* **2018,** *23* (7), 1654.

113. *Tin Catalyst Removal with Reaxis Tinex*; Reaxis: http://www.reaxis.com/data/uploads/pdfs/reaxistinex.pdf (accessed 05/01/2019).

114. 10. Scavenging A Tin Catalyst. https://www.silicycle.com/resource-center/applications-library/purification/metal-removal/10-scavenging-a-tin-catalyst (accessed 05/01/2019).

115. Bloodworth, A. J.; Davies, A. G., Organometallic reactions. I. The addition of tin alkoxides to isocyanates. *J. Chem. Soc.* **1965**, 5238-5244.

116. Pérez, L. M., Quantum Mechanical Short Course: Lecture 6. Simulation, T. A. M. U.-L. f. M., Ed. College Station, TX, 2016.

117. Marenich, A. V.; Cramer, C. J.; Truhlar, D. G., Universal Solvation Model Based on Solute Electron Density and on a Continuum Model of the Solvent Defined by the Bulk Dielectric Constant and Atomic Surface Tensions. *J. Phys. Chem. B* **2009,** *113* (18), 6378-6396.

118. Anslyn, E. V.; Dougherty, D. A., Modern Physical Organic Chemistry. Murdzek, J., Ed. University Science Books: Mill Valley, CA, 2006; p 378.

119. Wicks, Z. W.; Wicks, D. A.; Rosthauser, J. W., Two package waterborne urethane systems. *Prog. Org. Coat.* **2002,** *44* (2), 161-183.

120. Kaupmees, K.; Trummal, A.; Leito, I., Basicities of Strong Bases in Water: A Computational Study. *Croat. Chem. Acta* **2014,** *87* (4), 385-395.

121. *PubChem*. 1,8-Diazabicyclo[5.4.0]undec-7-ene. https://pubchem.ncbi.nlm.nih.gov/compound/1_8-Diazabicyclo_5.4.0_undec-7-ene (accessed 12/08/2019).

122. *PubChem*. 7-Methyl-1,5,7-triazabicyclo[4.4.0]dec-5-ene. https://pubchem.ncbi.nlm.nih.gov/compound/123583 (accessed 12/08/2019).

123. Sardon, H.; Engler, A. C.; Chan, J. M. W.; Garcia, J. M.; Coady, D. J.; Pascual, A.; Mecerreyes, D.; Jones, G. O.; Rice, J. E.; Horn, H. W.; Hedrick, J. L., Organic Acid-Catalyzed Polyurethane Formation via a Dual-Activated Mechanism: Unexpected Preference of N Activation over O Activation of Isocyanates. *J. Am. Chem. Soc.* **2013,** *135* (43), 16235-16241.

124. Coady, D. J.; Fukushima, K.; Horn, H. W.; Rice, J. E.; Hedrick, J. L., Catalytic insights into acid/base conjugates: Highly selective bifunctional catalysts for the ring-opening polymerization of lactide. *Chem. Commun.* **2011,** *47* (11), 3105-3107.

125. Lin, B.; Waymouth, R. M., Urea Anions: Simple, Fast, and Selective Catalysts for Ring-Opening Polymerizations. *J. Am. Chem. Soc.* **2017**.

126. Coutelier, O.; El Ezzi, M.; Destarac, M.; Bonnette, F.; Kato, T.; Baceiredo, A.; Sivasankarapillai, G.; Gnanou, Y.; Taton, D., N-Heterocyclic carbene-catalysed synthesis of polyurethanes. *Polym. Chem.* **2012,** *3* (3), 605-608.

127. Noh, H.-J.; Sadhasivam, T.; Jung, D.-S.; Lee, K.; Han, M.; Kim, J.-Y.; Jung, H.-Y., Poly(styrene)-supported N-heterocyclic carbene coordinated iron chloride as a catalyst for delayed polyurethane polymerization. *RSC Adv.* **2018,** *8* (65), 37339-37347.

128. Naray-Szabo, G.; Mika, L. T., Conservative evolution and industrial metabolism in Green Chemistry. *Green Chem.* **2018,** *20*, 2171-2191.

129. Basterretxea, A.; Jehanno, C.; Mecerreyes, D.; Sardon, H., Dual Organocatalysts Based on Ionic Mixtures of Acids and Bases: A Step Toward High Temperature Polymerizations. *ACS Macro Lett.* **2019,** *8* (8), 1055-1062.

130. Jiang, D. X.; Li, Y.; Li, J.; Wang, G. X., Prediction of the Aquatic Toxicity of Phenols to Tetrahymena Pyriformis from Molecular Descriptors. *International Journal of Environmental Research* **2011,** *5* (4), 923-938.

131. Jehanno, C.; Pérez-Madrigal, M. M.; Demarteau, J.; Sardon, H.; Dove, A. P., Organocatalysis for depolymerisation. *Polymer Chemistry* **2019,** *10* (2), 172-186.

132. Ma, C.; Xu, W.; Pan, J.; Xie, Q.; Zhang, G., Degradable Polymers for Marine Antibiofouling: Optimizing Structure To Improve Performance. *Ind. Eng. Chem. Res.* **2016,** *55* (44), 11495-11501.

133. Firdaus, M.; Meier, M. A. R., Renewable polyamides and polyurethanes derived from limonene. *Green Chem.* **2013,** *15* (2), 370-380.

134. Janvier, M.; Ducrot, P.-H.; Allais, F., Isocyanate-Free Synthesis and Characterization of Renewable Poly(hydroxy)urethanes from Syringaresinol. *ACS Sustainable Chem. Eng.* **2017,** *5* (10), 8648-8656.

135. Regalado, E. L.; Mendiola, J.; Laguna, A.; Nogueiras, C.; Thomas, O. P., Polar alkaloids from the Caribbean marine sponge Niphates digitalis. *Nat. Prod. Commun.* **2010,** *5* (8), 1187-1190.

136. Foster, G., Ethylene Supply in a Fluid Context: Implications of Shale Gas and Climate Change. *Energies* **2018,** *11*, 2967.

137. Methyl-α–D-glucopyranoside ≥99%. https://us.vwr.com/store/product/18599791/methyl-a-d-glucopyranoside-99 (accessed 12/08/2019).

138. Polyethylene glycol 1,450. https://us.vwr.com/store/product/7520906/polyethylene-glycol-1-450 (accessed 12/08/2019).

139. Wegener, G.; Brandt, M.; Duda, L.; Hofmann, J.; Klesczewski, B.; Koch, D.; Kumpf, R.-J.; Orzesek, H.; Pirkl, H.-G.; Six, C.; Steinlein, C.; Weisbeck, M., Trends in industrial catalysis in the polyurethane industry. *Appl. Catal., A* **2001,** *221* (1-2), 303-335.

140. Interesting Facts and Information about Carbon Dioxide (CO_2). http://www.uigi.com/carbondioxide.html (accessed 12/03/2019).

141. Aoyagi, N.; Furusho, Y.; Endo, T., Mild incorporation of CO2 into epoxides: Application to nonisocyanate synthesis of poly(hydroxyurethane) containing triazole segment by polyaddition of novel bifunctional five-membered cyclic carbonate and diamines. *J. Polym. Sci., Part A: Polym. Chem.* **2018,** *56*, 986-993.

142. Mikami, K.; Lonnecker, A. T.; Gustafson, T. P.; Zinnel, N. F.; Pai, P.-J.; Russell, D. H.; Wooley, K. L., Polycarbonates Derived from Glucose via an Organocatalytic Approach. *J. Am. Chem. Soc.* **2013,** *135* (18), 6826-6829.

143. Frisch, M. J.; Trucks, G. W.; Schlegel, H. B.; Scuseria, G. E.; Robb, M. A.; Cheeseman, J. R.; Scalmani, G.; Barone, V.; Mennucci, B.; Petersson, G. A.; Nakatsuji, H.; Caricato, M.; Li, X.; Hratchian, H. P.; Izmaylov, A. F.; Bloino, J.; Zheng, G.; Sonnenberg, J. L.; Hada, M.; Ehara, M.; Toyota, K.; Fukuda, R.; Hasegawa, J.; Ishida, M.; Nakajima, T.; Honda, Y.; Kitao, O.; Nakai, H.; Vreven, T.; Montgomery Jr., J. A.; Peralta, J. E.; Ogliaro, F.; Bearpark, M. J.; Heyd, J. J.; Brothers, E. N.; Kudin, K. N.; Staroverov, V. N.; Kobayashi, R.; Normand, J.; Raghavachari, K.; Rendell, A. P.; Burant, J. C.; Iyengar, S. S.; Tomasi, J.; Cossi, M.; Rega, N.; Millam, J. M.; Klene, M.; Knox, J. E.; Cross, J. B.; Bakken, V.; Adamo, C.; Jaramillo, J.; Gomperts, R.; Stratmann, R. E.; Yazyev, O.; Austin, A. J.; Cammi, R.; Pomelli, C.; Ochterski, J. W.; Martin, R. L.; Morokuma, K.; Zakrzewski, V. G.; Voth, G. A.; Salvador, P.; Dannenberg, J. J.; Dapprich, S.; Daniels, A. D.; Farkas, O.; Foresman, J. B.; Ortiz, J. V.; Cioslowski, J.; Fox, D. J. *Gaussian 09*, Wallingford, CT, 2009.

144. Hoff, E. A.; Abel, B. A.; Tretbar, C. A.; McCormick, C. L.; Patton, D. L., RAFT Polymerization of "Splitters" and "Cryptos": Exploiting Azole-N-carboxamides As Blocked Isocyanates for Ambient Temperature Postpolymerization Modification. *Macromolecules* **2016,** *49* (2), 554-563.

145. Sreerama, S. G.; Elupula, R.; Laurent, B. A.; Zhang, B.; Grayson, S. M., Use of MALDI-ToF MS to elucidate the structure of oligomeric impurities formed during 'click' cyclization of polystyrene. *React. Funct. Polym.* **2014,** *80*, 83-94.

146. Gao, L.; Oh, J.; Tu, Y.; Chang, T., Preparation of low molecular weight cyclic polystyrenes with high purity via liquid chromatography at the critical condition. *Polymer* **2018,** *135*, 279-284.

147. Cowie, J. M. G.; Arrighi, V., Polymer Chemistry: Chemistry and Physics of Modern Materials. 3rd ed.; CRC Press: Boca Raton, FL, 2008; pp 243-246.

148. Payne, M. E.; Grayson, S. M., Characterization of Synthetic Polymers via Matrix Assisted Laser Desorption Ionization Time of Flight (MALDI-TOF) Mass Spectrometry. *J. Visualized Exp.* **2018,** (136), 57174.

149. Keller, B. O.; Li, L., Three-Layer Matrix/Sample Preparation Method for MALDI MS Analysis of Low Nanomolar Protein Samples. *J. Am. Soc. Mass Spectrom.* **2006,** *17* (6), 780-785.

150. Cowie, J. M. G.; Arrighi, V., *Polymer Chemistry: Chemistry and Physics of Modern Materials*. 3rd ed.; CRC Press: Boca Raton, FL, 2008.

151. Kricheldorf, H. R., Cyclic polymers: Synthetic strategies and physical properties. *J. Polym. Sci., Part A: Polym. Chem.* **2010,** *48* (2), 251-284.

152. Kricheldorf, H. R., The role of self-dilution in step-growth polymerizations. *Macromol. Rapid Commun.* **2008,** *29* (21), 1695-1704.

153. Gooden, J. K.; Gross, M. L.; Mueller, A.; Stefanescu, A. D.; Wooley, K. L., Cyclization in Hyperbranched Polymer Syntheses: Characterization by MALDI-TOF Mass Spectrometry. *J. Am. Chem. Soc.* **1998,** *120* (39), 10180-10186.

154. Felder, S. E.; Redding, M. J.; Noel, A.; Grayson, S. M.; Wooley, K. L., Organocatalyzed ROP of a Glucopyranoside Derived Five-Membered Cyclic Carbonate. *Macromolecules* **2018**.

155. Roder, H.; Duncan, M. W.; Hunsucker, S. W., Quantitative matrix-assisted laser desorption/ionization mass spectrometry. *Briefings Funct. Genomics* **2008,** *7* (5), 355-370.

156. Bai, R.; Li, G.; Wang, S.; Mei, F. One-step method for preparation of diaryl carbonate and dimethyl ether. CN101239914A, 2008.

157. Ma, S.; Zhang, H.; Sablong, R. J.; Koning, C. E.; van Benthem, R. A. T. M., t-Butyl-Oxycarbonylated Diamines as Building Blocks for Isocyanate-Free Polyurethane/Urea Dispersions and Coatings. *Macromol. Rapid Commun.* **2018,** *39* (9).

158. Bolton, D. H.; Wooley, K. L., Hyperbranched aryl polycarbonates derived from A2B monomers versus AB2 monomers. *J. Polym. Sci., Part A: Polym. Chem.* **2002,** *40* (7), 823-835.

159. Montenegro-Burke, J. R.; Bennett, J. M.; McLean, J. A.; Hercules, D. M., Novel behavior of the chromatographic separation of linear and cyclic polymers. *Anal. Bioanal. Chem.* **2016,** *408* (3), 677-681.

160. Peña-Alvarez, M.; Qiu, L.; Taravillo, M.; Baonza, V. G.; Delgado, M. C. R.; Yamago, S.; Jasti, R.; Navarrete, J. T. L.; Casado, J.; Kertesz, M., From linear to cyclic oligoparaphenylenes: electronic and molecular changes traced in the vibrational Raman spectra and reformulation of the bond length alternation pattern. *Phys. Chem. Chem. Phys.* **2016,** *18* (17), 11683-11692.

161. Frisch, M. J.; Trucks, G. W.; Schlegel, H. B.; Scuseria, G. E.; Robb, M. A.; Cheeseman, J. R.; Scalmani, G.; Barone, V.; Petersson, G. A.; Nakatsuji, H.; Li, X.; Caricato, M.; Marenich, A. V.; Bloino, J.; Janesko, B. G.; Gomperts, R.; Mennucci, B.; Hratchian, H. P.; Ortiz, J. V.; Izmaylov, A. F.; Sonnenberg, J. L.; Williams; Ding, F.; Lipparini, F.; Egidi, F.; Goings, J.; Peng, B.; Petrone, A.; Henderson, T.; Ranasinghe, D.; Zakrzewski, V. G.; Gao, J.; Rega, N.; Zheng, G.; Liang, W.; Hada, M.; Ehara, M.; Toyota, K.; Fukuda, R.; Hasegawa, J.; Ishida, M.; Nakajima, T.; Honda, Y.; Kitao, O.; Nakai, H.; Vreven, T.; Throssell, K.; Montgomery Jr., J. A.; Peralta, J. E.; Ogliaro, F.; Bearpark, M. J.; Heyd, J. J.; Brothers, E. N.; Kudin, K. N.; Staroverov, V. N.; Keith, T. A.; Kobayashi, R.; Normand, J.; Raghavachari, K.; Rendell, A. P.; Burant, J. C.; Iyengar, S. S.; Tomasi, J.; Cossi, M.; Millam,

J. M.; Klene, M.; Adamo, C.; Cammi, R.; Ochterski, J. W.; Martin, R. L.; Morokuma, K.; Farkas, O.; Foresman, J. B.; Fox, D. J. *Gaussian 16 Rev. B.01*, Wallingford, CT, 2016.

162. Christensen, A. S.; Kubař, T.; Cui, Q.; Elstner, M., Semiempirical Quantum Mechanical Methods for Noncovalent Interactions for Chemical and Biochemical Applications. *Chem. Rev.* **2016,** *116* (9), 5301-5337.

163. Zakaznova-Herzog, V. P.; Malfait, W. J.; Herzog, F.; Halter, W. E., Quantitative Raman spectroscopy: Principles and application to potassium silicate glasses. *J. Non-Cryst. Solids* **2007,** *353* (44), 4015-4028.

164. Kealey, D.; Haines, P. J., INFRARED AND RAMAN SPECTROMETRY: PRINCIPLES AND INSTRUMENTATION. In *Analytical Chemistry*, BIOS Scientific Publishers Limited: Oxford, UK, 2002; p 237.

165. Lucotti, A.; Tommasini, M.; Chalifoux, W. A.; Fazzi, D.; Zerbi, G.; Tykwinski, R. R., Bent polyynes: ring geometry studied by Raman and IR spectroscopy. *J. Raman Spectrosc.* **2012,** *43* (1), 95-101.

166. Sriv, T.; Kim, K.; Cheong, H., Low-Frequency Raman Spectroscopy of Few-Layer 2H-SnS2. *Sci. Rep.* **2018,** *8* (1), 10194.

167. Laury, M. L.; Carlson, M. J.; Wilson, A. K., Vibrational frequency scale factors for density functional theory and the polarization consistent basis sets. *J. Comput. Chem.* **2012,** *33* (30), 2380-2387.

168. Xu, Q.; Barrios, C. A.; Cutright, T.; Zhang Newby, B.-m., Evaluation of toxicity of capsaicin and zosteric acid and their potential application as antifoulants. *Environ. Toxicol.* **2005,** *20* (5), 467-474.

169. Voo, Z. X.; Khan, M.; Narayanan, K.; Seah, D.; Hedrick, J. L.; Yang, Y. Y., Antimicrobial/Antifouling Polycarbonate Coatings: Role of Block Copolymer Architecture. *Macromolecules* **2015,** *48* (4), 1055-1064.

170. Harvey, A. C.; Madsen, J.; Douglas, C. W. I.; MacNeil, S.; Armes, S. P., Antimicrobial Graft Copolymer Gels. *Biomacromolecules* **2016,** *17* (8), 2710-2718.

171. Imbesi, P. M.; Gohad, N. V.; Eller, M. J.; Orihuela, B.; Rittschof, D.; Schweikert, E. A.; Mount, A. S.; Wooley, K. L., Noradrenaline-Functionalized Hyperbranched Fluoropolymer-Poly(ethylene glycol) Cross-Linked Networks As Dual-Mode, Anti-Biofouling Coatings. *ACS Nano* **2012,** *6* (2), 1503-1512.

172. Seetho, K. DEVELOPING NEW METHODOLOGIES FOR ANTI-FOULING POLYMERIC NETWORK SYNTHESES, ORTHOGONAL MODIFICATIONS, AND APPLICATIONS IN MARINE ENVIRONMENT. Dissertation, Texas A&M University, 2016.

173. Pollack, K. A.; Imbesi, P. M.; Raymond, J. E.; Wooley, K. L., Hyperbranched Fluoropolymer-Polydimethylsiloxane-Poly(ethylene glycol) Cross-Linked Terpolymer Networks

Designed for Marine and Biomedical Applications: Heterogeneous Nontoxic Antibiofouling Surfaces. *ACS Appl. Mater. Interfaces* **2014,** *6* (21), 19265-19274.

174. Gudipati, C. S.; Finlay, J. A.; Callow, J. A.; Callow, M. E.; Wooley, K. L., The Antifouling and Fouling-Release Performance of Hyperbranched Fluoropolymer (HBFP)-Poly(ethylene glycol) (PEG) Composite Coatings Evaluated by Adsorption of Biomacromolecules and the Green Fouling Alga Ulva. *Langmuir* **2005,** *21* (7), 3044-3053.

175. Pollack, K. A. MULTIPLY-COMPLEX, NON-TOXIC, ANTI-FOULING POLYMERS DESIGNED FOR MARINE AND BIOMEDICAL APPLICATIONS. Dissertation, Texas A&M University, 2014.

176. Tewksbury, J. J.; Reagan, K. M.; Machnicki, N. J.; Carlo, T. A.; Haak, D. C.; Calderon Penaloza, A. L.; Levey, D. J., Evolutionary ecology of pungency in wild chilies. *Proc. Natl. Acad. Sci. U. S. A.* **2008,** *105* (33), 11808-11811.

177. Sharma, S. K.; Vij, A. S.; Sharma, M., Mechanisms and clinical uses of capsaicin. *Eur. J. Pharmacol.* **2013,** *720* (1-3), 55-62.

178. N-vanillylnonanamide. Sigma-Aldrich: St. Louis, MO, 2014.

179. Constant, H. L.; Cordell, G. A.; West, D. P., Nonivamide, a Constituent of Capsicum oleoresin. *J. Nat. Prod.* **1996,** *59* (4), 425-426.

180. Capsaicin. Sigma-Aldrich: St. Louis, MO, 2014.

181. Gustafson, T. P.; Lonnecker, A. T.; Heo, G. S.; Zhang, S.; Dove, A. P.; Wooley, K. L., Poly(D-glucose carbonate) Block Copolymers: A Platform for Natural Product-Based Nanomaterials with Solvothermatic Characteristics. *Biomacromolecules* **2013,** *14* (9), 3346-3353.

182. Lonnecker, A. T.; Lim, Y. H.; Felder, S. E.; Besset, C. J.; Wooley, K. L., Four Different Regioisomeric Polycarbonates Derived from One Natural Product, D-Glucose. *Macromolecules* **2016,** *49* (20), 7857-7867.

183. David, R. L. A.; Kornfield, J. A., Facile, Efficient Routes to Diverse Protected Thiols and to Their Deprotection and Addition to Create Functional Polymers by Thiol-Ene Coupling. *Macromolecules* **2008,** *41* (4), 1151-1161.

184. Clark, J. H.; Jones, C. W., The preparation of alkyl iodides from alkyl chlorides and bromides using potassium iodide supported on alumina. *J. Chem. Res., Synop.* **1990,** (2), 39.

185. Gavva, N. R.; Bannon, A. W.; Surapaneni, S.; Hovland, D. N., Jr.; Lehto, S. G.; Gore, A.; Juan, T.; Deng, H.; Han, B.; Klionsky, L.; Kuang, R.; Le, A.; Tamir, R.; Wang, J.; Youngblood, B.; Zhu, D.; Norman, M. H.; Magal, E.; Treanor, J. J. S.; Louis, J.-C., The vanilloid receptor TRPV1 is tonically activated in vivo and involved in body temperature regulation. *J. Neurosci.* **2007,** *27* (13), 3366-3374.

186. Darre, L.; Domene, C., Binding of capsaicin to the TRPV1 ion channel. *Mol. Pharmaceutics* **2015,** *12* (12), 4454-4465.

187. N,N-Dimethylformamide, anhydrous ≥99.8%, DriSolv®. https://us.vwr.com/store/product/4596858/n-n-dimethylformamide-anhydrous-99-8-drisolv (accessed 02/19/2020).

188. Gonçalves, P. M. L.; Roberts, S. M.; Wan, P. W. H., Regioselective acylation of carbohydrate derivatives using lipases leading to a facile two-step procedure for the separation of some α- and β-glucopyranosides and galactopyranosides. *Tetrahedron* **2004,** *60* (4), 927-932.

189. Klausener, A.; Mueller, E.; Runsink, J.; Scharf, H. D., A simple preparation of methyl 2,6-dideoxy- and methyl 3,6-dideoxy-α-D-arabino-hexopyranoside by photochemical deoxygenation. *Carbohydr. Res.* **1983,** *116* (2), 295-302.

190. Brace, N. O., Amides as nucleophiles: reaction of alkyl halides with amides or with amides and water. A new look at an old reaction. *J. Org. Chem.* **1993,** *58* (7), 1804-11.

191. Landini, D.; Maia, A., Solvent effects in SN2 reactions promoted by macrocyclic polyethers and quaternary onium salts. *J. Supramol. Chem.* **2003,** *2* (1-3), 187-190.

192. Hoyle, C. E.; Lowe, A. B.; Bowman, C. N., Thiol-click chemistry: a multifaceted toolbox for small molecule and polymer synthesis. *Chem. Soc. Rev.* **2010,** *39* (4), 1355-1387.

193. Derboven, P.; D'Hooge, D. R.; Stamenovic, M. M.; Espeel, P.; Marin, G. B.; Du Prez, F. E.; Reyniers, M.-F., Kinetic Modeling of Radical Thiol-Ene Chemistry for Macromolecular Design: Importance of Side Reactions and Diffusional Limitations. *Macromolecules* **2013,** *46* (5), 1732-1742.

194. Rankin, J. M.; Zhang, Q.; La Gasse, M. K.; Zhang, Y.; Askim, J. R.; Suslick, K. S., Solvatochromic sensor array for the identification of common organic solvents. *Analyst* **2015,** *140* (8), 2613-2617.

195. Xu, J.; Boyer, C., Visible Light Photocatalytic Thiol-Ene Reaction: An Elegant Approach for Fast Polymer Postfunctionalization and Step-Growth Polymerization. *Macromolecules* **2015,** *48* (3), 520-529.

196. Fadeyi, O. O.; Mousseau, J. J.; Feng, Y.; Allais, C.; Nuhant, P.; Chen, M. Z.; Pierce, B.; Robinson, R., Visible-Light-Driven Photocatalytic Initiation of Radical Thiol-Ene Reactions Using Bismuth Oxide. *Org. Lett.* **2015,** *17* (23), 5756-5759.

197. Wang, S.; Kim, S.-H., New solvatochromic merocyanine dyes based on Barbituric acid and Meldrum's acid. *Dyes Pigm.* **2009,** *80* (3), 314-320.

198. Marcus, Y., Chemical Properties of Solvents. In *The Properties of Solvents*, Fogg, P. G. T., Ed. John Wiley & Sons Ltd: West Sussex, England, 1998; Vol. 4, pp 142 -162.

199. Zhang, J.; Lalevee, J.; Zhao, J.; Graff, B.; Stenzel, M. H.; Xiao, P., Dihydroxyanthraquinone derivatives: natural dyes as blue-light-sensitive versatile photoinitiators of photopolymerization. *Polym. Chem.* **2016,** *7* (47), 7316-7324.

200. Shih, H.; Fraser, A. K.; Lin, C.-C., Interfacial Thiol-ene Photoclick Reactions for Forming Multilayer Hydrogels. *ACS Appl. Mater. Interfaces* **2013,** *5* (5), 1673-1680.

201. Wacker, K. T.; Kristufek, S. L.; Lim, S.-M.; Kahn, S.; Wooley, K. L., Bio-based polycarbonates derived from the neolignan honokiol. *RSC Adv.* **2016,** *6* (85), 81672-81679.

202. Zhang, W.; Ye, M.; Zhan, J.; Chen, Y.; Guo, D., Microbial glycosylation of four free anthraquinones by Absidia coerulea. *Biotechnol. Lett.* **2004,** *26* (2), 127-131.

203. Shi, D.-H.; Huang, W.; Li, C.; Liu, Y.-W.; Wang, S.-F., Design, synthesis and molecular modeling of aloe-emodin derivatives as potent xanthine oxidase inhibitors. *Eur. J. Med. Chem.* **2014,** *75*, 289-296.

204. de Melo, C. E. A.; Nandi, L. G.; Dominguez, M.; Rezende, M. C.; Machado, V. G., Solvatochromic behavior of dyes with dimethylamino electron-donor and nitro electron-acceptor groups in their molecular structure. *J. Phys. Org. Chem.* **2015,** *28* (4), 250-260.

205. Marcus, Y., Solvent Effects. In *The Properties of Solvents*, Fogg, P. G. T., Ed. John Wiley & Sons Ltd: West Sussex, England, 1998; Vol. 4, pp 58 - 62.

206. Li, Q.; Batchelor-McAuley, C.; Lawrence, N. S.; Hartshorne, R. S.; Compton, R. G., Electrolyte tuning of electrode potentials: the one electron vs. two electron reduction of anthraquinone-2-sulfonate in aqueous media. *Chem. Commun.* **2011,** *47* (41), 11426-11428.

207. Murschell, A. E.; Kan, W. H.; Thangadurai, V.; Sutherland, T. C., Anthraquinone derivatives as electron-acceptors with liquid crystalline properties. *Phys. Chem. Chem. Phys.* **2012,** *14* (13), 4626-4634.

208. Gao, A.; Zhang, H.; Sun, G.; Xie, K.; Hou, A., Light-induced antibacterial and UV-protective properties of polyamide 56 biomaterial modified with anthraquinone and benzophenone derivatives. *Mater. Des.* **2017,** *130*, 215-222.

209. Nissim, R.; Batchelor-McAuley, C.; Li, Q.; Compton, R. G., The anthraquinone mediated one-electron reduction of oxygen in acetonitrile. *J. Electroanal. Chem.* **2012,** *681*, 44-48.

210. Zeng, L.; Liu, T.; He, C.; Shi, D.; Zhang, F.; Duan, C., Organized Aggregation Makes Insoluble Perylene Diimide Efficient for the Reduction of Aryl Halides via Consecutive Visible Light-Induced Electron-Transfer Processes. *Journal of the American Chemical Society* **2016,** *138* (12), 3958-3961.

211. Briggs, E. A.; Besley, N. A., Density Functional Theory Based Analysis of Photoinduced Electron Transfer in a Triazacryptand Based K+ Sensor. *J. Phys. Chem. A* **2015,** *119* (12), 2902-2907.

212. Anslyn, E. V.; Dougherty, D. A., Modern Physical Organic Chemistry. Murdzek, J., Ed. University Science Books: Mill Valley, CA, 2006; pp 955 - 956.

213. Nuzhdin, K. B.; Feldman, V. I., Structure and photochemistry of "bridged" bifunctional radical cations: Amidoesters vs. amides. *Radiat. Phys. Chem.* **2008,** *77* (4), 416-427.

214. Shkrob, I. A.; Marin, T. W., Electron Localization and Radiation Chemistry of Amides. *J. Phys. Chem. A* **2012,** *116* (7), 1746-1757.

215. Eastland, G. W.; Rao, D. N. R.; Symons, M. C. R., Radiation generation of radical cations of amides. An electron spin resonance study. *J. Chem. Soc., Faraday Trans. 1* **1986,** *82* (9), 2833-42.

216. Pérez, L. M., Quantum Mechanical Short Course: Lecture 2. Simulation, T. A. M. U.-L. f. M., Ed. College Station, TX, 2016.

217. Chen, R.; Tang, Y.; Wan, Y.; Chen, T.; Zheng, C.; Qi, Y.; Cheng, Y.; Huang, W., Promoting Singlet/triplet Exciton Transformation in Organic Optoelectronic Molecules: Role of Excited State Transition Configuration. *Sci. Rep.* **2017,** *7* (1), 6225.

218. Kim, H.; Kim, H.; Lambert, T. H.; Lin, S., Reductive Electrophotocatalysis: Merging Electricity and Light To Achieve Extreme Reduction Potentials. *J. Am. Chem. Soc.* **2020,** *142* (5), 2087-2092.

219. Kajjam, A. B.; Giri, S.; V, S., Triphenylamine-based donor–π–acceptor organic phosphors: synthesis, characterization and theoretical study. *Mater. Chem. Front.* **2017,** *1* (3), 512-520.

220. Lakowicz, J. R., Introduction to Fluorescence. In *Principles of Fluorescence Spectroscopy*, 3rd ed.; Springer Science+Business Media, LLC: New York, NY, 2006; pp 8-9.

221. Banerjee, S.; Both, A. K.; Sarkar, M., Probing the Aggregation and Signaling Behavior of Some Twisted 9,9'-Bianthryl Derivatives: Observation of Aggregation-Induced Blue-Shifted Emission. *ACS Omega* **2018,** *3* (11), 15709-15724.

222. Korth, M., Density Functional Theory: Not Quite the Right Answer for the Right Reason Yet. *Angew. Chem. Int. Ed.* **2017,** *56* (20), 5396-5398.

223. Wang, C.-C.; Lai, Y.-H.; Ou, Y.-M.; Chang, H.-T.; Wang, Y.-S., Critical factors determining the quantification capability of matrix-assisted laser desorption/ionization- time-of-flight mass spectrometry. *Philos. Trans. R. Soc. A* **2016,** *374* (2079), 20150371.

224. Goldschmidt, R. J.; Wetzel, S. J.; Blair, W. R.; Guttman, C. M., Post-source decay in the analysis of polystyrene by matrix-assisted laser desorption/ionization time-of-flight mass spectrometry. *J. Am. Soc. Mass Spectrom.* **2000,** *11* (12), 1095-1106.

225. Gruendling, T.; Weidner, S.; Falkenhagen, J.; Barner-Kowollik, C., Mass spectrometry in polymer chemistry: a state-of-the-art up-date. *Polym. Chem.* **2010,** *1* (5), 599-617.

226. Smolira, A.; Wessely-Szponder, J., Importance of the matrix and the matrix/sample ratio in MALDI-TOF-MS analysis of cathelicidins obtained from porcine neutrophils. *Appl. Biochem. Biotechnol.* **2015,** *175* (4), 2050-2065.

227. Aksenov, A. A.; Bier, M. E., The Analysis of Polystyrene and Polystyrene Aggregates into the Mega Dalton Mass Range by Cryodetection MALDI TOF MS. *J. Am. Soc. Mass Spectrom.* **2008,** *19* (2), 219-230.

APPENDIX A

SUPPORTING INFORMATION FOR CHAPTER 2

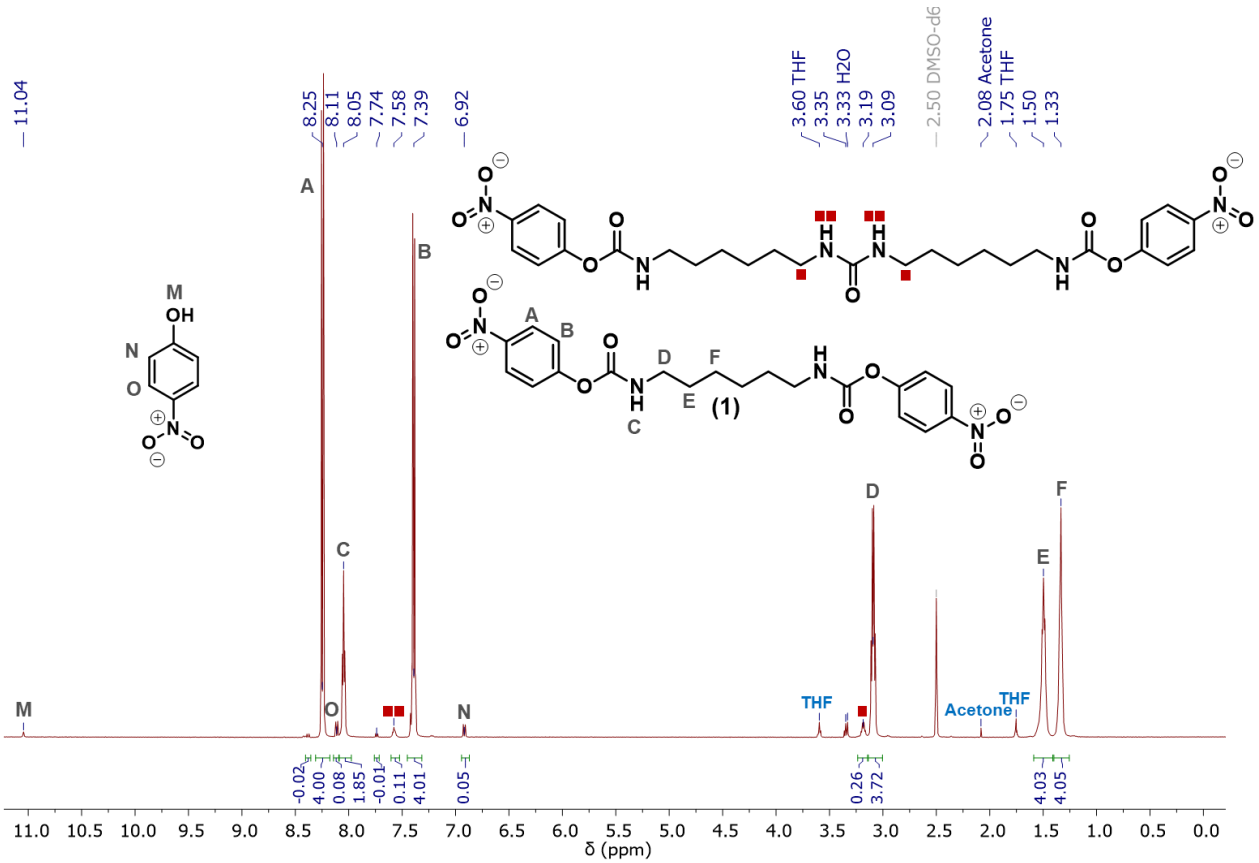

Figure A-1. ^{1}H-NMR (500 MHz, DMSO-d_6) of **1**. The composition of urea (red boxes) at 3.19 and 7.58 ppm integrates to 7% relative to carbamate.

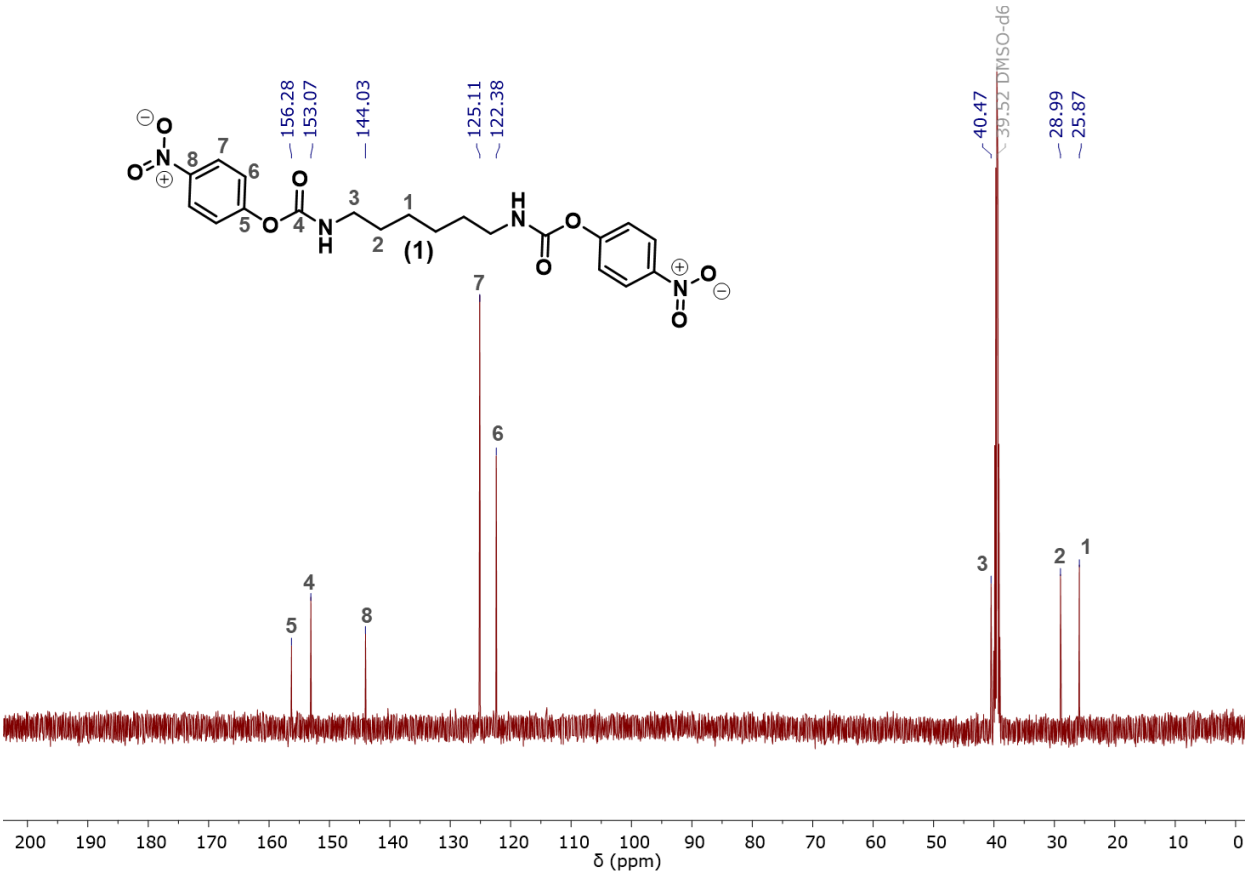

Figure A-2. ^{13}C-NMR (125 MHz, DMSO-d_6) spectrum of **1**, d1 = 1 s.

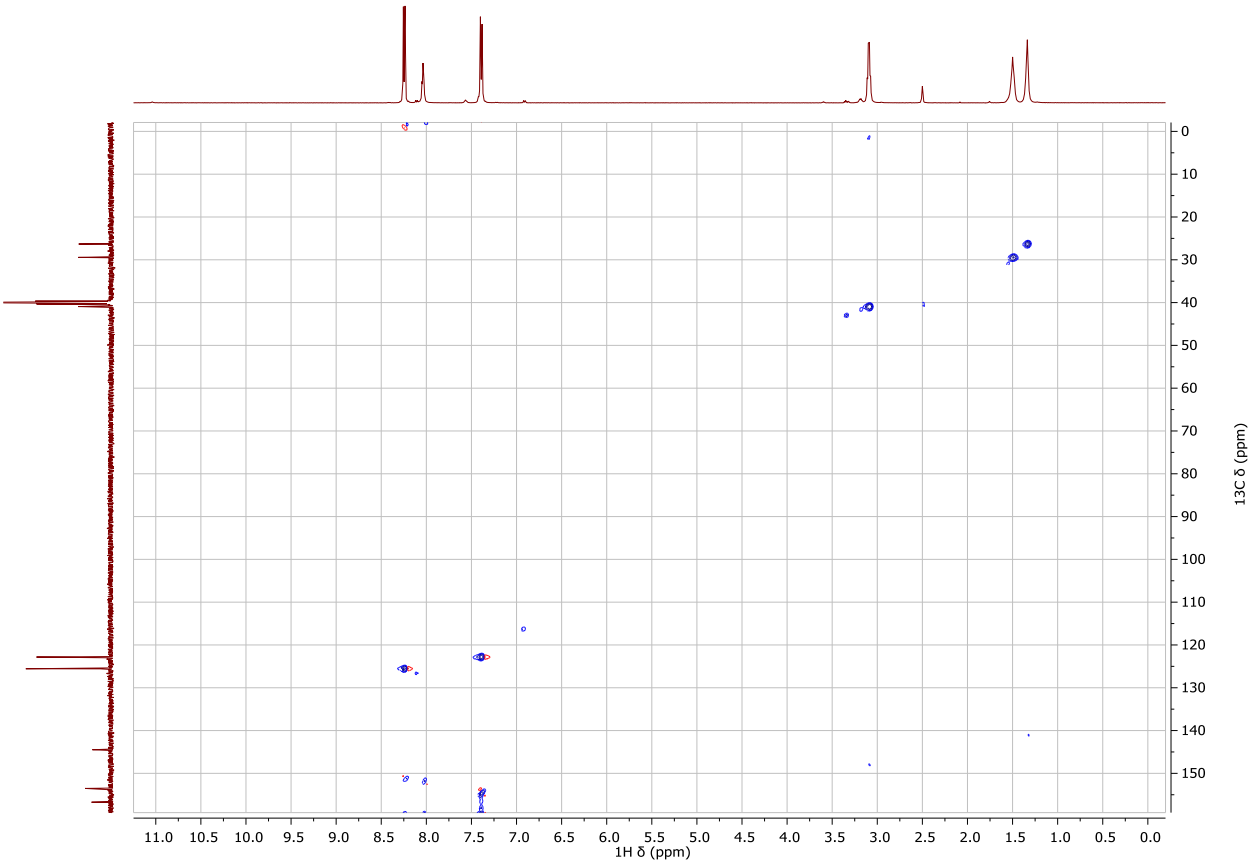

Figure A-3. ^{1}H-^{13}C-HMQC NMR (500-125 MHz, DMSO-d_6) spectrum of **1**.

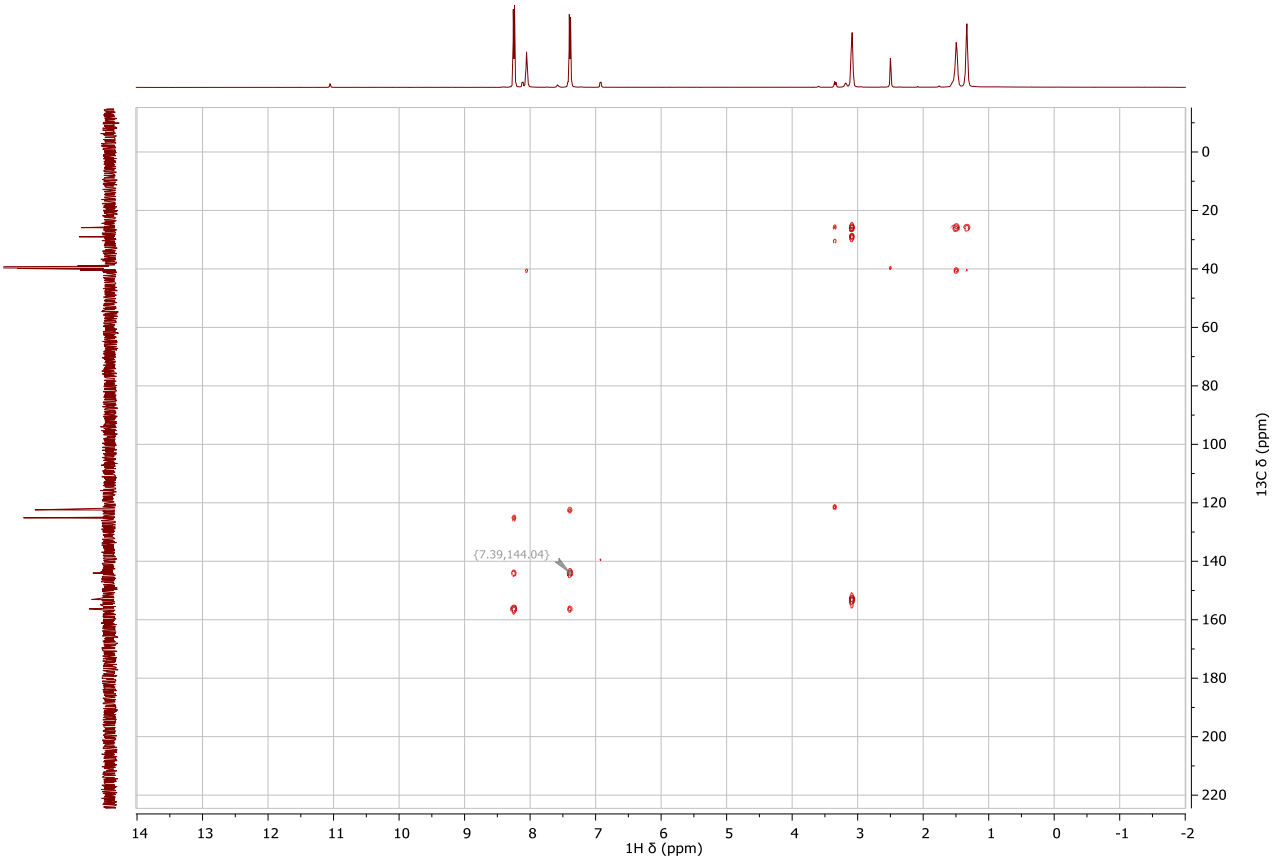

Figure A-4. ^{1}H-^{13}C-gHMBC NMR (500 – 125 MHz, DMSO-d_6) spectrum of **1**. This spectrum was acquired on a Varian NMRS500 instrument.

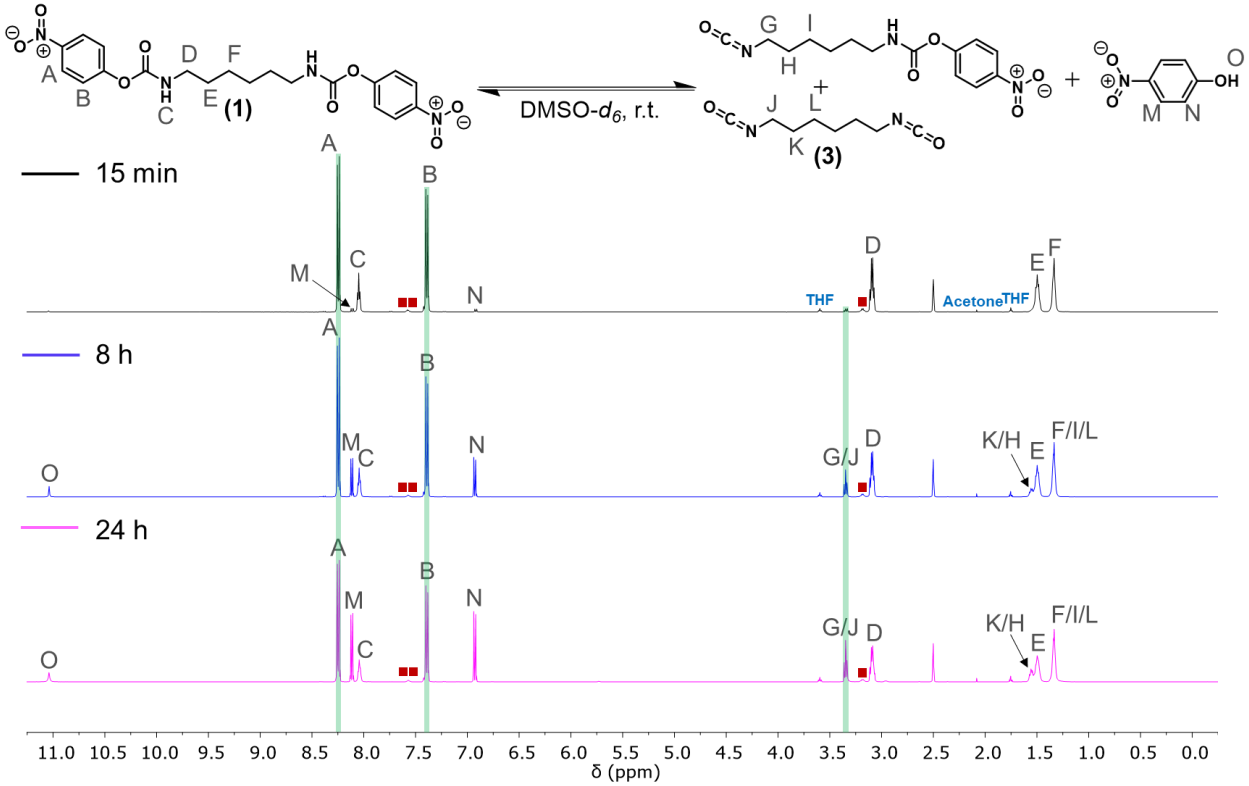

Figure A-5. ^{1}H-NMR (500 MHz, DMSO-d_6) spectra showing the autodissociation of dicarbamate **1** at room temperature for *ca.* 15 min, 8 h, and 24 h after dissolution. A small amount of urea (red boxes) was visible (see Figure A-1). The d1 was set for 10 s.

Table A-1. Integration table for the ^{1}H NMR spectra acquired during dicarbamate autodissociation shown in Figure A-5. The peaks are listed as normalized relative to the A peak in each time point. The percent of dissociated dicarbamate at 15 min, 8 h, and 24 h was determined to be 1%, 15%, and 28%, respectively, based on the relative integrations of the normalized aromatic B proton resonances adjacent to the carbamate group at 7.44 to 7.35 ppm and the *p*-nitrophenol N peaks between 6.97 and 6.90 ppm. The d1 was set for 10 s.

	15 min		**8 h**		**24 h**	
Range (ppm)	Normalized	Absolute	Normalized	Absolute	Normalized	Absolute
8.28 - 8.20	4.00	80600	4.00	70500	4.00	61500
8.15 - 8.09	0.08	1630	0.71	12600	1.49	22900
8.08 - 8.00	1.82	36800	1.81	31900	1.81	27800
7.44 - 7.35	4.00	80600	3.99	70300	3.98	61200
6.97 - 6.90	0.05	1030	0.71	12500	1.52	23300
3.37 - 3.31	0.11	2180	0.79	13900	1.56	23900

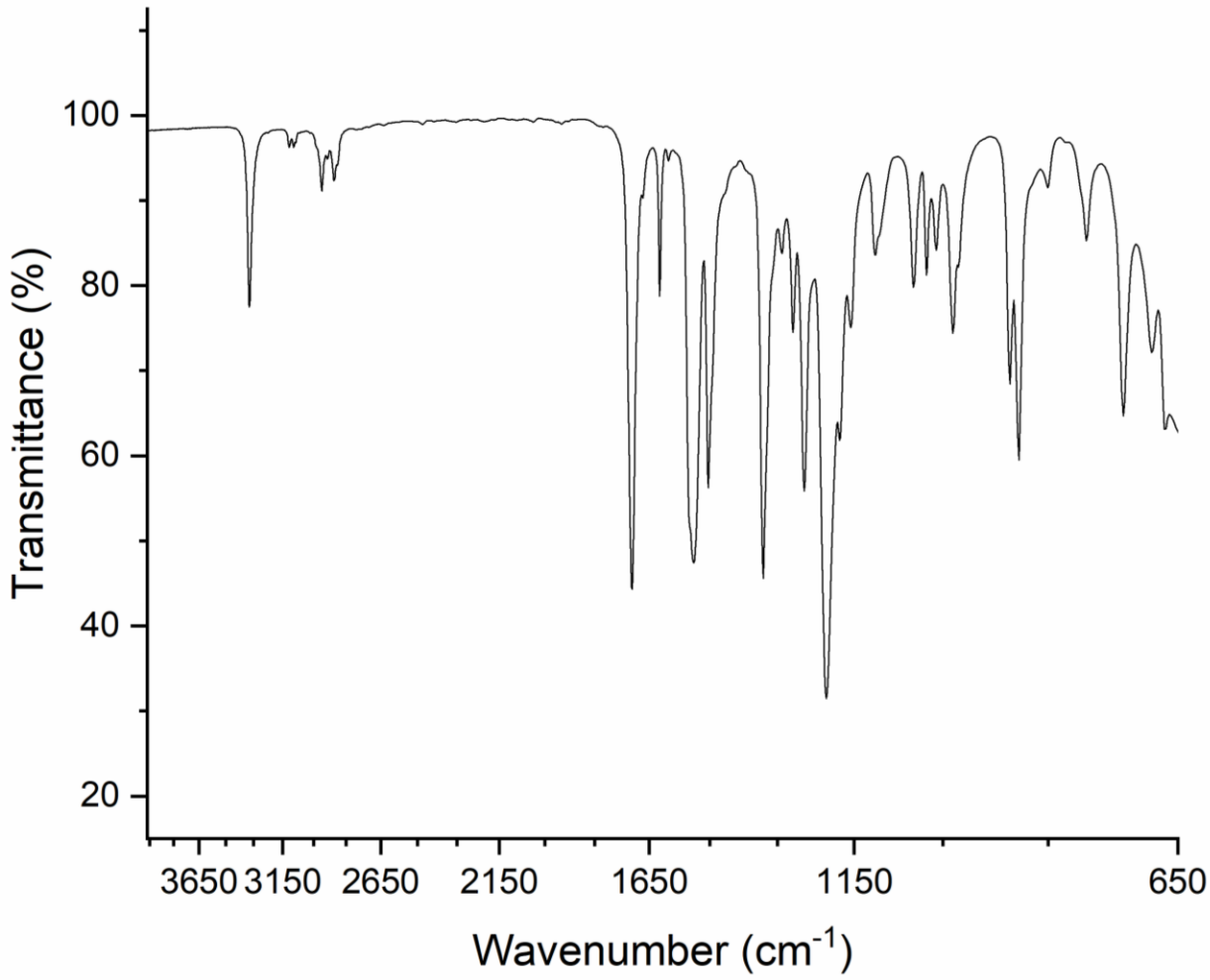

Figure A-6. FTIR spectrum of **1**.

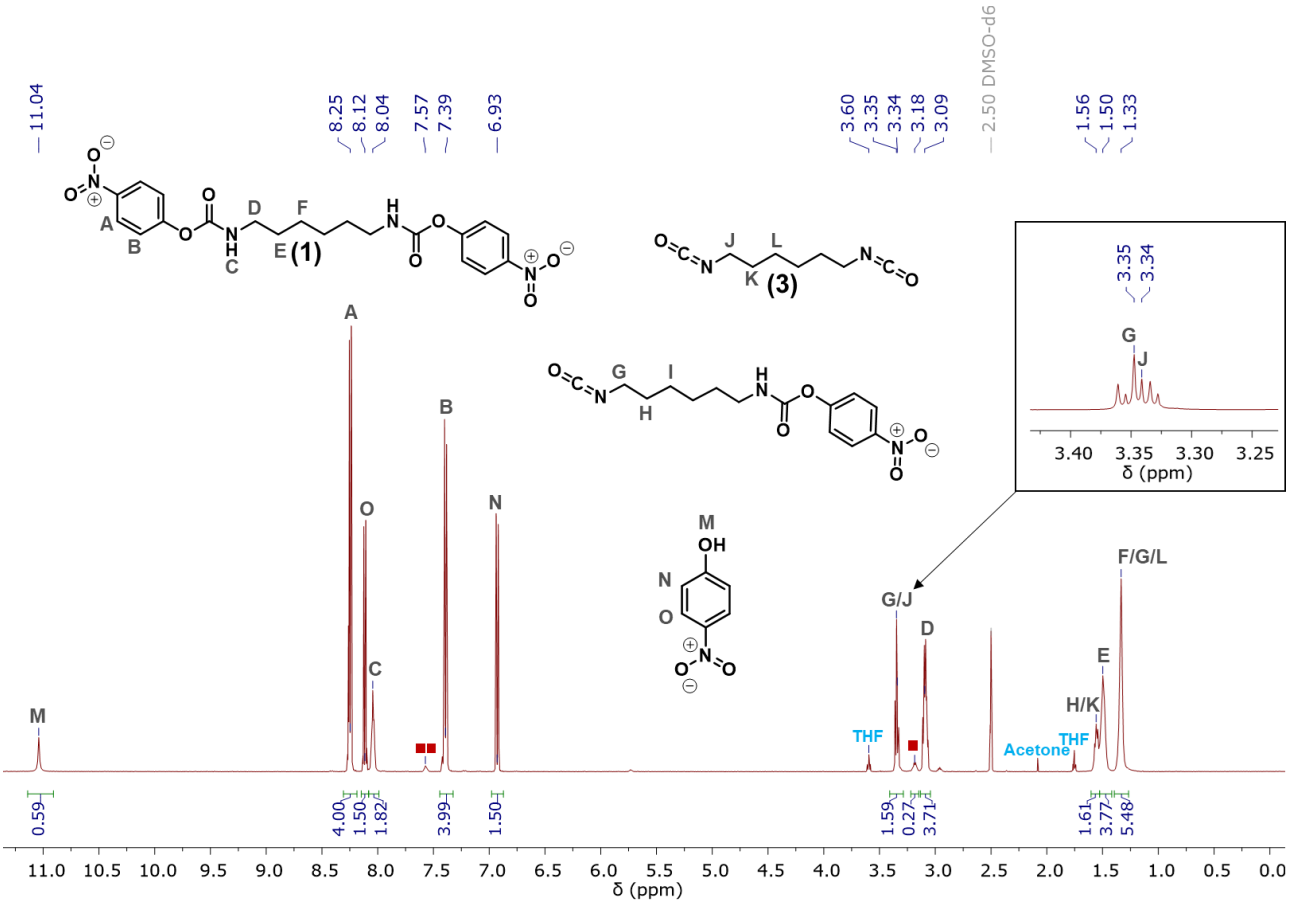

Figure A-7. ^{1}H-NMR (500 MHz, DMSO-d_6) spectrum of **1** at 24 h. The presence of urea (red boxes) can be observed.

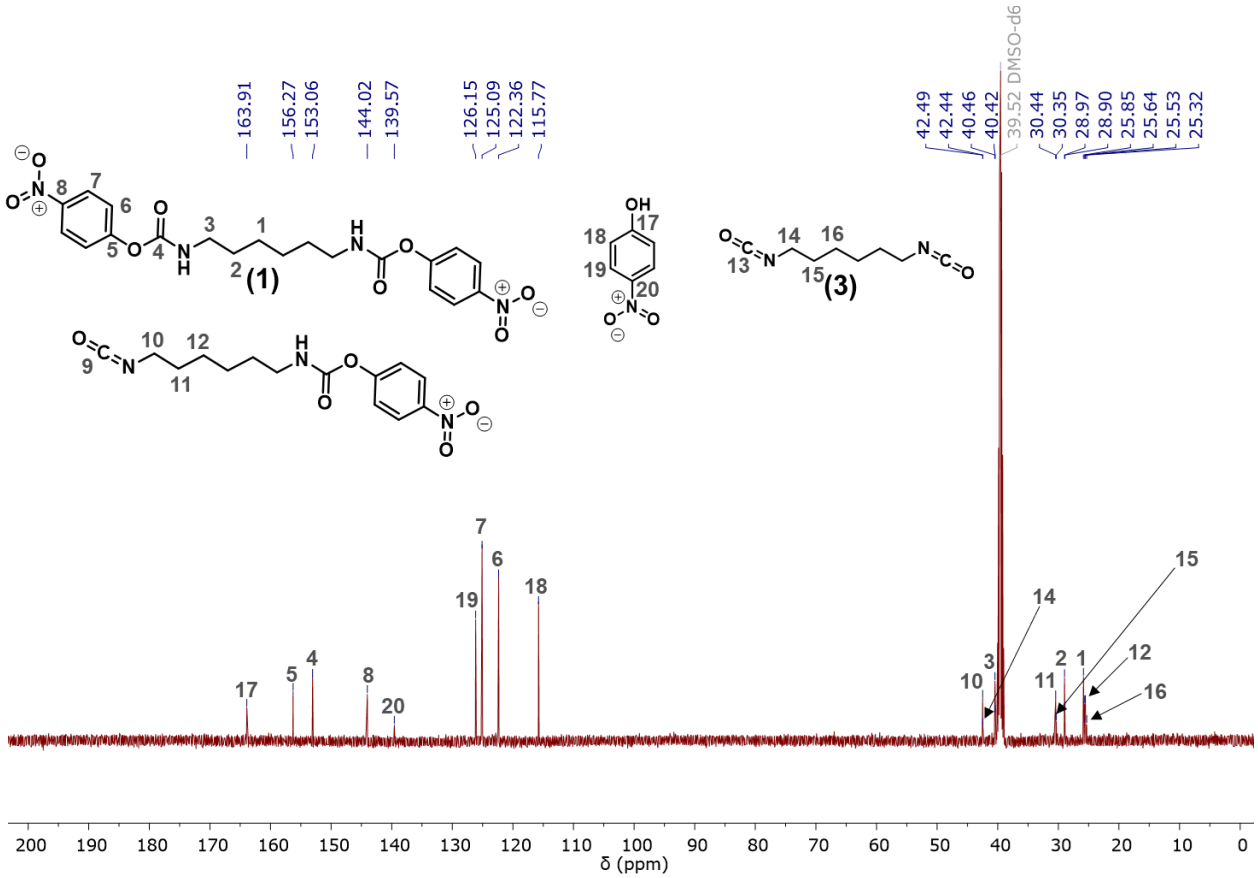

Figure A-8. ^{13}C-NMR (125 MHz, DMSO-d_6) spectrum of dicarbamate **1** at 24 h, d1 = 3 s.

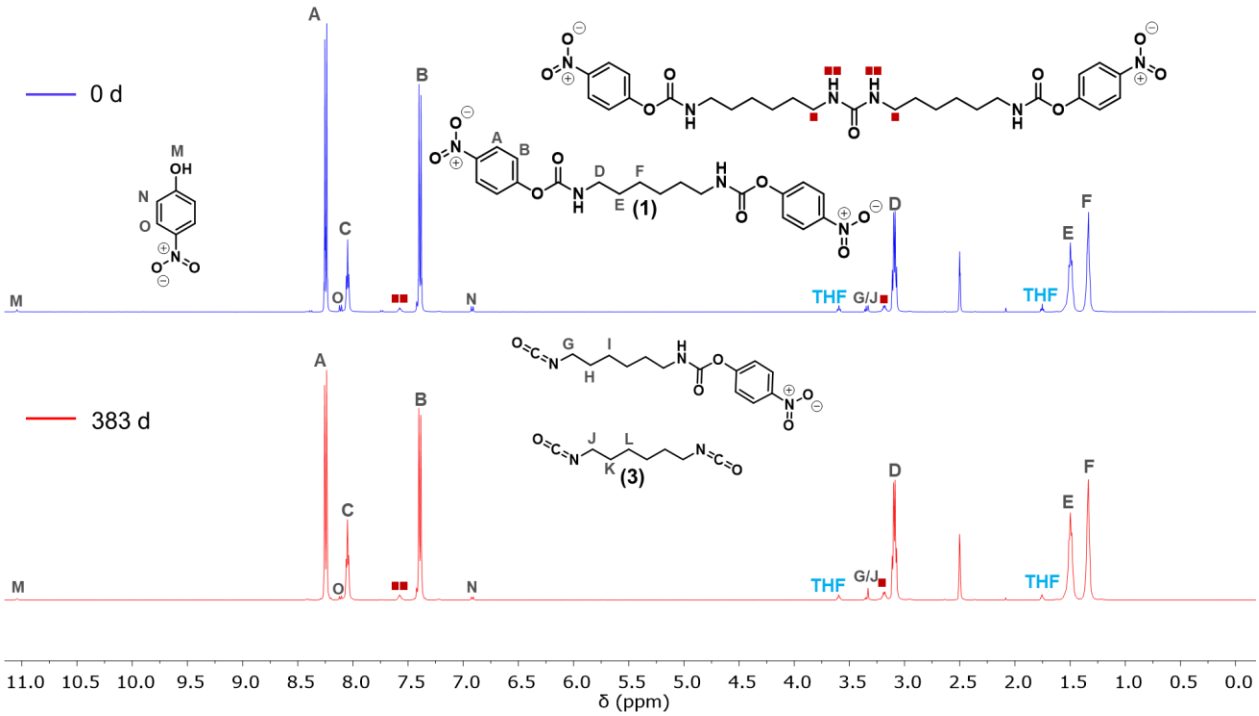

Figure A-9. Long-term stability of **1** (over 383 d) as measured by ^{1}H-NMR (500 MHz, DMSO-d_6) spectroscopy**.** A solid sample of **1** was stored in a vial with a cap under ambient conditions before being dissolved in DMSO-d_6 and acquiring the spectra. The relaxation delay was 10 s for both runs.

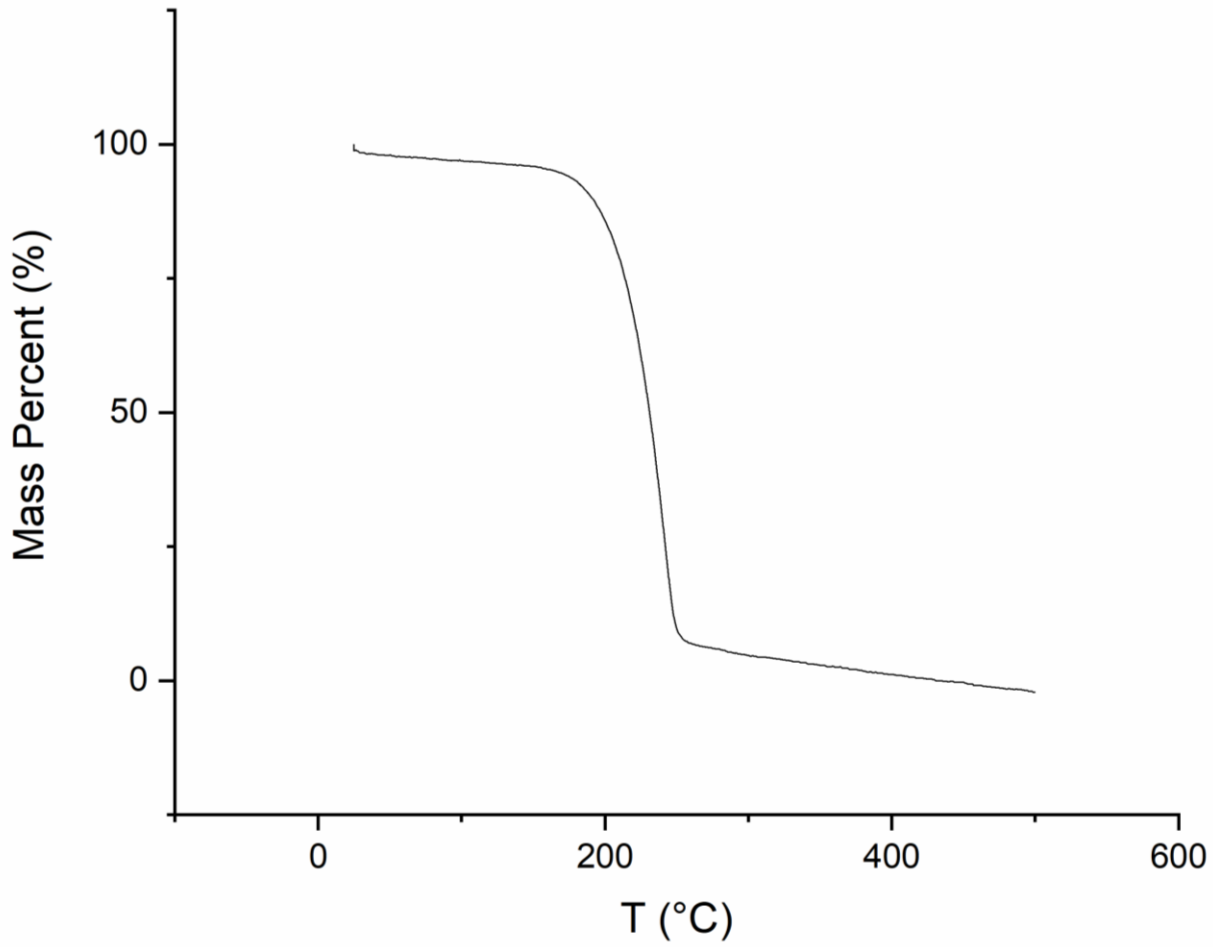

Figure A-10. TGA of **1**.

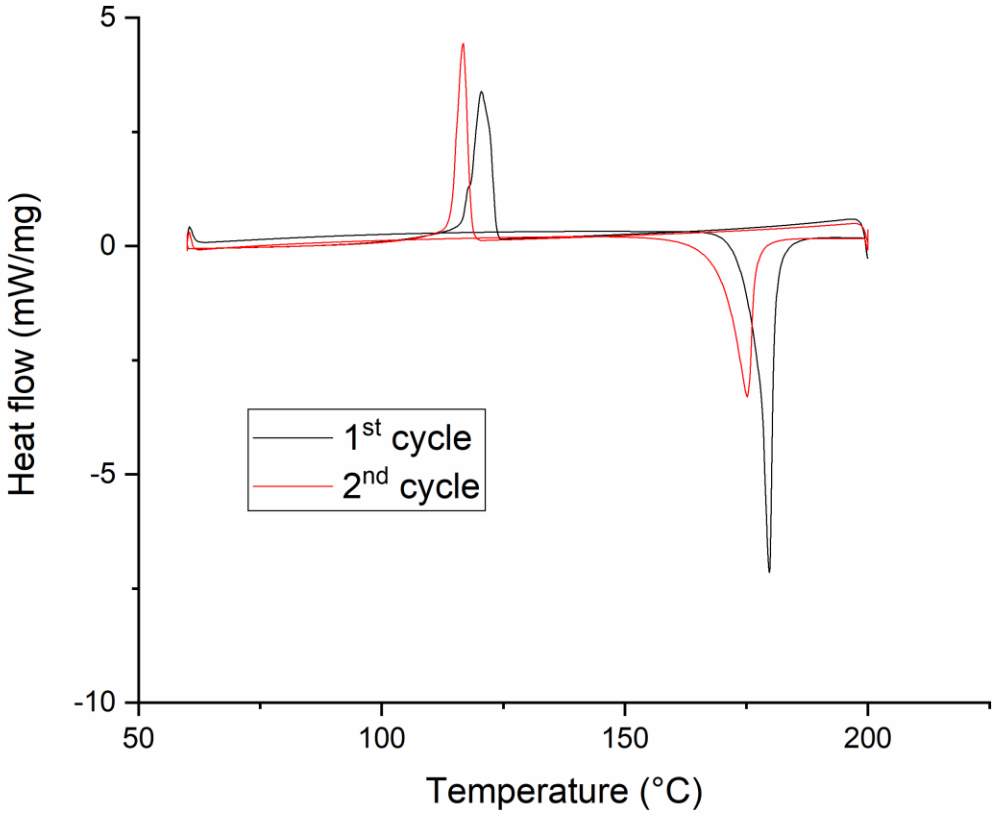

Figure A-11. DSC thermogram of **1** during the first and second heating and cooling cycles. Note the exothermic event on both of the cooling ramps. Because of hysteresis in the second cycle, the T_m is was reported from the first heating cycle.

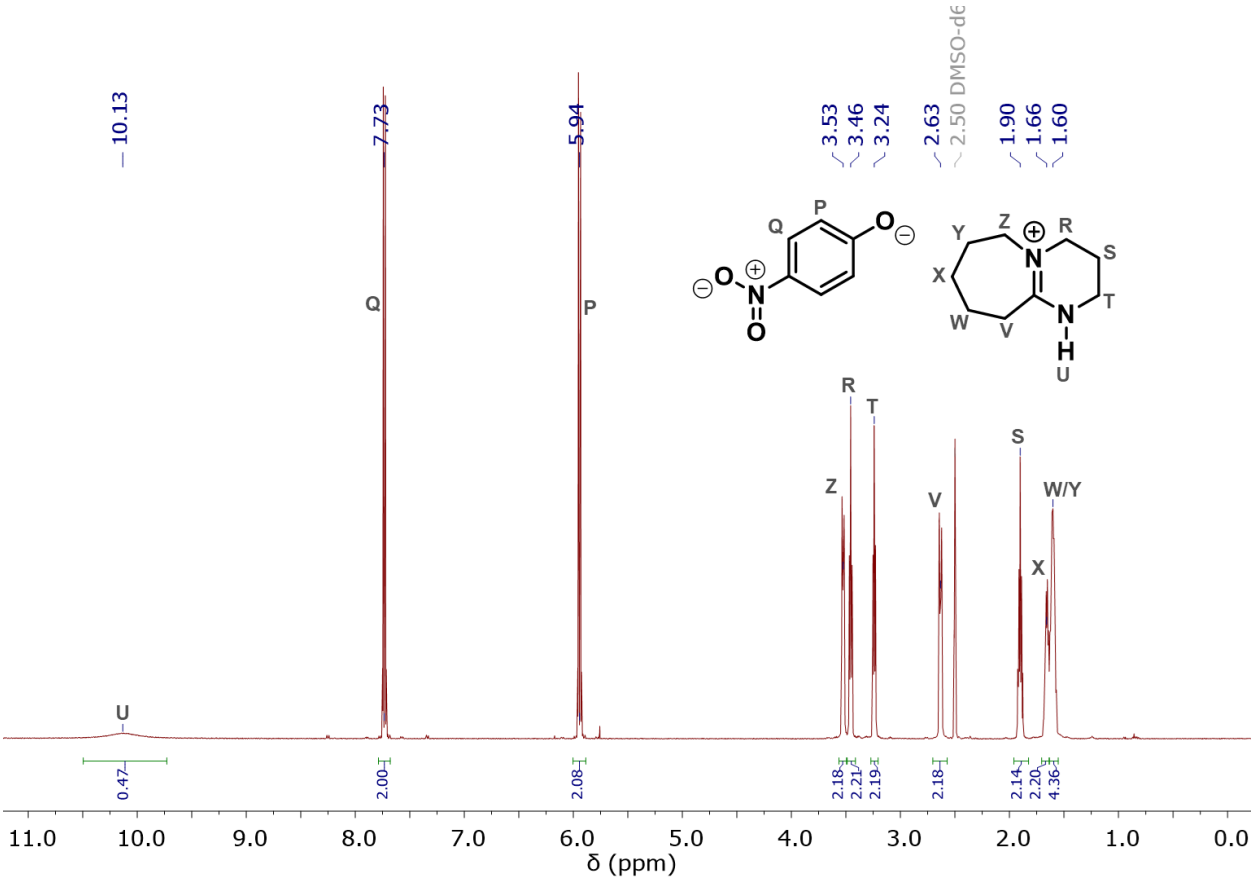

Figure A-12. ^{1}H-NMR (500 MHz, DMSO-d_6) spectrum of the DBU-H *p*-nitrophenoxide salt **4** with d1 = 10 s.

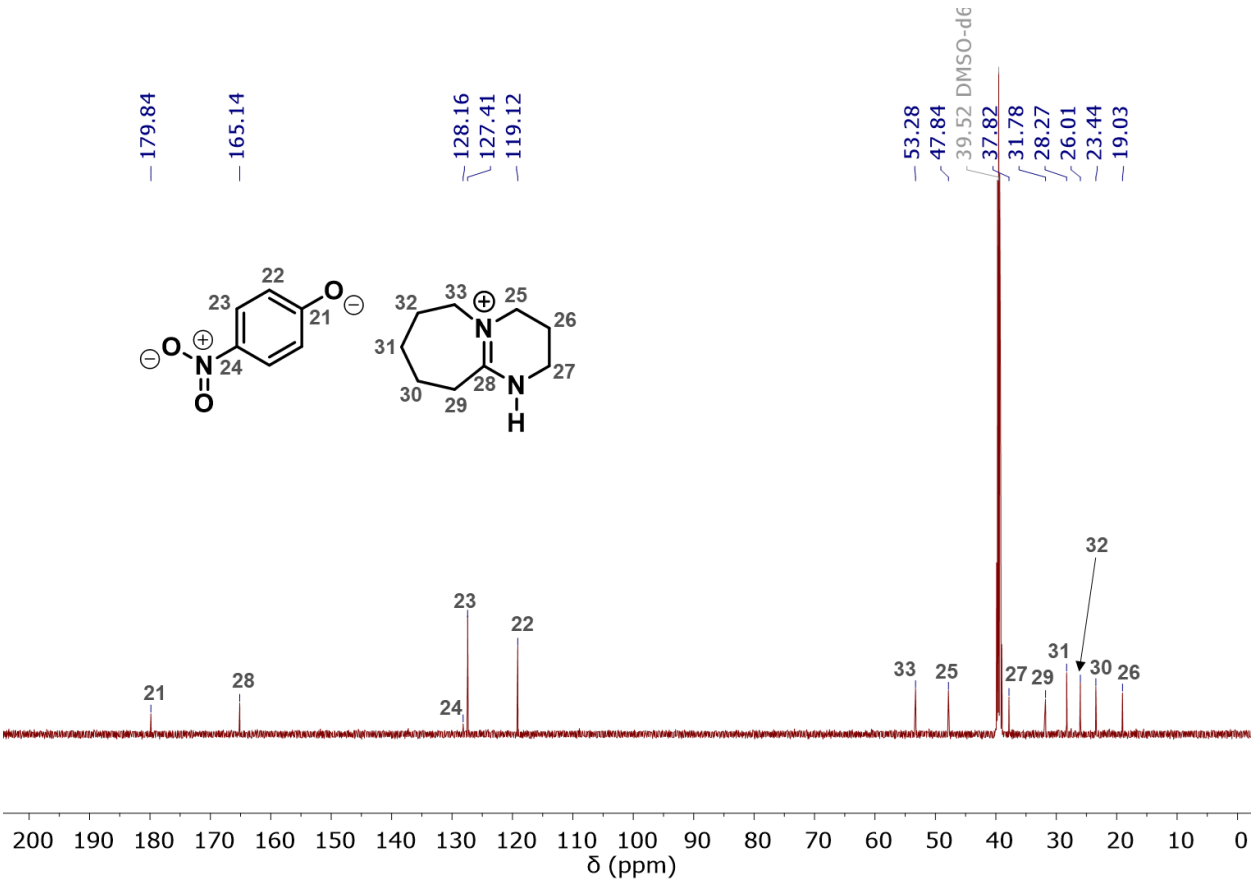

Figure A-13. ^{13}C-NMR (125 MHz, DMSO-d_6) spectrum of DBU-H *p*-nitrophenoxide salt **4** with nt = 512 and d1 = 3 s.

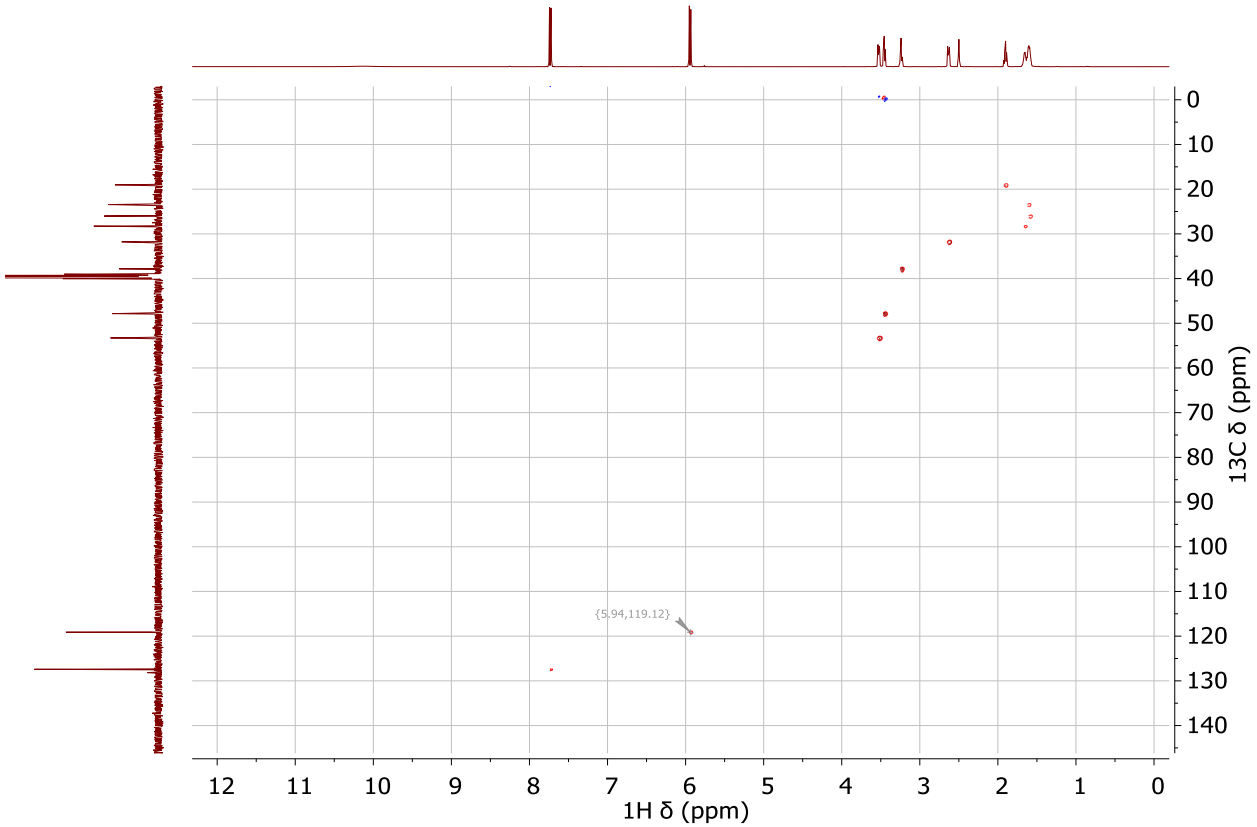

Figure A-14. ^{1}H - ^{13}C HMQC NMR (125 MHz, DMSO-d_6) spectrum of DBU-H *p*-nitrophenoxide salt **4** with nt = 32 and ni = 200.

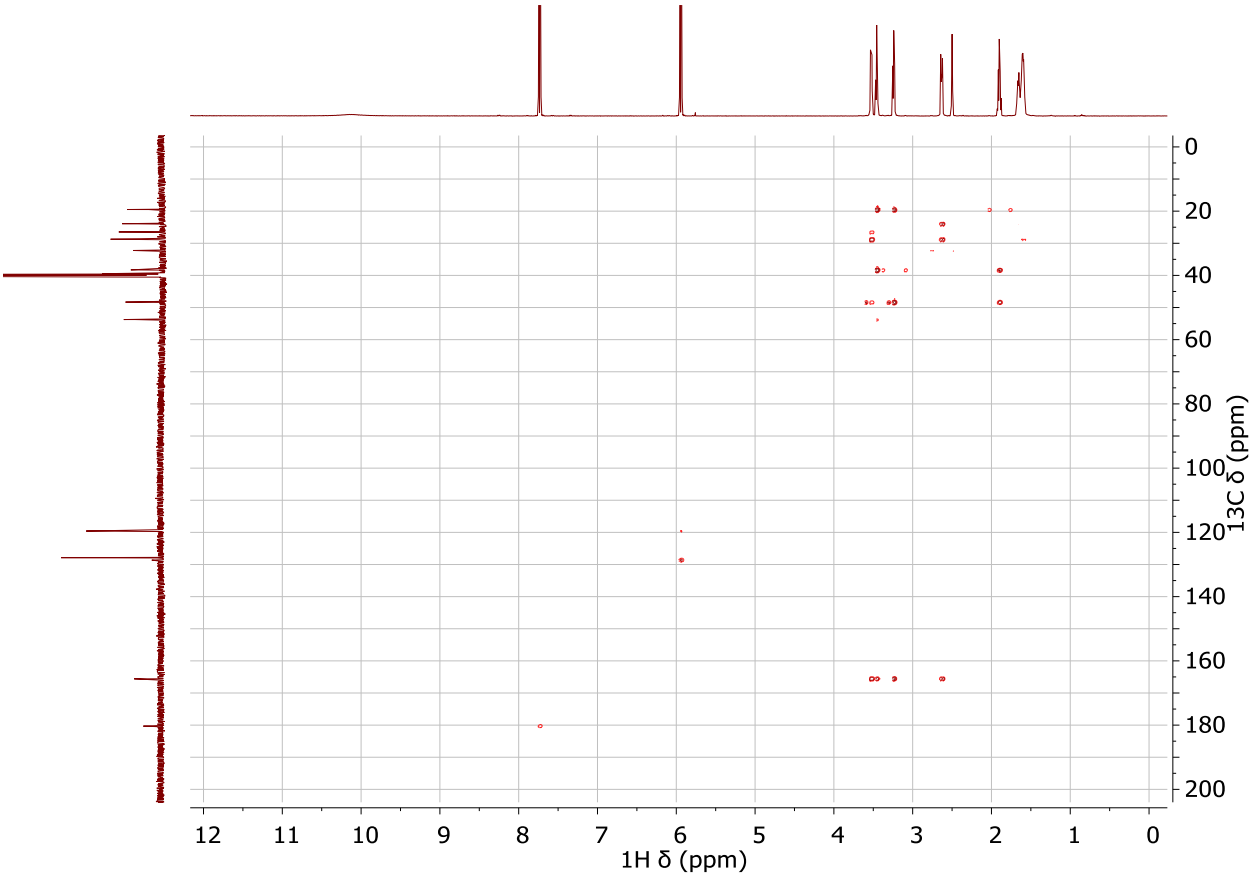

Figure A-15. ^{1}H - ^{13}C HMBC NMR (125 MHz, DMSO-d_6) spectrum of **4** with nt = 50 and ni = 200.

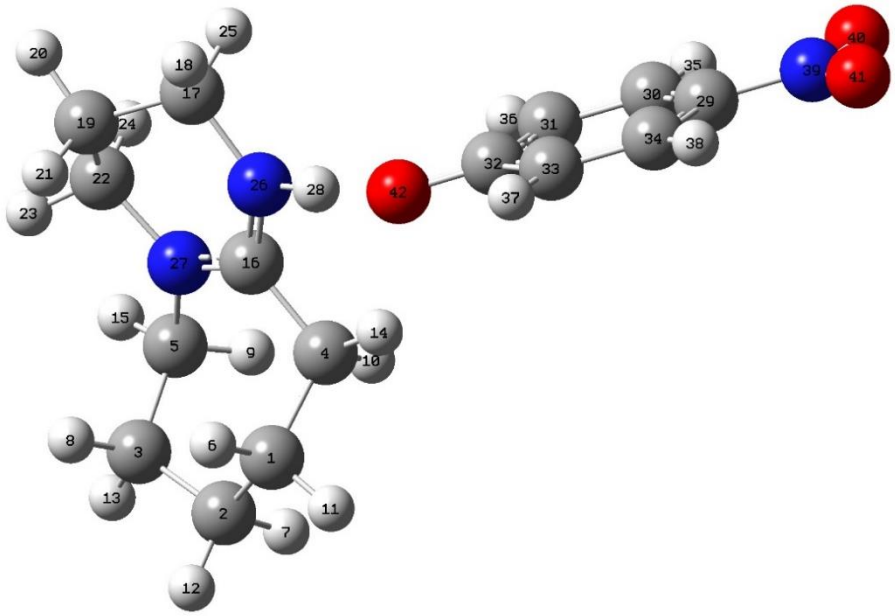

Figure A-16. Computationally optimized structure of **4**: NMR calculations for **4** were carried out using the GIAO method.

Table A-2. Calculated ^{1}H-NMR Shifts (Reference shielding = 31.89 ppm)

Shift (ppm)	Degeneracy	Atom Index
12.54	1	28
8.26	2	38,35
6.44	2	37,36
3.85	1	9
3.54	1	24
3.45	2	18,23
3.31	1	25
3.21	1	15
2.63	1	10
2.58	1	14
2.00	2	20,21
1.93	1	12
1.81	1	11
1.73	1	13
1.65	1	7
1.59	1	8
1.53	1	6

Table A-3. Calculated $_{13}$C-NMR Shifts (Reference Shielding = 185.38 ppm)

Shift (ppm)	Degeneracy	Atom Index
189.72	1	32
176.63	1	16
139.49	1	29
136.40	1	34
136.18	1	30
126.51	1	33
124.56	1	31
59.94	1	5
54.49	1	22
43.24	1	17
38.65	1	4
35.46	1	2
32.15	1	3
31.02	1	1
25.35	1	19

Table A-4. XYZ matrix for optimized structure of **4**.

C	1.157964646622	-1.222065286997	-0.000115189186
C	-0.212602625254	-1.225419661905	-0.000103640011
C	-0.992083655382	0.000223200894	0.000009922469
C	-0.212401145801	1.225735745617	0.000109397078
C	1.158166269330	1.222154060795	0.000118828699
C	1.870309257445	-0.000013830765	0.000006053502
H	1.711636390562	-2.152584685297	-0.000193603348
H	-0.755358442655	-2.165443383130	-0.000172584900
H	-0.754998991472	2.165850582139	0.000174622738
H	1.711990627032	2.152582501455	0.000193888830
O	-2.250168568856	0.000325744656	-0.000002933586
N	3.281269549684	-0.000131217681	0.000018054828
O	3.894890447128	1.090306343088	0.000386498394
O	3.894706891617	-1.090672002869	-0.000250425508

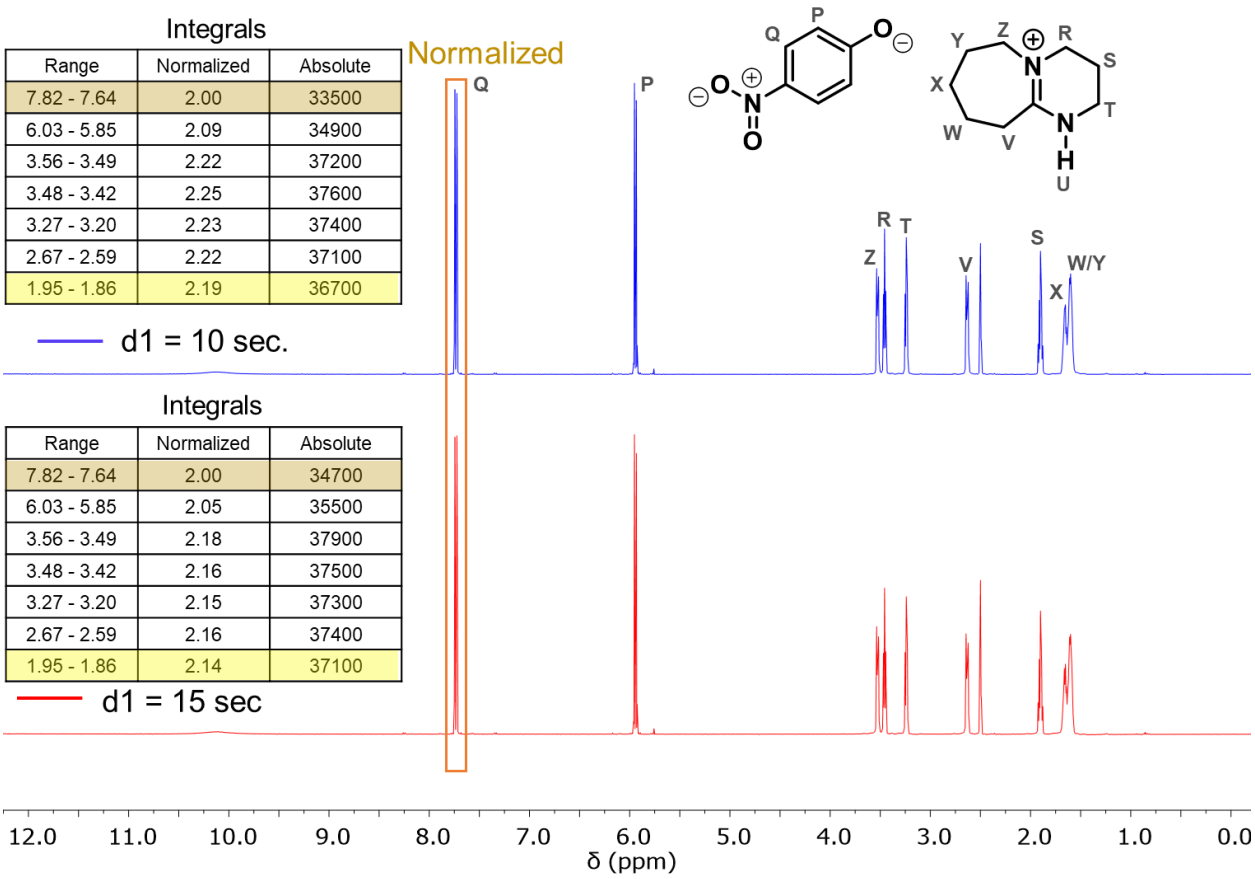

Figure A-17. ^{1}H-NMR (500 MHz, DMSO-d_6) spectroscopy relaxation experiment to determine the optimal relaxation delay time for use in acquiring NMR spectra of **4** in DMSO-d_6 at a concentration of 14 mg/mL. The range (ppm) highlighted in yellow shows a 5.5% difference by integration. This is the highest percentage difference between corresponding peaks in both spectra indicating that the protons are relaxed sufficiently.

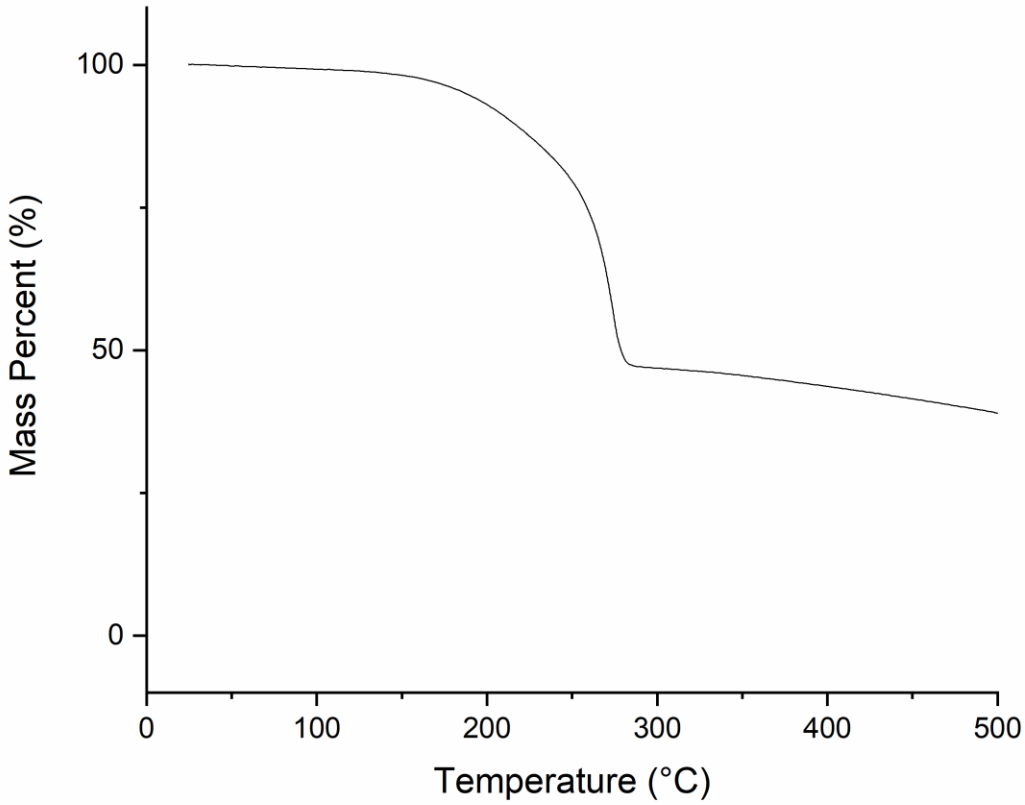

Figure A-18. TGA of **4**.

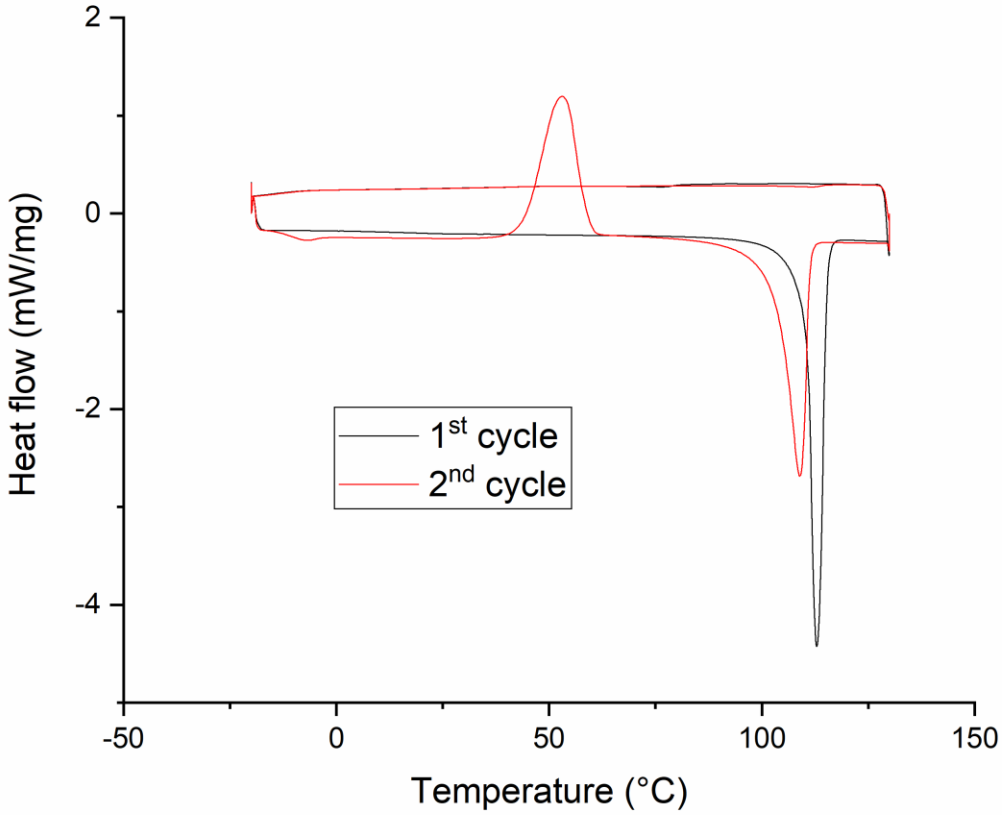

Figure A-19. DSC of **4** showing both the first and second heating and cooling cycles. Because of the hysteresis and anomalous exothermic event (*ca.* 50 °C) on the heating cycle of the second run, the T_m was reported from the first run.

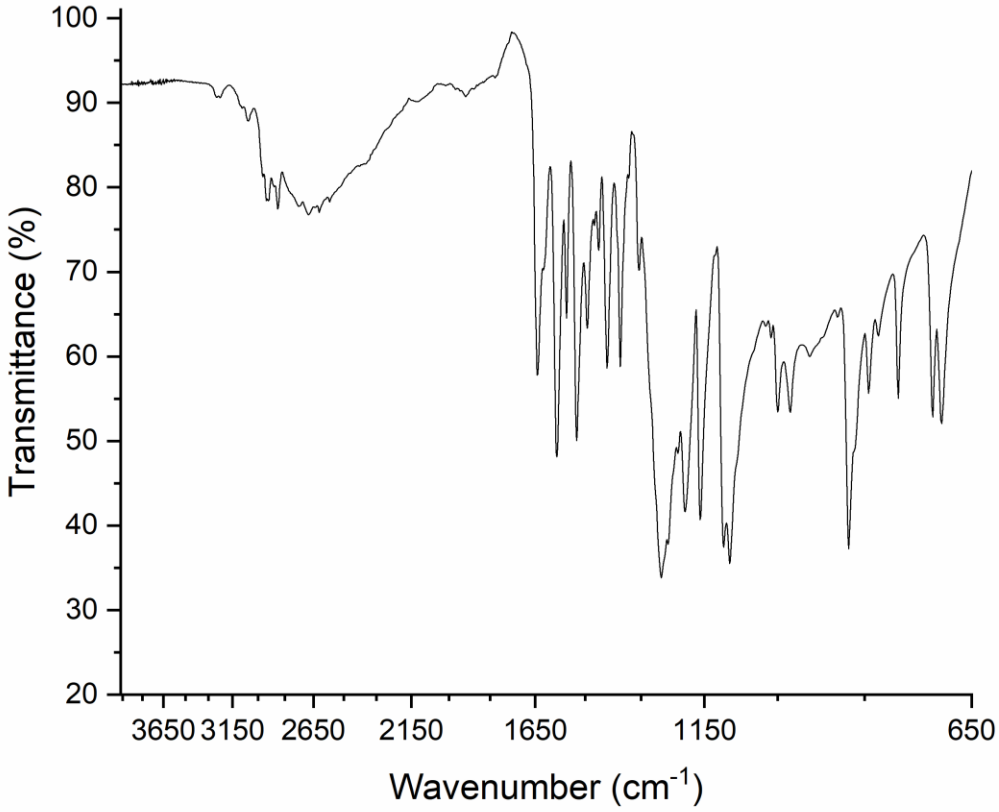

Figure A-20. ATR-FTIR spectrum of **4**.

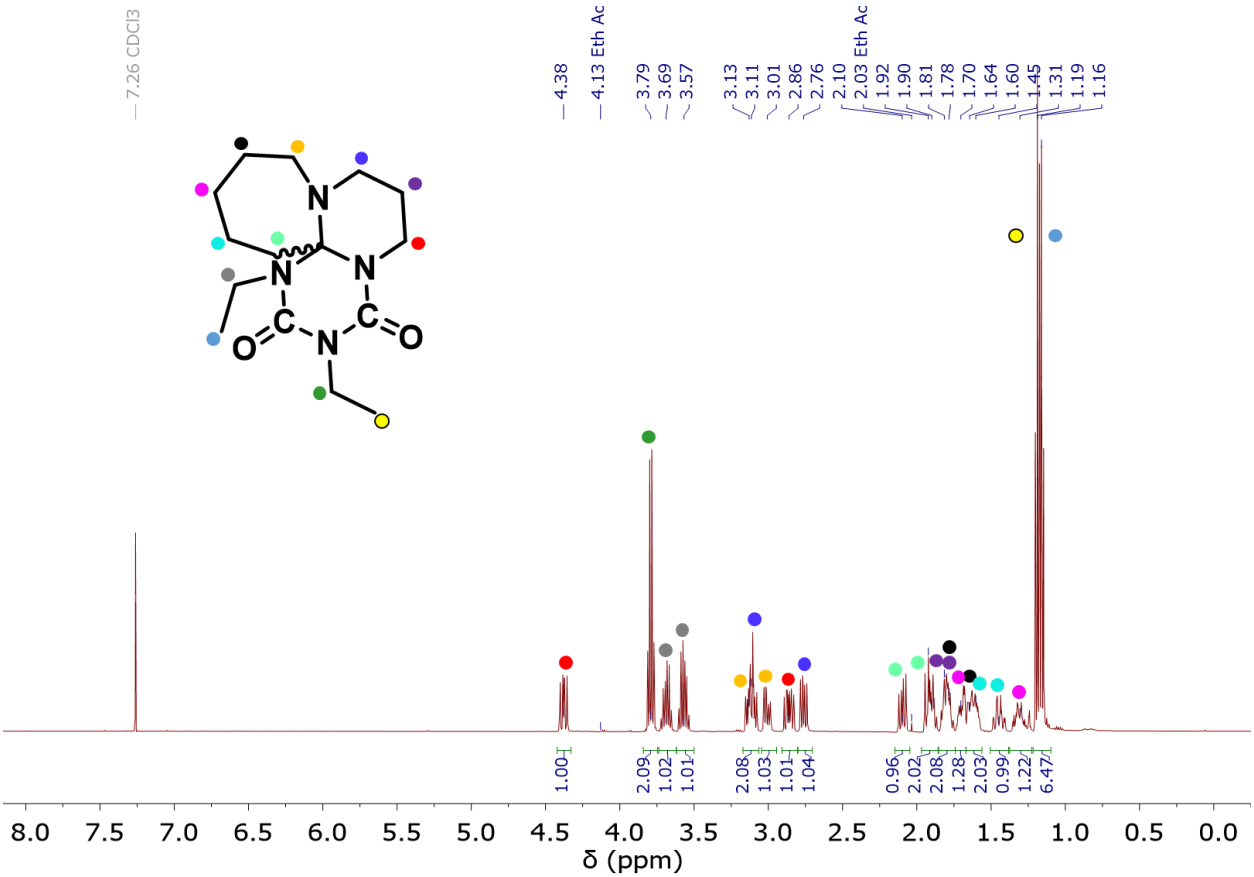

Figure A-21. ^{1}H-NMR spectrum (500 MHz, $CDCl_3$) of DBU ethyl isocyanate cyclodimer adduct **5**, d1 = 1 s.

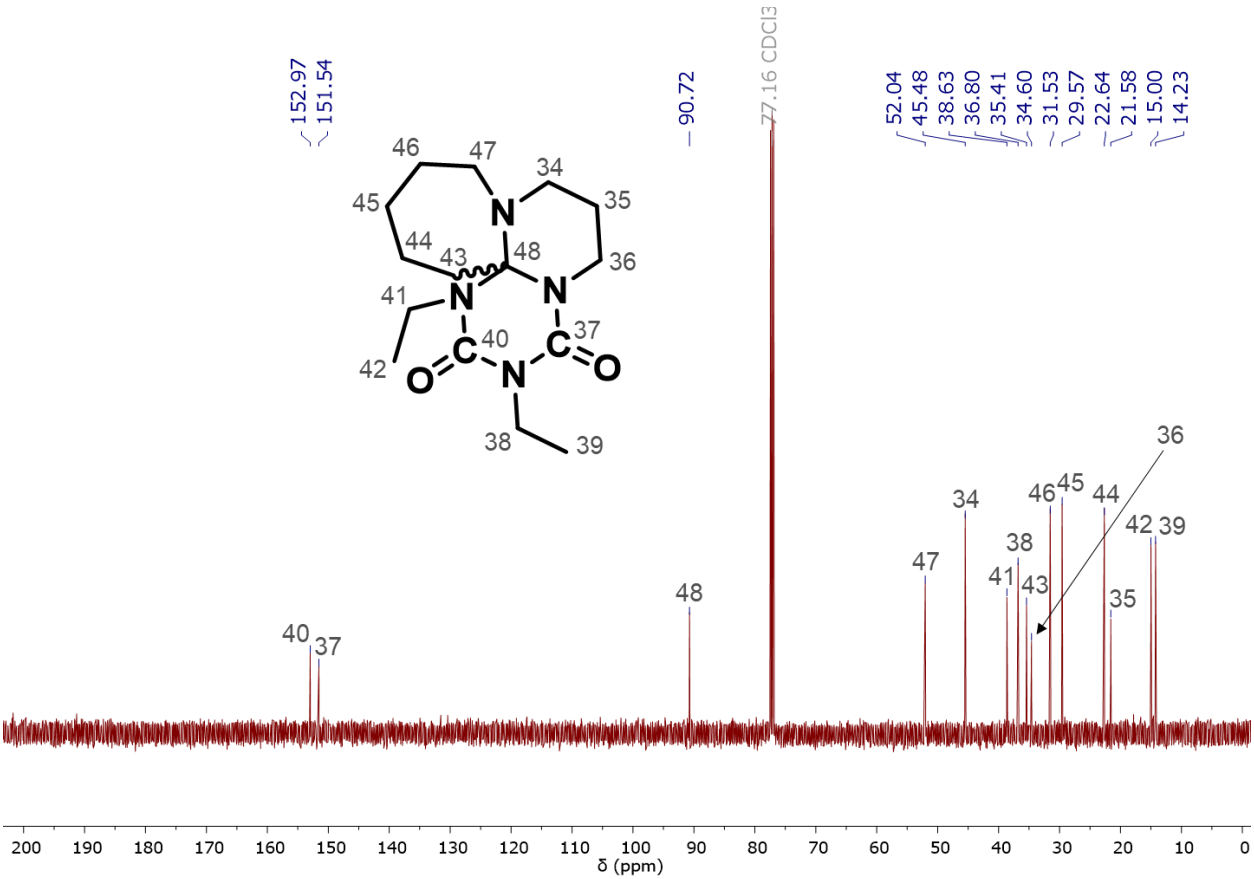

Figure A-22. ^{13}C-NMR spectrum (125 MHz, $CDCl_3$) of **5**.

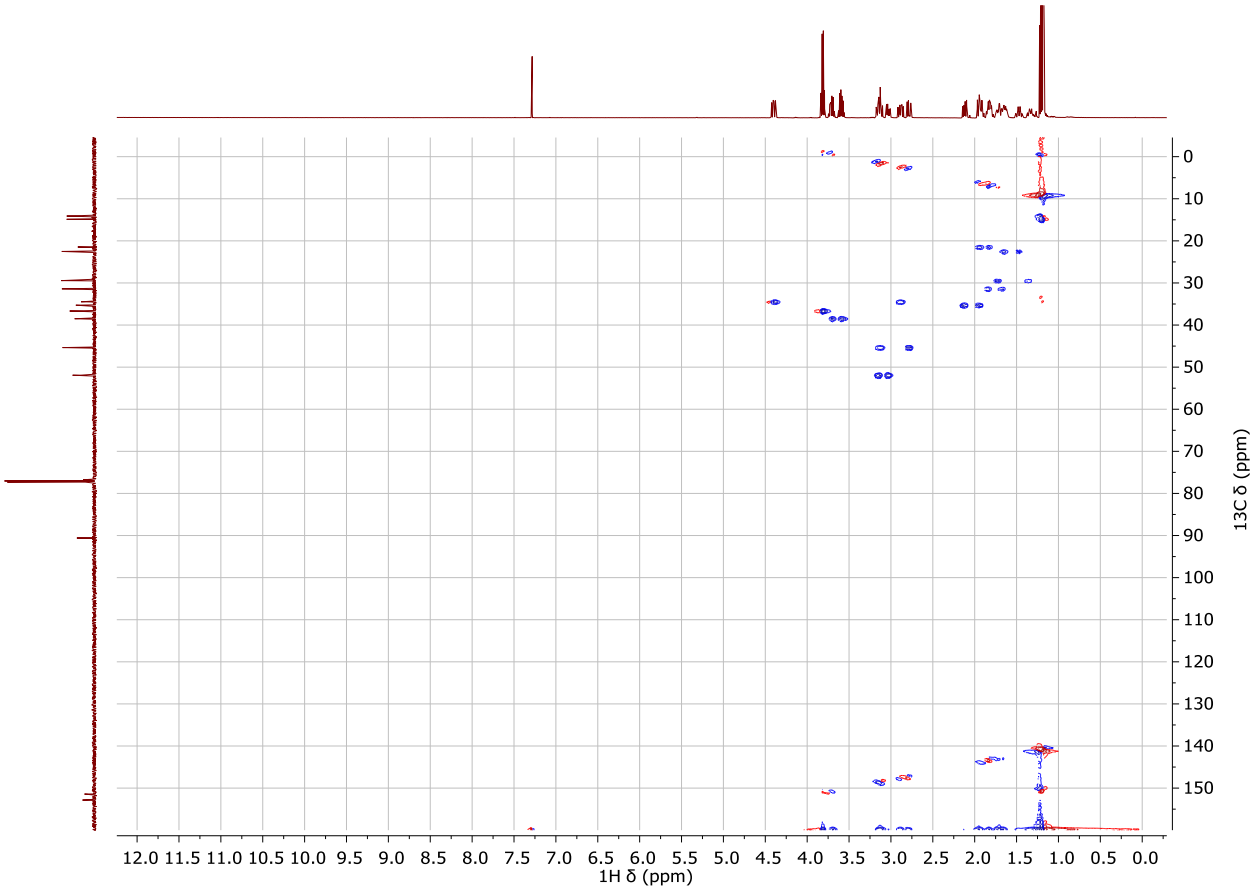

Figure A-23. ^{1}H-^{13}C HMQC spectrum (500 MHz-125 MHz, $CDCl_3$)of **5**.

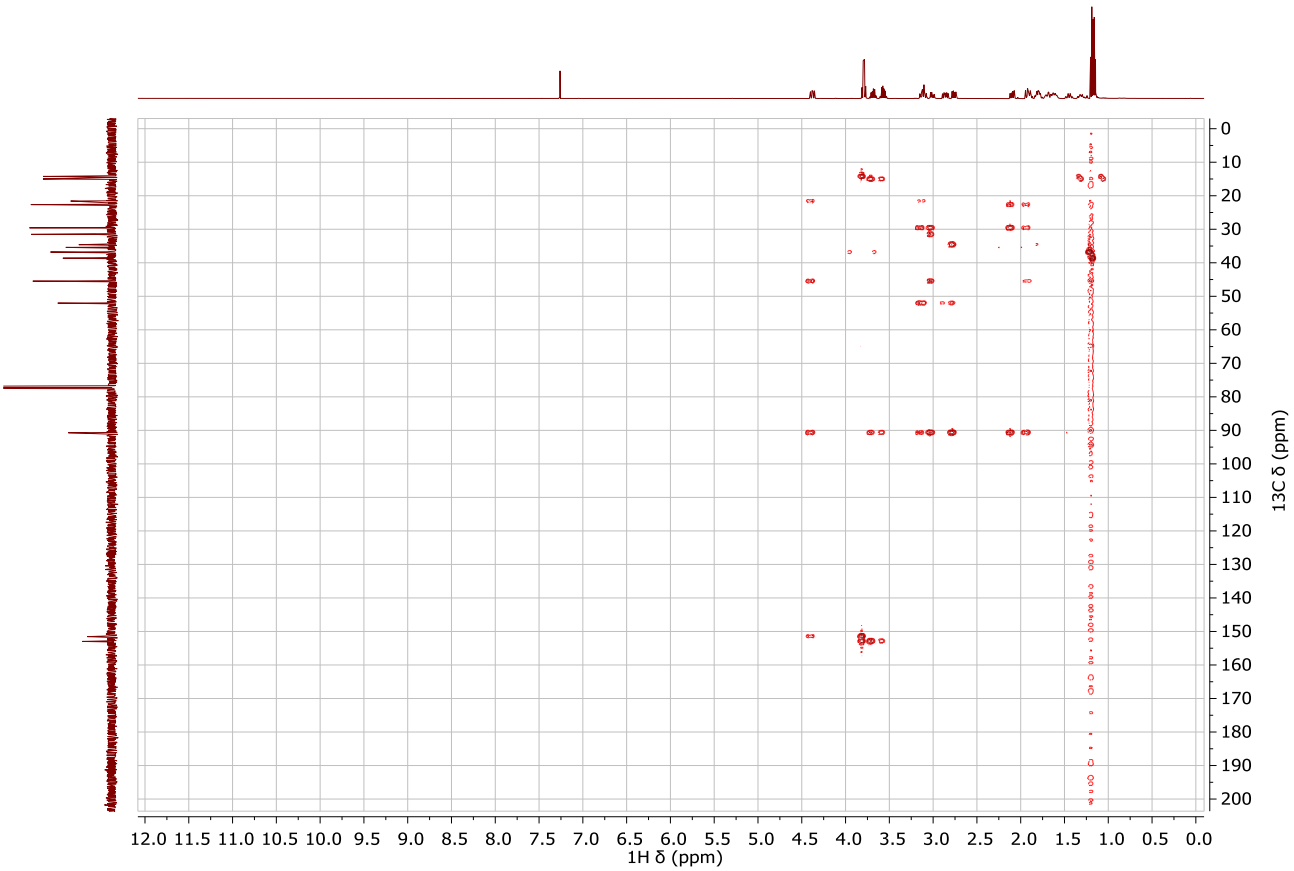

Figure A-24. ^{1}H-^{13}C HMBC (500 MHz-125 MHz, $CDCl_3$) spectrum of **5**.

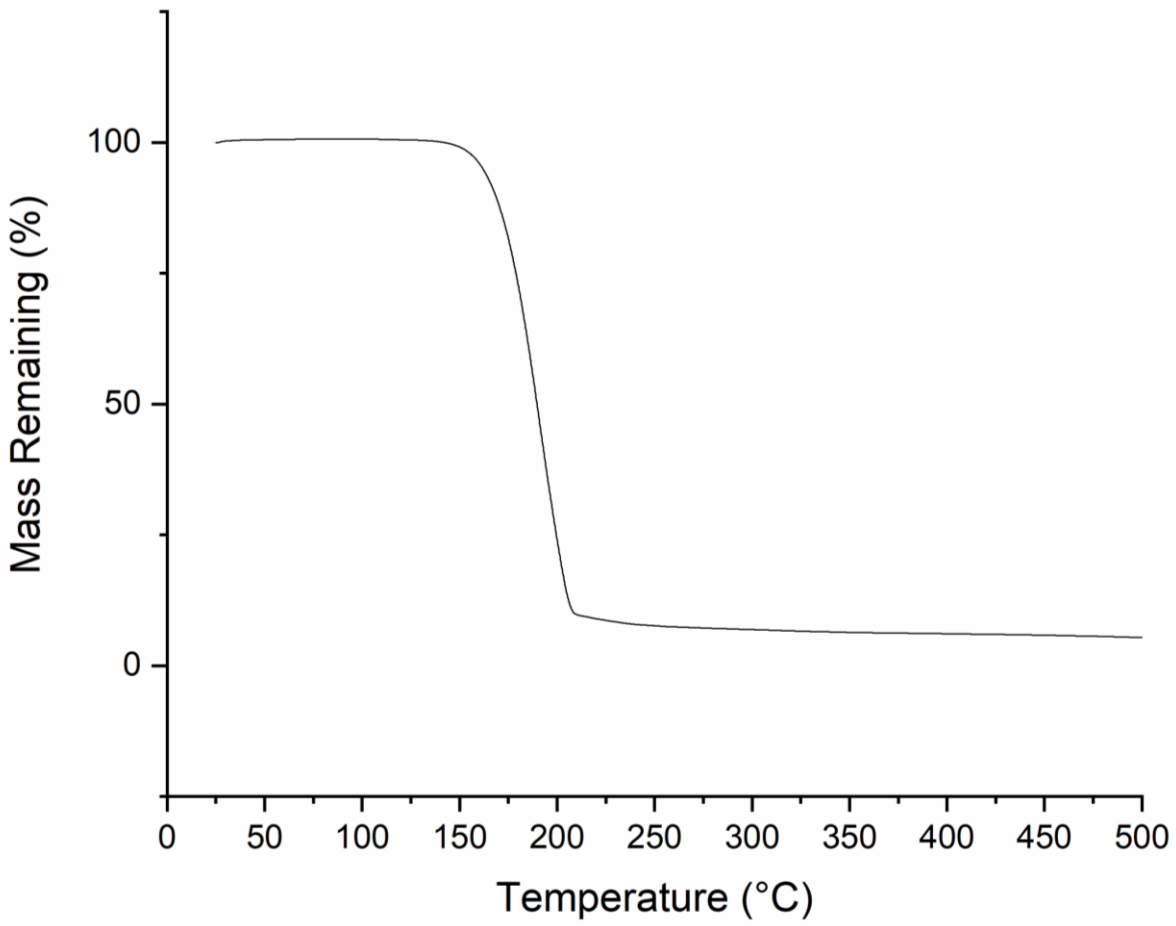

Figure A-25. TGA of **5**.

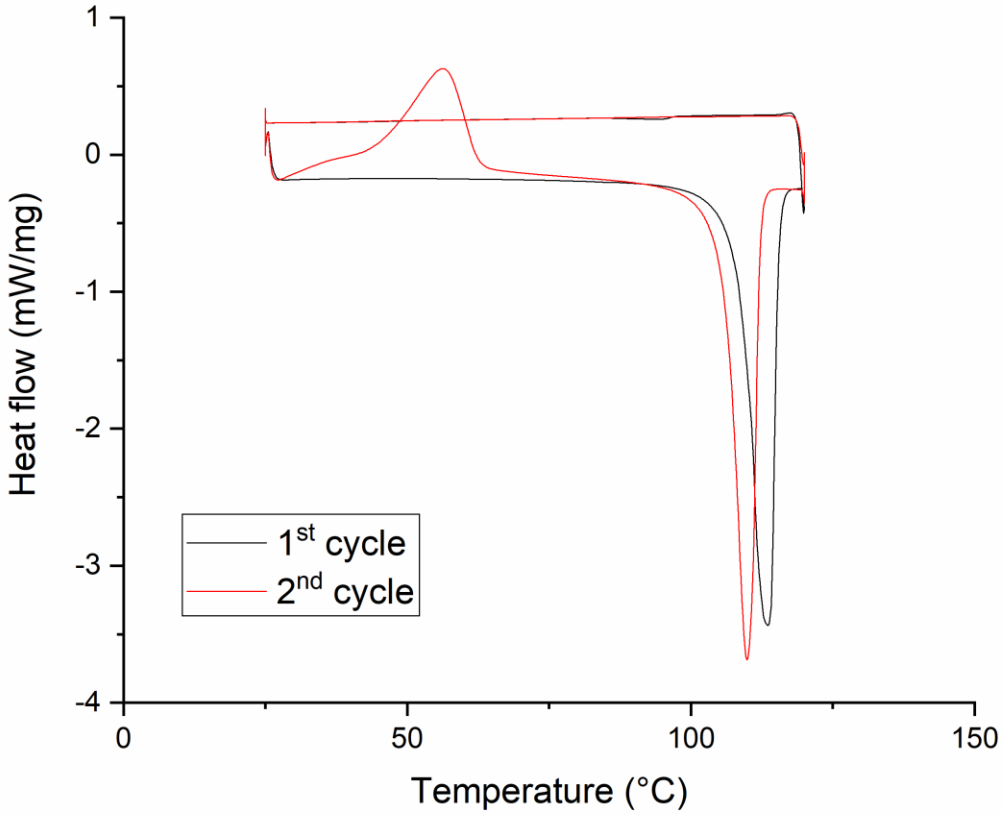

Figure A-26. DSC of **5** during the first and second heating and cooling cycles. Note the anomalous exothermic event in the second cycle. Because of hysteresis over the two cycles, the T_m was reported from the first heating cycle.

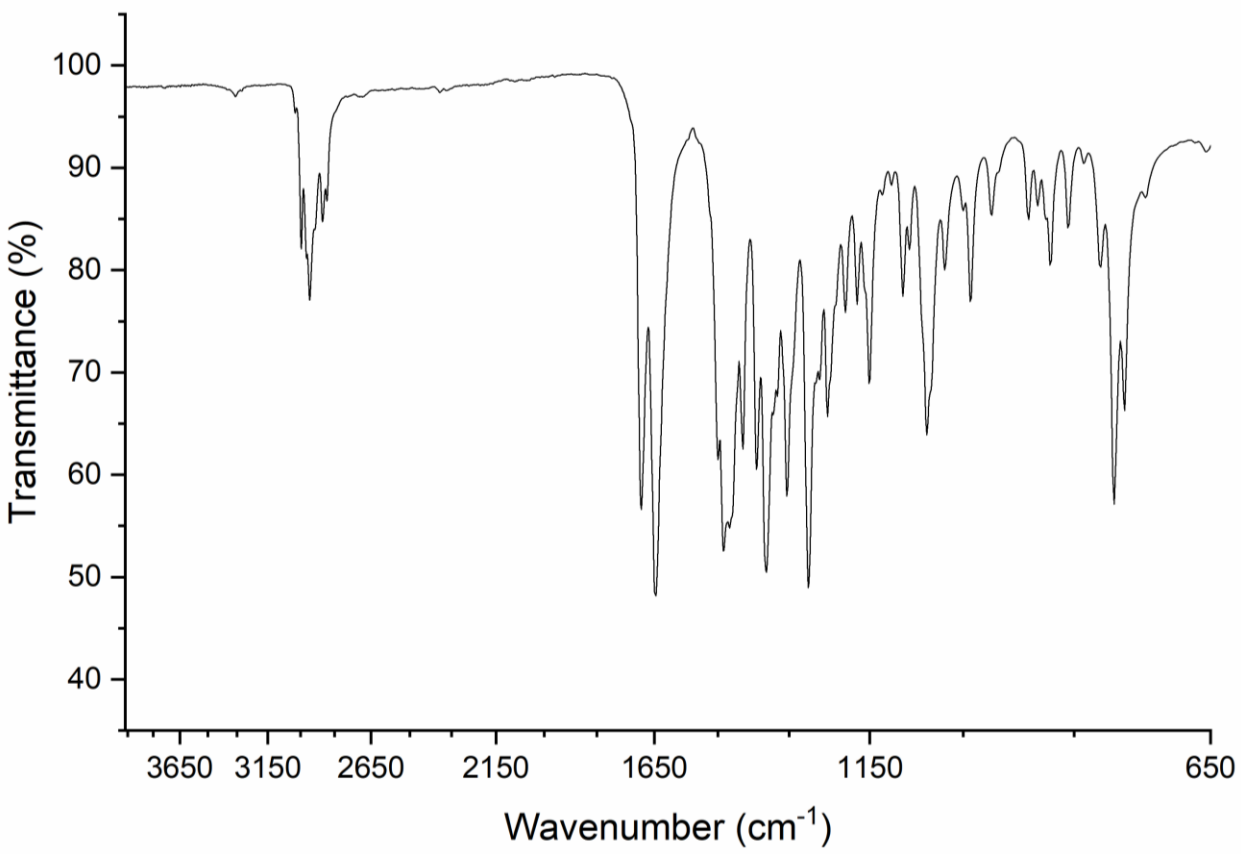

Figure A-27. ATR-FTIR spectrum of **5.**

Dicarbamate Dissociation Study with DBU

Table A-5. Integration table of ^{1}H NMR spectra acquired during dicarbamate dissociation in the presence of different amounts of DBU 15 to 20 min after DBU addition. The peaks are listed as normalized relative to the A peak (8.20 to 8.28 ppm) in each spectrum. The percent dissociation was calculated from the *p*-nitrophenol N peaks (6.95 to 6.90 ppm) for the neat system and *p*-nitrophenoxide Q peaks (6.48 to 5.89 ppm) for the systems with DBU taken as a percentage of the dicarbamate (**1**) B peaks (8.28 to 8.20 ppm). The percent dissociations are 1%, 60%, 81%, and 93% for 0, 0.48, 0.99, and 2.0 equivalents of DBU, respectively.

	DBU Equivalents							
	0		**0.48**		**0.99**		**2.0**	
Range (ppm)	Normalized	Absolute	Normalized	Absolute	Normalized	Absolute	Normalized	Absolute
8.28–8.20	4.00	97500	4.00	82000	4.00	25000	4.00	10300
7.44–7.35	4.00	97500	4.08	83500	3.94	24600	4.30	11100
6.95–6.90	0.06	1500	0.00	6.95	–0.30	–1900	0.00	–12.5
6.48–6.22	-0.15	–3740	6.03	124000	–1.14	–7110	0.41	1060
6.22–6.07	-0.09	–2150	0.06	1190	16.86	105000	2.22	5720
6.04–5.89	-0.08	–2060	0.01	275	–0.82	–5130	56.80	146000
3.37–3.31	0.11	2660	5.83	119000	16.63	104000	41.49	107000
3.13–3.04	3.70	90100	3.81	78100	3.95	24700	6.62	17100

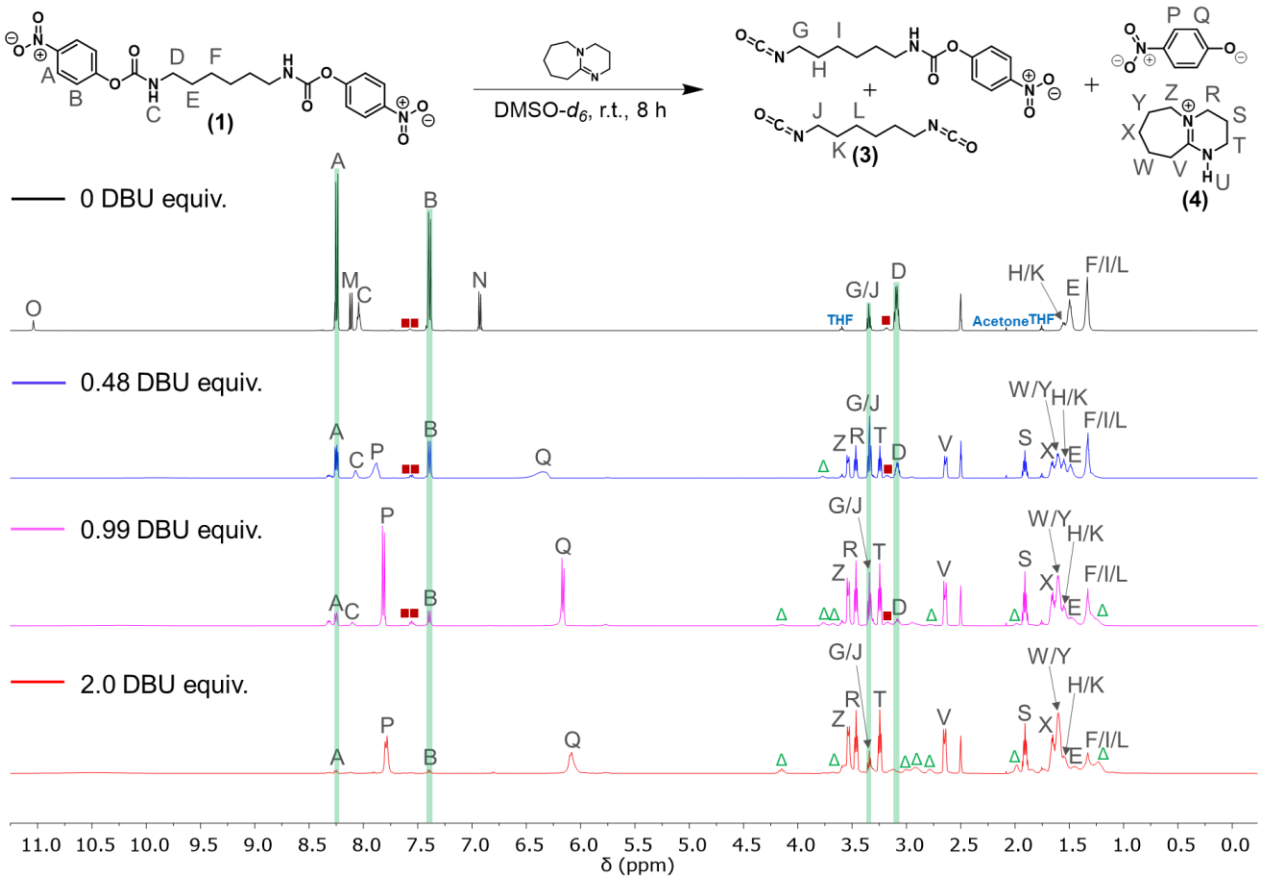

Figure A-28. ^{1}H-NMR (500 MHz, DMSO-d_6) spectra of DBU-promoted dissociation of dicarbamate **1** at room temperature over 8 h showing that 2.0 equivalents of DBU are needed to ensure complete conversion of dicarbamate. Also note the disappearance of the residual DBU signals and the formation of the expected DBU-H *p*-nitrophenoxide salt by-product peaks in the spectra of the mixture with 2.0 DBU equivalents. The spectrum of the sample with 0.99 DBU equivalents also shows the isocyanate cyclodimer by-product (Δ) with DBU. A small amount of urea (red boxes) was also visible in all spectra, except that of the reaction mixture with 2.0 DBU equivalents (see Figure A-1).

Table A-6. Integration table of ^{1}H NMR spectra acquired during dicarbamate dissociation in the presence of different amounts of DBU, 8 h after DBU addition. The peaks are listed as normalized relative to the A peak (8.22 to 8.28 ppm) in each spectrum.

	DBU Equivalents							
	0		**0.48**		**0.99**		**2.0**	
Range (ppm)	Normalized	Absolute	Normalized	Absolute	Normalized	Absolute	Normalized	Absolute
8.28–8.22	4.00	70400	4.00	31100	4.00	13300	4.00	3480
7.45–7.35	4.00	70300	4.05	31400	4.31	14400	4.70	4080
6.97–6.90	0.71	12500	0.00	–2.05	0.00	12.4	0.21	180
6.56–6.27	–0.19	–3380	6.32	49100	0.39	1290	0.85	743
6.26–6.12	–0.09	–1590	0.03	253	21.57	71900	6.98	6070
6.19–5.98	–0.14	–2460	0.02	120	19.40	64600	84.77	73700
3.37–3.32	0.78	13700	4.86	37800	10.50	35000	22.82	19800
3.13–3.04	3.70	65100	3.78	29400	4.86	16200	14.04	12200

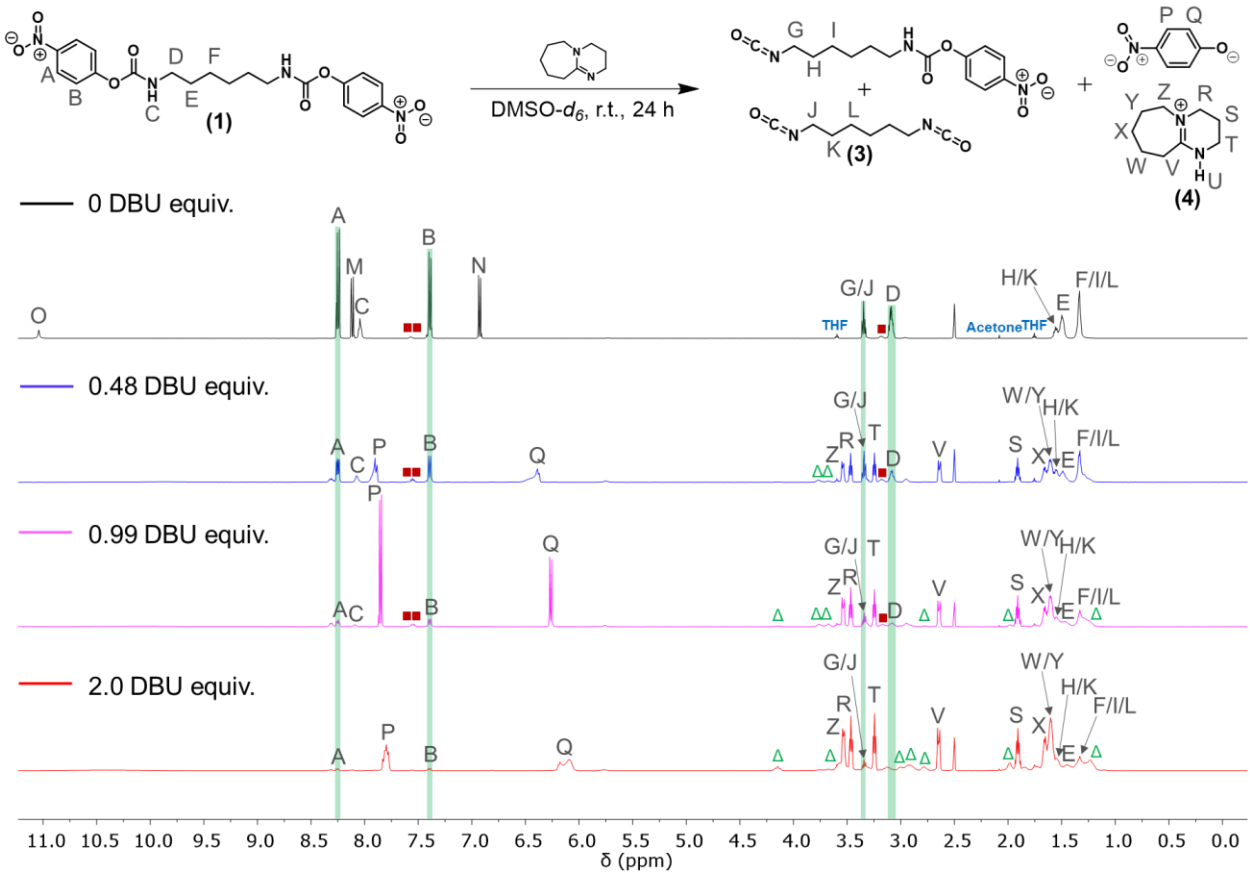

Figure A-29. ^{1}H-NMR (500 MHz, DMSO-d6) spectra showing DBU-promoted dissociation of dicarbamate **1** in DMSO-d_6 at room temperature over 24 h as a function of DBU equivalents. The spectrum of the reaction mixture with 0.99 DBU equivalents shows both the isocyanate cyclodimer by-product and excess DBU (Δ). A small amount of urea (red boxes) was also visible in all spectra, except that acquired of the reaction mixture with 2.0 DBU equivalents (see Figure A-1).

Table A-7. Integration table of ^{1}H NMR spectra acquired during dicarbamate dissociation in the presence of different amounts of DBU, 24 h after DBU addition. The peaks are listed as normalized relative to the A peak (8.20 to 8.28 ppm) in each spectrum.

	DBU Equivalents							
	0		**0.48**		**0.99**		**2.0**	
Range (ppm)	Normalized	Absolute	Normalized	Absolute	Normalized	Absolute	Normalized	Absolute
8.28–8.20	4.00	55900	4.00	26900	4.00	7600	4.00	2570
7.44–7.35	3.99	55700	4.01	26900	4.54	8620	4.59	2950
6.95–6.90	1.52	21300	–0.01	–52.2	–0.47	–893	–0.09	–61.1
6.57–6.35	–0.17	–2440	7.12	47900	–2.06	–3920	–0.01	–8.53
6.31–6.23	–0.06	–809	0.00	25.7	24.99	47500	1.13	724
6.22–6.02	–0.16	–2190	–0.04	–296	–1.44	–2730	103.67	66700
4.25–4.05	–0.17	–2310	0.01	98.6	–0.75	–1420	17.36	11200
3.37–3.31	1.57	21900	3.89	26100	7.79	14800	21.86	14100
3.13–3.04	3.69	51600	3.78	25400	5.00	9510	15.16	9760

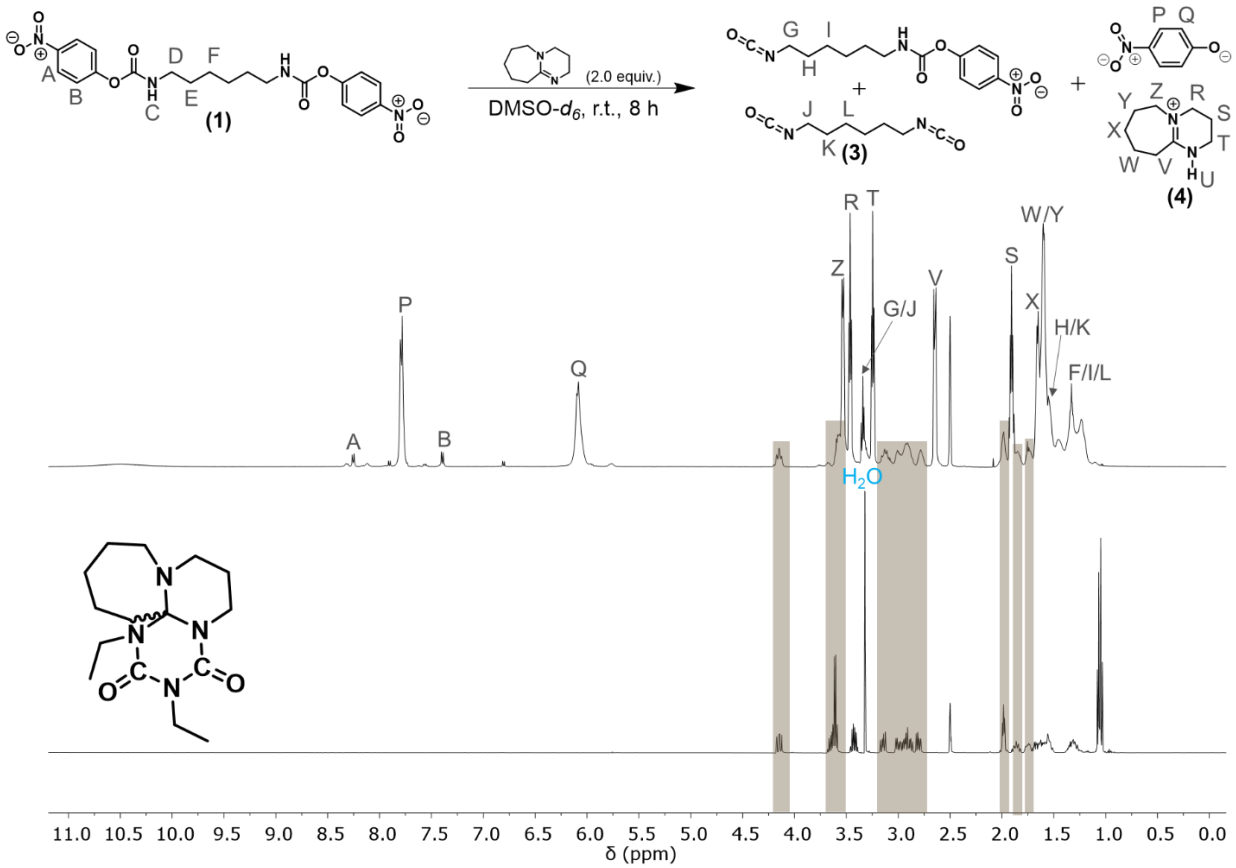

Figure A-30. ^{1}H-NMR(500 MHz, DMSO-d6) spectra comparing **1** with 2.0 equivalents of DBU added after 8 h with the d1 set for 10 s (top) and **5** in DMSO-d_6 with d1 = 1 s (bottom). of DBU added after 8 h with the d1 set for 10 s (top) and; 5 in DMSO-d6 with d1 = 1 s (bottom).

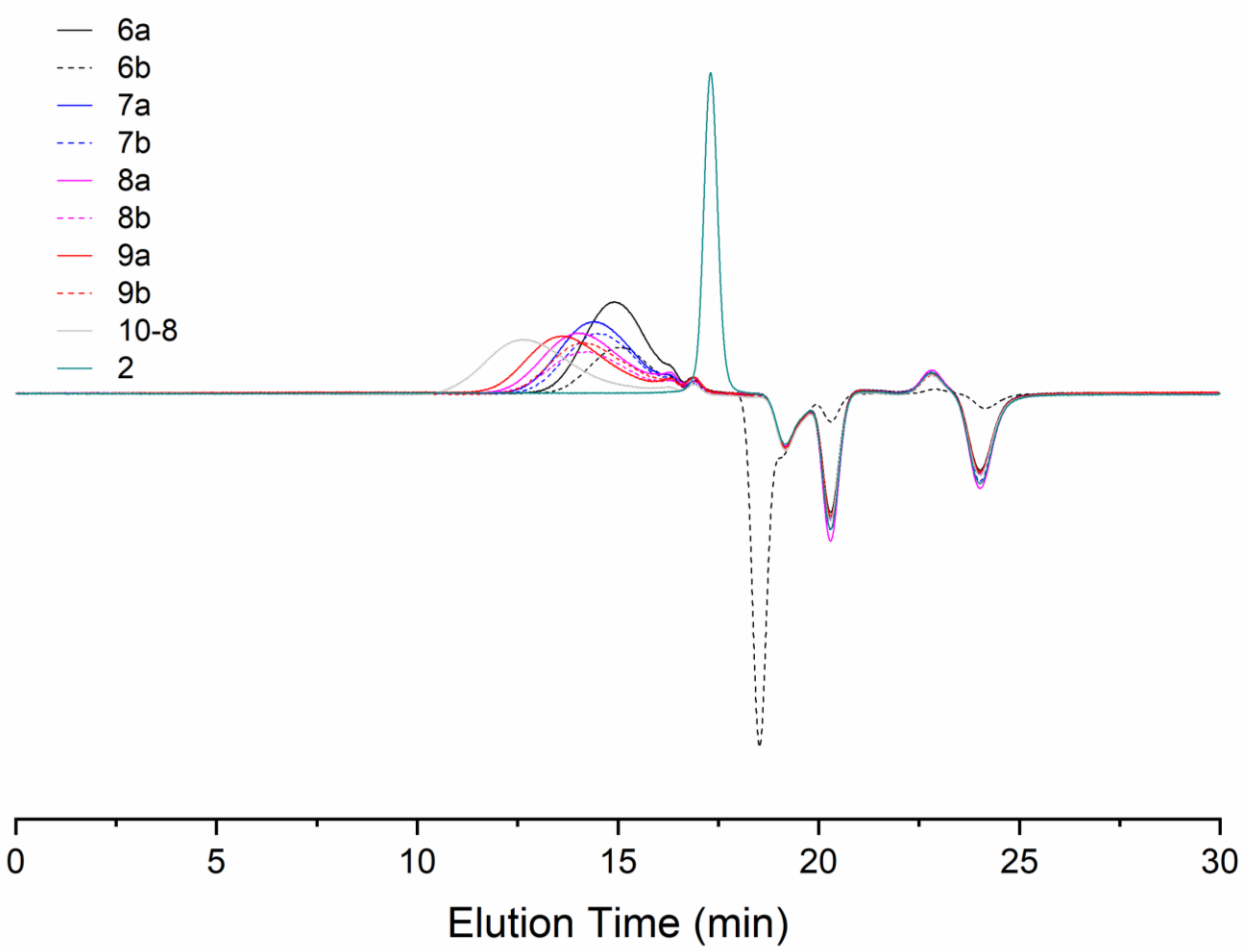

Figure A-31. DMF SEC of PUs **6** to **9**, **10-8**, and 4,6-*O*-benzylidene-α-(D)-glucopyranoside **2**. An acetone flow marker (negative peak) was added to the **6b** sample.

MALDI-TOF MS

Linear Mode

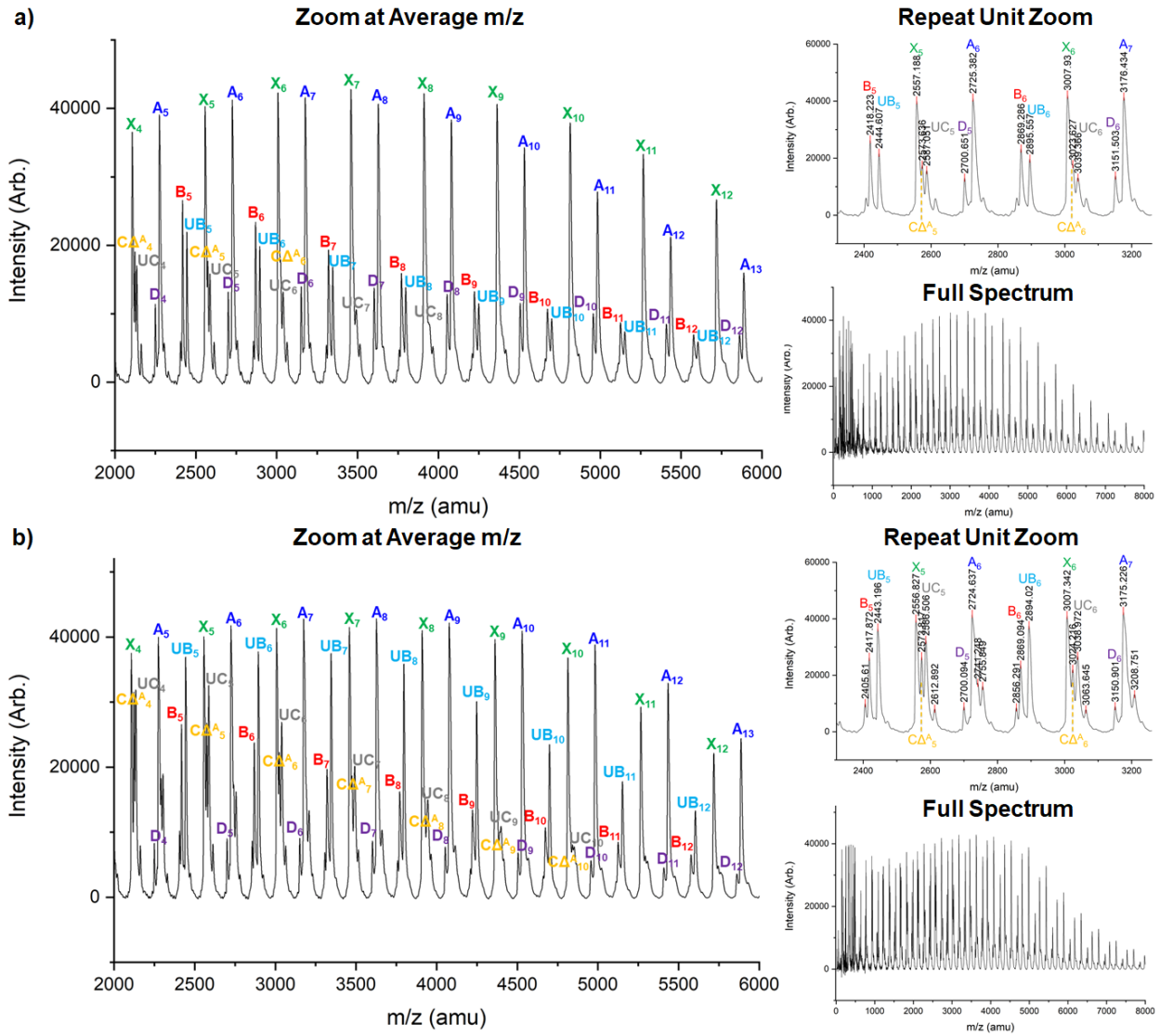

Figure A-32. The MALDI-TOF MS spectra for polymers synthesized with different DBU addition rates: a) PU **8a**, DBU addition rate = 5.6 μL/min; b) PU **9b**, DBU addition rate = rapid. The composition of uretdione and Δ-adduct populations was found to correlate with DBU addition rate.

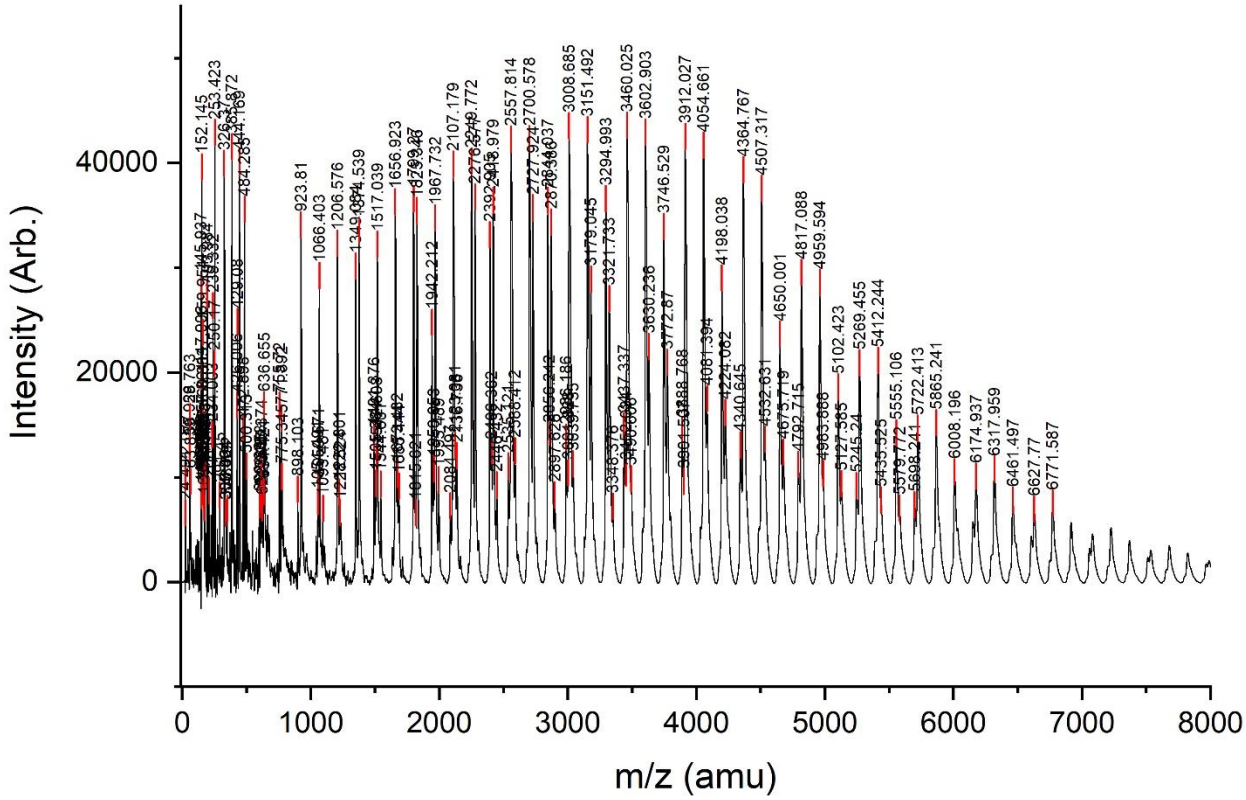

Figure A-33. Linear mode MALDI-TOF spectrum of PU **6a.**

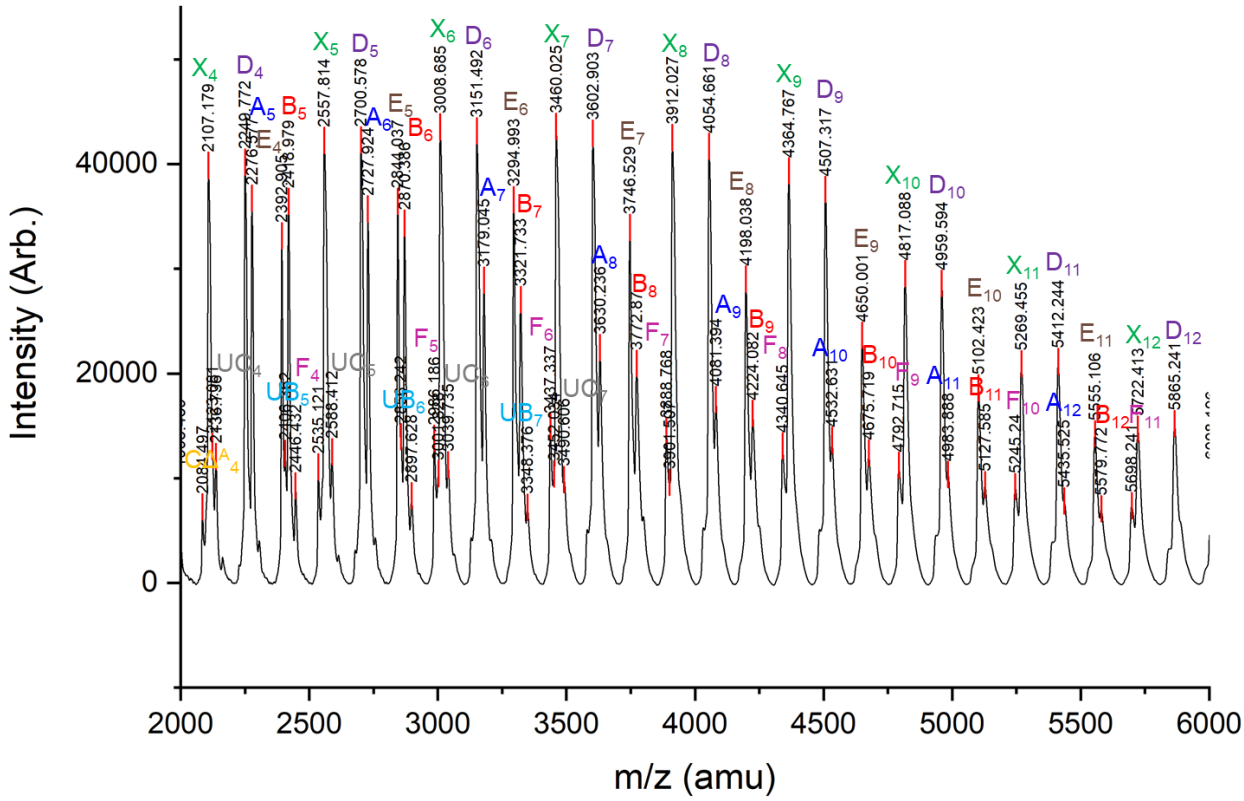

Figure A-34. Expanded linear mode MALDI-TOF spectrum of PU **6a** with peak assignments.

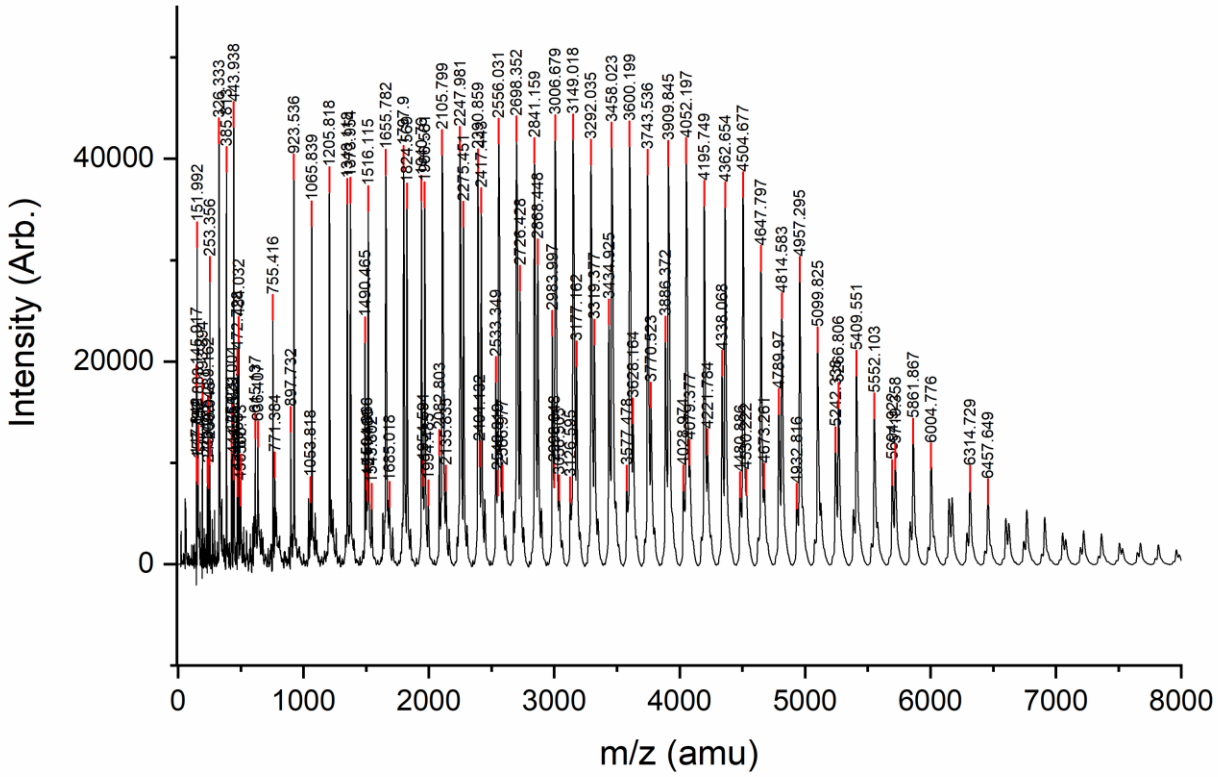

Figure A-35. Linear mode MALDI-TOF spectrum of PU **6b**.

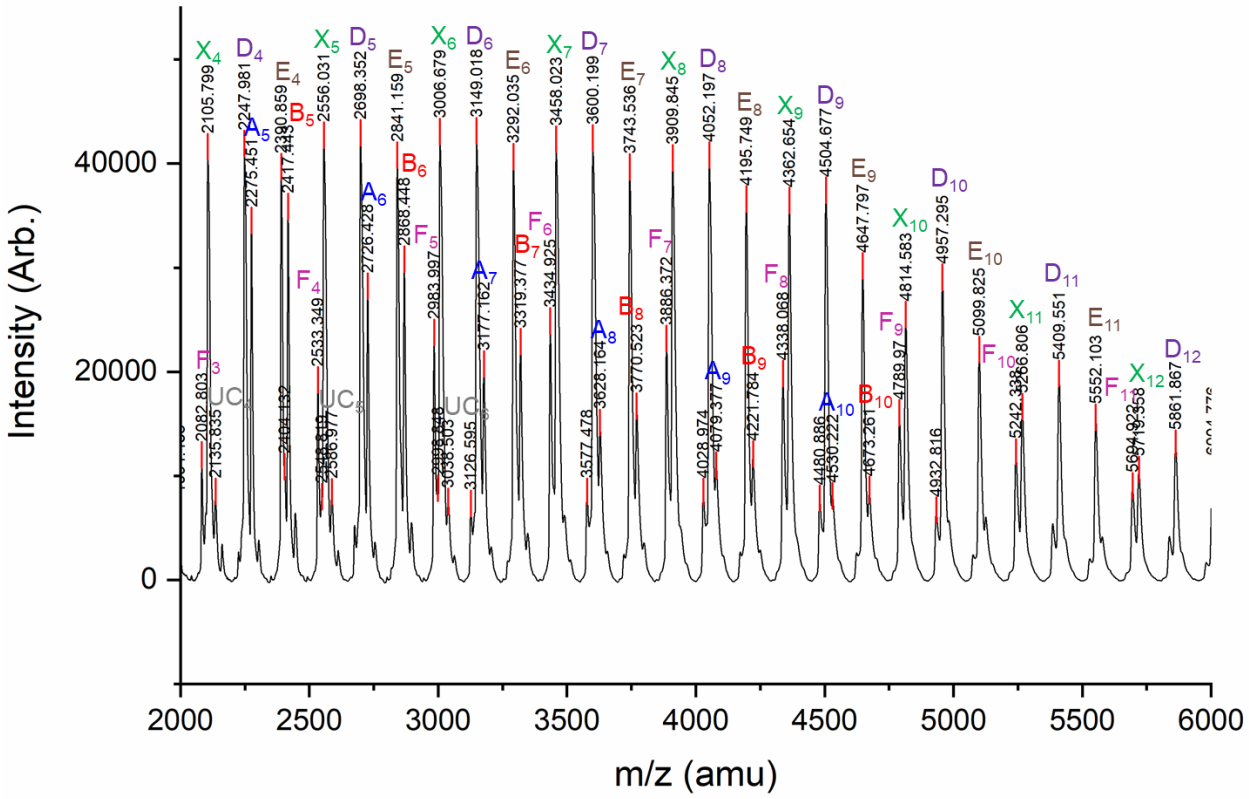

Figure A-36. Expanded linear mode MALDI-TOF spectrum of PU **6b** with peak assignments.

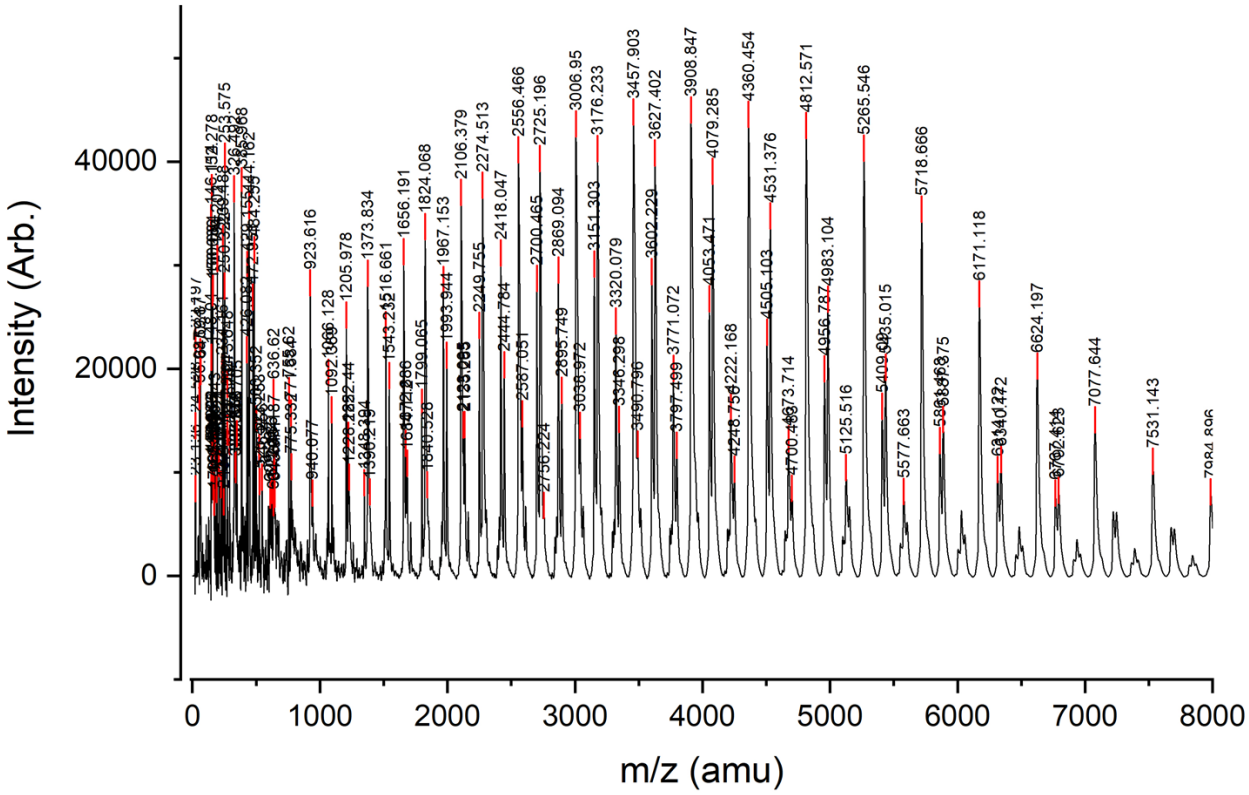

Figure A-37. Linear mode MALDI-TOF spectrum of PU **7a**.

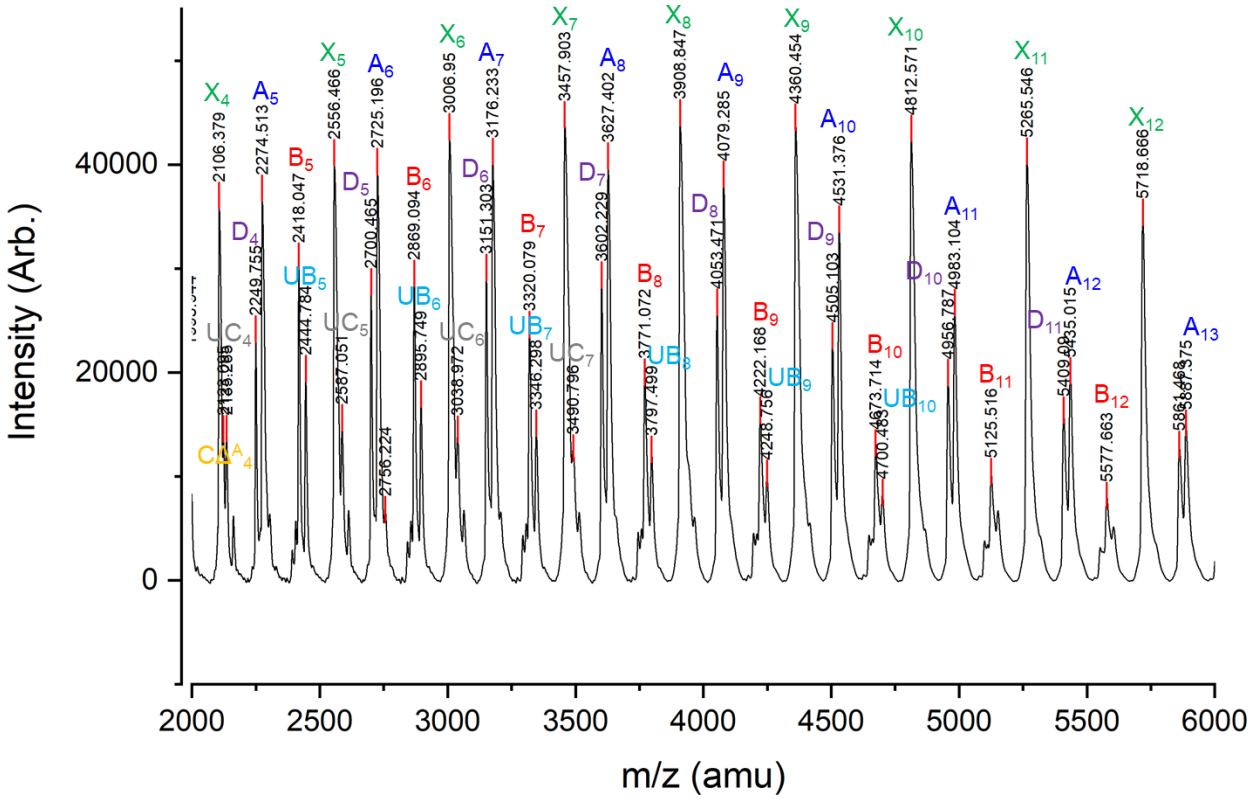

Figure A-38. Expanded linear mode MALDI-TOF spectrum of PU **7a** with peak assignments.

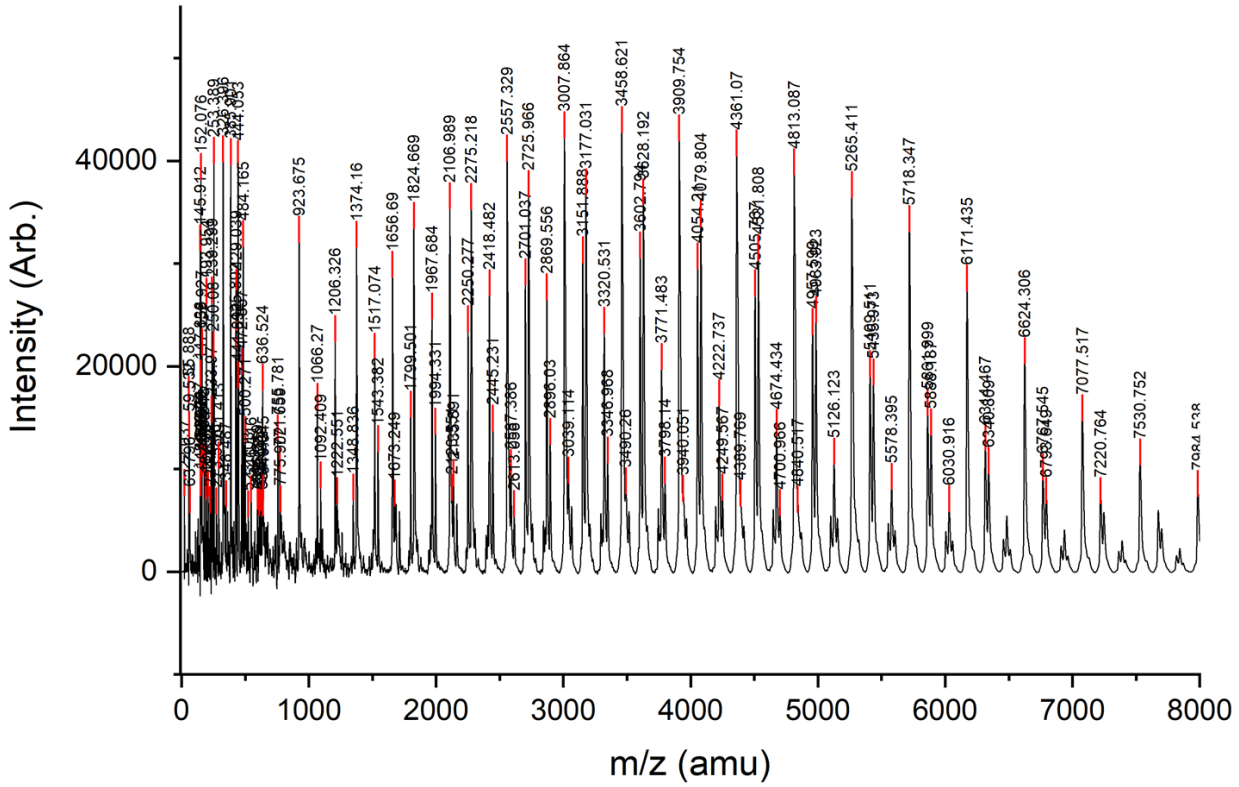

Figure A-39. Linear mode MALDI-TOF spectrum of PU **7b.**

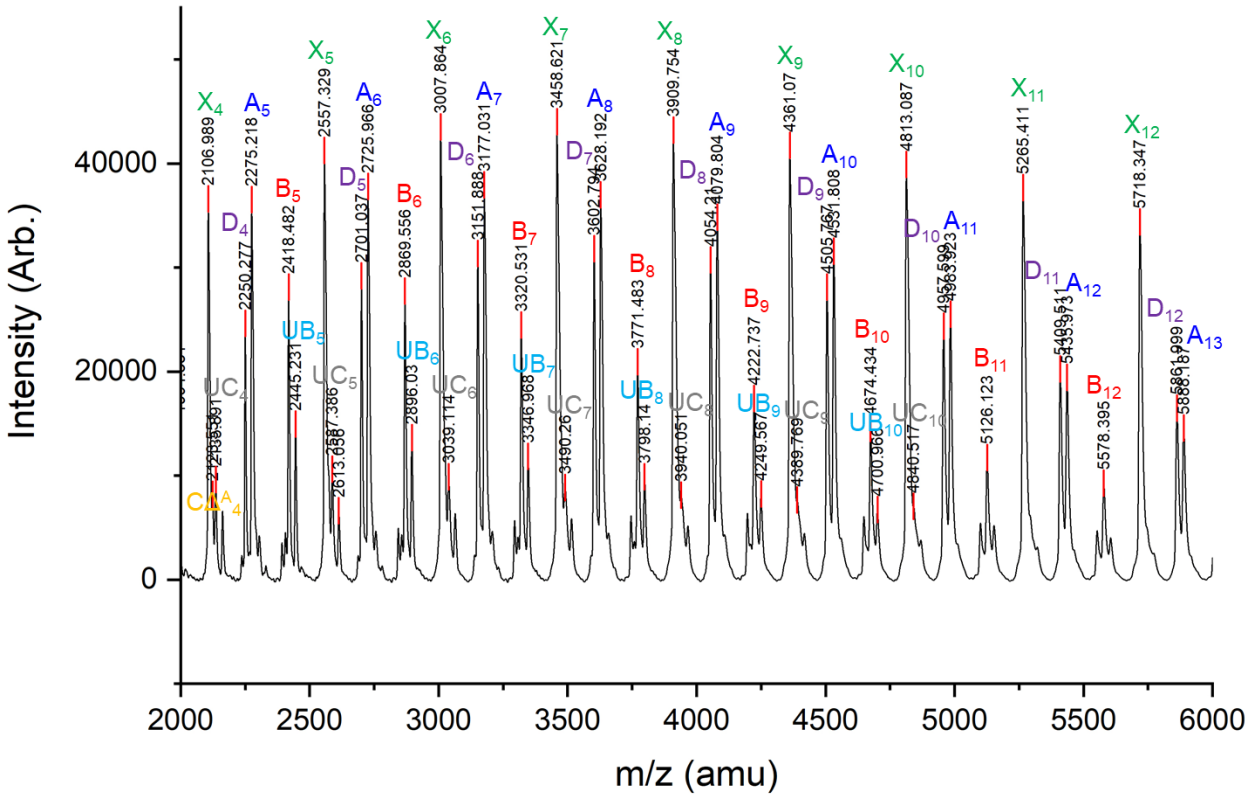

Figure A-40. Expanded linear mode MALDI-TOF spectrum of PU **7b** with peak assignments.

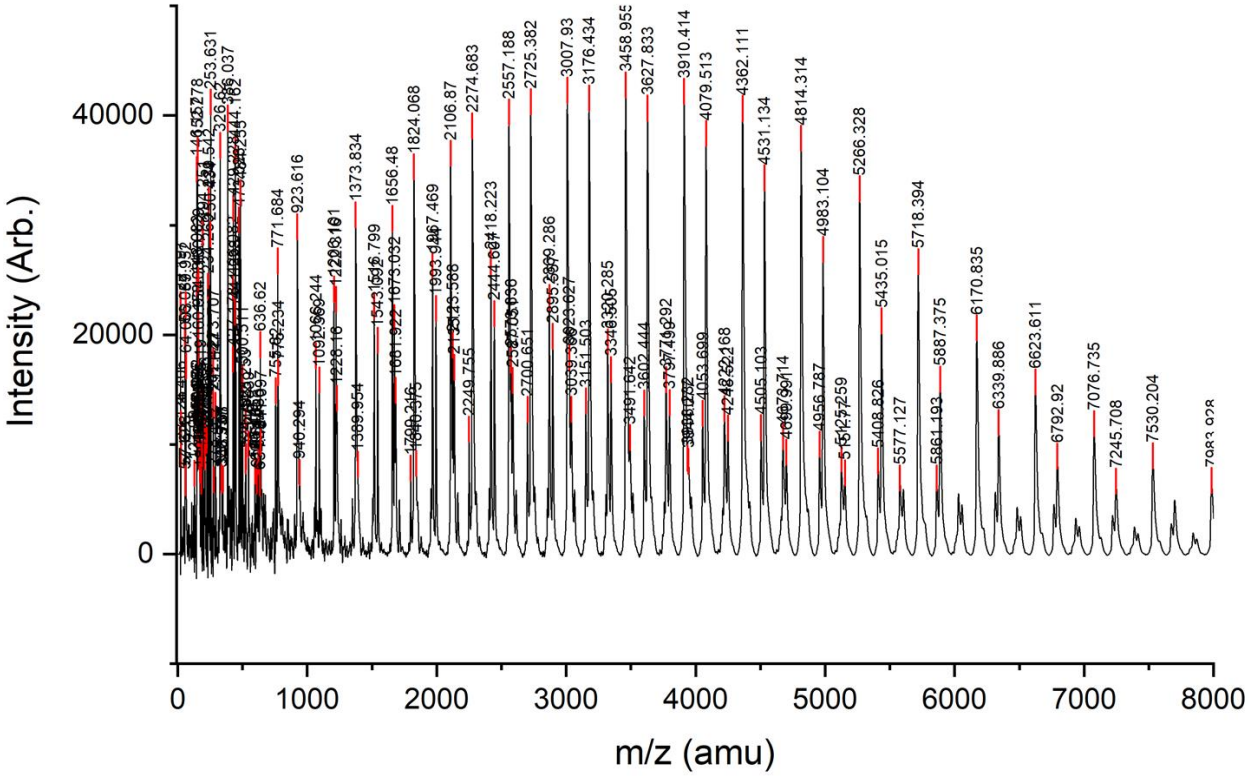

Figure A-41. Linear mode MALDI-TOF spectrum of PU **8a**.

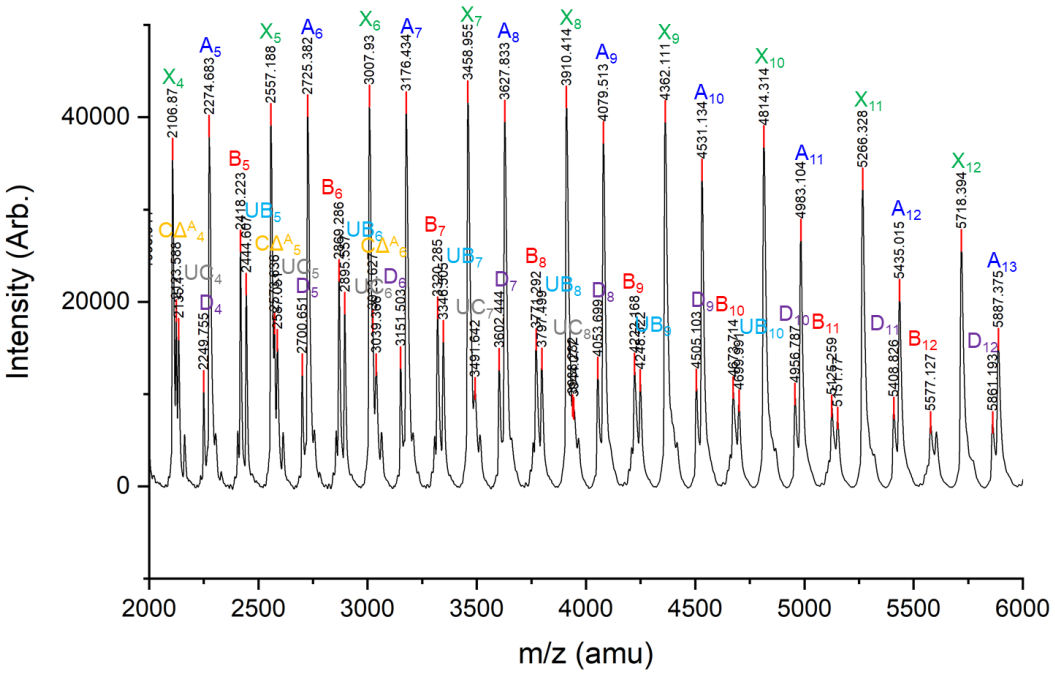

Figure A-42. Expanded linear mode MALDI-TOF spectrum of PU **8a** with peak assignments.

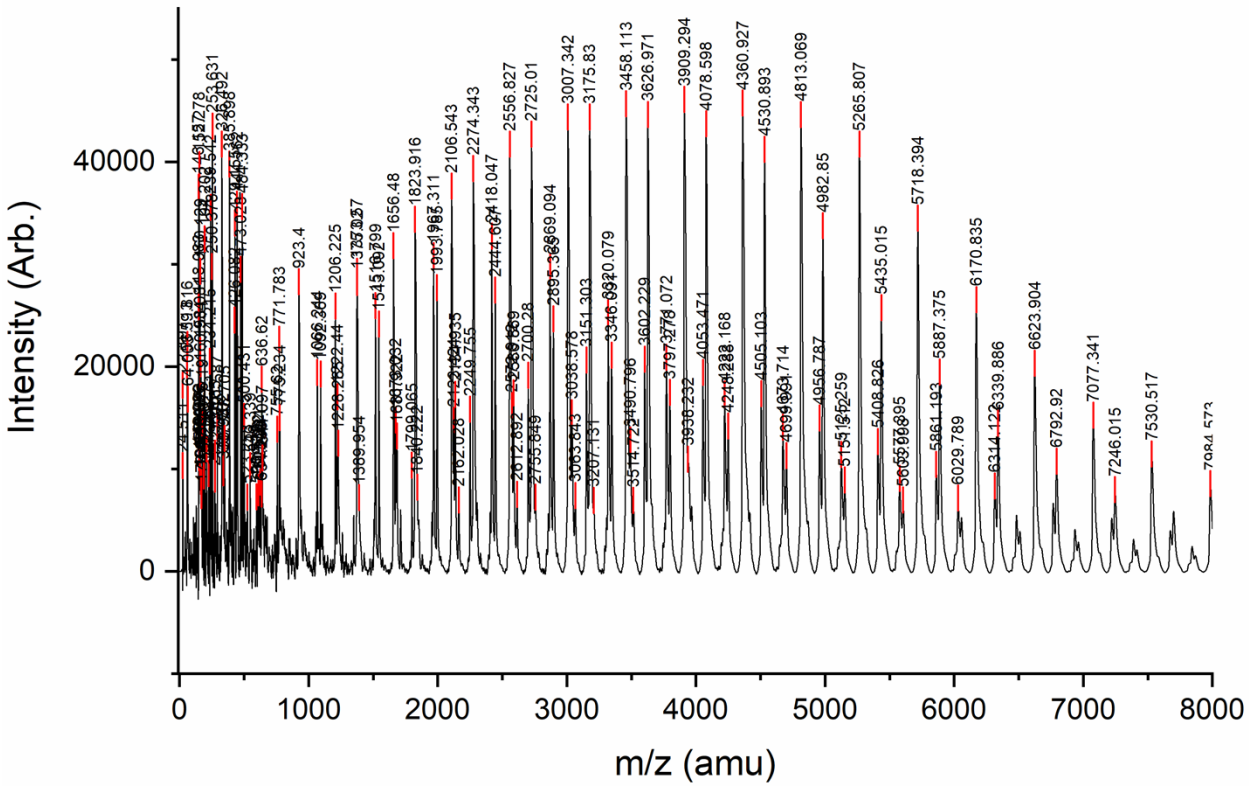

Figure A-43. Linear mode MALDI-TOF spectrum of PU **8b.**

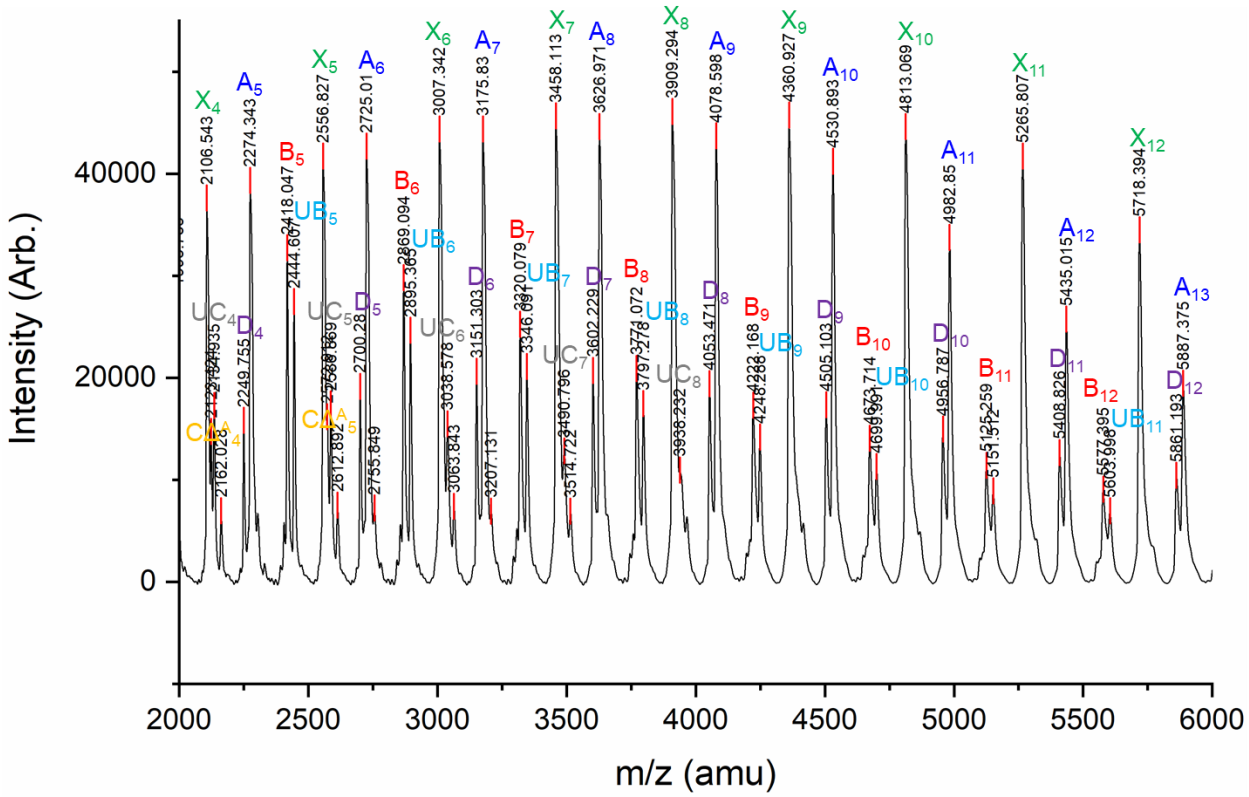

Figure A-44. Expanded linear mode MALDI-TOF spectrum of PU **8b** with peak assignments.

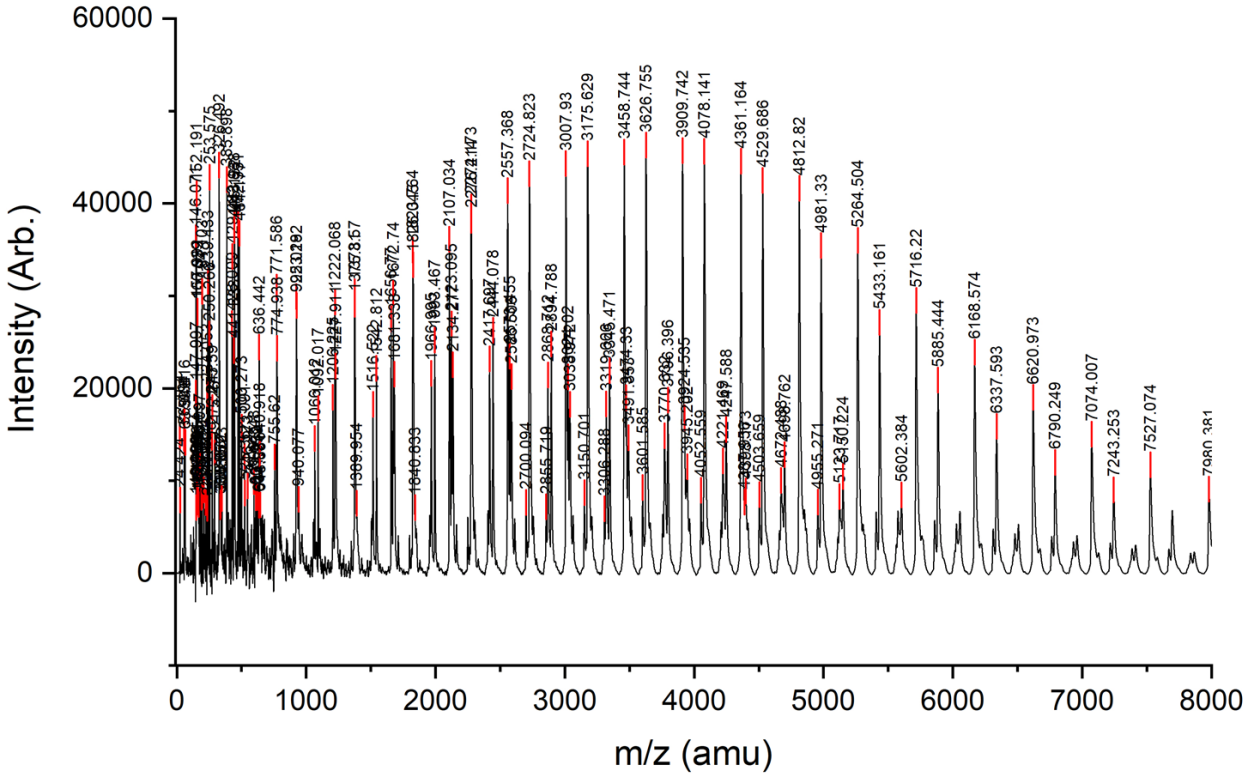

Figure A-45. Linear mode MALDI-TOF spectrum of PU **9a**.

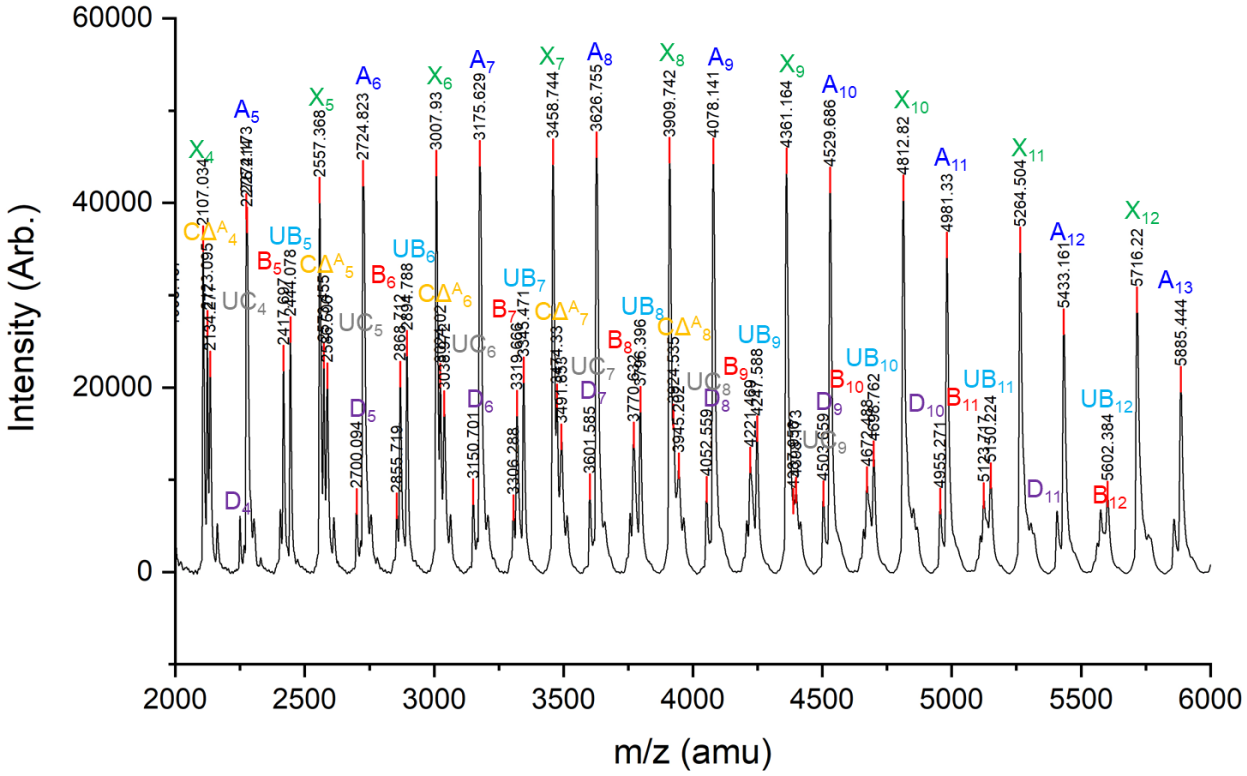

Figure A-46. Expanded linear mode MALDI-TOF spectrum of PU **9a** with peak assignments.

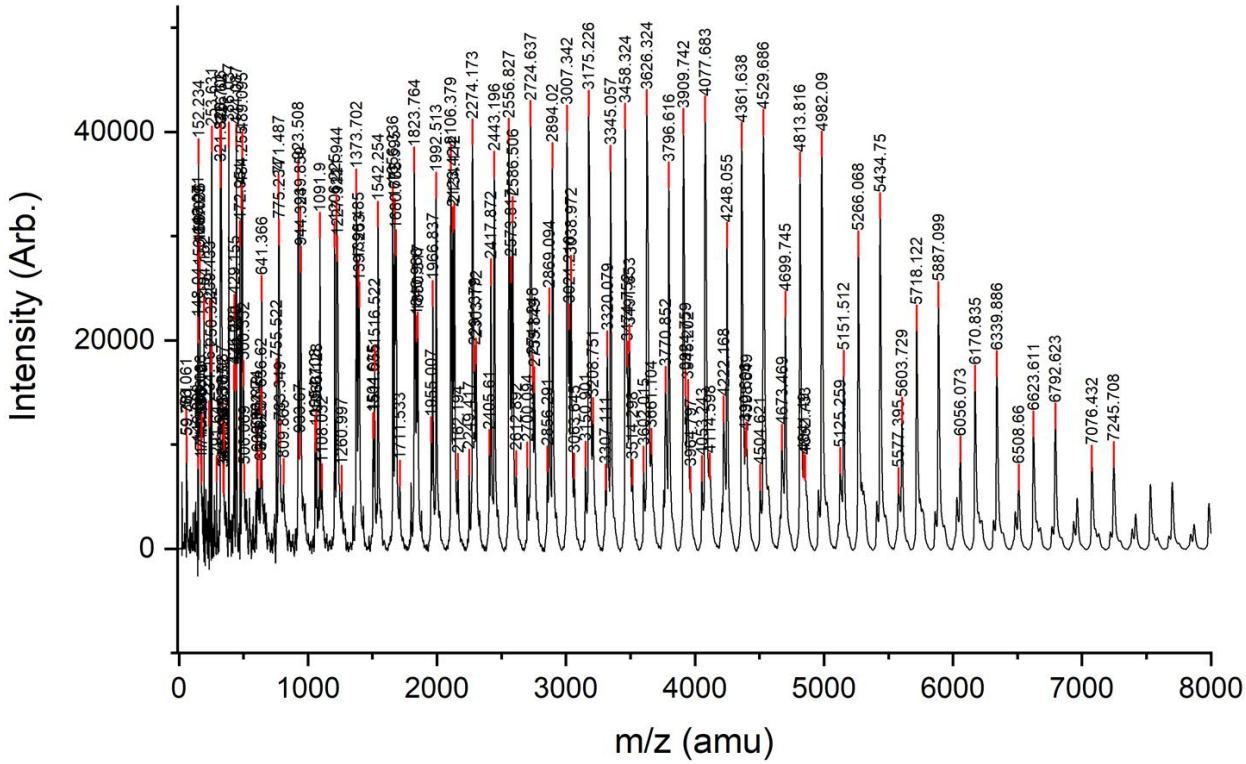

Figure A-47. Linear mode MALDI-TOF spectrum of PU **9b**.

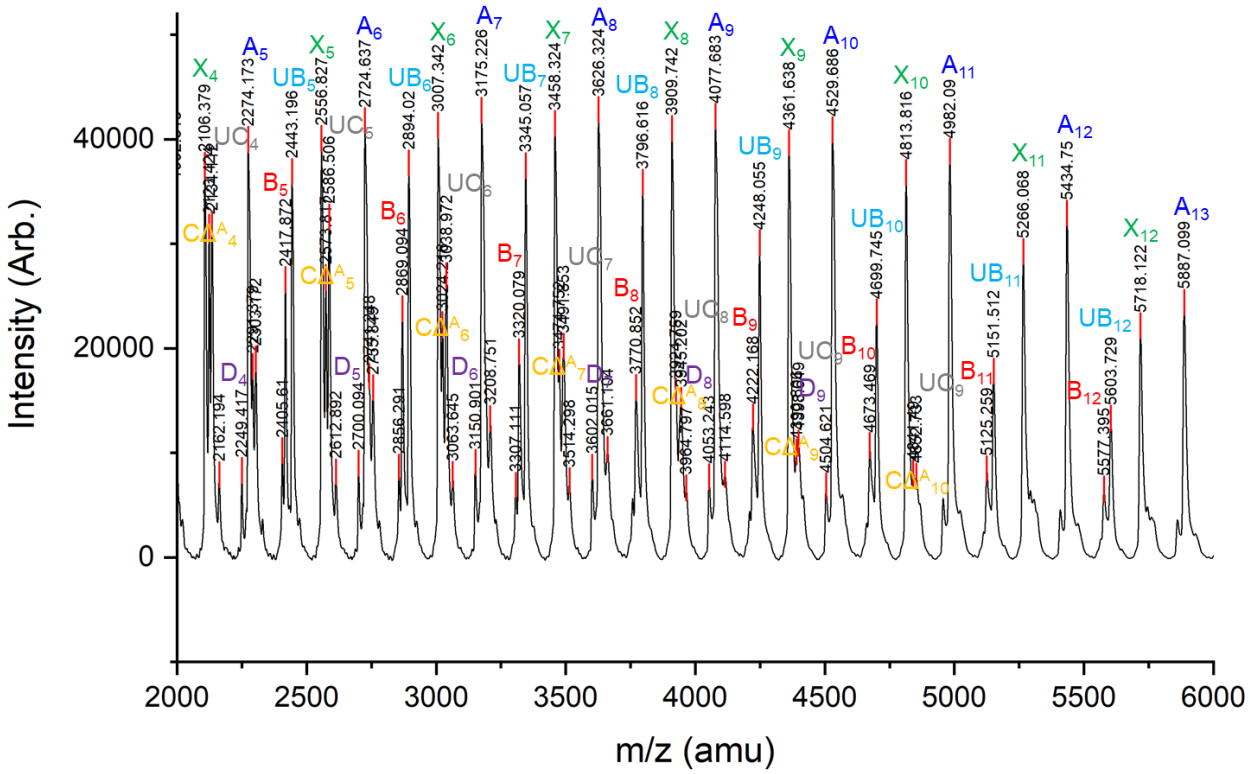

Figure A-48. Expanded linear mode MALDI-TOF spectrum of PU **9b** with peak assignments.

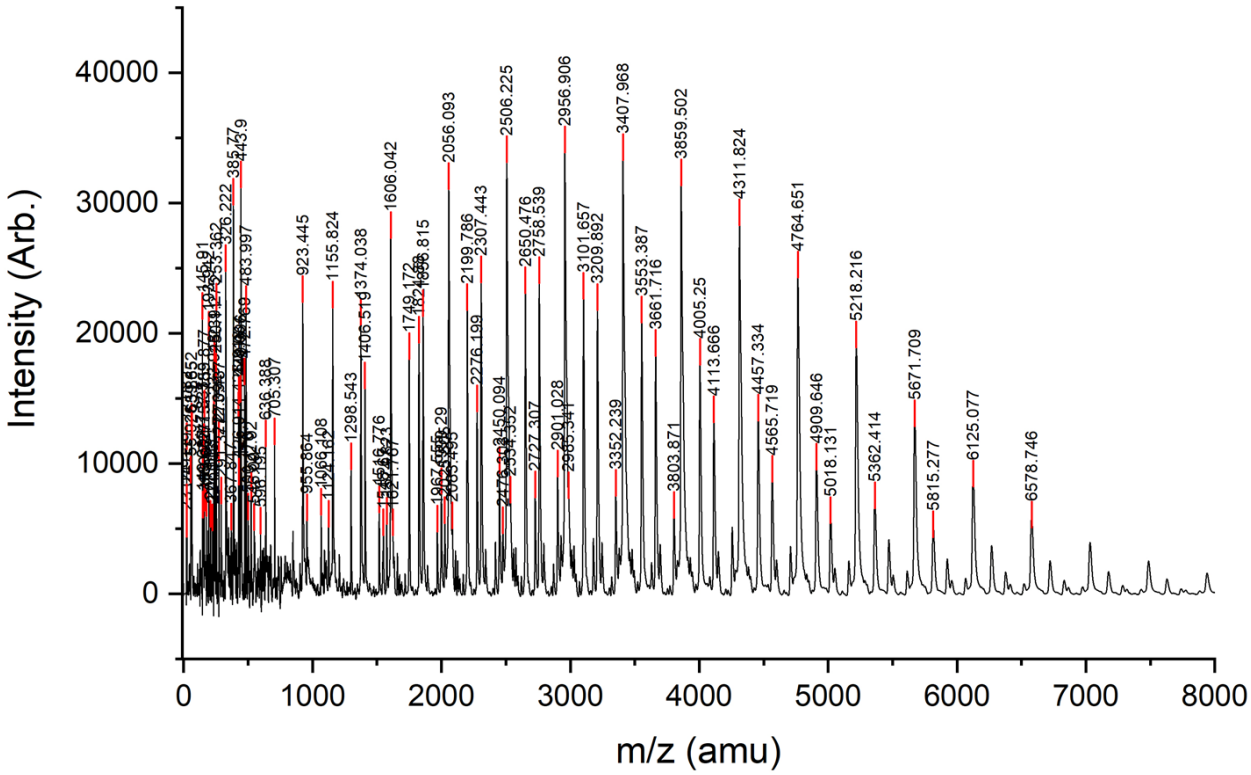

Figure A-49. Linear mode MALDI-TOF spectrum of PU **10-1a**.

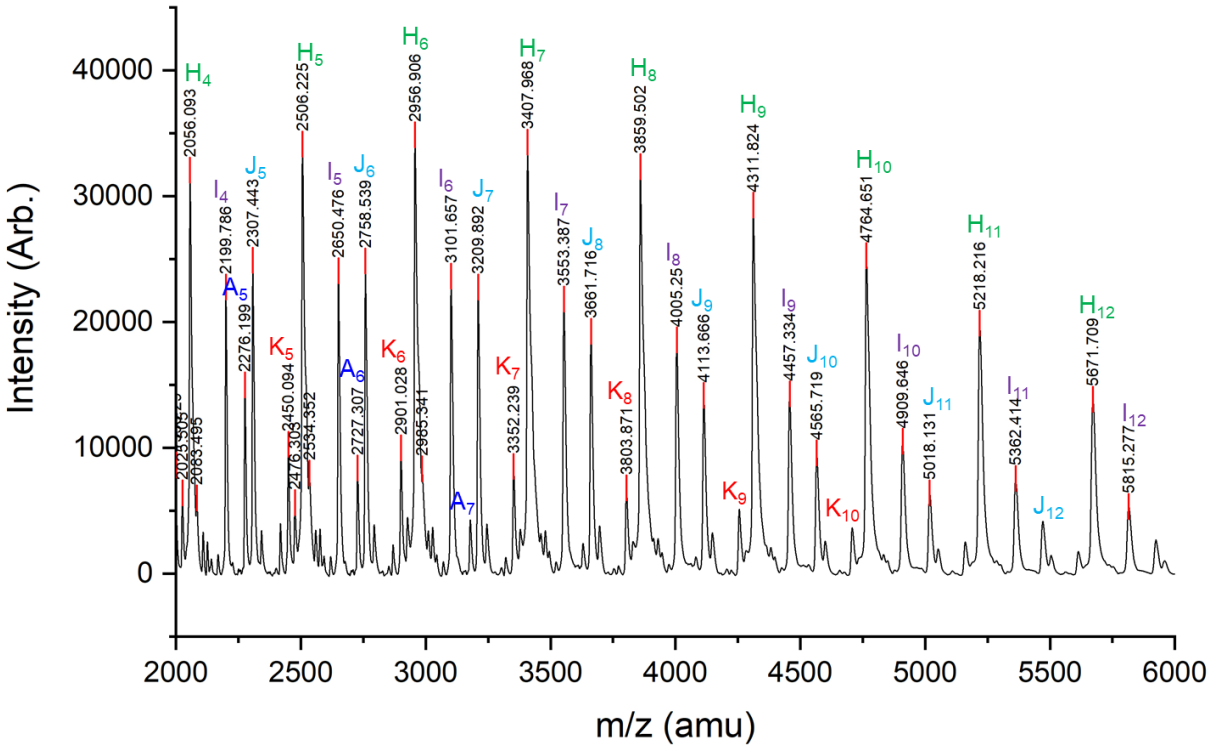

Figure A-50. Expanded linear mode MALDI-TOF spectrum of PU **10-1a** with peak assignments.

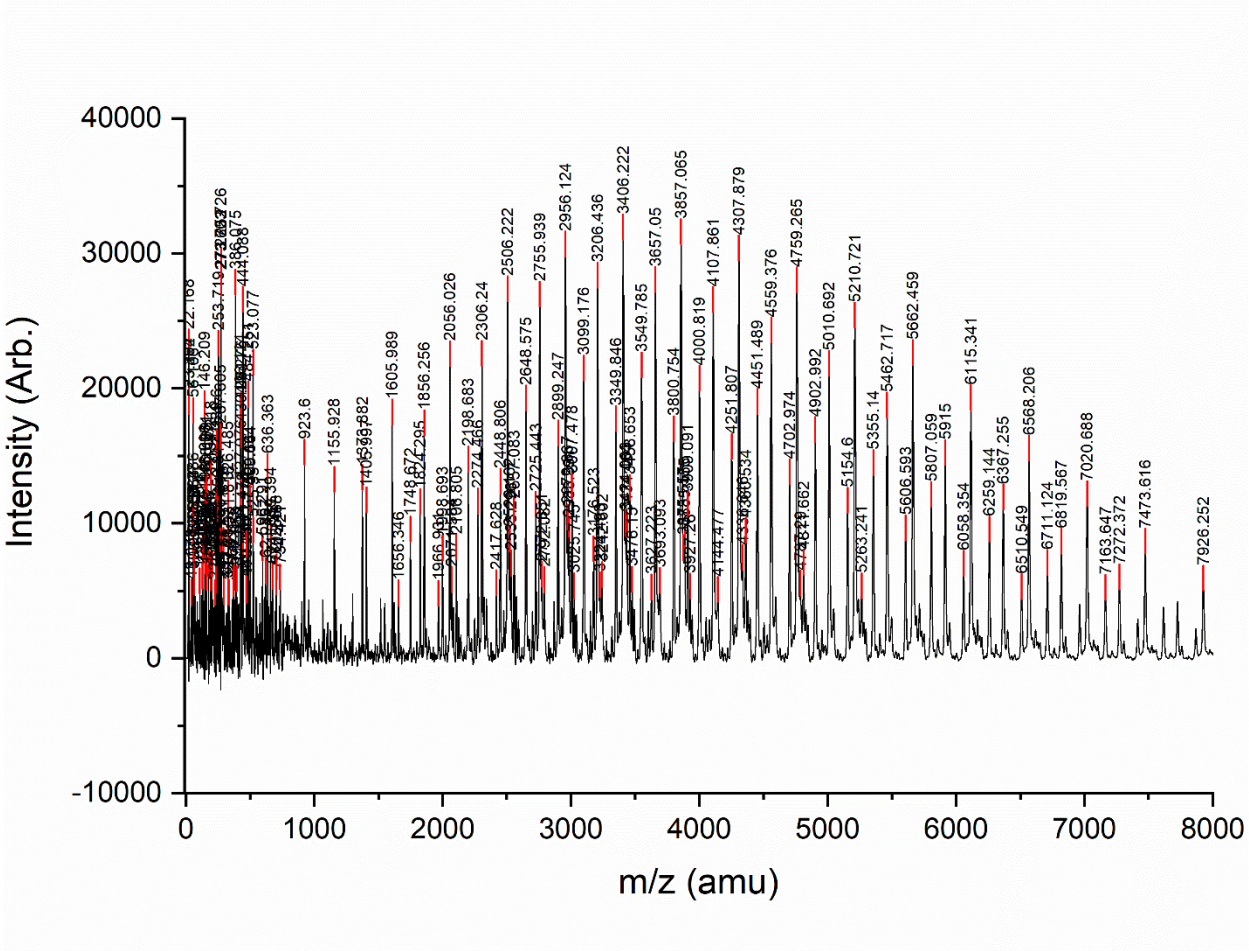

Figure A-51. Linear mode MALDI-TOF spectrum of PU **10-1b**.

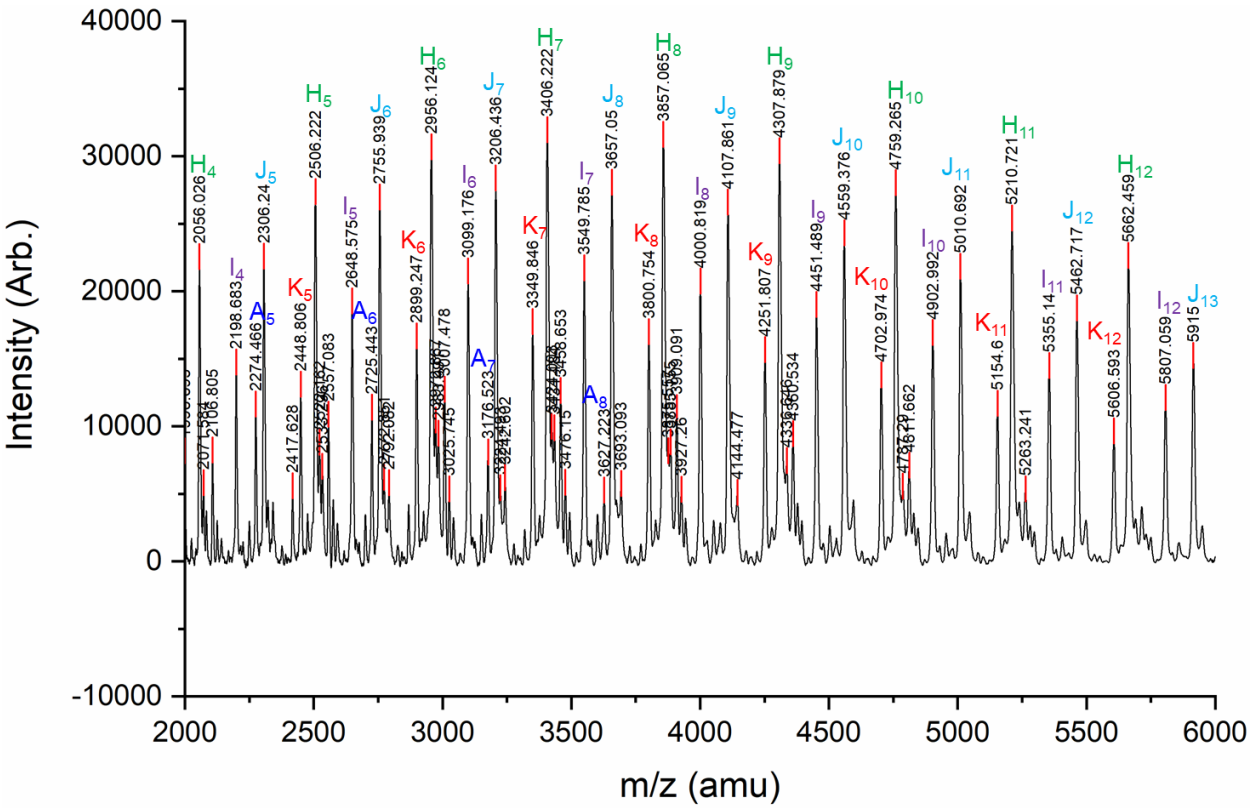

Figure A-52. Expanded linear mode MALDI-TOF spectrum of PU **10-1b** with peak assignments.

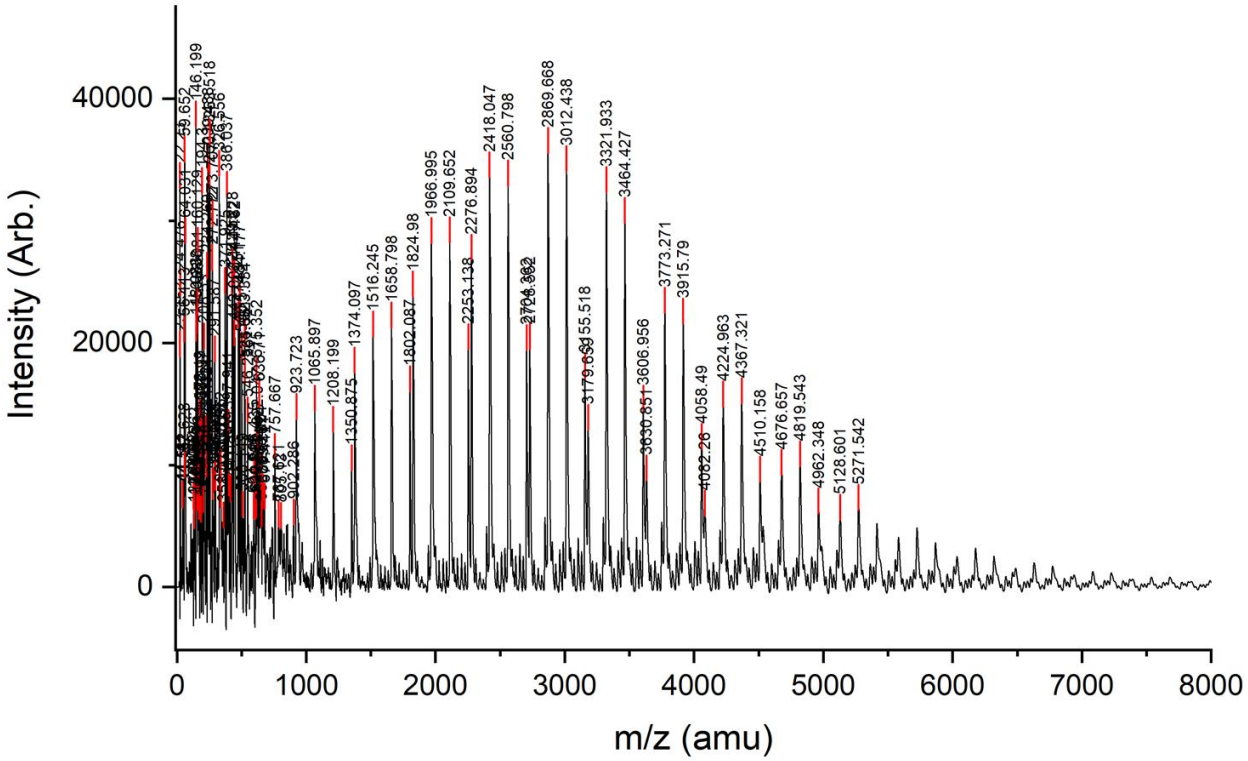

Figure A-53. Linear mode MALDI-TOF MS of PU **10-8a**.

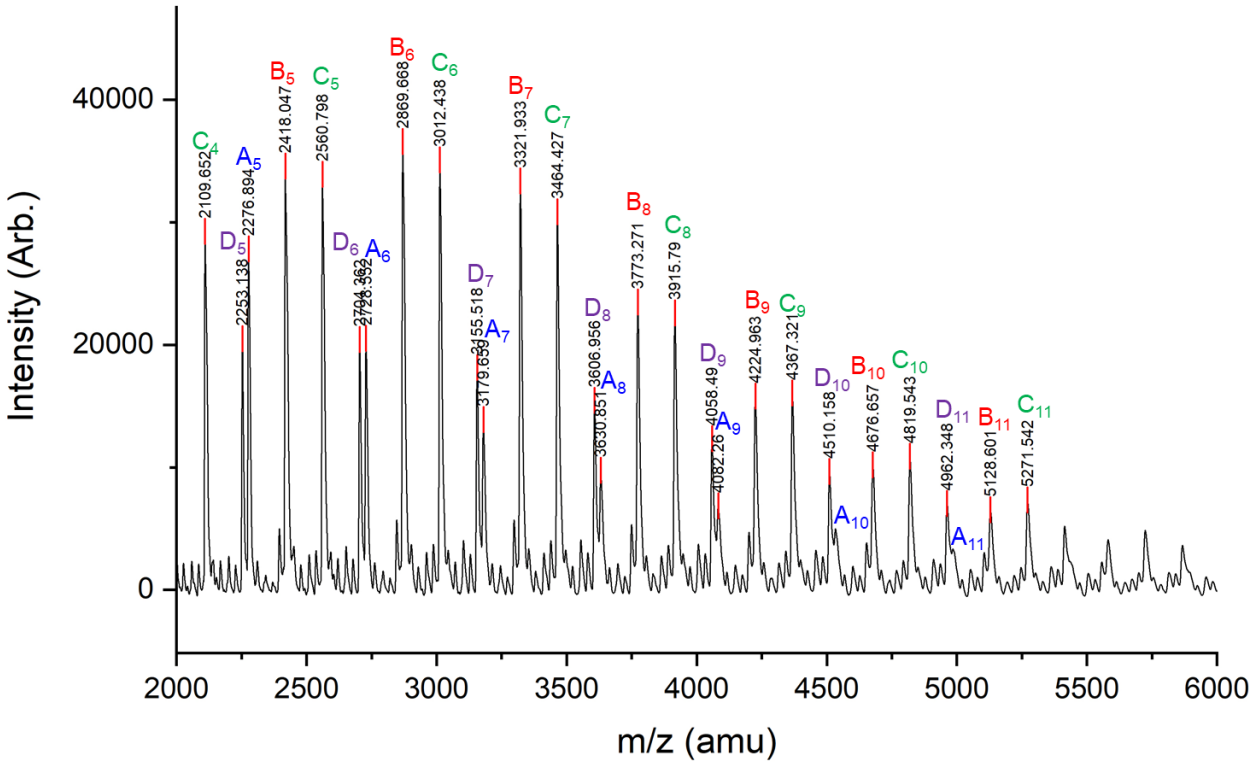

Figure A-54. Expanded linear mode MALDI-TOF MS of PU **10-8a** with peak assignments.

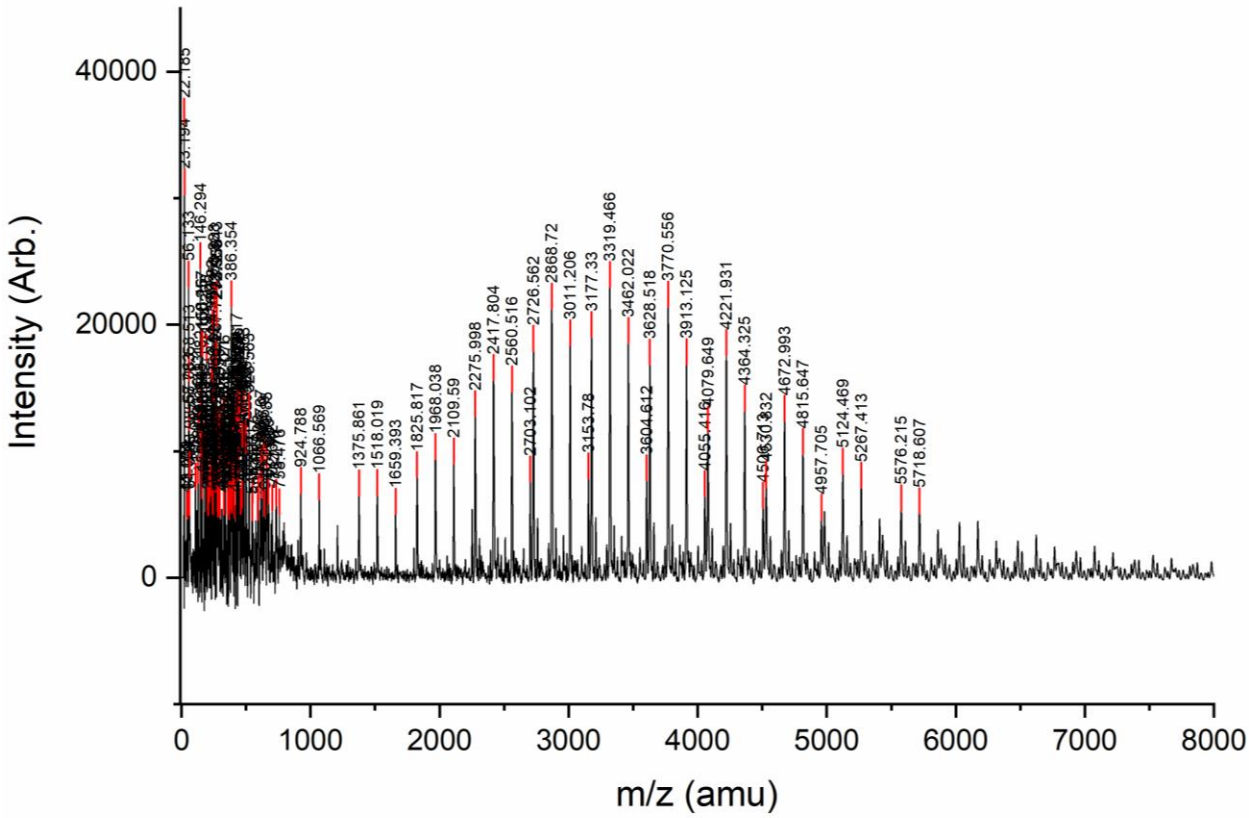

Figure A-55. Linear mode MALDI-TOF MS of PU **10-8b**.

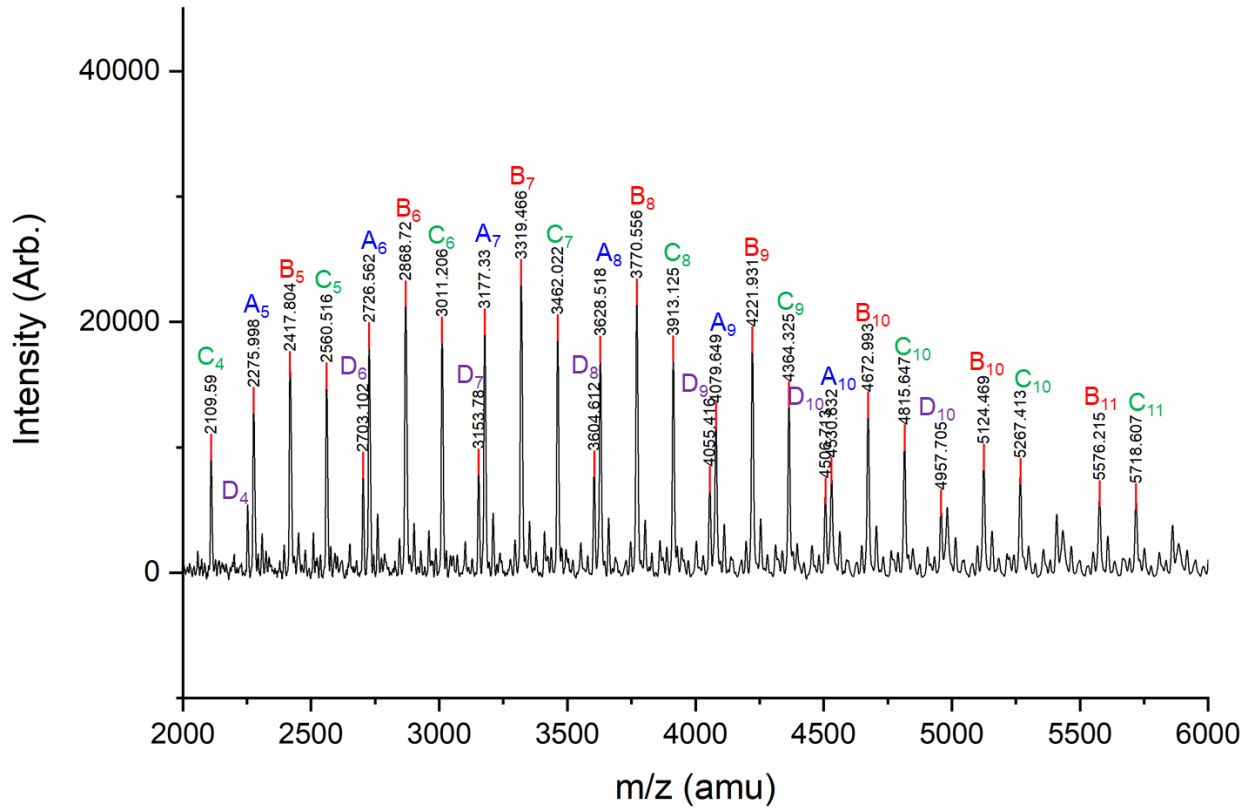

Figure A-56. Expanded linear mode MALDI-TOF MS of PU **10-8b** with peak assignments.

ATR-FTIR of Polymers 6 to 10

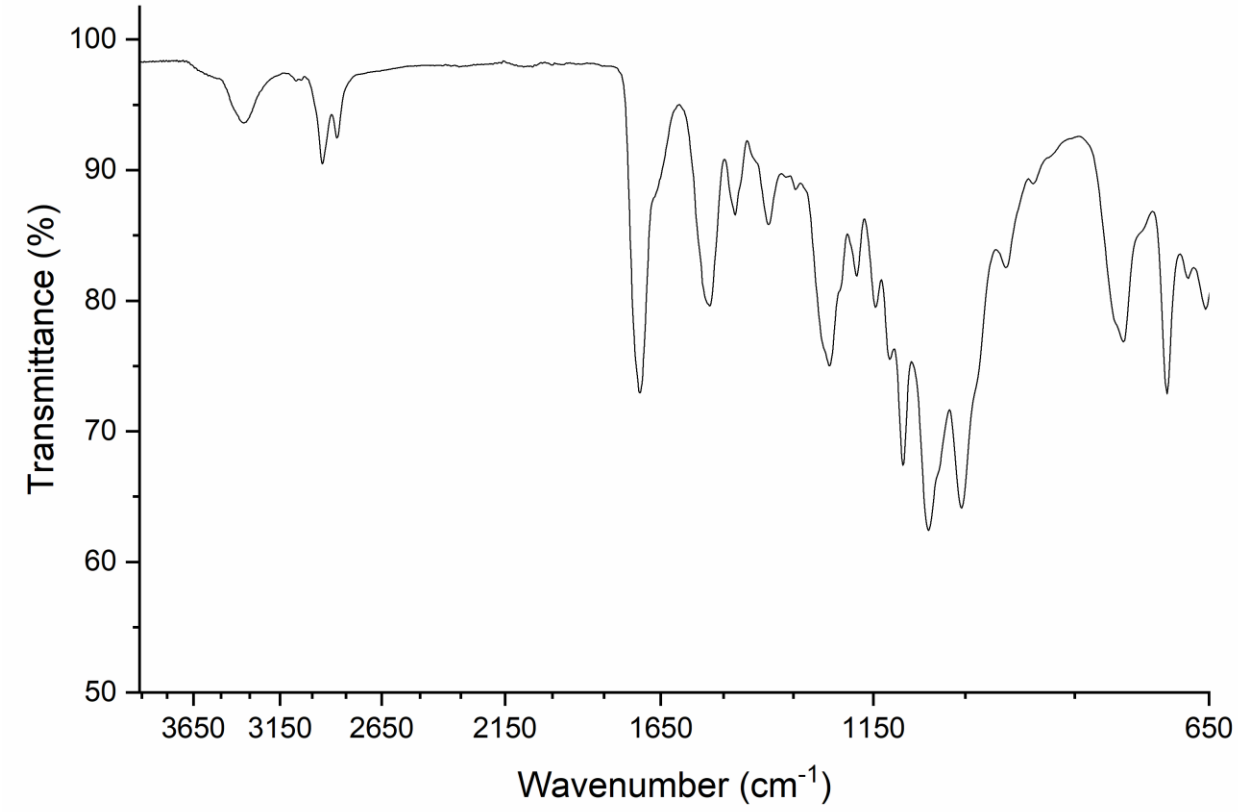

Figure A-57. Transmittance ATR-FTIR spectrum of polymer **6a**.

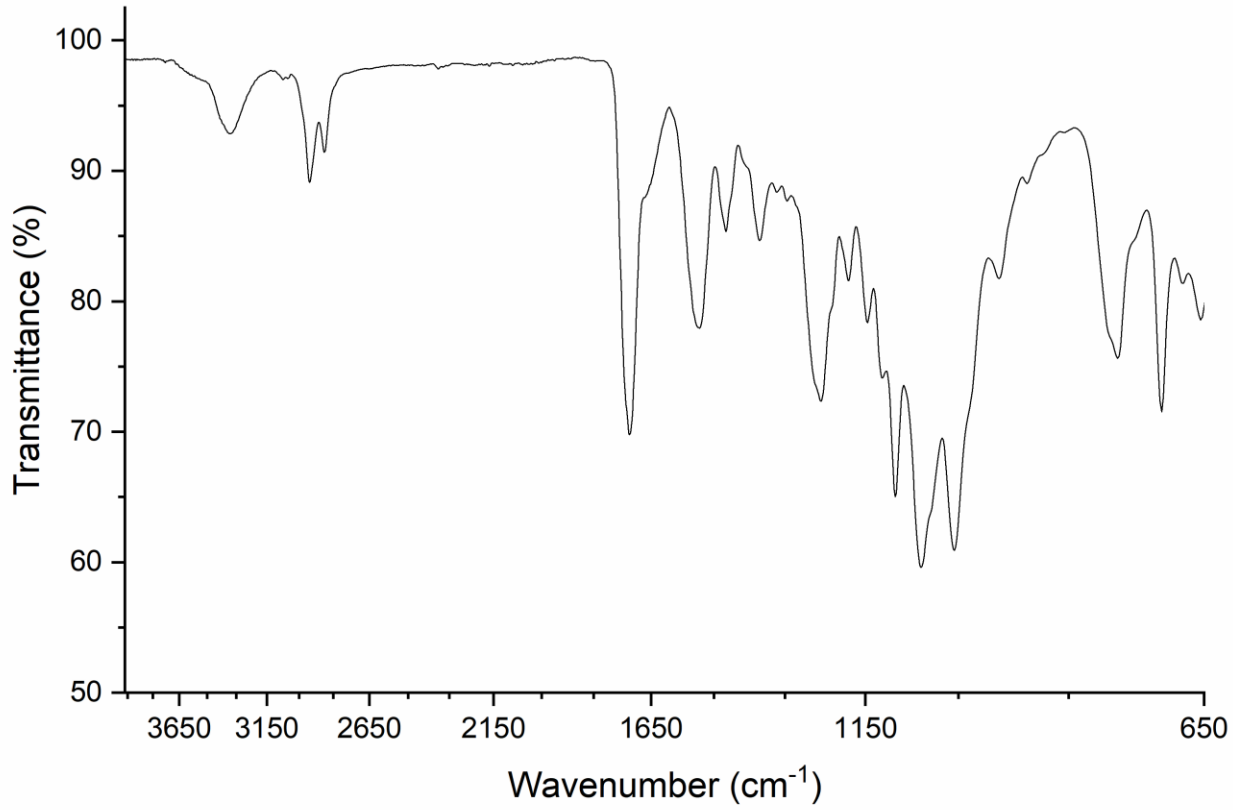

Figure A-58. Transmittance ATR-FTIR spectrum of polymer **6b**.

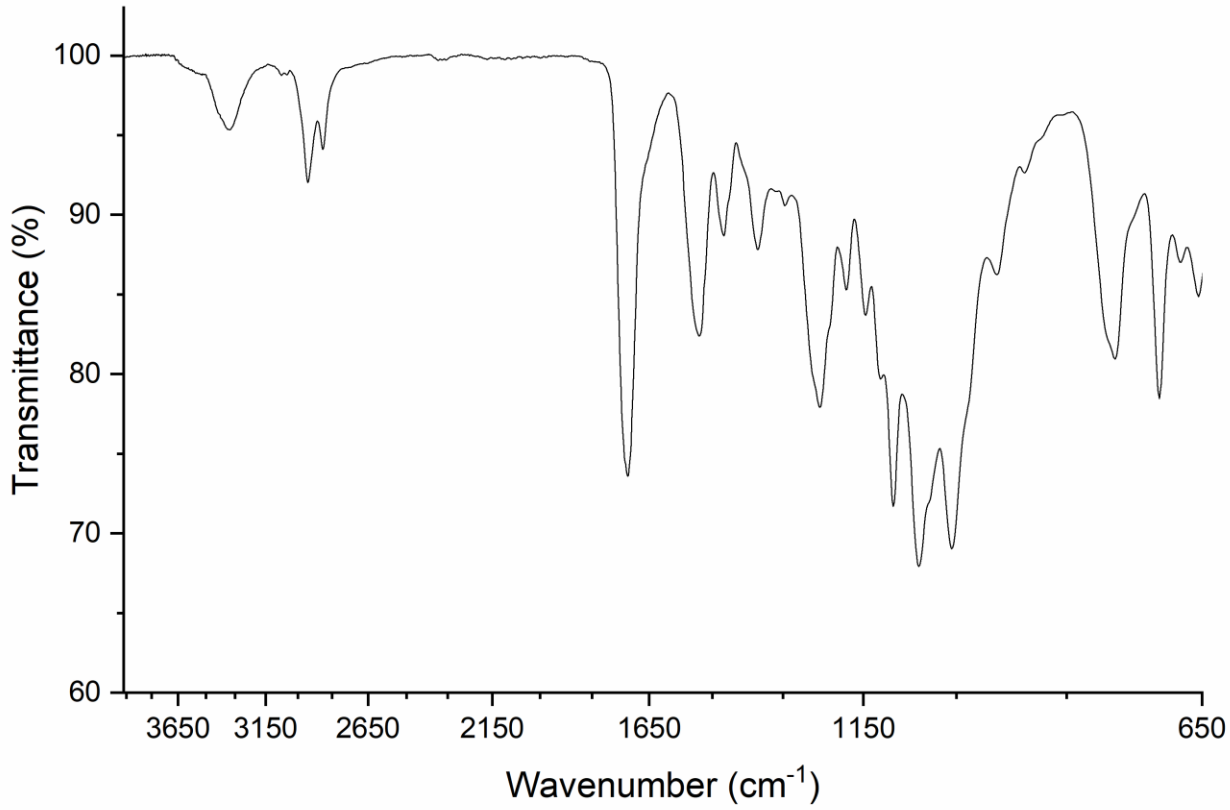

Figure A-59. Transmittance ATR-FTIR spectrum of polymer **7a**.

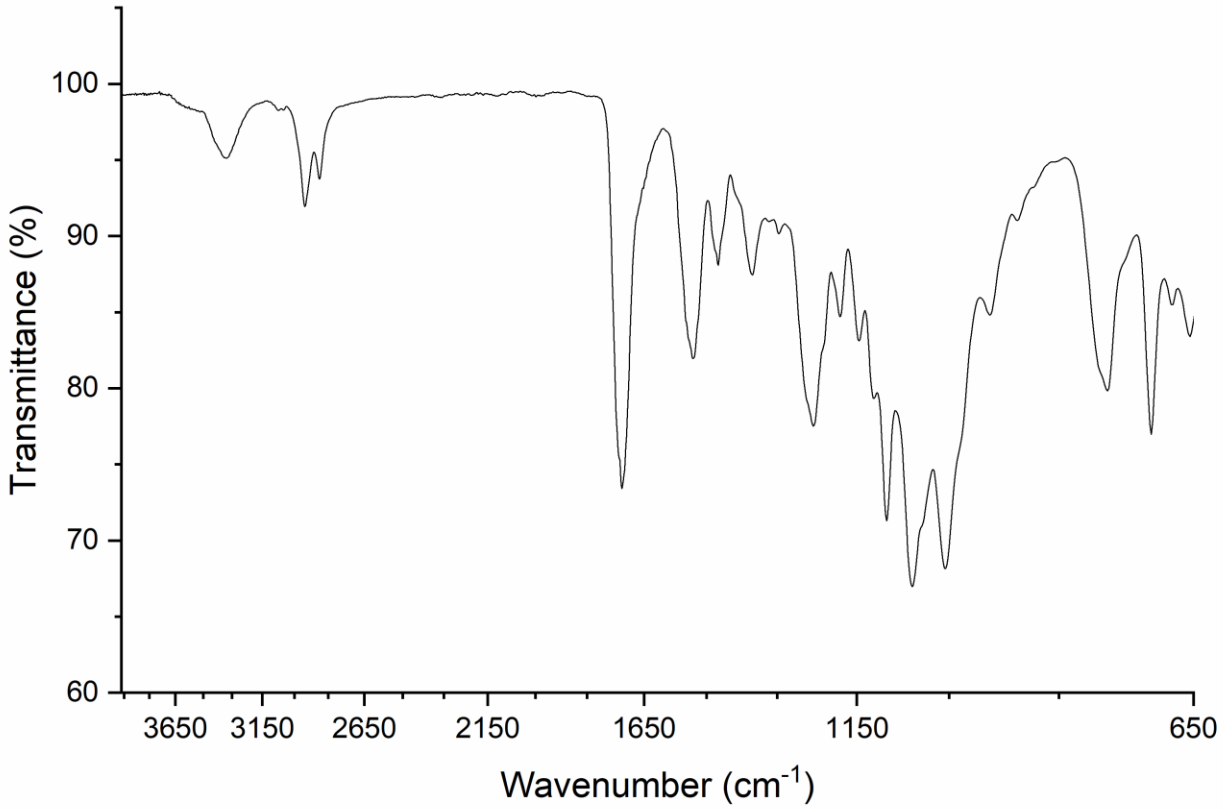

Figure A-60. Transmittance ATR-FTIR spectrum of polymer **7b**.

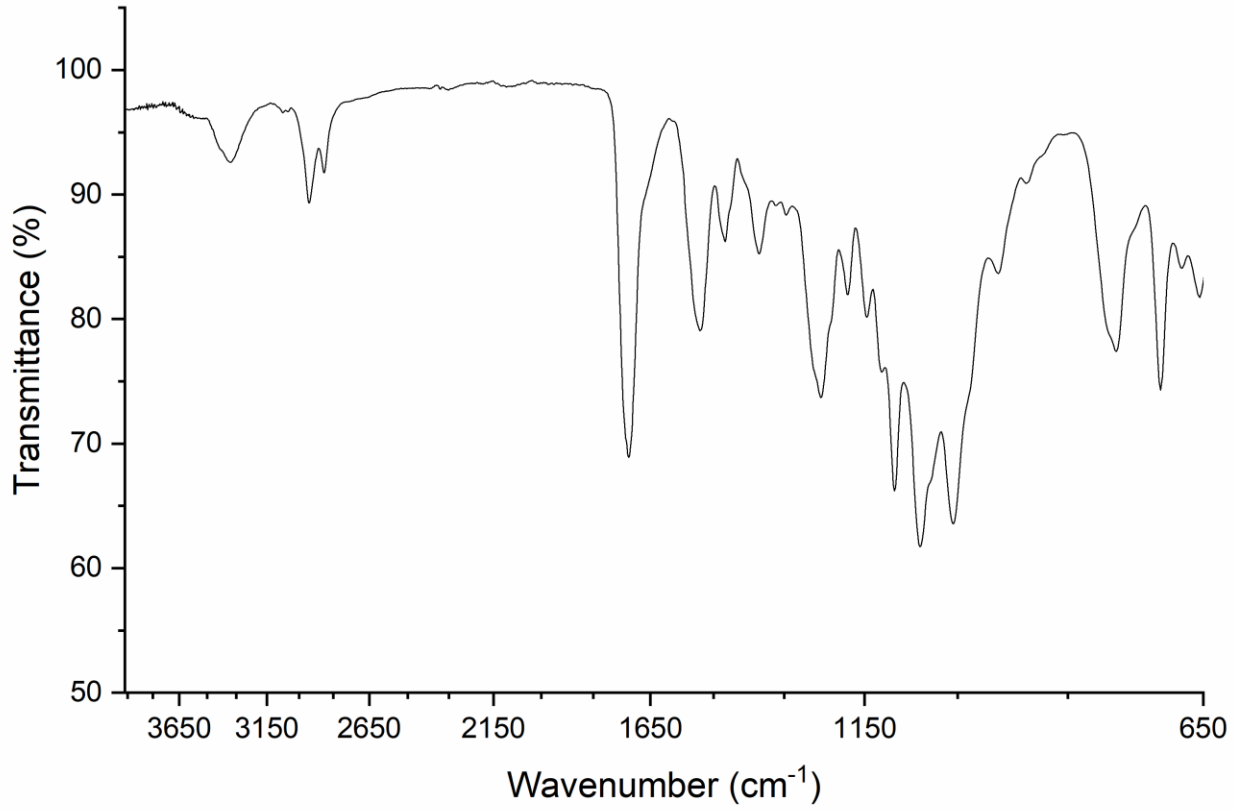

Figure A-61. Transmittance ATR-FTIR spectrum of polymer **8a**.

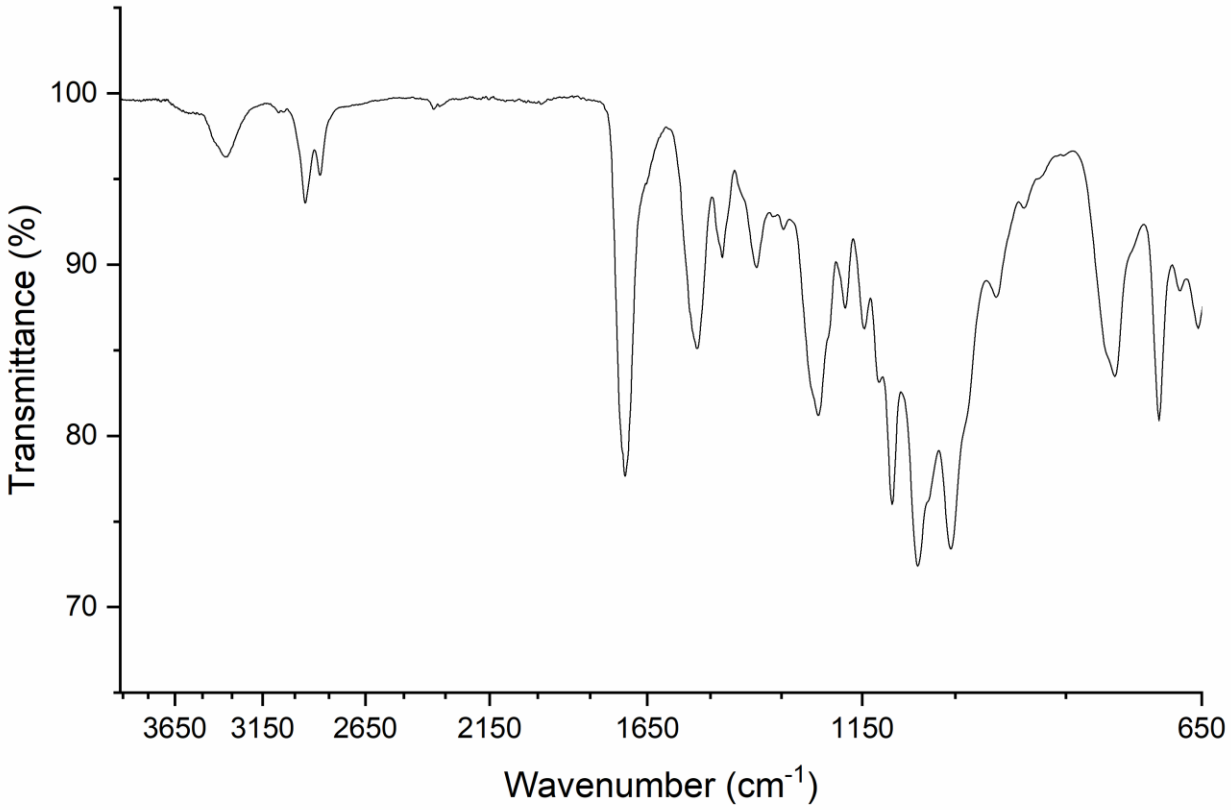

Figure A-62. Transmittance ATR-FTIR spectrum of polymer **8b**.

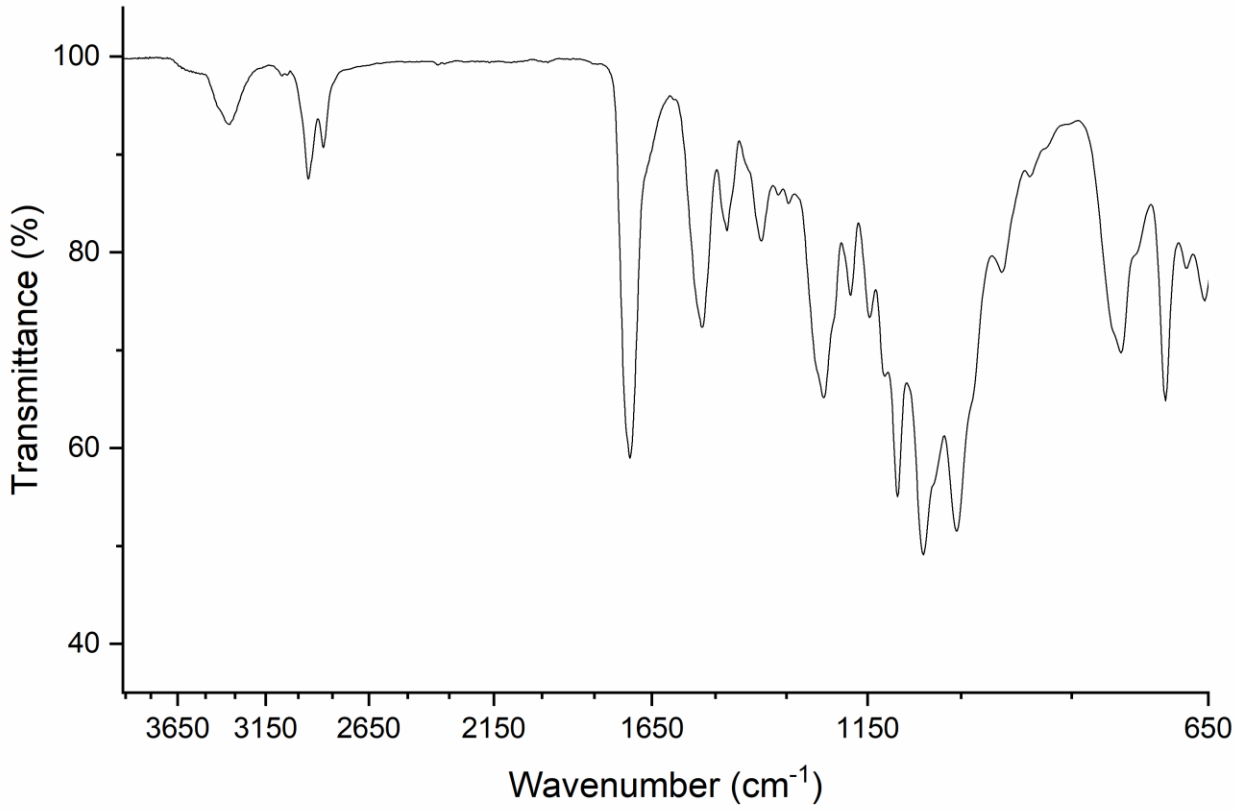

Figure A-63. Transmittance ATR-FTIR spectrum of polymer **9a**.

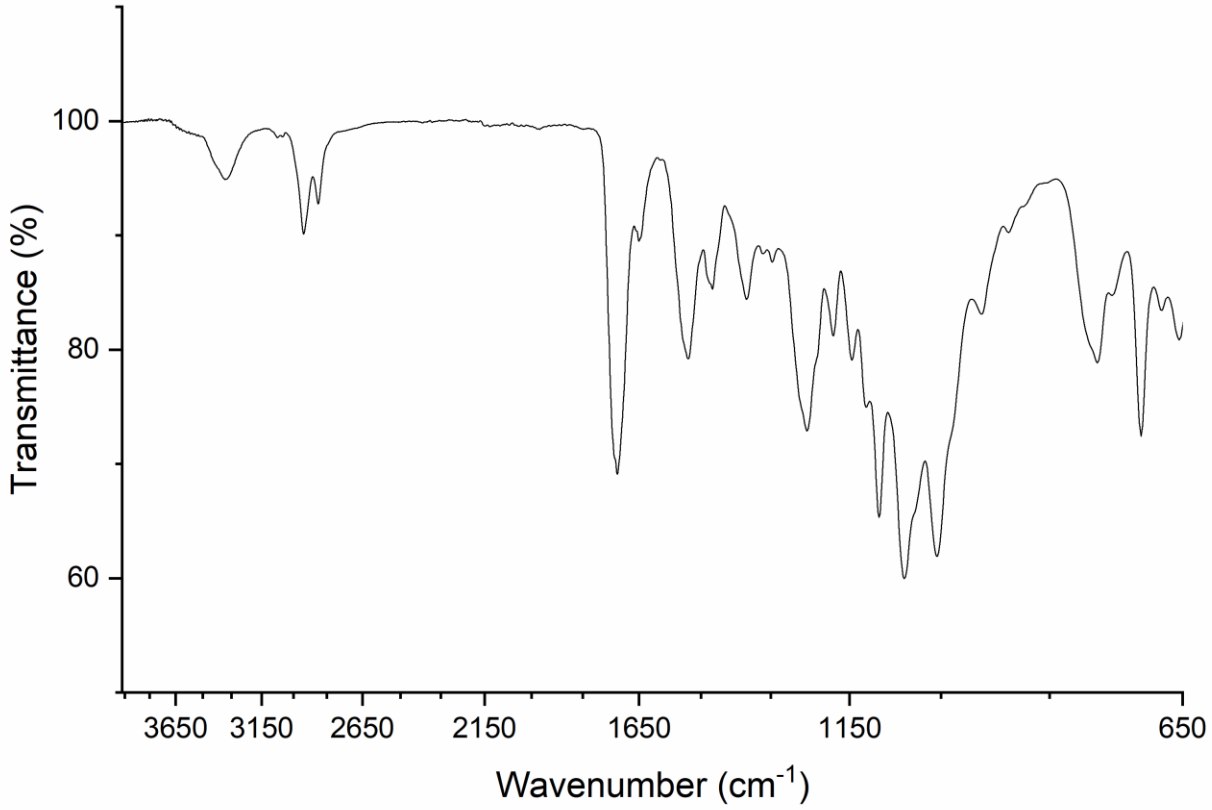

Figure A-64. Transmittance ATR-FTIR spectrum of polymer **9b**.

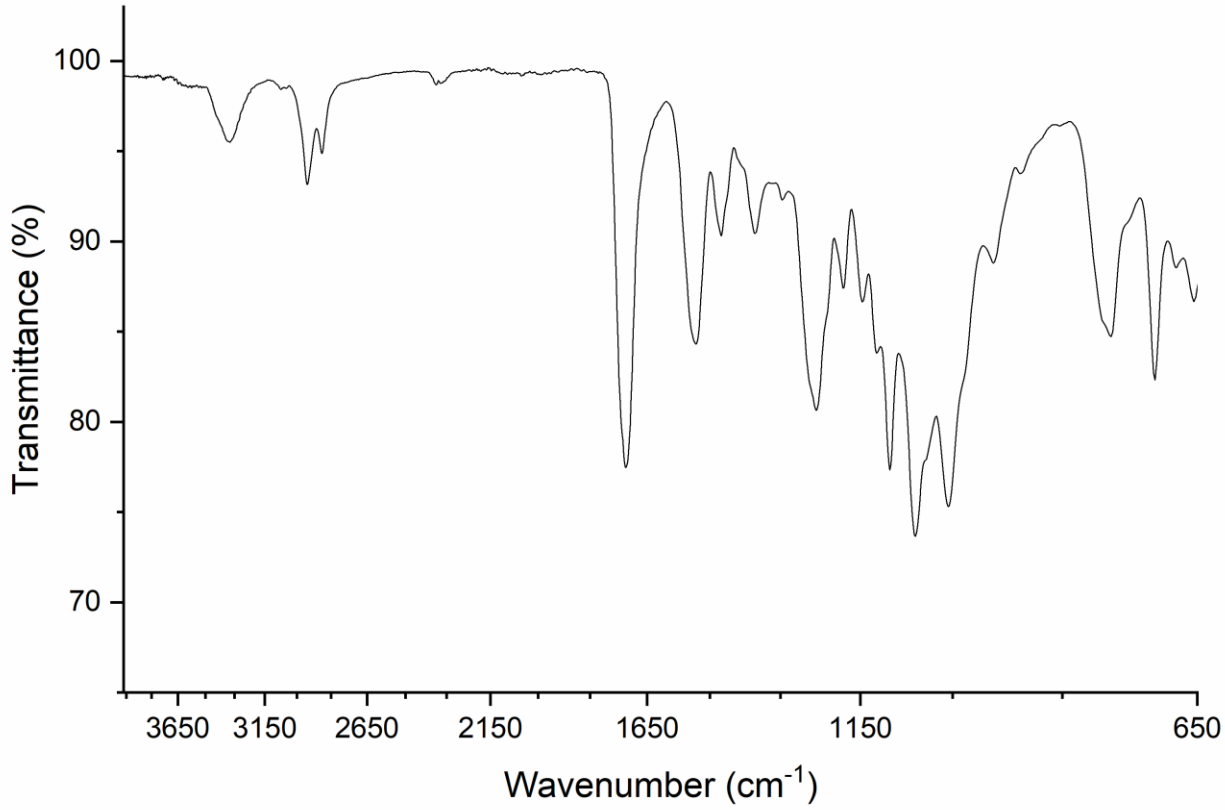

Figure A-65. Transmittance ATR-FTIR spectrum of polymer **10-1a**.

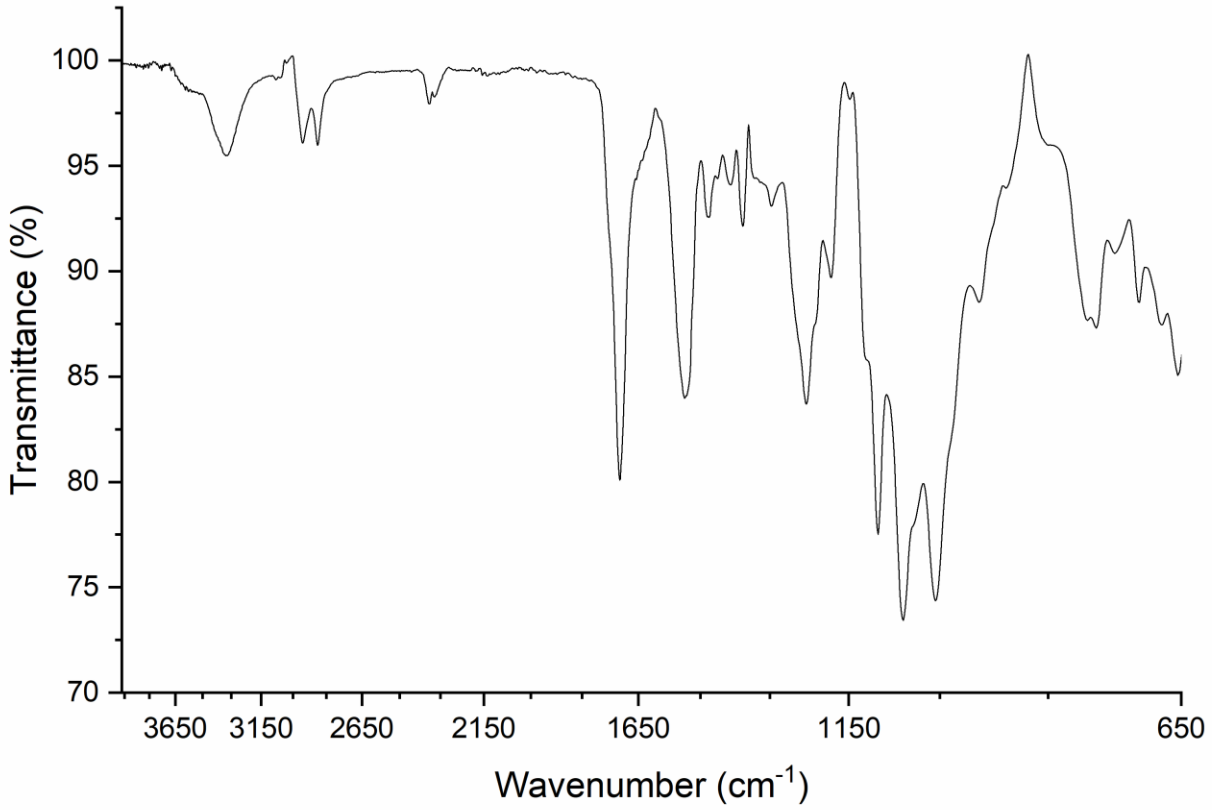

Figure A-66. Transmittance ATR-FTIR spectrum of polymer **10-1b**.

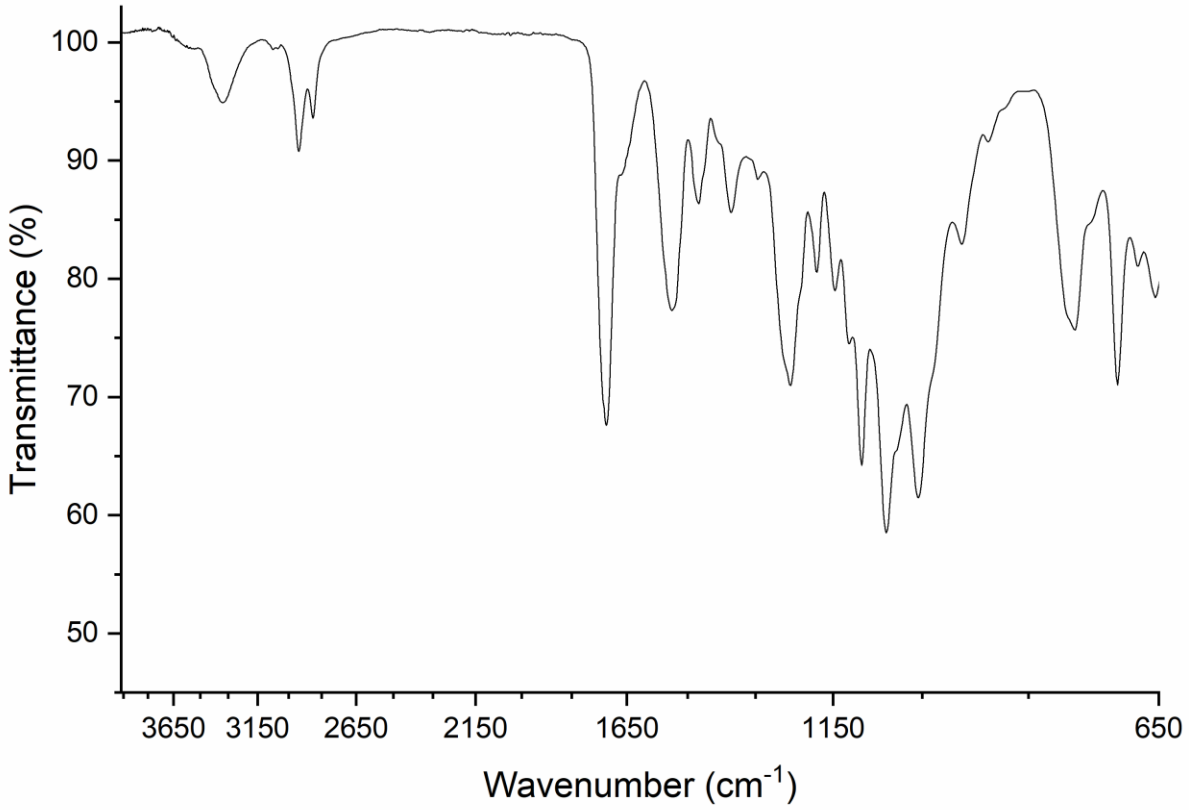

Figure A-67. Transmittance ATR-FTIR spectrum of polymer **10-8a**.

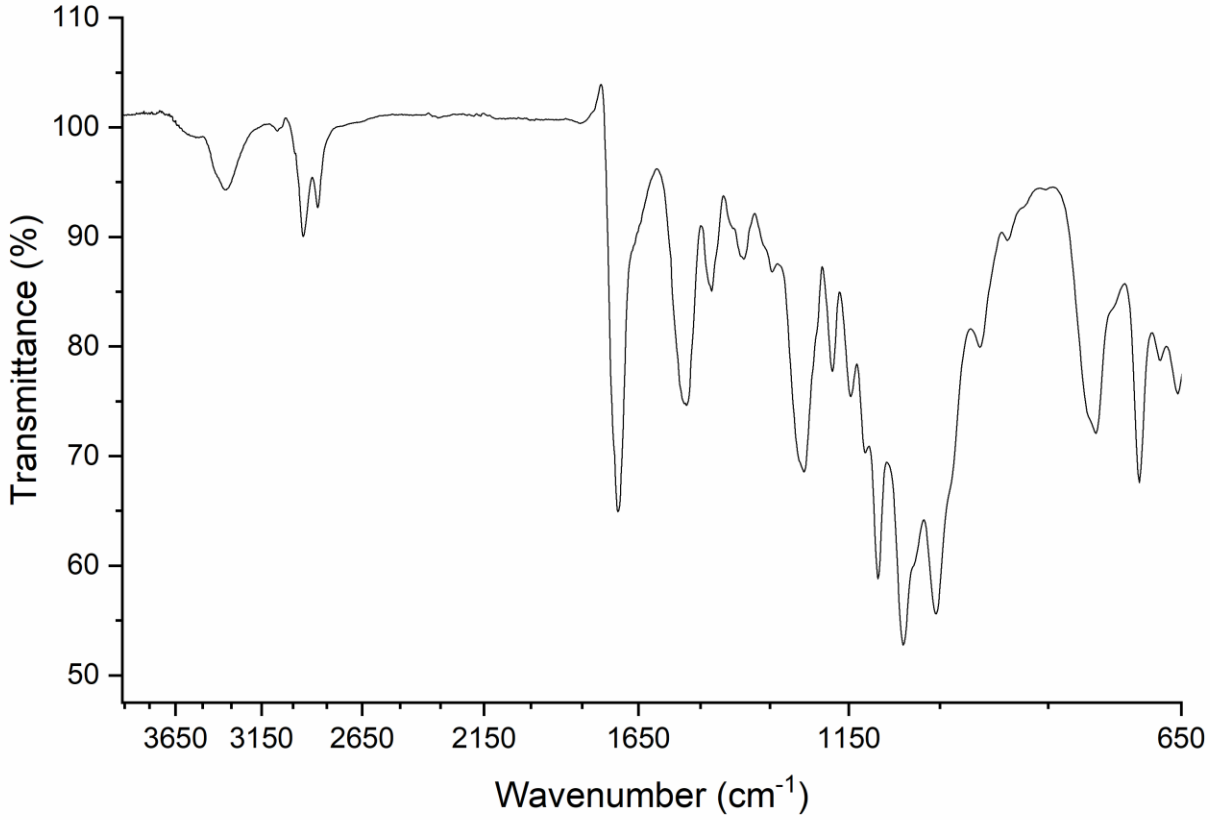

Figure A-68. Transmittance ATR-FTIR spectrum of polymer **10-8b**.

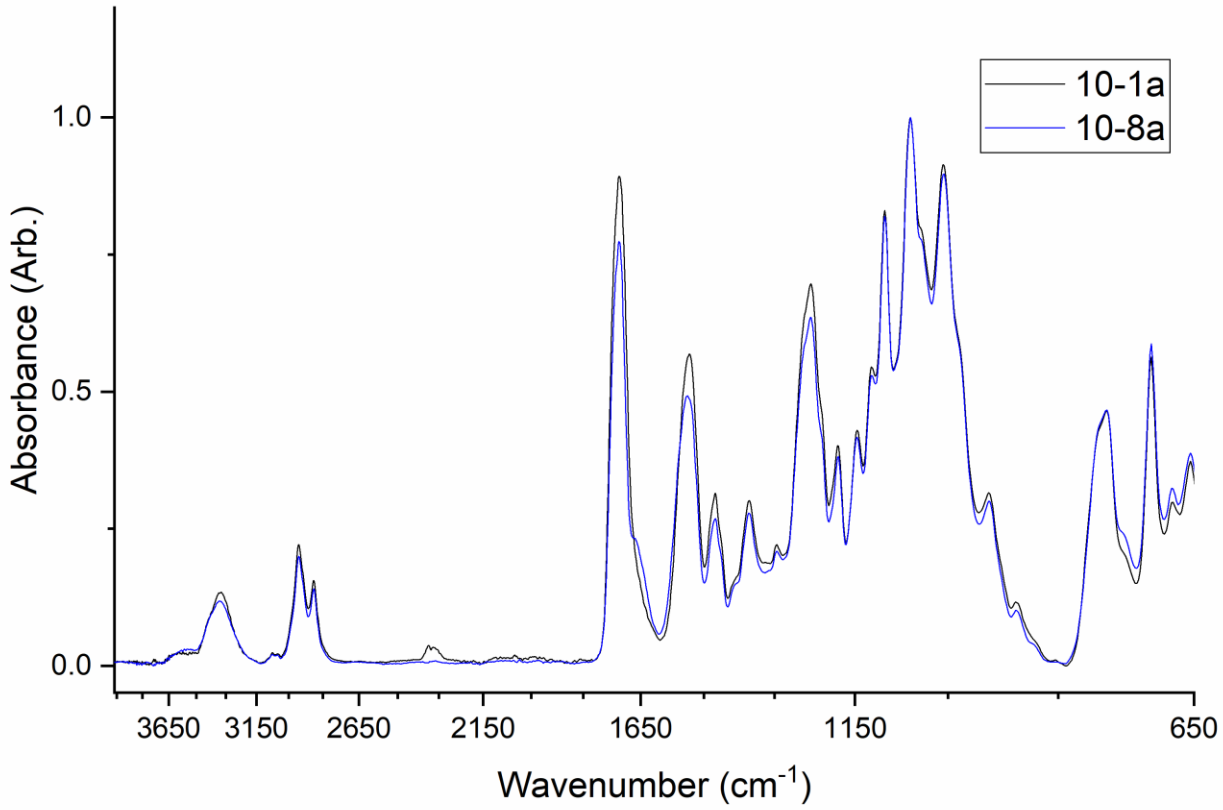

Figure A-69. Baseline-subtracted and normalized absorbance ATR-FTIR spectra of polymers **10-1a** and **10-8a**.

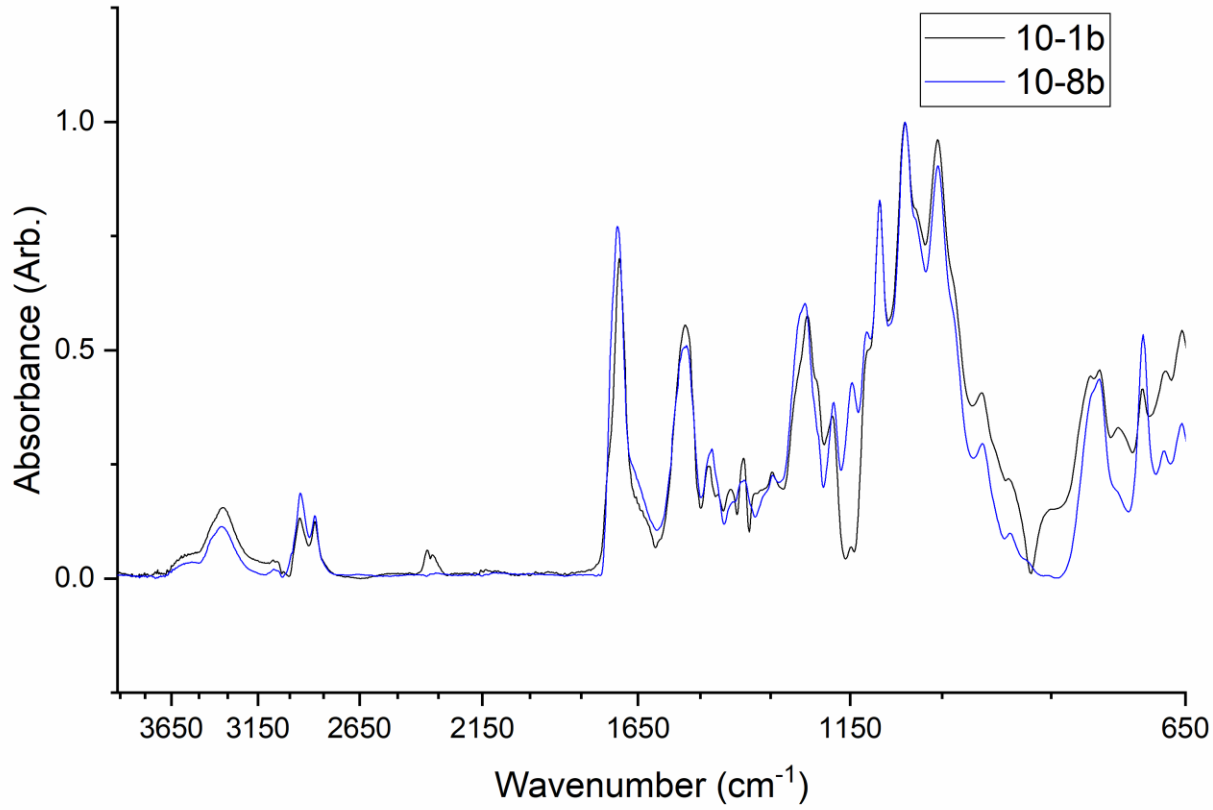

Figure A-70. Baseline-subtracted and normalized absorbance ATR-FTIR spectra of polymers **10-1b** and **10-8b**.

NMR Spectroscopy of Polymers 6a, 7a, 8a, 9b, and 10-8

Table A-8. Integration ranges and values for the ^{1}H-NMR spectra in Figure 2-7. In each system, the integration values were normalized to the ρ protons.

	6a		**7a**		**8a**		**9b**		**10-8**	
Range (ppm)	Normalized	Absolute	Normalized	Absolute	Normalized	Absolute	Normalized	Absolute	Normalized	Absolute
7.51–7.37	2.00	32400	2.00	28700	2.00	37200	2.00	31200	2.00	33800
7.37–7.27	3.00	48600	2.99	42800	2.97	55100	2.99	46500	2.92	49400
5.59–5.52	0.31	5050	0.17	2450	0.17	3130	0.20	3120	0.12	2020
5.52–5.42	1.12	18200	1.03	14800	1.10	20400	1.07	16700	1.19	20100
5.42–5.28	1.09	17600	1.18	16900	1.23	22900	1.16	18100	1.52	25700
5.01–4.87	1.23	20000	1.47	21000	1.44	26700	1.42	22200	1.42	23900
4.87–4.72	0.85	13700	0.92	13200	0.93	17300	0.93	14500	1.01	17000
4.72–4.60	0.20	3320	0.14	2030	0.10	1880	0.12	1890	0.03	514
4.39–4.32	0.00	–15.9	0.00	65.4	0.03	537	0.10	1510	0.03	590
4.32–4.22	1.02	16500	0.99	14200	0.98	18200	1.00	15700	0.89	15100
4.22–4.09	0.16	2640	0.08	1190	0.07	1210	0.08	1240	0.04	683
3.97–3.83	0.91	14800	0.94	13400	0.99	18400	0.99	15400	1.02	17200
3.83–3.71	1.14	18500	1.07	15400	1.08	20100	1.12	17500	1.01	17100
3.71–3.55	1.04	16800	1.06	15200	1.06	19700	1.24	19400	1.05	17700
3.44–3.30	3.01	48800	3.05	43800	3.01	55900	3.06	47700	2.94	49700
3.19–2.88	3.88	62800	3.65	52400	3.74	69500	3.83	59800	4.55	76900
2.86–2.57	0.37	5990	0.47	6680	0.37	6900	0.47	7260	0.31	5310
1.48–1.32	3.00	48700	2.57	36900	2.72	50600	3.02	47100	3.64	61500
1.32–0.96	5.30	85900	5.43	77900	5.06	94000	5.12	79700	6.40	108000

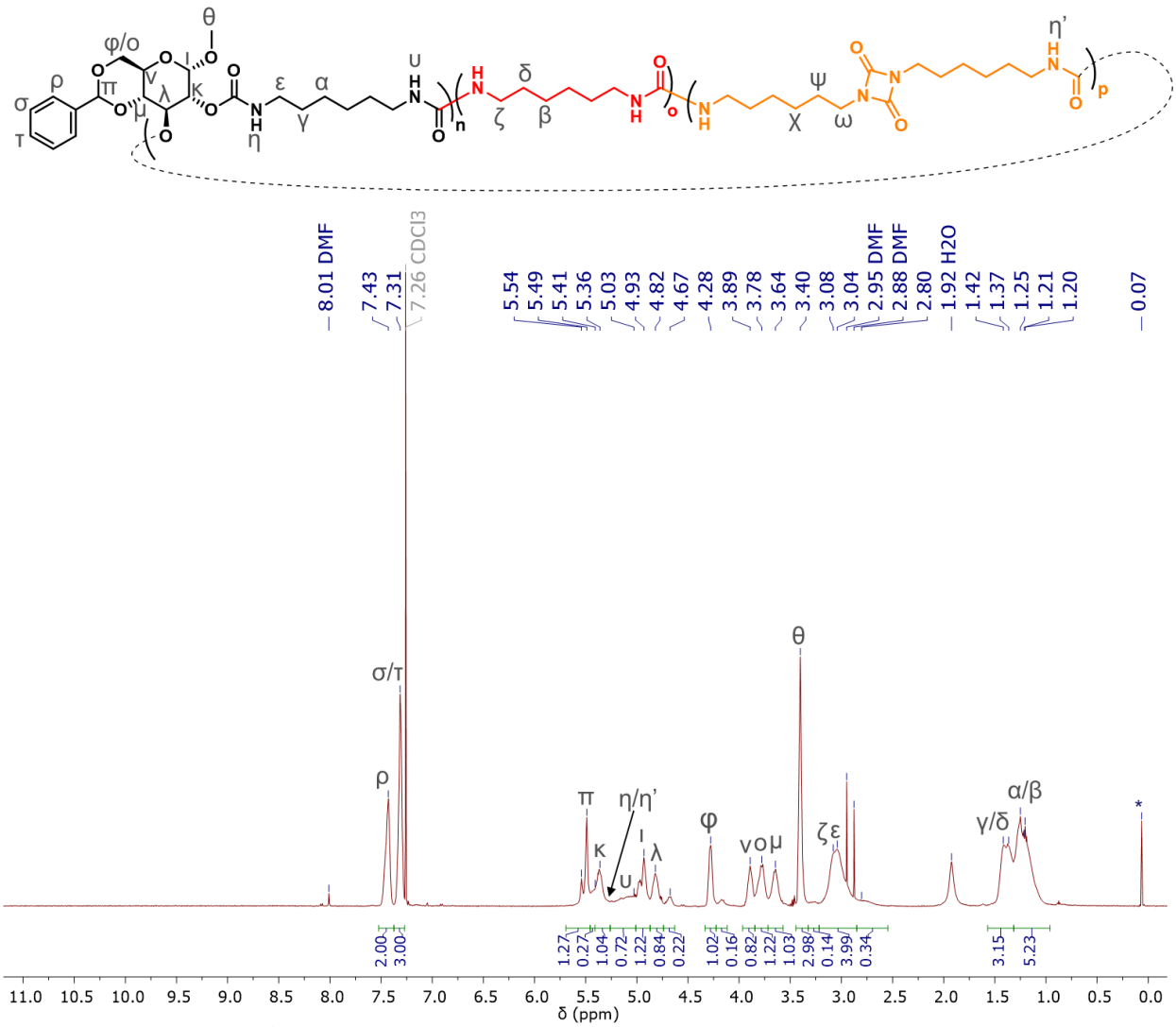

Figure A-71. ^{1}H-NMR (500 MHz, $CDCl_3$) spectrum of **6a.** *Grease impurity.

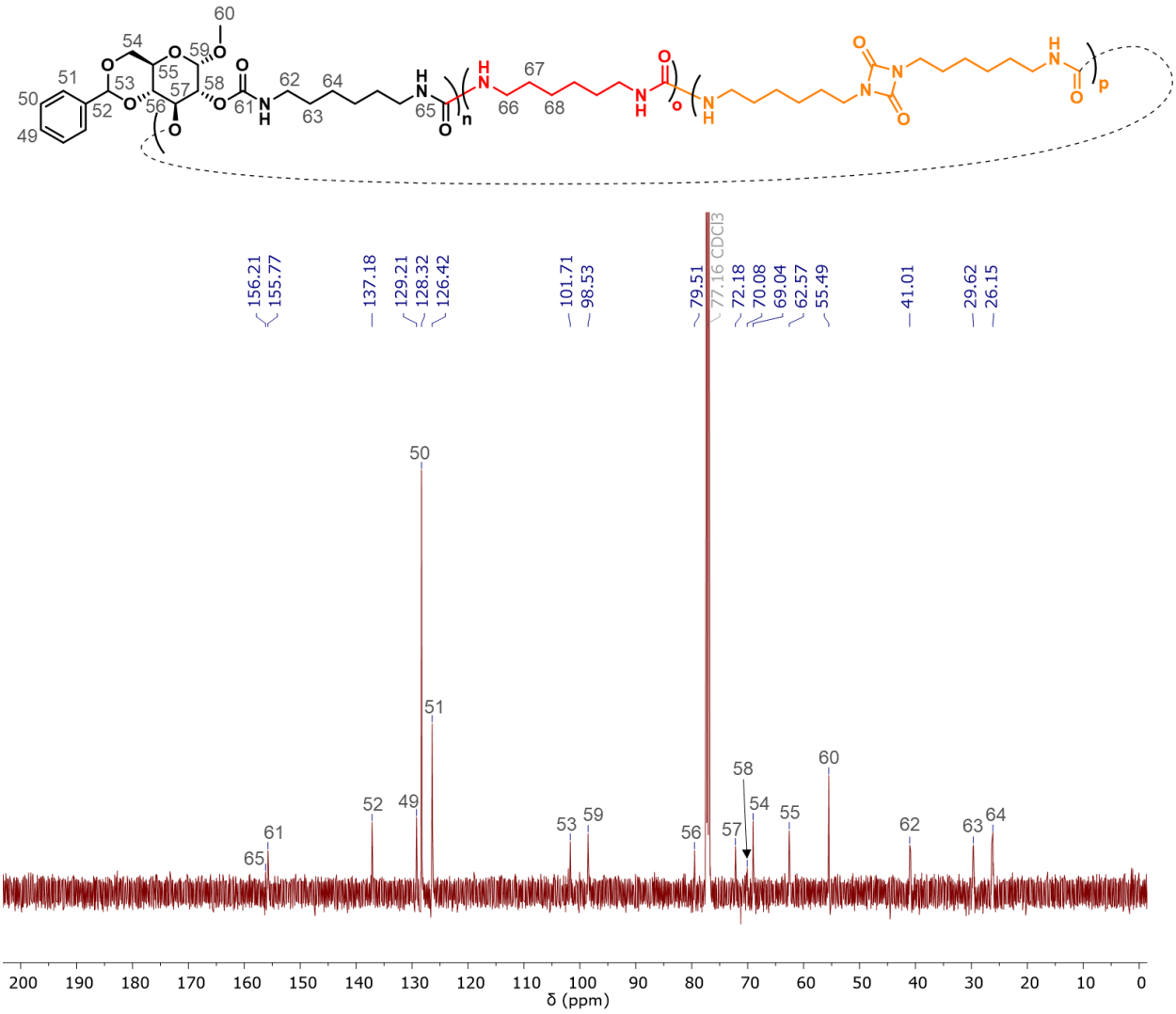

Figure A-72. ^{13}C-NMR (125 MHz, $CDCl_3$) spectrum of **6a**, ns = 2000, d1 = 8 s.

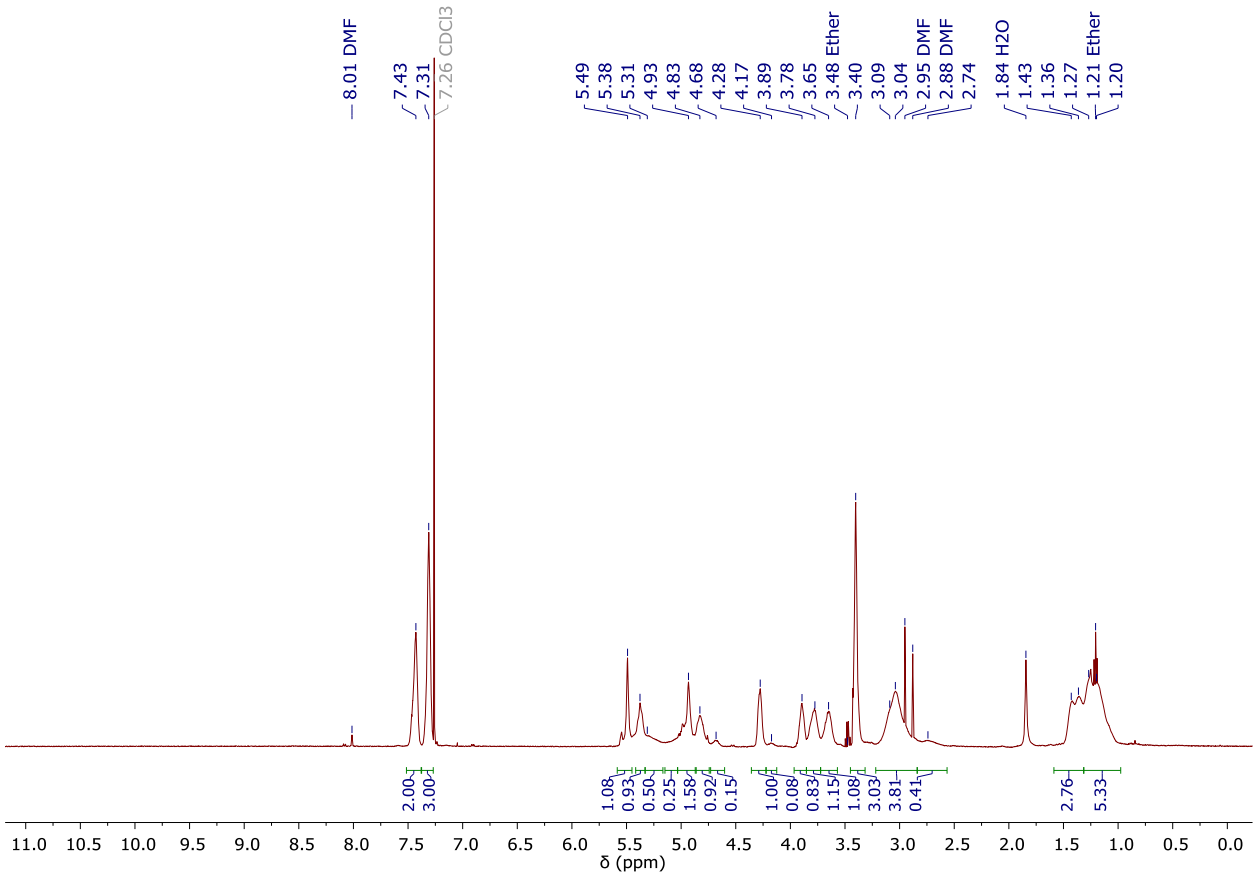

Figure A-73. ^{1}H-NMR (500 MHz, $CDCl_3$) spectrum of **7a.**

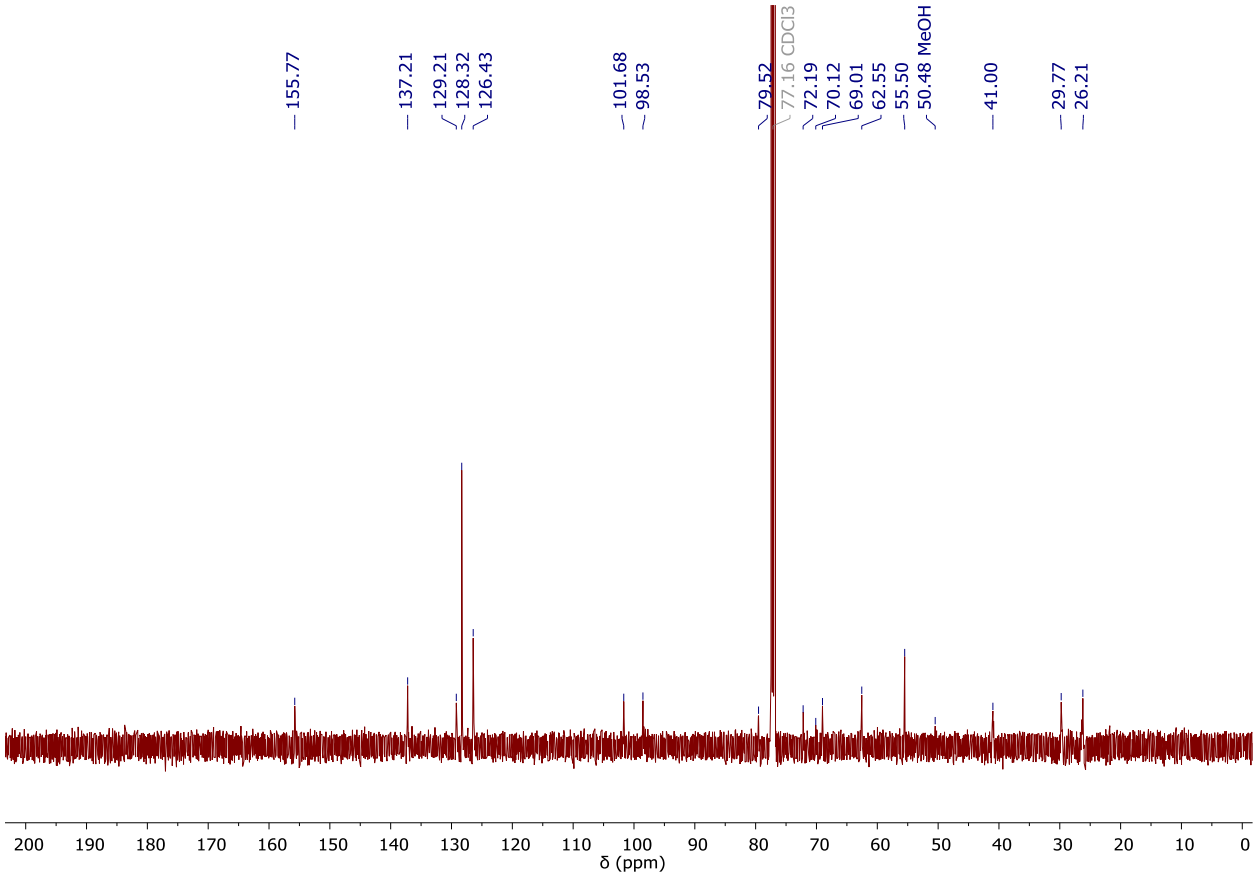

Figure A-74. ^{13}C-NMR (125 MHz, $CDCl_3$) spectrum of **7a**, ns = 1152, d1 = 8s 3C-NMR (125 MHz, CDCl3) spectrum of 7a, ns = 1152, d1 = 8s.

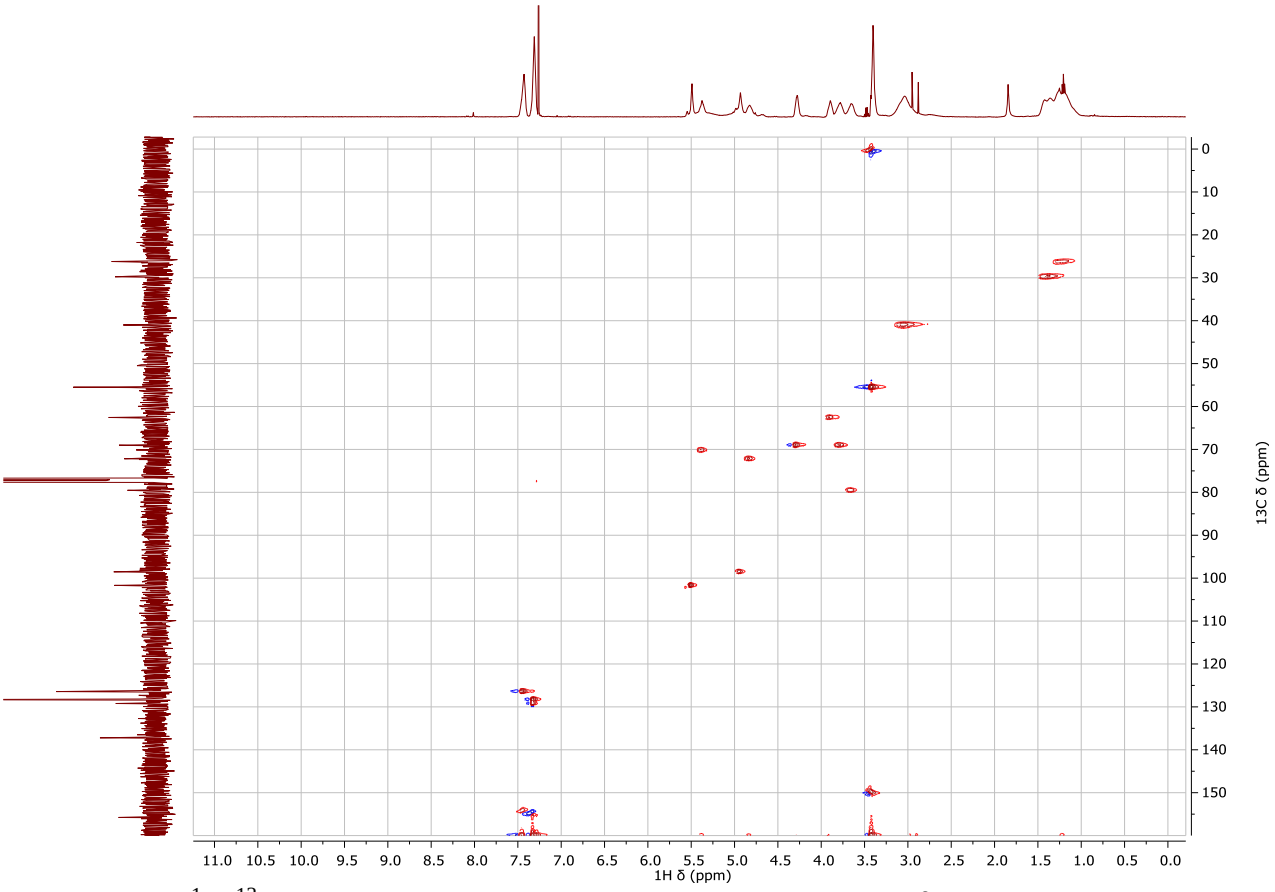

Figure A-75. ^{1}H-^{13}C HMQC (500 MHz-125 MHz, $CDCl_3$) spectrum of **7a** in $CDCl_3$, nt = 32, ni = 200.

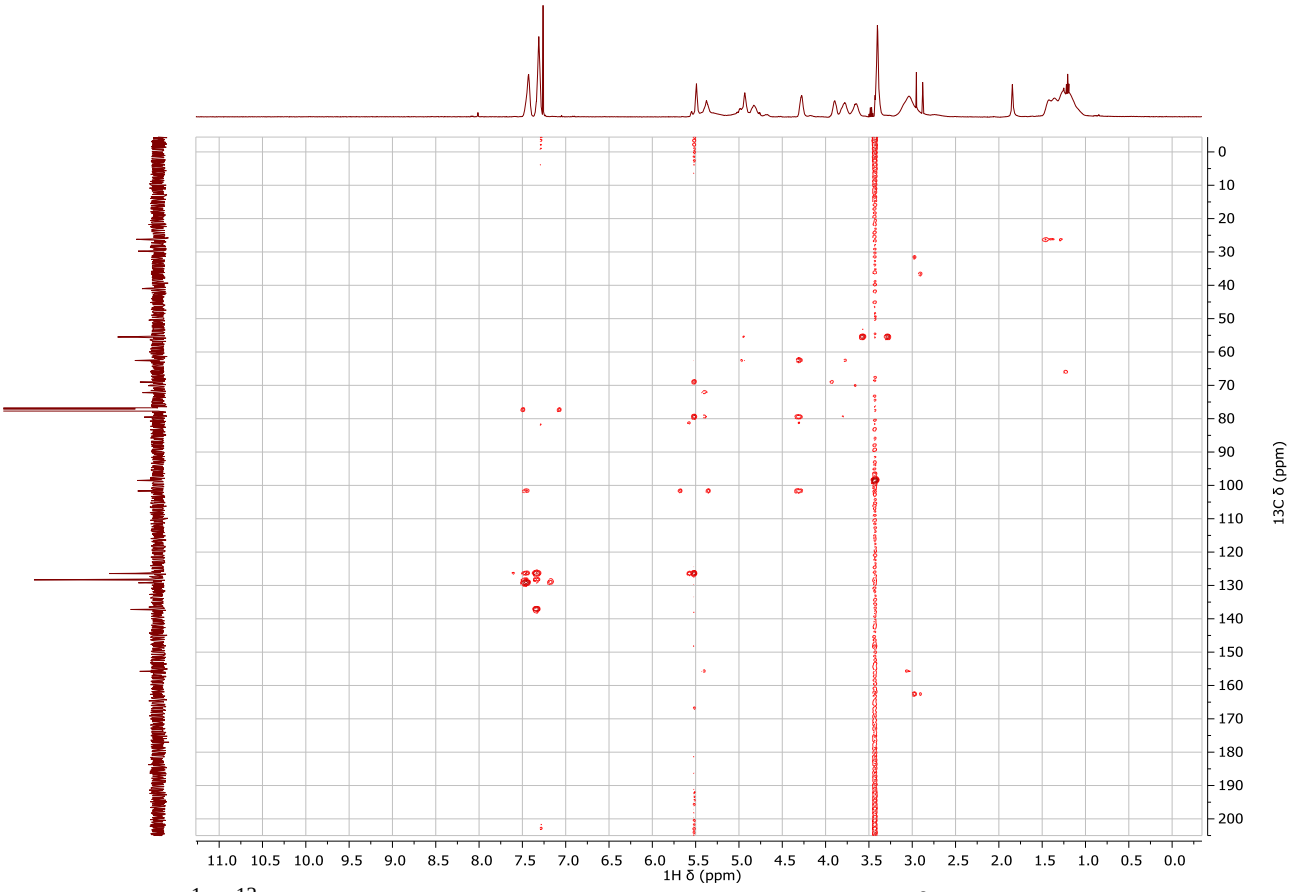

Figure A-76. ^{1}H-^{13}C HMBC (500 MHz-125 MHz, $CDCl_3$) spectrum of **7a.**

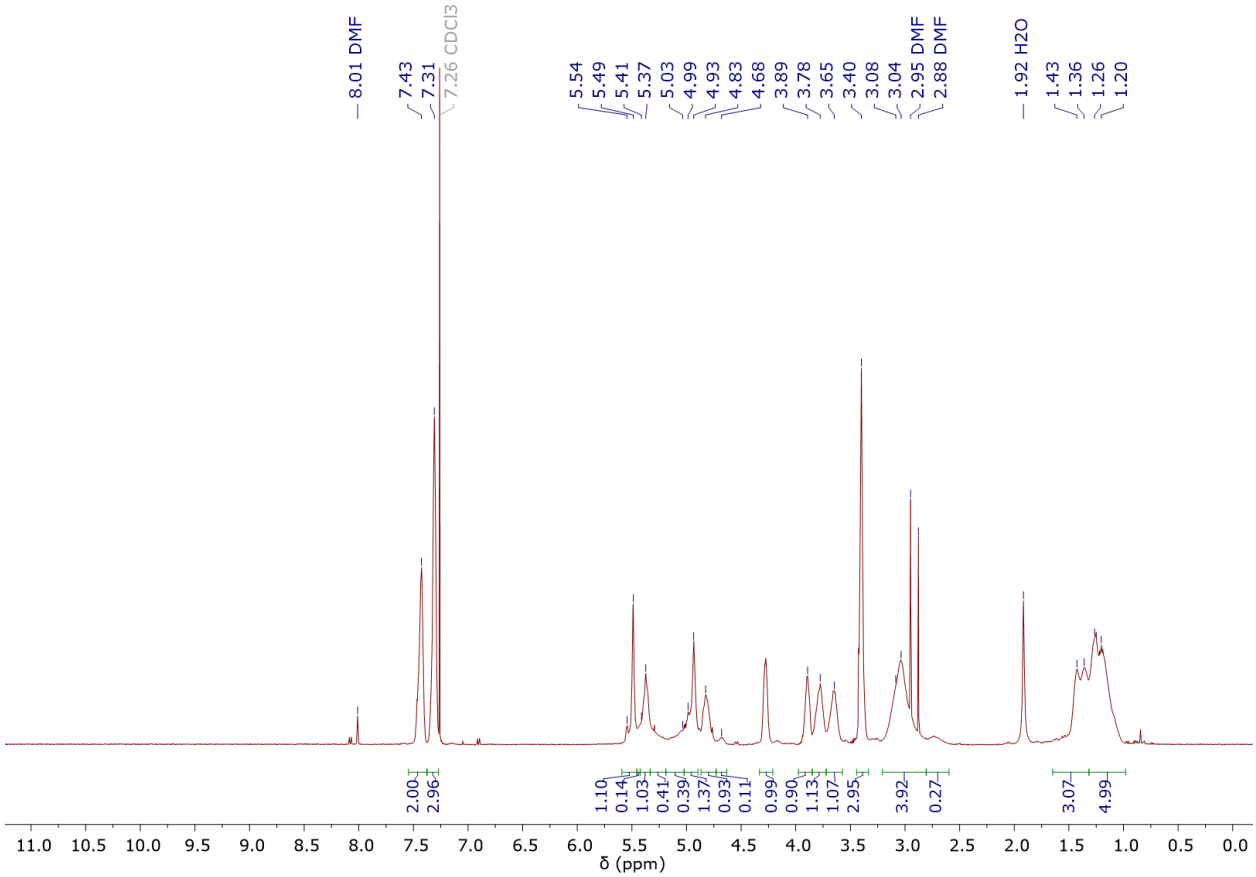

Figure A-77. ^{1}H (500 MHz, $CDCl_3$) NMR spectrum of **8a**.

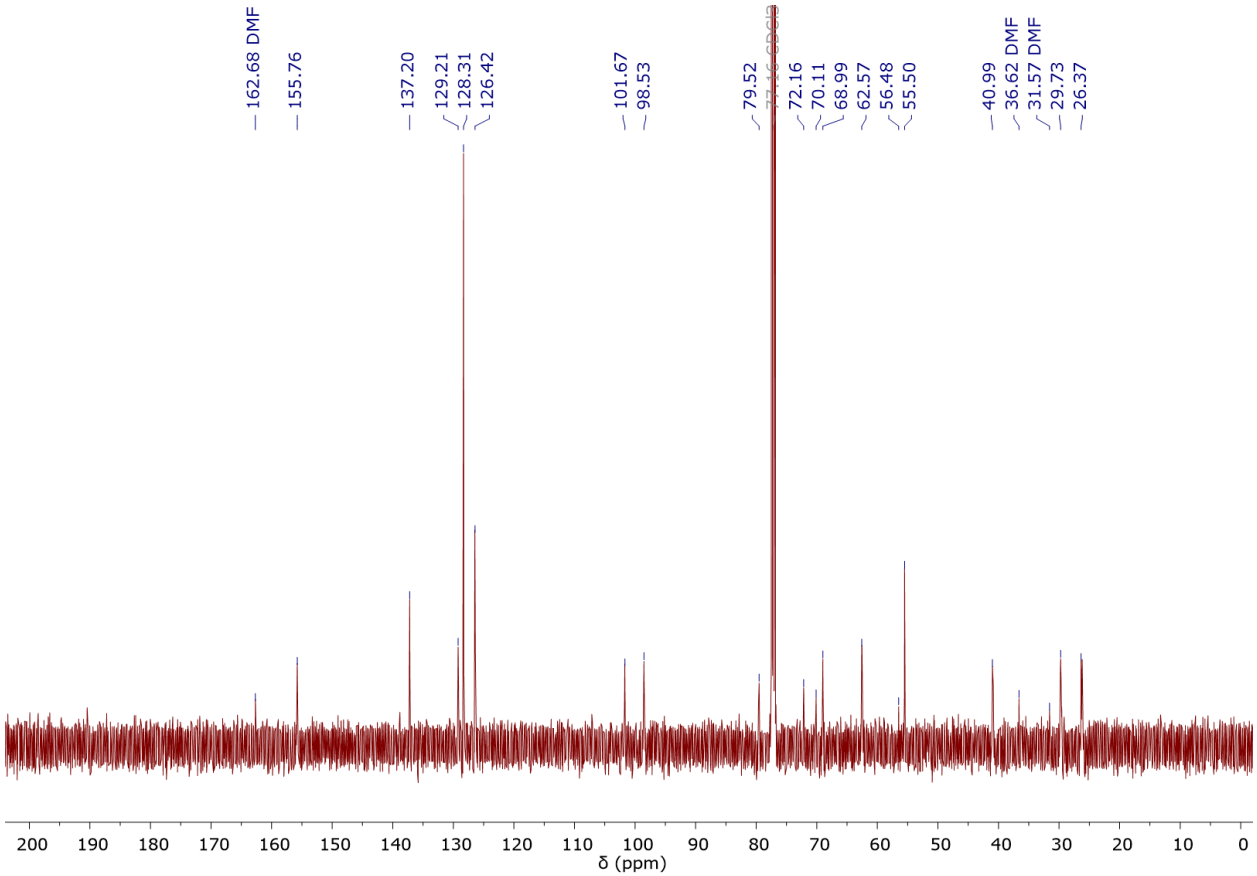

Figure A-78. ^{13}C (125 MHz, $CDCl_3$) NMR spectrum of **8a**.

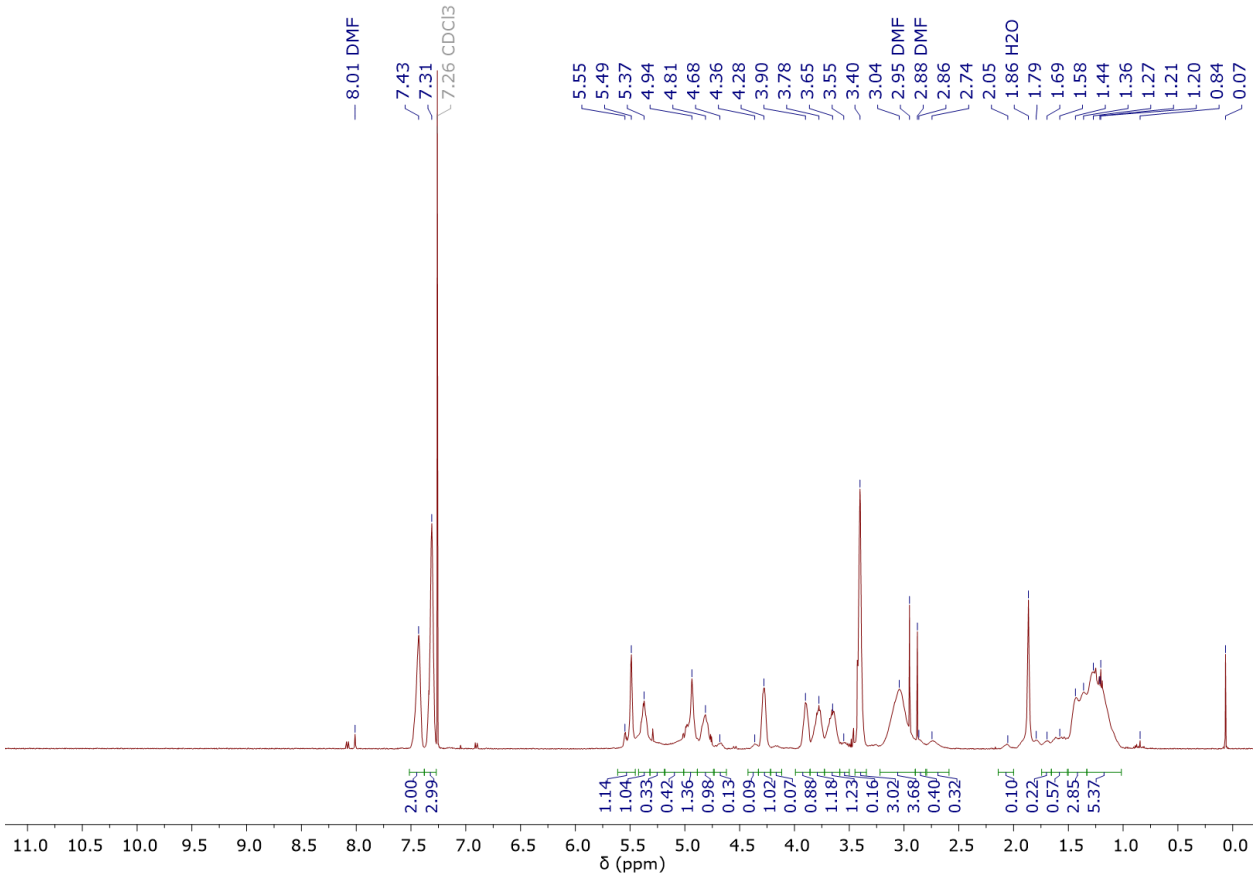

Figure A-79. ^{1}H (500 MHz, $CDCl_3$) NMR spectrum of **9b**.

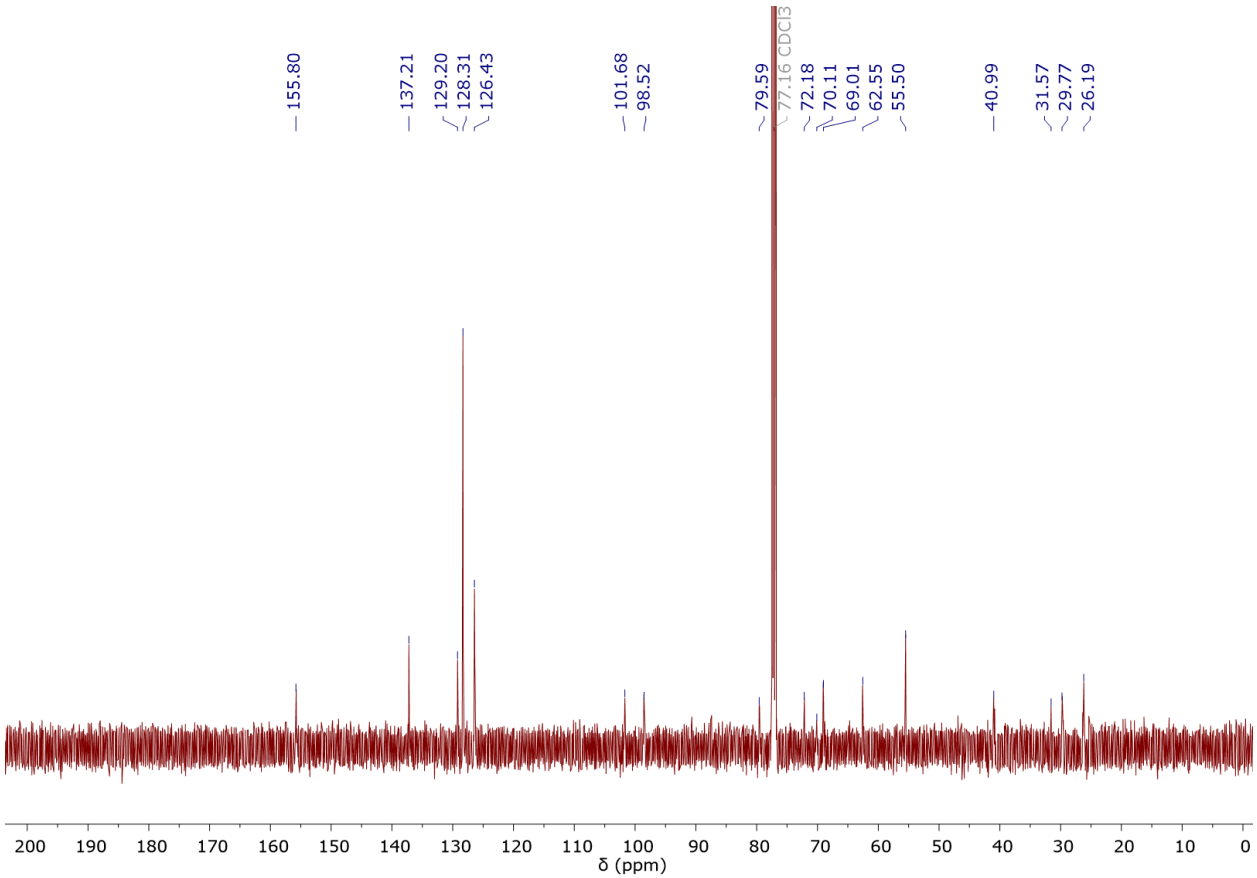

Figure A-80. ^{13}C (125 MHz, $CDCl_3$) NMR spectrum of **9b**, nt = 1152.

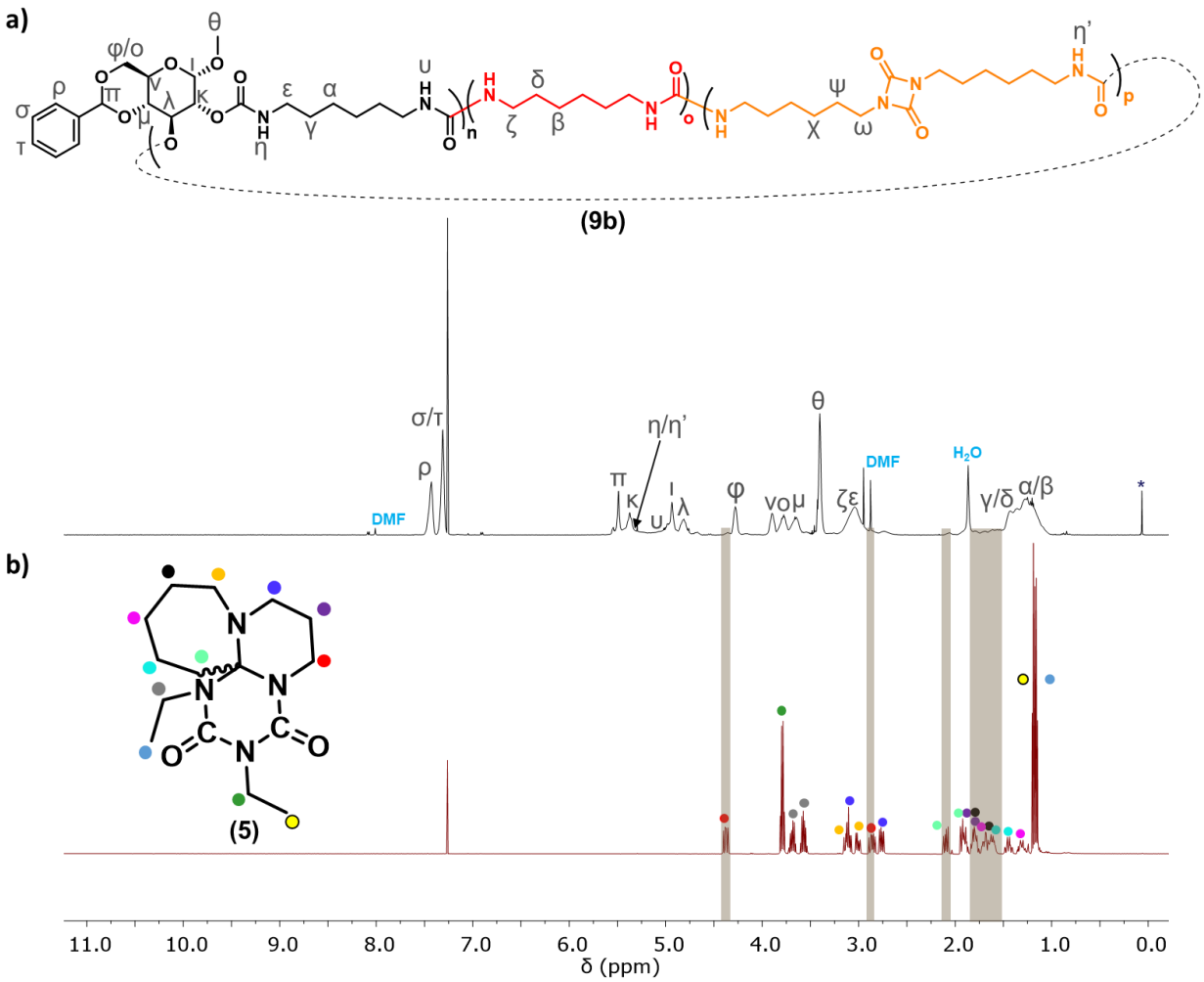

Figure A-81. ^{1}H (500 MHz, $CDCl_3$) NMR spectra of a) polymer **9b** (d1 = 10 s) and b) ethyl isocyanate cyclodimer **5** (d1 = 1 s) showing the correlation of certain peaks (highlighted) in the **9b** spectrum.

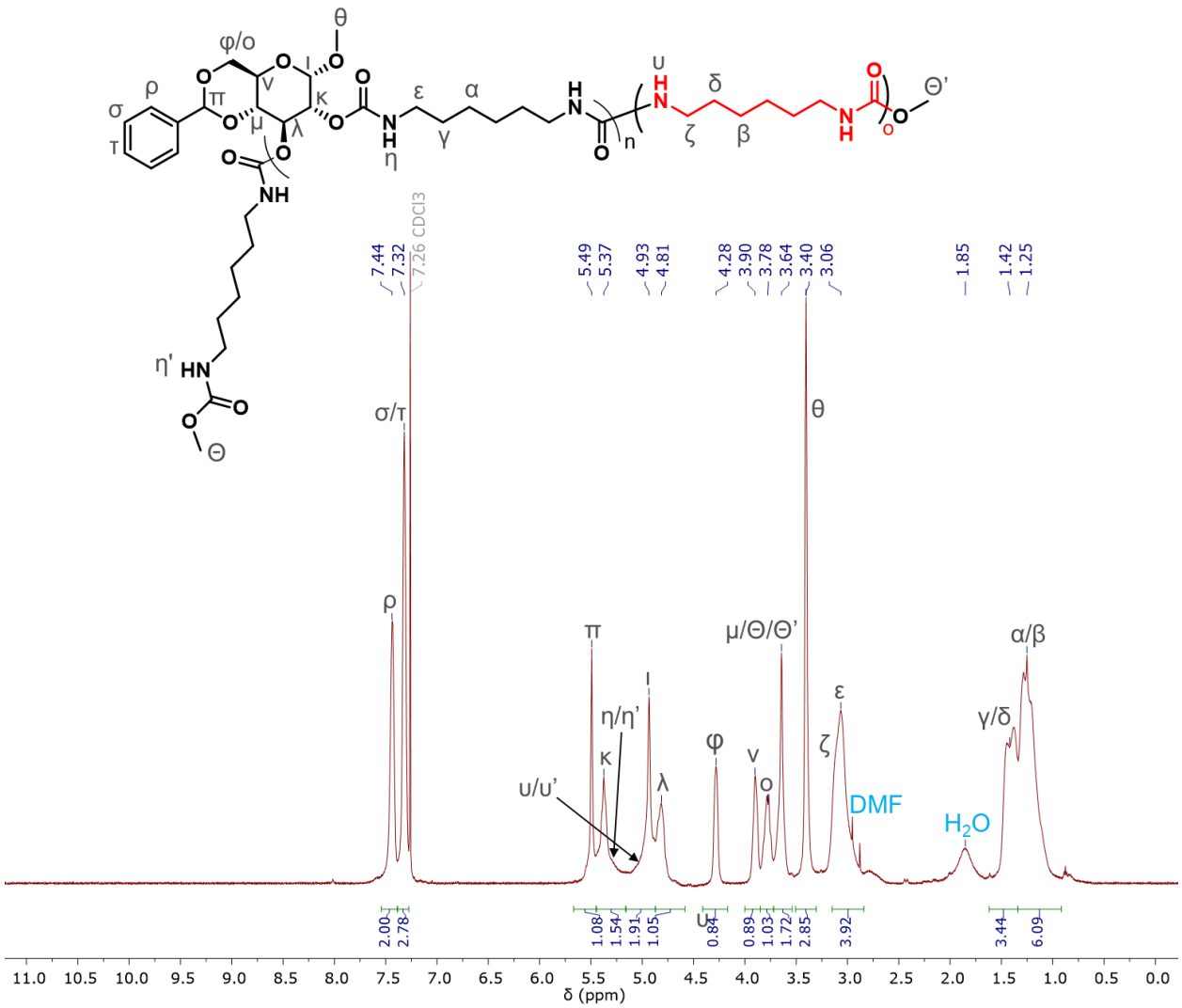

Figure A-82. ^{1}H (500 MHz, $CDCl_3$) NMR spectrum of **10-1a**.

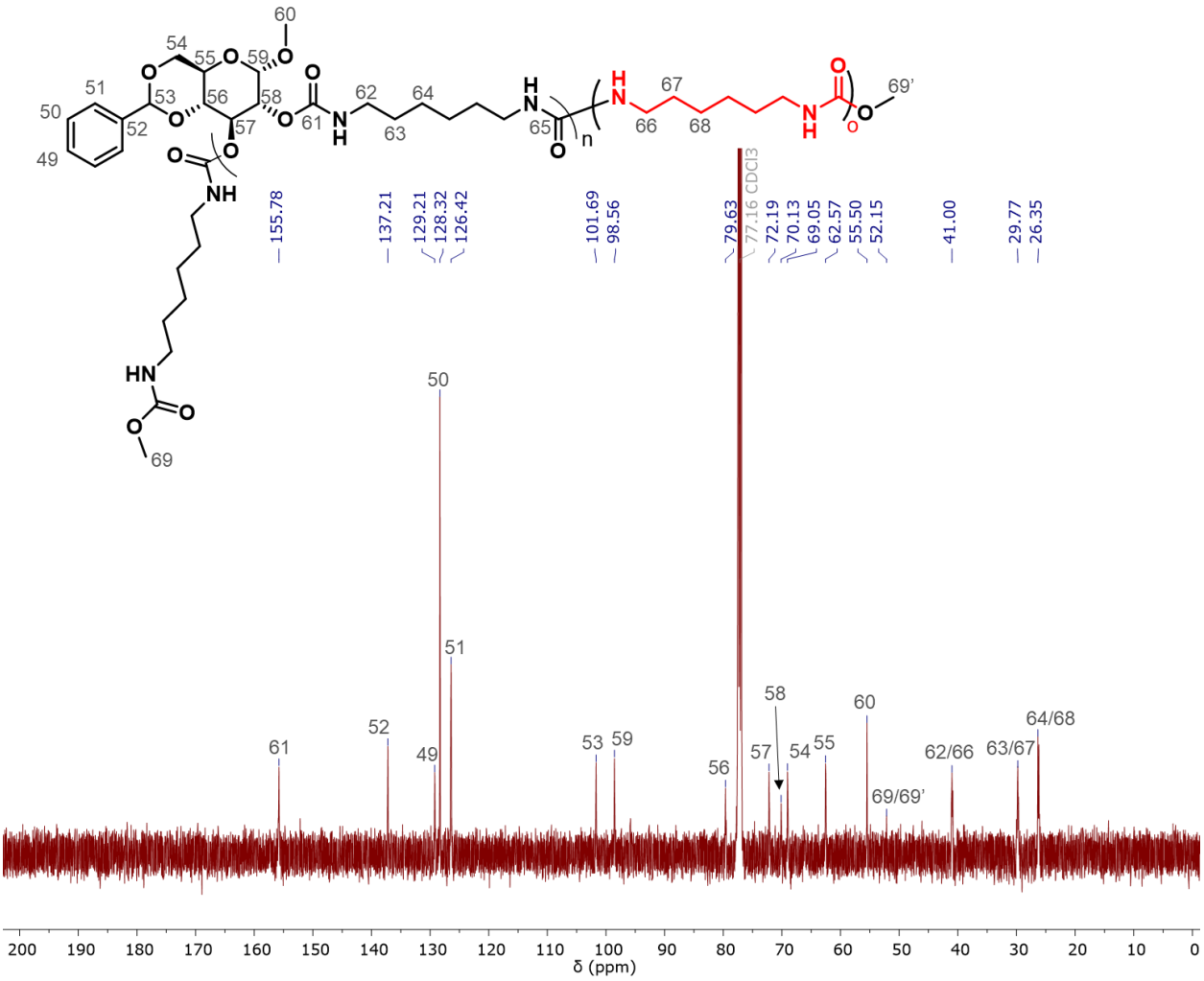

Figure A-83. ^{13}C (125 MHz, $CDCl_3$) NMR spectrum of **10-1a** with d1 = 3 s and nt = 2000.

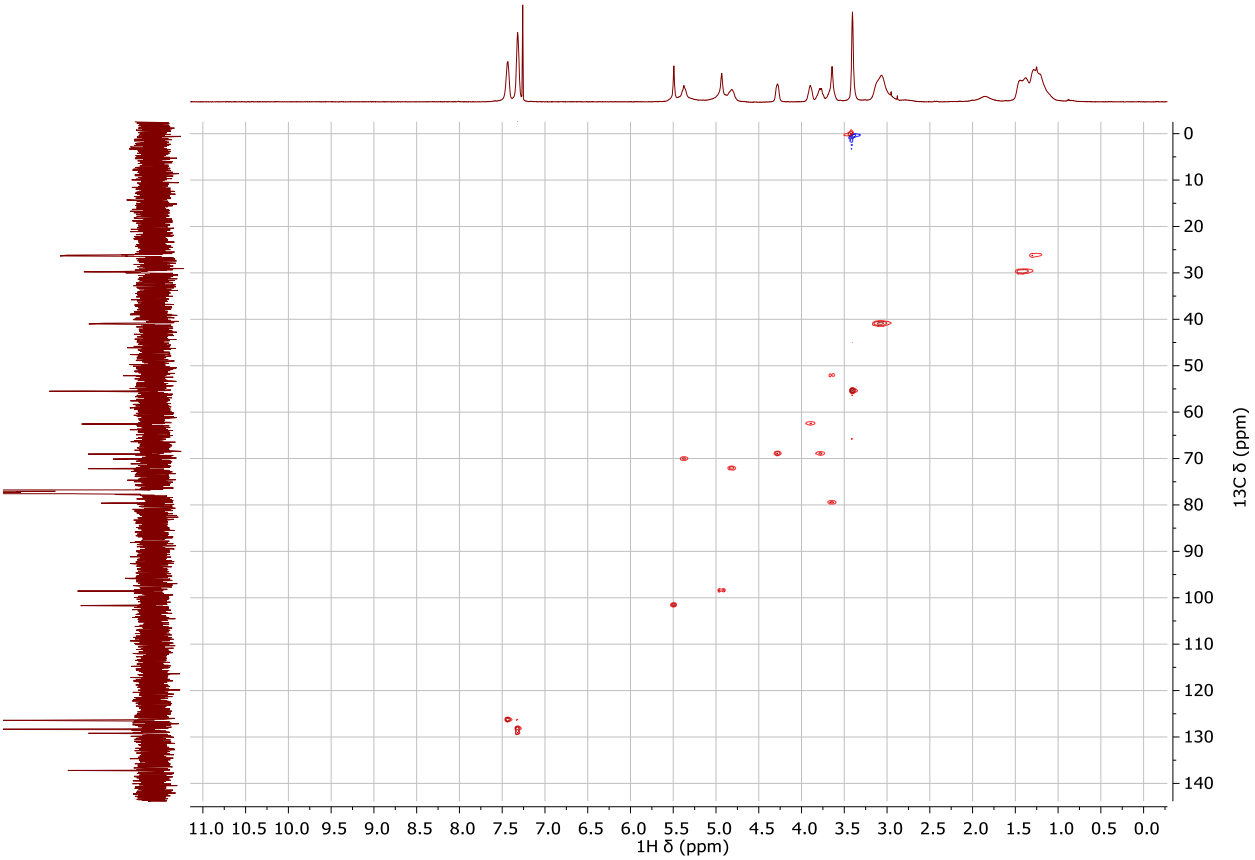

Figure A-84. ^{1}H-^{13}C HMQC (500 MHz-125 MHz, $CDCl_3$) spectrum of **10-1a** with nt = 32.

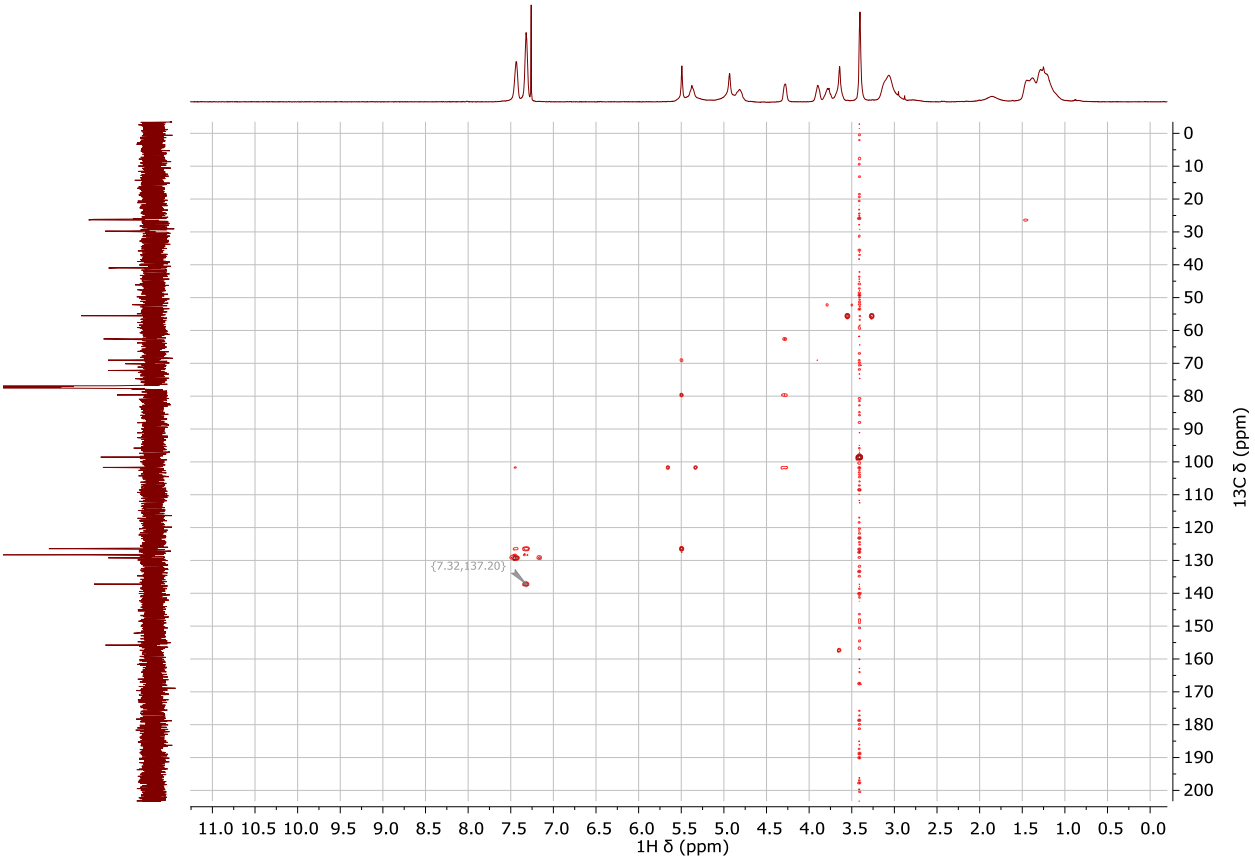

Figure A-85. ^{1}H-^{13}C HMBC (500 MHz-125 MHz, $CDCl_3$) spectrum of **10-1a** with nt = 56.

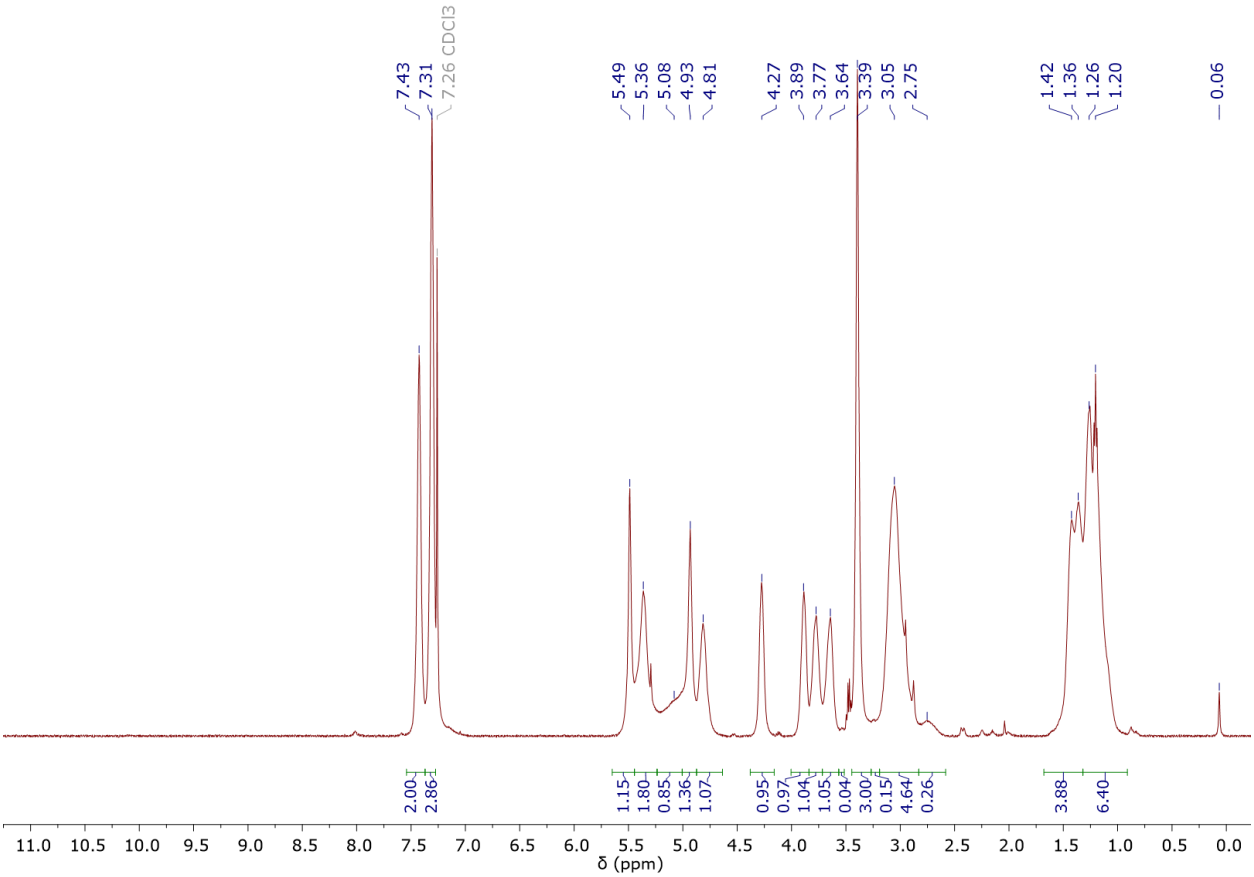

Figure A-86. ^{1}H (500 MHz, $CDCl_3$) NMR spectrum of **10-8**. 1H (500 MHz, $CDCl_3$) NMR spectrum of **10-8**.

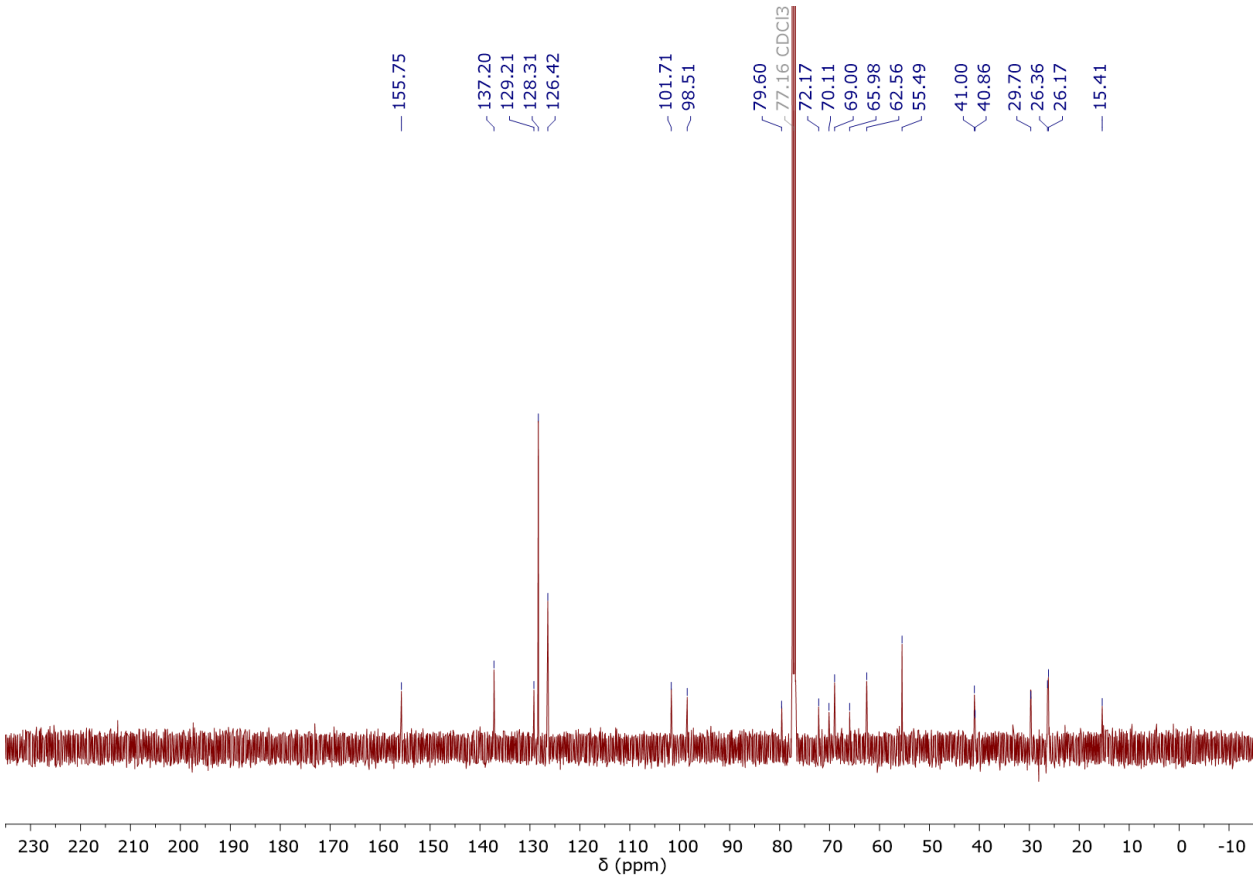

Figure A-87. ^{13}C (125 MHz, $CDCl_3$) NMR spectrum of **10-8**.

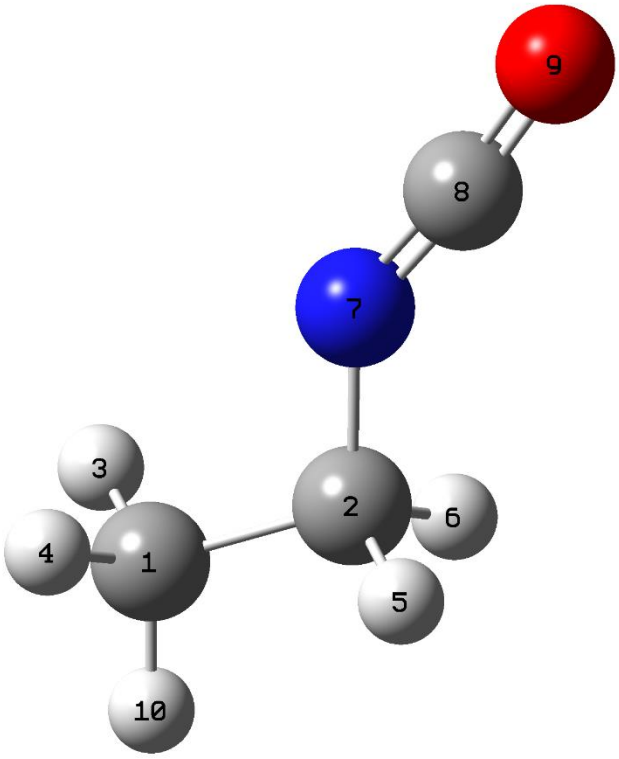

Figure A-88. Structures of ethyl isocyanate and the TMS reference optimized at the B3LYP level of theory with the 6-311++G(d,p) basis set using the SMD parameter with $CHCl_3$. Subsequently, NMR calculations were carried out using the GIAO method with the same solvation parameters.

Table A-9. Calculated ^{1}H-NMR Shifts in $CHCl_3$

Shift (ppm)	Degeneracy	Atoms
3.71	2	5,6
1.18	2	3,4
0.97	1	10

Table A-10. XYZ matrix for optimized ethyl isocyanate molecule

C	1.599116102300	0.113172065495	-0.242351107227
C	1.937485736968	-1.268884783786	0.295658747621
H	2.261306076341	0.385583651778	-1.068112433694
H	1.690696083918	0.871608249760	0.539296274689
H	1.262900932217	-1.537664305221	1.113074175108
H	1.831853382110	-2.022281408063	-0.489648052694
N	3.306724614292	-1.312157049335	0.794811484604
C	4.090001590440	-2.060097974127	1.298863502718
O	4.943816581987	-2.703033231051	1.796226133561
H	0.569558539425	0.122162404550	-0.610552084689

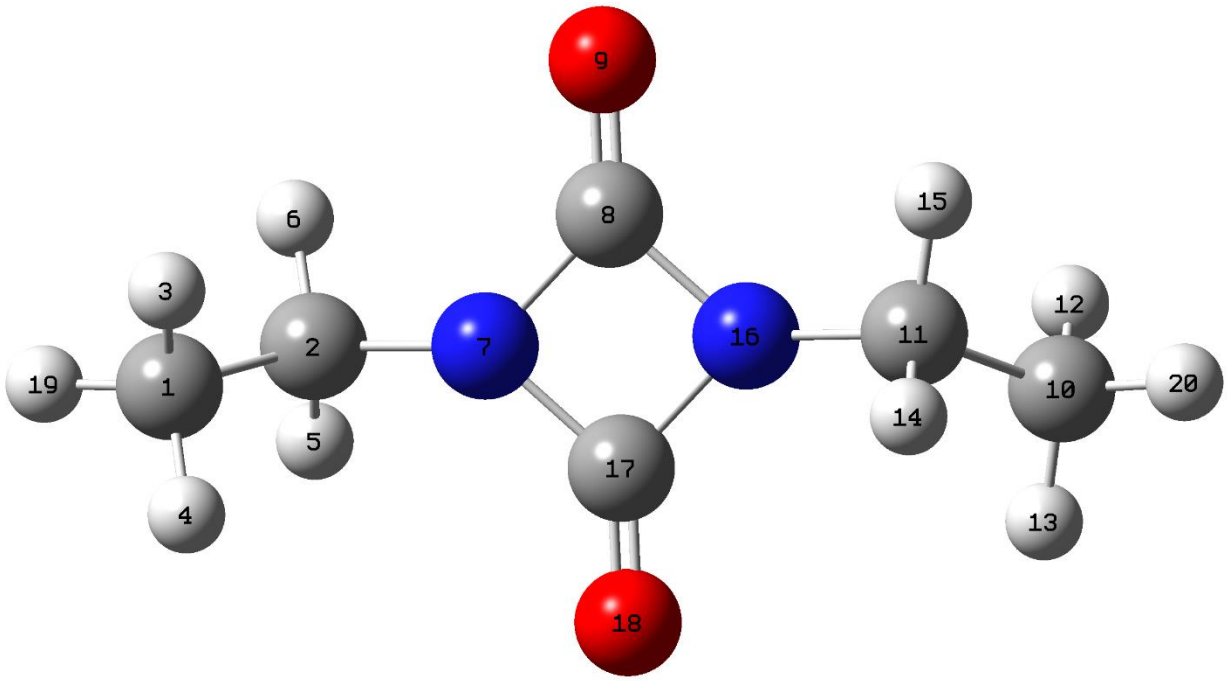

Figure A-89. Structures of ethyl uretdione and the TMS reference optimized at the B3LYP level of theory with the 6-311++G(d,p) basis set using the SMD parameter with $CHCl_3$. Subsequently, NMR calculations were carried out using the GIAO method with the same solvation parameters.

Table A-11. Calculated ^{1}H-NMR Shifts in $CHCl_3$

Shift (ppm)	Degeneracy	Atoms
3.26	4	15,6,5,14
1.39	1	13
1.23	1	4
1.08	4	3,12,20,19

Table A-12. XYZ matrix for optimized ethyl uretdione molecule

C	2.171150780624	-2.447195815118	3.755319484356
C	0.776640159605	-2.058537290226	3.274871374255
H	2.871469606934	-1.616408693384	3.636534956409
H	2.554825795125	-3.305911410831	3.198435257879
H	0.075035114696	-2.886282717700	3.410831535530
H	0.396134030270	-1.206951039857	3.844023106384
N	0.751889538098	-1.673360417068	1.864603668947
C	0.448426222226	-0.455660275725	1.218919929152
O	0.516295623399	0.697819451838	1.535430208859
C	-1.244695145066	-1.033323685389	-2.081420135324
C	0.061342594942	-0.729366035585	-1.355536631937
H	-2.083852540801	-0.517609145434	-1.607559722828
H	-1.454674400453	-2.105720634797	-2.086937502888
H	0.904533010708	-1.221096898271	-1.850842280455
H	0.259597166467	0.344811013922	-1.356583112845
N	0.028895645312	-1.132435726119	0.050249193394
C	0.340756503935	-2.353184603780	0.695720394277
O	0.278619665871	-3.506722878593	0.378889893114
H	2.135935363962	-2.717533787910	4.814535598207
H	-1.175748485853	-0.696748739974	-3.119775454486

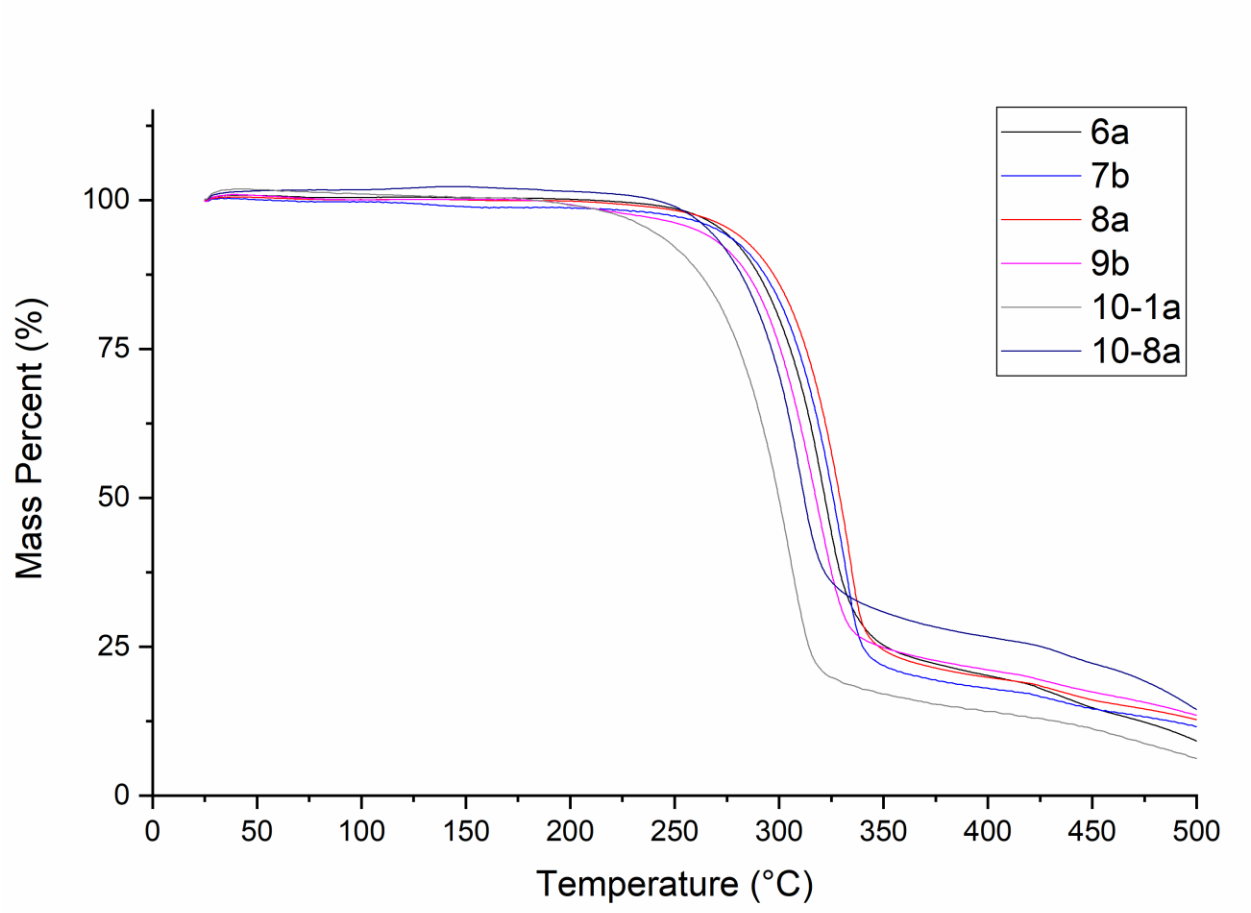

Figure A-90. TGA of polymers **6a**, **7b**, **8a**, **9b**, **10-1a**, and **10-1b**.

Table A-13. T_d values for PUs **6a**, **7b**, **8a**, **9b**, **10-1a**, and **10-8a**. There is an anomaly in the **9b** system where some mass was initially lost at 191 °C before the main thermal decomposition event at 289 °C

Polymer Index	T_d (°C)	Mass Loss at 375 °C (%)
6a	289–336	78
7a	289–335	84
8a	292–345	79
9b	289–335	77
10-1a	265–320	85
10-8a	266–324	72

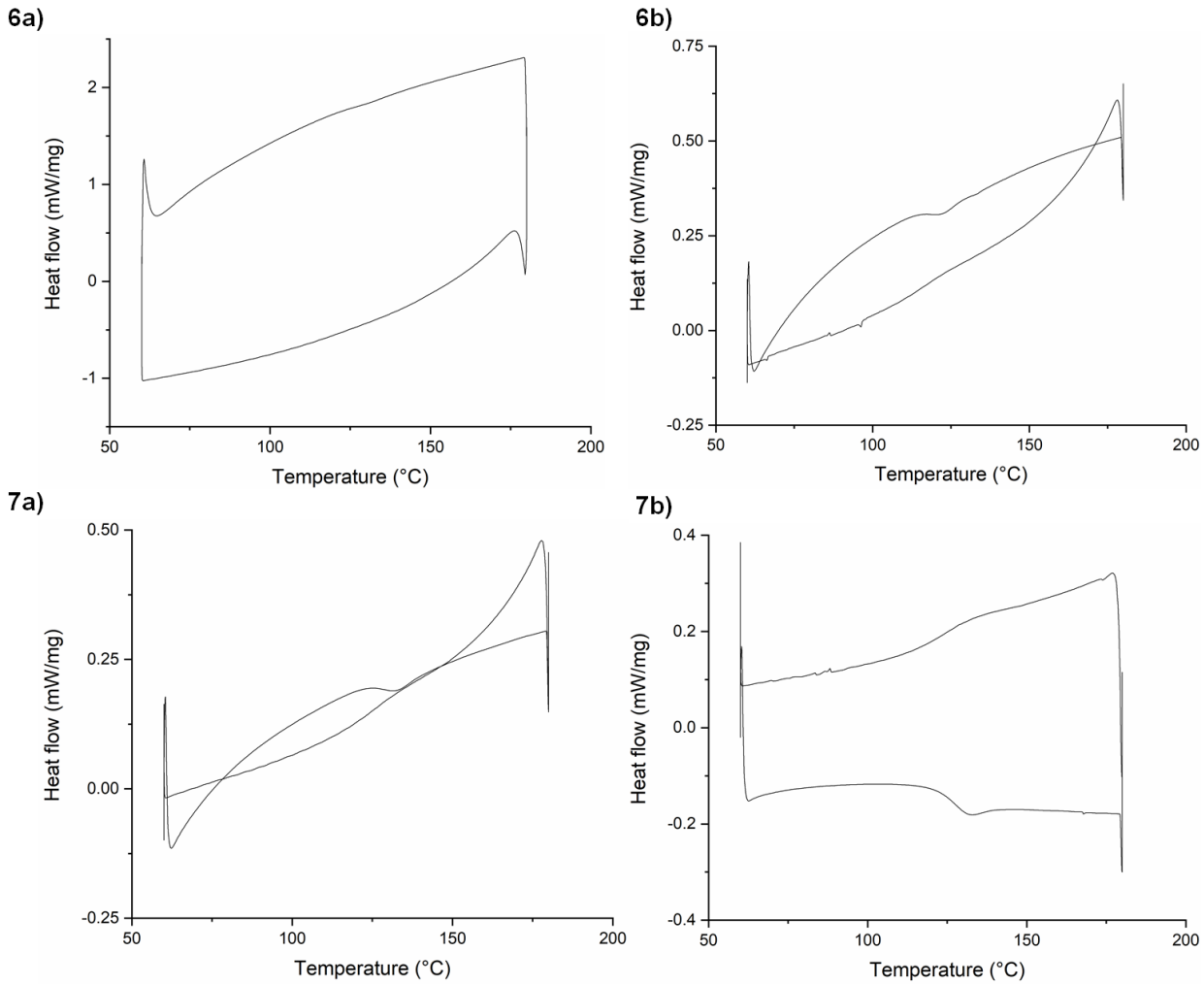

Figure A-91. DSC thermograms of polymers **6a**, **6b**, **7a**, and **7b** during the second heating and cooling cycle.

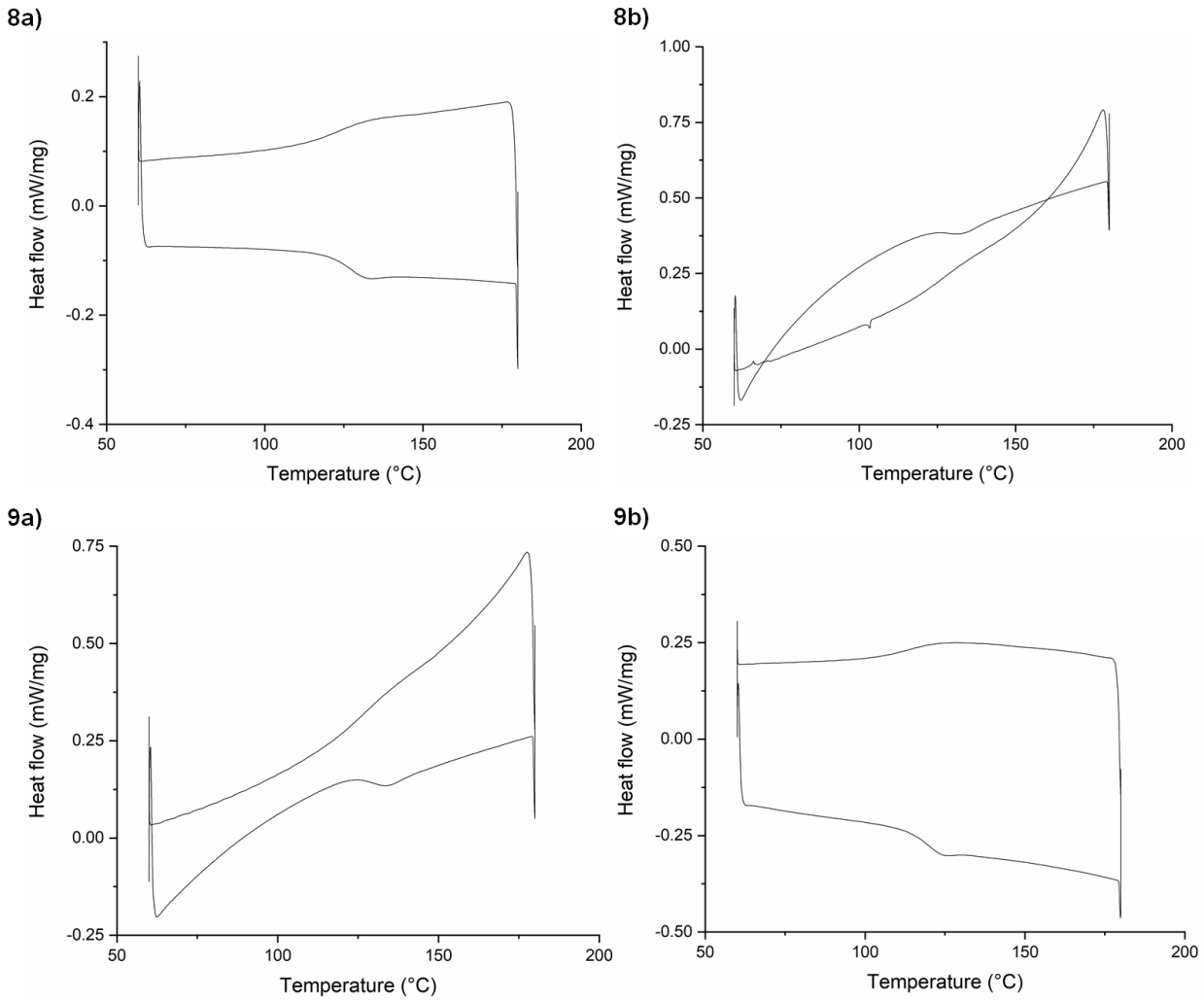

Figure A-92. DSC thermograms of polymers **8a**, **8b**, **9a**, and **9b** during the second heating and cooling cycle.

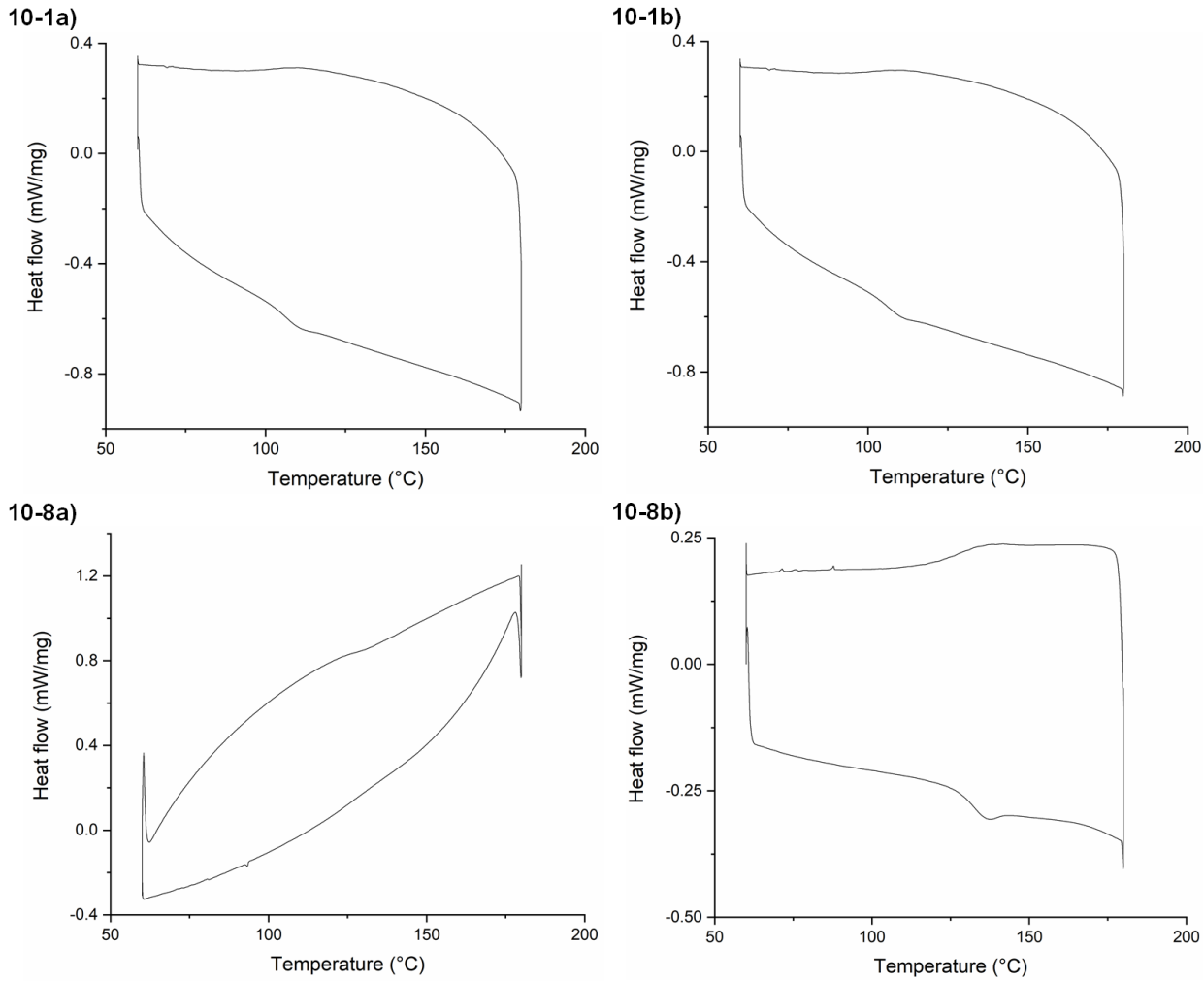

Figure A-93. DSC thermogram of polymers **10-1a**, **10-1b**, **10-8a**, and **10-8b** on the second heating and cooling cycle.

Table A-14. T_g values for polymers **6** to **10**. Values were determined as the midpoint of the tangent line of the inflection of the second heating cycle.

Polymer Index	T_g (°C)
6a	127
6b	118
7a	129
7b	126
8a	125
8c	128
9a	129
9b	118
10-1a	106
10-1b	107
10-8a	126
10-8b	131

Molecular Modeling TMS References

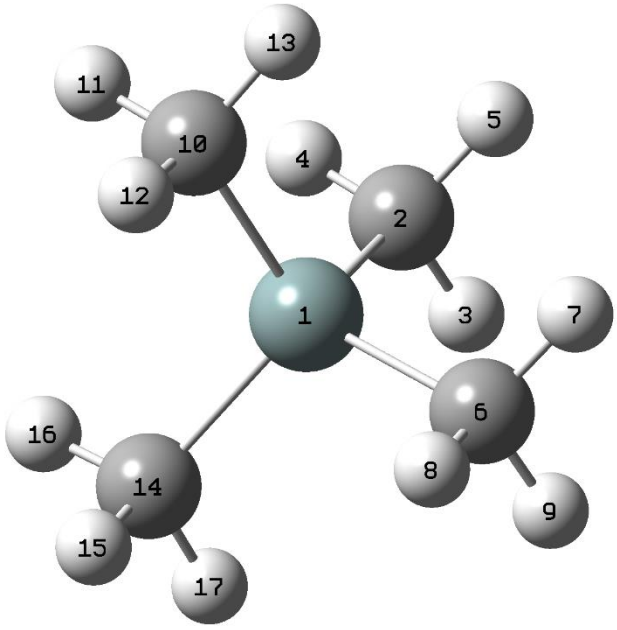

Figure A-94. Computationally optimized structure of TMS using the B3LYP level of theory with the 6-311++G(d,p) basis set using the SMD parameter with DMSO. Subsequently, NMR calculations were carried out using the GIAO method. The values for hydrogen and carbon were averaged to 31.89 ppm and 185.37 ppm, respectively, when used as references for other calculations.

Table A-15. Calculated NMR Shifts for Both Nuclei in DMSO

Nuclei	Shift (ppm)	Degeneracy	Atom Index
^{1}H	31.89	12	16,8,15,11,4,9,12,17,3,13,5,7
^{13}C	185.30	1	2
^{13}C	185.41	3	6,14,10

Table A-16. XYZ Matrix for Optimized TMS Structure in DMSO

Si	1.058097137211	-0.836918020053	-0.001905458176
C	-0.830625394066	-0.834535175574	0.002080075771
H	-1.225265833376	0.187741650196	-0.010635842441
H	-1.234760247195	-1.357014404653	-0.871873194983
H	-1.224909456906	-1.331220508742	0.895605113910
C	1.682380628055	0.053337903347	1.542650436719
H	1.333755800849	-0.446034701763	2.453738860883
H	2.777391610764	0.077234815113	1.577369991423
H	1.327424799824	1.089421711985	1.577442831724
C	1.682674450620	-2.619739530761	-0.003252289929
H	1.321366000933	-3.164279546227	-0.882873092591
H	2.777472496779	-2.660477041273	-0.015161642909
H	1.340681263222	-3.162797542392	0.884731091984
C	1.687696274698	0.054613648828	-1.543100144433
H	2.782999689713	0.092402737239	-1.561274512272
H	1.360357500345	-0.448550039377	-2.459997139657
H	1.320525778862	1.086278384526	-1.583545008943

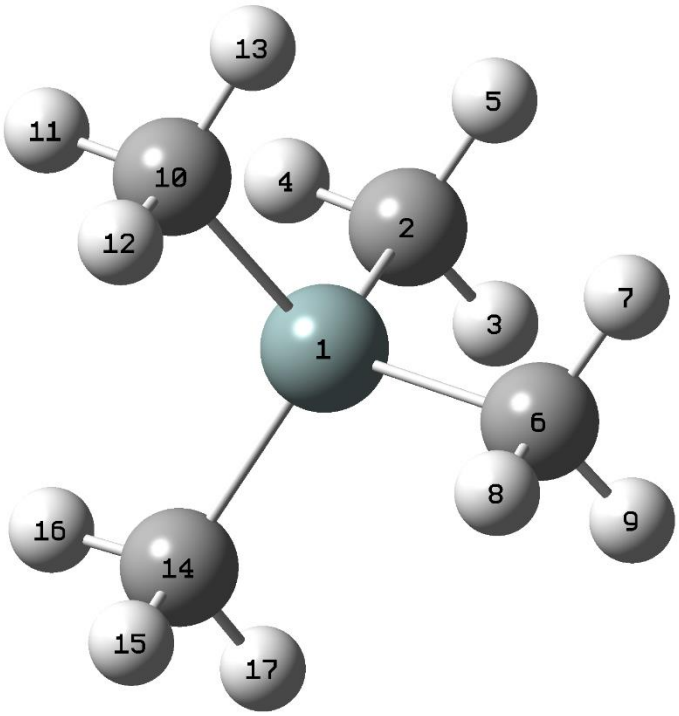

Figure A-95. Computationally Optimized Structure of TMS using the B3LYP level of theory with the 6-311++G(d,p) basis set using the SMD parameter with chloroform. Subsequently, NMR calculations were carried out using the GIAO method. The values of hydrogen and carbon were averaged to 31.91 ppm and 184.99 ppm respectively when used as references for other calculations.

Table A-17. Calculated NMR Shifts for Both Nuclei in $CHCl_3$

Nuclei	Shift (ppm)	Degeneracy	Atom Index
^{1}H	31.91	12	6,5,7,4,11,12,9,13,15,3,17,8
^{13}C	184.97	3	2,10,6
^{13}C	185.06	1	14

Table A-18. XYZ Matrix for Optimized TMS Structure in chloroform

Si	-0.001028588919	-0.000411868325	0.000257304562
C	0.795243612931	0.465749696892	-1.649326387889
H	1.417767109804	-0.348969040150	-2.035276011514
H	0.040523253755	0.692699196249	-2.410279673245
H	1.435027922102	1.349069275344	-1.545626995174
C	1.353208033502	-0.355575983160	1.269398847934
H	1.988801030211	0.522576608415	1.427899314657
H	0.929356085851	-0.635052364545	2.240227838382
H	2.000892857964	-1.176944102362	0.943935367766
C	-1.075246886202	1.431311779475	0.606307332252
H	-1.865871093944	1.667556196843	-0.114375735805
H	-1.558899219491	1.194153388170	1.560260360615
H	-0.481954516834	2.340247676270	0.754301981241
C	-1.070653011087	-1.540336444095	-0.228095510382
H	-1.530393561681	-1.851153633183	0.716646097810
H	-1.880195810003	-1.363898711166	-0.944960442357
H	-0.480078607959	-2.384943380673	-0.599745108853

APPENDIX B

RESOLUTION OF G_n AND C_n PEAKS

The X peaks in Figure 2-11 were verified to contain overlapping polymer populations by further examination with the more-precise reflectron mode of MALDI-TOF MS. This increase in precision is enabled by a longer flight path for the ionized species to the TOF detector but reduces the intensity of all peaks significantly and is less quantitative due to postsource decay.[148,223,224] Figure B-1 shows the expanded spectra of **6a** and **7a** acquired in reflectron mode, where the isotopic splitting pattern at high m/z matches that of the A_n, species except at high m/z where there is an expected loss in resolution.[223]

The X population in Figure 2-11 was assigned to include two overlapping species, C and G, that are resolved in reflectron mode, but appear as one peak in linear mode. The reflectron spectra in Figure B-2 show isotopic splitting patterns for bot h a linear, diol-terminated species (G) and a cyclic PU containing two urea linkages (C). The newly identified linear species, G_n, remains pronounced relative to C_n for polymer **7a**, even at high m/z. Without an internal standard, the amounts of either species can only be inferred relative to the other and Figure 2-11 does not necessarily imply that there are more G_n chains in **7a** than in **6a**. Because species G_n is slightly lower in mass than C_n, as shown in Tables 2-3 and 2-4, the broadened peak observed in linear mode appears biased to a slightly lower mass than expected. Thus X_n is labeled as $X_n = C_n + G_n$.

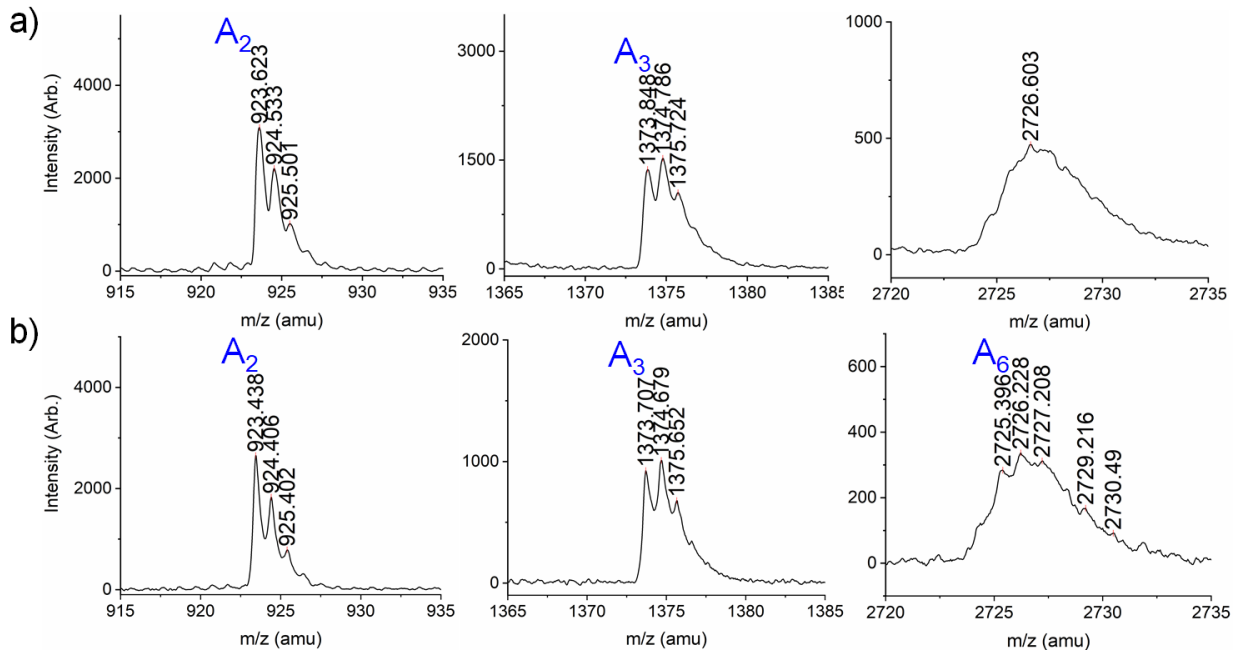

Figure B-1. MALDI-TOF MS spectra acquired in reflectron mode shows that species A_n has the expected isotopic splitting pattern for both a) **6a** and b) **7a**. Note that at high m/z, isotopic resolution is lost.

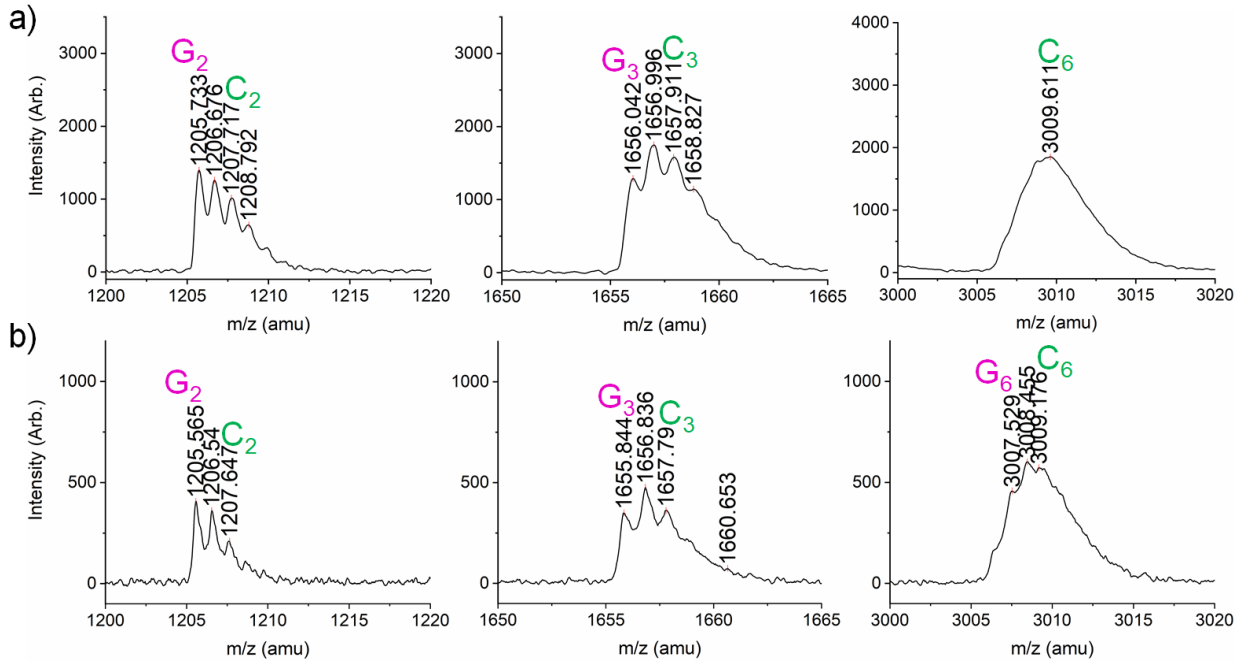

Figure B-2. MALDI-TOF spectra acquired in reflectron mode shows the presence of a linear species that is lower in mass but unresolvable with C in linear mode. This G species is less pronounced in a) **6a** where species C_n appears more favored, while b) in **7a**, G_n is relatively more pronounced.

APPENDIX C

DETERMINATION OF AGGREGATE FORMATION BY PULSED ION EXTRACTION DELAY ADJUSTMENT

The unusually high molar mass determined by SEC (see Table 2-2) and the observed error for peaks in the linear MALDI-TOF MS spectra for PUs **10-8a** and **10-8b** (see Figures A-53 and S55) were determined to be the result of aggregation by adjusting the PIE delay time. As shown in Figure C-1, the reflectron spectra of **10-8a** displayed a loss of isotopic information and the each of the broadened peaks appear centered at a higher m/z.

One possible explanation for this anomaly was the formation of doubly charged dimer aggregates that contain two Na^+ counterions. It has been reported that metastable aggregates can undergo postsource decay during acceleration leading to peak broadening and inaccurate m/z measurements.[223,224] By extending the PIE delay, more collisions during the initial MALDI "plume" can occur before the ionized species are accelerated into the TOF chamber, thereby suppressing aggregate formation.[223,224] Therefore, we hypothesized that isotopic information should be mostly restored by extending the PIE delay time if aggregation was indeed causing this anomaly.

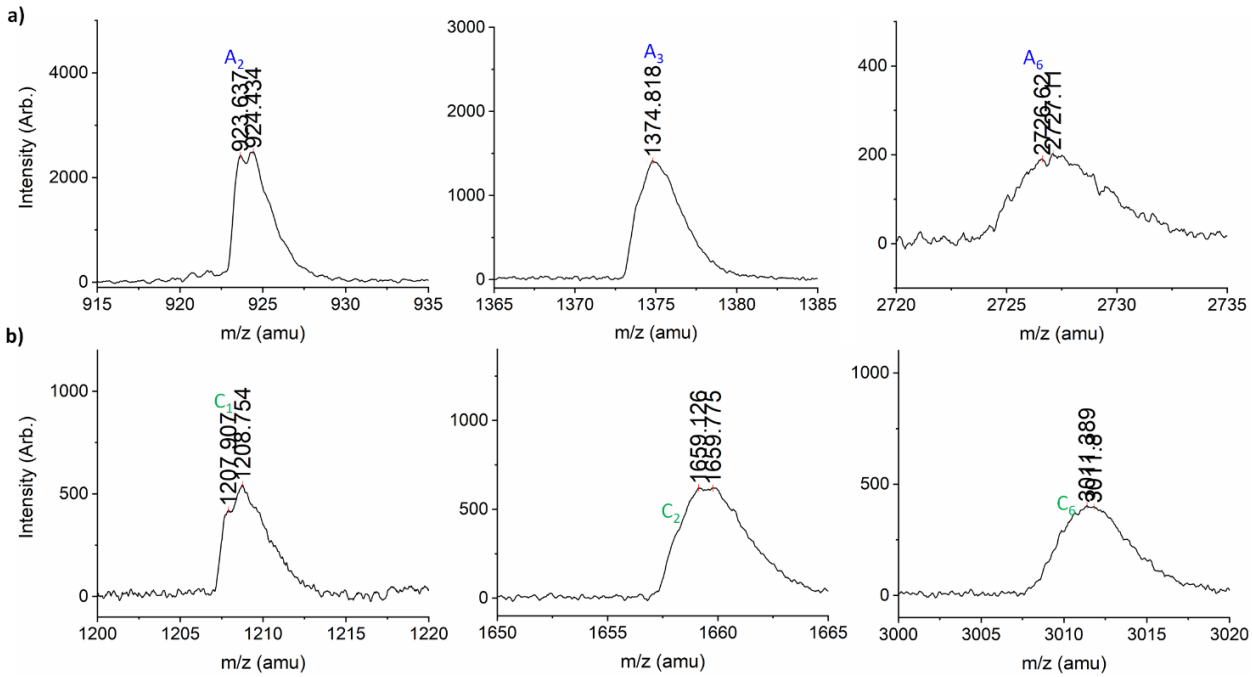

Figure C-1. Reflectron MALDI-TOF MS of PU **10-8a** expanded and centered on a) the A_n and b) the C_n peaks. Note that the absence of G_n species from the dicarbamate systems.

As shown in Figure C-2, extending the PIE delay time from 110 ns to 300 ns did indeed restore isotopic resolution, confirming that aggregate formation was occurring under the default MALDI-TOF MS conditions for PUs **10-8**. If the effect observed in Figure C-1 was merely caused by macrocycles being twice as large with two counterions, then extending the PIE delay time would result in a shift of all peaks to an m/z corresponding to the cycle that is twice as large, as more collisions would annihilate the extra counterion. This result is not observed in Figure C-3 (compare with Figure A-58) where the PIE delay time in linear mode was increased from 220 ns to 300 ns and can be ruled out.

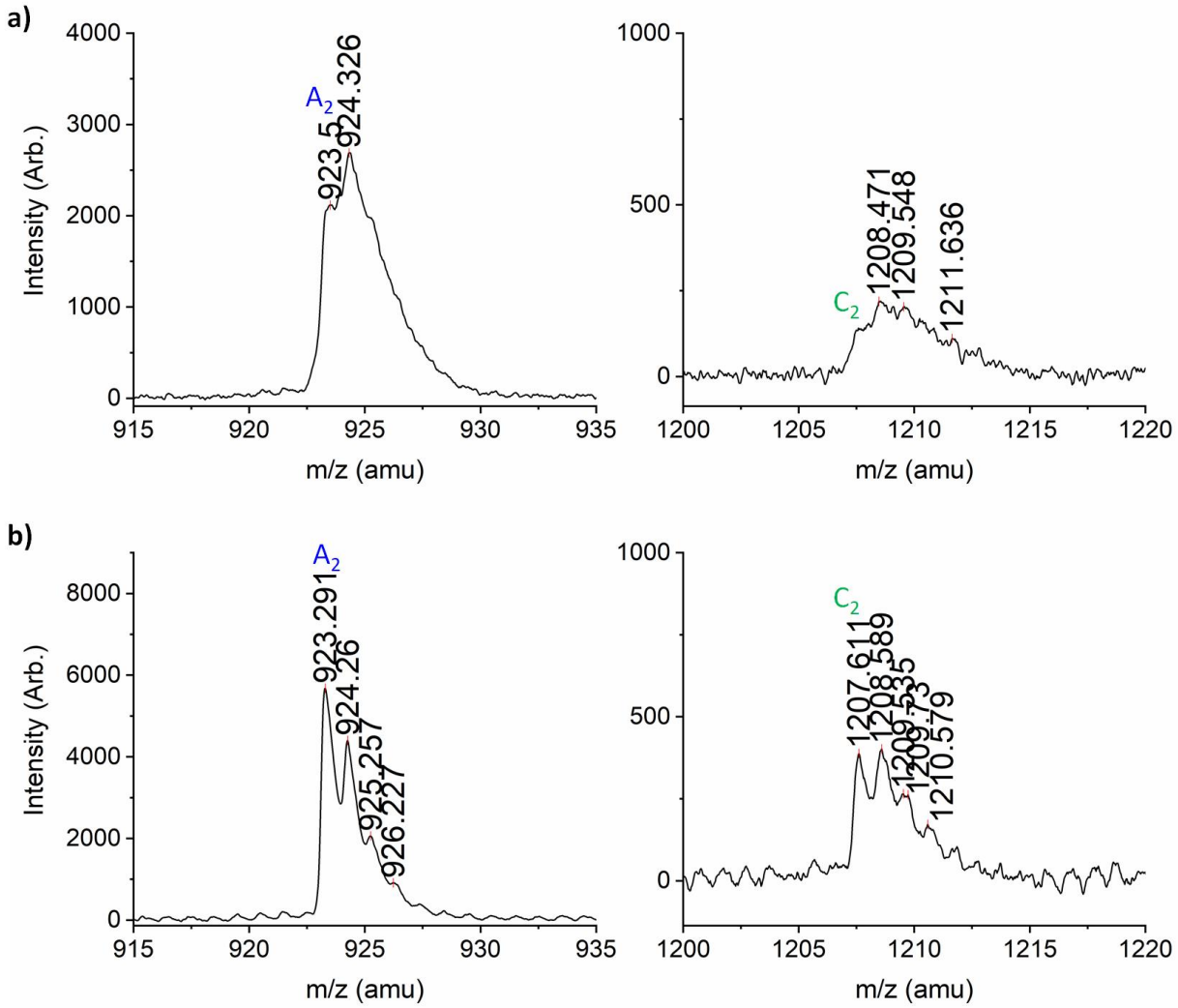

Figure C-2. MALDI-TOF spectra of the A_2 and C_2 peaks acquired in reflectron mode of PU **10-8b** where a) the PIE delay time was set at the default 110 ns and b) the PIE was extended to 300 ns, showing a significantly reduced aggregation error and a restoration of isotopic information.

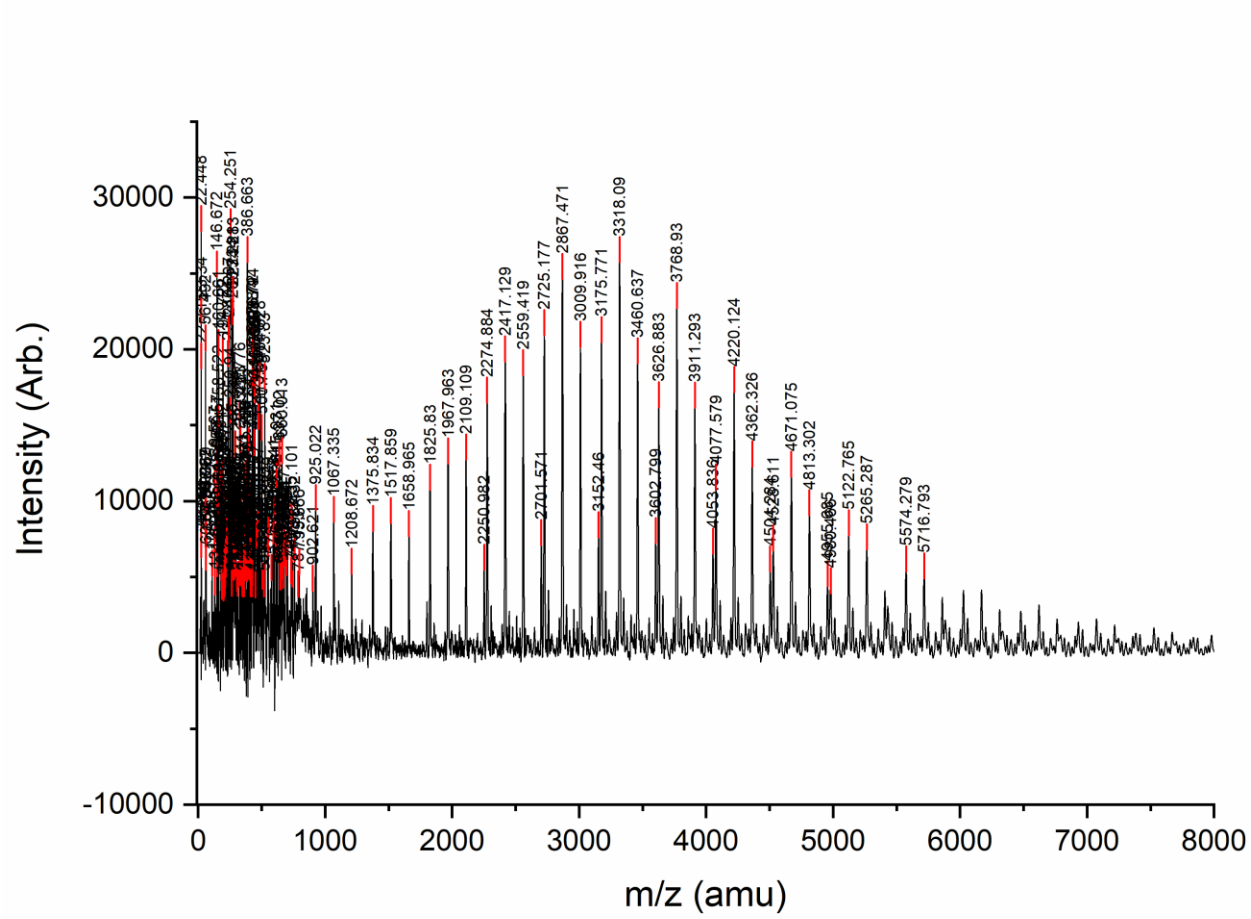

Figure C-3. MALDI-TOF MS linear spectrum of PU **10-8b** run with PIE delay set for 300 ns (default is 220 ns for linear mode) shows that no shift of the average molar mass to a higher m/z occurred. indicating that no single polymer chain was doubly charged.

Aggregation was observed in the linear and reflectron spectra of both of the **10-8** PUs, but was never observed in any of the dicarbamate-derived systems. This phenomenon, in reflectron mode, was also observed in Figure C-3 for **10-1b** but not **10-1a**, but no significant deviation from the expected average masses for either system was observed in linear mode (see Figures A-49 and A-51). Thus, aggregation apparently occurred to a lesser extent in the **10-1** systems. Two possible contributions for the observation of this phenomenon in PUs **10-8** are as follows: 1) a more-homogeneous polymer system with fewer by-products allows for more uniform packing and raises the probability of one species interacting with an identical species or

2) the $Mn(acac)_2$ catalyst present in this system could be inducing a self-assembly of these macrocycles into aggregates at high conversion, as the number of chains in the system are reduced relative to the amount of Mn^{2+}. Further investigation is needed to explore the cause of this phenomenon.

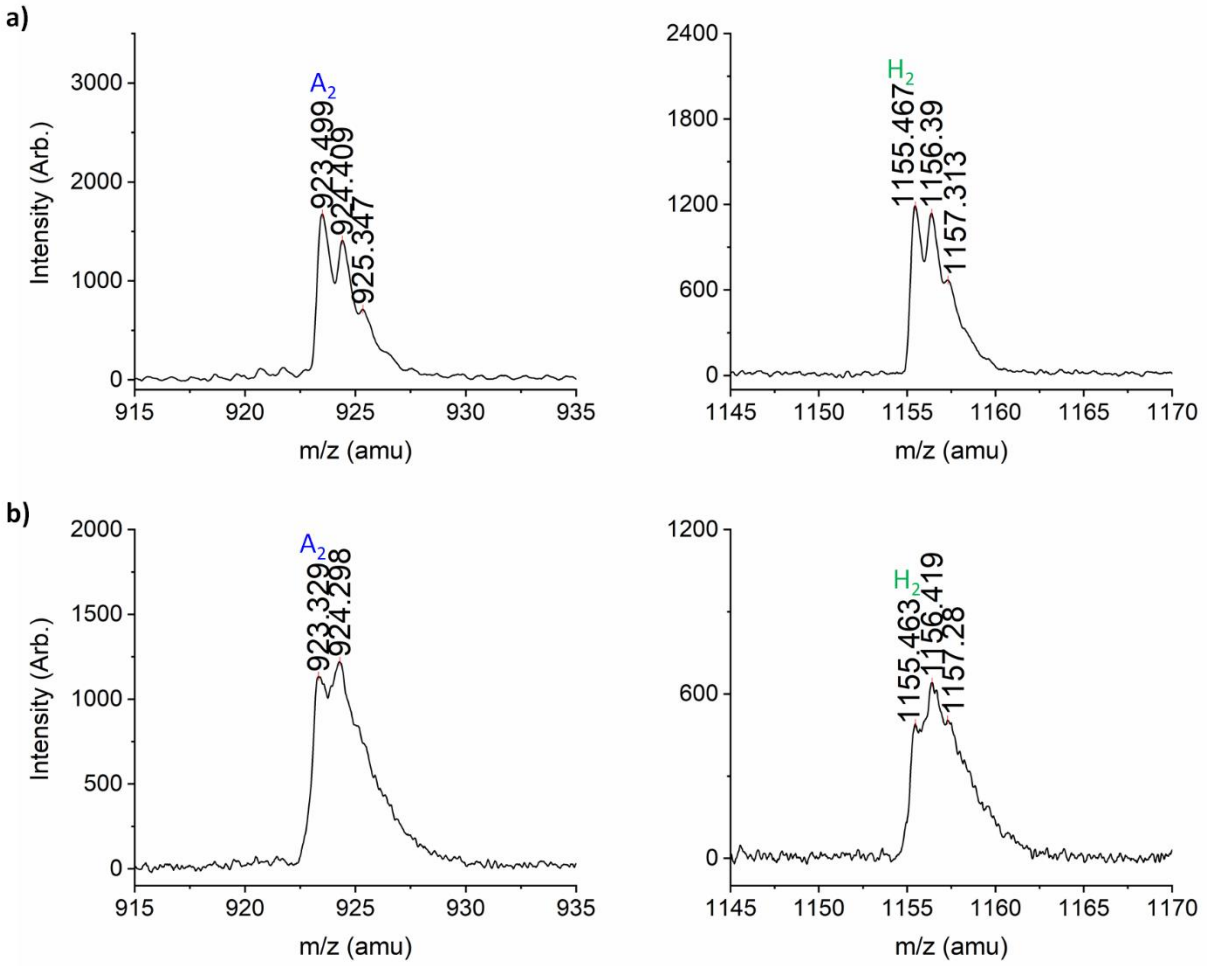

Figure C-4. MALDI-TOF MS reflectron spectra showing the A_2 and H_2 peaks of a) **10-1a** showing no sign of aggregation and b) **10-1b** showing some aggregation.

APPENDIX D

DISCREPANCY BETWEEN POLYURETHANES 8a AND 9b

In the duplicate reaction (**9a**) (see Figure A-46), the results are similar, aside from a few changes in relative intensity for sub-populations UB, UC, and $C\Delta^A$. Notably, not as many high-molar-mass species of $C\Delta^A$ are detectable. The rest of the populations appear nearly identical to that of **9b**. This result explains the discrepancy seen in both the SEC-derived molar mass distributions and ATR-FTIR results from Table 2-2 and Figure 2-14. It is possible that the amount of Δ-adduct seen in **9a** is simply too low for the ATR-FTIR to detect given that MALDI-TOF is able to detect picomoles of analyte.[149] Again, this discrepancy in composition is attributed to the inherent inhomogeneity and nonequilibrium conditions present with a rapid addition of DBU.

APPENDIX E

COMPARISON BETWEEN POLYURETHANES 8a AND 9b

Figure A-32 shows the comparison between polymers **8a** (DBU added at a rate of 5.6 µL/min) and **9b** (rapid DBU addition), where the former was expected to have an intermediate composition of Δ adducts between **7a** and **9b**. Indeed, the Δ adduct ($C\Delta^{A}_{n}$) population in **8a** is more pronounced than that of **7a**, but is not near as intense as that of **9b**. The UBn population, corresponding to a cyclic species with one uretdione, of **8a** also appears to be more intense than that of **7a** but not near as pronounced as that of **9b**. The UC_n population, corresponding to a cyclic species with a uretdione and one urea linkage, appears almost identical between **8a** and **9b**. The spectrum of the **8b** duplicate reaction appears almost identical to **8a** (see Figure A-44). The nearly identical spectra, and in turn nearly identical composition of functional groups, correlates to the very similar molar masses determined by SEC in Table 2-2.

APPENDIX F

MATRIX-ASSISTED LASER DESORPTION/IONIZATION – TIME-OF-FLIGHT IONIZATION OPTIMIZATION FOR POLYURETHANE 10-8

Recognizing the possibility that PU **10-8** could exhibit "mass bias" for lower-m/z species in MALDI-TOF MS, we optimized the matrix:analyte ratio.[225] It is generally accepted that higher-molar-mass analytes require a higher matrix:analyte ratio to "lift" them into the gas phase and that increasing the matrix:analyte ratio can minimize mass bias in a MALDI-TOF spectrum.[226,227] The matrix:analyte ratio used for all samples throughout this work was 25:1 (mg:mg) and had been previously determined from optimization of similar PUs as the ones discussed herein. Thus, we decided to verify that this ratio is indeed optimal for **10-8** by screening ratios of 25:1 and 50:1. Figure F-1 shows no change in the polymer distribution upon increasing the matrix:analyte ratio to 50:1. Moreover, the whole distribution in Figure 2-17 is Gaussian, which further indicates that there is no ionization error due to mass bias. We therefore concluded that the matrix:analyte ratio is optimal and that all species present are ionizing.

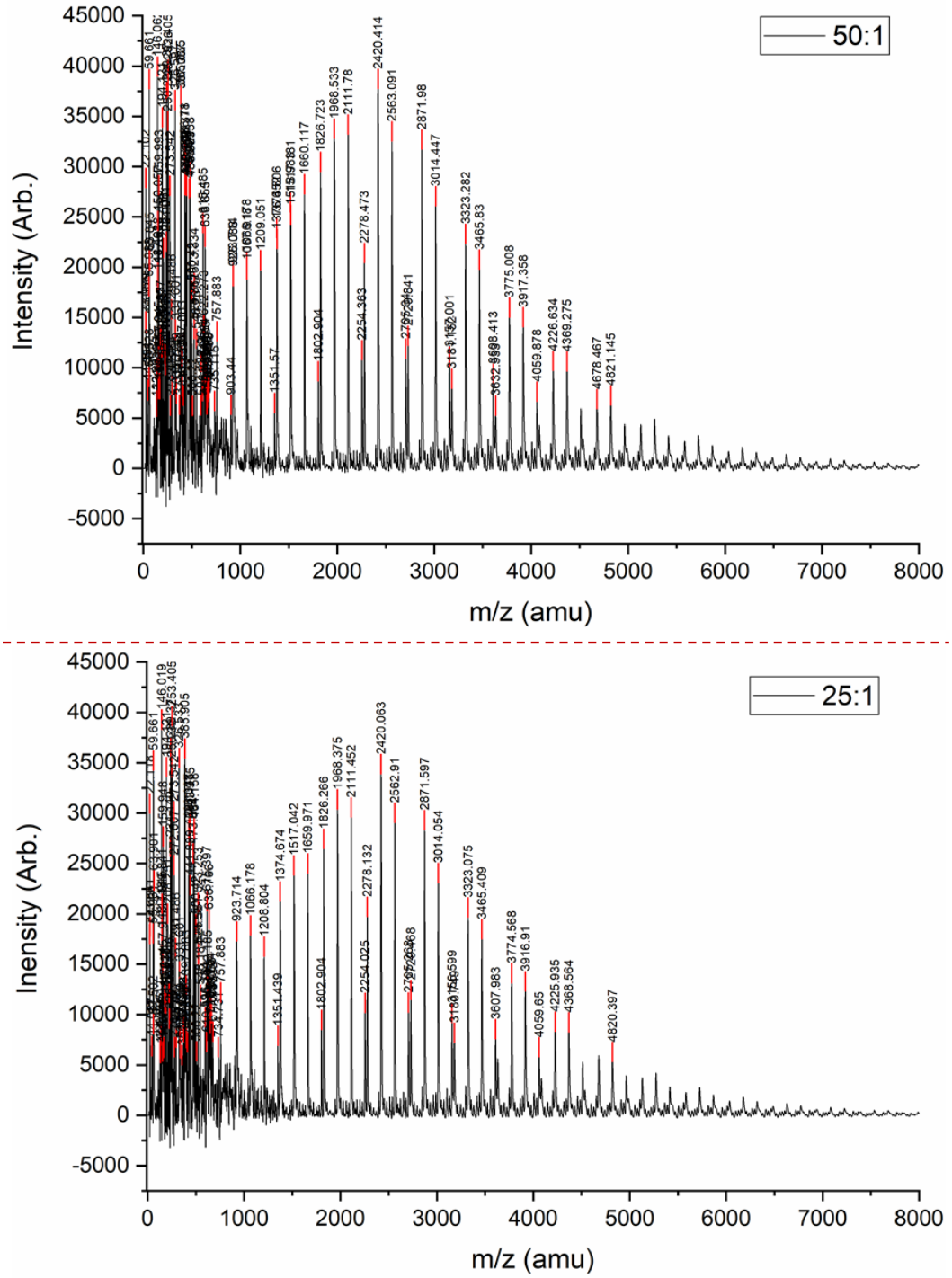

Figure F-1. Screening of matrix:analyte (mg:mg) ratio for MALDI-TOF MS of PU **10-8a** by showing no significant difference between the 25:1 condition, used on all samples, and the 50:1 condition.

APPENDIX G

PREDICTED FOURIER TRANSFORM INFRARED AND SUPPLEMENTAL MATRIX-ASSISTED LASER DESORPTION-IONIZATION – TIME-OF-FLIGHT MASS SPECTRA FOR CHAPTER 3

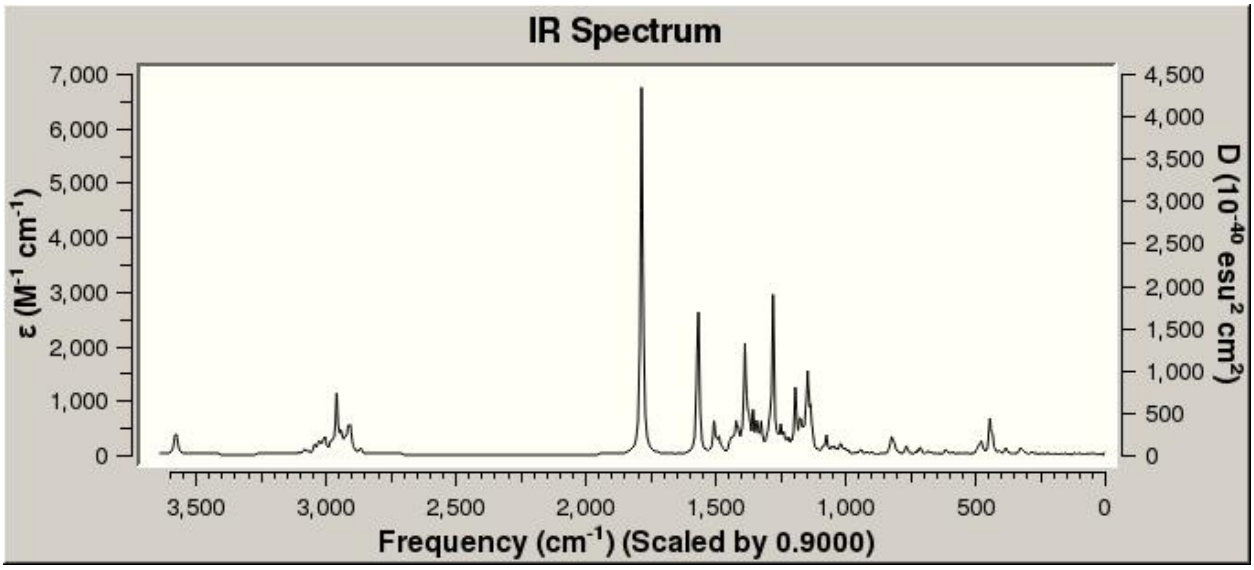

Figure G-1. The predicted FTIR spectrum for the H_1 species that was optimized by HF/6-311++G(d,p).

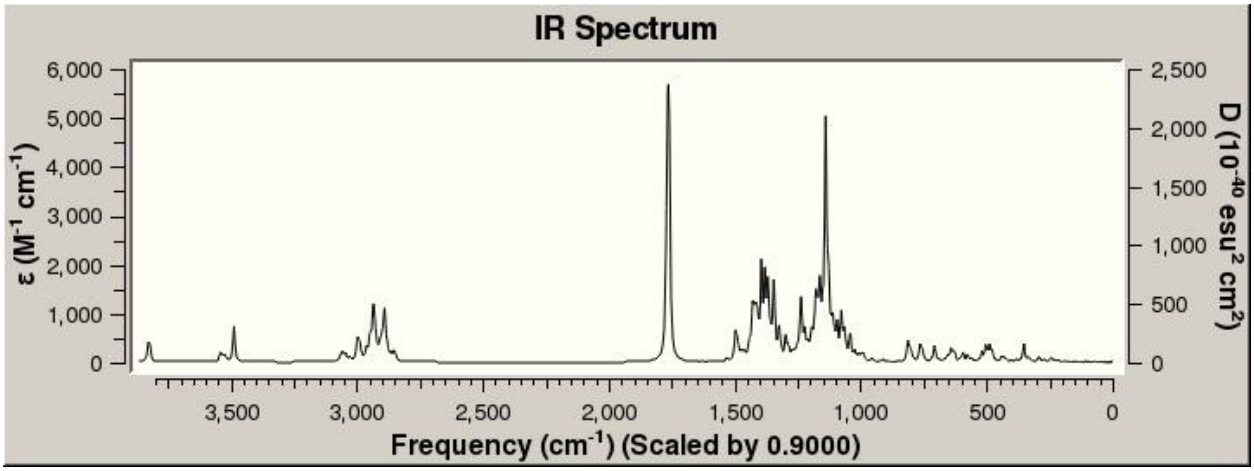

Figure G-2. The predicted FTIR spectrum for the G_2 species that was optimized by HF/6-311++G(d,p).

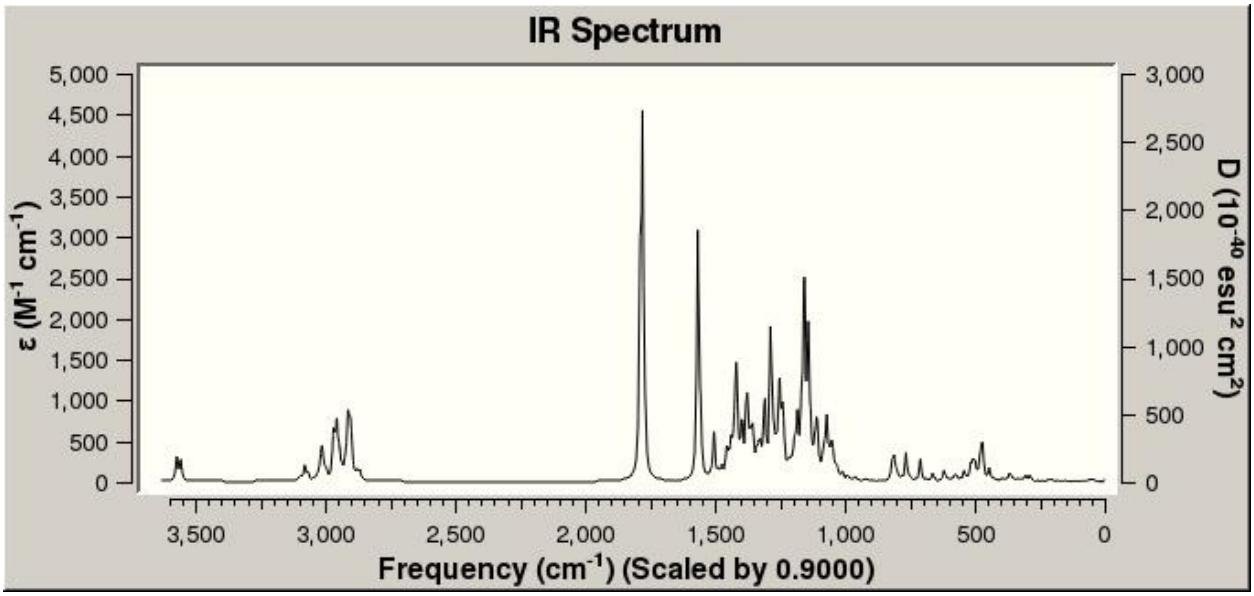

Figure G-3. The predicted FTIR spectrum for the A_2 species that was optimized by HF/6-311++G(d,p).

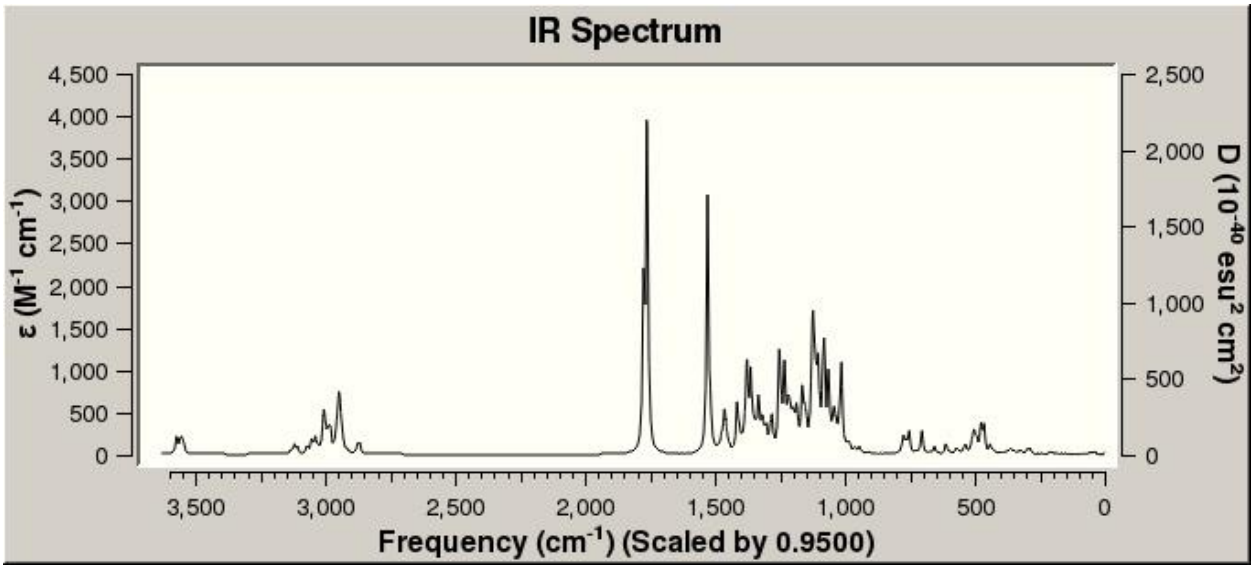

Figure G-4. The predicted FTIR spectrum for the A_2 species that was optimized by cam-B3LYP/6-311++G(d,p).

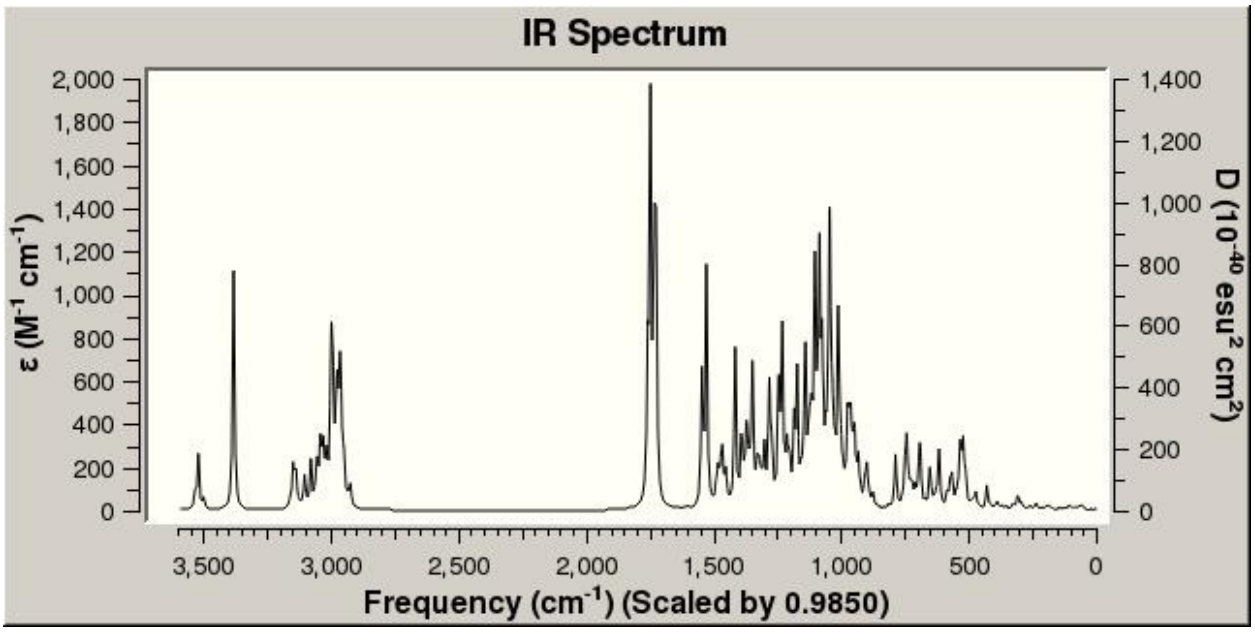

Figure G-5. The predicted FTIR spectrum for the A_2 conformer 102 that was first conformationally sampled in Materials Studio and then optimized by BP86/3-21G* incorporating the d3bj empirical dispersion correction.

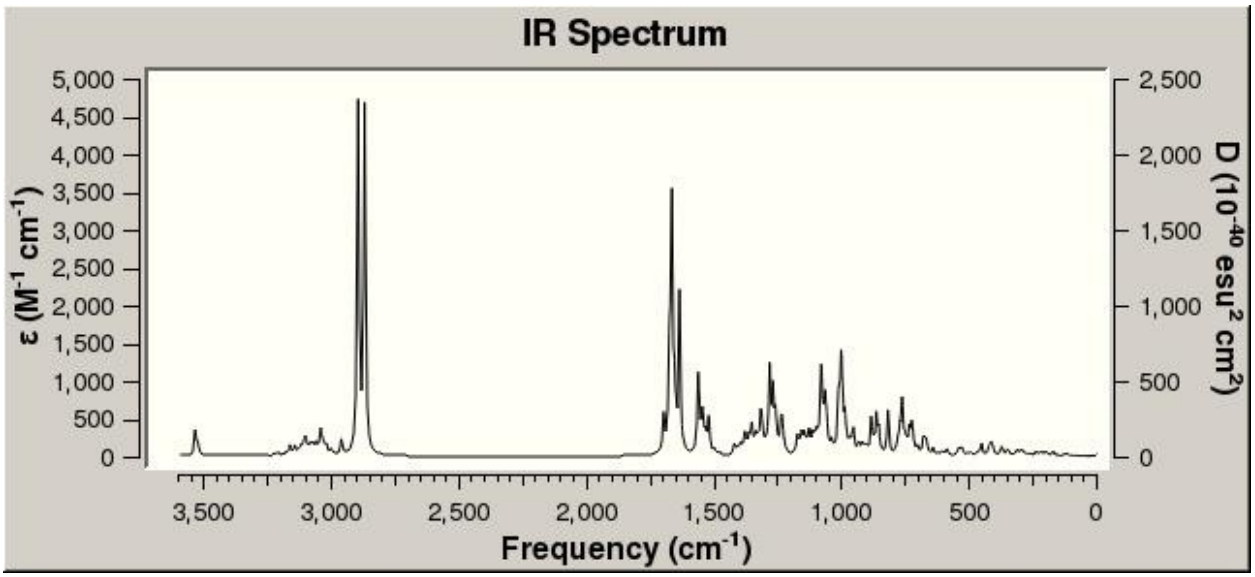

Figure G-6. The predicted FTIR spectrum for the A_2-Mn(II) complex that was optimized using BP86/3-21G* and incorporated the d3bj empirical dispersion correction.

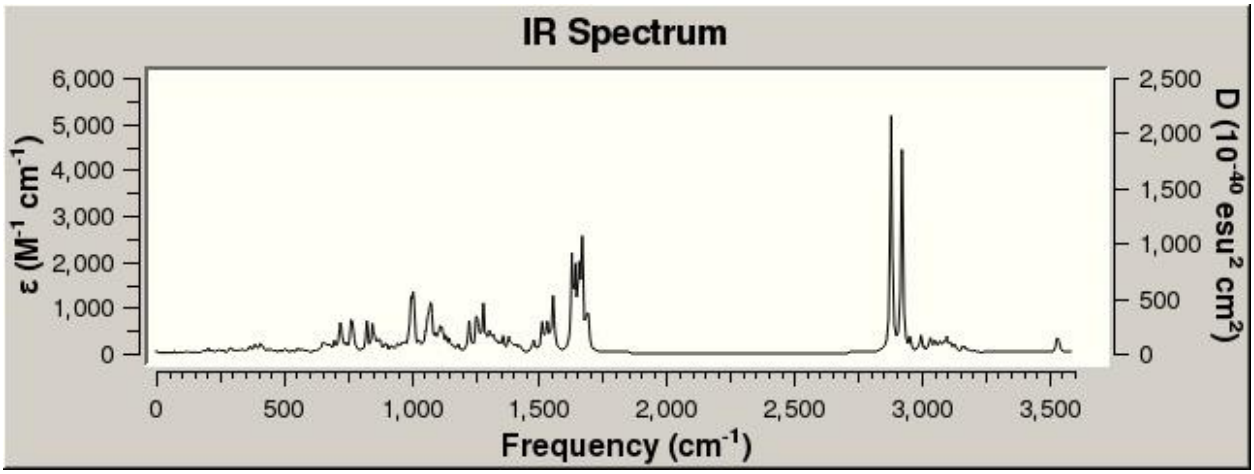

Figure G-7. The predicted FTIR spectrum for the A_2-Mn(II)-DMF complex that was optimized using BP86/3-21G* and incorporated the d3bj empirical dispersion correction.

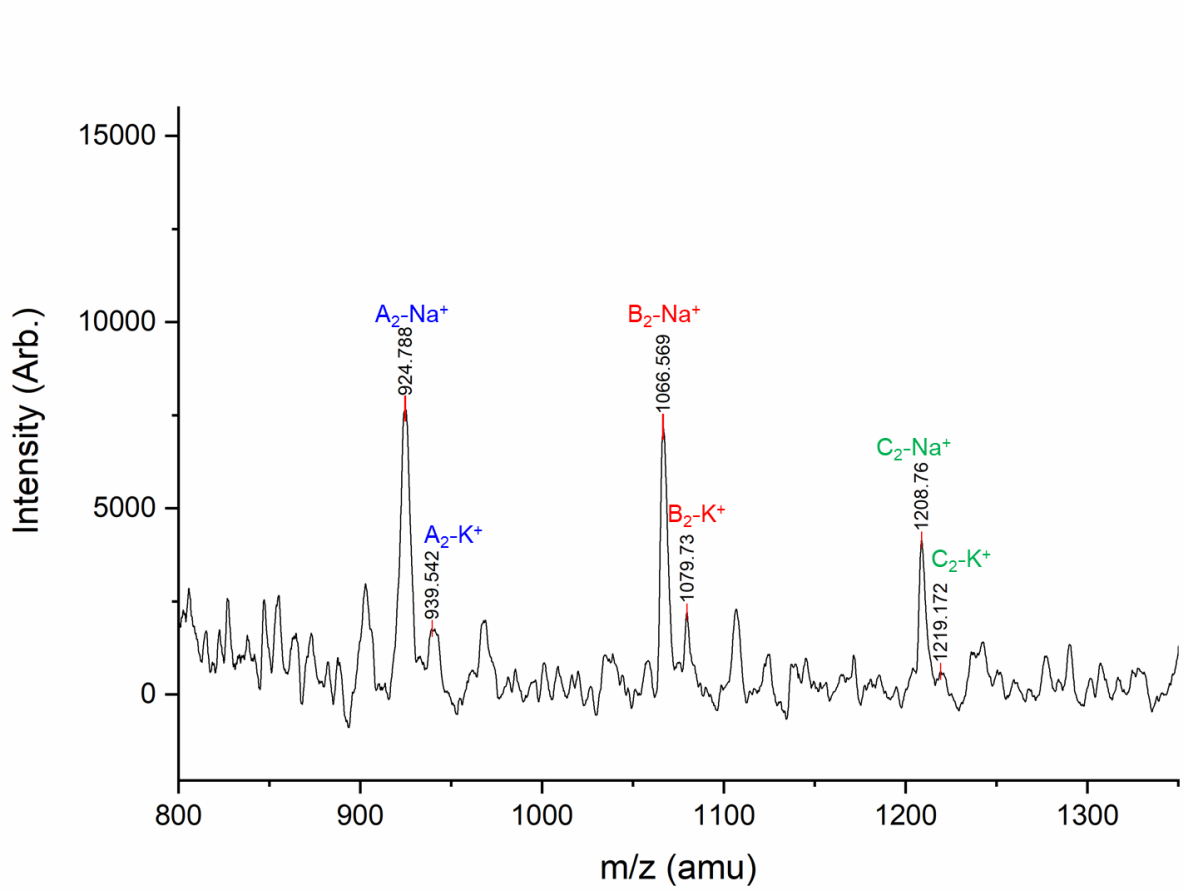

Figure G-8. The MALDI-TOF MS spectrum of PU **10-8b** focused on the A_2 species indicating K^+ cations are present

APPENDIX H

SUPPLEMENTAL MATERIALS FOR CHAPTER 4

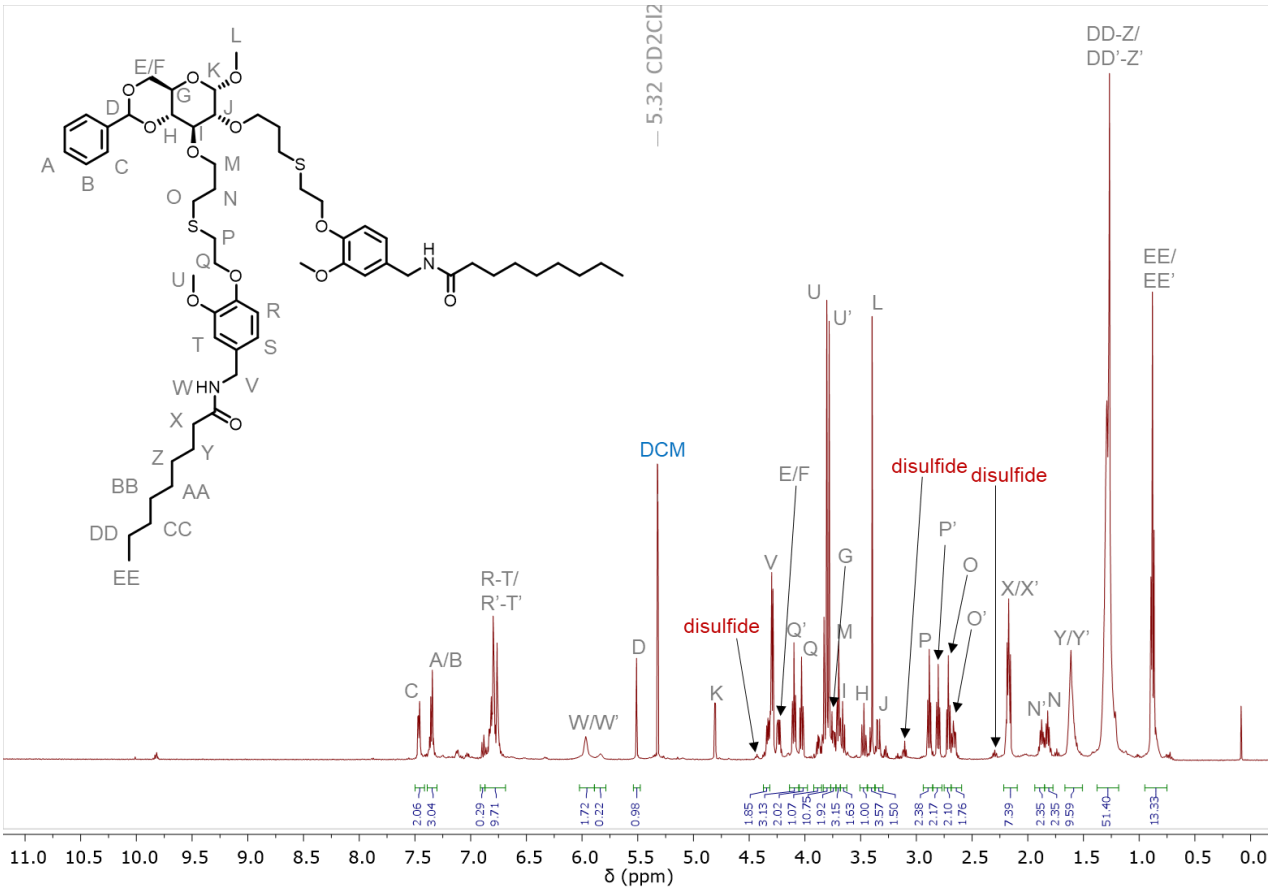

Figure H-1. ^{1}H-NMR spectrum of methy 4,6-*O*-benzylidene-2,3-*O*-bis(3-thiopent-5-*O*-pseudocapsaicin)-α-(D)-glucopyranoside (**20**) product in CD_2Cl_2 indicating intended product but also presence of disulfide.

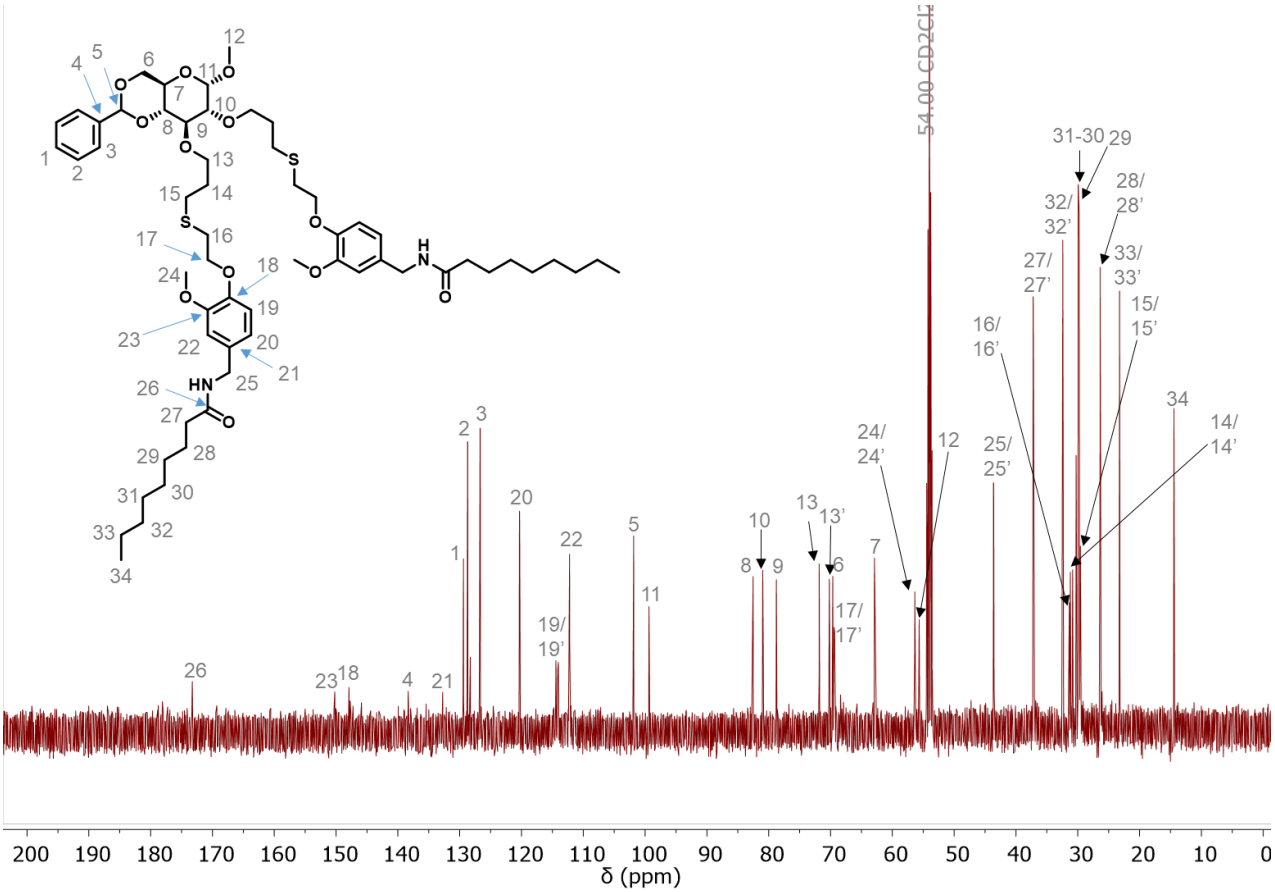

Figure H-2. ^{13}C-NMR spectrum of 4,6-*O*-benzylidene-2,3-*O*-bis(3-thiopent-5-*O*-pseudocapsaicin)-α-(D)-glucopyranoside (**20**) product in CD_2Cl_2 indicating intended product.

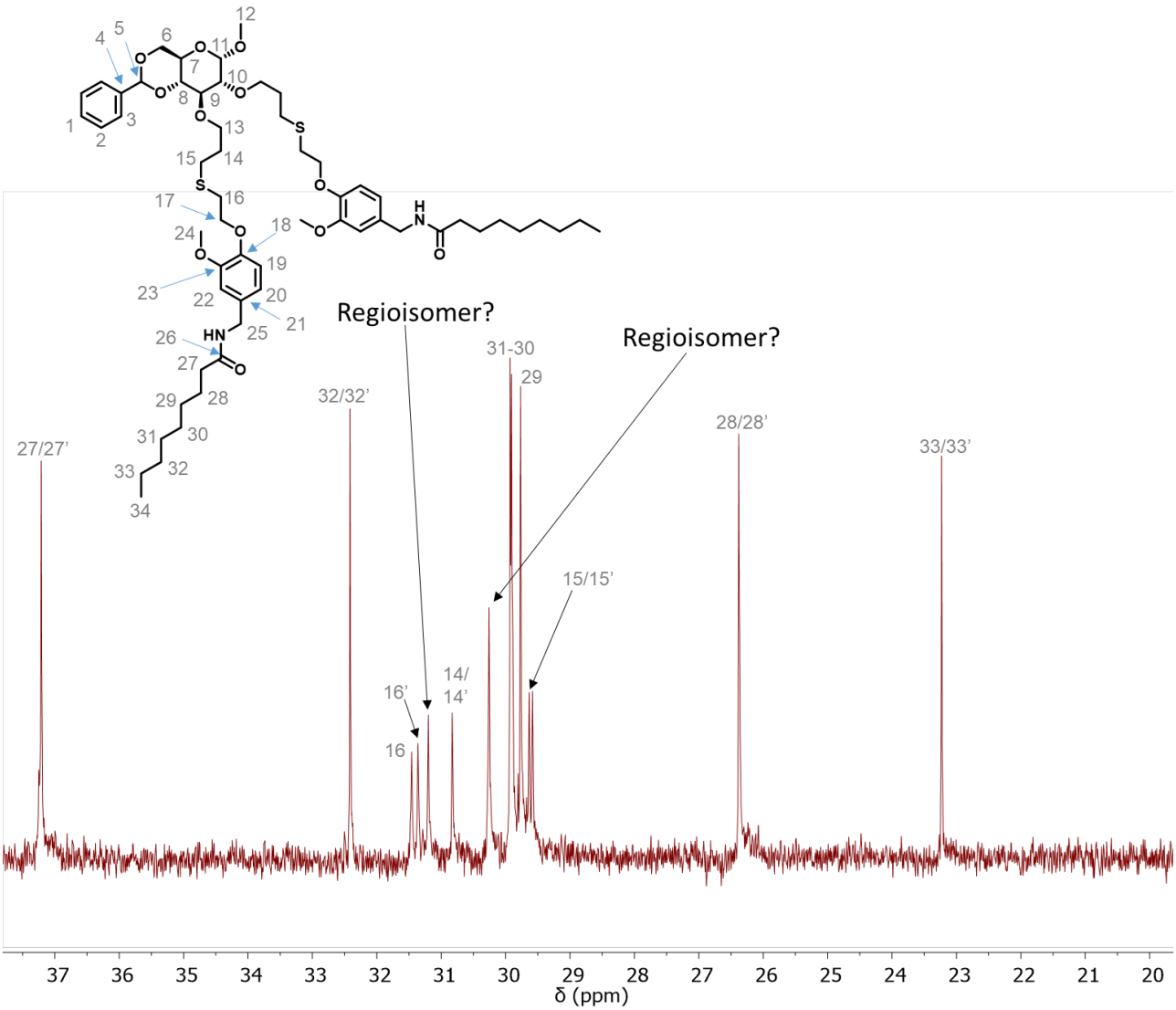

Figure H-3. An enlarged area of the ^{13}C-NMR spectrum of 4,6-*O*-benzylidene-2,3-*O*-bis(3-thiopent-5-*O*-pseudocapsaicin)-α-(D)-glucopyranoside (**20**) product in CD_2Cl_2 has two unknown peaks that could be regioisomers.

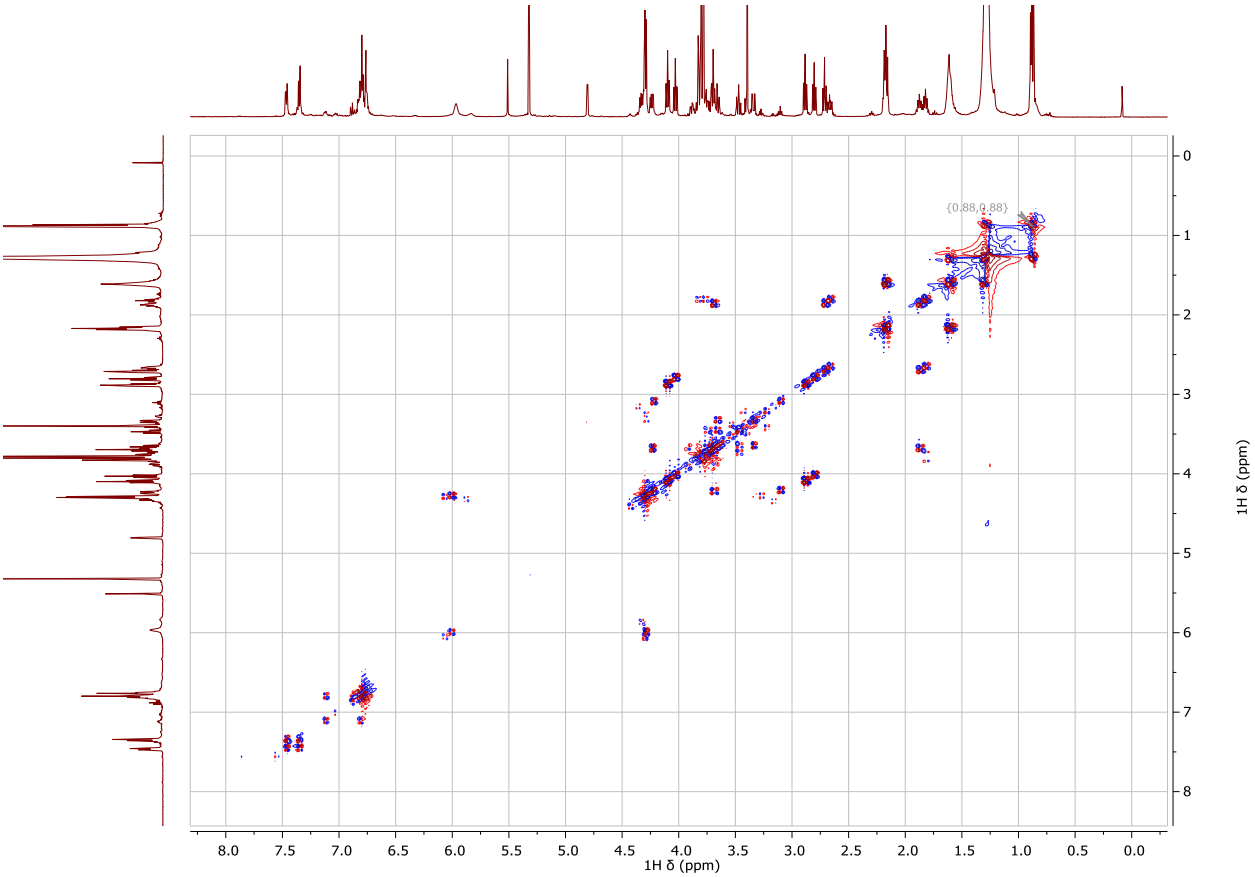

Figure H-4. ^{1}H-^{1}H DQ-COSY spectrum of 4,6-*O*-benzylidene-2,3-*O*-bis(3-thiopent-5-*O*-pseudocapsaicin)-α-(D)-glucopyranoside (**20**) product.

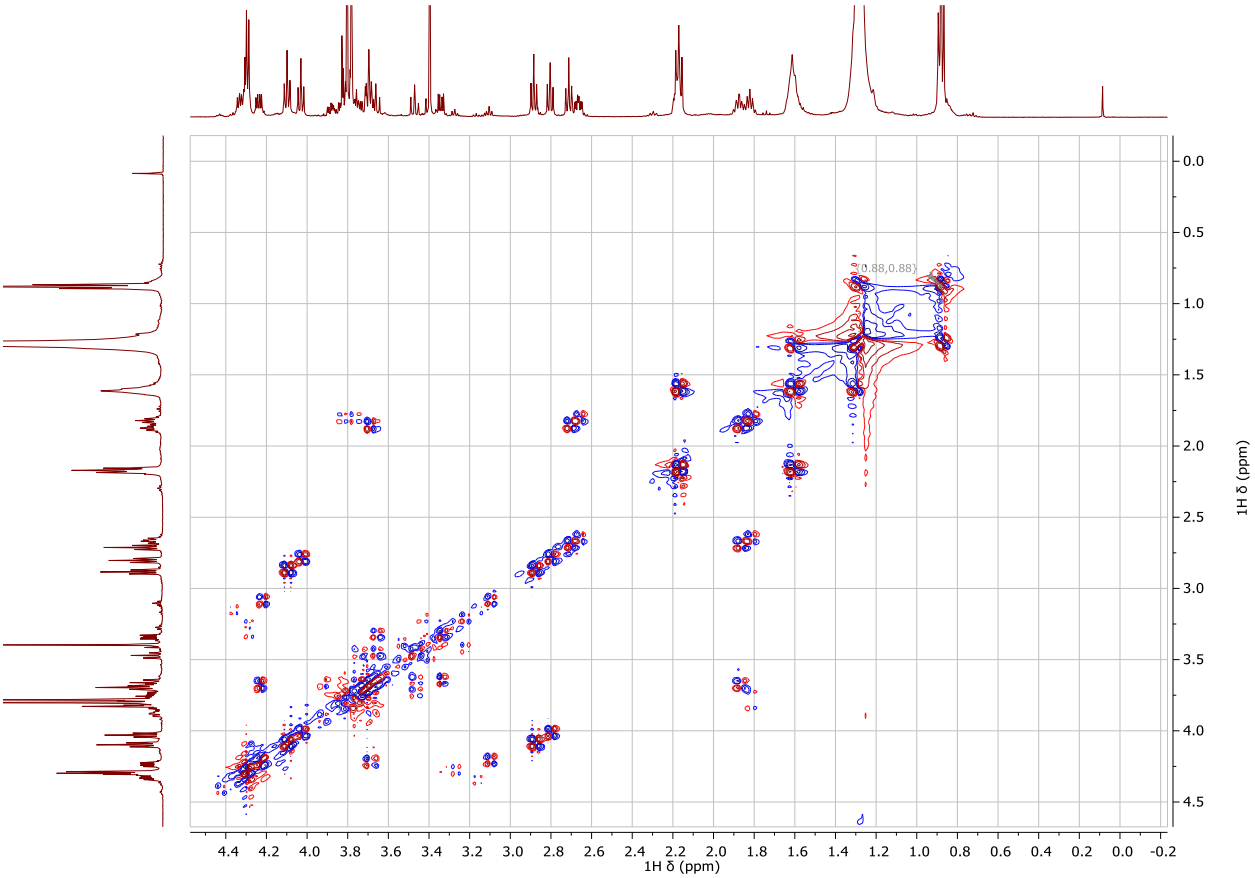

Figure H-5. Enlarged ^{1}H-^{1}H DQ-COSY spectrum of 4,6-*O*-benzylidene-2,3-*O*-bis(3-thiopent-5-*O*-pseudocapsaicin)-α-(D)-glucopyranoside (**20**) product at low ppm.

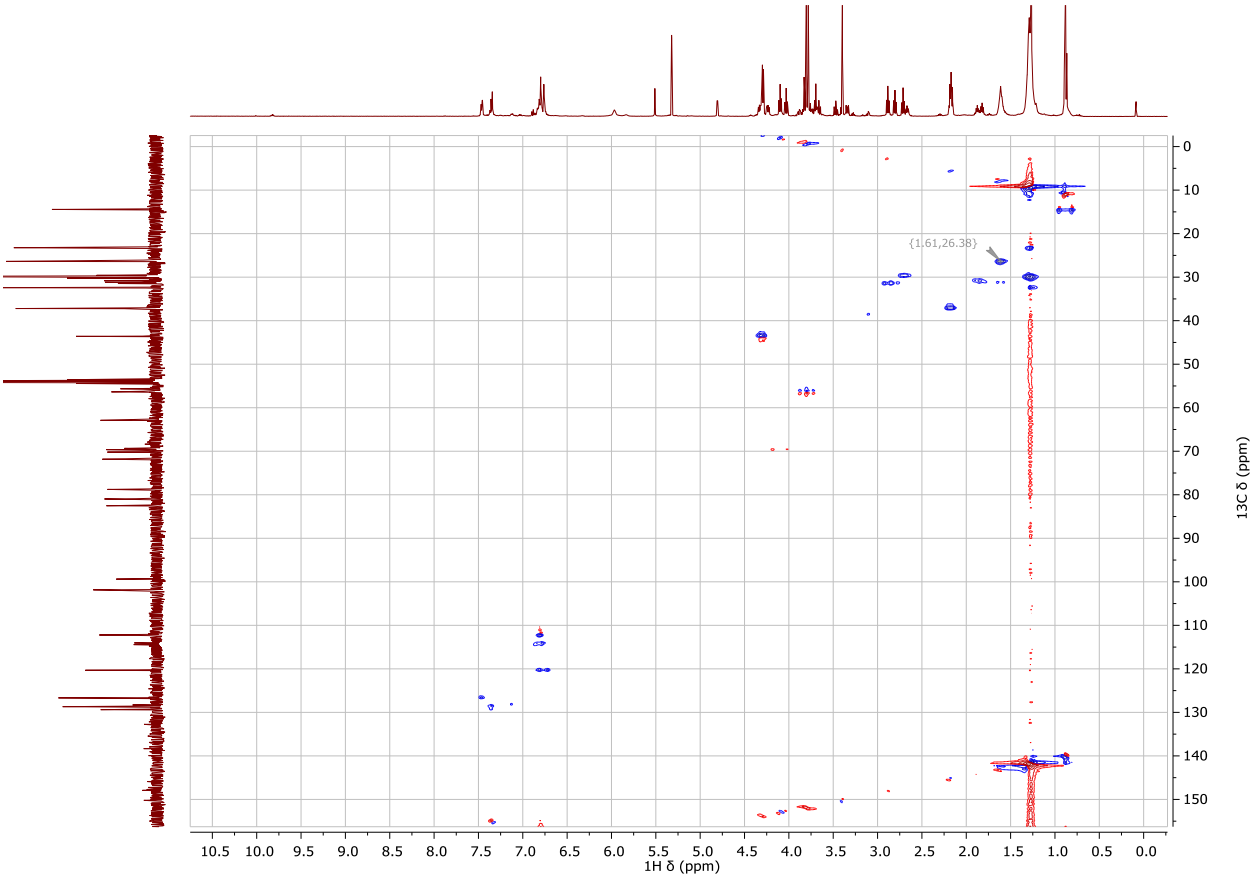

Figure H-6. ^{1}H-^{13}C HMQC NMR spectrum of 4,6-*O*-benzylidene-2,3-*O*-bis(3-thiopent-5-*O*-pseudocapsaicin)-α-(D)-glucopyranoside (**20**) product.

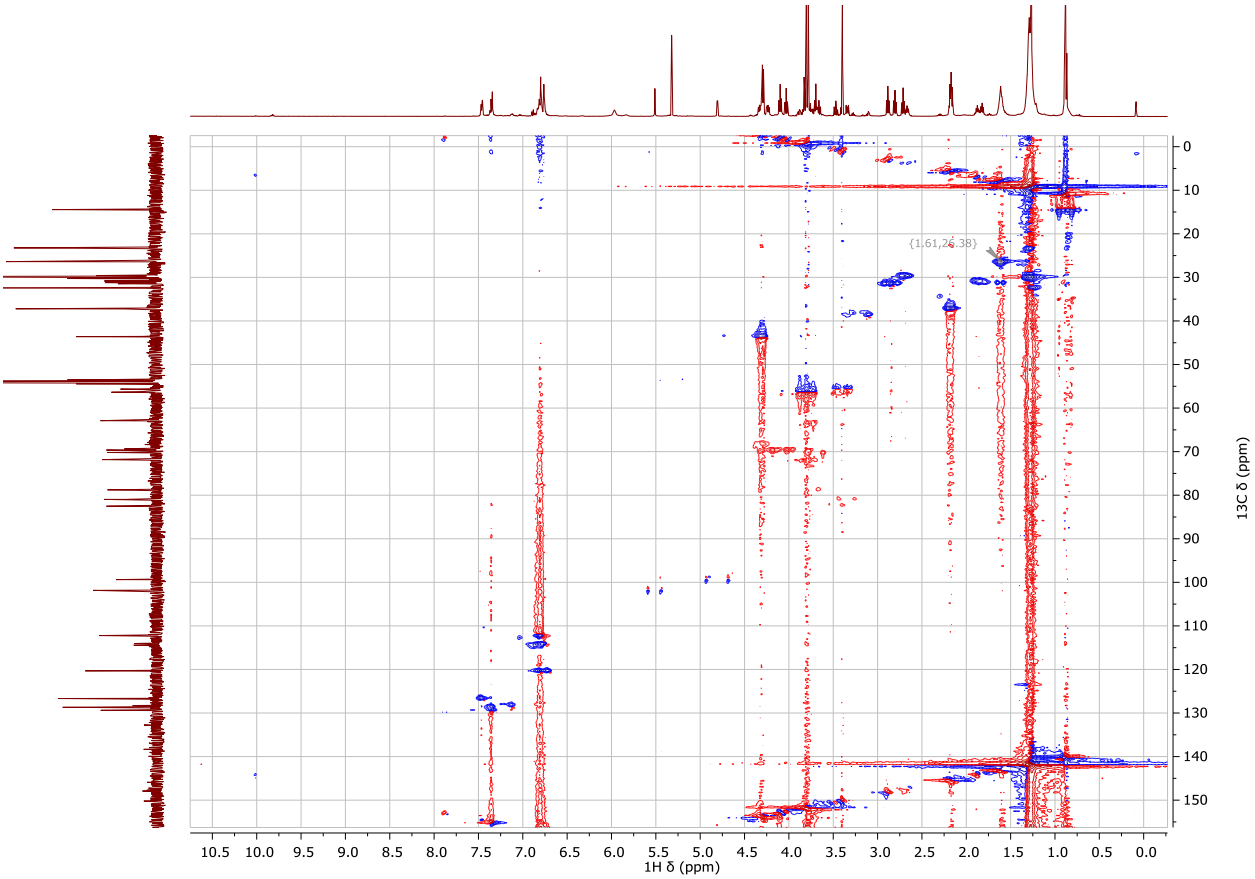

Figure H-7. ^{1}H-^{13}C HMQC NMR spectrum of 4,6-*O*-benzylidene-2,3-*O*-bis(3-thiopent-5-*O*-pseudocapsaicin)-α-(D)-glucopyranoside (**20**) product with intensity increased.

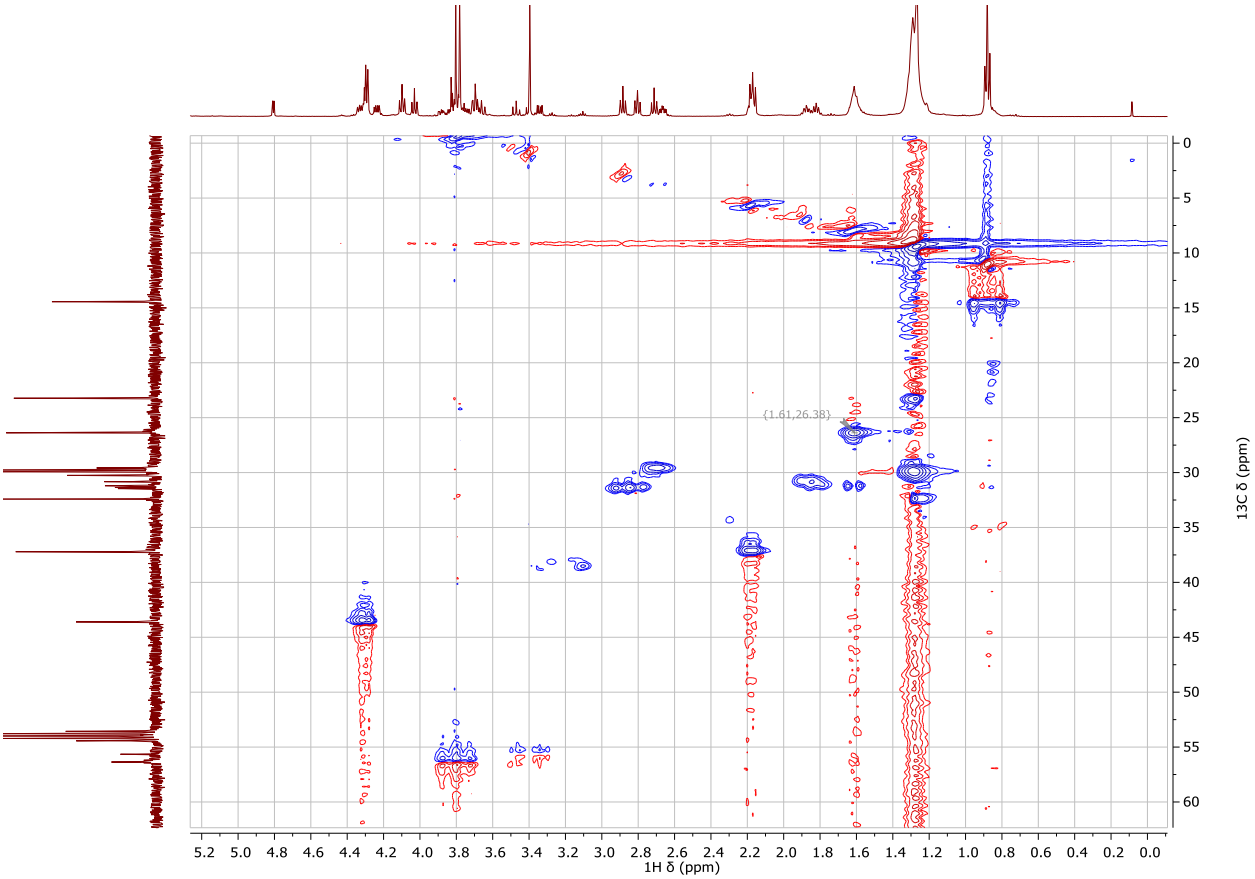

Figure H-8. A focused ^{1}H-^{13}C HMQC NMR spectrum of 4,6-*O*-benzylidene-2,3-*O*-bis(3-thiopent-5-*O*-pseudocapsaicin)-α-(D)-glucopyranoside (**20**) product at low ppm with intensity increased.

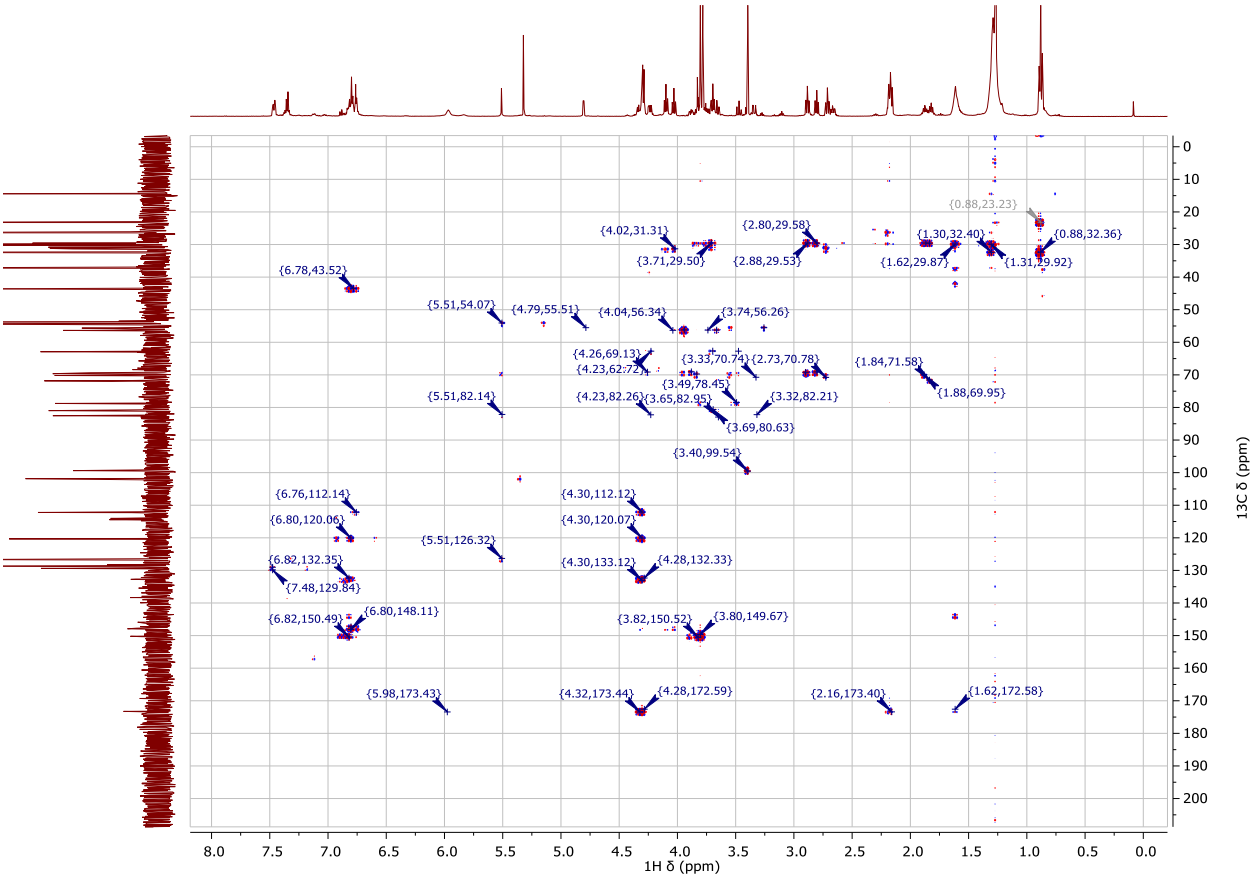

Figure H-9. ^{1}H-^{13}C HMBC NMR spectrum of 4,6-*O*-benzylidene-2,3-*O*-bis(3-thiopent-5-*O*-pseudocapsaicin)-α-(D)-glucopyranoside (**20**) product.

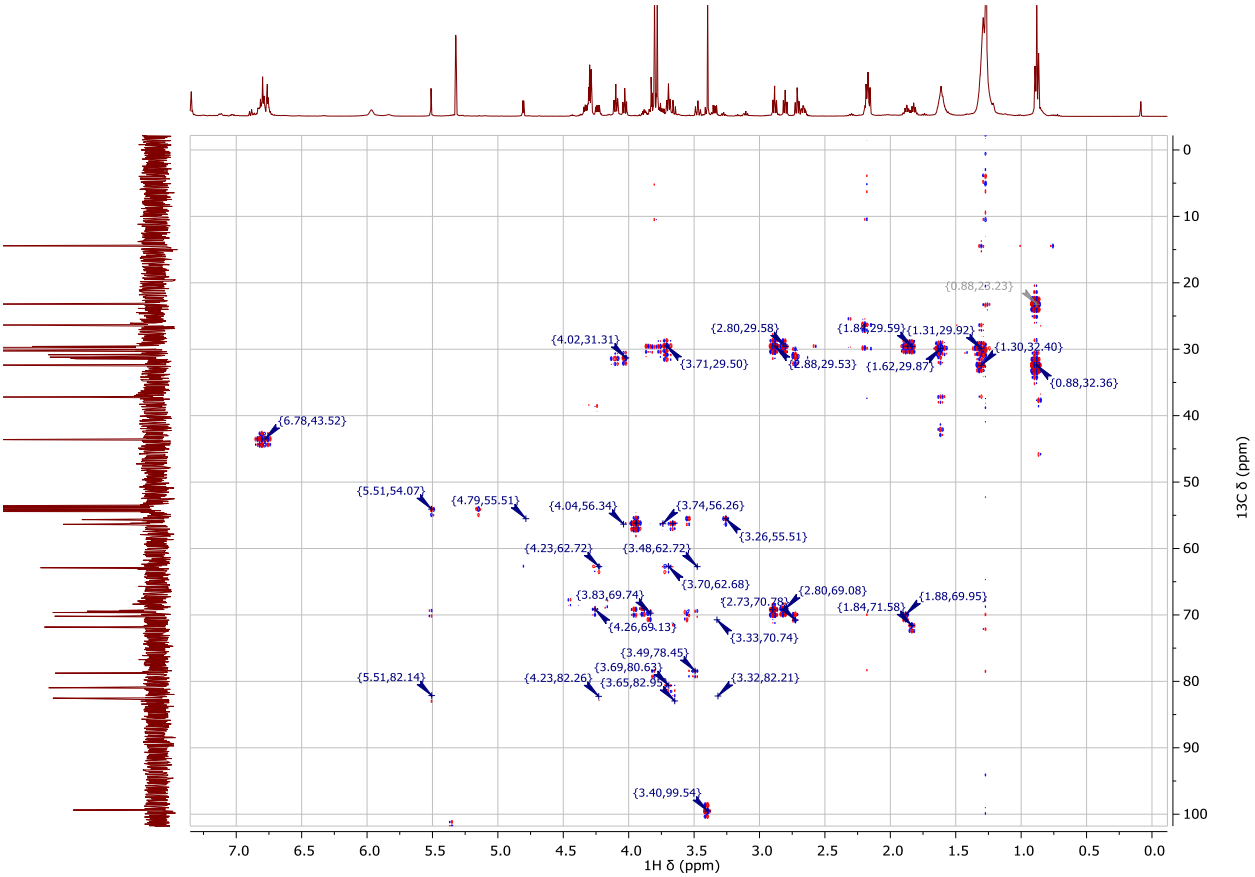

Figure H-10. An expanded ^{1}H-^{13}C HMBC NMR spectrum of 4,6-*O*-benzylidene-2,3-*O*-bis(3-thiopent-5-*O*-pseudocapsaicin)-α-(D)-glucopyranoside (**20**) product at low ppm.

APPENDIX I

SUPPLEMENTARY MATERIALS FOR CHAPTER 5

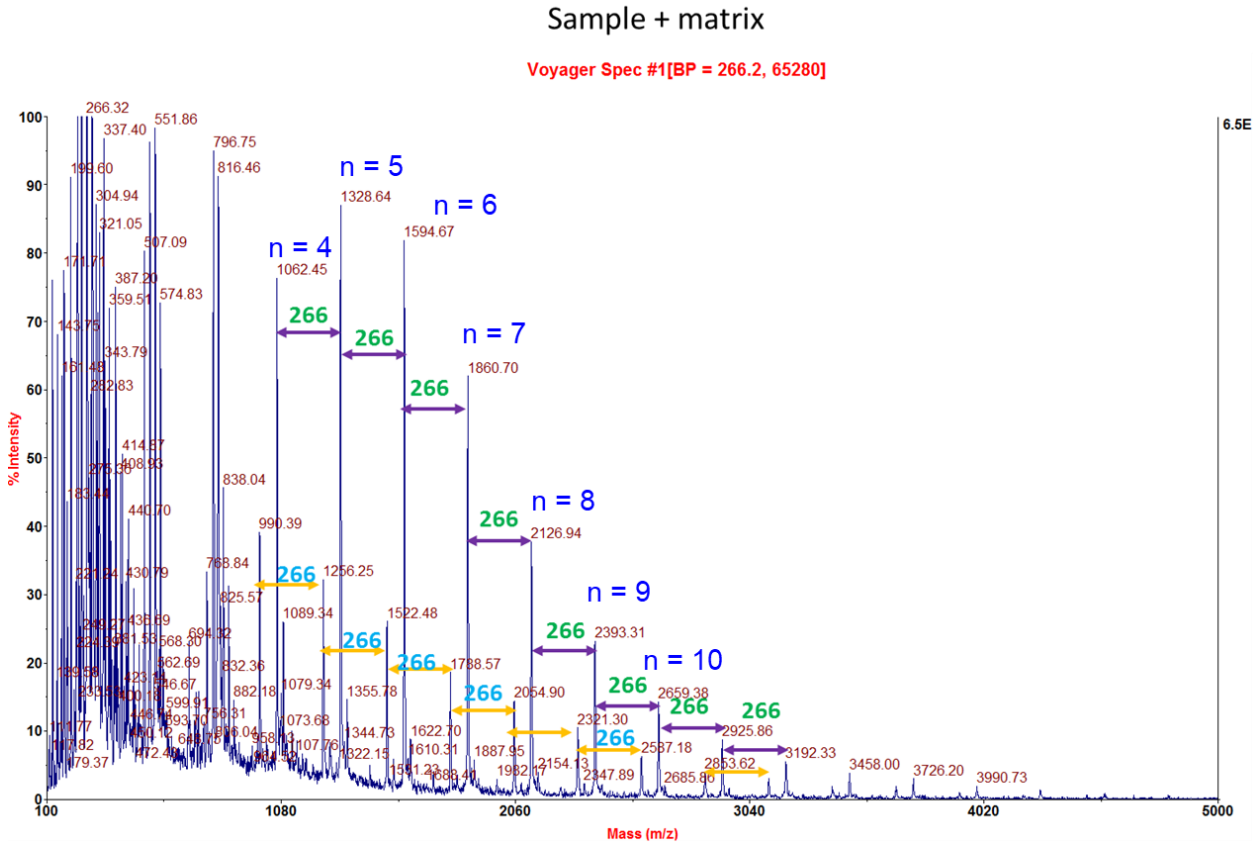

Figure I-1. MALDI-MS performed on **26** by Yohannes Rezenom in Dr. Russel's group using the HABA matrix indicated that the low-molar-mass oligomer first produced was, on average, a pentamer.

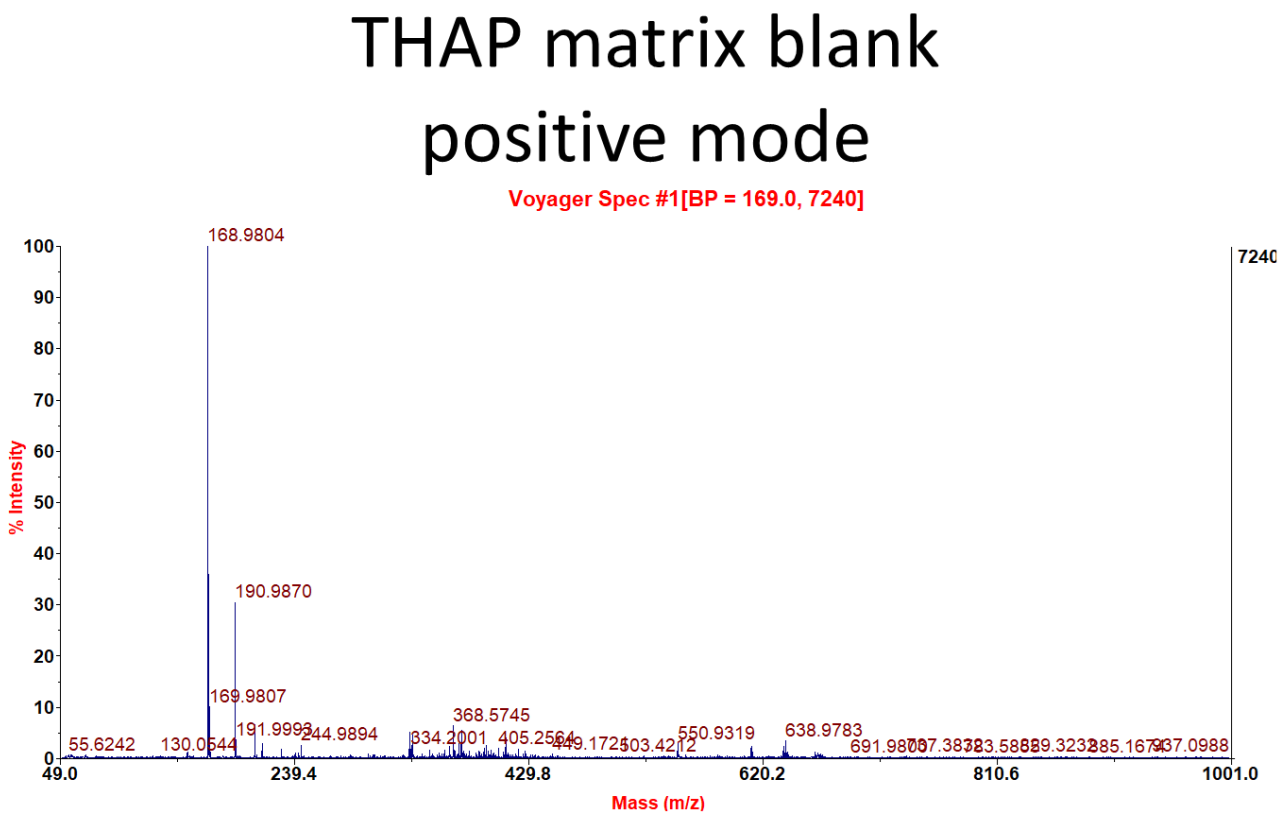

Figure I-2. The "blank" spectrum from MALDI-TOF MS with only the THAP matrix being run. This was the control spectrum acquired before running a sample of **22** on the instrument.

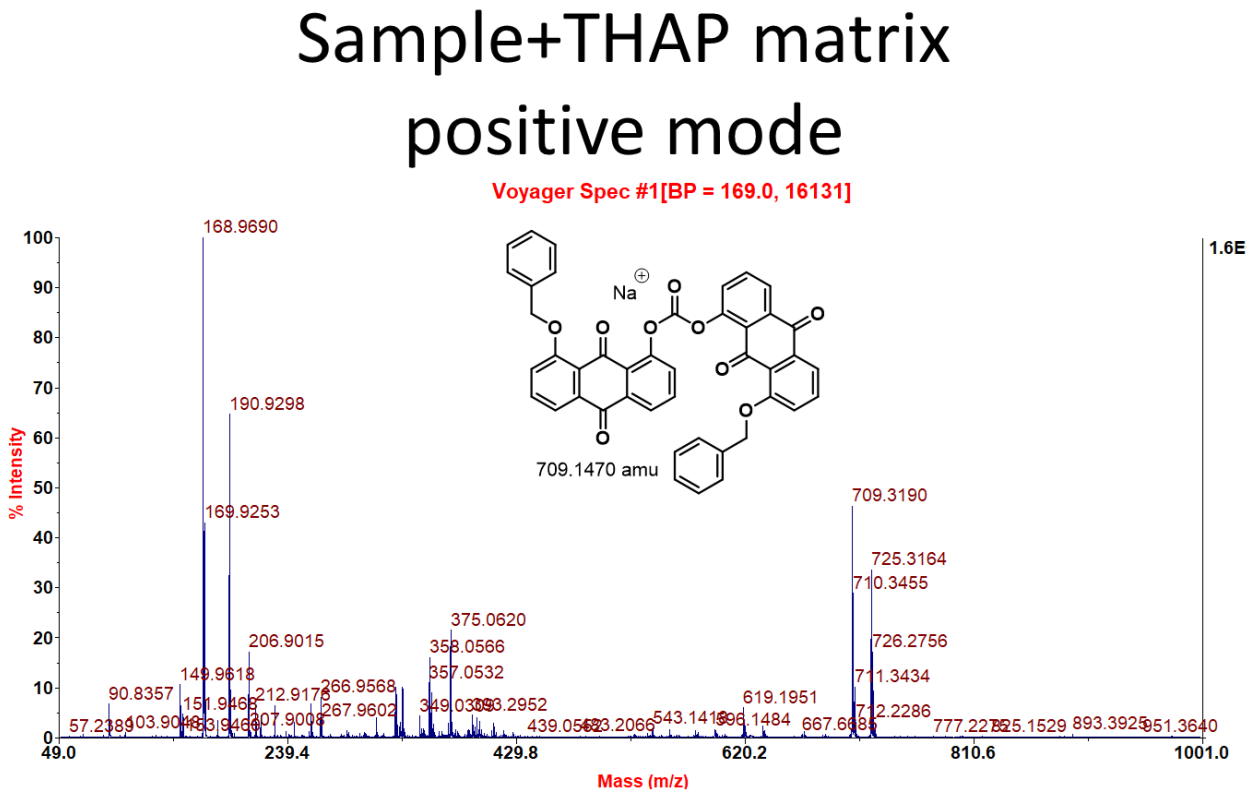

Figure I-3. The MALDI-TOF MS showing product **22** ionizing well with both a sodium counterion and a potassium counterion in close agreement with the predicted isotopic mass. A THAP matrix was used.

Sample + THAP matrix zoom in positive mode

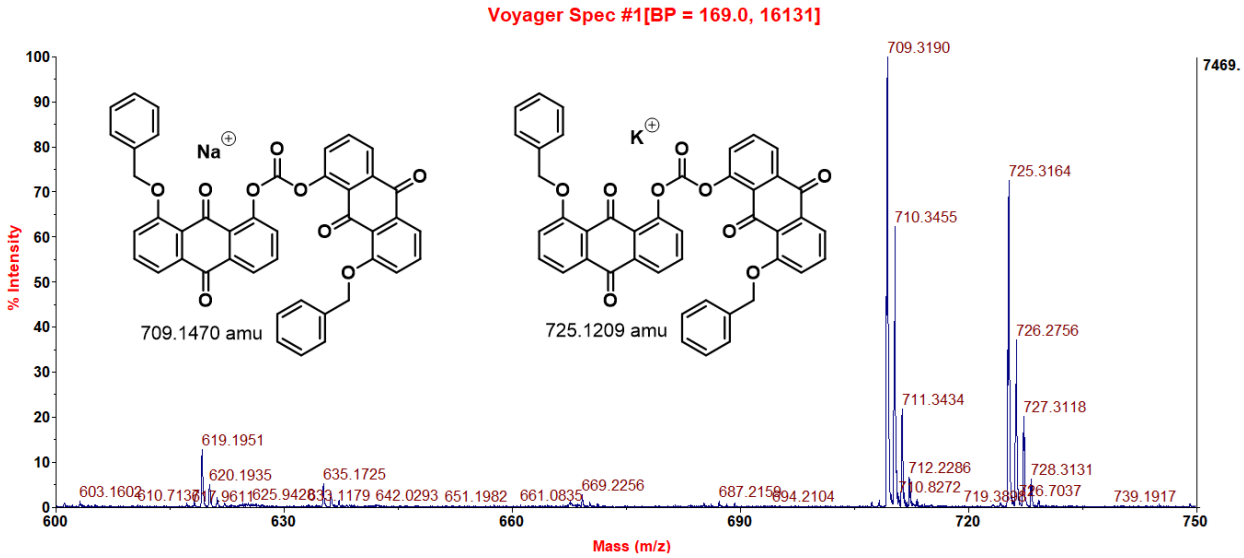

Figure I-4. The focused view of the MALDI-TOF MS showing product **22** ionizing well with both a sodium and potassium counterion in close agreement with the predicted isotopic mass. A THAP matrix was used.

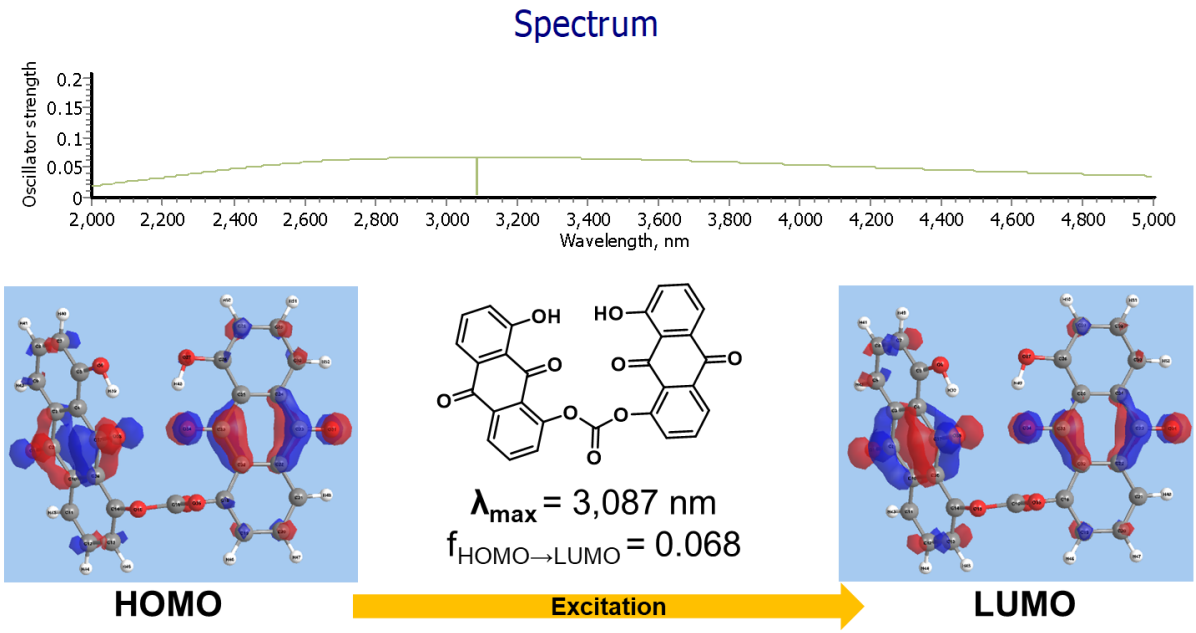

Figure I-5. The predicted UV-VIS spectrum of bis(1,8-DHA)carbonate (**23**) radical anion in the gas phase with the spectral window expanded into the near-IR region. The structure was optimized using the same conditions prior to this calculation.

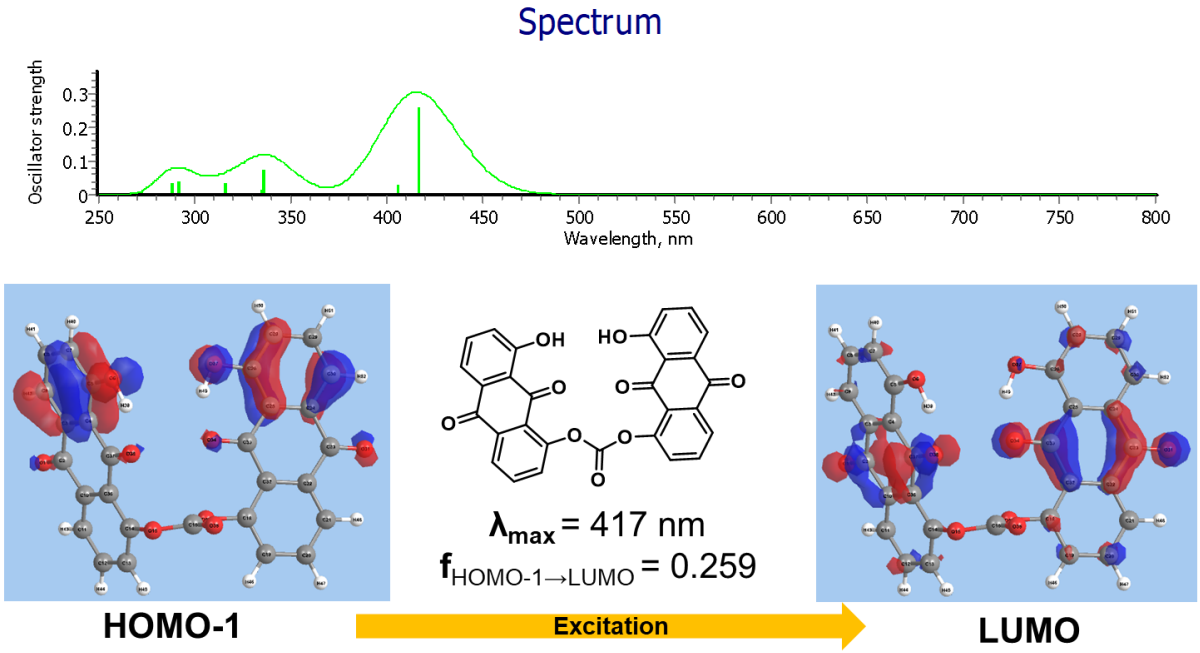

Figure I-6. Predicted UV-VIS spectrum of **23** with DMAc solvation using the SMD for energetic calculations. The structure was optimized using the same conditions prior to this calculation.

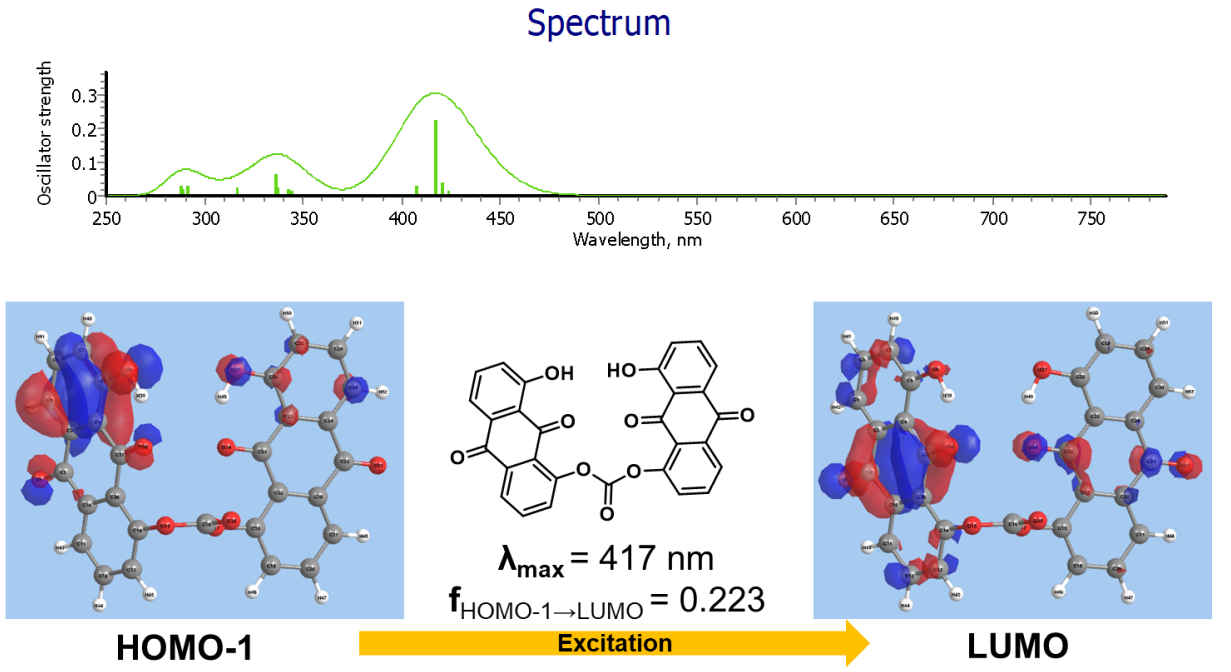

Figure I-7. Predicted UV-VIS spectrum of **23** with DCM solvation using the SMD for energetic calculations. The structure was optimized using the same conditions prior to this calculation.

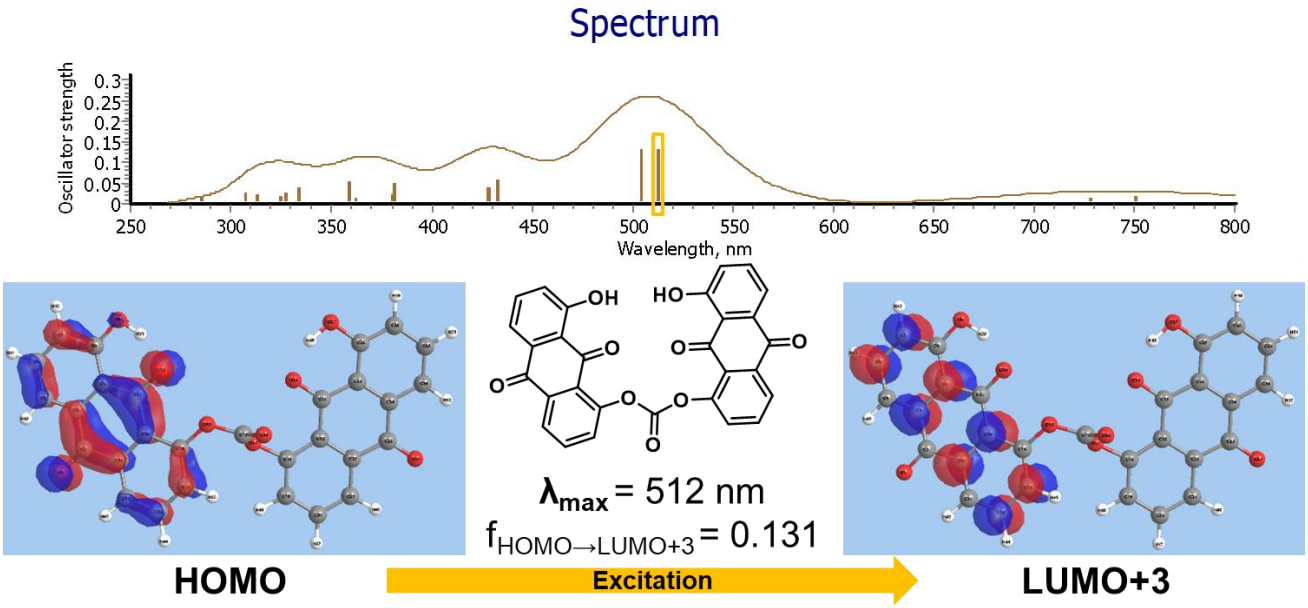

Figure I-8. Predicted UV-VIS spectrum of **23** in the gas phase as a diradical dianion (T_1^{2-}). The structure was optimized using the same conditions prior to this calculation.

Table I-1. Gibbs free energy values for the bis(1,8-DHA)carbonate (**23**), in the gas phase and with implicit solvation, as a singlet, radical anion, diradical dianion, and a neutral triplet. The SMD was used.

Spin State	Charge	G_{gas} (kcal/mol)	G_{DMAc} (kcal/mol)	G_{DCM} (kcal/mol)
Singlet	none	0.0 (norm)	0.0 (norm)	0.0 (norm)
Doublet	1–	–48.3	–76.0	–72.3
Triplet	2–	–38.6	–147.9	–139.5
Triplet	none	56.1	54.2	55.5

Table I-2. Gibbs free energy values for DMAc, in the gas phase and with implicit solvation, as a singlet and as a radical cation. The SMD was used.

Spin State	Charge	G_{gas} (kcal/mol)	G_{DMAc} (kcal/mol)
Singlet	none	0 (norm)	0 (norm)
Doublet	1+	191.0	135.6

Table I-3. Gibbs free energy values for DCM, in the gas phase and with implicit solvation, as a singlet and as a radical cation. The SMD was used.

Spin State	Charge	G_{gas} (kcal/mol)	G_{DCM} (kcal/mol)
Singlet	none	0 (norm)	0 (norm)
Doublet	1+	252.0	200.3

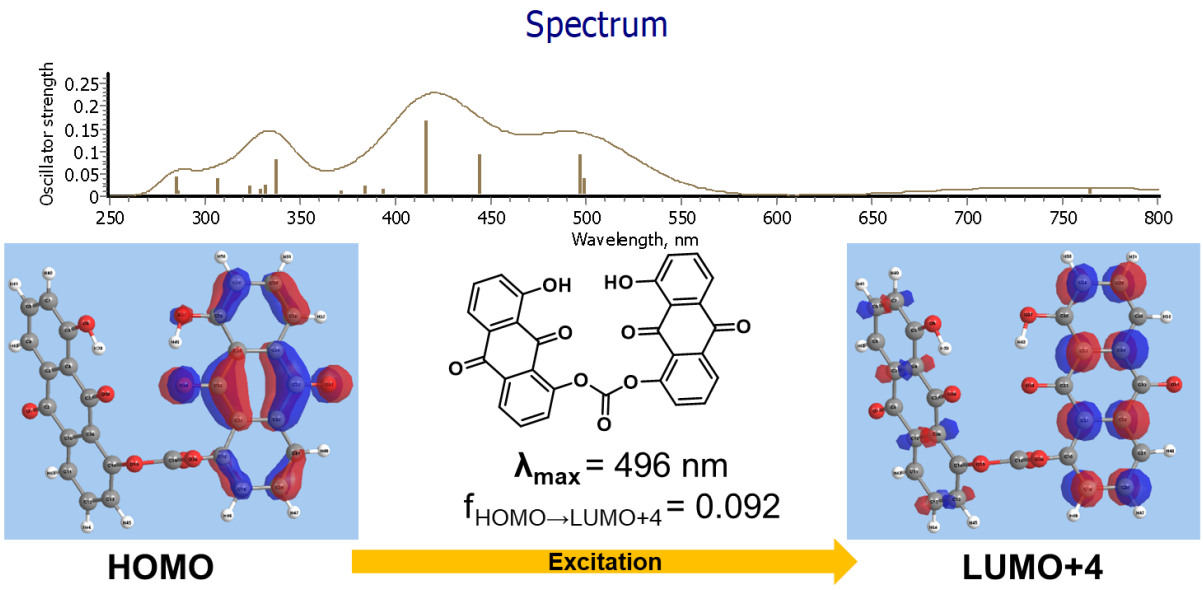

Figure I-9. Predicted UV-VIS spectrum of **23** as a radical anion (D_0^-) with solvation in DMAc using the SMD for energetic calculations. The structure was optimized using the same conditions prior to this calculation.

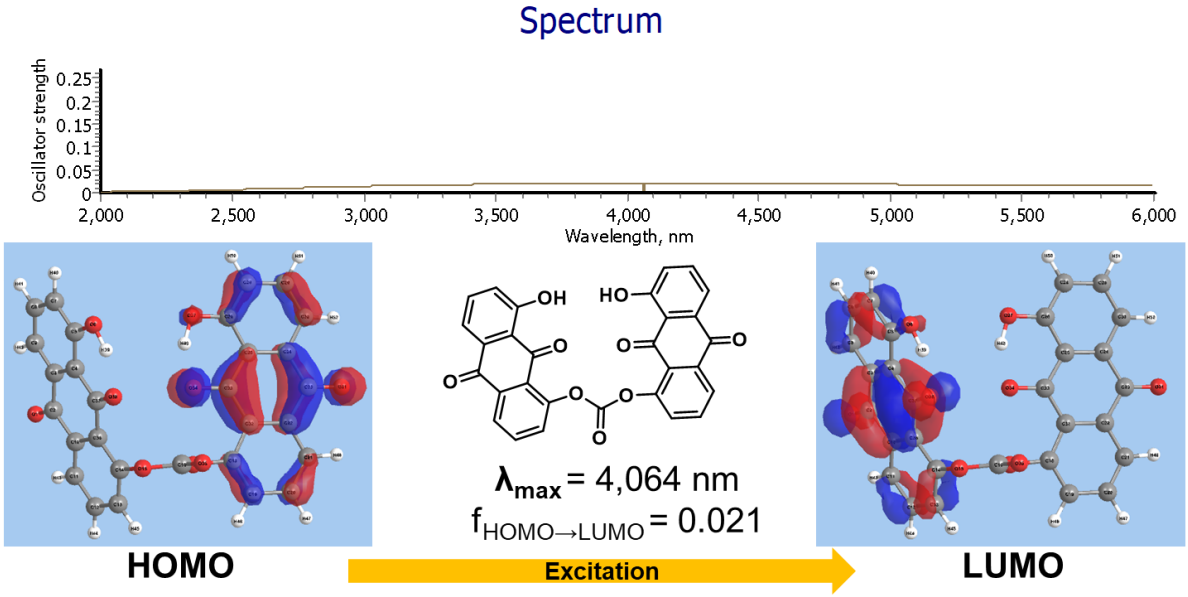

Figure I-10. Predicted UV-VIS spectrum of **23** as a radical anion (D_0^-) with solvation in DMAc using the SMD showing the significantly decreased excitation at 4064 nm relative to this excitation in the gas phase. The structure was optimized using the same conditions prior to this calculation.

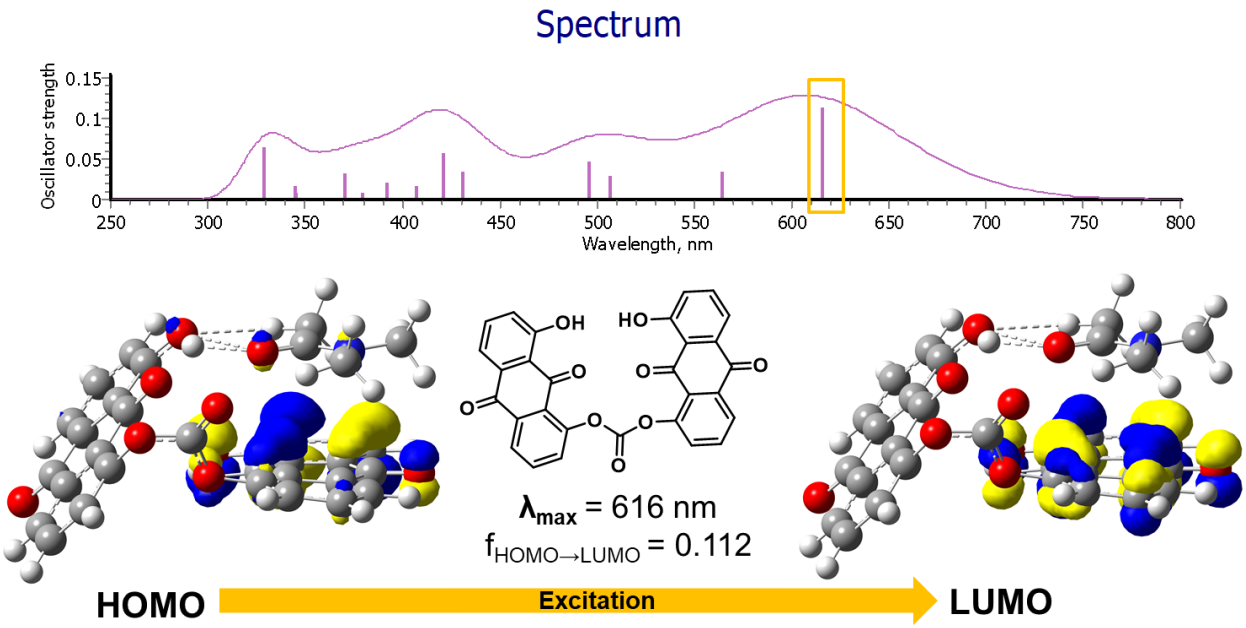

Figure I-11. The excitation at 616 nm between the HOMO-1 and the LUMO of DMAc and **23**, optimized together, shows some intramolecular charge transfer character. This binary system was optimized initially as a T_1 in an attempt to approximate the geometry of the S_1 excited state and limit the number of potential local minima. The gd3bj empirical dispersion parameter was incorporated into this system in DMAc using the PCM solvation parameter.

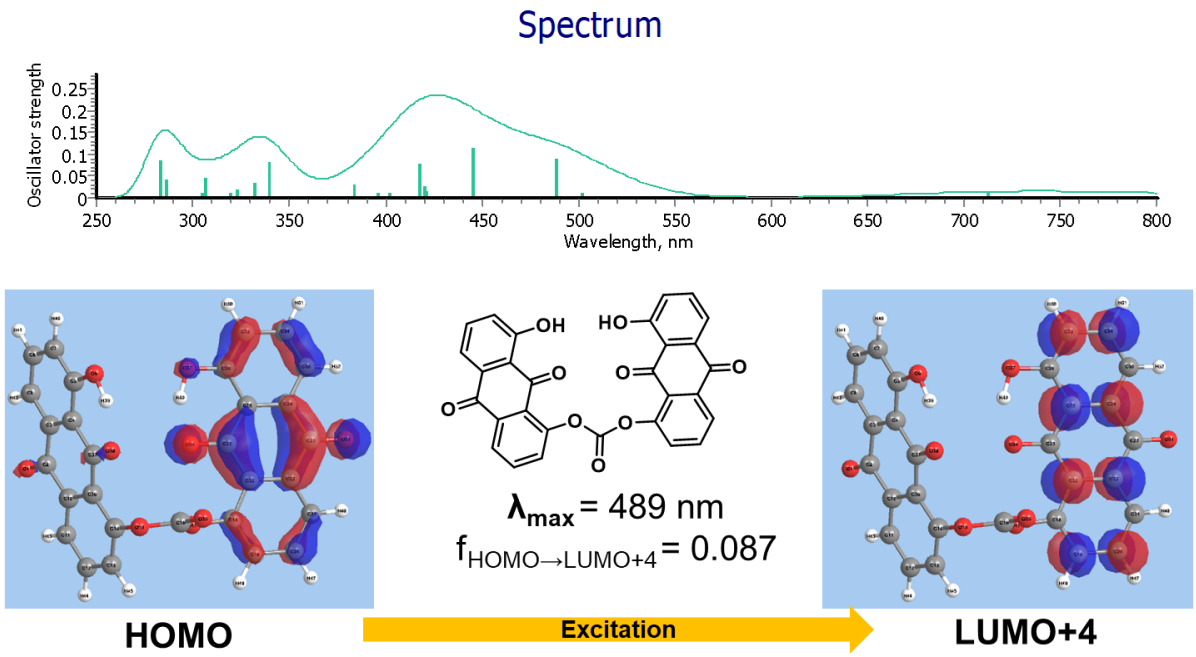

Figure I-12. The UV-VIS spectrum of **23** in DMAc using the PCM shows an even worse correlation to the experimental λ_{max} at 555 nm relative to the radical anion in the gas phase. The structure was optimized using the same parameters.

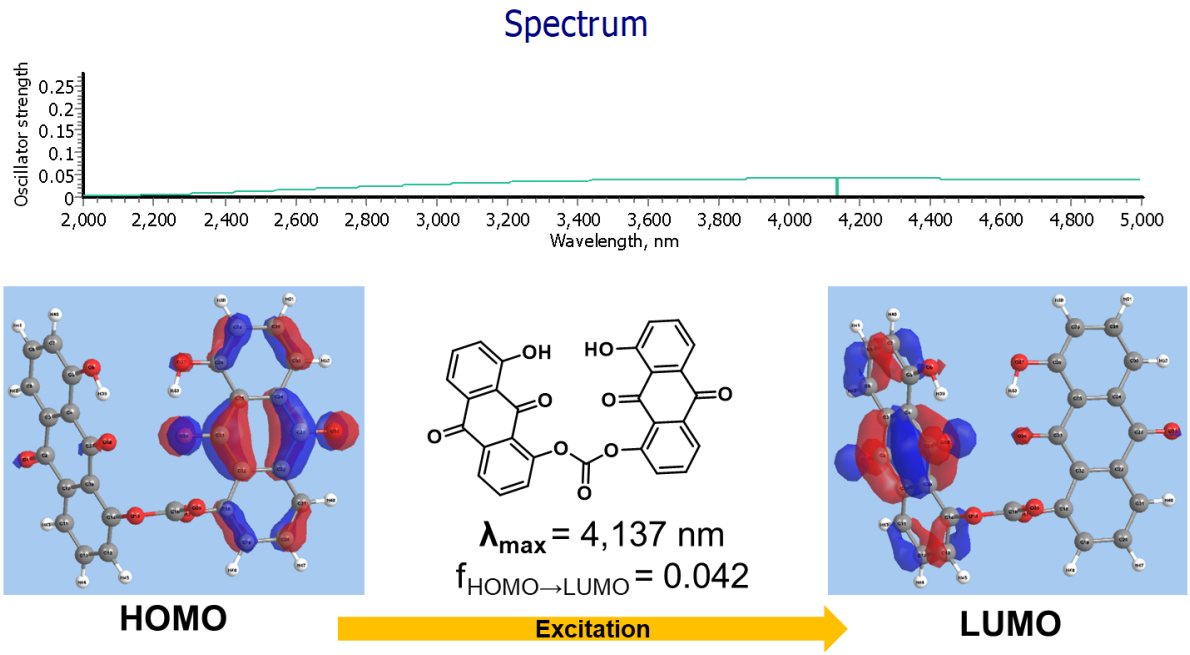

Figure I-13. The UV-VIS spectrum of **23** in DMAc using the PCM shows a much weaker excitation at 4137 nm. The structure was optimized using the same parameters.

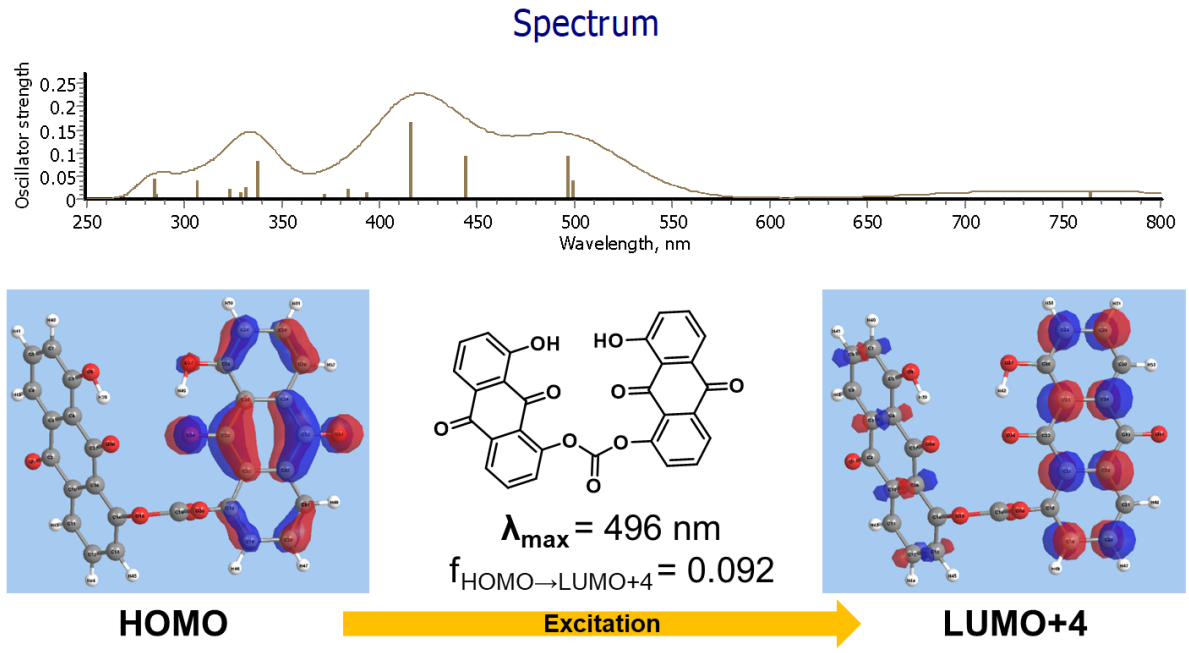

Figure I-14. The UV-VIS spectrum of **23** in DMAc using the SMD shows an even worse correlation to the experimental λ_{max} at 555 nm relative to the radical anion in the gas phase. The structure was optimized using the same parameters.

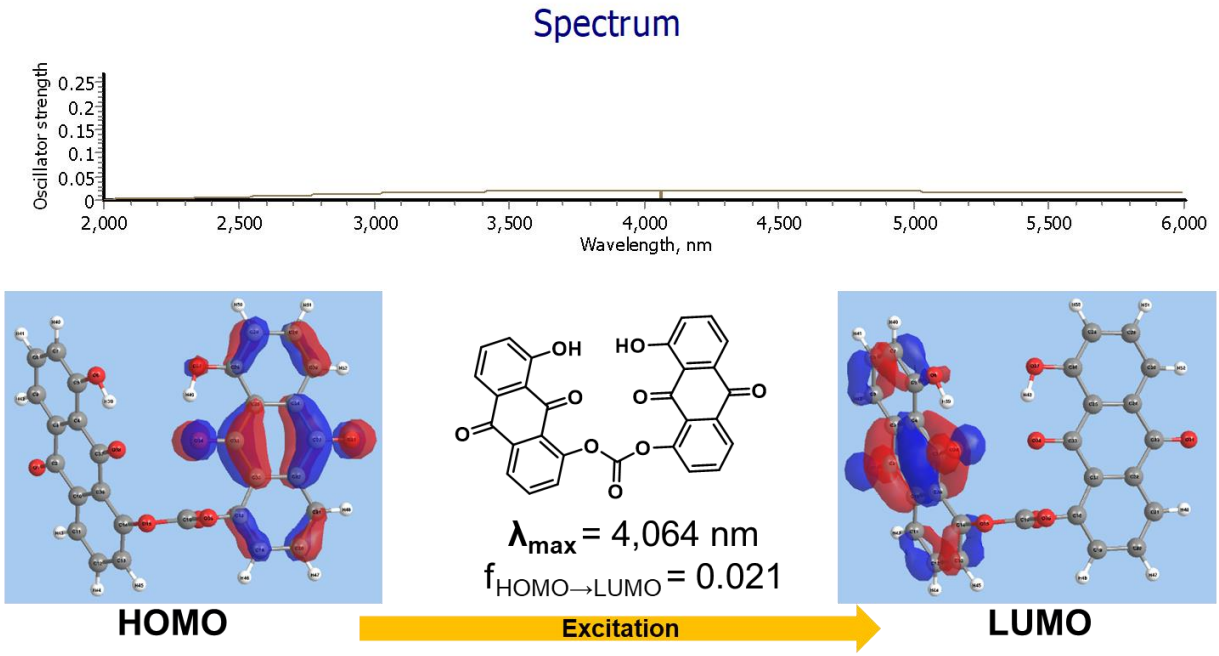

Figure I-15. The UV-VIS spectrum of **23** in DMAc using the SMD shows a much weaker excitation at 4064 nm relative to the gas phase radical anion. The structure was optimized using the same parameters.

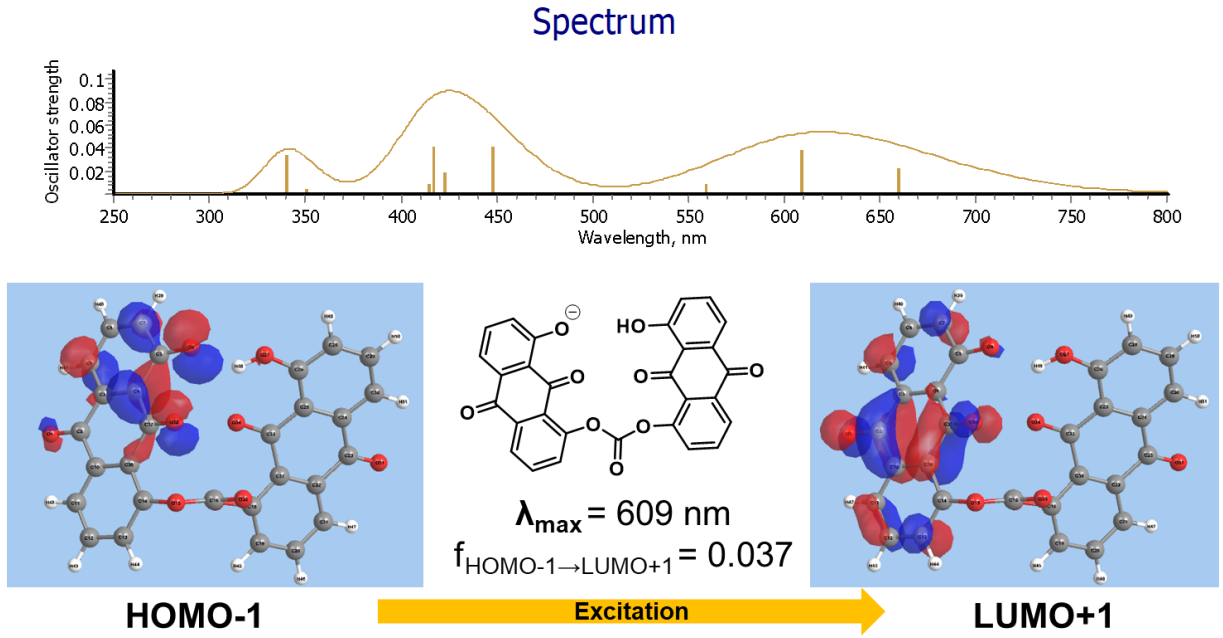

Figure I-16. The UV-VIS spectrum of the deprotonated **23** anion in the gas phase shows has an excitation at 609 nm. The structure was optimized using the same parameters.

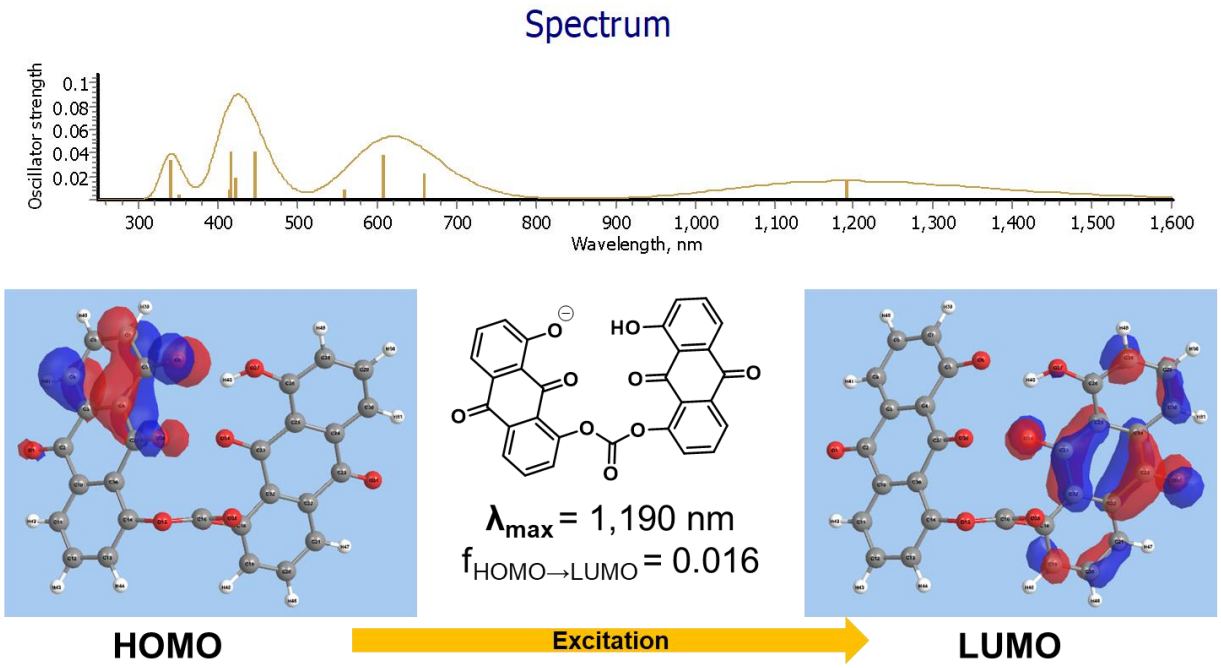

Figure I-17. The expanded UV-VIS spectrum of the deprotonated **23** anion in the gas phase shows has an excitation at 1190 nm in the near IR. The structure was optimized using the same parameters.

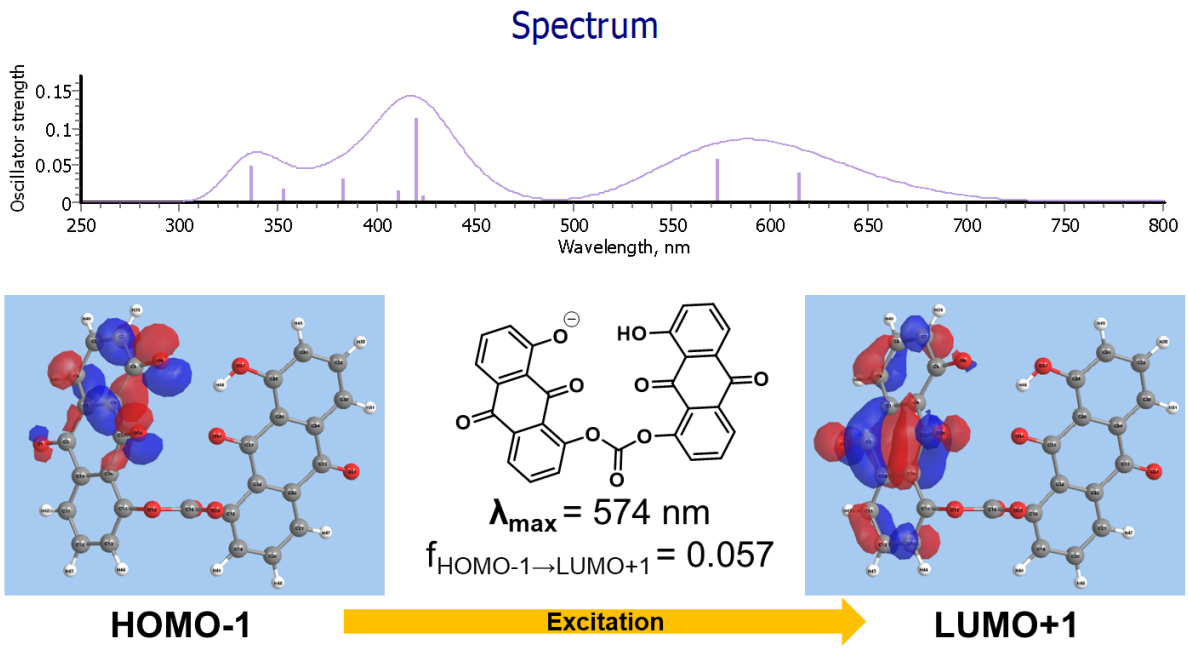

Figure I-17. The UV-VIS spectrum of the deprotonated **23** anion with DMAc solvation (PCM) shows has an excitation at 574 nm. This value is close to the experimentally observed λ_{max} of **23** in DMAc at 555 nm. The structure was optimized using the same parameters.

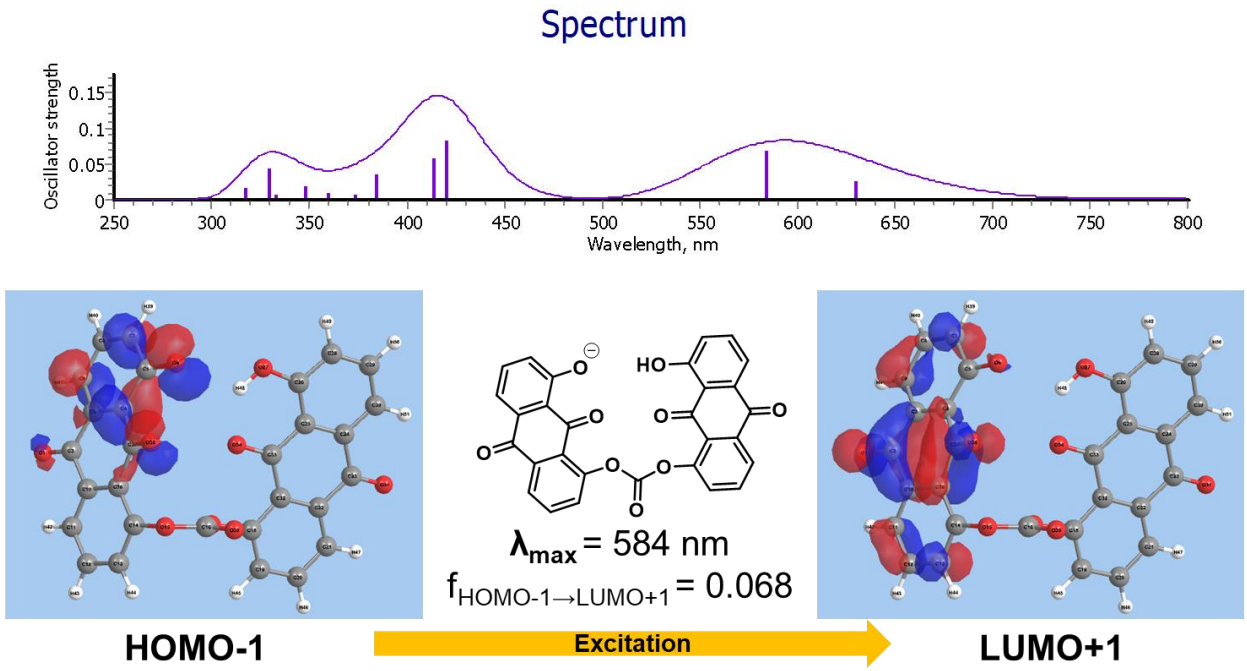

Figure I-18. The UV-VIS spectrum of the deprotonated **23** anion with DMAc solvation (SMD) shows has an excitation at 584 nm. This value is further away from the experimentally observed λ_{max} of **23** in DMAc at 555 nm. The structure was optimized using the same parameters.

Table I-4. Gibbs free energy values, in the gase phase and with implicit solvation, for **23** in its ground state and for the deprotonated anion of **23**. SMD was the implicit solvation model used.

Compound	Charge	G_{gas} (kcal/mol)	G_{DMAc} (kcal/mol)
23	none	0.0 (norm)	0.0 (norm)
23 Anion	1–	340.2	305.8

Table I-5. Gibbs free energy values, in the gas phase and with implicit solvation, for DMAc in its ground state and for the protonated cation of DMAc. SMD was the implicit solvation model used.

Compound	Charge	G_{gas} (kcal/mol)	G_{DMAc} (kcal/mol)
DMAc	None	0.0 (Norm)	0.0 (Norm)
DMAc-H	1+	–216.8	–267.2

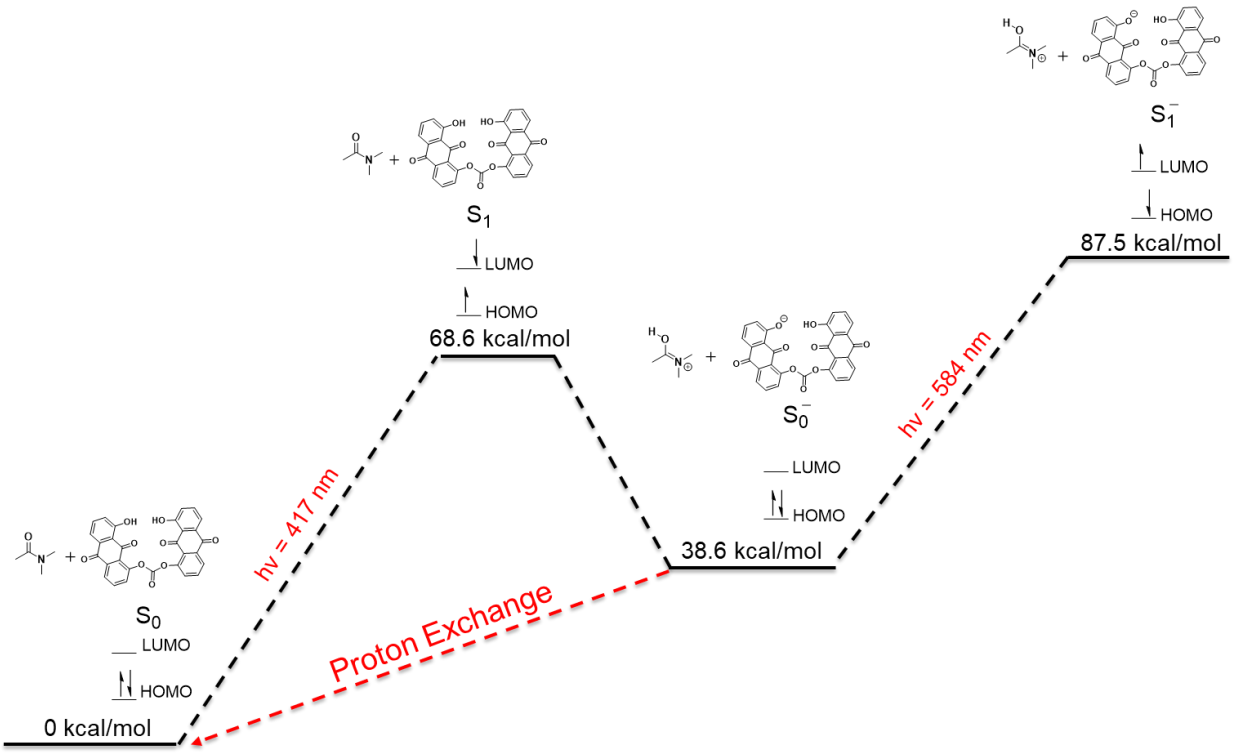

Figure I-19. The normalized Gibbs free energy values of **23** and DMAc shows that although an excited-state deprotonation is theoretically possible, the Gibbs free energy value of the resulting anion is higher than the neutral ground state by 38.6 kcal/mol. The proton exchange to return to the ground state is competing with a second excitation of the anion. The relative rates of these two processes are not yet known.